RESPONSE OF UNSATURATED SOILS UNDER MONOTONIC AND DYNAMIC LOADING OVER MODERATE SUCTION STATES

by

ARITRA BANERJEE

Presented to the Faculty of the Graduate School of

The University of Texas at Arlington

in Partial Fulfillment of the Requirements

for the Degree of

DOCTOR OF PHILOSOPHY

THE UNIVERSITY OF TEXAS AT ARLINGTON

May 2017

This work is dedicated to my grandmother, who had recently passed away and to my beloved parents.

ACKNOWLEDGEMENTS

First of all, I would like to express my deepest gratitude to my research advisor, Dr. Anand J Puppala for offering me the opportunity to pursue my doctoral research under his esteemed guidance. I am especially thankful to him for providing me with excellent research facilities and a very friendly working environment. I am indebted to him forever for his excellent guidance, invaluable remarks, motivation, and wholehearted support during the entire period of this research.

I would also like to convey my gratitude to Dr. Laureano R. Hoyos for his suggestions, expert guidance, and careful review of my dissertation. Furthermore, I am also grateful to Dr. Xinbao Yu and Dr. Shih-Ho (Simon) Chao for their willingness to serve on my dissertation committee. I would like to thank them for their valuable advice and insightful comments.

Furthermore, I would like to thank the Department of Civil Engineering for their financial support through the EGTA scholarships. I would also like to thank the University of Texas at Arlington and the Carrizo Oil and Gas, Inc. for selecting me for the Carrizo Oil and Gas, Inc. Graduate Research Fellowship. The work described in this dissertation was funded by the National Science Foundation's grant # 1039356. Their financial support is gratefully acknowledged. I would extend a vote of thanks to Mr. Mark Thomas and D&S Engineering Labs for helping me with obtaining the silty soil for this research. I would also like to thank Mr. Paul Shover, Mr. Peter Goguen, Mr. Manuel Abundez and GCTS Testing

Systems for their help in modifying the equipment. I am grateful to Dr. J. S. Vinod from University of Wollongong, Australia for his suggestions during final phase of the experimental research.

I would like to express my thanks to my colleagues Dr. Aravind Pedarla, Dr. Ujwalkumar Patil, Dr. Tejo Bheemasetti, Dr. Pinit Ruttanaporamakul, Dr. Raju Acharya, Dr. Alejandro Pino, Dr. Nan Zhang, Santiago, Minh Hai, Haifeng, Sayantan, Jasaswee, Ali, Dany, Anu, Leila, Tom, Puneet, Sarat, Rinu, Manikanta, Carlos, Minh Tran, Kaleisha, Manaf, and Leo for their sincere support and encouragement during this research work.

I would also like to thank my parents for their continuous support and encouragement all along. Finally, I would like to thank the God Almighty without whose blessing nothing would have been possible.

April 12, 2017

ABSTRACT

RESPONSE OF UNSATURATED SOILS UNDER MONOTONIC AND DYNAMIC LOADING OVER MODERATE SUCTION STATES

Aritra Banerjee

The University of Texas at Arlington, 2017

Supervising Professor: Anand J. Puppala

The understanding of the mechanical behavior of the unsaturated soils has been significantly enhanced due to the recent advancement of technology and modifications to the conventional testing devices. However, the implementation of the concepts of unsaturated soil has lagged, mainly due to the risks associated with the development of civil infrastructure based on practically untested theories and the limited reliable prediction methods for compacted, expansive, residual, and collapsible soils, which requires reliable and comprehensive experimental data. Moreover, the tests on unsaturated soils are enormously time consuming and often exorbitantly expensive, which further hinders the use of unsaturated soil mechanics in practical applications.

Additionally, the liquefaction of cohesionless soils has predominantly been considered only for saturated soils. However, the soils with high degree of saturation, yet partially saturated, which are mostly near the ground surface and have low overburden pressure, may liquefy during earthquakes. Since plenty of unsaturated cohesionless soils are present near high seismic activity zones, the susceptibility of these soils to liquefy needs to be studied. Addressing these problems has been the main objective of the present dissertation research.

The characteristics of compacted soils were studied by performing an elaborate series of suction-controlled monotonic triaxial tests on compacted silty soil specimens following the hydrostatic compression (HC) and the conventional triaxial compression (CTC) stress paths at varying net mean stresses and matric suction levels. The multistage triaxial tests were performed on the silty soil specimens at varying suction levels using a new approach to address the issues related to soil variability and to significantly reduce the testing time while maintaining the reliability of the test results. The Barcelona Basic Model (BBM) framework was used to reproduce experimental test results both from suction-controlled single-stage and multistage triaxial tests. Hence the BBM was indirectly used to demonstrate the utility of multistage triaxial tests in replicating test results or predictions similar to single-stage triaxial testing.

The influence of suction, unit weight, and wetting and drying of the compacted specimens of silty soil on the resilient modulus was also studied by performing a comprehensive series of suction-controlled repeated load triaxial (RLT) tests over a wide range of suction to address the issue of repeatability of RLT tests.

In this dissertation research, the tendency of the soil in unsaturated condition to liquefy was studied by performing cyclic triaxial tests on suction-equilibrated silty sand specimens. A series of cyclic triaxial tests were performed in undrained conditions at varying suction states and cyclic stress ratios to assess the liquefaction potential of the soil at varying relative densities and matric suction levels.

The findings from this dissertation research would assist in the development of future constitutive models for predicting the response of dilatant soils in unsaturated conditions subjected to monotonic and dynamic loading.

TABLE OF CONTENTS

LIST OF ILLUSTRATIONS

LIST OF TABLES

Chapter 1

INTRODUCTION

1.1 General

Unsaturated soils, which are neither completely dry nor fully saturated, are prevalent at shallow depth in regions having arid and semi-arid climatic conditions. Around one-third of the earth's surface is situated in these regions, where the potential evaporation exceeds the precipitation (Barbour, 1998). However, as per theories of classical soil mechanics and geotechnical engineering, the basic assumption for most of the analysis for any geotechnical problem is that the soil is either completely dry or fully saturated and these are only the extreme conditions of the soils (Fredlund and Rahardjo, 1993). Contrary to this assumption, the unsaturated soils are a general case, which can characterize the special cases that lie in between dry soil (0 percent saturation), and fully saturated soil (100 percent saturation). Despite the abundance of unsaturated soils around the world, limited research has been conducted in this field.

Generally, the soil beneath the ground water table is considered to be saturated, while the soil above the water table (also known as the vadose zone) is considered to exist in unsaturated condition. The soil below the water table consists of soil solids and pore water, which is commonly referred to as the two-phase system. In the vadose zone, the soil exists in a four-phase system (Fredlund and Morgenstern, 1977). The four-phase system comprises of soil solids, pore water,

pore air and the air-water interface, known as contractile skin (Paddy, 1969). The interactions of the contractile skin with the various phases result in the generation of surface tension. The study of unsaturated soil involves the principles of mechanics, hydraulics, and interfacial physics. The fundamentals of interfacial physics control the behavior of the air-water interface or the contractile skin (Fredlund et al., 2012). The behavior of contractile skin and multiphase interactions have significant influence on the overall response of the unsaturated soil, which primarily results in the difference in the behaviors of unsaturated and saturated soils (Lu and Likos, 2004). Because of the complexity of the material properties and the requirement of sophisticated equipment to characterize the behavior of unsaturated soils, limited research has been conducted, resulting in a lack of knowledge.

The seasonal variations of temperature and moisture regime cause fluctuations in the depth of the water table (Fredlund et al., 2012). These seasonal variations and precipitation result in stresses being induced to the soil, which also alters its properties and behavior. The variation in the properties of the soil may result in changes in its shear strength, stiffness, bearing capacity, and others. The negligence or oversimplification of the relations, required to accurately study the behavior of unsaturated soils, has resulted in incorrect predictions of strength and volume changes of soil when it is subjected to various kinds of loads, such as structural and climatic loads. Since the volume changes of expansive soils create severe distress to civil infrastructure, the study of the behavior of expansive soils

motivated the unsaturated soil research (Jones and Holtz, 1973; Lu and Likos, 2004). Similarly, the collapsible soils undergo enormous settlement on wetting, due to the weakening of cementation bonds and the collapse of the initially loose fabric, which also emphasized the need to study the behavior of unsaturated soils.

Initially, the soil system is at equilibrium state. However, as the external forces are applied, in the form of structural loads, surcharge, and rapid drawdown, the soil attempts to regain its equilibrium by balancing the components of the stresses applied and the stresses arising from the interaction of the phases. These stresses and interactions include the pore water pressure, pore air pressure, changes in osmotic suction due to chemical imbalance, water vapor pressure in the air, dissolved air in the water, contractile skin, an adsorbed double layer of water on the surface of soil particle and absorbed water into the soil solids, and the interactions among the soil solids (Murray and Sivakumar, 2010). Some of these interactions may be insignificant and, therefore, may be ignored, but the contribution of each phase and interaction to the general behavior of the soil in unsaturated condition is pivotal.

The determination of the stress variables responsible for influencing the behavior of unsaturated soil has been debated over years. The pioneering studies, like those of Bishop (1959), Coleman (1962), and Bishop and Blight (1963) aimed at the development of a single relationship which could define the effective stress in unsaturated soils as a modified version of the classical effective stress equation

for saturated soils established by Terzaghi (1936, 1943). Fredlund and Morgenstern (1977) introduced the concept of two-independent stress state variables (i.e., net mean stress and matric suction) to define the effective stress of unsaturated soils. This approach has been widely adopted and validated by many researchers (Ho and Fredlund, 1982; Escario and Saez, 1986; Fredlund and Rahardjo, 1993; Houston et al., 2008; Nyunt et al. 2011, Leong et al., 2013; Rosone et al., 2016). Recently, an attempt has been made to comprehend the fundamentals of unsaturated soil mechanics, and constitutive models have been developed to predict the strength and volume change responses of soils subjected to monotonic loading. Researchers such as Alonso et al. (1990) have developed pioneering constitutive drivers for unsaturated soils demonstrating compressible behavior, which has been widely used by other researchers.

In the field, the subgrade soils, on which pavements are constructed, are mostly unsaturated and are subject to seasonal variations of moisture content and hence induced suction. The resilient modulus is primarily used in the mechanistic pavement design methods to characterize the resilience of pavement materials (Han and Vanapalli, 2015). The resilient modulus of subgrade soil is highly dependent on the applied stresses, moisture regime, soil type, soil fabric/particle arrangement and testing protocols (Puppala, 2008). Although matric suction is an important parameter for determination of resilient modulus of the subgrade soil, little attention

has been given to either controlling or measuring suction during resilient modulus testing.

Furthermore, the liquefaction of a soil is basically assumed to be in saturated cohesionless soils. Many studies have been conducted after the pioneering work of Seed and Idriss (1971) on saturated soils. However, rarely has the assessment of liquefaction potential been conducted on soils which are almost saturated. These soils, which have a high degree of saturation (but are not completely saturated) may undergo significant loss of strength, thereby resulting in excessive subsidence, which is also known as cyclic mobility. The aspects of unsaturated soils, which affects the mechanical and hydrological responses of soils under static and dynamic loading conditions, have been the primary focus of this dissertation.

1.2 Problem Statement and Research Objectives

A comprehensive study, using an innovative triaxial setup, was conducted to characterize the mechanical response of unsaturated soils when subjected to monotonic and dynamic stresses under varying levels of suction. Emphasis was placed on the effects of matric suction on the response of unsaturated soil under monotonic and dynamic loads. It is anticipated that the experimental evidence observed from these studies, pertaining to the behavior of dilatant geomaterials under monotonic loads, will enable the future enhancement of advanced constitutive models. The liquefaction tests conducted under the unsaturated condition may be helpful in broadening the scope of our understanding regarding

the conditions which are susceptible to cause liquefaction. Finally, the effect of matric suction and the density of the soil on the resilient modulus of the silty soil is investigated using suction controlled, repeated load triaxial tests (RLTTs), to explore the capability of this technique to address the issues regarding the repeatability of these tests. Thereby, minimizing the uncertainty in the values of resilient modulus, which are used to design the pavement thickness.

The main objective of this dissertation work was therefore to modify an advanced triaxial setup, so that it could perform suction-controlled monotonic and dynamic triaxial tests on unsaturated soil specimens at varying suction states, using the axis translation technique. The experimental setup was also used to induce high suction (above 10 MPa) using a relative humidity apparatus that works on the principle of the vapor pressure technique. The resilient modulus tests were performed on these specimens having high induced suction, to study the effect of a wide range of suction on resilient modulus of silty soil.

The research for this dissertation was divided into six major tasks, which are discussed briefly in the following section.

The first task comprised of literature review, soil selection, and preliminary tests on selected soils. Simultaneously, the triaxial setup was modified to successfully perform a wide range of tests. Initially, the system was calibrated and tests were performed on replicated specimens to verify the repeatability of the tests. Thereby, the proper functioning, operation, control, and data acquisition system of

the modified triaxial setup were ascertained. After performing the literature review to define the problem statement, the appropriate soils were selected. The preliminary tests on the selected soils were conducted, such as the sieve analysis, including hydrometer analysis for fines present in the soil; specific gravity; Atterberg's limit; Proctor compaction; and Soil Water Characteristic Curve (SWCC).

The second task included a series of triaxial tests, following the Conventional Triaxial Compression (CTC) stress path, on saturated and unsaturated specimens of silty soil under drained conditions. The net confining pressures of 100, 200 and 400 kPa were used, and the matric suction was varied from 0 to 750 kPa using the axis translation technique.

The third task was to determine the applicability of multistage triaxial tests at the same matric suction, with varying net mean stresses. These tests were performed under the same conditions as those of the conventional (or single-stage) triaxial tests. The results from the multistage tests were compared to those of the single-staged tests, to confirm their applicability to low suction states (matric suction between 0 and 250 kPa).

The fourth task included the calibration and validation of the fundamental version of the Barcelona Basic Model (BBM) framework using the experimental data obtained from the series of triaxial tests performed. The deviator stress

responses obtained from triaxial tests were compared with the predictions made from the calibrated BBM framework.

The fifth task was the development of a new test sequence to determine the resilient modulus of subgrade soil, which had been equilibrated to a constant suction level, by using the axis translation technique (matric suction less than 500 kPa) and the vapor pressure technique (suction more than 10 MPa). This task also included the development of a prediction model, capable of predicting the resilient modulus of soil based on its SWCC parameters and the value of induced-suction.

The sixth and final task was comprised of a series of suction-controlled triaxial tests, under cyclic loading sequence in undrained conditions to determine the liquefaction potential of the silty sandy soil. These tests were performed to ascertain the resistance to liquefaction due to induced matric suction and to determine the upper limit for induced matric suction at which cyclic stresses do not cause liquefaction.

Figure 1.1 represents a flow chart of the major research tasks performed.

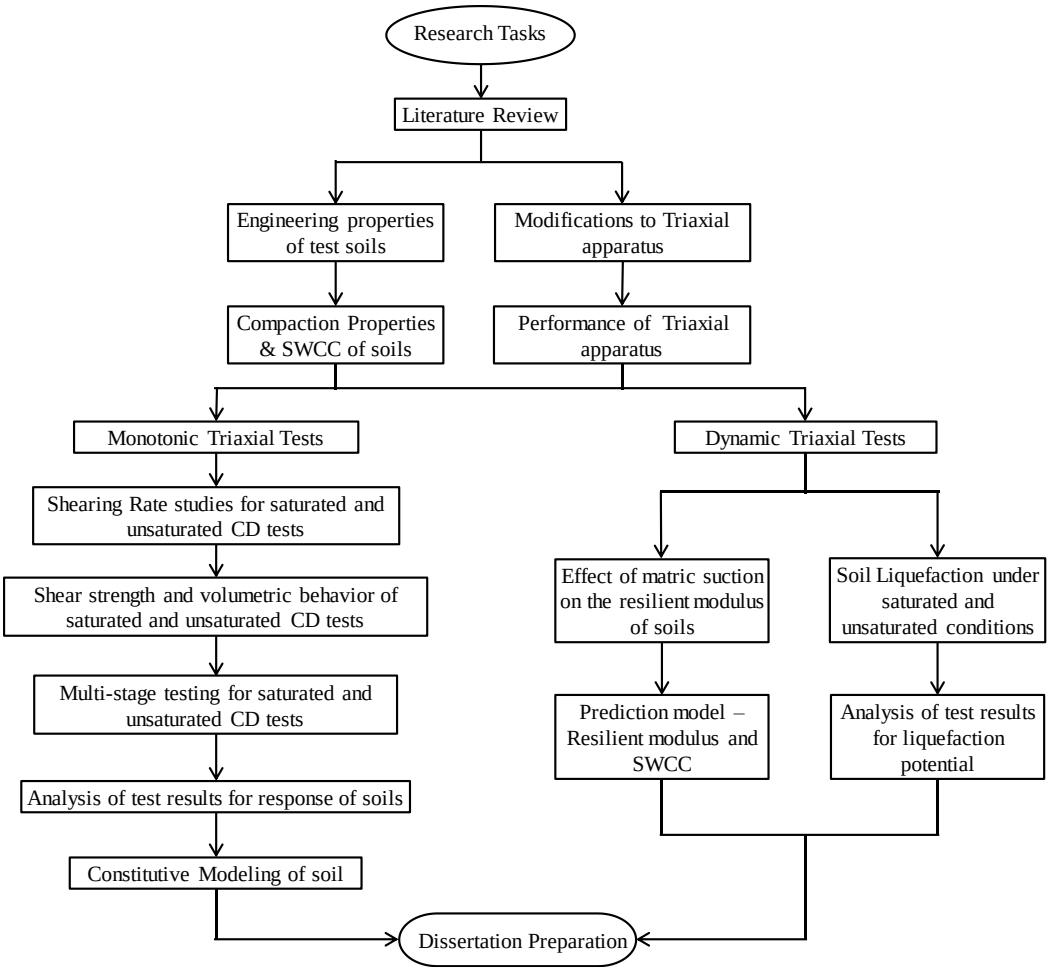

Figure 1.1 Flowchart for the tasks involved in the research

1.3 Organization of Dissertation

The dissertation is divided into seven chapters.

The first chapter introduces the problems that are caused by unsaturated soils and describes the significance of devising an advanced triaxial setup which is capable of performing suction-controlled monotonic and dynamic triaxial tests on

soil specimens. The research objective and the tasks involved in the research are also discussed in this chapter.

Chapter 2 includes a synopsis of the fundamental concepts involved in unsaturated soils. The overview primarily emphasizes the matric suction in soils, modifications to the conventional triaxial testing setup, the shear strength of unsaturated soils, triaxial tests of saturated and unsaturated soil specimens, the resilient modulus of soils and the liquefaction potential of cohesionless soils. It also includes prior developments in the triaxial testing of unsaturated soils for determination of shear strength and soil volume change response under monotonic loading. A review of the literature was performed on the application of triaxial test apparatus to determine the resilient modulus of subgrade soils and the liquefaction potential of saturated and unsaturated soils.

Chapter 3 discusses the primary features of the modified suction-controlled triaxial testing device used in this research. This chapter includes an elaborate explanation of the basic laboratory experiments performed on the test soils, such as the sieve analysis (including hydrometer test), specific gravity, Atterberg's limit, Proctor compaction, maximum and minimum void ratio, and Soil Water Characteristic Curve (SWCC). The technique employed to prepare compacted soil specimens is also discussed, as is the procedure followed to perform the conventional (or single-staged) triaxial test on unsaturated specimens under monotonic loading. The results from the series of single-staged triaxial tests under

monotonic loading following the conventional triaxial compression (CTC) stress path under drained conditions are also presented in this chapter. These tests include the determination of strain rate for shearing of saturated and unsaturated specimens, repeatability tests, and the influence of matric suction and net confining pressure (or net mean stress) on the response of saturated and unsaturated specimens of compacted silty soil.

Chapter 4 describes the procedure used to perform a multistage triaxial test of unsaturated specimens of compacted silty soil at constant suction and varying confining pressures. The results of these tests were analyzed and compared with those of single-stage tests, thereby recommending a convenient, yet effective methodology to perform the multistage triaxial test. This chapter also presents a succinct discussion regarding the basic elasto-plastic framework of the Barcelona Basic Model (BBM), as postulated by Alonso et al. (1990). Initially, the model parameters were calibrated using the experimental data obtained from the triaxial tests on compacted silty soil specimens. The calibrated model was then used to predict the stress-strain response at varying suction levels, and was compared with those obtained from the experimental single stage and multistage triaxial tests.

Chapter 5 discusses the determination of the resilient modulus of suction equilibrated specimens of silty soil using a modified triaxial setup. Low-to-medium suction levels (0–300 kPa) were applied, using the axis-translation technique, while high suction levels (suction greater than 10 MPa) were applied using the vapor

pressure technique. The vapor pressure technique was applied using an automated relative humidity apparatus. The working principle of the automated relative humidity apparatus is discussed in this chapter. The overall modifications to the triaxial setup and the procedure for conducting a resilient modulus test on specimens equilibrated at constant suction are also described. The experimental results of the resilient modulus of specimens of silty soil under varying suctions and dry densities are discussed. The effect of suction on resilient modulus of soils was investigated by modifying the prediction model presented by Han and Vanapalli (2015). The model was calibrated and then the predictions were compared against experimental results from this study and studies available from the literature.

Chapter 6 focuses on the liquefaction assessment of unsaturated soil, using the modified triaxial testing device. In the past, the presence of highly compressible air in unsaturated soils has been assumed to implicitly safe against cyclic shear. This is the primary reason for the lack of research on liquefaction analysis and the shear strength reduction of unsaturated soils subjected to dynamic stresses. After the pioneering work of Seed and Idriss (1971), the liquefaction potential of saturated cohesionless soils was investigated by many researchers. In this chapter, an attempt to develop a correlation by considering the liquefaction resistance developed in silty sandy soil due to induced matric suction, is described. To achieve this, a comprehensive series of cyclic triaxial tests was performed on saturated and

unsaturated specimens of loose silty sand for varying cyclic stress ratio and varying degrees of saturation under undrained conditions. The term “liquefaction resistance factor” is used to quantify the resistance to liquefaction caused by the induced matric suction.

Chapter 7 summarizes the major conclusions obtained from this research and suggests the future scope of research in the field of experimental geomechanics and constitutive modeling of unsaturated soils. Finally, the novelty of this research work is briefly discussed.

Chapter 2

UNSATURATED SOIL MECHANICS FUNDAMENTALS

2.1 Introduction

The fundamental concepts involved in unsaturated soils are complex involving solid mechanics, hydraulics, and interfacial physics (meniscus). Therefore, this chapter is devoted to the explanation of the theories of unsaturated soil mechanics.

The concept of thermodynamics plays an important role in the behavior of unsaturated soils, as it controls the meniscus formed at air and water interface (Lu and Likos, 2004). It involves the knowledge of vapor pressure, evaporation, precipitation, suction, and cavitation. The thermal agitation causes the water molecules, present within the soil, to escape from the air-water interface. Higher temperature results in higher kinetic energy, which causes a larger number of water molecules to escape from the liquid phase to vapor phase. The vapor pressure increases till the number of molecules of water leaving and entering the water phase attains equilibrium, which is known as the saturated vapor pressure (Giancoli, 1985). The evaporation of water from the soils causes the air-water interface to initially develop and gradually curve due to the pressure difference between the air and water phases in the soil (Fredlund et al., 2012).

The rate of evaporation primarily depends on the temperature, vapor pressure, water content and concentration of salts. The suction developed due to the

presence of dissolved solutes in pore water is known as osmotic suction. The concentration of salts decreases the vapor pressure and results in an increase of osmotic suction, which results in a slower rate of evaporation at a given temperature (Fredlund and Rahardjo, 1993). Conversely, precipitation results in an increase in water content and decrease in vapor pressure, resulting in decrease in the soil suction.

The behavior of the soil depends on the equilibrium of the inter-molecular and intra-molecular forces/stresses existing among the soil solids, pore water pressure, pore air pressure, and the air-water interface (Laloui, 2010). Since the principles of thermodynamics affect these forces/stresses, the behavior of soil varies significantly due to drying or wetting of soil (Fredlund et al., 2012). In other words, the behavior of saturated and unsaturated soils is significantly different due to thermodynamics. Henceforth, the constitutive relations or parameters required to predict the behavior of unsaturated soils are different from that required for saturated soils.

2.2 Saturated and Unsaturated Soils

A brief overview of the saturated and unsaturated soils is provided in this section, in order to clarify their differences. Figure 2.1a shows a schematic diagram of the location of saturated and unsaturated soils and their phase diagrams. The variation of pore water pressure with depth, with reference to ground water table and capillary fringe, is shown in Figure 2.1b. Generally, it is assumed that the

ground water table defines the separation of the unsaturated and saturated soil mediums. There is an additional layer above the water table which is almost saturated, known as the capillary fringe. This layer has minuscule and discontinuous pore air voids and the pore water pressure is negative (shown in Fig. 2.1b). The soil above the water table, consisting of the capillary fringe and the unsaturated soil, is commonly referred to as the vadose zone. The vadose zone media has a negative pore water pressure.

The saturated soil, which lies beneath the water table, has no air voids and forms a two-phase system consisting of soil solids and pore water. In this layer, the pore water pressure is positive and increases linearly with depth from the ground water table level.

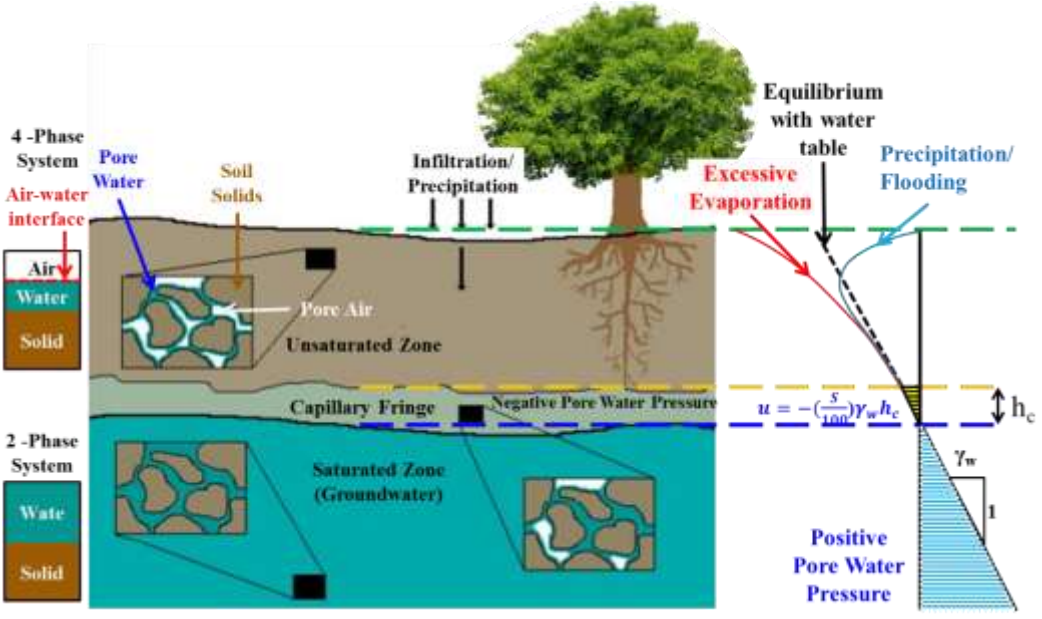

Figure 2.1 Schematic diagram of the variation of pore water pressure with depth (modified from MSU, n.d.)

The unsaturated soil layer, which lies above the capillary fringe, has a four-phase system comprising of soil solids, pore water, pore air, and the air-water interface, commonly known as the meniscus. The degree of saturation and the soil suction determines the continuity of the pore water and pore air. At a very low degree of saturation (less than 20% or 30%), the pore air phase is generally continuous and is referred to as "Pendular saturation" (Bear, 1979; Lu et al., 2009).

For a higher degree of saturation (greater than 85% or 90%) the air voids are occluded within continuous water phase (Schuurman, 1966; Fredlund and Morgenstern, 1977). This state is referred to as "insular air saturation" or "capillary regime" (Bear, 1979; Lu et al., 2009). Whereas, the transition state, where both air and water phases are continuous, is known as "Funicular saturation" (Lu et al., 2009). The variation of pore water pressure in the unsaturated zone is predominantly dependent on the climatic conditions.

Near the ground surface (in the vadose zone), the increase in temperature causes excessive evaporation which results in an increase in the magnitude of the negative pore water pressure. Conversely, precipitation or very high humidity condition has an opposite effect. The variation of pore water pressure in this zone is thus non-linear (Fredlund et al., 2012). This non-linearity, coupled with negative values and the time varying nature of pore water pressure result in difficulties in measurement of these pressures in the field (Fredlund and Rahardjo, 1993).

High temperature conditions over a prolonged period of time increases the pore water pressure, causing desaturation induced volume shrinkage cracks. This is referred to as desiccation cracking (Omidi et al., 1996; Kodikara et al., 2000). On the other hand, when there is precipitation under these circumstances, the sudden decrease in the magnitude of pore water pressure might cause surficial failure, especially on steep slopes.

The behavior of soil also depends on its brittleness. Brittleness is the tendency of a material (i.e., soil in this case) to fail upon application of small amount of load without significant deformation. Brittleness affects the post-peak softening, which is the decrease in strength of soil from the peak strength to residual or critical state strength upon shearing. The influence of suction on brittleness and post-peak softening have been investigated in Chapter 3.

2.3 Soil Suction in Unsaturated Soils

Soil suction is defined as the free energy state of the soil-water (Edlefsen and Anderson, 1943), which can be computed in terms of the partial vapor pressure of the pore water. The total suction (ψ) of a soil has mainly two components: matric suction ($u_a - u_w$) and osmotic suction (π). The suction developed due to the combined effects of capillarity and short-range adsorption is collectively known as matric suction (Krahn and Fredlund, 1972; Lu and Likos, 2004). The word *matric* reflects the prior usage of the term *matrix*, which symbolizes the suction due to interactions between pore water and soil solids (Lu and Likos, 2004).

The suction developed due to the presence of dissolved solutes is known as osmotic suction. Generally, in non-plastic soils, the matric suction is a major component of total suction. Expansive soils demonstrate high activity due to mineral composition and dissolved solutes. Hence, osmotic suction component constitutes a considerable portion of total suction (Blatz et al., 2008).

2.4 Surface Tension

Air-water interface exhibits a phenomenon called surface tension. Surface tension arises from unbalanced intermolecular forces acting on molecules of the liquid phase, which is water in this case (Lu and Likos, 2004). Figure 2.2 shows a schematic diagram of the generation of surface tension from unbalanced forces at the air-water interface. Any water molecule present in the liquid phase (away from the air-water interface) experiences equal tensile forces from all directions due to hydrogen bonds between adjacent water molecules. Therefore, no unbalanced forces are present and the water molecule is in static equilibrium.

Conversely, any water molecule at or very near to the air-water interface experiences tensile forces from adjacent water molecules, but as these forces are not equally distributed, they result in unbalanced forces and the resultant tension acts towards the interior of water body (as shown in Fig. 2.2). This resultant unbalanced force leads to the phenomenon of surface tension. The same property causes a water droplet to appear as a spherical mass (due to gravity it gets distorted).

Surface tension acts as an elastic membrane at the air-water interface and it acts tangentially to the air-water interface (Figure 2.3).

The pressure difference (Δu) across a warped three-dimensional surface with radii of curvature of two orthogonal principal planes, R_1 and R_2 and surface tension, T_s (Figure 2.3) is given by the following relation:

$$\Delta u = T_s \left(\frac{1}{R_1} + \frac{1}{R_2} \right) \tag{2.1}$$

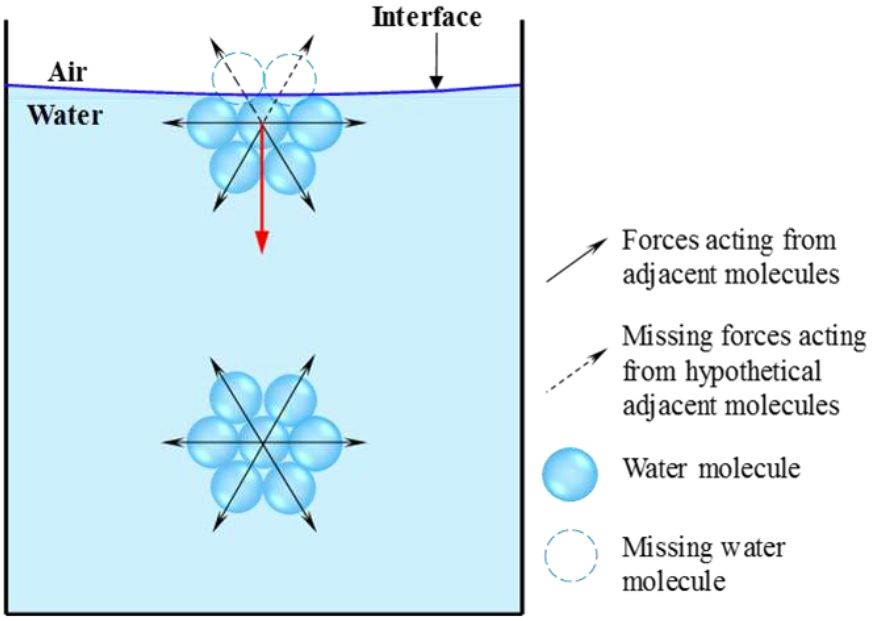

Figure 2.2 A schematic of the surface tension at air-water interface

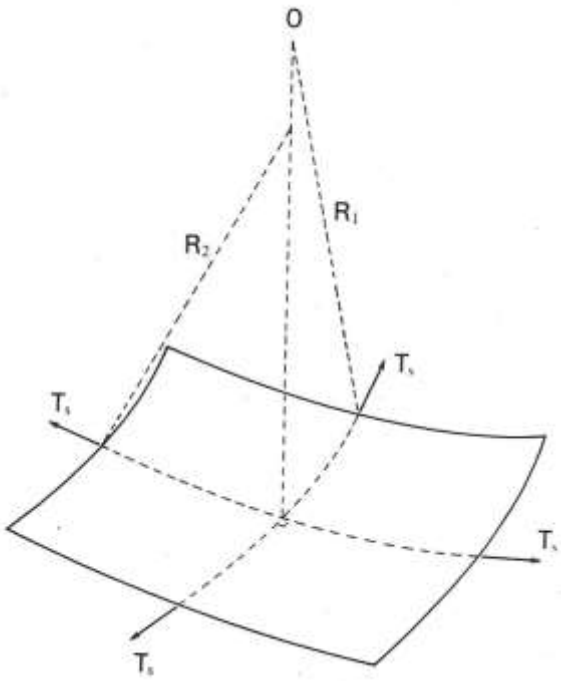

Figure 2.3 Surface tension on a warped membrane (Fredlund and Rahardjo, 1993)

When the radius of curvature is the same in all directions ($R_1 = R_2 = R_s$), the equation 2.1 reduces to:

$$\Delta u = \frac{2T_s}{R_s} \tag{2.2}$$

In unsaturated soils, this pressure difference is the matric suction ($u_a - u_w$) which causes the contractile skin of the air-water interface to curve, in accordance with the following relationship:

$$(u_a - u_w) = \frac{2T_s}{R_s} \tag{2.3}$$

2.5 Capillary Phenomenon

Capillarity occurs when liquid rises in narrow tubes or is drawn into small openings such as those between grains of a soil (Allaby, 2004). Generally, the capillary force comprises of two components: (*i*) the surface tension acting along the water-soil particle contact line, and (*ii*) the pressure difference across the bridge acting on the cross-sectional area (Pietsch and Rumpf, 1967; Schubert, 1984; Kim and Sture, 2008). Capillary action causes the water to move (against gravity) from water table into the soil pores. The height up to which the waterfront rises above the water table is known as the height of capillary rise, which depends on the dimension of the pore spaces. Generally, the fine-grained soils with small pore size, have a higher capillary rise as compared to that for coarse-grained soils. Physically, the maximum capillary height represents the decrease in pressure head across the air-water interfaces in the soil pores.

The rate of capillary rise depends on the hydraulic conductivity of the soil medium. When the capillary rise is greater than the air-entry head (explained in section 2.6.2) for that soil, the unsaturated hydraulic conductivity determines the rate of capillary rise. The unsaturated hydraulic conductivity depends on the degree of saturation and it maybe 5 to 7 orders of magnitude lower than that of saturated hydraulic conductivity (Lu and Likos, 2004).

The capillarity can be demonstrated by the capillary tube model, where the water rises in the tube of small diameter when the tube is immersed in water. The

capillary tube model can be used to predict the air-entry suction in the soil (Fredlund and Rahardjo, 1993; Lu and Likos, 2004). Since the in-situ soil is comprised of particles of different sizes and has complex geometries, analytical solutions for the height of capillary rise is too complicated. Hence, direct measurement of the height of capillary rise is the most reliable method, though often empirical relations, based on soil types, are used in real practice.

2.6 Soil Water Characteristic Curve (SWCC)

2.6.1 *General*

The soil-water characteristic curve (SWCC) provides a relationship between the water content (w) and the suction (ψ) for a specific soil. It portrays the thermo-dynamic capability of pore water in the soil with respect to that of the free water as a function of the measure of water adsorbed by the soil system (Lu and Likos, 2004). The SWCC mainly depends on the soil type, gradation, void ratio, presence of salt concentration, temperature, and drying or wetting cycle of testing. The SWCC is used to develop correlation with various parameters, like shear strength, stiffness, and permeability.

The fundamentals and behavioral understanding of the SWCC have been developed by the agriculture-related research communities, like soil science and agronomy. Due to the varied disciplines using the water content – soil suction relationship, various other terminologies have been used to define the relationship, like Soil Water Retention Curve (SWRC), and moisture retention curve. Also, the

amount of water in a soil can be defined using various terms, such as gravimetric water content (w), volumetric water content (θ), degree of saturation (S), ratio of the volume of water to the original volume of the specimen (V_w/V_o).

Gravimetric water content, w is mostly used in geotechnical engineering and is defined as:

$$\textit{Gravimetric water content, } w = \frac{M_w}{M_s} \tag{2.4}$$

where,

M_w = mass of water, and

M_s = mass of soil solids.

Volumetric water content, θ is usually used in the field of agricultural engineering and deals with the volumes of water, voids, and solids. It is defined as:

$$\text{Volumetric water content, } \theta = \frac{V_w}{V_v + V_s} \tag{2.5}$$

where,

V_w = volume of water

V_v = volume of voids, and

V_s = volume of soil solids.

The degree of saturation, S is the ratio of the volume of water, V_w to the volume of voids, V_v.

$$\text{Degree of Saturation, } S = \frac{V_w}{V_v} \tag{2.6}$$

Other terms to represent the amount of water present in soil include the dimensionless gravimetric water content, Θ, which is defined as the ratio of gravimetric water content at any degree of saturation, w to the initial saturated gravimetric water content, w_{sat}:

$$\text{Dimensionless gravimetric water content, } \Theta = \frac{w}{w_{sat}} \tag{2.7}$$

Each of the above terms has their own advantages and disadvantages for determination of the amount of water in the soil. The gravimetric water content is most commonly used measure of water content of a soil sample in which the reference is made with respect to the mass of soil solids (which remains constant). However, it does not account for the changes in volume of soil and the degree of saturation. The volumetric water content is often used in transient seepage in unsaturated soils, but volume measurements are complicated and its usage is quite unfamiliar to geotechnical engineers. The degree of saturation properly designates the air-entry value and controls the behavior of unsaturated soils. Though it involves the measurement of volume of soil solid, it does not incorporate the overall change in volume of the soil sample (Fredlund and Rahardjo, 1993).

The SWCC can be portrayed in terms of matric suction, osmotic suction and/or total suction. For practical considerations, the soil suction is considered to vary from zero to 10^6 kPa or 1 GPa. The Gibbs free-energy state equations for water vapor forms the basis for the upper limit of the soil suction (Gibbs, 1873; Edlefsen

and Anderson, 1943). The Gibbs free-energy state equation is a thermodynamic relationship between partial water vapor pressure (i.e., relative humidity) and the soil suction. The relative humidity (RH) is defined as the ratio of the partial pressure of water vapor to the saturation pressure of pure water vapor at a given temperature condition. Hence, the Gibbs free-energy state equation is presented in the following (Sposito, 1981):

$$\psi = -\frac{RT}{\nu_{wo}\,\omega_v}\ln\left(\frac{u_v}{u_{vo}}\right) = -\frac{RT}{\nu_{wo}\,\omega_v}\ln(RH) \tag{2.8}$$

where,

ψ = total suction, kPa,

T = Absolute temperature, K,

R = Universal gas constant (8.31432 J mol^{-1} K^{-1}),

ν_{wo} = Specific volume of water (i.e. reciprocal of density, m^3/kg),

ω_v = molecular mass of water vapor (18.016 kg/kmol),

u_v = partial pressure of water (or pore-water) vapor (kPa), and

u_{vo} = saturation pressure of pure water vapor (kPa).

The lowest and highest suction states provide important information about the soil and hence the suction values need to be plotted on a single graph on a logarithmic scale. Generally, the matric suction denotes the lower suction range (till 1500 kPa), while the total suction represents the higher suction range.

A typical SWCC is shown in Figure 2.4, where the various states of saturation are delineated by the air-entry value of the soil and the residual soil suction. Also, the effect of initial density of the SWCC is shown in Figure 2.5.

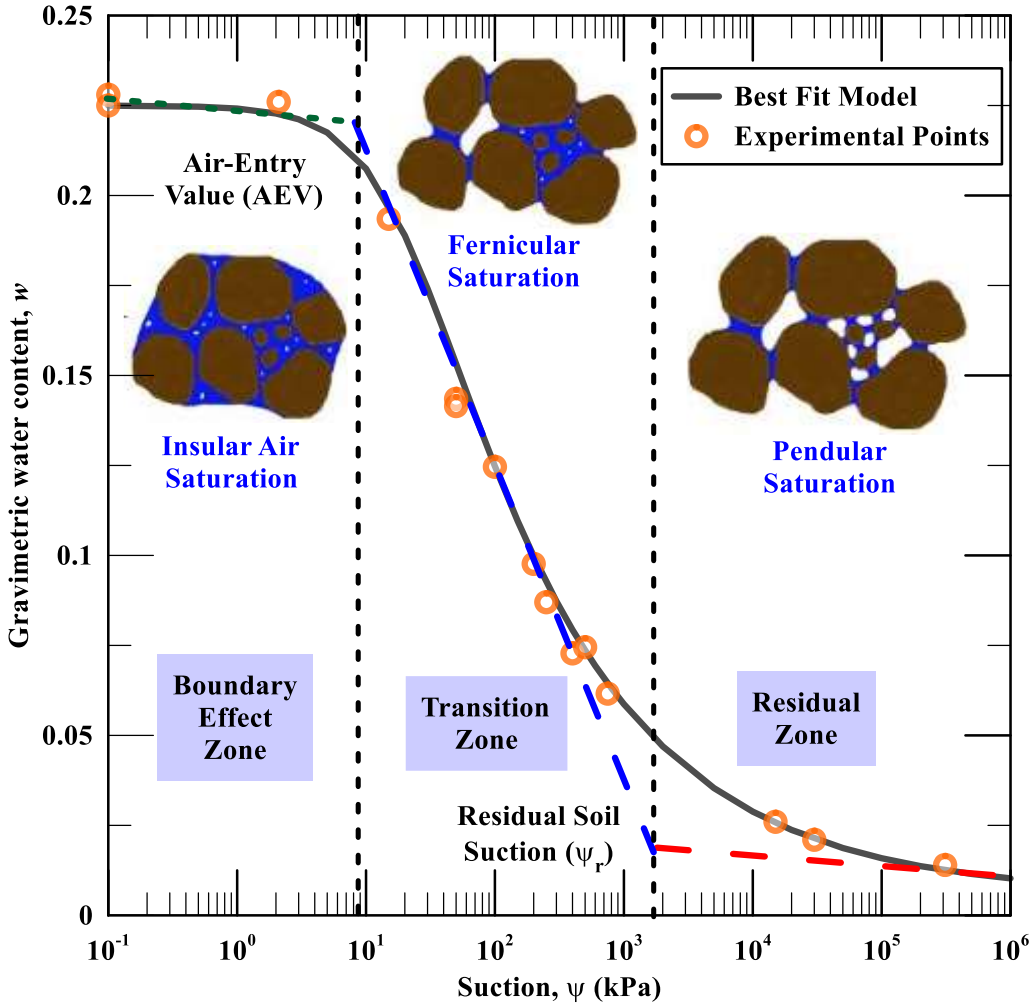

Figure 2.4 A typical Soil Water Characteristic Curve

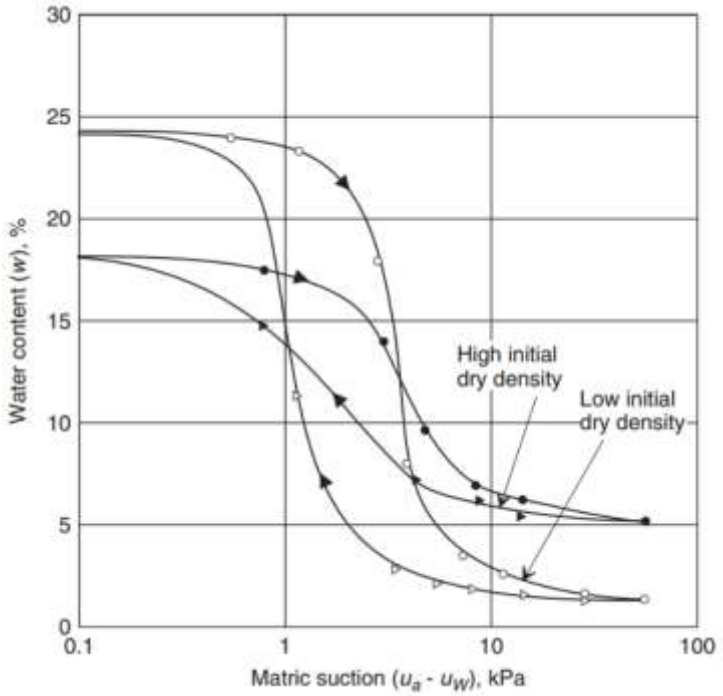

Figure 2.5 Effect of initial density on SWCCs (Croney and Coleman, 1954)

2.6.2 *Air-Entry Value*

Air entry value (AEV) of a soil is defined as the value of matric suction at which upon drying, the pore water is replaced by the air entering the soil (Lu and Likos, 2004). The AEV demarcates the boundary effect zone, which has insular air saturation, from the transition zone, which comprises of fernicular saturation. The permeability of the soil until the AEV is almost same as the saturated hydraulic conductivity, but upon further desaturation, the permeability decreases exponentially (Fredlund and Rahardjo, 1993). The AEV is determined by the intersection of the extrapolated portion of the linear part of the SWCC and the saturated portion of the SWCC as shown in Figure 2.4.

2.6.3 *Residual Soil Suction*

The suction at and beyond which the drying of soil barely decreases its water content is termed as residual soil suction. As per Vanapalli et al. (1998), beyond the value of the residual suction, the water is present in the soil system by means of adsorption and not by capillarity. The pore water phase becomes intermittent and isolated with thin films of water, which is difficult to remove with an increase in suction. The permanent wilting point is generally assumed to be the water content of the soil at residual suction state(van Genuchten, 1980).

The residual soil suction is obtained by the intersection of the extrapolated section of the linear portion of the SWCC and the tangent extended from the SWCC at the maximum suction, which is practically considered as 1 GPa (as shown in Fig. 2.4).

2.6.4 *Hysteresis Effect*

The drying and wetting cycles of the SWCCs are significantly different (as shown in Figure 2.6). In many scenarios, it becomes essential to evaluate the properties of soil separately for drying and wetting cycles. The Geotechnical engineers need to consider the conditions which the soil will experience in real conditions and accordingly use the properties of either of the two cycles (Tami et al., 2004). The drying cycle is easier to perform and hence most commonly conducted in the laboratory. The hysteresis behavior of the drying and wetting cycles has been studied in detail by (Pham et al., 2002, 2003a; b).

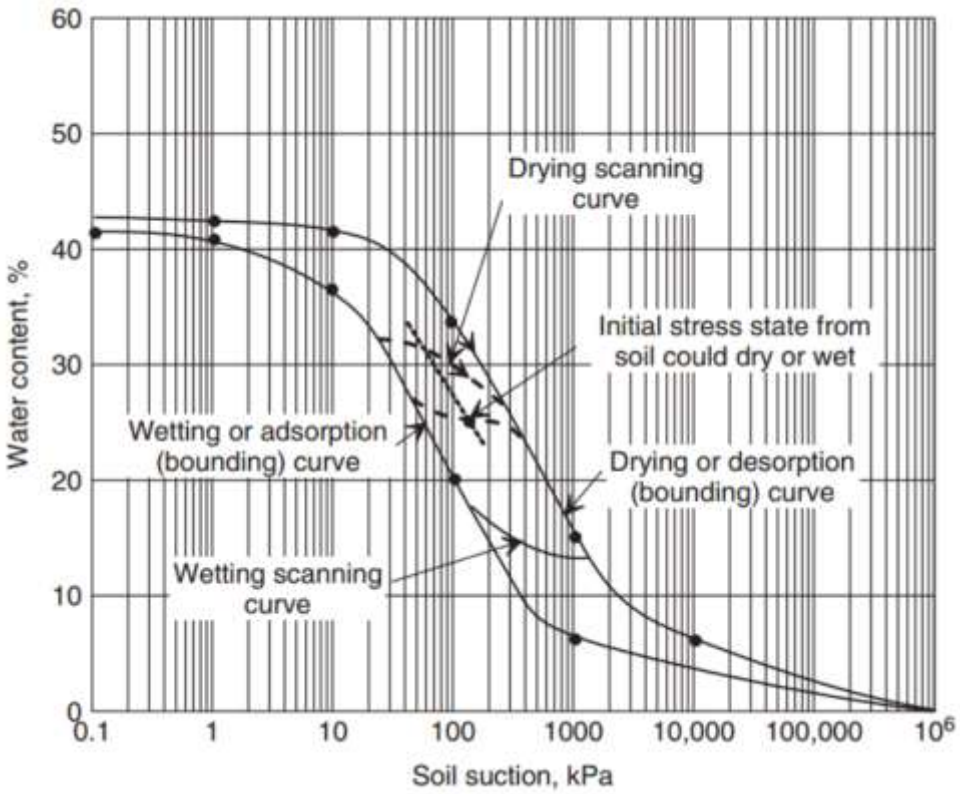

Figure 2.6 Schematic of SWCCs depicting hysteresis due to drying and wetting cycle (Fredlund and Rahardjo, 1993)

2.6.5 *Techniques for SWCC Measurement*

There are many techniques to determine the SWCC of a soil. Some of the techniques and equipment are suitable for laboratory testing, while the others are appropriate for use in the field. Some suction measurement devices measure total suction, while other record the matric or osmotic suction. The suction measurement techniques are broadly classified into two categories: (*i*) direct measurement techniques, where the suction is directly measured from the equilibrium of the soil-water system; (*ii*) indirect measurement techniques, where another parameter is

measured which has been equilibrated within the soil-water system. Correlations and/or calibration charts are then used to determine the suction from that measured parameter. Table 2.1 lists some of the most commonly used suction measurement devices and their limitations.

Table 2.1 Techniques to determine the various types of suction (modified from Lu and Likos, 2004; Murray and Sivakumar, 2010)

Suction Component Measured	Device / Technique	Typical range (kPa) (Area of Usage)	Limitations
Matric Suction	Pressure plate and Tempe cell	0 – 1,500 (Lab)	Long equilibration time and induced suction limited by AEV of ceramic disc
	Contact filter paper method	3000 – 100,000 (Lab)	Very sensitive to measurements
	Tensiometer	0 –100 (Lab and Field)	Cavitation at absolute zero pressure limits the range
	Electrical/thermal conductivity sensors	0 – 400 (Lab and Field)	High failure rate; fragile and needs regular calibration
Osmotic Suction	Electrical conductivity of pore water extracted using pore fluid squeezer	Entire range (Lab)	Sensitive to extraction pressure; otherwise other equipment is required to determine the total and matric suction
Total Suction	Thermocouple psychrometer	100 – 8,000 (Lab and Field)	Sensitive to temperature fluctuations
	Chilled mirror hygrometers	1,000 – 450,000 (Lab)	Sensitive to dust and temperature
	Non-contact filter paper method	3,000 – 100,000 (Lab and Field)	Calibration is sensitive to time for equilibration
	Relative humidity apparatus	5000 – 500,000 (Lab)	High suction range

2.6.5.1 Fredlund's SWCC Device

The Fredlund's SWCC device (Figure 2.7) is similar to the pressure plate device, with the added advantage that the overburden pressure can be applied and the entire SWCC can be obtained without disassembling the device. It works based on the principle of axis-translation technique. It can induce matric suction up to the air-entry value of the ceramic disk (generally, 500 kPa or 1500 kPa).

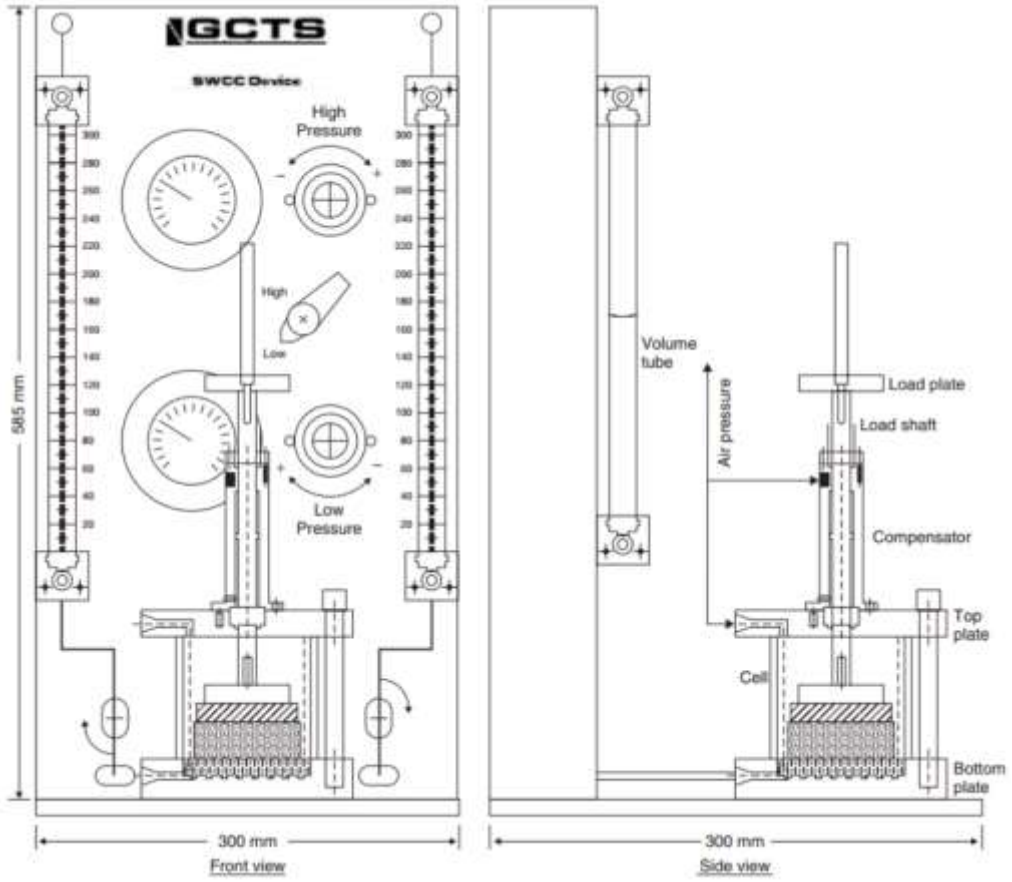

Figure 2.7 Fredlund's soil water characteristic curve device (Padilla et al., 2005)

2.6.5.2 Filter paper technique

The filter paper technique is an indirect method of measuring suction. The suction measurement is based on the moisture equilibration between the filter paper and the adjacent soil. Contact and non-contact filter paper techniques can be used to measure the matric and total suction, respectively. The ‘contact’ here refers to the direct interaction of the filter paper with the soil-water system within an enclosed space.

The filter paper absorbs moisture until the equilibrium has been achieved with the water content of soil for contact technique, and the relative humidity inside the container for non-contact technique. After equilibrium has been achieved between the filter paper and the relative humidity in the enclosed space, the adsorbed water content provides the correlation with the suction in the filter paper, based on the calibration charts. This technique is used to measure both total and matric suction for a soil specimen. The calibration chart has been shown in Figure 2.8 for the most commonly used filter paper, i.e., Whatman 42.

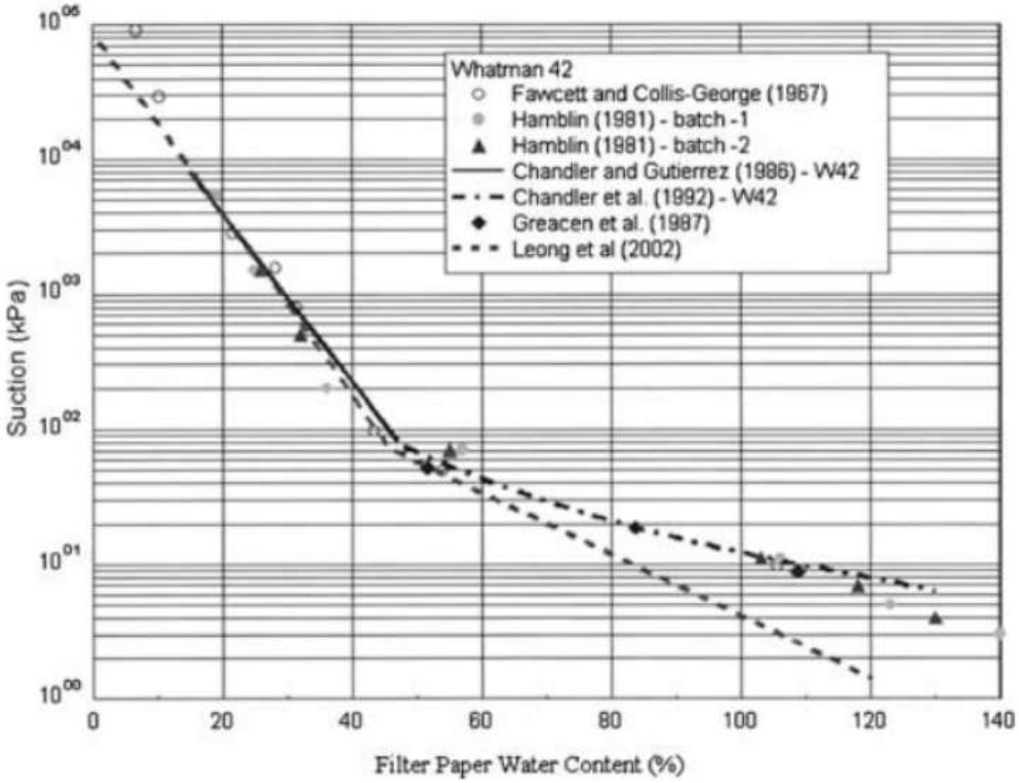

Figure 2.8 Calibration curves for Whatman No. 42 filter paper (Marinho and Oliveira, 2006)

2.6.5.3 Dew point potentiometer

The WP4C dew point potentiometer measures water potential by determining the relative humidity of the air above a sample in a closed chamber, using the principle of the chilled-mirror technique (ASTM D 6836; Leong et al., 2003; Thakur et al., 2005). The sealed block chamber comprises of the following: (*i*) a mirror; (*ii*) an optical sensor which is used to detect the dew formation on the mirror; (*iii*) a temperature sensor which measures the dew point temperature of the air; (*iv*) a thermopile to measure the temperature of the sample; and (*v*) a fan, which

enhances the equilibration of the sample with the chamber environment (Thakur et al., 2005).

Figure 2.9 WP4 chilled water Potentiameter

2.6.6 *Mathematical Models for SWCC*

The measurement of SWCC over the entire suction range and at close intervals is not practical, due to the high expenditure, lack of replicates of soil specimens, and time constraints. Henceforth, closed-form empirical relationships are mostly used to obtain best-fit curves using the discrete data points obtained from the laboratory tests. Some of the empirical relationships commonly used have been tabulated in Table 2.2.

A dimensionless parameter, Θ, is often used and is obtained by normalizing the volumetric water content with respect to saturated and residual condition, and is expressed as below:

$$\Theta = \frac{\theta - \theta_r}{\theta_s - \theta_r} \quad (2.9)$$

where,

θ = volumetric water content at any degree of saturation

θ_s = saturated volumetric water content

θ_r = residual volumetric water content

The normalized water content, Θ, varies from zero, for the residual condition, to 1, in case of the saturated condition. Also, if the residual water content is zero, the dimensionless parameter for water content Θ converges to the value of the degree of saturation, *S*.

Many other empirical relationships have also been developed in order to facilitate the SWCC modeling, including Leong and Rahardjo (1997), Sillers and Fredlund (2001), Houston et al. (2006), Pham and Fredlund (2008), and Gould et al. (2012). Recently other tools have being used in the form of data mining, neural networks and genetic programming based tools for determining soil suction-water content relationships (Johari and Javadi, 2011; Ahangar-Asr et al. 2012).

Table 2.2 Empirical models used to best fit SWCC data

Reference	Equation for Model	Parameters Involved
Brooks and Corey (1964)	$\Theta = \begin{cases} 1, & \psi < \psi_b \\ \left(\frac{\psi_b}{\psi}\right)^{\lambda}, & \psi \geq \psi_b \end{cases}$	ψ = soil suction; ψ_b = air-entry suction value of soil; λ = Pore size distribution index that varies with type of soil and its texture
Van Genuchten (1980)	$\Theta = \left[\frac{1}{1+\left(\frac{\psi}{\alpha}\right)^{n}}\right]^{m}$	α, n and m are fitting parameters based on AEV of soil, the rate of water extraction from the soil for suction greater than AEV and residual water content, respectively.
Fredlund and Xing (1994)	$\theta = C(\psi)\theta_s \left[\frac{1}{ln\left\{e + \left(\frac{\psi}{a}\right)^{n}\right\}}\right]^{m}$ where $C(\psi) = \left[1 - \frac{ln\left(1 + \frac{\psi}{\psi_r}\right)}{ln\left(1 + \frac{10^6}{\psi_r}\right)}\right]$	ψ = suction θ_s = saturated volumetric water content a, n, m are the fitting parameters based on AEV of soil, the rate of water extraction from the soil for suction greater than AEV and residual water content, respectively e = the natural logarithmic constant $C(\psi)$ = correction factor based on the suction corresponding to residual water content

2.7 Shear Strength

The shear strength of soil describes the magnitude of maximum shear stress it can sustain, and hence is an essential parameter for geomechanics and geotechnical engineers (Holtz and Kovacs, 1981). The safety of many engineering structures depends on the strength of underlying soil. Applications of shear strength of soil include problems like bearing capacity, slope stability, lateral earth pressure, pavement design and foundation design (Holtz and Kovacs, 1981; Lu and Likos, 2004). The general concepts associated with the shear strength of soil remain similar for saturated and unsaturated conditions. For instance, the increase in cohesion, internal friction angle of the soil and application of confining pressure increases the strength in both cases. Similarly, the concepts of dilation and changes in the shear strength of soil with strain are similar for both saturated and unsaturated conditions (Fredlund and Rahardjo, 1993).

2.7.1 *Shear Strength of Saturated Soil*

Most of the theories of shear strength were postulated after considering the limitations of the equation of shear strength of saturated soils to predict the strength of unsaturated soil. Henceforth, a brief review of the shear strength relations for saturated soils is presented.

The Mohr-Coulomb theory of shear strength of saturated soil, initially advocated by Coulomb (1776) and later generalized by Mohr (1914), is the most widely used relationship. Coulomb assumed that the normal stress acting on any

plane had a linear relationship with the shear strength available on that plane, which is known as Coulomb's law and is expressed as follows:

$$\tau = c + \sigma \tan \varphi \tag{2.10}$$

where, *c* and φ are cohesion and angle of internal friction of the soil, respectively.

The relation for total strength parameter (Eqn. 2.10) was modified, as it was postulated by Terzaghi that shear strength is a function of effective stresses. The modified relation is as follows:

$$\tau = c' + \sigma' \tan \varphi \tag{2.11}$$

where, *c'* and φ' are effective cohesion and effective angle of internal friction of the soil, respectively. The parameters, *c'* and φ' are known as the effective shear strength parameters. A typical Mohr-Coulomb Failure Envelope for a saturated over consolidated clay is shown in Fig. 2.10. Three hypothetical triaxial tests, i.e. A, B, and C, were performed on replicates of the same specimen at varying effective confining pressures, which failed at an effective axial stress of $\sigma_1'_A$, $\sigma_1'_B$, and $\sigma_1'_C$, respectively. Therefore, at failure, a shear stress of τ_f and a normal stress of σ'_f were acting along the failure plane.

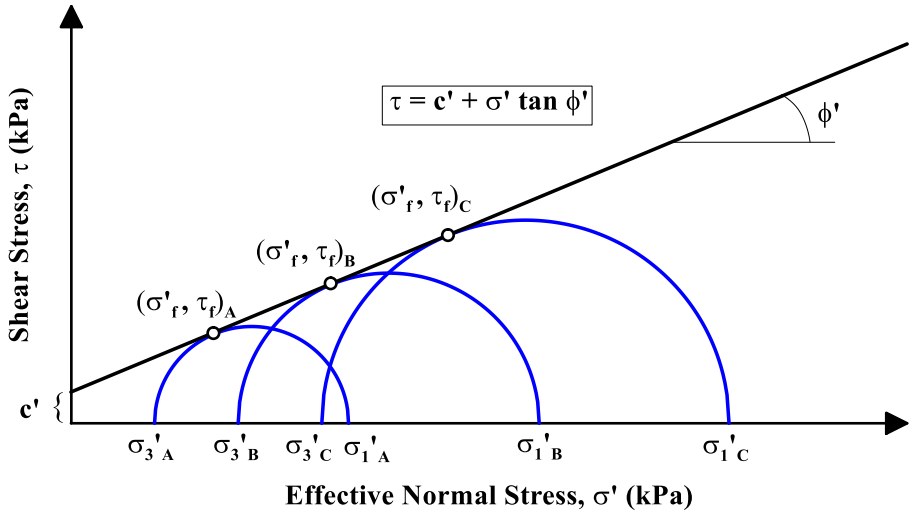

Figure 2.10 A typical Mohr-Coulomb Failure Envelope for saturated OC clayey soils

Other relations are available for shear strength of saturated soils, but those are beyond the scope of this discussion.

2.7.2 *Shear Strength of Unsaturated Soil*

The strength and deformation attributes of unsaturated soil are complex and unpredictable. Material behavior is affected by alteration in wetting, drying, loading and unloading, and furthermore by time. The debate over the most suitable stress state variables applicable for unsaturated soil has impeded the development of the subject.

The success of the concept of classical effective stress introduced by Terzaghi (1936), given mathematically by equation 2.11, drove researchers to endeavor an extension of the equation to unsaturated soils. Attempts have been

made to use a single-value stress state variable, to predict the behavior of unsaturated soils. Due to the limitations of the single-valued stress state variable approach, the independent stress variable approach was proposed. Meanwhile, researchers have worked on the development of modified stress-variable approaches.

2.7.2.1 Bishop's effective stress

Bishop (1959) proposed such an equation for effective stress, σ′:

$$\sigma' = (\sigma - u_a) + \chi(u_a - u_w) \tag{2.12}$$

where,

σ is the total stress,

u_a is the pore air pressure,

u_w is the pore water pressure, and

χ is a soil parameter related to the degree of saturation of the soil and the wetting or drying cycle.

The parameter ($\sigma - u_a$) is referred to as the net normal stress, while ($u_a - u_w$) is known as matric suction. The parameter, χ is a material variable and is generally considered to vary between zero, in the case of dry soil and unity, in the case of saturated soil.

When the expression for effective stress for unsaturated soil is integrated with the classical Mohr-Coulomb failure criterion, the shear strength, τ_f of unsaturated soil is expressed as below:

$$\tau_f = c' + \left[(\sigma - u_a)_f + \chi_f (u_a - u_w)_f\right] tan\,\varphi' \quad (2.13)$$

where, c' and φ' are effective cohesion and effective angle of internal friction of the saturated soil, respectively.

However, it was observed that the relationship between χ and degree of saturation, S is not unique; and the soil type and stress path had a noteworthy effect on the relationship. Thus, the use of Equation 2.12, and Equation 2.13 were debated by many researchers including Jennings and Burland (1962), Bishop and Blight (1963), Burland (1964), Blight (1967), and Fang (1977). Jennings and Burland (1962) argued that Equation 2.13 could not comprehensively clarify the volumetric behavior of most unsaturated soils below a certain degree of saturation and collapse upon wetting. While, Coleman (1962), Bishop and Blight (1963), Burland (1964), and Blight (1967) postulated a theory that the mechanical behavior of unsaturated soil is independently correlated to the net normal stress and the matric suction. Similar observations were made by Matyas and Radhakrishna (1968), Aitchison and Woodburn (1969), Barden et al. (1969), Brackely (1971), and Escario and Juca (1989). Thus, the limitations of the parameter χ to capture the behavior of unsaturated soil, its lack of one to one correspondence with the degree of saturation and the difficulties associated with the determination of χ in the laboratory, demonstrates the shortcomings of the Bishop's approach.

2.7.2.2 Independent two-stress state variable approach

The limitations of the single-value stress state variable approach resulted in the consideration for an independent two-state stress variable approach. Fredlund and Morgenstern (1977) postulated the use of net normal stress and matric suction as independent stress state variables, for capturing the response of unsaturated soil. A series of "null" triaxial tests showed that when the net normal stress and the matric suction are kept constant while varying other parameters, the volume of the soil specimen practically remained the same (Fredlund, 1973). These "null" triaxial tests supported the proposed approach. The shear strength at failure, τ_f, provided by the modified Mohr-Coulomb failure criterion (Fredlund and Morgenstern, 1977) is as follows:

$$\tau_f = c' + (\sigma - u_a)_f \tan \varphi' + (u_a - u_w)_f \tan \varphi^b \qquad (2.14)$$

where, c' and φ' are effective cohesion and effective angle of internal friction of the saturated soil, respectively, and φ^b is the friction angle, which is due to the contribution of the matric suction on the shear strength of the soil. Due to lack of experimental evidence, initially, the value of φ^b was considered as a constant for a specific soil by Fredlund et al. (1987). This assumption led to the conclusion that the soil strength increases consistently with the increase in suction. However, the increase in shear strength due to matric suction decreases with increase in suction, which became evident with additional experimental results over a wide range of suction and on different types of soils (Escario and Saez, 1986; Gan et al., 1988).

Equation 2.14 can be simplified to:

$$\tau_f = c' + c"(\sigma - u_a)_f \tan \varphi' \tag{2.15}$$

where c'' is the capillary cohesion, which arises due to capillary effect, and is as follows:

$$c" = (u_a - u_w)_f \tan \varphi^b \tag{2.16}$$

Also, total apparent cohesion is the sum of c' and c''.

The extended Mohr-Coulomb failure envelope, based on independent two-state stress variable approach, is shown in Figure 2.11. Instead of a two-dimensional plot between effective stress and shear stress, as in the case of saturated soil; the extended MC failure envelope requires a three-dimensional plot, among the net normal stress, matric suction, and shear stress. Additionally, MC failure envelope transforms from a line (for saturated soils) to a surface (for unsaturated soils).

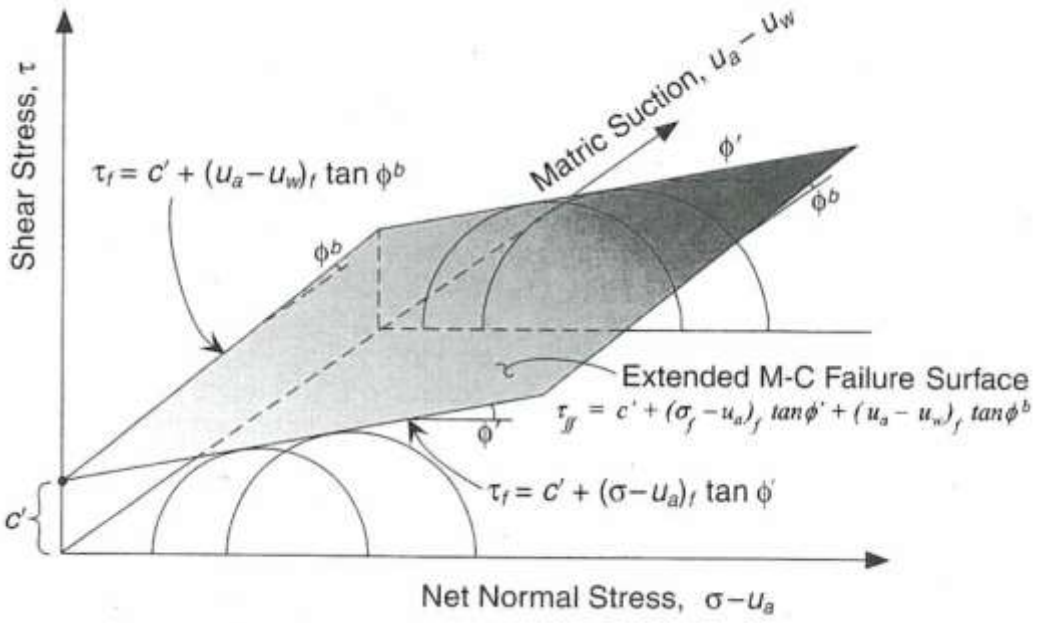

Figure 2.11 Extended Mohr-Coulomb Failure Envelope (Fredlund and Morgenstern, 1977; Fredlund and Rahardjo, 1993; Lu and Likos, 2004)

2.7.2.3 Alternative approaches

The concept of suction stress was introduced by Lu and Likos (2006) to facilitate the use of the suction stress characteristic curve. Suction stress is composed of four components, which originate from different water retention mechanisms: (*i*) van der Waals attraction, (*ii*) electric double layer forces, (*iii*) tensile pore water pressure, and (*iv*) surface tension (Lu and Likos, 2006; Lu et al., 2009).

Van der Waals forces occur due to attractive or repulsive forces between molecules or atomic groups that do not have covalent or ionic bonds (Lu and Likos, 2006; Lu et al., 2009). The correlations in the fluctuating polarizations of adjacent

molecules are the main cause for generation of these forces. The Van der Waals forces decrease exponentially when the distance between the molecules increases or when the degree of saturation increases.

Electric double layer forces arise between charged objects across liquids, like water. The first layer refers to the charged surface, and the charges originate from the adsorbed ions. The second layer corresponds to the diffused layer, which consists of neutralizing charge comprising of depleted co-ions or counter-ions. The potential difference between these two layers generates the difference in ionic concentration. This difference results in osmotic pressure (Lu and Likos, 2006; Lu et al., 2009).

The van der Waals forces and the electric double layer forces can be safely neglected in sands and non-plastic silts. Capillarity, which includes the latter two mechanisms, is the major reason for sand and non-plastic silt to exhibit cohesiveness or attractive forces (Lu and Likos, 2006; Lu et al., 2009).

However, very limited studies have been conducted independently to validate this hypothesis of suction stress concept. The concept of independent two-stress state variable approach by Fredlund and Morgenstern (1977) is still most widely used relationship for shear strength of unsaturated soils.

Various researchers have attempted to develop alternative approaches, which enables the development of constitutive models for predicting the behavior of unsaturated soils, including Alonso et al. (1990), Wheeler and Sivakumar (1995),

Houlsby (1997), Chiu and Ng (2003), Gallipoli et al. (2003), Datcheva and Schanz (2003); Khalili et al. (2005), Russell and Khalili (2006), Yang et al. (2008), Morvan (2010), and Manzanal et al. (2011).

2.8 Types of Triaxial Tests

The most common triaxial test performed in the laboratory follows the Conventional Triaxial Compression (CTC) stress path, where a constant effective confining pressure is maintained, while the soil specimen is loaded axially. The axial loading may be stress controlled or strain controlled. Strain-controlled tests can be continued even after the specimen has failed; thereby the post-peak or the residual behavior can be determined. However, strain controlled test setups are more expensive than stress controlled test setups. Based on the drainage conditions allowed during application of confining pressure and shearing, the triaxial tests are classified into three categories:

1. Unconsolidated Undrained (UU) Tests:

No drainage is allowed during the entire testing process. So, the soil is not allowed to consolidate and no volume changes are allowed during shearing. The testing procedure for cohesive soils has been explained through ASTM D2850-15 standards. The total stress path is obtained during this test. This a quick test, generally completed within 30 - 45 minutes. Field applications of UU tests include the scenarios where the rate of loading (during consolidation and shearing) is much faster than the rate of dissipation of excess pore water pressure. The rapid

construction of an embankment of soft clay; construction of footing and super-structure on a clay deposit; bearing capacity of deep foundations, like piles, on soft clay may be considered (Holtz and Kovacs, 1981).

For unsaturated specimens, the procedure for conducting the unconsolidated undrained test is similar to that for saturated specimens. The sample is not consolidated and it is sheared at its original suction state. The pore air and pore water valves are closed throughout the test. Since air pressure is not applied, conventional triaxial setup may be used to conduct UU test of unsaturated specimens (Fredlund et al., 2012).

2. Consolidated Undrained (CU) Tests:

Drainage is permitted during the application of confining pressure, thereby allowing the consolidation of the soil specimen. However, the drainage is not allowed during the loading stage. The generation of excess pore water pressure is measured during the loading phase. The testing procedure for cohesive soils has been explained through ASTM D4767-11 standards. The total stress path is directly obtained from this test; while the effective stress path may be calculated by deducting the excess pore pressure measured during shearing. This is a slower test when compared to UU test (Holtz and Kovacs, 1981).

Field application includes situations where the soil is allowed to consolidate, and then the additional form of loading is applied. Examples include the rapid drawdown of an embankment dam and slopes of reservoirs; rapid

construction of a structure on top of an embankment or raising the height of an existing embankment (Holtz and Kovacs, 1981).

For unsaturated specimens, the pore-air and pore-water lines are open during consolidation and target values of cell pressure, pore air pressure, and pore water pressures are gradually applied. While during shearing, the pore air and pore water valves are closed and their values are measured (Fredlund et al., 2012). Consolidated Undrained tests on unsaturated specimens were conducted by Soranzo (1988), Saeedy and Mollah (1988), Schoenemann and Pyles (1988) and Khosravi et al. (2011).

3. Consolidated Drained (CD) Tests:

Drainage is allowed throughout the consolidated drained (CD) test. In other words, the drainage valves are open during application of confining pressure (i.e., consolidation) and loading. Thus, the soil specimen is allowed to consolidate for the confining pressure applied, and then the soil is loaded gradually, to allow proper dissipation of excess pore water pressure. Henceforth, the volume change of specimen is permitted during the test and it is recorded via proper volume measurement devices. It is of primary importance to determine the proper rate of loading so that the excess pore water pressure can properly dissipate, during the loading sequence. The testing procedure has been explained through ASTM D7181-11 standards.

The effective stress path and the drained shear strength parameters can be computed from this test. As there is no generation of excess pore water pressure during the loading sequence, the total stress path is same as the effective stress path. This is the slowest among the UU, CU and CD tests and usually takes days to complete a test, and the duration is highly dependent on the permeability of the soil (Holtz and Kovacs, 1981).

Practical applications of CD tests comprise of the cases where the loading rate is smaller than the rate of dissipation of excess pore water pressure generated during shearing. The CD tests are mostly applicable for long term stability analyses. Examples of CD tests include slow construction of embankment over soft clay; stability analysis of embankment having steady seepage condition; long-term stability of a natural slope or an excavation (Holtz and Kovacs, 1981).

For unsaturated specimens, the pore air and pore water lines are open throughout the stages of consolidation and shearing (Fredlund et al., 2012). The respective targets of cell pressure, pore air pressure, and pore water pressures are gradually applied throughout the test. CD tests on unsaturated specimens were performed by Blight (1967), Satija and Gulhati (1979), Escario (1980), Ho and Fredlund (1982), Saeedy and Mollah (1988), Rahardjo et al. (1995), Rampino et al. (1999, 2000), Rahardjo et al. (2004), Kayadelen et al. (2007), Houston et al. (2008), Khalili and Zargarbashi (2010), Rahardjo et al. (2013, 2014), Ishikawa et al. (2014), Patil (2014), Ma et al. (2016) and Rosone et al. (2016).

There are additional two categories of triaxial testing, which are as follows:

1. Constant Water (CW) Tests:

The Constant water (CW) test is same as the consolidated undrained test for saturated specimens. However, for unsaturated specimens, the CW test is categorized as a separate test. The consolidation of the unsaturated specimen is carried out in a similar way as the consolidated drained or consolidated undrained test. In other words, the pore air and pore water drainage valves are kept open during consolidation to permit the change in volume of the specimen and to prevent generation of excess pore water pressure (Fredlund et al., 2012). Henceforth, the induced matric suction prior to the commencement of consolidation is maintained after the specimen has been consolidated.

During shearing, the pore water drainage valves are closed, but the pore air pressure value is kept open (Fredlund et al., 2012). Therefore, the pore air pressure is maintained at the same level as after consolidation. However, the pore water pressure is not controlled during shearing, which results in varying matric suction. The behavior of matric suction is dependent on previous stress history of the soil, its preconsolidation pressure and the effective confining pressure. CW tests were performed on unsaturated soils by Satija and Gulhati (1979), Rahardjo et al. (2004), and Li and Zhang (2015).

2. Unconfined Compression (UC) Tests:

The unconfined compression (UC) test procedure is comparable to that of the UU test, with the exception that the confining pressure is not applied in UC test. It is one of the most basic tests to estimate the strength of a soil specimen. Generally, an axial load is applied monotonically from a simple loading frame to shear the specimen (Fredlund et al., 2012).

Table 2.3 summarizes the drainage conditions and pressures which are controlled or measured during the various types of the triaxial tests.

Table 2.3 Types of triaxial tests for soils (modified from Fredlund et al., 2012)

Test Method	**Consolidation Stage**	**Shearing Stage**				
		Drainage		**Pore Air Pressure**	**Pore Water Pressure**	**Soil Volume Change**
		Pore Air	**Pore Water**			
CD	Yes	Yes	Yes	Controlled	Controlled	Measured
CW	Yes	Yes	No	Controlled	Measured	Measured
CU	Yes	No	No	Measured	Measured	No change
UU	No	No	No	N/A	N/A	No change
UC	No	No	No	N/A	N/A	N/A

2.9 Methods to Control Suction

2.9.1 Axis Translation Technique

The application and control of matric suction are pivotal for any suction-controlled triaxial test. As already mentioned in Section 2.2, the measurement and the control of high magnitudes of negative pore water pressure are limited due to cavitation (Fredlund and Rahardjo, 1993).

Cavitation is the process of vapor nucleation in water when the absolute pore-water pressure is less than the vapor pressure of water (Lu and Likos, 2004). Due to entrapment of air within the liquid (water) phase, the continuity of the liquid phase is lost. This causes erroneous pore water pressure readings. Since the matric suction is the difference between pore-air and pore water pressures, inaccurate pore water pressure would make it difficult/problematic to control matric suction.

Hilf (1956) introduced the concept of using the axis-translation technique to measure and control matric soil suction. The term "axis translation" refers to the procedure of increasing the pore air pressure above the atmospheric pressure, while maintaining a constant pore water pressure at or near the atmospheric pressure (Lu and Likos, 2004). This concept alleviated the problem caused due to cavitation at a pore-water pressure below absolute zero pressure, i.e. –1 atm with reference to the atmospheric pressure. Henceforth, the datum of determining air pressure is shifted from atmospheric pressure to a higher value. Using axis-translation technique, the matric suction higher than 1 atm ≈ 101.3 kPa can be applied or controlled, which is required for many soil types and applications.

2.9.1.1 High-air entry ceramic disk

In conventional saturated tests, the porous stone and the filter paper prevent the soil from entering the water line, but the flow of water is allowed either from or to the specimen, due to the high permeability of the porous stone and filter paper. However, due to the presence of pressurized air in unsaturated testing using axis

translation technique, the use of low air entry porous stone to separate the saturated pore water pressure line from the unsaturated soil is not feasible. Henceforth, a very low permeable and hydrophilic material, known as High Air-Entry (HAE) ceramic disk is essential to isolate the saturated pore water pressure line from the pressurized air present in the unsaturated soil.

The HAE ceramic material generally has uniform pore sizes. After saturation of the ceramic disk, due to the hydrophilic nature of the ceramic material, the water can flow through it, but the passage for air flowing through it is prevented till the air pressure exceeds the air-entry value of the material. The HAE disks are made of materials like sintered ceramics and have an air-entry value up to 1500 kPa (Lu and Likos, 2004).

The contractile skin which forms at the interface of air and water present in pores of the HAE disk, resists the flow of air through the disk. This resistance is dependent on the surface tension, T_s, of the contractile skin (Fredlund and Rahardjo, 1993). The contractile skin acts as a thin membrane connecting the minute pores of radius, R_s, on the ceramic disc surface (as shown in Figure 2.12). The matric suction is induced due to the difference between air pressure, u_a, above the contractile skin and water pressure, u_w, below the contractile skin.

The maximum matric pressure, which can be controlled across the contractile skin of the HAE disc is known as its air-entry value, $(u_a - u_w)$ (Lu and

Likos, 2004). The air-entry value can be represented by the Young-Laplace equation, which is applicable for the capillary tube model (Lu and Likos, 2004):

$$(u_a - u_w)_d = \frac{2T_s}{R_s} \quad (2.17)$$

It is evident from Equation 2.17, that as the size of the largest pore of the HAE disc decreases the air-entry value increases. The pore sizes of the ceramic material are dependent upon the casting process and sintering technique of the ceramic material (Fredlund et al., 2012).

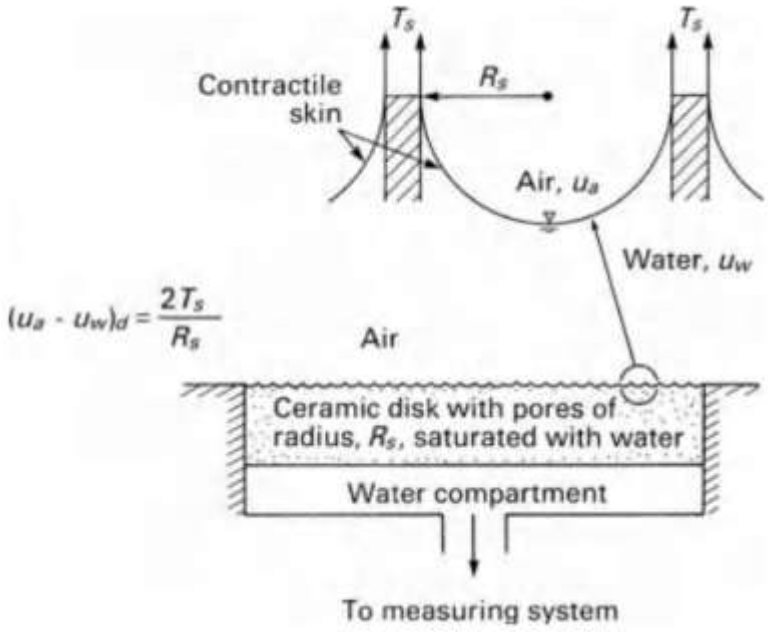

Figure 2.12 Schematic representation of the air-water interface in HAE disc (Fredlund and Rahardjo, 1993)

The HAE ceramic disc can be attached to conventional triaxial equipment to perform unsaturated soil testing. The HAE disc is generally mounted on the base pedestal and it is glued to the stainless-steel ring, which fits in the base pedestal.

Figure 2.13 shows the schematic section and plan of two types of shapes for HAE ceramic discs and the glue which attaches the steel ring to the HAE disc. The proper bond between the glue and the ring is pivotal for maintaining a suitable seal, thereby assuring that water passes only through the ceramic disc and there is no leakage.

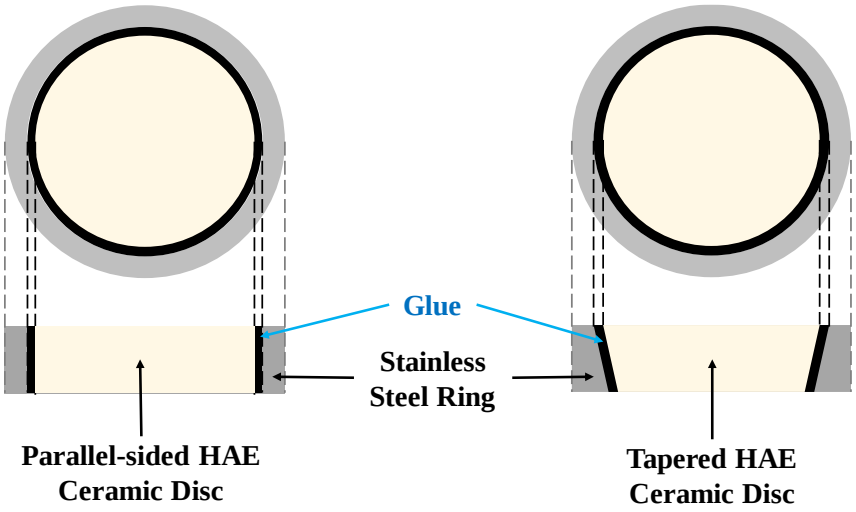

Figure 2.13 High air-entry disk ring arrangement

2.9.1.2 Saturation of HAE ceramic disc

The saturation of the ceramic disc is essential, before any test. The permeability of each ceramic disc is dependent on its air-entry value. So, different water pressure for varying duration of time should be applied to different types of HAE ceramic discs in order to saturate the disc.

Sivakumar (1993) suggested a technique to saturate the ceramic disc having AEV of 500 kPa. The saturation process was started by placing the disc in a chamber as shown in Fig. 2.14. The ceramic disc was fitted to the base pedestal

which had the facility to flush water from beneath the ceramic disc. The drainage lines were saturated and the chamber was sealed. The chamber was filled with de-aired water and pressurized beyond the air-entry value of the ceramic disk. After maintaining the pressure for a couple of days, one of the drainage lines was opened, and the water was allowed to flow for a day. Subsequently, the applied pressure in the chamber was gradually reduced to atmospheric pressure, i.e., zero pressure, and the water was removed. This process was repeated by introducing fresh de-aired water and re-pressuring the water to 600 kPa and maintaining it for a day. Then, one of drainage lines was again opened for another day; and finally, the pressure was gradually reduced. Thereafter, the HAE disc was removed.

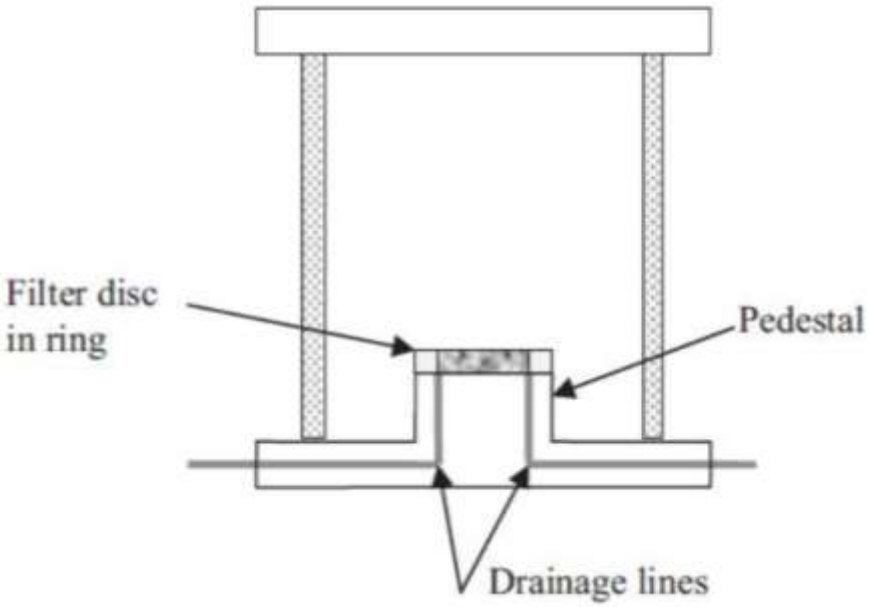

Figure 2.14 Chamber to saturate a ceramic filter disc (Brown, 2009; Sivakumar and Murray, 2010)

Another approach for saturating the HAEV ceramic disc was presented by Bishop and Henkel (1962), Fredlund (1973), Hoyos (1998), and Laikram (2007). The ceramic disc, having AEV of 500 kPa was installed in the test cell (Hoyos, 1998; as shown in Fig. 2.15a) or cavity of the custom-made saturation chamber (Laikram, 2007; as shown in Fig. 2.15b). The drainage lines were saturated and the connection below the ceramic disc was flushed to eliminate any air bubbles trapped beneath the HAE disc. Next, the triaxial assembly was set up and de-aired water was filled till 25 mm (approximately 1 inch) above the top surface of the ceramic disc. Air pressurized to 600 kPa was applied from the top onto the surface of the water, which indirectly pressurizes the water. One of the drainage valves, connected to the base of the ceramic disc was opened and the rise of water level in the attached burette was recorded. The high pressure dissolved the air into the water and the HAE disc became saturated. Subsequently, the air pressure was gradually released to prevent any dissolved air to diffuse into the ceramic disk.

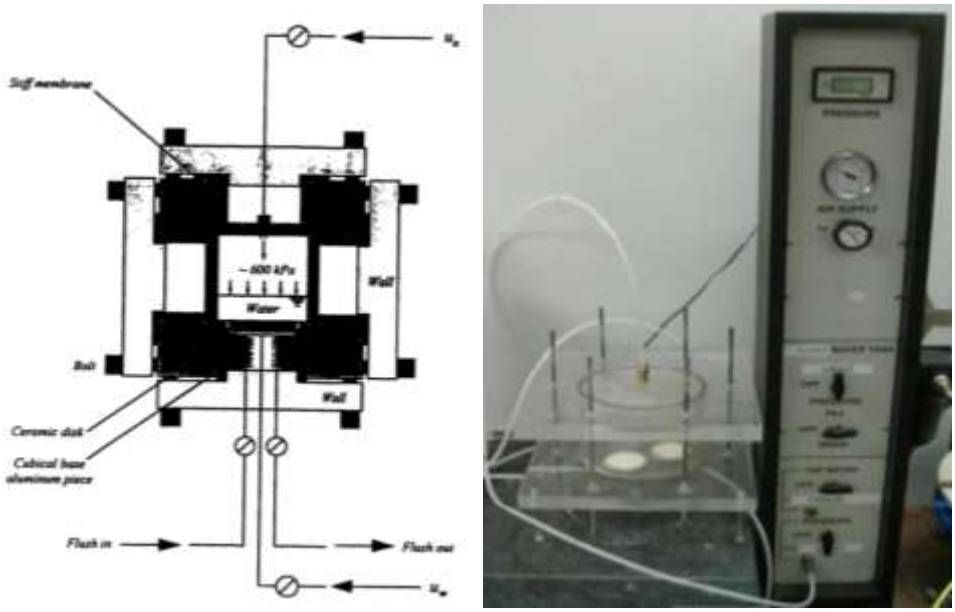

(a) (b)

Figure 2.15 Saturation of HAEV ceramic disc in (a) test cell (Hoyos, 1998); (b) custom-built saturation chamber (Laikram, 2007)

2.9.1.3 Limitations of axis-translation technique

Olson and Langfelder (1965) had reasoned that by increasing the air pressure acting on the soil specimen, the soil solids and the pore water become compressed isotropically. However, as these are practically incompressible, the air pressure increase resulted in an insignificant alteration in the curvature of the contractile skin. Thereby, the value of matric suction ($u_a - u_w$) would have remained almost constant. Henceforth, they concluded that the axis-translation technique would be suitable for soils having only continuous air-water interface. Later, Bocking and Fredlund (1980) had similar observations and it was concluded that

based on the rate of increase of air pressure, the actual value of matric suction might momentarily increase beyond its applied value.

Also, it was concluded that if the specimen contains occluded pore-air, which make it highly compressible, then, the actual matric suction might be over-estimated. In addition, the diffusion of air through the ceramic disc is a major limitation for the duration of each test. The dissolved air above the ceramic disc might diffuse through the HAE ceramic disk into the base chamber, where it enlarges and accumulates due to relatively lower pressure. This might obstruct the flow of water through the ceramic disc.

2.9.2 Osmotic Suction Technique

The osmotic suction method achieves control of matric suction by allowing the pore water to equilibrate with a salt solution of known osmotic potential, and the soil specimen is separated from the salt solution by a semi-permeable membrane (Zur, 1966). The semi-permeable membrane is permeable to water molecules but impermeable to salt molecules. The experimental setup by Cui and Delage (1996), demonstrating the procedure of inducing suction using osmosis is shown in Fig. 2.16.

The osmotic suction technique was initially adopted by researchers from biological sciences for controlling the osmotic pressure of plant nutrient solutions by using Polyethylene Glycol, commonly referred by its acronym, PEG (Legerwerff et al., 1961). Later, the suction control by means of the osmotic suction

technique was adopted in the field of soil sciences (Painter, 1966; Zur, 1966). In geotechnical engineering, this technique was also adopted to control suction in triaxial setups (Delage et al., 1987; Cui and Delage, 1996; Ng et al., 2007) and suction controlled tests in oedometer (Delage et al., 1992; Dineen and Burland, 1995; Tarantino and Mongiovi, 2000).

The main benefit of this technique is that the cavitation is prevented while maintaining a negative pore water pressure within the soil. The disadvantages include the long duration of each test may not be feasible, as the semi-permeable membrane is delicate. Also, the migration of soil salts, which are dissolved in pore-water in the soil, into the salt solution may affect the soil water chemistry and soil properties (Murray and Sivakumar, 2010).

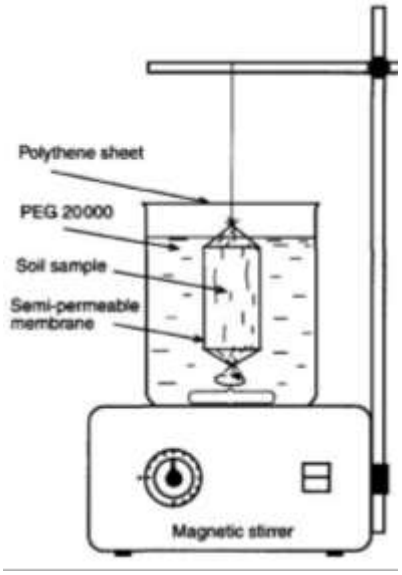

Figure 2.16 Osmotic suction technique to impose suction in soil specimen (Cui and Delage 1996)

2.9.3 Vapor Equilibrium Technique

The vapor equilibrium technique was introduced by researchers for application in soil sciences. This technique controls the soil suction by controlling the relative humidity, which could be achieved by two methods: (*i*) isopiestic method, and (*ii*) two-pressure method. The isopiestic or "same pressure" method depends on achieving the vapor pressure equilibrium for salt or acid solutions in a closed thermodynamic environment (Lu and Likos, 2004). The "two-pressure" method relies on the control of relative humidity by changing the pressure or temperature; or by mixing vapor-saturated gas with a dry gas (Lu and Likos, 2004). The control of soil suction in unsaturated soil testing using the vapor pressure technique was conducted by Esterban and Saez (1988); Oteo-Mazo et al. (1995), Delage et al. (1998), Al-Mukhtar et al. (1999), Blatz and Graham (2000); Cunningham et al. (2003), Blatz and Graham (2003), Likos and Lu (2003), Nishimura and Vanapalli (2005), Nishimura et al. (2008), Nishimura et al. (2010) and Patil (2014). In this approach, the soil specimen is placed in a thermodynamically sealed system controlled by the air flowing through a desiccator where an aqueous solution results in a controlled partial vapor pressure generated by the salt solution of known concentration. The transfer of water from the soil specimen with the vapor from the relative humidity apparatus, until the soil suction is in equilibrium with the partial vapor pressure. The "two-pressure" humidity control method was used by Likos and Lu (2003) to develop a system which could

be modified to be used along with a triaxial device to test specimen under high suction states (Figure 2.17).

The vapor equilibrium technique has similar advantages like the osmotic suction technique, with an added advantage that this technique could be used for very high suction states like 4 to 600 MPa (Murray and Sivakumar, 2010). However, the lower suction levels (less than 4 MPa) cannot be applied using this technique. Also, the suction equilibration time is very high, and it takes up to 1 – 2 months to attain equilibrium for standard triaxial specimens.

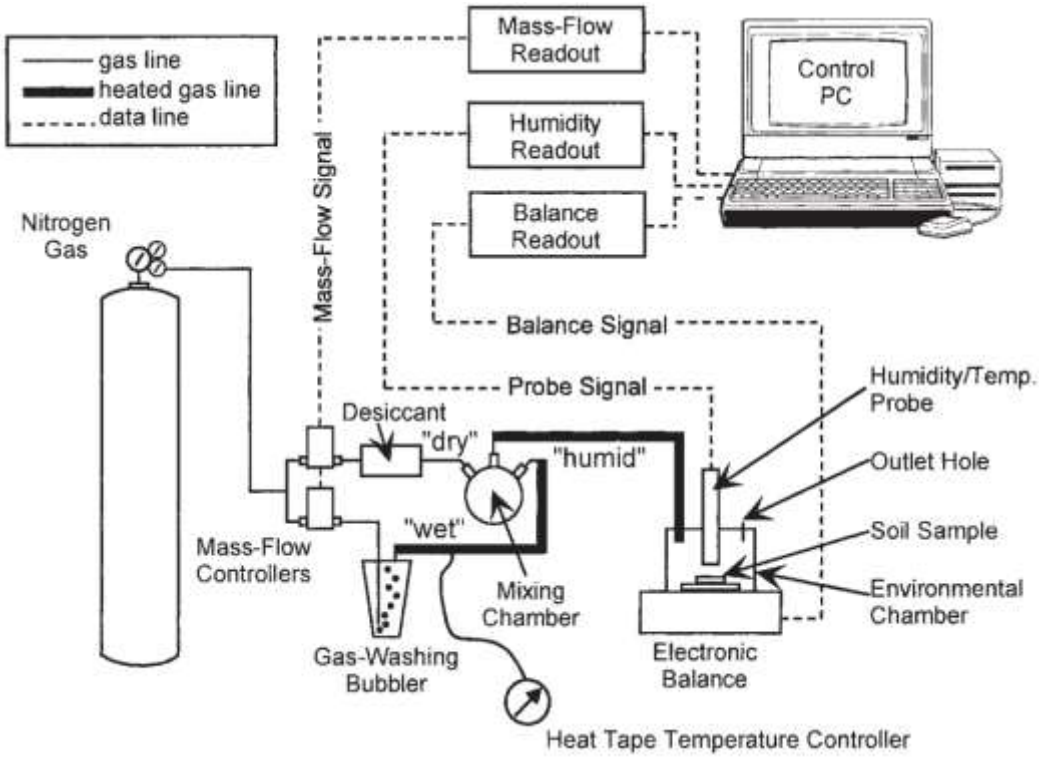

Figure 2.17 General Layout of automatic humidity control system (Likos and Lu, 2003)

2.10 Modified Unsaturated Soil Triaxial Testing System

The conventional triaxial testing device has been altered to incorporate unsaturated soil testing by many researchers. The modifications introduced include the precise measurement of the volume changes in soil, the volume of water flowing into or out of the soil specimen and the volume of air inflow or outflow to control the required suction. The modifications also comprise of the independent control and measurement of pore air and pore water pressures over a wider range, minimizing the errors due to the expansion of triaxial cell with an increase in pressure, and flushing devices to remove air from the base of the high air-entry ceramic disk during a test.

The advent of computer technology, sensors, and mechanical devices has enabled these modifications to be incorporated into soil testing. Some of these modified triaxial devices and the tests conducted have been discussed in the next section.

2.10.1 Independent Pore Water and Pore Air Pressures Control and Measurement

The triaxial tests on unsaturated soils were performed by Bishop and Donald (1961) using a modified version of the conventional triaxial setup, where the pore air and pore water pressures were individually controlled or measured. The tests confirmed that the pore water pressure could be measured through a saturated ceramic disk, which was attached and sealed to the base pedestal. However, the pore water pressure measurement was restricted to less than 90 kPa below

atmospheric pressure, to prevent cavitation. The pore air pressure was applied through a porous stone at the top of the soil specimen.

Bishop and Blight (1963) verified the application of axis translation technique to induce matric suction in the testing of unsaturated soil. The matric suction induced were in excess of 1 atm, which was till then the maximum induced matric suction. Blight (1967) performed consolidated drained (CD) tests on unsaturated soil specimens and concluded that the shear strength increases with increase in suction and net confining pressure. Satija and Gulhati (1979) had performed a series of consolidated drained (CD) and constant water (CW) triaxial tests, where the pore air and pore-water pressures were controlled or measured throughout the tests. A similar set of CD triaxial tests were performed by Escario (1980), which employed the axis translation technique.

Later, many researchers had conducted triaxial tests with independent control of pore air and pore water pressures. The primary modifications required for unsaturated soil testing were presented by Fredlund and Rahardjo (1993), which included the HEA disk and independent control of pore air and pore water pressures (Fig. 2.18). A similar test setup was used by Rahardjo et al. (2004) to perform a series of CD and CW triaxial tests on compacted sandy clay specimens. They concluded that the specimens exhibited characteristics of an overconsolidated soil with post-peak softening and dilatancy at higher suction levels. Also, they observed that the matric suction reduces on shearing of specimens in CW tests.

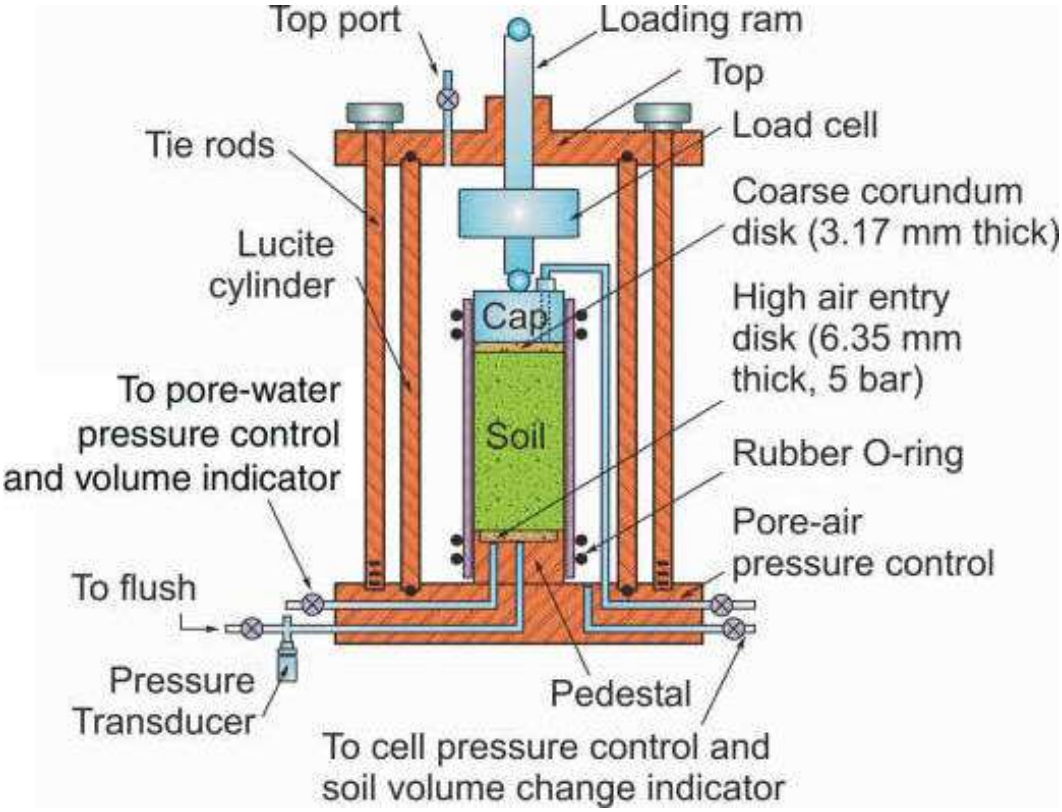

Figure 2.18 Modified triaxial setup for unsaturated soil testing (Fredlund and Rahardjo, 1993)

Meanwhile, Sharma et al. (1998) used a porous stone to apply air pressure at one end of the specimen but also used HAE disk at both ends of the specimen to apply pore water pressure. This technique aided in reducing equilibration time but exposed the tests to the possibility of air bubbles to be entrapped in the center of the soil specimen, owing to movement of waterfront from both ends of the specimen. A similar approach was adopted by researchers such as Barrera (2002), and Rojas et al. (2008), where the pore air and pore water pressures were applied

from both ends of the specimens by installing a HAE ceramic disc at the core of the base pedestal, with an annular ring of porous stone (as shown in Fig. 2.19).

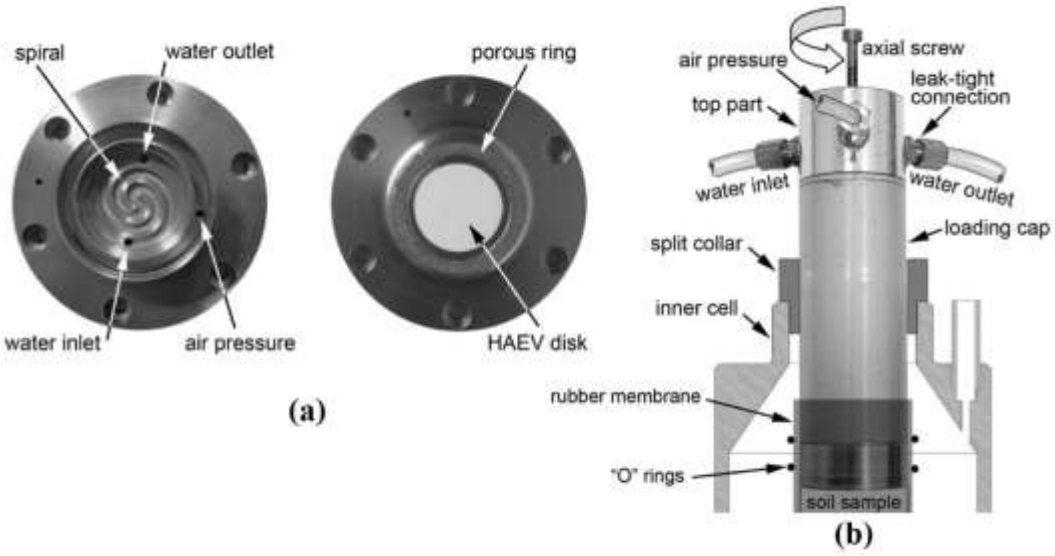

Figure 2.19 Modifications to (a) base platen, and (b) top cap assembly (Rojas et al., 2008)

Rampino et al. (1999, 2000) developed a new setup to perform suction controlled triaxial tests by adopting the axis translation technique. Various compacted specimens of silty sands were tested at suction levels varying from 0 to 400 kPa. The deviator stress and the volumetric strain response demonstrated post-peak softening and dilation after initial compaction, which showed that the specimen behaved as dense sand.

Ishikawa et al. (2014) performed tests on a medium-sized triaxial equipment (as shown Fig. 2.20) for studying the mechanical behavior of unsaturated subbase course materials using pressure membrane method with hydrophilic microporous

filters, instead of HAE ceramic discs. The main motive of using pressure membranes and installing water supply on both ends of the soil specimen was to reduce the testing time by developing double drainage, as was confirmed by Ishikawa et al. (2010) and Nishiumura et al. (2012). The pore air and pore water pressure applied to the specimen from the top cap and the bottom pedestal, respectively, were controlled independently. Additional tests were performed on the same setup by Zhang et al. (2014) to study the strength characteristics of subbase course material subjected to the variation in the degree of saturation and the loading strain rate.

The soil selected was a subbase course material, comprising of natural crusher-run made from angular, crush, hard andesite stone. The consolidated drained triaxial tests on the compacted specimens showed initial compression (up to less than 1%) and subsequent, dilation for all specimens. Similarly, the deviator stress response showed post-peak softening behavior. Also, the strain rate for shearing demonstrated that the higher strain rates resulted in higher peak deviator stress and the dilation initiated at a lower axial strain, with higher dilation angle.

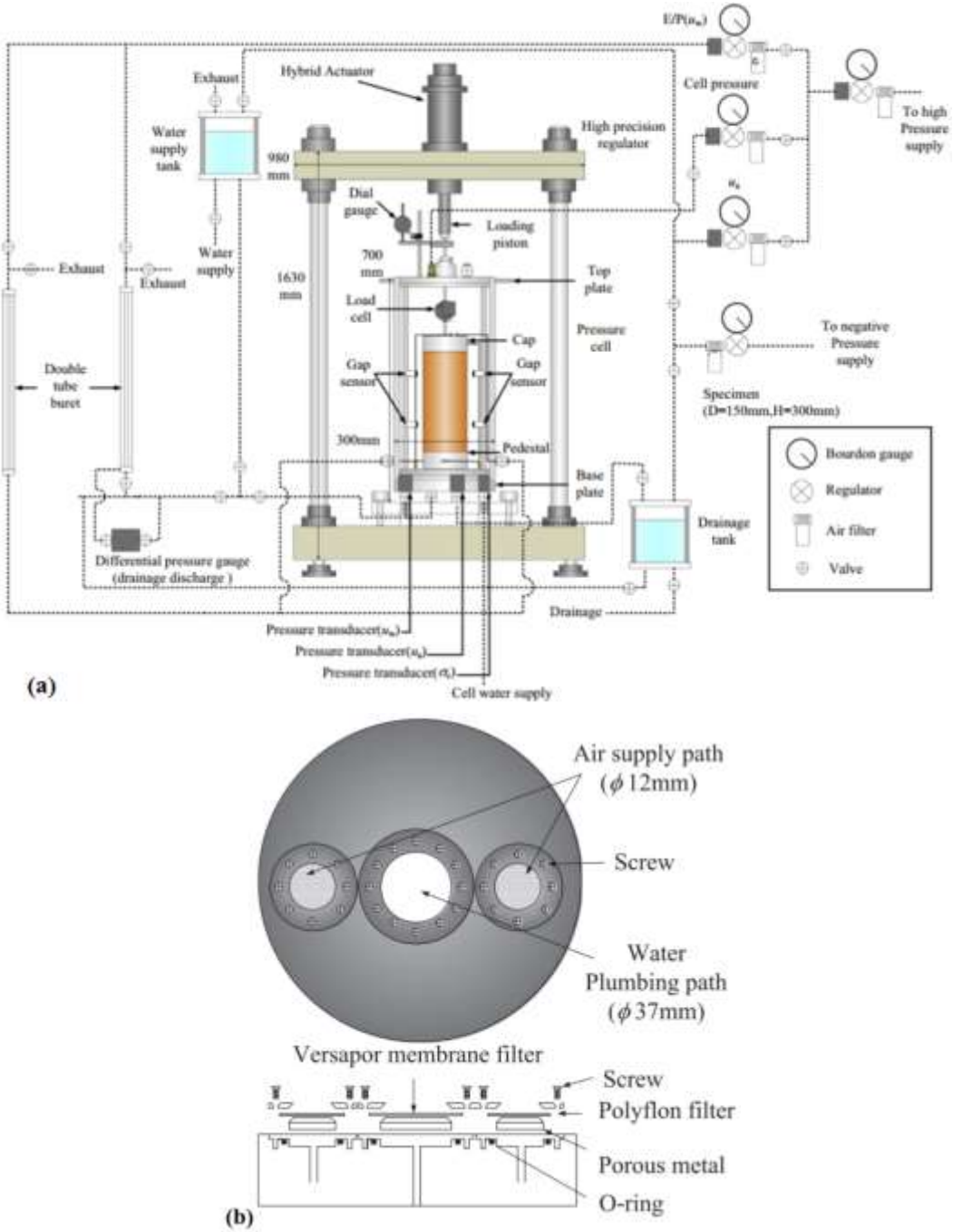

Figure 2.20 (a) General setup of medium-sized triaxial apparatus and (b) Structure of top cap and base pedestal (Ishikawa et al., 2014)

Rosone et al. (2016) conducted a series of suction controlled drained triaxial test on unsaturated specimens of scaly clay on a modified triaxial device using axis translation technique. The independent control of air pressure from the top cap and water pressure through the combination of two HAE ceramic discs (AEV of 500 kPa and 1500 kPa) at the base pedestal enabled the control of matric suction.

The experimental program was defined on the basis of two-independent stress state variable approach by Fredlund and Morgenstern (1977). The matric suction induced on the specimens varied from 50 to 500 kPa. All the specimens, except for the 500 kPa suction specimens, were dynamically compacted on the dry side of optimum (2% drier than optimum moisture content) and subjected to net mean stress of 50 kPa and matric suction of 50 kPa before the required suction was induced. Due to the excessive time required to equilibrate specimens from a matric suction of 50 kPa to 500 kPa, the specimens to be tested at a matric suction of 500 kPa were directly subjected to a suction of 500 kPa and net mean stress of 50 kPa.

The response of the compacted specimens to shearing showed an increase in deviator stress to its peak value with a corresponding increase in axial strain when suction was less than 500 kPa. However, for specimens subjected to 500 kPa, slight post-peak softening was observed. Some of these unsaturated tests were performed using multistage triaxial testing sequence, which is discussed in Section 2.11.3.

Elaborate analyses of the test results were performed and yield curves were estimated using the isotropic consolidation data. The shear strength envelope at saturated and unsaturated condition was generated using the two-independent stress state variable approach by Fredlund and Morgenstern (1977). Additionally, the apparent cohesion was estimated for the soil over a wide range of suction states by using the macropore degree of saturation as Bishop's effective stress parameter, χ.

It was observed that at high suction (greater than 9 MPa), the use of macropore degree of saturation as χ, predicted that the apparent cohesion decreased to zero, due to excessive desaturation (Rosone et al., 2016). Moreover, the apparent cohesion was also predicted over the suction range considered in the study (0 - 500 kPa) by using the hyperbolic envelope. Using this approach, it was detected that the rate of increase of apparent cohesion gradually decreased after matric suction of 100 kPa, which was near the AEV of the soil (Rosone et al., 2016).

2.10.2 Volume Measurement

The various volume measurements required to be measured accurately include (*i*) the volume of the soil specimen, (*ii*) the volume of water flowing into or out of the specimen through the HAE disc, and (*iii*) the volume of air flowing in or out of the specimen to maintain the required soil suction. Researchers have attempted to capture the volume changes in the soil and volume of air and water supply to maintain suction accurately, by various methods which have been discussed in this section.

Initial problems regarding the expansion of triaxial cell with an increase in cell pressure were addressed by Bishop and Donald (1961), where the use of double-walled triaxial cell was suggested. Mercury was used as an internal cell fluid, while water was utilized as the external cell fluid. The application of equal pressures to both the cells prevented any expansion of the inner cell. The schematic plot of the modified triaxial setup is shown in Fig. 2.21.

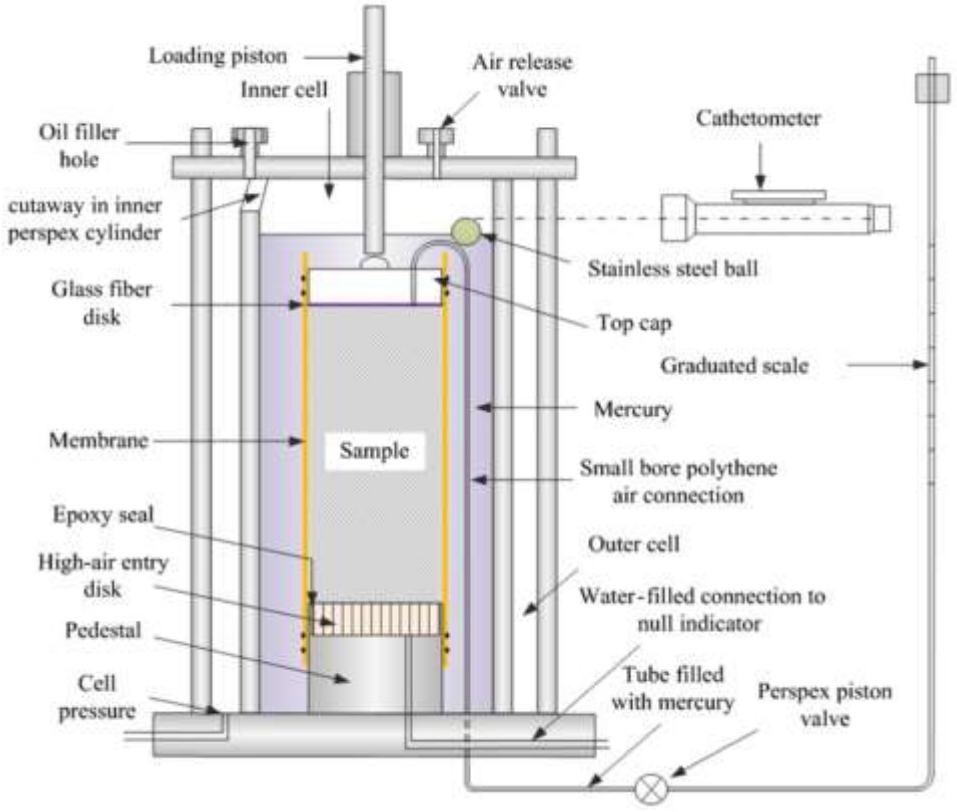

Figure 2.21 Schematic plot of triaxial setup for unsaturated soils (modified from Bishop and Donald, 1961; adopted from Li and Zhang, 2015)

Ng et al. (2002) developed a simple triaxial device by installing a highly accurate differential pressure transducer in a Bishop and Wesley (1975) type

triaxial cell. The differential pressure transducer measured the alterations in the volume of soil by measuring the pressures difference between the water inside in the inner cell and that in a reference tube. The schematic representation of the setup is shown Fig. 2.22.

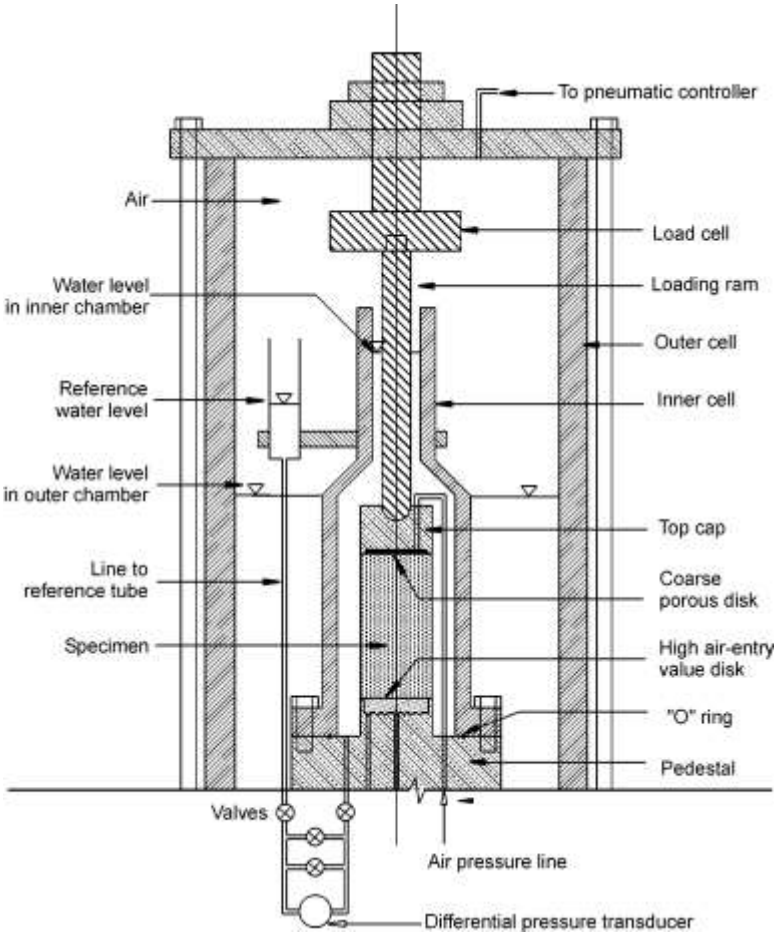

Figure 2.22 Schematic of new triaxial setup to measure the volume change of the specimen (Ng et al., 2002)

Kayadelen et al. (2007) attempted to evaluate the critical state parameters with respect to matric suction for highly plastic clayey soils, for which a series of

triaxial tests were conducted on a modified triaxial equipment (Fig. 2.23). In Fig. 2.23, the numerals refer to the various components of the triaxial setup. The axis-translation technique was adopted to control suction and prevent cavitation.

Furthermore, the pore air and pore water pressures were independently controlled and measured (Kayadelen et al., 2007). It was assumed by the authors that the difference between overall soil and pore water volume changes causes the air volume change. However, this assumption has major limitations as the expansion of triaxial cell and the pipes connecting the pressure lines were neglected and their effect was included in the air volume change.

The volume change transducer connected to the pore water line measured the volume of water flowing in or out of the soil specimen. An additional volume change transducer was attached to the constant pressure device and inlet for the triaxial cell, which recorded the volume change of the soil specimen. To prevent the diffusion of air through the rubber (or latex) membrane into the cell water, the soil specimen was enclosed within two latex membranes with two slotted aluminum sheets separated by silicone grease. A similar approach was recommended by Alonso et al. (1990) to prevent air diffusion from the specimen to the confining liquid in the cell.

The triaxial tests were conducted on specimens with induced matric suction up to 400 kPa, which was at a degree of saturation of approximately 75%. The

consolidated drained tests conducted on the residual clayey soil specimens showed a compressive behavior.

Figure 2.23 Modified triaxial testing equipment (Kayadelen, 2007)

Houston et al. (2008) performed a series of consolidated drained (CD) triaxial tests on four types of compacted soil specimens (sandy silty clay, lean clay, silty sand, and poorly graded sand) to study the unsaturated soil properties using a modified triaxial device, similar to the equipment used by Padilla et al. (2006). The errors in volume change measurement due to the expansion of triaxial cell with higher pressure was addressed by using a double-walled triaxial cell. The volume change of the soil specimen was measured by measuring the volume of water flowing into the inner cell which applied the confining pressure. Since the inner

cell experienced same pressure on the inside and outside, it did not deform, thereby the errors due to cell expansion were minimized.

The authors also suggested the equilibration of the soil specimen outside the triaxial cell to minimize the time required to attain equilibrium in unsaturated soils. The tests conducted mostly showed initial compression and then dilation for sandy silty clay, silty sand, and poorly graded sand, while only compression was observed for lean clay.

Many researchers have resorted to the alternative ways of determination of volume change using strain gauges (Thom et al., 2008) and radial strain belts and submersible displacement transducers (Cabarkapa and Cuccovillo, 2006). Other researchers like Burrage et al. (2011) attempted to develop a cost effective modified triaxial device to test unsaturated specimens, by using calibration charts to determine the errors introduced due to cell expansion in a single triaxial cell, etc.

Li and Zhang (2015) proposed only minor modifications to a conventional triaxial testing device to make unsaturated soil testing affordable. It was suggested that in lieu of controlling suction, the use of high suction tensiometers would enable to record the changes in matric suction during constant water triaxial tests. Furthermore, the volume measurements were done using photogrammetry-base methods. The triaxial setup used this purpose is shown in Fig. 2.24a. The schematic diagram showing the location of targets (as shown in Fig. 2.24b), which were high-contrast observation points, which could be automatically detected by the

photogrammetry software. The images taken during testing enabled the authors to recreate a three-dimensional model of the soil specimen.

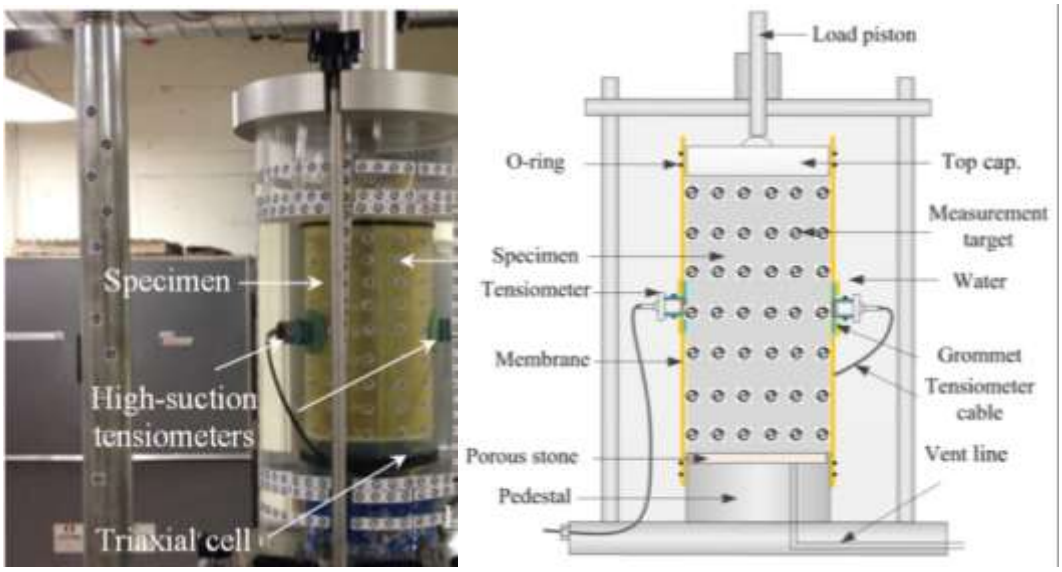

(a) (b)

Figure 2.24 Proposed triaxial testing system: (a) photograph of the setup; (b) schematic plot (after Li and Zhang, 2015)

The soil selected for the test comprised of a combination of Fairbanks silt and Kaolin in the ratio of 85:15. Constant Water (CW) triaxial tests were conducted on compacted specimens having initial suction up to 500 kPa. The deviator stress response showed post-peak softening for all specimens subjected to a low net confining pressure of 5 kPa and for all specimens having initial suction greater than 150 kPa for all net confining pressures. However, for specimens subjected to net confining pressure of 200 kPa with initial suction less than 150 kPa, an increase in deviator stress was observed with a corresponding increase in axial strain. The rate

of decrease of deviator stress with respect to axial strain increased drastically with increase in initial suction and decrease in net confining pressure.

The volume change behavior was observed to be initially compressive (up to an axial strain of 1%), and then dilatant behavior was observed for all specimens when subject to a net confining pressure of 5 kPa (Li and Zhang, 2015). Whereas, only when the specimens were subjected to a net confining pressure of 200 kPa and sheared, the specimens having an initial suction of more than 150 kPa, demonstrated dilatancy, after initial compression. The remaining specimens (initial suction less than 150 kPa) showed only compression during shearing. It was also noted that the matric suction reduced gradually with an increase in net mean stress, during isotropic consolidation and the decrease was more noticeable for specimens having higher initial suction.

Ma et al. (2016) performed a series of consolidated drained triaxial test on unsaturated silty soil using a suction-controlled double cell triaxial apparatus. The pore air pressure was applied from the top cap, while the pore water was applied from the base pedestal. The volumetric strains during shearing were computed using a differential pressure transducer, which measured the difference in pressure due to varying levels of water between the inner cell and reference tube. A similar approach was used earlier by Ng et al. (2002). The axial deformation was computed using a strain gauge. The radial deformation was determined from the axial and volumetric deformations. The tests were conducted on various specimens having

low suction, from 15 to 90 kPa. The stress-strain response during shearing demonstrated post-peak softening. The volume change response showed initial compression till the axial strain reached 5%, and then dilation. It was noted that the dilation angle increased with increase in induced suction and net confining pressure. However, the increase in net confining pressure decreased the tendency of the specimen to dilate.

2.10.3 *True Triaxial Testing*

The true triaxial setup is capable of testing soil specimens along multi-axial stress paths under suction-controlled stress paths (Hoyos et al., 2008). It comprises of cubical specimens within rigid loading plates (as in Matsuoka et al., 2002) or flexible loading membranes (as in Hoyos, 1998; Macari and Hoyos, 2001).

The response of soils under varying suction and net confining pressure under varying stress paths like hydrostatic compression (HC), triaxial compression (TC) and conventional triaxial compression (CTC) have been performed using true triaxial setups by Hoyos (1998), Macari and Hoyos (2001), Matsuoka et al. (2002), Hoyos et al. (2005); Laikram (2007), and Perez-Ruiz (2009)

2.10.4 Osmotic Suction Technique in Triaxial Setup

Cui and Delage (1996) had assembled a modified triaxial device which utilized the osmotic technique to induce suction in soil specimens (as shown in Fig. 2.25). A semi-permeable membrane, which only allowed water molecules to pass through, was kept on the top and at the base of the soil specimen and Poly Ethylene

Glycol (PEG) solution, of required concentration, was circulated at the both ends of the specimen. The imbalance of the suction caused the exchange of water molecules through the semi-permeable membrane, which ceased upon achievement of equilibrium between the soil and the PEG solution. Earlier, Delage et al. (1987) had utilized osmotic technique to modify a triaxial equipment to perform suction controlled tests.

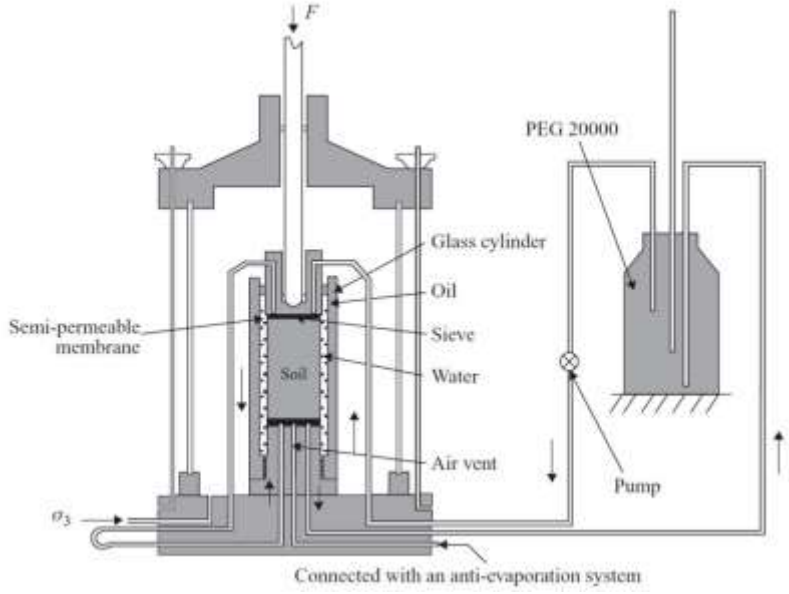

Figure 2.25 A modified triaxial setup with osmotic technique (Cui and Delage, 1996)

Ng et al. (2007) performed a study to compare the differences in suction induced by axis-translation technique and osmotic technique. A series of consolidated drained triaxial tests were conducted on compacted specimens of high plasticity clays, with an air-entry value of 60 kPa. The tests were conducted at low suction range 0 kPa to 165 kPa with net confining pressure varying from 25 kPa to

100 kPa. The osmotic suction was induced by using a PEG solution of known concentration. It was observed that deviator stress increases with increase in shearing and there is no evidence of post- peak softening.

Furthermore, it was calculated that there was no variation in the angle of internal friction due to axis translation and osmotic techniques. However, the value of φ^b was observed to be slightly higher for test series using the axis-translation technique as compared to those in the series of tests using the osmotic technique by 3° to 4°. The reason for the difference was speculated to be due to lower specific volume and a higher degree of saturation for the series of tests conducted using the axis translation technique than those in the series of tests using the osmotic technique.

2.10.5 Vapor Equilibrium Technique in Triaxial Setup

Blatz and Graham (2000) developed a new triaxial apparatus which could control high suction states using the vapor pressure technique. The vapor pressure technique was applied using an ionic solution, having the target suction value, which was placed in a desiccator. The desiccator was attached to the base of the specimen, whereas, the top of the specimen was connected to the desiccator via a pump and flow meter, which regulated the flow of vapor through the specimen.

As the vapor flowed through the specimen, the water was absorbed or released to the vapor from the specimen, which depended on the suction gradient between the ionic solution and the specimen. It also utilized the thermocouple

psychrometry for measurement of suction. The volume changes in the soil specimens were computed from the height and the diameter of the specimens, which were measured by linear displacement transducers. The modified triaxial setup is shown in Fig. 2.25. Similar techniques were applied by Cunningham (2003), Nishimura and Fredlund (2003), Nishimura and Vanapalli (2005), Nishimura et al. (2008), and Patil et al. (2016) to perform triaxial tests on specimens having high induced suction. An Auto-RH system was developed by Likos and Lu (2003), which has the capability of being integrated with a traditional triaxial setup for testing soil specimens under high suction states.

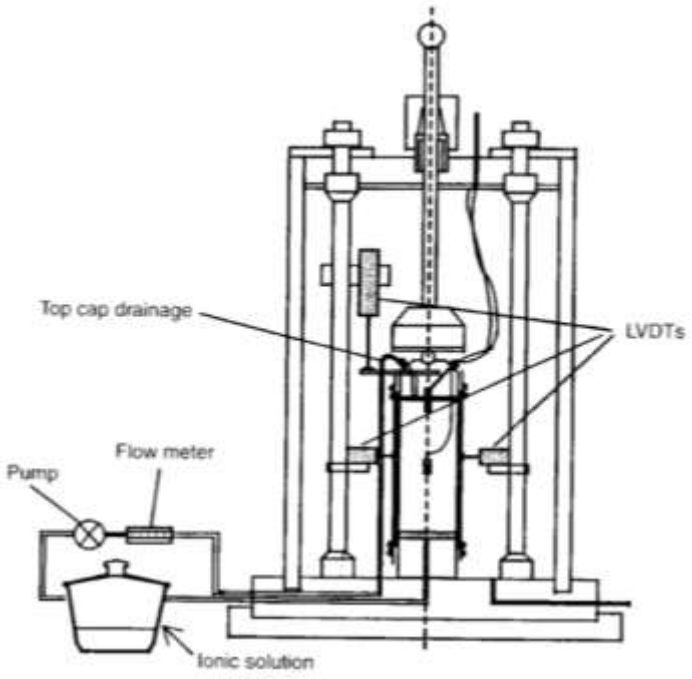

Figure 2.26 Modified triaxial setup for inducing high suction states in soils (Blatz and Graham, 2000)

2.10.6 *Synopsis of Modifications to Unsaturated Triaxial Testing Device*

The advent of technology and knowledge of fundamental theories involved in unsaturated soil has enabled the modifications to be introduced into the conventional triaxial device. These modifications have resulted in significant development of experimental unsaturated soil mechanics, especially by controlling suction and accurate measurements of volumetric changes. Nevertheless, detailed experimental research of unsaturated soils under varying suction states and loading conditions are very limited.

Also, the various methodologies to apply suction in soils have their own advantages and disadvantages, which have been explained briefly in Section 2.9. Therefore, based on the requirements of testing conditions, the appropriate technique should be judiciously selected.

2.11 Multistage Triaxial Testing

2.11.1 *Introduction*

The predominant objective of performing a triaxial test is to determine the shear strength parameters of the soil. Generally, three triaxial tests at different values of confining pressure conditions, are conducted to obtain the shear strength of any saturated soil specimen. The shear strength parameters are determined by drawing the Mohr's circles at varying confining pressures and the common tangent to theses circles, which is known as Mohr-Coulomb Failure Envelope (shown in Fig. 2.10). However, the soil variability of the replicates may result in erroneous

determination of failure envelope, which would lead to errors in computation of the shear strength parameters of the soil (Parry and Nadarajah, 1973; Sharma et al., 2011).

Additionally, often there is a lack of acceptable replicates at a given site to perform triaxial tests on three different specimens. Therefore, the need of alternative testing methodologies arises which addresses these issues. This lead to the development of multistage triaxial tests. The feasibility of performing multistage tests for saturated soils was initiated by De Beer (1950), Taylor (1950), Fleming (1952), Kenney and Watson (1961), Lumb (1964), Sridharan and Rao (1972) and Parry and Nadarajah (1973). The applicability of multistage triaxial tests for unsaturated soils was introduced by Ho and Fredlund (1982) and the following sections cover others who performed same tests on unsaturated soils.

2.11.2 *Multistage Testing on Saturated Soils*

The multistage triaxial tests of saturated specimens refer to the test in which a saturated specimen is initially consolidated and sheared to a pre-failure state of stress and strain, consolidated to a higher effective confining pressure and sheared again. In multistage tests, these repeated cycles of consolidation and shearing are performed on the same specimen. Though these tests have been introduced decades ago, there is a lack of usage of multistage triaxial tests among geotechnical engineers primarily due to problems regarding the premature failure of specimens

during shearing at initial confining pressures (Sharma et al., 2011). Also, there are no available standards describing the procedure to perform these tests.

Kenney and Watson (1961) performed one of the first investigations into the drained and undrained behaviors of saturated clays, using conventional and multistage triaxial tests. They concluded that the effective shear strength parameters from both types of tests were comparable, but the effective stress path and induced pore pressure showed significant differences.

Sridharan and Rao (1972) attempted a new approach to minimize the strains induced in the specimen by using Kondner's hyperbolic stress-strain relationship (Kondner, 1963). The relationship enabled in predicting the state of stress at failure from the stress-strain and the pore water pressure response observed during undrained tests. Sridharan and Rao (1972) suggested that initially, the soil behavior needed to be checked for its corresponding comparison with the Kondner's stress-strain relationship. The specimen was consolidated and sheared in undrained conditions only till an axial strain of 2% to 4% for all confining pressures, except for the highest confining pressure. Similar specimens were consolidated and sheared at two higher confining pressures and the Kondner's relationship was used to determine the failure stresses at each confining pressure. The authors reported that satisfactory results for shear strength parameters and pore-water pressure response were observed from multistage tests, in comparison to conventional tests.

It was also reported that the Kondner's relationship over-estimated the values of deviator stress and pore pressure at failure.

Parry and Nadarajah (1973) performed a series of conventional and multistage triaxial tests under undrained conditions on remolded kaolin and soft silty clay specimens. The multistage included 5 stages, instead of three stages which are generally used. It was concluded that shear strength parameters obtained from multistage tests showed similar results as compared to those from obtained from conventional tests. Thereby, multistage triaxial tests were deemed to be suitable for practical purposes.

In contrast, the authors observed that the variation of stress paths obtained from both the type of tests was significantly different, especially for higher confining pressure. This may be due to the high number of alternating stages of confining pressure and shearing, which substantially alters the soil fabric. It was strongly suggested that the multistage tests be used routinely for soft lightly overconsolidated and low sensitive clays (Parry and Nadarajah, 1973).

Nambiar et al. (1985) performed a series of conventional and multistage triaxial tests under undrained conditions on submarine kaolinitic clay to determine the influence of the ratio between the second confining pressure and the initial confining pressure during the multistage test, and to assess the validity of the procedure of multistage tests. Multistage triaxial tests were performed using

procedures from Kenney and Watson (1961) and Sridharan and Rao (1972) on fine-grained carbonate soil.

The soil behavior was obtained from conventional consolidated undrained tests. It was observed that the stress-strain and pore pressure generation for soil during undrained shearing followed the Kondner's hyperbolic stress-strain relationship (Kondner, 1963). The multistage tests conducted in accordance with the approach developed by Sridharan and Rao (1972) demonstrated better correspondence in results obtained from conventional tests.

Therefore, Nambiar et al. (1985) concluded that for successfully conducting a multistage triaxial tests for the submarine deposit, the following steps needed to be considered: (*i*) verification that the failure condition of the selected soil could be predicted by Kondner's hypothesis (Kondner, 1963); (*ii*) the ratio of effective confining pressure for successive stages of multistage test be at least two; and (*iii*) the shearing of the specimen was to be continued till only 2% to 4% of axial strain and finite strains be used in Kondner's hypothesis to determine the strain at failure.

Soranzo (1988) performed multistage consolidated undrained triaxial tests on normally consolidated alluvial clay and overconsolidated colluvial clay. To overcome the difficulty of selecting the point at which the shearing needed to be stopped for initial confining pressure, the Kondner's hyperbolic criterion (Kondner, 1963) was used. However, the results from multistage tests were not compared to any conventional triaxial test results, due to lack of replicates. Also, the use of

multistage tests for brittle, highly overconsolidated, cemented or sensitive soils, which show failure at axial strains less than 4%, was discouraged as it might be difficult to accurately judge the point at which the shearing needed to be stopped.

Saeedy and Mollah (1988) investigated the applicability of multistage triaxial tests to accurately determine the shear strength parameters of saturated specimens of silty sand and clayey sand. A series of consolidated drained and consolidated undrained conventional and multistage triaxial tests were performed at varying degree of saturation. Most of the specimens showed slight post-peak softening behavior. The peak deviator stress from multistage tests showed good correspondence with that obtained from conventional tests. It was recommended to stop shearing before specimen failure for initial two confining pressures. This was suggested to be highly critical for all specimens, especially for brittle, or strongly cemented soils.

Schoenemann and Pyles (1988) observed that the unloading of the specimen after shearing for each confining pressure in multistage undrained tests resulted in the development of positive excess pore pressures, which decreased the effective confining pressure. The termination point of shearing for initial confining pressures was identified as the moment at which the stress path alters its direction to establish a tangential path or a K_f line.

Sharma et al. (2011) developed a new methodology for performing multistage triaxial tests under drained conditions on saturated specimens of weakly

cemented sands, which demonstrated a brittle behavior. The termination point for the shearing of earlier stages is selected based on the point at which the slope of volumetric strain with respect to axial strain became zero. After each shearing sequence, the deviator stress was reduced to zero before the next confining pressure was applied.

The comparison of test results from conventional and multistage tests demonstrated errors in the determination of cohesion and angle of internal friction were approximately 6% and 5%, respectively. The bender elements were used to determine the shear wave velocity throughout the test, which showed that minor degradation of the specimen was observed during shearing.

2.11.3 *Multistage Testing on Unsaturated Soils*

The motivation behind finding an alternative for conventional tests of saturated specimens is intensified in the case of unsaturated soils, due to the longer time required to complete each test. As there are two independent parameters controlling the behavior of unsaturated soils, the multistage triaxial test for unsaturated soil specimens could be performed in two ways: (*i*) keeping net confining pressure ($\sigma_3 - u_a$) constant and varying matric suction ($u_a - u_w$), or (*ii*) maintaining constant matric suction ($u_a - u_w$) and varying net confining pressure ($\sigma_3 - u_a$). The first approach is useful for obtaining the shear strength with varying matric suction. However, the time required to complete a test is too long due to the long equilibration time between successive suction states. Whereas, the second

approach determines the shear strength with varying net confining pressure (similar to saturated specimens) at constant suction and it drastically reduces the duration of the test.

Ho and Fredlund (1982) introduced the multistage triaxial testing of unsaturated specimens. The specimens were initially equilibrated to a low suction state, consolidated, and sheared at constant suction and net confining pressure under drained conditions before failure. Subsequently, the axial stress was decreased to isotropic consolidation state and then the second matric suction was induced on the specimen. Thereafter, the specimen was axially loaded before failure and again unloaded.

The final value of matric suction was induced and the specimen was sheared beyond failure. The net confining pressure was kept at a constant level throughout the test, while the matric suction was increased after each shearing stage. Figure 2.27 illustrates the ideal stress-strain curve for a multistage test using the cyclic stress approach.

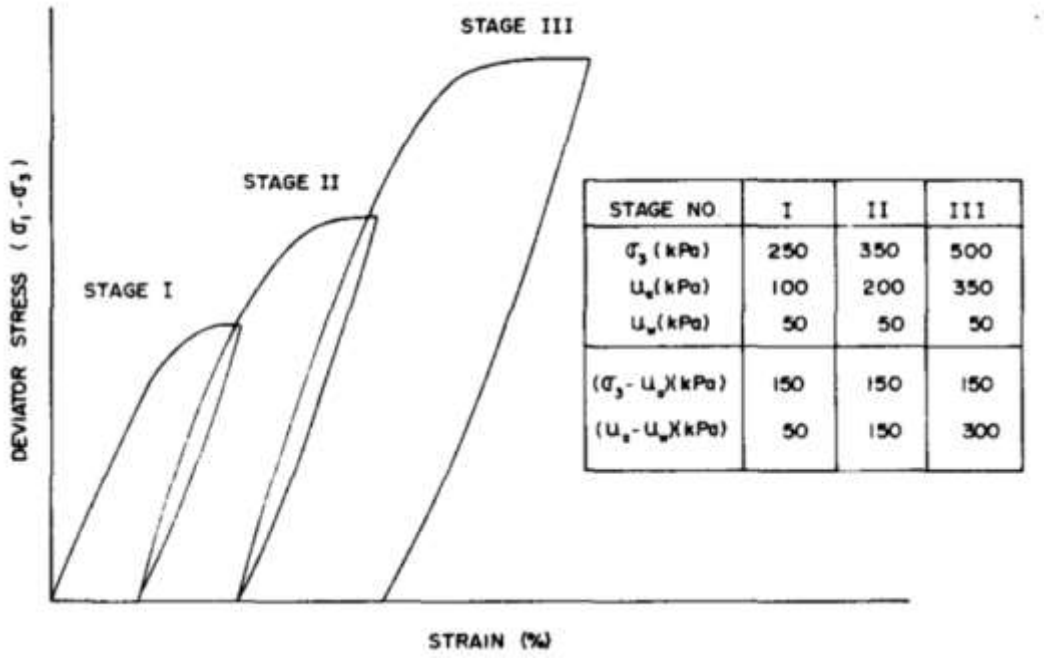

STAGE NO	I	II	III
σ_3 (kPa)	250	350	500
u_a (kPa)	100	200	350
u_w (kPa)	50	50	50
$(\sigma_3 - u_a)$ (kPa)	150	150	150
$(u_a - u_w)$ (kPa)	50	150	300

Figure 2.27 Ideal deviator stress response for a multistage triaxial test using the cyclic stress approach (Ho and Fredlund, 1982)

The multistage tests were performed on residual unsaturated soils like decomposed granite and rhyolite. The results from the multistage tests showed the potential of mitigating the problems due to soil variability and extracting maximum information from a single test. However, the results also demonstrated major disadvantages due to delay in the termination of the shearing process for the initial stages.

The delayed termination had caused a significant decrease from expected strength in the successive stage. The limitation of not removing the entire load after shearing in the earlier stages was also established. The creep of the residual stresses from the previous stages resulted in significant deformations, which was evident

from the decrease in deviator stress during suction equilibration. The deformations caused the specimen to fail in the final without reaching the strength level from the previous stage which was at a lower suction state (as shown in Fig. 2.28). So, it was concluded that multistage tests were appropriate for unsaturated soils when the specimen had not reached its failure in the initial stages and when the cyclic stress approach was used to perform the test.

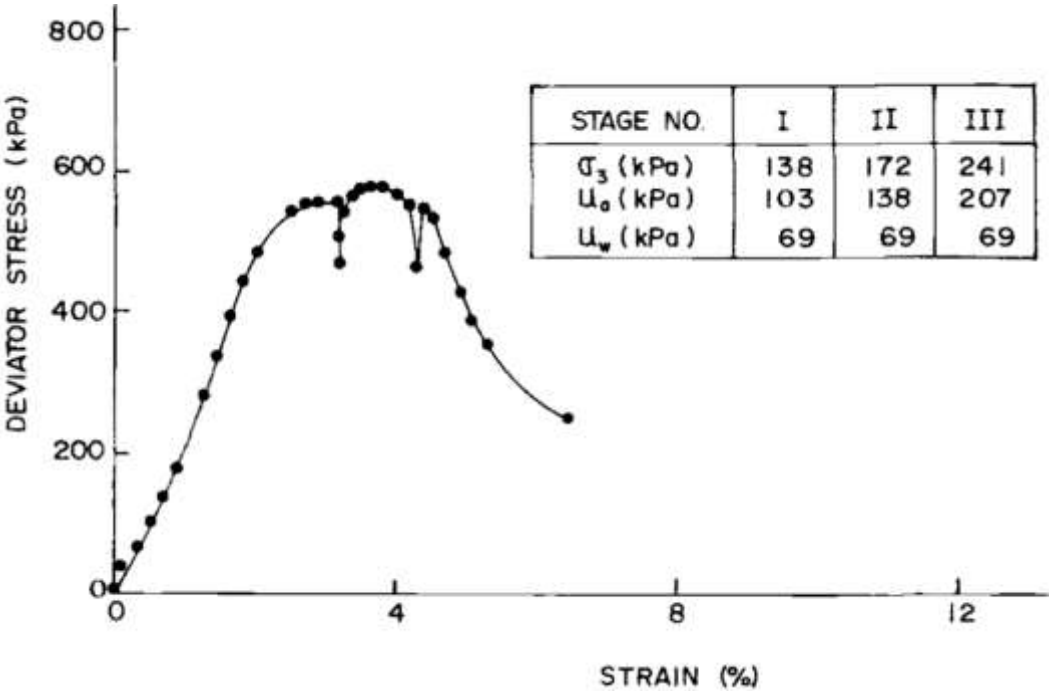

Figure 2.28 Deviator stress response for a multistage triaxial test where the cyclic stress approach was not used (Ho and Fredlund, 1982)

Rahardjo et al. (1995) assessed the shear strength characteristics of residual soils under unsaturated conditions using a series of multistage, consolidated drained (CD) triaxial tests. Both the methods of multistage triaxial tests were used: (*i*) constant net confining pressure and varying suction, and (*ii*) constant suction and

varying net confining pressure. 12 samples of silts and clayey soils from different depths were selected for the study. To negate the effect of hysteresis associated with the wetting and drying curves of SWCC, the specimens were initially saturated and thereafter, the required matric suction was applied.

The cyclic stress approach was also used in this study. Specimens were subjected to 3 to 5 stages of multistage tests and mostly a small increase in the suction or net mean stress were introduced for the successive stages. Due to lack of replicates, the accuracy of multistage tests was not confirmed by comparing their results with that obtained from the conventional tests. However, the shear strength parameters of unsaturated soils from two nearby sites showed similar results, which validates the repeatability of these tests. Similar tests were performed by Noor and Jais (2014) on residual soils to establish a correlation between the minimum mobilized friction angle and the axial strain. The comparison between the deviator stress response obtained from conventional tests was similar to that from multistage tests.

Ng et al. (2007) performed a comparison between conventional and multistage triaxial tests on unsaturated highly expansive clay, by adopting the axis translation technique. The cyclic stress approach was used for multistage tests (Ho and Fredlund, 1982). Also, during multistage tests, at each stage, the suction was maintained at a constant value, while the net confining pressure was increased for successive stages. The results showed a continuous increase in deviator stress, till

it reached its peak, with an increase in axial strain, i.e. no post-peak softening was observed. The multistage tests showed similar results when compared to conventional triaxial tests, with an average error of 3% in the computed shear strength, based on two-independent stress state variable approach by Fredlund and Morgenstern (1977).

Multistage tests were performed for suction of 50 and 100 kPa, with varying net confining pressure of 25, 50 and 100 kPa. However, the conventional tests were performed only on parameters for the final stage. Furthermore, since the air-entry value of the expansive clay selected for the study was 60 kPa and multistage tests were conducted at suction levels of 50 and 100 kPa, so the tests were conducted at a high degree of saturation (approximately greater than 85%). Therefore, a meticulous comparison was not be provided with a limited number of replicates tested over similar saturation level.

Khalili and Zargarbashi (2010) endeavored to investigate the variation of the effective stress parameter, χ along drying and wetting paths, for which a series of multistage tests were conducted on saturated and unsaturated soil specimens under drained conditions. A variety of soils, like lean clay, sand-clay mixture, low plasticity silt and a mixture of sand and kaolin were chosen for the study. The following stress path was followed: (*i*) the specimen was sheared to reach the CSL (*ii*) matric suction was induced in the specimen, which enhanced the effective stress acting on the specimen and the stress path moved away from the CSL, (*iii*) the steps

(*i*) and (*ii*) were repeated several times, (*iv*) matric suction was reduced to enforce the specimen to undergo unloading along the CSL at constant values of net mean stress and axial strain. The variations of the effective stress parameter, χ with suction along wetting and drying curves were computed from the slope of CSL on $p'-q$ space and the values of deviator stress, q, net confining stress, $\sigma_{3,\ net}$, and suction, s. The relationship is as follows:

$$\chi = \frac{[1-M_{cr}/3]\ q-M_{cr}\ \sigma_{3,net}}{M_{cr}\ s} \qquad (2.18)$$

It was observed that the degree of saturation didn't represent a satisfactory correlation with the effective stress parameter. By extending the Khalili and Khabbaz (1998) model for the effective stress parameter, the variation of χ during the transition from drying to wetting was computed using the results from the multistage test. This helped in the determination of hysteresis of the effective stress of unsaturated soils due to the wetting-drying cycles. However, during this study, the axial load was not reduced after shearing, which may have caused creep to affect the results.

Khosravi et al. (2011) evaluated a new methodology to determine the termination point during shearing in a multistage triaxial test on unsaturated specimens of compacted silty sand. Before performing a multistage test, a consolidated undrained triaxial test was conducted on a saturated specimen, to obtain the CSL of the saturated specimen. It was assumed that the CSL on p'-q

space is unique for both saturated and unsaturated soil, as observed by Khalili et al. (2004). For the tests on unsaturated specimens, the suction stress was computed by using the effective stress parameter, χ and it was presumed that χ was equal to the degree of saturation.

This assumption by Khosravi et al. (2011) has been criticized as it has been observed to be not true for many soils (Jennings and Burland, 1962; Bishop and Blight, 1963; Burland, 1964; Blight, 1967; Fang, 1977; Khalili and Zargarbashi, 2010; and also explained in Section 2.7.2.1). Nevertheless, the shearing stage in the multistage test was terminated when the stress path of the ongoing test reached the CSL, which had been obtained from the CU test on the saturated specimen.

These multistage tests were conducted using the cyclic stress approach (Ho and Fredlund, 1982) and the net confining pressure was kept constant, while the suction was increased in the successive stages. It was concluded that the multistage test demonstrated a consistent trend with the CSL obtained from the saturated test when the failure points were plotted in the p'-q space. Therefore, apart from the assumptions, the CSL of the specimen needs to be known before initiation of the multistage test. This results in a major limitation, as the main reason to perform these tests were to reduce soil variability from replicates and to address the issue of scarcity of identical specimens.

Handoko et al. (2013) had performed a multistage test on sandy soil where the cyclic stress approach was used and for each successive stage, the suction was

increased, but the net confining pressure was kept constant. The shearing stage was terminated after the equilibrium was obtained, i.e. once the deviator stress reaches a constant value, the shearing was stopped, and then the specimen was axially unloaded. This approach may cause premature failure of the specimen and result in a reduction of strength for subsequent stages. Also, the results from the multistage test were not compared to that obtained from any conventional triaxial test.

Similar tests were performed by Oh and Lu (2015) to estimate the shear strength parameters of unsaturated specimens of well-graded sand and high plasticity silts at varying suction levels. These parameters were utilized to perform slope stability analysis of failed slopes.

Rahardjo et al. (2013, 2014) had performed a series of multistage triaxial test on recycled materials like Recycled Concrete Aggregate (RCA) and Reclaimed Asphalt Pavement (RAP), under drained conditions in saturated and unsaturated conditions. Since these materials have a brittle nature, the strain induced at failure is very low and likewise, the margin for error in termination of the shearing during the initial confining pressure levels are very small.

For unsaturated specimens, the multistage tests were performed at same net confining pressure and with increasing the suction level for successive stages. The multistage tests helped in studying the influence of grain size distribution and porosity of the strength of recycled materials. The shear strength parameters were

utilized for slope stability analysis Rahardjo et al. (2014). Similar multistage tests were performed on residual silty soil by Leong et al. (2013).

Rosone et al. (2016) performed an elaborate series of consolidated drained (CD) triaxial test on unsaturated specimens of scaly clay. Apart from the series of conventional triaxial test on unsaturated specimens, using the axis-translation technique, three specimens were tested using multistage testing, where the suction was maintained at a constant level, while the net confining stress was increased. The multistage test consisted of two stages and its result was compared to a conventional test, where the specimen was subjected to the same matric suction and net confining pressure as the final stage of the multistage test.

Figure 2.27 shows the comparison between the multistage test and the conventional test, both tests were performed at a matric suction of 50 kPa. The multistage test response showed very good correspondence with that obtained from the single stage test. This validated the use of the multistage test for determining the shear strength of the scaly clay. Though the deviator stresses were not removed entirely, the successive stage didn't show any decrease of strength due to creep, which may be due to three reasons.

Firstly, a partial reduction in deviator stress was performed after shearing was terminated. Secondly, the duration for equilibration was quite less when the suction was maintained constant, as compared to duration required to achieve equilibrium after increasing suction. Finally, the scaly clays were overconsolidated

due to its complex geological history and soil structure, so their stiffness may induce lesser volumetric changes with similar stresses.

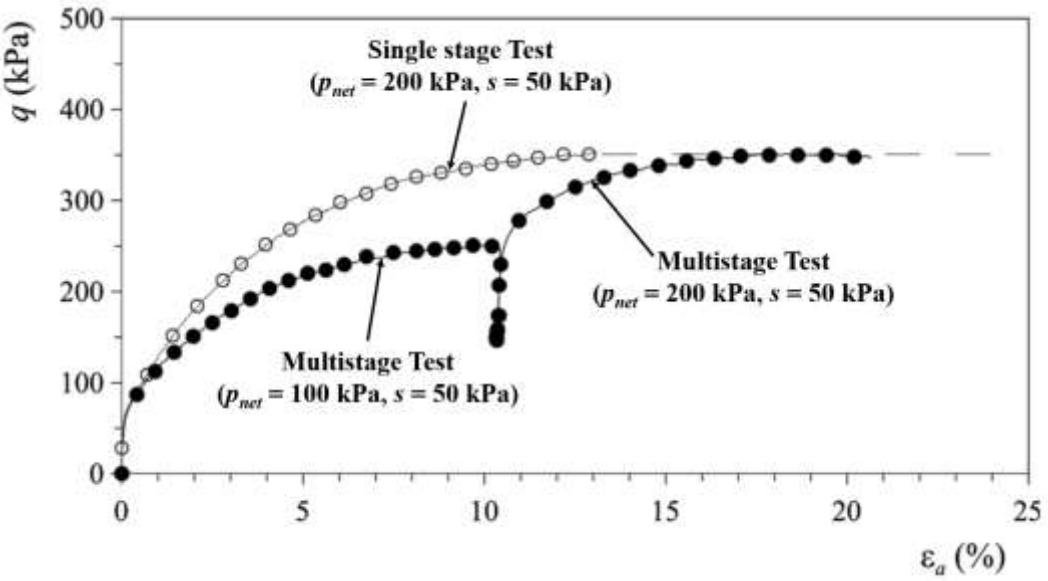

Figure 2.29 Comparison between response of multistage triaxial test and single stage test at suction of 50 kPa (Rosone et al., 2016)

Ferreira et al. (2016) validated the use of multistage triaxial tests, instead of single stage triaxial tests to estimate the shear strength parameters of unbound granular non-traditional material like processed steel slag. Additionally, the effect of saturation of the granular material was studied using the multistage testing procedure. The specimens were tested in unsaturated conditions in drained conditions, but the suction was neither controlled, nor measured.

Initially, three stages of alternating consolidation and shearing to a limited axial strain, using the cyclic stress approach by (Ho and Fredlund, 1982) were applied. Subsequently, the specimens were unloaded axially, saturated and sheared

till failure. Similarly, single stage tests were conducted on unsaturated and saturated specimens and the results were compared. The maximum difference in peak angle of internal friction was computed to be less than 10%, with an average difference of less than 5%.

2.11.4 *Synopsis of Multistage Triaxial Testing*

The multistage triaxial testing has been identified as a possible substitute for the single-stage triaxial testing in case of lack of proper replicates, to address the issue of soil variability among various soil specimens and to reduce testing cost and time required to complete a test. It has been identified that the selection of the termination point for the shearing stage is the most critical part of the test. This becomes even more significant for brittle geomaterials. The various approaches used to select the termination point of the shearing stage are shown in Fig. 2.28, where σ_d is the deviator stress, and ε_a and ε_v are the axial and volumetric strains, respectively. Table 2.4 summarizes the various approaches used for multistage triaxial tests.

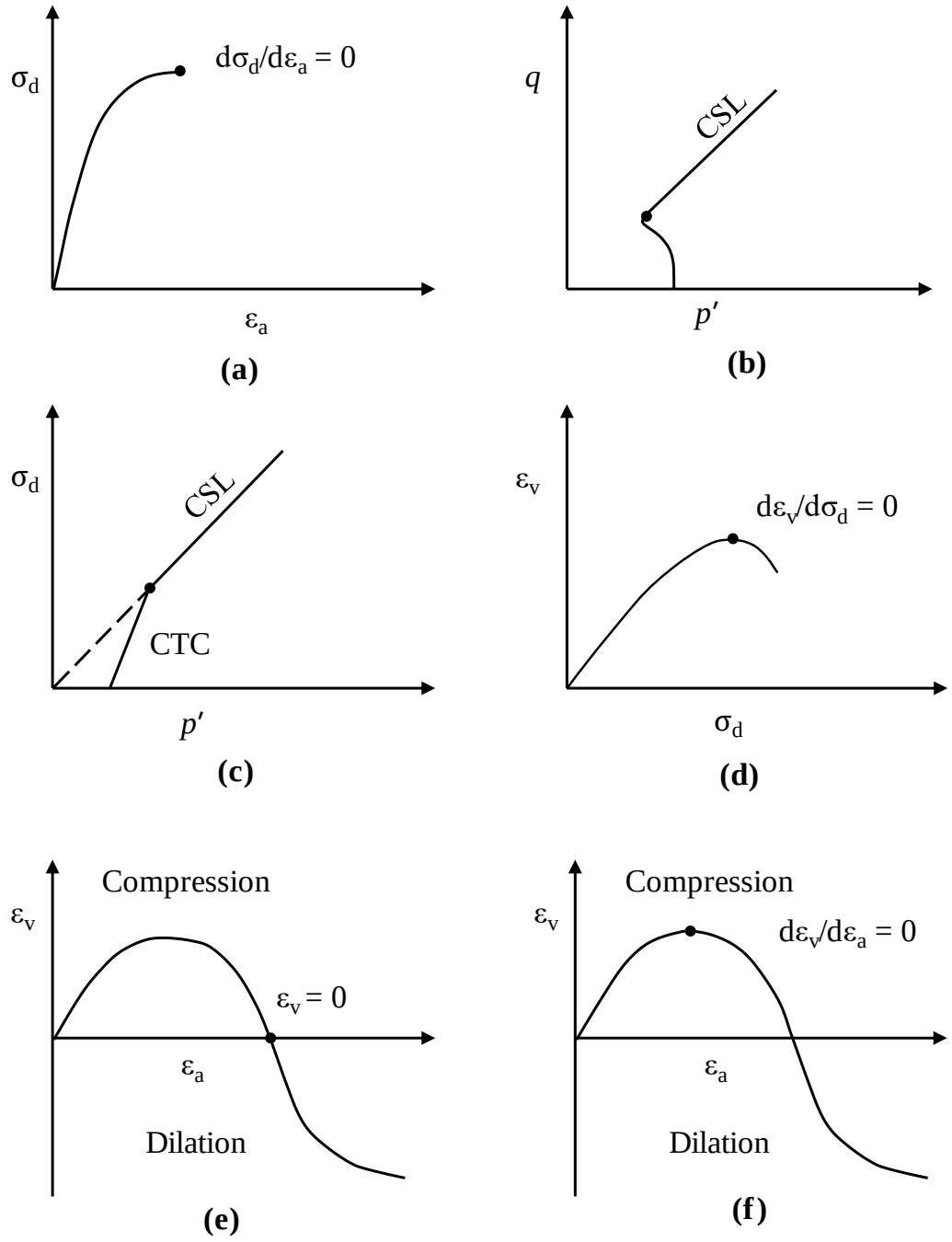

Figure 2.30 Schematic of various approaches to determine termination of shearing in the multistage triaxial test.

Table 2.4 Comparison of methodology followed for suction controlled multistage triaxial test

Reference	Comparison with single-stage response	Method for termination of shearing stage	Approach after termination of shearing stage	Variable for successive stage
Ho and Fredlund (1982)	No	$d\sigma_d/d\xi_a = 0$ (Fig. 2.28a)	Cyclic	Matric suction
Rahardjo et al. (1995)	No	$d\sigma_d/d\xi_a \approx 0$ (Fig. 2.28a)	Cyclic	(*i*) Matric suction (*ii*) Net confining pressure
Ng et al. (2007)	Yes (Final Stage)	N/A	Cyclic	Net confining pressure
Khalili and Zargarbashi (2010)	No	Reaching CSL (Fig. 2.28c)	No Unloading	Matric suction
Khosravi et al. (2011)	No	Reaching CSL (Fig. 2.28c)	Cyclic	Matric suction
Leong et al. (2013)	No	$d\sigma_d/d\xi_a = 0$ (Fig. 2.28a)	Cyclic	Matric suction
Handoko et al. (2013)	No	$d\sigma_d/d\xi_a = 0$ (Fig. 2.28a)	Cyclic	Matric suction
Rahardjo et al. (2013, 2014)	No	$d\sigma_d/d\xi_a = 0$ (Fig. 2.28a)	Cyclic	Matric suction
Rosone et al. (2016)	Yes (Final Stage)	N/A	No Unloading	Net confining pressure

2.12 Summary

This chapter describes various topics from the literature related to the dissertation subject topic. First, the difference between saturated and unsaturated soils by considering the mechanics involved in governing the behavior of unsaturated soils is described. The importance of surface tension, capillarity, and soil suction in unsaturated soils are presented. The influence of soil water characteristic curve, air-entry value, residual soil suction, and the hydraulic hysteresis on the response of unsaturated soils are discussed.

The concept of shear strength of unsaturated soil is introduced and the methods to determine the shear strength are described. An elaborate discussion on the determination of shear strength using triaxial tests is presented. The various techniques to apply, control, and measure soil suction are described in brief. A review of the past and recent advances in triaxial test equipment for determination of the hydromechanical response of unsaturated soils is presented in detail. The chapter also caters to the applicability of multistage triaxial tests for determination of shear strength of saturated and unsaturated soil specimen.

Chapter 3

MONOTONIC TRIAXIAL TEST – SINGLE-STAGE TESTS

3.1 Introduction

The mechanical response of the soil in saturated and unsaturated condition, when subjected to monotonic stresses under the drained condition, has been studied and detailed in this chapter. Table 3.1 lists the various triaxial tests performed as a part of this chapter.

Table 3.1 Series of single-stage triaxial tests performed in this dissertation research

Sl. #	Type of Triaxial Test	# of Tests	Research Variables	Assessment Focus
1	Consolidated drained triaxial test (CTC stress path) – saturated specimen	4	Axial Rate of shearing – 0.01, 0.05, 0.25, and 0.50%.min for effective confining pressure of 400 kPa	Appropriate rate of shearing for saturated specimens
2	Consolidated drained triaxial test (CTC stress path) – saturated specimen	3	Effective Confining pressure: 100, 200, and 400 kPa	Stress-strain response and shear strength parameters of saturated soil
3	Suction-controlled isotropic triaxial consolidation (HC stress path)	10	Net confining pressure: 100, 200, and 400 kPa Matric Suction: 50, 250, and 750 kPa. Additional Test: CD_200_500	Consolidation behavior (effect of matric suction on elastic stiffness parameter κ, suction-induced stiffness, λ, and yield stress, σ_{yield}).
4	Consolidated drained triaxial test (CTC stress path) – unsaturated specimen	3	Axial Rate of shearing – 0.001, 0.003, and 0.010%.min for CD_400_250	Appropriate rate of shearing for saturated specimens
5	Consolidated drained triaxial test (CTC stress path) – unsaturated specimen	10	Net confining pressure: 100, 200, and 400 kPa Matric Suction: 50, 250, and 750 kPa. Additional Test: CD_200_500	Stress-strain response and shear strength parameters of unsaturated soil

Prior to discussing the results of the triaxial tests, the properties of the soil used in this study have been specified. Additionally, the modifications made to a conventional triaxial testing device have been succinctly described.

3.2 Basic Properties of Test Soil

The soil used in the study was obtained from a site in Denison, Texas near the Red River at the border of Texas and Oklahoma (Fig. 3.1). The soil was air-dried, mixed thoroughly, and stored in buckets for future use. From the sieve analysis and hydrometer test, it was determined that the soil primarily comprises of silt (86%), with a small amount of clay (10%), and sand (4%). The grain size distribution is shown in Fig. 3.2. The soil was found out to be non-plastic from Atterberg Limit tests, which were conducted in accordance to ASTM D4318-10e1. Accordingly, the soil was classified as silt of low plasticity (ML) as per the Unified Soil Classification System (USCS). The specific gravity of the soil solids was obtained to be 2.68, by conducting specific gravity test using a pycnometer, as per ASTM D854-14. The standard proctor tests were conducted as per ASTM D698-12e2 (shown in Fig. 3.3), and the maximum dry density of 1.70g/cm^3 was obtained at an optimum moisture content of 14.8%. The physical and mechanical properties of the soil are listed in Table 3.2.

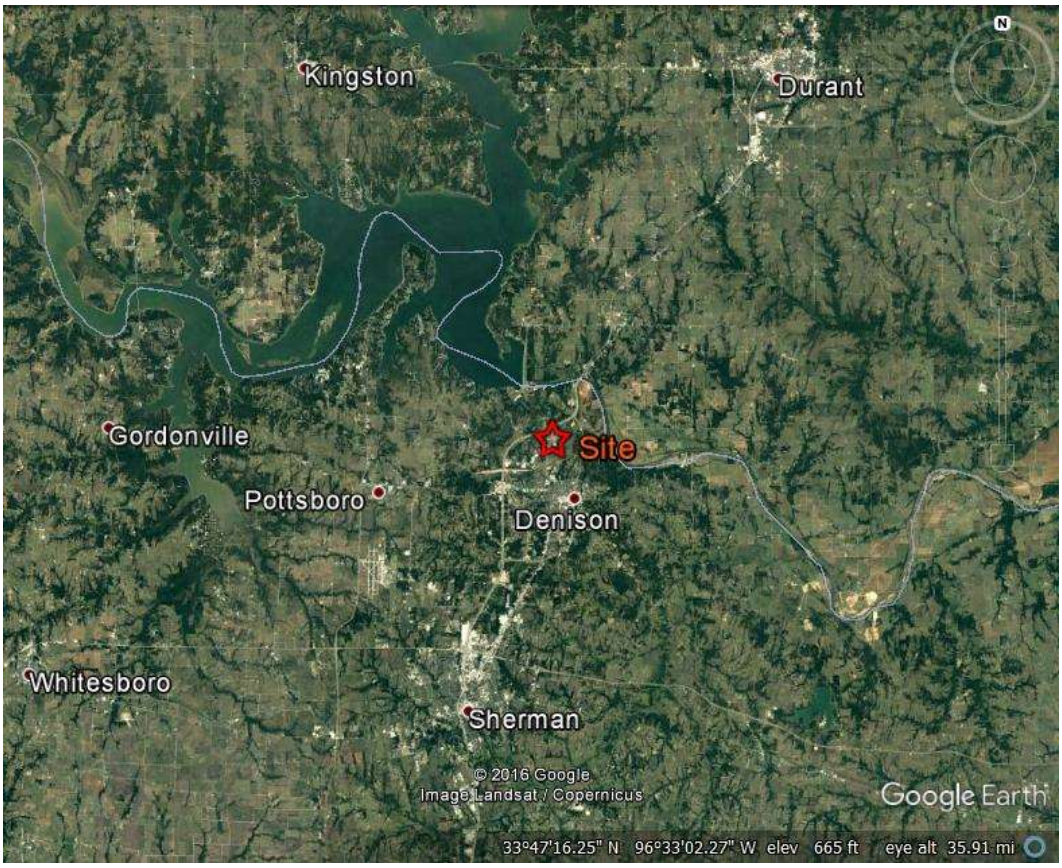

Figure 3.1 Site Location for the silty soil used in the study (from Google Earth, 2016)

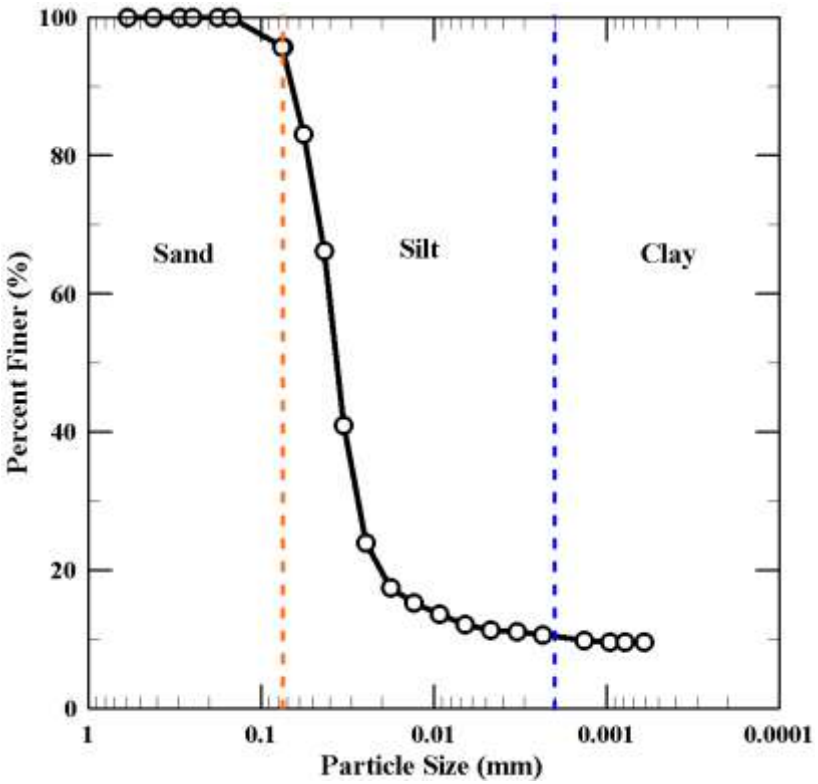

Figure 3.2 Grain size distribution of the silty soil used in the study

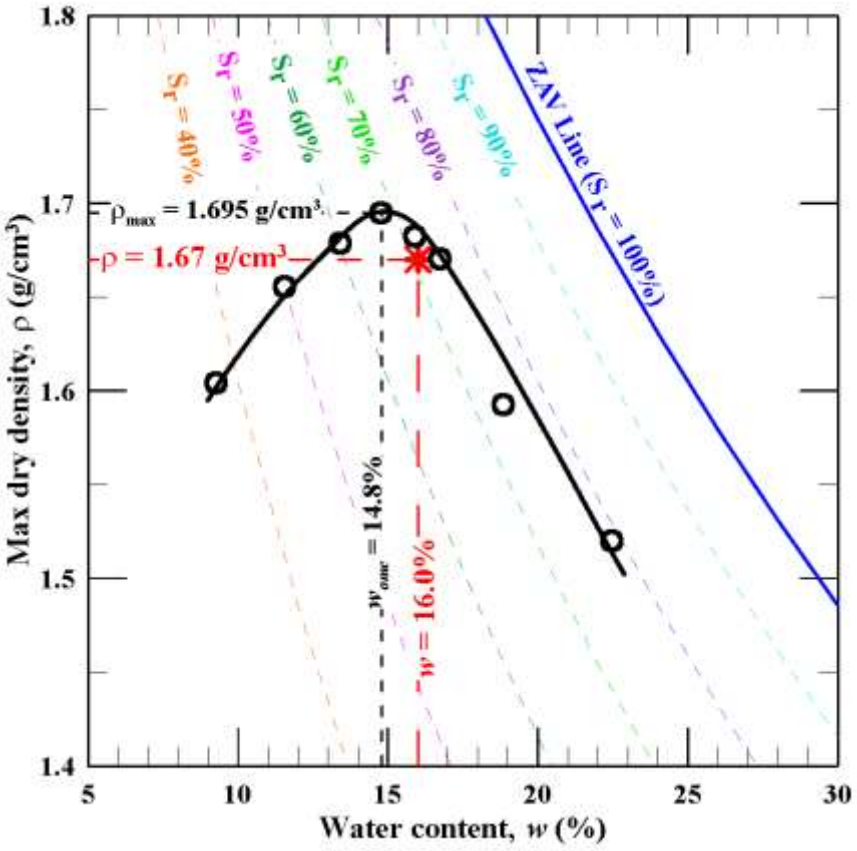

Figure 3.3 Standard Proctor Compaction curve for the silty soil used in the study

Table 3.2 Properties of the silty soil used in the study

Parameters	**Value**
Sand (%)	4
Silt (%)	86
Clay (%)	10
USCS classification	ML
Maximum dry unit weight, $\gamma_{d,\,max}$, (kN/m^3)	16.8
Optimum moisture content, w_{opt} (%)	14.8
Plasticity Index, PI (%)	NP (Non-Plastic)
Specific Gravity, G_s	2.68

3.3 Specimen Preparation

The expectation of procuring many homogenous undisturbed specimens without any vegetative matter or stones is quite unrealistic. The homogeneity of the specimens is essential to obtain a coherent relationship among the variables involved in determining the behavior of soil when subjected to mechanical stresses. Therefore, remolded specimens are used for performing fundamental and theoretical-based research to understand the behavior of soil (Wulfsohn et al., 1998).

3.3.1 *Specimen Preparation Technique*

The remolded specimens for the triaxial test can be prepared using compaction methods like static or dynamic compaction, wet or dry pouring, or moist tamping. The selection of compaction techniques is essential, as the compaction technique has a significant influence on the soil fabric or the microstructure of the soil, which thereby influences the mechanical and hydraulic response of the soil (Cox, 1978; Lawton et al., 1989; Alonso and Gens, 1992; Vanapalli et al., 1999; Wood et al., 2008; Yamamuro et al., 2008).

The compaction energy is another variable to be considered to achieve a target density at a selected moisture content. Sivakumar and Wheeler (2000) had concluded that the compaction energy causes the expansion of the initial yield surface of the specimen. The initial state at different suction levels is expected to be dependent on the compaction energy applied to prepare the specimen. However,

the slope of the normal compression and critical state lines are affected marginally (Sivakumar and Wheeler, 2000).

The moisture content at which the soil is compacted has a major influence on the behavior of the soil. It affects the initial state, the stress path, the slopes of normal compression line, and the critical state line of the compacted soil specimen. Therefore, soils compacted at different moisture contents behave differently, due to the difference in soil fabric. The soil fabric refers to the alignment of the solid soil particles, the pore air, and pore water voids. The difference in moisture content and compaction energy affects the size of the pore air voids, which upon wetting should collapse to the size of largest pore filled with water, under the given stress condition. This leads to the overall collapse of the specimen (Vatsala and Murthy, 2010).

The problem of segregation of silts and the coarse particles is a possibility in wet pouring method (Ladd, 1978). Moreover, it is difficult to maintain a specific dry density of soil throughout the specimen. Similarly, the other compaction methods, except the static compaction technique were determined to be unsuitable for preparing soil specimens for this research.

Hence, the static compaction technique had been used in this study to prepare specimens of 142.8 mm height and 71.4 mm diameter. As per ASTM D7181-11, the recommended aspect ratio for the triaxial specimen is between 2 to 2.5, to negate the end effect of the end platens (in the case of short specimens) and

excessive buckling (in the case of slender specimens). The end effect is due to static friction which develops between the ends of soil specimen and top cap and bottom pedestal. The friction generates a pseudo confining pressure towards the ends of the specimen. As per ASTM D7181-11, the minimum diameter of the specimen is restricted by the maximum size of the particle (d_{max} = 0.25 mm in this case) or 33 mm, whichever is higher. Since the soil was predominantly silty with no coarse sand and D/d_{max} being very large (much greater than 6, as per the requirements of ATSM D7181-11), the specimen diameter was not of any concern.

Toll (1990) had mentioned the problems regarding compaction of soil specimens on the dry side of optimum. The soil, especially the ones having a significant proportion of silt, tend to flocculate and form aggregated fabric. These aggregated particles become stronger with induced suction and each aggregated unit behaves as an individual particle, which alters the overall behavior of the soil specimen when subjected to shear (Toll, 1990). Henceforth, in this research, the soil specimens were prepared on the wet side of optimum, where this problem does not arise.

The air-dried sample of silty soil was mixed thoroughly with 16.0% water (1.2% wet of optimum) and stored in sealed bags at constant temperature and humidity in the 100% relative humidity chamber for a few days. After ensuring that the target water content of 16% has been achieved (by conducting moisture content

tests on the equilibrated sample), the soil specimen for the triaxial test was prepared in three equal lifts.

It is well-known that the compaction energy applied for a specific layer also compacts the lower layers. Henceforth, to achieve the same density throughout the specimen, the lower layers were relatively under-compacted as compared to the ones on top. Each layer was compressed statically in a split compaction mold by using a 44.5 kN (10000 lbf) load frame, shown in Fig. 3.4. A constant axial strain rate of 1 mm/min was used to achieve the target height for each layer. After compaction of each layer, a thorough inspection was performed regarding the height of soil compacted. Subsequently, the surface was scarified to provide for proper interlocking between the interface of adjacent layers. The properties of the compacted specimens are listed in Table 3.3.

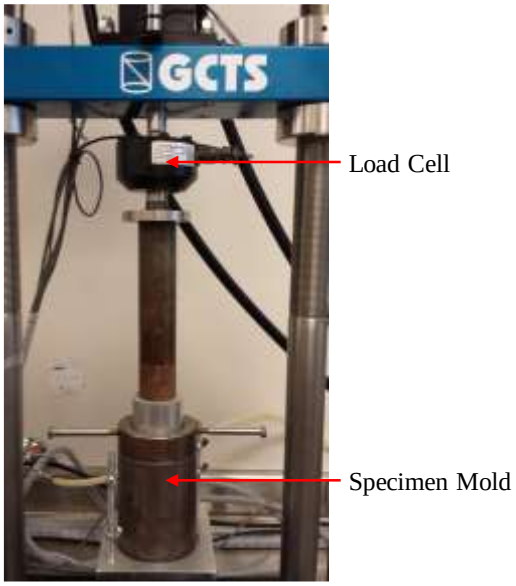

Figure 3.4 Static compaction setup to prepare standard specimens for triaxial tests

Table 3.3 Properties of compacted specimens

Parameters	**Value**
Dry Unit Weight, γ_d (kN/m^3)	16.4
Degree of saturation, S_r (%)	71
Matric Suction (kPa)	26
Void ratio, *e*	0.60
Porosity, *n* (%)	37.5
Water Content, *w* (%)	16.0
Height of Specimen (mm)	142.8
Diameter of Specimen (mm)	71.4

The compression curves for each layer of a typical triaxial test specimen is shown Fig. 3.5. It clearly shows that the lowest layer (Layer 1) was subjected to the least stress, whereas the top layer (Layer 3) was subjected to the maximum stress. However, the stresses applied on the top surface is also partly experienced by all the layers. Figure 3.5 demonstrates the principle of undercompaction by Ladd (1978). It can also be proven mathematically, that the compaction energy applied per unit volume was higher for the top layer (with two layers of soils below it) as compared to the layers below it. The work done (*W*) or the energy (*E*) applied to the soil is as follows:

$$W = \int_a^b F\, ds = \int_a^b \sigma \text{ x } A\, ds = A \int_a^b \sigma\ ds \qquad (3.1)$$

where,

F is the Force applied to the specimen

s is displacement caused due to the application of the force *F*

a and *b* are the initial and the final displacements during compaction

A is the cross-section area of the specimen

σ is the axial stress applied to the specimen

Energy per unit volume (*E*) of the specimen is defined as the ratio of work done to compact the specimen (*W*) to the volume of soil compacted (*V*).

$$E = \frac{W}{V} \tag{3.2}$$

The work done and energy per unit volume was computed from Fig. 3.5 and Equations 3.1 and 3.2, as shown in Table 3.4. The area under each curve was approximated by computing the integral of the best-fit curve (third order polynomial) over the displacement for each curve. It was observed that the compaction effort for the third lift was almost twice that of the first one, while compaction effort for the second lift was almost 50% more than that of the first one. All the specimens for triaxial tests were prepared using the same approach as described above.

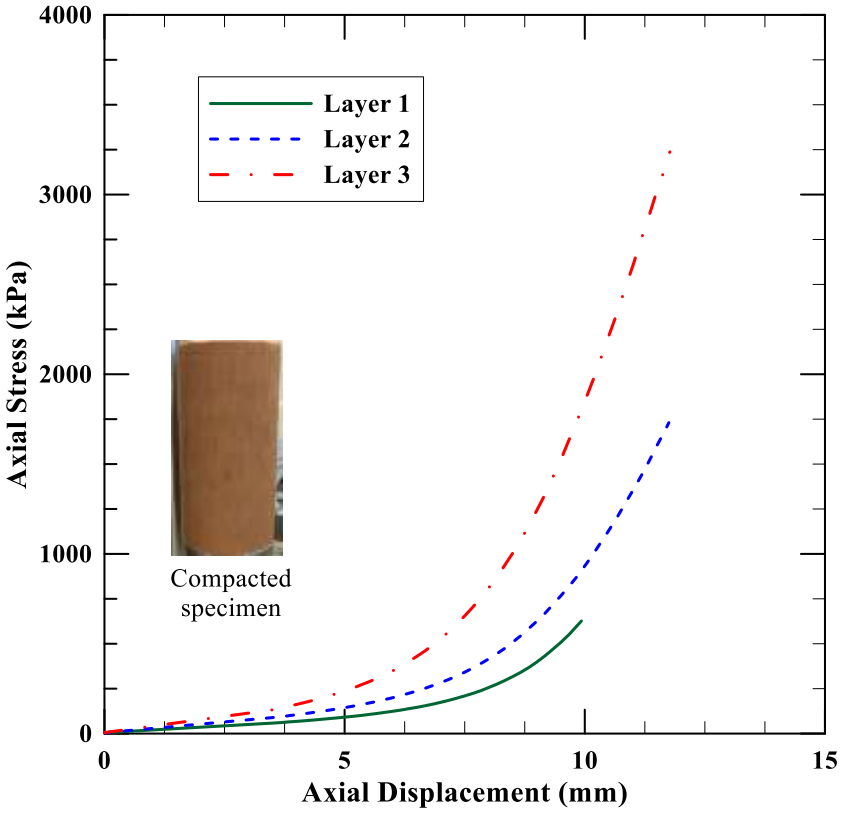

Figure 3.5 Compaction curves for each layer of a specimen for triaxial test during static compaction

Table 3.4 Computation of Energy per unit volume for each lift during static compaction

Particulars	**Layer 1**	**Layer 2**	**Layer 3**
Height of each lift (mm)	47.6	95.2	142.8
Area of cross-section (cm^2)	40.039	40.039	40.039
Volume of soil compacted (cm^3)	190.59	381.17	571.76
Area under the curve, $\int_a^b \sigma \ ds$ (kN/m)	1.559	4.658	9.003
Work Done, W (kJ)	6.242×10^{-3}	1.865×10^{-2}	3.605×10^{-2}
Energy per unit volume (kJ/m^3)	32.756	48.934	63.050
Factor (E_i/E_1)	1.00	1.49	1.93

3.4 Soil Water Characteristic Curve (SWCC)

The drying cycle of the soil-water characteristic curve (SWCC) of the test soil at its target dry density was obtained by using the Fredlund device, commonly known as Tempe Cell, and the relative humidity apparatus. The Tempe Cell was used for matric suction below 500 kPa and it works on the principle of axis-translation technique. The experimental points in the residual zone of the SWCC were obtained from the automatic relative humidity apparatus, which works on the principle of vapor pressure technique. Additional SWCC data points were obtained by using the filter paper technique and the potentiometer.

3.4.1 *SWCC using Tempe Cell*

The specimen for determination of SWCC using a Tempe Cell (Fig. 3.6) is similar in size to the one used in an oedometer. The final diameter of the SWCC specimen is 63.5 mm (2.5 in) and its height is 25.4 mm (1 in). Air-dried silty soil was mixed thoroughly with 16% water and after equilibration for more than two days, the moist soil was placed in the stainless-steel ring of inner dimension 63.5 mm (2.5 in) and height 31.75 mm (1.25 in). The soil was compacted using static compaction at a rate of 0.5 mm/min to achieve the target density of 1.67 g/cm^3.

The compacted specimen placed in the steel ring was placed on top a steel plate and a previously saturated porous stone of 101.6 mm (4 in) diameter. Another saturated porous stone was placed on top of soil specimen with filter paper at the interface between soil and porous stones (at the top and bottom). A steel plate was

kept on top of the top porous stone and the top steel plate was tightened to the bottom steel plate using a combination of rods and screws. The entire assembly was placed in a small reservoir to saturate the soil specimen, without allowing any volumetric changes. To prevent air bubbles getting trapped in the soil, initially, the soil was allowed to absorb water through capillary action by filling water till the bottom porous stone. Later, the entire reservoir was filled with water. After saturating the specimen for more than a day, the assembly was removed from the water and the soil within the ring was weighed for its saturated mass. Subsequently, the specimen was placed in the Tempe Cell with a saturated ceramic disk for obtaining the SWCC over the drying curve.

The ceramic disk (AEV = 5 bar) of the Tempe cell was saturated before placing the specimen. The ceramic disk was placed in a container and de-aired water was partially filled to the middle of the ceramic disk for allowing the air bubble to move upwards. After 12 hours, the entire ceramic disk was submerged in de-aired water for 24 hours.

To ensure the ceramic disk was fully saturated, it was placed in the Tempe cell and fixed to the base plate and the drainage pipes were properly flushed with de-aired water. The chamber for the Tempe cell was attached to the base plate and the ceramic disk was submerged in approximately 38 mm (1.5 in) of de-aired water. The Tempe cell was sealed and the air pressure was applied from the top onto the surface of the water. This pressurized the water and forced it to flow through the

ceramic disk. Since the air-entry value (AEV) of the ceramic disk was 5 bar. The air pressure was gradually increased to 600 kPa (greater than the AEV), which forced the water to flow through the ceramic disk at a much faster rate. After 3 hours, the air pressure was gradually released and the water remaining above the ceramic disk was removed. Meanwhile, throughout the saturation process, the rate of water flow with respect to applied pressure was noted, in order ensure that there were no cracks in the ceramic disk.

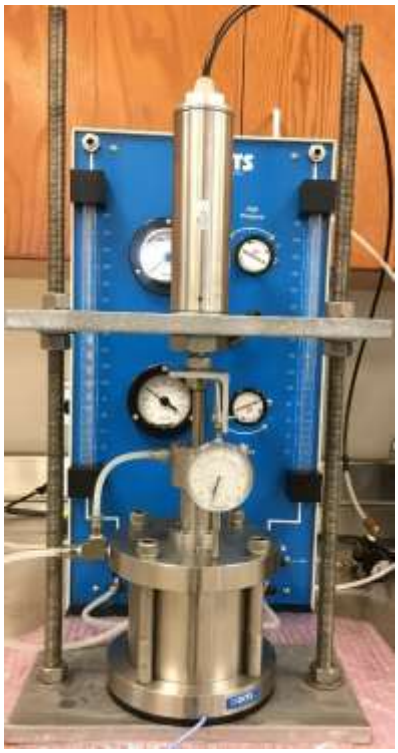

Figure 3.6 Tempe Cell (Fredlund's device) used to determine the SWCC of the silty soil.

After setting up the assembly for Tempe cell with saturated soil specimen, the chamber was sealed and the appropriate air pressure was applied. After the water levels in the graduated column stabilized (generally after 1-3 days), the next air pressure was applied. This process was continued till the air pressure reached 400 kPa. After stabilization of water in the vertical column, the pressure was gradually released and the soil specimen was removed, weighed, and dried in the oven for determination of the water content. Throughout the test, the drainage pipes were regularly flushed to prevent accumulation of diffused air beneath the ceramic disk. The water content corresponding to each of the earlier air pressures were computed based on the difference in water level in the graduated column.

3.4.2 *SWCC using Auto RH apparatus*

The automatic relative humidity apparatus (Fig. 3.7) was used to determine the SWCC of the soil at high suction states (greater than 10 MPa). It works on the principle of vapor equilibrium technique. The specimen like the ones used for SWCC tests using a Tempe cell were also prepared for this test. To negate the effect of hysteresis between the drying and wetting curves, the specimen was fully saturated, similar to the method used for specimens tested on a Tempe Cell. Gradually the saturated specimen was dried in the air by keeping it on a weighing balance. The weight of the specimen was continuously monitored to estimate the water content of the soil. Since the SWCC obtained from Tempe Cell was already known before starting this test, once the specimen reached a water content

corresponding to a suction of 500 kPa, the specimen was removed from the stainless ring and transferred to the acrylic chamber whose humidity is monitored by the RH probe from the auto-RH apparatus (as shown in Fig. 3.7). The same auto-RH setup was used by Patil (2014) and additional information on RH apparatus may be obtained from Patil (2014). At this point, the relative humidity was set to induce a total suction greater than 15 MPa. After equilibrating the specimen for approximately 3 weeks inside the chamber, the weight of the specimen was observed to be constant. Consequently, the specimen was removed, its mass was noted and it was dried in an oven to obtain the moisture content. Similar procedure was adopted for obtaining additional SWCC data points at higher suction levels (≈ 30 MPa and 310 MPa).

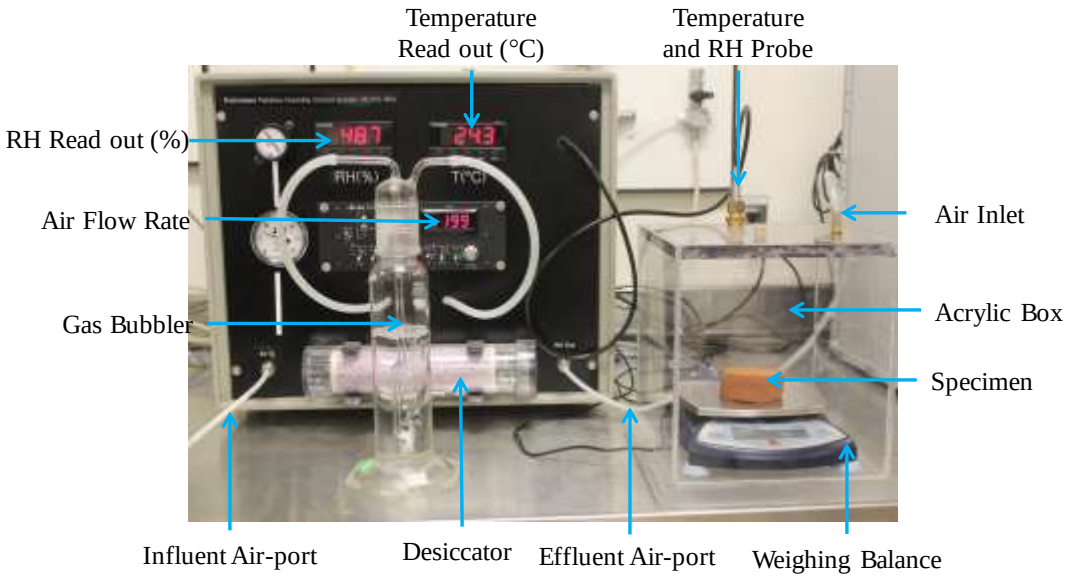

Figure 3.7 Auto-RH apparatus used to determine the SWCC of the silty soil.

3.4.3 *SWCC using WP4C and Filter Paper Technique*

The SWCC of the silty soil was also obtained using WP4C dew point potentiometer, shown in Fig. 3.8. It measures the water potential by determining the relative humidity of the air above the surface of the specimen in a closed chamber within the potentiometer. The chilled mirror technique is used to determine the relative humidity. It has been observed to work in the suction range of 500 kPa to 200 MPa. After the instrument determines the soil suction of the specimen, the water content of the specimen was measured immediately, by measuring the moist soil mass using a high precision balance, having an accuracy of 0.0001 g (as shown in Fig. 3.8) and placing the specimen in a clean oven. The dry mass was recorded after a day. The tests were conducted in accordance to ASTM D6836-16.

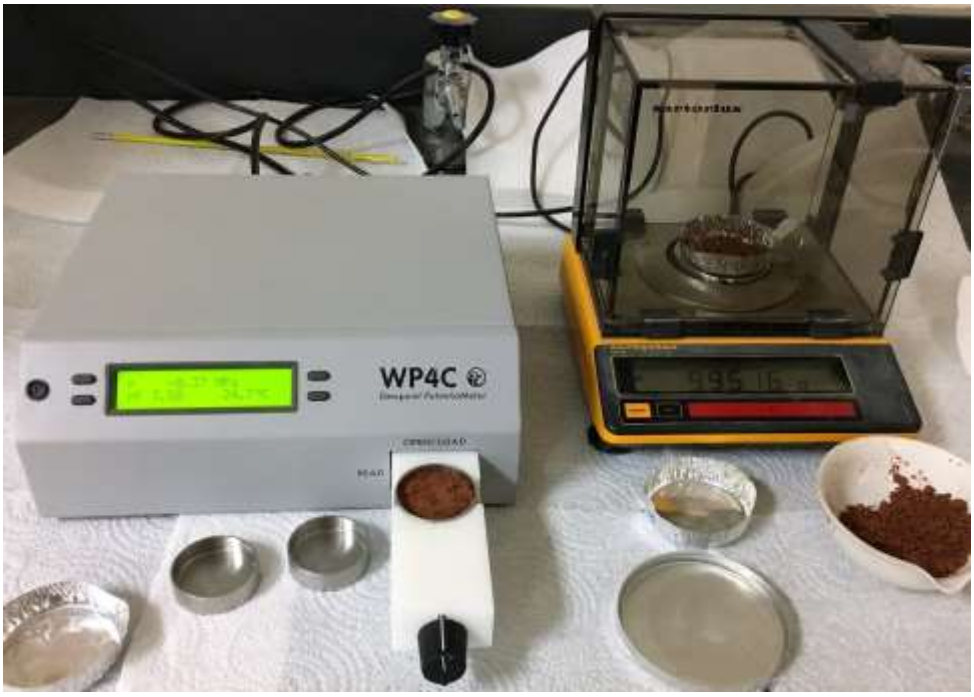

Figure 3.8 SWCC of silty soil used in the study

Similarly, the filter paper technique (contact method) was used to determine the SWCC of the soil at a suction range of 35 kPa to 250 kPa. The setup used is shown in Fig. 3.9. These tests were conducted to validate the results obtained from the other techniques and to confirm that negligible salts were present in the test soil, which may result in osmotic suction.

Figure 3.9 SWCC of silty soil used in the study

3.4.4 *SWCC on Silty Soil and Mathematical Modeling*

The drying curve of the SWCC is shown in Fig. 3.10. The SWCC model parameters proposed by Van Genuchten (1980) and Fredlund and Xing (1994) were used to develop best-fit curves for these experimental data points. The details of the major SWCC models have been described in Section 2.6.6. The SWCC model parameters used to define the best-fit curves based on experimental data points have been tabulated in Table 3.5. The residual volumetric water content, θ_r = 0.07, corresponds to the volumetric water content at the residual suction, Ψ_r of 1900 kPa. The air-entry value (AEV) of the compacted specimen was determined to be 5 kPa.

Table 3.5 Parameters for selected SWCC models

Van Genuchten (1980)	Fredlund and Xing (1994)
α = 0.07	α = 18
n = 1.0	n = 0.8
m = 0.45	m = 1.0
θ_s = 0.376	θ_s = 0.376
θ_r = 0.070	Ψ_r = 1900 kPa

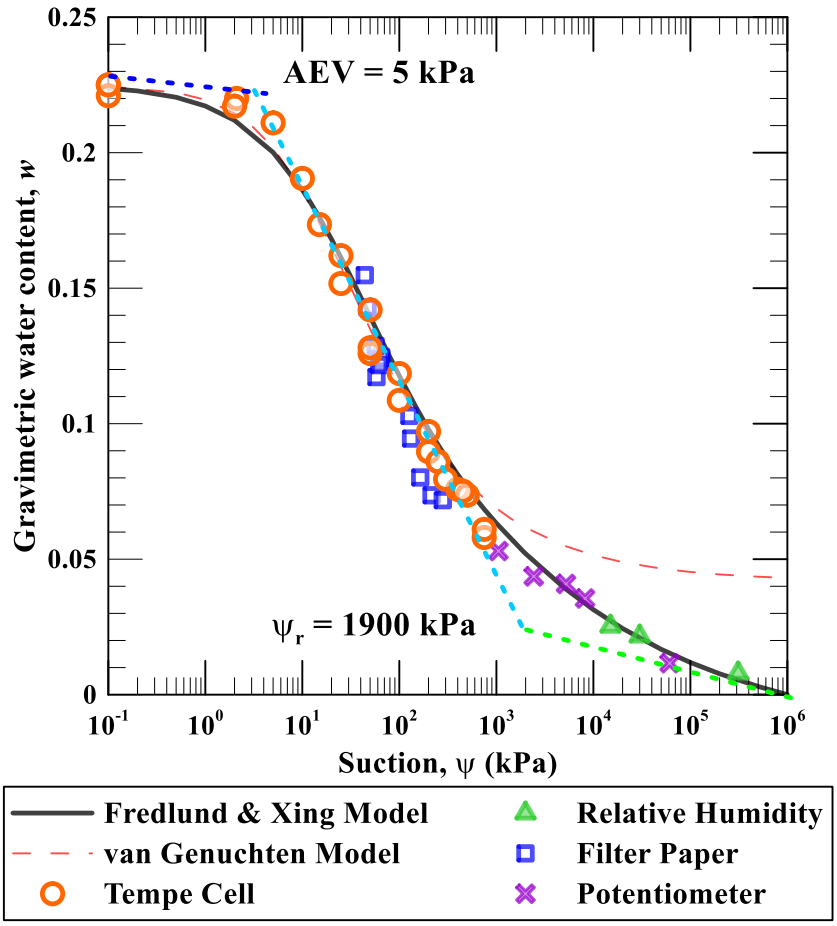

Figure 3.10 SWCC of silty soil used in the study

3.5 Modification to Conventional Triaxial Testing Device

The conventional triaxial device needed a few additional features to efficiently perform suction-controlled triaxial tests. These include the modifications to the base pedestal to incorporate ceramic disks, an arrangement to apply air pressure, double-walled triaxial cell, volume change device, and flushing device. The fully automated double-walled triaxial test setup used throughout this research is shown in Fig. 3.11. The major components of the setup include (a) double-walled triaxial cell; (b) load frame; (c) pressure control panel; (d) process/data controller system; (e) User Interface/Software; (f) volume change device; and (g) air flushing device. A schematic diagram of the triaxial setup is shown in Fig. 3.12. Figure 3.13 shows the closer view of the triaxial assembly.

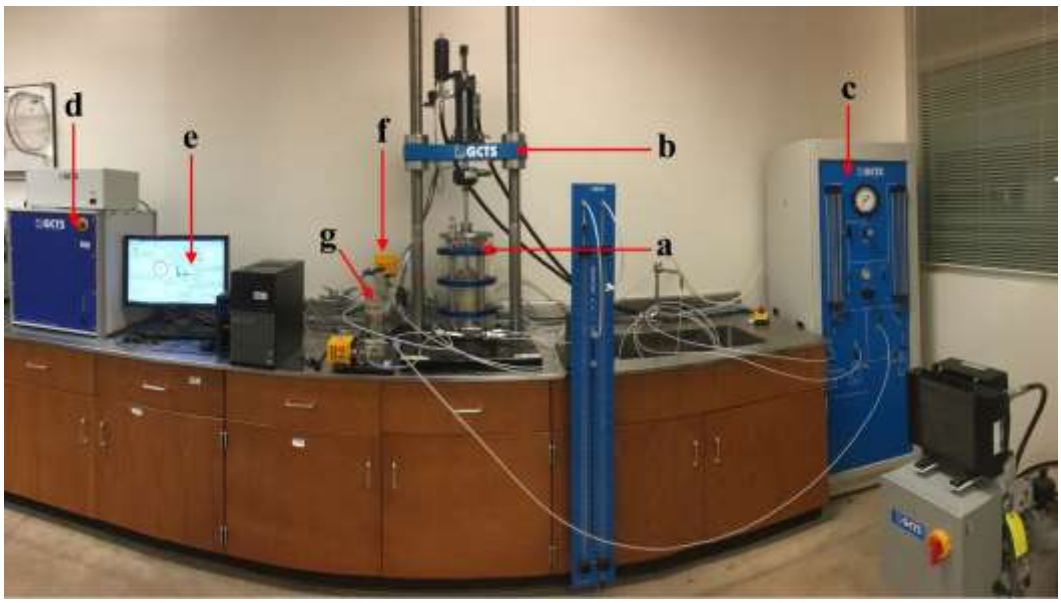

Figure 3.11 Panoramic view of the fully automated double-walled triaxial test setup

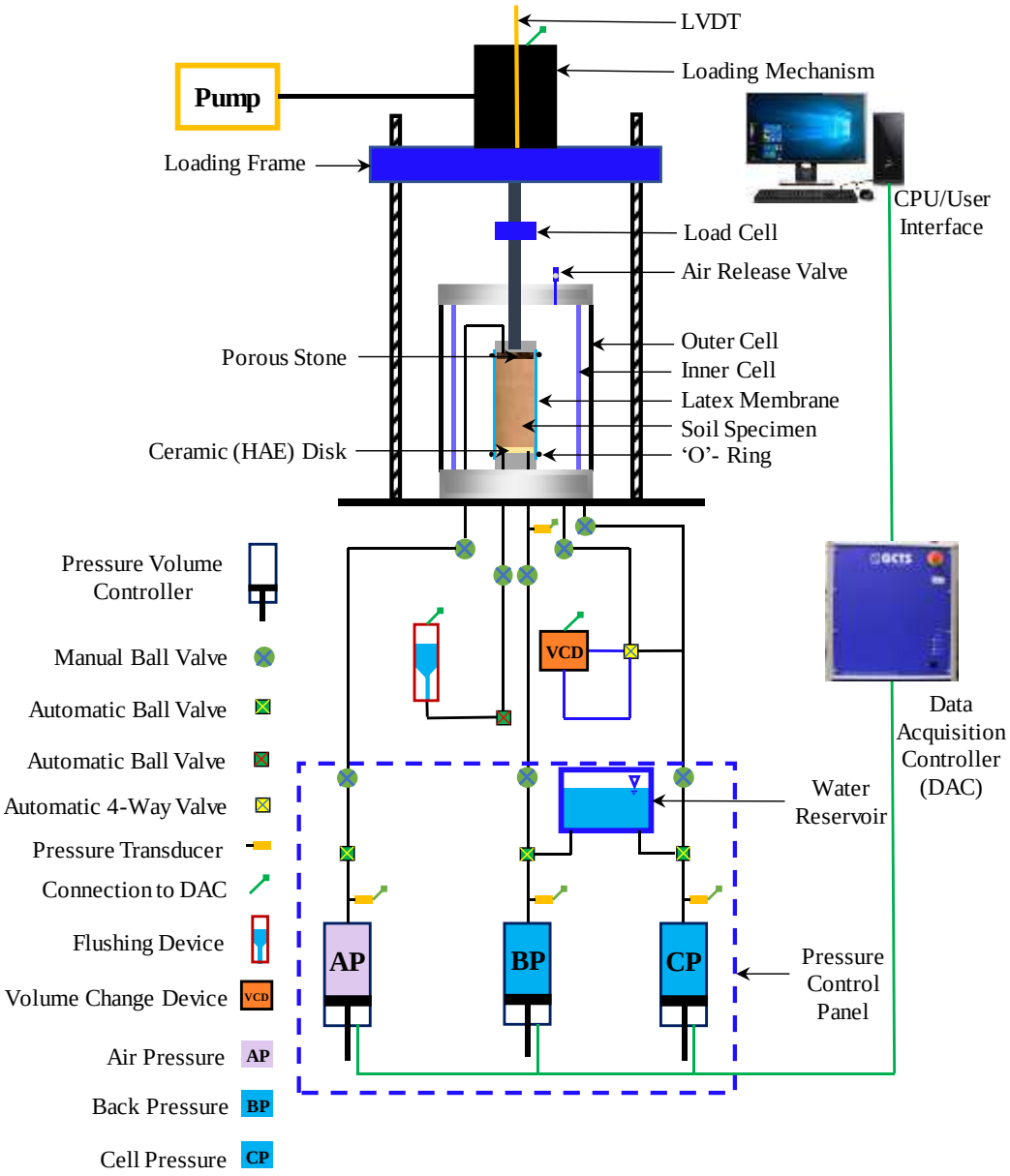

Figure 3.12 A schematic diagram of the fully automated double-walled triaxial setup

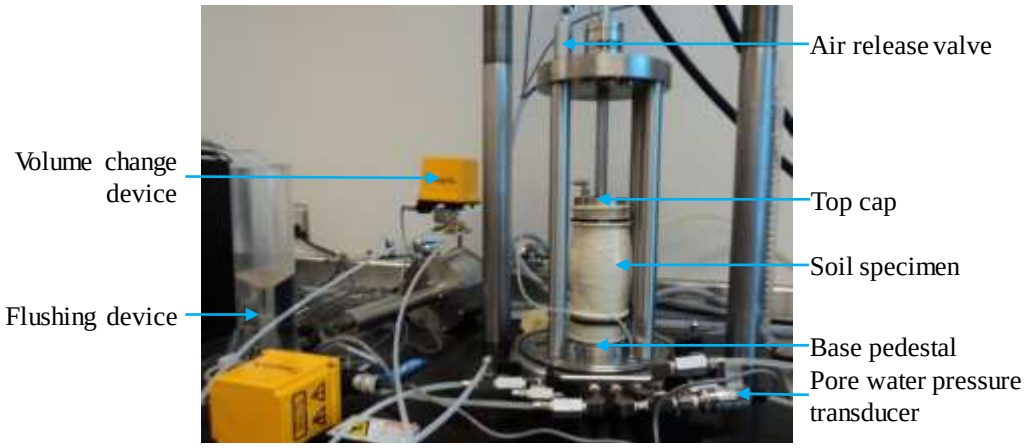

Figure 3.13 A closer view of the experimental setup after the completion of a test

3.5.1 *Modifications to Base pedestal to implement axis-translation technique*

The major limitation of traditional triaxial equipment to perform tests on unsaturated specimens is the control and measurement of suction having a magnitude greater than 100 kPa (1 atm). Since the cavitation occurs when pore water pressure falls below absolute zero (or -100 kPa), the axis translation technique (Hilf, 1956) is used to allow the modified triaxial equipment to control suction in excess of 100 kPa in magnitude. In the axis-translation technique, the air pressure is increased beyond atmospheric pressure and pore water pressure is kept at or near the atmospheric pressure.

However, porous stones would allow the passage of air through it to the saturated pore water pressure lines, which would result is an erroneous measurement of pore water pressure. To prevent such a problem, an artificially manufactured High Air Entry (HAE) disk was used in this research to separate the

soil specimen and the pore water pressure line. The base pedestal was fitted with three HAE ceramic disks of higher air entry value than the matric suction to be applied. Whereas, the top cap was fitted with a traditional porous stone to allow the passage of air to the soil specimen. The modified base plate assembly is shown in Figure 3.14. It shows the connections of the various ports present in the base plate.

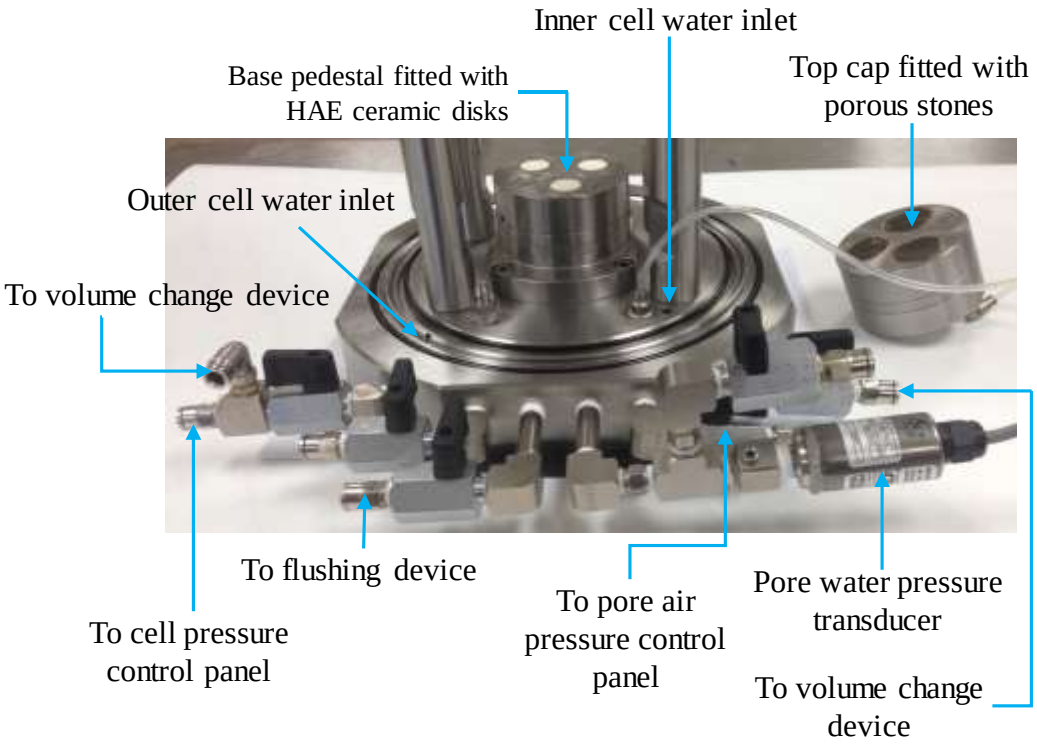

Figure 3.14 The modified assembly of base plate along with base pedestal and top cap

The HAE ceramic disks were attached to steel rings using an epoxy to prevent any leakage at the interface of the two materials (Fig. 3.15a). The stainless-

steel ring was fitted with ‘O’-rings (Fig. 3.15b) and these HAE disks encased in the ring were fitted securely into the base pedestal (Fig. 3.16).

(a)

(b)

Figure 3.15 (a.) Top View, (b.) Perspective View of the ceramic disks used to maintain matric suction via axis translation technique

Figure 3.16 The assembled base pedestal fitted with ceramic disks

3.5.2 *Double-walled Triaxial Cell*

Generally, the single-walled cell is used to perform triaxial tests on both saturated and unsaturated specimens. However, the difference in pressure on either side of the cell results in the expansion of the cell during testing. The volume change in the soil specimen is generally computed from the measurement of water flowing towards or away from the cell. The expansion of the cell with an increase in pressure results in water flowing into the cell to maintain the target confining pressure. This causes an error in the measurement of the change of soil volume during testing, if proper corrections are not applied, which requires an elaborate calibration at regular intervals. To mitigate this problem, the double-walled cell was used in this research (Fig. 3.15).

The double-walled cell comprised of an inner and outer cell, which were connected via pipes. Any pressure which was applied to the outer cell automatically was applied to the inner cell. Hence, the inner cell was subjected to same external and internal pressures, thereby preventing differential pressures, cell expansion, and leakage of water; and reducing system compliance errors. An automatic volume change device was used to accurately measure the volume of water entering the inner cell. These features enabled the accurate measurement, control, and data collection of pressures and changes in specimen volume throughout the test.

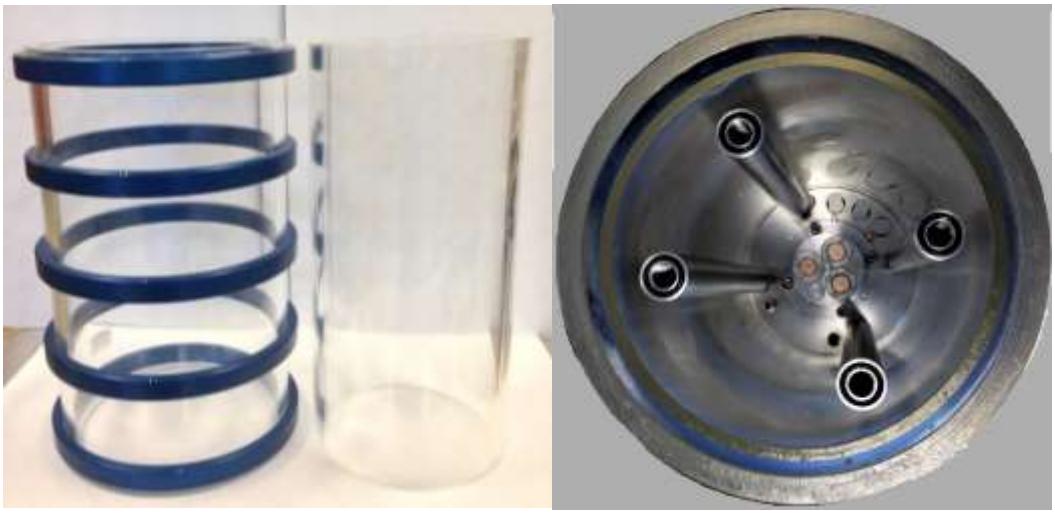

Figure 3.17 Double-walled triaxial cells

3.5.3 *Automatic Volume Change Device*

The volume change of the specimen is accurately measured by using the automatic volume change device (Fig. 3.18). The volume change device measures the volume of water flowing in or out of the inner cell. Any change in volume of the specimen would result in a change in the volume of water in the inner cell. Thus, the volume change of the specimen is computed by measuring the change in the volume of water in the inner cell. The volume change device consists of a computer controlled four-way valve, programmed to automatically reverse the flow after reaching its capacity. Thus, providing the infinite capacity to measure the change in volume of the soil specimen. The volume change device has a rolling diaphragm, which eliminates sliding friction (GCTS, 2010). Hence, the differential pressure across the volume change device is negligible, which would result in equal pressure

in the inner and outer cells. The accuracy of volume measurement by the VCD is 0.01 cm^3.

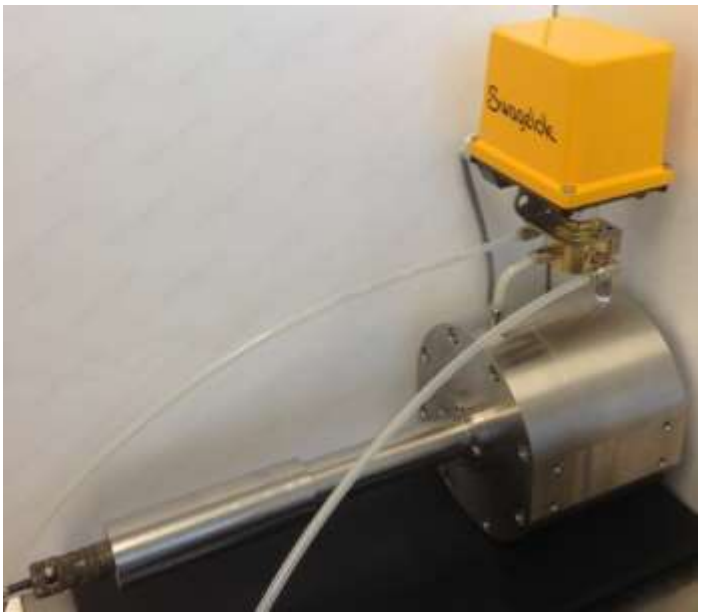

Figure 3.18 Automated volume change device

3.5.4 *Flushing Device*

The removal of diffused air beneath the ceramic disk is a major concern while performing a triaxial test on an unsaturated soil specimen. The ceramic disk allows a steady diffusion of air through it to the saturated water lines beneath the ceramic disk, due to the concentration difference, which arises because of the difference in density between the free air and the dissolved air present in the water (Fredlund and Rahardjo, 1993). The Fick's law of diffusion governs the diffusion of air.

An automatic flushing device is used to remove the diffused air which may accumulate beneath the ceramic disk over time. The presence of air beneath the ceramic disk reduces the permeability of the ceramic disk and may hinder the suction equalization process. In cases of undrained testing, the diffused air affects the matric suction values and results in erroneous pore water pressure measurements. Henceforth, it is of primary importance to flush the pore water pressure lines periodically.

The change in the volume of pore water is also essential, which could be determined by deducting the diffused air from the total change in volume of pore water. The flushing device (shown in Fig. 3.19) consists of a differential pressure transducer with a range of 7 kPa (Fig. 3.20) and is used to measure the height of water in the water column (or reservoir), with an accuracy of 0.08 cm height of water. The top surface of the reservoir is open to the atmosphere.

Figure 3.19 Automated Flushing Device

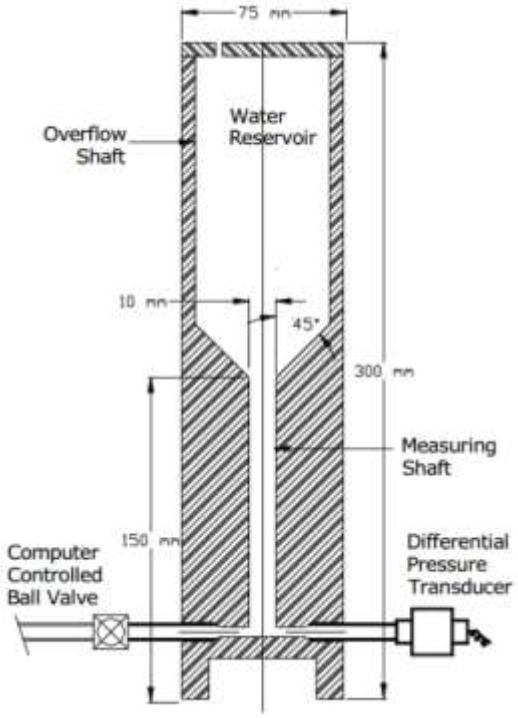

Figure 3.20 A schematic of automatic flushing device (from GCTS, 2010)

During flushing, the total volume of the combination of diffused air and water passing through the flushing device is known from the back pressure volume controller. When the diffused air reaches the water column (or reservoir), it escapes from the water surface and is released at the atmospheric pressure. Thereby, the difference in total volume of diffused air and water and the remaining height of water in the reservoir provides the information regarding the volume of diffused air.

The procedure for flushing involves the opening of the ball valve and passing enough deaired water from the back pressure volume controller to the

flushing device via the grooves present beneath the ceramic disks. As the diffused air reaches the atmospheric pressure, it escapes from the surface of the water in the reservoir and the remaining water results in an increase in the height of water in the reservoir, which is recorded by the pressure transducer.

3.5.5 *Saturation of Ceramic Disc*

The saturation of ceramic disk prior to the commencement of triaxial test is pivotal. The ceramic disks were fitted to the base pedestal of the triaxial setup and after placing the triaxial cell, the chamber was sealed. The cell was partially filled with de-aired water, to a height of approximately 30 mm (as shown in Fig. 3.21). One end of the pore water pressure line, which was connected in parallel to the pore pressure transducer, was connected to the volume change device to enable accurate measurement of the volume of water flowing through the ceramic disks. While the other end was closed using the manual valve. The connection from the other end of the volume change device was connected to a burette as a supplementary volume measurement system.

The air pressure line from the pressure control panel was connected to the air release valve on top of the triaxial cell (as shown in Fig. 3.21a) and gradually the air pressure was increased to a value greater than the air-entry value of the ceramic disk. The water gradually flows through the ceramic disk and its rate is recorded. The rate of water flow was compared with the applied air pressure and the permeability of the ceramic disk was estimated, to ensure that there was no

leakage in the base pedestal assembly and ceramic disks have no cracks. Once the rate of water flow was consistent with the expected values, the air pressure was maintained for more than 2 hours to ensure complete saturation of all the ceramic disks.

Consequently, the air pressure was gradually decreased to atmospheric pressure and the water from the triaxial was drained out. The connections to the pore water pressure line were changed from the volume change device to the back pressure control panel and the ceramic disk was flushed using the automatic flushing device. Thereafter, the ball valve of the flushing device was closed and a pore water pressure of 5 kPa was applied to the ceramic disk, to ensure that while placing the soil sample, the ceramic disk remains saturated. Similar approaches had been used by Hoyos (1998), Laikram (2007), and Patil (2014).

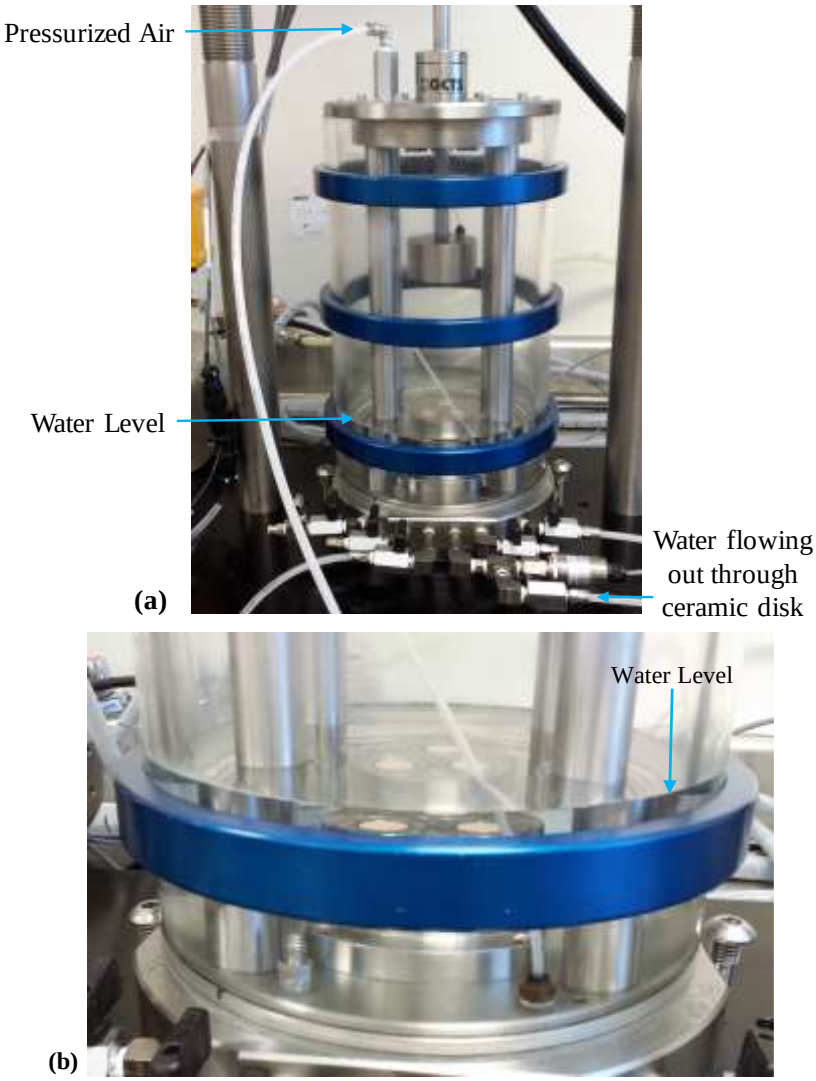

Figure 3.21 Setup for saturation of HAE ceramic disks

3.6 Saturated Soil Triaxial Testing

3.6.1 *General*

A series of independent tests at the same net confining pressure were performed at varying shearing rates to determine the suitable shearing rate for all triaxial tests on saturated specimens. An elaborate explanation has been provided

in Section 3.9.2. The most appropriate axial shearing rate was obtained to be 0.05%/min. Three consolidated drained (CD) triaxial tests were performed following the conventional triaxial compression (CTC) stress path for saturated specimens. The compacted specimens were weighed and the height was measured in orthogonal directions. The diameter was measured in orthogonal directions at three equally spaced locations along the longitudinal axis of the compacted specimen and the average of these readings was recorded.

The base pedestal fitted with a saturated porous stone was attached to the base plate of the triaxial setup and the pore pressure lines (or pipes) were saturated using manual control. A moist filter paper was placed on the previously saturated porous stone to prevent migration of fine particles into the pore pressure line. Additionally, the filter paper prevented the clogging of the porous stone. The compacted specimen was mounted on the base pedestal with the porous stone. Another filter paper was placed on the top of the specimen. The top cap fitted with another porous stone was carefully placed on the compacted specimen. The entire assembly of the base pedestal, compacted soil specimen, and the top cap was enclosed using a latex membrane and three 'O'- rings at both the ends of the assembly. The double-walled cells were placed and the entire chamber was sealed. Initially, the outer cell and later the inner cell was filled with de-aired water by applying a 15 kPa pressure from the pressure control panel. Since the air release valve was open, the soil specimen did not experience any significant confining

pressure. Once the inner cell is almost filled, the pressure was reduced to 5 kPa and after its filled, the air release valve was closed. Subsequently, the cell pressure was increased to 15 kPa and a back pressure of 5 kPa was introduced. Thus, an effective confining pressure of 10 kPa was maintained. A seating stress of 5 kPa was applied to the axial actuator to maintain proper contact with the top surface of the specimen.

3.6.2 *Saturation of the Specimen*

The first stage of a saturated triaxial test is the process of saturation, where the soil is gradually saturated while maintaining positive effective confining pressure throughout the process. Since the degree of saturation of specimen is 71% prior to saturation, most of the pore air was removed by applying a suction of 10 kPa to the top of the specimen, while allowing the water-front to slowly move towards the top of the specimen. This procedure was conducted as per the guidelines of ASTM D7181-11. After the water-front reached near the top of the specimen, the applied suction was removed. When the water comes out through the top porous stone, due to the back pressure of 5 kPa, the valve to the top cap was closed.

Subsequently, the specimen was saturated using back pressure approach. Bishop and Henkel (1957) introduced the use of back pressure approach to saturate the specimen. Black and Lee (1973) demonstrated the influence of soil type and initial degree of saturation, prior to back pressure approach, on the final back pressure required to saturate the specimen. The specimen was saturated by either

dissolving the pore air into the pore water or by collapsing the air bubbles due to the introduction of high back pressure. According to ASTM D7181-11, the specimen is considered to be fully saturated when the Skempton's pore-water parameter, *B*, is greater than 0.95. The *B*-value is the ratio of increase in pore water pressure (Δu) due to an increase of cell pressure ($\Delta\sigma_3$) and is defined using the following expression:

$$B - \text{value} = \frac{\Delta u}{\Delta \sigma_3} \tag{3.3}$$

To check the *B*-value, the drainage valve connected to the base of the specimen was closed, and the cell pressure was increased by 15 kPa. The generation of excess pore water pressure (Δu) due to incremental cell pressure ($\Delta\sigma_3$) was recorded after the stabilization of the pore water pressure. The *B*-value was calculated using Equation 3.3.

In this research, the criterion for complete saturation was set at a *B*-value of 0.96. The *B*-value was checked after both the cell and pore pressure have stabilized. If the criterion for full saturation was not met, the drainage valve was opened and both the cell pressure and the back pressure were gradually increased by an equal increment of 15 kPa/h. The pressures were increased gradually to allow proper pore pressure equalization throughout the specimen. It was observed that the final value of the back pressure required for complete saturation was in excess of 1300 kPa.

Theoretically, Lowe and Johnson (1960) demonstrated the final back pressure required to achieve the target degree of saturation by computing the additional back pressure required (ΔP) to increase the degree of saturation from an initial value of S_i to a final value S, using Henry's coefficient of solubility, H.

$$\Delta P = \frac{P_i(S-S_i)(1-H)}{1-S(1-H)} \tag{3.4}$$

where, P_i = the initial absolute pressure corresponding to S_i. For full saturation (S = 100%), the Equation 3.4 reduces to the following expression:

$$\Delta P_{S=100\%} = 49P_i\,(1-S_i) \tag{3.5}$$

where, $\Delta P_{S=100\%}$ is the additional back pressure required to achieve complete saturation from an initial degree of saturation of S_i. Since the initial degree of saturation prior to initiation of the application of back pressure for saturation is approximately 91%. As per Equation 3.5, the theoretical additional back pressure required for complete saturation is around 600 kPa.

However, it would take approximately 4.5 months to saturate the specimen (Black and Lee, 1973). To hasten the process to less than two days, an additional back pressure of 1600 kPa (total back pressure = 1700 kPa) is required. This pressure is slightly higher than the actual pressure required to saturate the specimen. However, due to the multitude of variables involved like type of soil and its permeability, the predicted values are quite similar to the observed values.

3.6.3 *Isotropic Consolidation of the Specimen*

The consolidation stage involves the dissipation of excess pore water pressure generated due to the application of the target effective pressure at which the shearing would be conducted. During consolidation, the volume of the soil specimen undergoes changes due to the dissipation of excess pore water pressure. The target consolidation stress was achieved by ramping up the cell pressure while maintaining constant back pressure. The target cell pressure was reached in 30 seconds and the change of volume of soil specimen and the volume of water flowing out of the specimen was recorded and plotted.

Subsequently, when both the volumes reach a constant value and the volume of water flowing out of the specimen was the same as the change in volume of the soil specimen, the consolidation was assumed to be completed. This was generally observed after 10 hours. To ensure that the primary consolidation was practically completed for all tests, 24 hours of consolidation was implemented. Similar procedure was used to consolidate the specimens to an effective confining pressure of 100, 200, and 400 kPa. These samples were then tested to study the behavior of the compacted soil during shearing at varying effective confining pressures.

3.6.4 *Shearing under Drained conditions*

After consolidation, the specimen was sheared monotonically following the Conventional Triaxial Compression (CTC) stress path in drained conditions. For

consolidated drained (CD) test following CTC stress path, both the cell pressure and the back pressure were maintained at a constant value, while the specimen was loaded axially under constant axial strain rate (strain controlled test) or under constant axial stress rate (stress controlled test). The post-peak response could only be obtained from a strain-controlled test, since in stress-controlled tests, the test gets terminated after reaching peak stress. Therefore, in this research, strain controlled tests were conducted on all the specimens.

The determination of appropriate strain rate is essential for consolidate drained tests. Since the shearing rate influences the peak deviator stress and the volume change response of soil specimen, an independent study was conducted to study the influence of axial strain rate on the mechanical behavior of compacted specimen of silty soil. The independent strain rate study has been elaborated in Section 3.9. The most appropriate strain rate for a saturated specimen was determined to be 0.05%/min, which was obtained by determining the fastest strain rate which practically had a negligible effect on the mechanical response of the soil during shearing. This shearing rate was selected since it allowed proper dissipation of excess pore water pressure throughout the specimen.

Three saturated specimens were sheared at varying effective confining pressure of 100, 200, and 400 kPa at constant axial strain rate of 0.05%/min to study the mechanical response of the soil under drained conditions. The deviator stress response was carefully analyzed to determine the strength of the saturated soil at

the peak stress state and the critical state. The deviator stress and induced volumetric strain responses of saturated specimens to shearing at the effective confining pressures of 100, 200, and 400 kPa are shown in Fig. 3.22 and Fig. 3.23, respectively. The volumetric strains of the specimen showed initial compression response followed by dilation type response for all the values of effective confining pressure applied. It can be observed from Fig. 3.23 that the value of axial strain required to initiate dilation increases with an increase in effective confining pressure. Henceforth, an increase in effective confining pressure generates a higher tendency for the soil to compress than to dilate. In these tests, it was also observed that the specimens failed, without any distinct shear planes, by bulging at the center.

The peak shear strength parameters were obtained by plotting the Mohr Circle at peak stress (Fig. 3.24). Figure 3.25 shows the Mohr Circle plot for saturated specimens of silty soil at the critical state. The peak effective cohesion was obtained as 4.8 kPa and the peak effective angle of internal friction was 34.0°. The cohesion at critical state was computed to be 2.7 kPa and the corresponding angle of internal friction was 33.6°. The slope of the critical state line was determined to be 1.356 and slope of individual p'-q stress path was calculated to be 3:1. In saturated condition, the soil depicted a minor post-peak softening response, as observed by the small difference in values of peak strength and strength at the critical state.

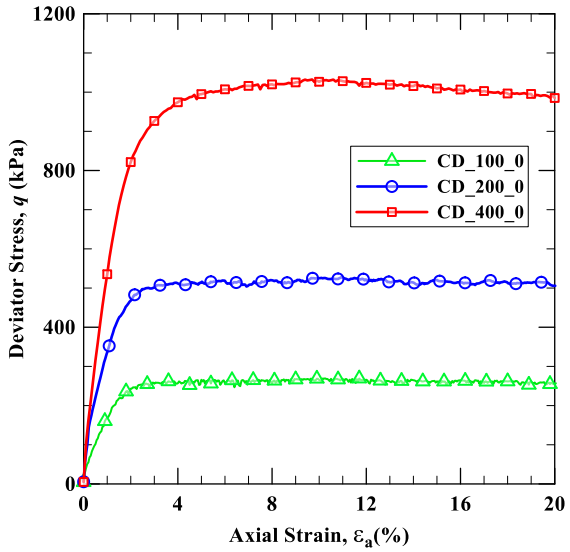

Figure 3.22 Deviator stress response of saturated silt for varying effective confining pressure

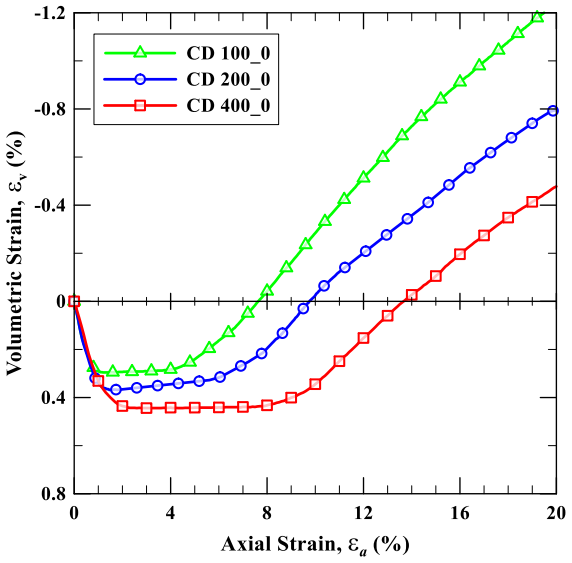

Figure 3.23 Volume change response of saturated silt for varying effective confining pressure

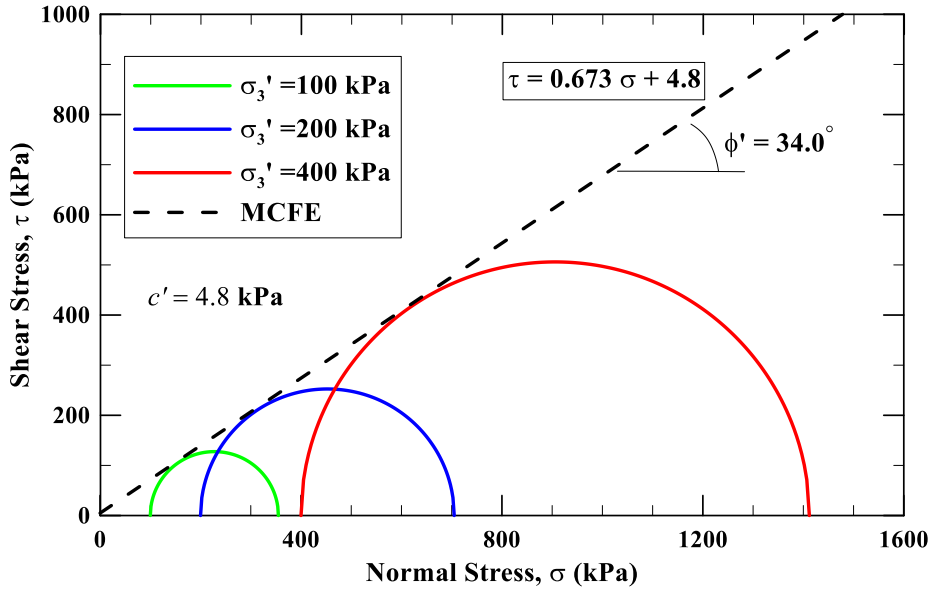

Figure 3.24 Determination of peak shear strength parameters for saturated silt specimen using Mohr-Coulomb failure criterion

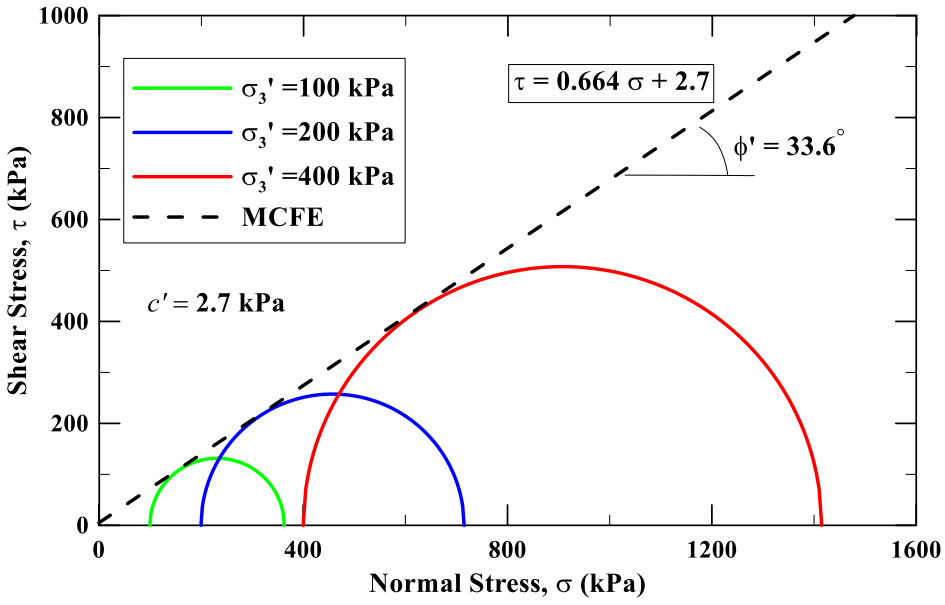

Figure 3.25 Determination of critical shear strength parameters for saturated silt specimen using Mohr-Coulomb failure criterion

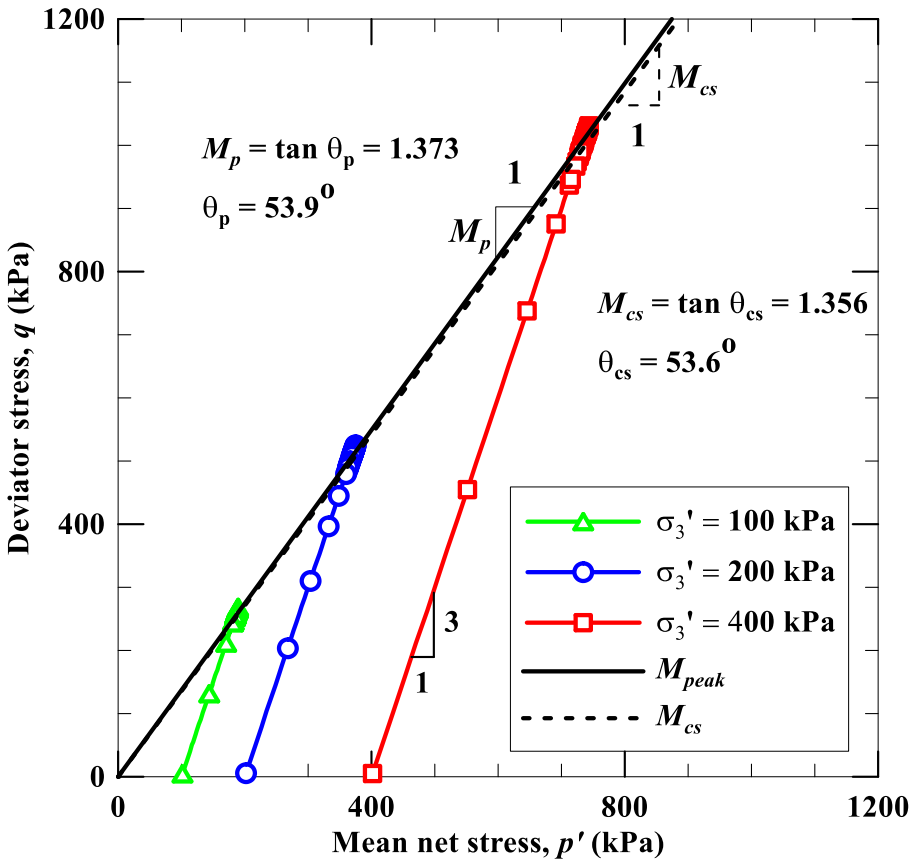

Figure 3.26 Stress Paths, PSL and CSL for saturated silt specimens

3.7 Unsaturated Soil Triaxial Testing

3.7.1 *General*

The modifications to the triaxial device as explained in section 3.5 enabled the testing of unsaturated specimens. An independent series of triaxial tests were performed on specimen subjected to a matric suction of 250 kPa and the net confining pressure of 400 kPa with varying shearing strain rate, to determine the suitable shearing rate at which all the unsaturated specimens could be sheared under

drained conditions. This independent test series is explained in detail in Section 3.9.3. The optimum axial strain rate for shearing was obtained to be 0.003%/min, which had been selected based on the response of deviator stress and volumetric strain during shearing and the consideration of an appropriate practical duration for the completion of an unsaturated triaxial test.

A series of suction-controlled triaxial tests under drained conditions following the CTC stress path were performed and matric suction was induced within the soil specimen using the principle of axis-translation technique.

3.7.2 *Stress Variables and Shear Strength of Unsaturated Soils*

The identification of the appropriate stress variables which controls the behavior of unsaturated soil is essential prior to testing of unsaturated soils. As explained in section 2.7.2, the independent two-stress state variable approach by Fredlund and Morgenstern (1977) has been one of the most widely accepted theories for determination of effective stress acting on an unsaturated soil. The stress state variables, i.e., net normal stress ($\sigma - u_a$), and matric suction ($u_a - u_w$), were considered as independent parameters which primarily controlled the behavior of unsaturated soils.

The independent two-stress state variable approach can be integrated with the Mohr-Coulomb failure criterion, and the shear strength at failure, τ_f, of unsaturated soil can be estimated using the following relation:

$$\tau_f = c' + (\sigma - u_a)_f \tan \varphi' + (u_a - u_w)_f \tan \varphi^b \qquad (3.6)$$

where, c' and φ' are effective cohesion and effective angle of internal friction of the saturated soil, respectively, and φ^b is the friction angle, which is due to the contribution of the matric suction on the shear strength of the soil.

Alternatively, the parameters net mean stress, p', deviator stress, q and the matric suction, s are used to study the behavior of unsaturated soils, which are expressed as follows:

$$p = \frac{\sigma_1 + 2\sigma_3}{3} - u_a \tag{3.7}$$

$$q = \sigma_1 - \sigma_3 \tag{3.8}$$

$$s = u_a - u_w \tag{3.9}$$

where, σ_1 and σ_3 are the major and minor principal stresses, which are assumed to be the axial and radial stresses acting on the specimen. The parameters, u_a and u_w are the pore air and pore water pressure, respectively.

3.7.3 *Testing Procedure*

The axis translation technique was used to apply and control the matric suction inside the specimen during the tests. Independent control of pore air and pore water pressures facilitated in the application of matric suction, following the axis translation technique (Hilf, 1956).

The following stages are performed to determine the shear strength and volume change behavior of unsaturated specimen.

Stage 1: Pre-equilibration

The compacted specimen could take several weeks to achieve the required matric suction. This would result in an enormous delay in completion of a test. Henceforth, before mounting the specimen in the triaxial cell, the specimen was pre-equilibrated to the desired suction outside the test chamber. After specimen preparation, they were carefully placed on the weighing scale and its mass was recorded (Fig.3.27a). Subsequently, the specimen was enclosed in a custom made acrylic chamber for 24 hours to allow proper moisture equilibration throughout the specimen (Fig. 3.27b). Meanwhile, the water content of the remaining soil was determined and the dry mass of the soil specimen was recorded. Since, the final water content required for the achieving the target suction to be applied during testing was known from the drying curve of the SWCC (Fig. 3.10), the target moist mass of soil was computed.

The specimen was gradually dried by removing the chamber for 12 hours while recording the mass of soil at regular intervals (Fig. 3.27c). Subsequently, for the next 24 hours, the specimen was kept inside the chamber, which is air-tight and the specimen was allowed equilibrate (Fig. 3.27b). Thus, the mass of the specimen, thereby, the water content and inherent matric suction, was continuously monitored. Again, if the target water content or suction was not achieved then the

process of gradual drying (Fig. 3.27c) and suction equilibration (Fig. 3.27b) was repeated for 12 hours and 24 hours, respectively.

When the target water content was about to be reached, the drying process was continued very slowly by allowing only the bottom 1 inch (or 25 mm) to be exposed to the surrounding air (Fig. 3.27d). In this case, the specimen is rotated every 3 hours to prevent excessive differential water content from the top to the bottom of the soil. A similar approach was used by other researchers such as Houston et al. (2008) and Patil (2014).

The target water content during this stage is different from the water content required during testing. To account for possible errors in SWCC and difference in its drying and wetting curves (hysteresis effect), the target water content for this stage (pre-equilibration outside the triaxial cell) was set at 0.5% on the wetter side of actual target water content. For a target suction of 50 kPa, the criterion of 0.5% wetter than the target water content corresponds to the suction of approximately 43 kPa, while the same criterion increases the difference in suction from 750 kPa (target suction) to 580 kPa.

(a) (b)

(c) (d)

Figure 3.27 Suction equilibration outside the triaxial cell

After the target suction or the corresponding water content (for the pre-equilibration stage) had been achieved the specimen was kept in the chamber for 2 days to ensure complete moisture equilibration.

Stage 2: Suction equalization

Once the desired matric suction was approximately achieved, the mass and dimensions were carefully measured and the specimen was mounted on the base pedestal fitted with saturated HAE ceramic disk in the triaxial cell. Previously, the pore water pressure lines were filled with de-aired water and the base pedestal was flushed thoroughly. The double-walled cell was placed and the chamber was sealed. The inner and outer triaxial cells were also filled with de-aired water and a cell pressure of 20 kPa was applied with pore water pressure of 5 kPa maintained through the bottom pedestal and an initial pore air pressure of 15 kPa applied at top of specimen via porous stone. Therefore, the initial net confining pressure, $(\sigma_3 - u_a)$ being applied was 15 kPa.

The cell pressure and pore air pressure were gradually increased, at a constant rate of 10 kPa/hr, to attain the desired matric suction. Hence, the matric suction was imposed using the axis-translation technique. Sivakumar (1993) suggested that the suction equilibration was completed when the water content change was less than 0.04%/day or 0.5 cm^3/day, which was followed by Ng et al. (2013). In this research, the suction was considered to be equilibrated when the

change in water content was less than 0.04%/day for specimens at suction till 250 kPa (i.e., 50 and 250 kPa). While for specimens equilibrated at suctions above 250 kPa (i.e., 500 kPa and 750 kPa), the criterion was set at 0.03%/day, as small change in water content at higher suction levels results in significant change in induced suction. It generally required 5-7 days to achieve equilibration for the required matric suction, since the specimens were pre-equilibrated at a nearby suction level.

The suction equalization process was facilitated by using different types of ceramic disks during testing. The 5-bar HAE ceramic disk was used for performing tests on specimens having a matric suction of 50 kPa and 250 kPa. However, for higher suction levels (500 kPa and 750 kPa), 15-bar HAE ceramic disk was used.

Stage 3: Isotropic Consolidation

Once the required matric suction was achieved, the isotropic consolidation stage was commenced. In the case of axis translation technique, the matric suction was maintained by controlling the pore air pressure and pore water pressure at a constant value, while the cell pressure was gradually increased at the rate of 5 kPa/h to its required value to attain the requisite net confining pressures. Each specimen was consolidated for more than 24 hours to ensure complete dissipation of pore air and water pressure. During this stage, the volume change of the specimen is recorded carefully.

Stage 4: Shearing

After isotropic consolidation, the specimen was sheared monotonically by axially loading at constant axial strain rate (strain controlled test) of 0.003%/min, while a constant net confining pressure and matric suction was maintained throughout the test. The conventional triaxial compression (CTC) stress path under drained conditions was followed during the shearing stage.

A schematic representation of the sequences involved in the unsaturated triaxial test is shown in Fig. 3.28. In this case, the test was performed at a matric suction of 250 kPa at a net confining pressure of 200 kPa. It also shows the values of axial and radial stresses, pore air pressure, pore water pressure, net confining pressure and the matric suction acting on the specimen at the end of each stage of unsaturated soil testing.

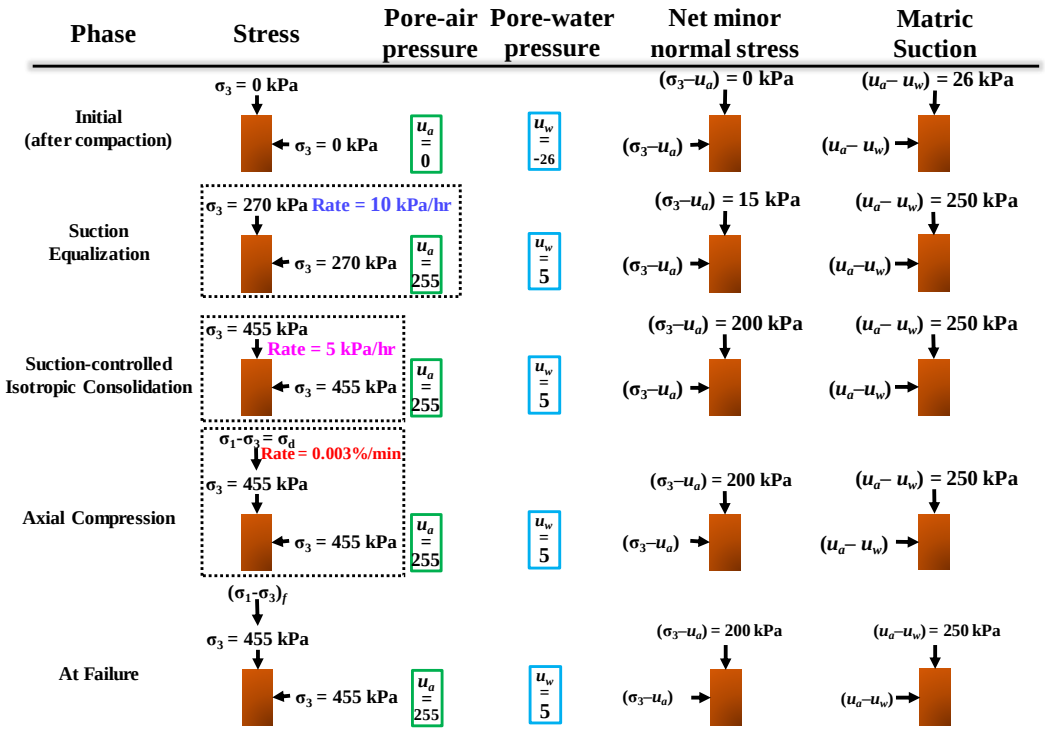

Figure 3.28 Schematic of procedure to perform an unsaturated triaxial test at net confining pressure of 200 kPa and matric suction of 250 kPa under drained conditions

The stress path involved during suction pre-equilibration, suction equalization and isotropic consolidation for specimens subjected to varying matric suction (s = 50, 250 and 750 kPa) and consolidated to a net mean stress of 200 kPa is shown in Fig. 2.29. Similar tests were conducted for the net mean stress of 100 kPa and 400 kPa.

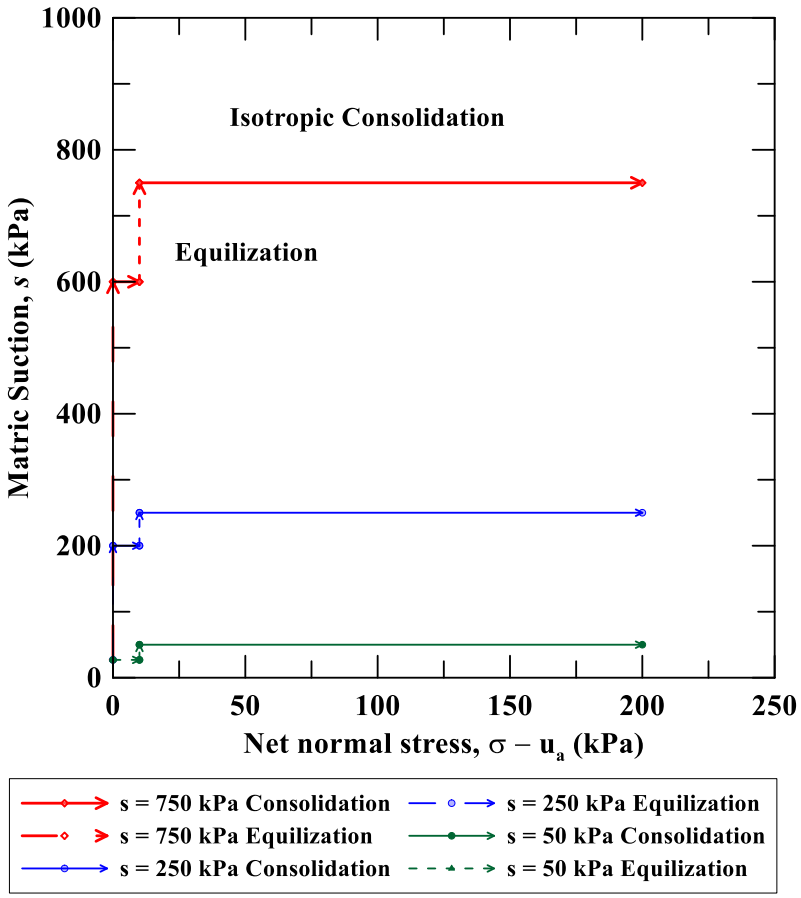

Figure 3.29 Stress paths involved in suction equalization and consolidation process for specimens consolidated to a net mean stress of 200 kPa

3.7.4 *Test Program*

An exhaustive series of triaxial tests were performed to investigate the effect of the increase of net confining pressure and matric suction on the mechanical response of soil when subjected to the loading in the form of hydrostatic compression (HC) and conventional triaxial compression (CTC).

The following values of stress variables were considered during the series of single-stage monotonic triaxial tests:

Net confining pressure, $(\sigma_3 - u_a)$: 100, 200 and 400 kPa

Matric suction, $(u_a - u_w)$: 0 (saturated), 50, 250 and 750 kPa

One independent test was also performed at a net confining pressure of 200 kPa at an induced matric suction of 500 kPa (not shown in Fig. 3.30).

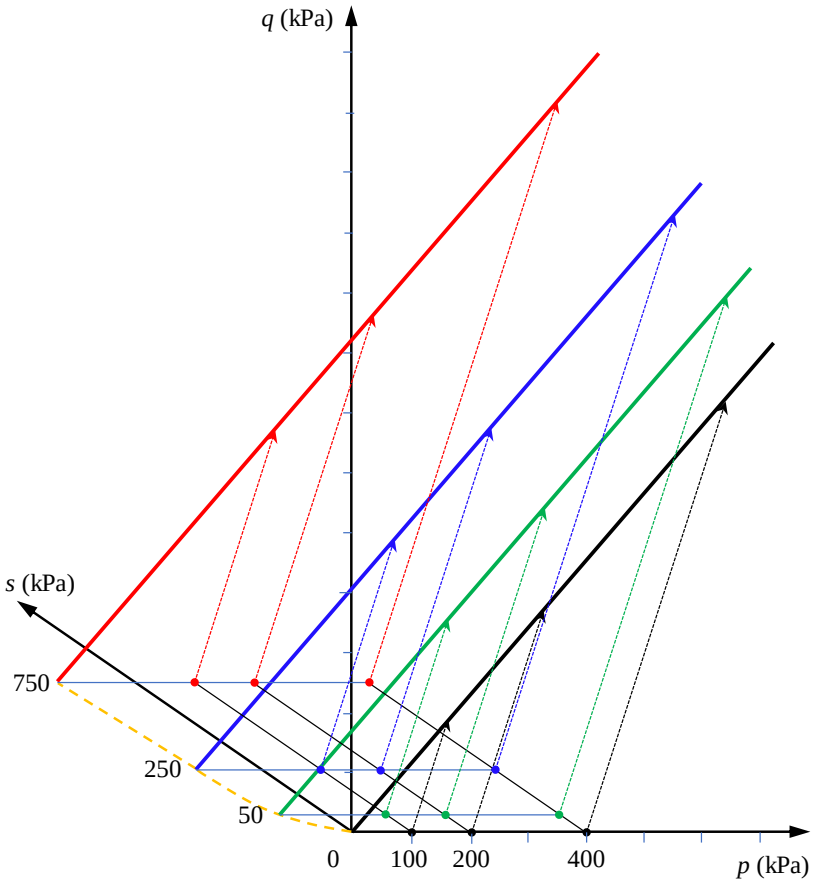

Figure 3.30 Saturated and suction-controlled CTC stress paths in *p*:*q*:*s* space

3.8 Mechanical Response under Suction-controlled isotropic consolidation

A series of suction-controlled isotropic consolidation tests were performed on compacted specimens of silty soil under varying matric suction. The response of unsaturated soil (s = 50, 250 and 750 kPa), when subjected to a net mean stress of 200 kPa following hydrostatic compression (HC) stress path, is shown in Fig. 3.31.

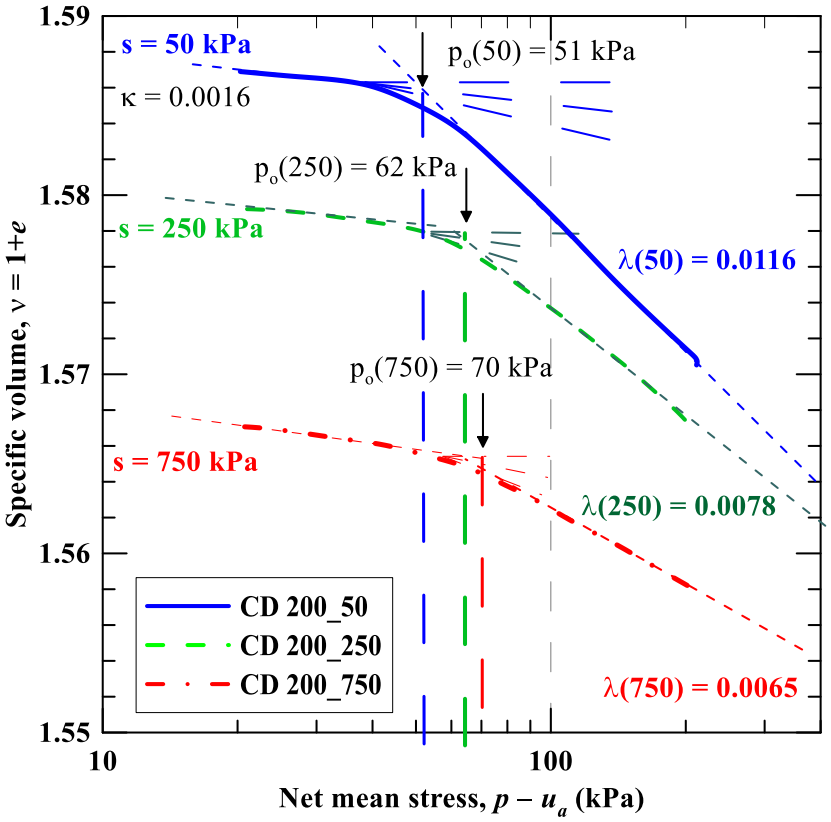

Figure 3.31 Response of silty soil from suction-controlled HC test at s = 50, 250 and 750 kPa

The plots in Fig. 3.31 provide the information regarding the yielding at each suction level. Yield stress is defined as the stress at which the soil experiences its maximum past stress. When the stresses are higher than the yield stress, the soil reaches its virgin state. The variation of suction had a minor, but suction has a vital impact on the yield stress of the soil specimen, which proves the existence of the loading collapse (LC) locus. The increase of suction from 50 kPa to 750 kPa increased the yield stress from 51 to 70 kPa. This variation of yield stress due to suction is critical for constitutive modeling of unsaturated soils. The slope of the virgin section of the curve defined by the volumetric stiffness parameter, $\lambda(s)$ is shown to decrease with increase in suction, which indicates the stiffness of the soil increasing with increase in suction. The slope of the reloading curve, referred to as the elastic rebound index, κ showed an increase in slope of 0.0012 at 50 kPa matric suction to 0.0019 at 750 kPa matric suction. However, since the BBM model assumes a constant value of the elastic rebound index, κ, the average value of 0.0016 was assumed for all cases. The details regarding the BBM modeling and its parameters are explained in section 4.6.

3.9 Independent Strain Rate Studies

3.9.1 *General*

The effect of strain rate during shearing in a triaxial test has been initially recognized by researchers including Taylor (1943) and Casagrande and Wilson (1951). Further research was conducted in evaluating the effect of strain rate on the

behavior of saturated soils by many researchers (Crawford, 1959; Richardson and Whitman, 1963; Bjerrum, 1967,1973; Alberro and Santoyo, 1973; Vaid and Campenella, 1977; Kavazanjian and Mitchell, 1980; Graham et al., 1983; Lefebvre and LeBouef, 1987; Sheahan et al., 1996; Zhu and Yin, 2000, Cheng and Yin, 2005, Sorensen et al. 2007; Diaz-Rodriguez et al., 2009). In this research, the determination of appropriate strain rate for shearing of unsaturated soil specimens is essential, prior to performing the series of triaxial tests on saturated specimens.

A similar effect of strain rate on the mechanical behavior of unsaturated soils was recognized by Arenson and Springman (2005); Zhang et al. (2014b); Patil, (2014).

3.9.2 *Saturated Soil Specimens*

The appropriate rate of shearing was determined by performing triaxial tests on four replicate compacted specimens of silty soil. The rates of shearing selected for the study were 0.01%/min (slowest), 0.05%/min, 0.25%/min and 0.50%/min (fastest). Figures 3.32 and 3.33 show the influence of axial strain rates on the behavior of saturated silty soil during shearing for an effective confining pressure of 400 kPa under drained conditions.

The appropriate shearing rate was determined by analyzing the stress-strain (Fig. 3.32) and volumetric response (Fig. 3.33). It was observed that higher the strain rate, higher was the peak stress achieved. Additionally, the peak stress and the initiation of dilation was reached at a smaller axial strain. This was due to the

generation of excess pore water pressure, which results in an apparent increase in strength. Also, the higher strain rates prevent the generation of creep and proper stress distribution within the specimen.

The differences between the peak stresses can be observed to be much higher than that of critical state stresses for any pair of strain rates. Henceforth, it can be concluded that the strain rate is critical for studies which deal with peak stress. Researchers had earlier observed that the variation of strain rates, within a moderate range, does not affect the critical state strength of clays (Sheahan et al., 1996; Sorensen et al., 2007; Díaz-Rodríguez et al., 2009).

For a drained test, the dissipation of excess porewater pressure is essential. Therefore, the slower strain rates provide a response which is closer to the true response. However, slower the strain rate, the higher is the time required for the completion of a test. Hence, the optimal rate of shearing is obtained by attaining a balance between achieving the response which is closest to the ideal response and the time required to complete a test. In this case, the optimal rate of shearing for performing the monotonic triaxial tests on saturated silty soil specimens was selected to be 0.05%/min.

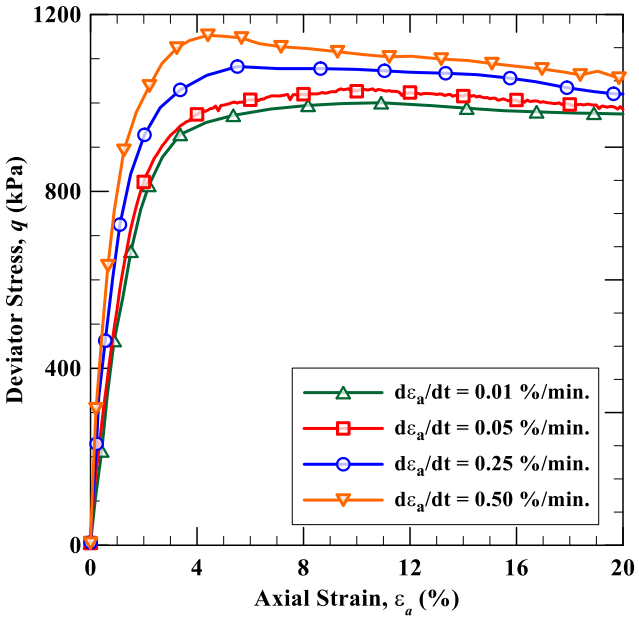

Figure 3.32 Stress-strain response of saturated soil at varying strain rates for 400 kPa effective confining pressure

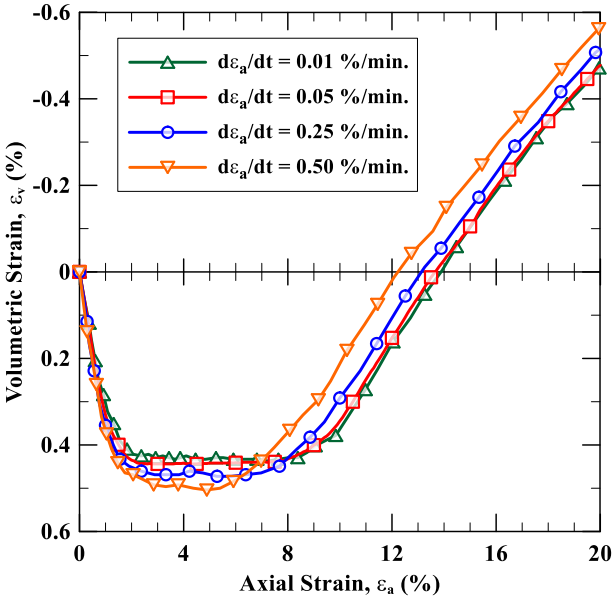

Figure 3.33 Volume change response of saturated soil at varying strain rates for 400 kPa effective confining pressure

3.9.3 *Unsaturated Soil Specimen*

For unsaturated specimens, apart from the dissipation of excess pore water pressure, the pore air pressure also should be properly dissipated, to obtain the true response of soil during shearing. Since the permeability of unsaturated specimens is more than one order of magnitude lower than that of saturated specimens (Meerdink et al., 1996; Vanapalli et al. 1997; Trinh et al. 2010), it is expected that the optimum strain rate for unsaturated specimens is much slower than that of saturated specimens.

The study of the effect of rate of shearing on unsaturated specimens was conducted by analyzing the stress-strain and volumetric response of compacted silty soil. The rates of shearing selected for this task were 0.001%/min (slowest), 0.003%/min and 0.01%/min (fastest). It was observed that the response of soil to the slower rate of shearing (0.001%/min and 0.003%/min) was similar. Whereas, the fastest shearing rate showed increasing deviator stress response and faster rate volume change for any given axial strain level. To account for the time required to shear the specimen, the fastest rate of shearing which almost depicts the true nature of soil behavior to shearing was selected as the appropriate rate of shearing for all unsaturated specimens. In this case, the appropriate shearing rate was determined to be 0.003%/min.

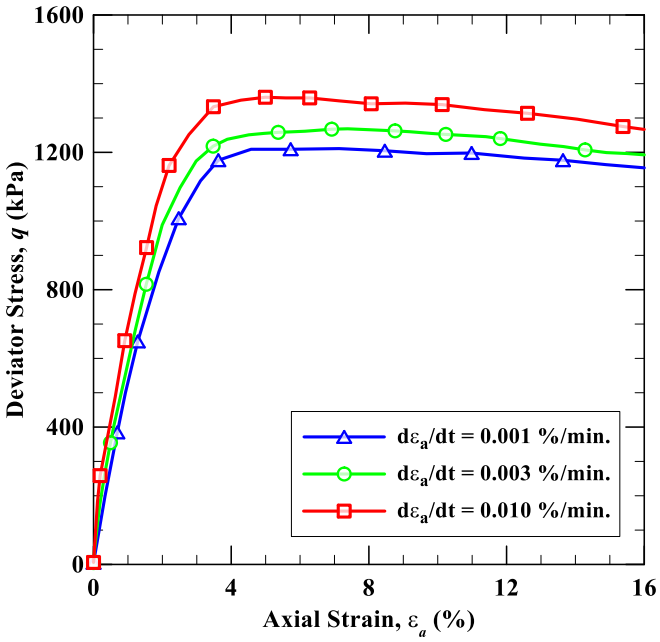

Figure 3.34 Stress-strain response of unsaturated soil at varying strain rates for 400 kPa mean net stress and 250 kPa matric suction

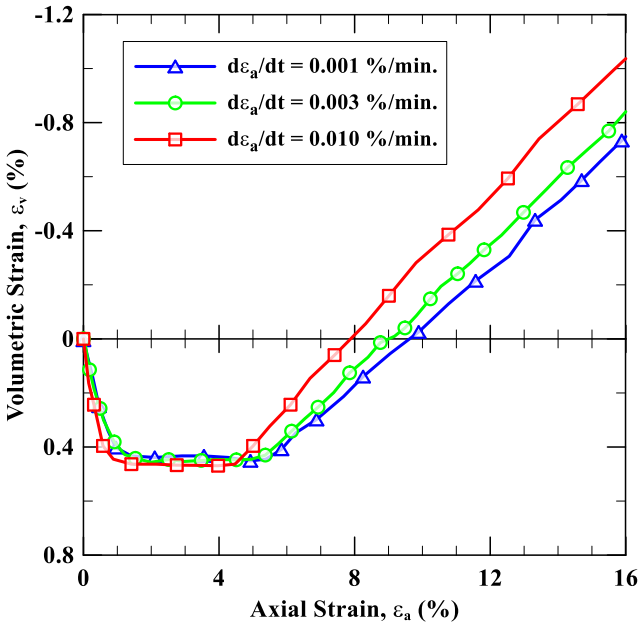

Figure 3.35 Volume change response of unsaturated soil at varying strain rates for 400 kPa mean net stress and 250 kPa matric suction

3.9.4 *Synopsis of Strain Rate Studies*

The variation of strain rate affects the deviator stress and volumetric strain responses of both saturated and unsaturated soils. It plays an important role in the determination of the peak deviator stress, which aids in the accurate estimation of peak shear strength of soils. The higher strain rates resulted in the development of higher peak deviator stress, which is achieved at a smaller strain. Also, the initiation of dilation occurred at a smaller strain.

However, it was observed the strain rate had a minimal effect on the deviator stress at critical state. Henceforth, for the saturated specimen, the variation of deviator stress at critical state between the selected strain rate of 0.05%/min and a slower strain rate 0.01%/min was computed to be 2%, while at peak stress the difference was 4%. Similarly, for the unsaturated specimen, 3% variation in deviator stress at critical state was observed between the selected strain rate of 0.003% and a slower strain rate of 0.001%/min, whereas for peak stress, the difference was 6%. Similar observations were made by Zhang et al. (2014b); Patil (2014) for unsaturated soils, where it was concluded that the maximum deviator stress was higher for higher strain rate, whereas, at the critical state, the deviator stress was observed to be similar for varying strain rates.

3.10 Mechanical Response under Suction-controlled Shearing

The results of the shearing stage for all the unsaturated specimens have been discussed in this section. Additionally, the detailed analysis of the data was

performed to study the effect of matric suction on other parameters, such as stiffness.

The compression of soil is represented as positive volumetric strain, while, the dilation is represented by a negative sign, which is the general sign convention followed for soils. Additionally, the nomenclature followed to represent each test is "CD_x_y", where, CD denotes the Consolidated Drained test; x and y represent the net confining pressure ($\sigma_3 - u_a$) and the matric suction ($u_a - u_w$) applied in kPa during the test, respectively.

3.10.1 *Effect of Net Confining pressure at Constant Matric Suction*

The deviatoric stress response of the unsaturated specimens during shearing in drained conditions at constant induced matric suction of 50, 250 and 750 kPa has been shown in Fig. 3.36, Fig. 3.38, and Fig. 3.40, respectively. The volumetric strain response of the specimen during shearing in drained condition at constant induced matric suction of 50, 250 and 750 kPa has been shown in Fig. 3.37, Fig. 3.39, and Fig. 3.41, respectively. It can be observed that the strength of the specimen increases with an increase in confining pressure.

The soil specimens show dilative behavior after initial compression, which occurs because of the particle rearrangement, due to sliding and rolling of particles. During compression, the particle rearrangement results in better interlocking, which causes an increase in strength. However, it is evident from Fig. 3.40 and Fig. 3.41 that as the particles start to slide over each other, which initiates strain

localization, and the soil specimen starts to dilate. This results in loss of interlocking, which decreases the strength of the soil. The dilation of soil is a typical behavior of over-consolidated soils.

Strain localization was mainly observed in specimens having an induced suction of 750 kPa, where distinct failure plane was observed. The development of strain localization induces a collapse in the strength of the soil, which is evident from shearing of specimens consolidated to 100 and 200 kPa at an induced suction of 750 kPa (Fig. 3.40).

As the net confining pressure increases, the slope of the volumetric strain curve during dilation decreases, which means that the dilation angle also decreases with an increase in net confining pressure. An elaborate analysis of dilation angle has been presented in Section 3.10.12. Due to the increase in net confining pressure, the soil also achieves greater initial compression prior to dilation.

The response of deviator stress at all suction levels (s = 50, 250 and 750 kPa) showed that the increase in net confining pressure resulted in an increase in initial stiffness of the specimen.

The post-peak softening behavior is defined as the decrease in deviator stress after attaining the peak deviator stress. The specimens at the induced suction of 50 kPa, showed a slight post-peak softening behavior after attaining peak stress (Fig. 3.36). However, the softening behavior is clearly evident at the suction of 750 kPa (Fig. 3.40).

Fig. 3.40 shows that the specimen subjected to higher net confining pressure shows higher ductility, as compared to the specimens sheared at lower net confining pressure, at the same matric suction. Similar behavior was observed by Rahardjo et al. (2004), and Li and Zhang (2015), where higher net confining pressure showed an increase in ductility (explained in section 2.11.1) of the soil specimen.

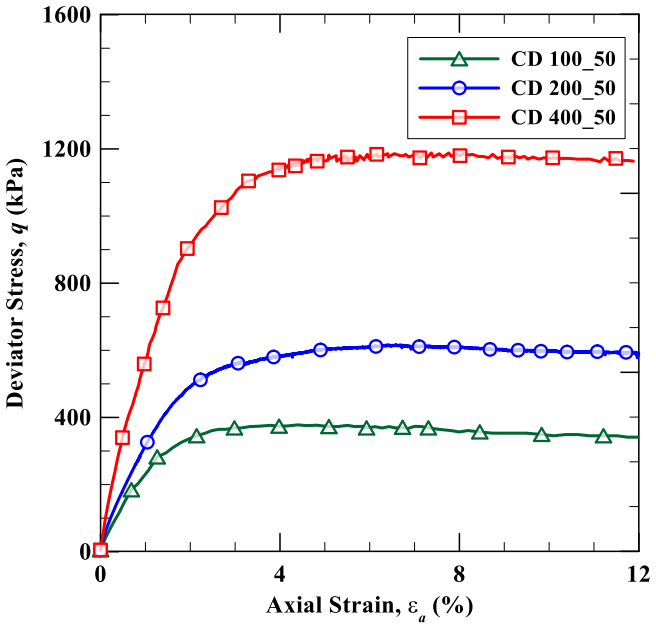

Figure 3.36 Deviatoric stress response of consolidated specimen at induced matric suction of 50 kPa under drained condition

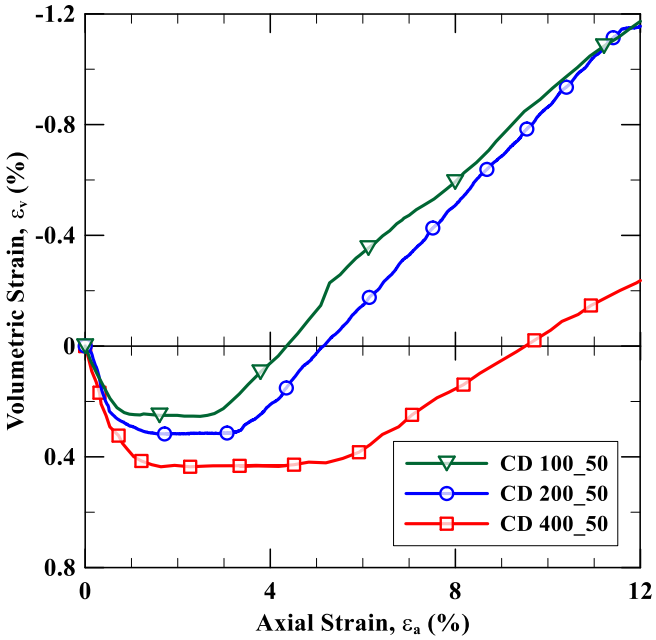

Figure 3.37 Volumetric strain response of consolidated specimen at induced matric suction of 50 kPa under drained condition

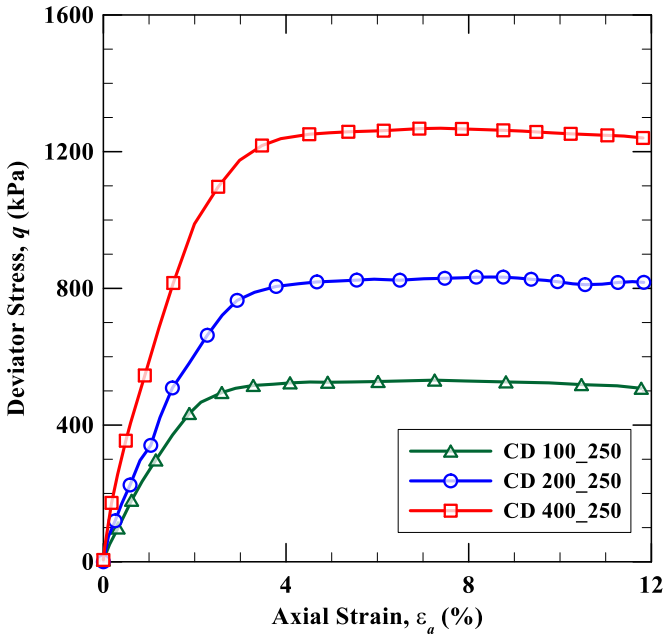

Figure 3.38 Deviatoric stress response of consolidated specimen at induced matric suction of 250 kPa under drained condition

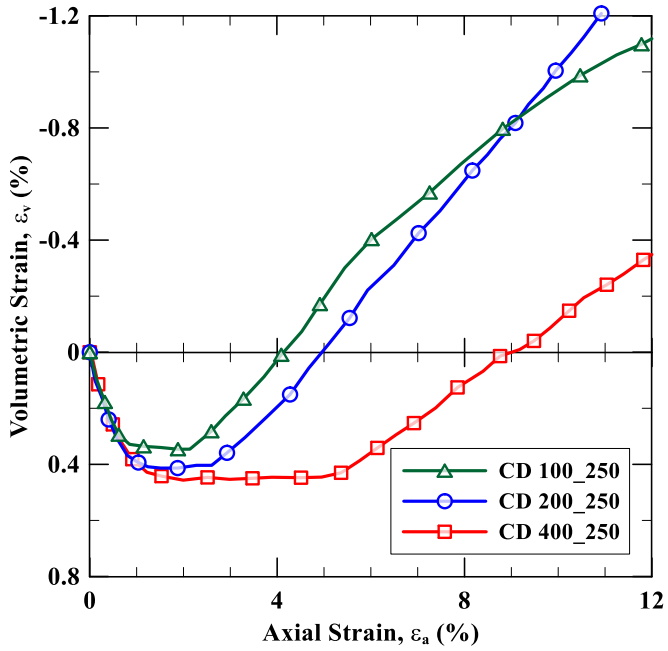

Figure 3.39 Volumetric strain response of consolidated specimen at induced matric suction of 250 kPa under drained condition

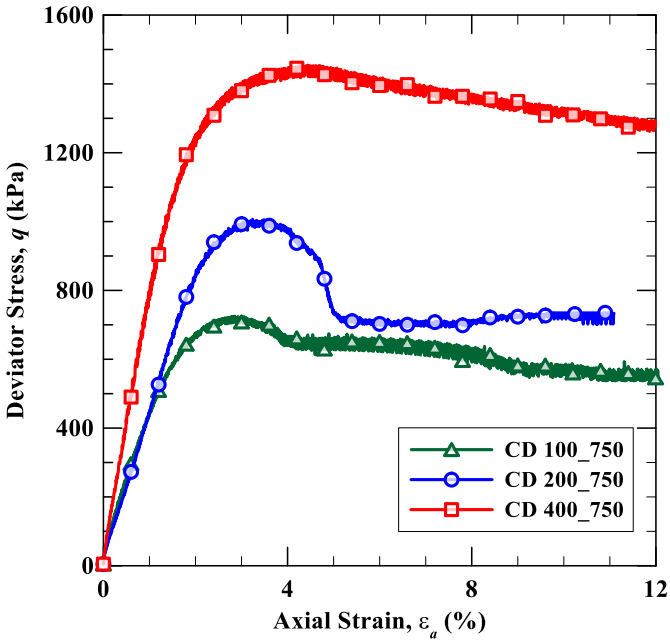

Figure 3.40 Deviatoric stress response of consolidated specimen at induced matric suction of 750 kPa under drained condition

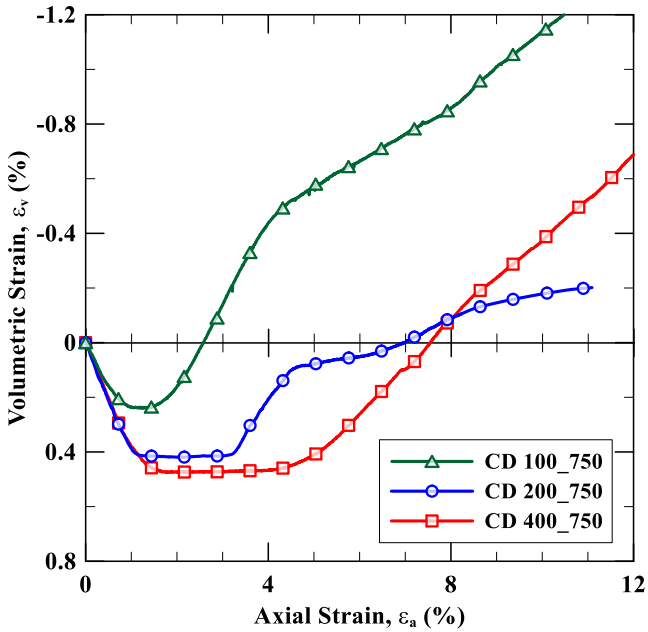

Figure 3.41 Volumetric strain response of consolidated specimen at induced matric suction of 750 kPa under drained condition

3.10.2 *Effect of Suction at Constant Net Confining pressure*

The comparison of deviator stress response of specimens sheared at constant net confining pressure, but varying induced matric suction is shown in Figs. 3.42, 3.44, and 3.46. The comparison of the volumetric strain response of specimens sheared at constant net confining pressure, but varying induced matric suction is shown in Figs. 3.43, 3.45 and 3.47. These plots also include the response of saturated soil specimens (suction, s = 0 kPa).

Figure 3.42 shows the increase of peak deviator stress with an increase of suction from s = 0 kPa to 750 kPa. This clearly indicates that the peak strength increases significantly due to suction. The increase of suction results in the attainment of peak stress at a smaller axial strain. In other words, with an increase in suction a smaller deformation mobilizes the peak strength. This has direct practical applications for the stability of slopes, where an increase in suction would mean that lesser sliding of the slip surfaces of the slope is required to attain the peak strength.

However, when the stresses in critical stresses are compared, it shows that the rate of increase in stress decreases with increase in suction. This is especially evident for an increase in suction from 250 kPa and 750 kPa, where the deviator stresses at critical state are almost the same. The effect of suction on the initial stiffness of soil can be clearly seen in Fig. 3.42, where the stiffness increases with increase in suction. Additionally, the increase of suction increases the brittleness of

the soil, and the specimen demonstrates greater post-peak softening, which is mobilized within less axial strain.

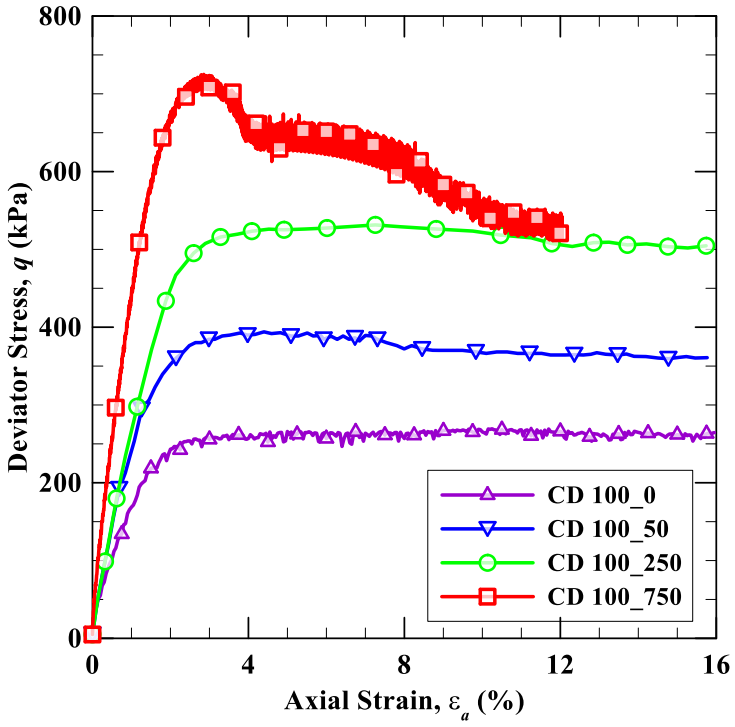

Figure 3.42 Deviator stress response of specimen consolidated to a net confining pressure of 100 kPa under drained condition

The response of volumetric strain at a constant net confining pressure ($\sigma_3 - u_a$ = 100 kPa) for varying matric suction (s = 0, 50, 250 and 750 kPa) is shown in Fig. 3.43. It can be observed that the initial compression is similar at all suction levels. However, the dilation increases with increase in suction, which is evident from the slope of volumetric strain curve after the initiation of dilation. Additionally, the initiation of dilation is dependent on the induced matric suction.

The dilation is initiated at relatively earlier axial strain with increasing value of induced matric suction.

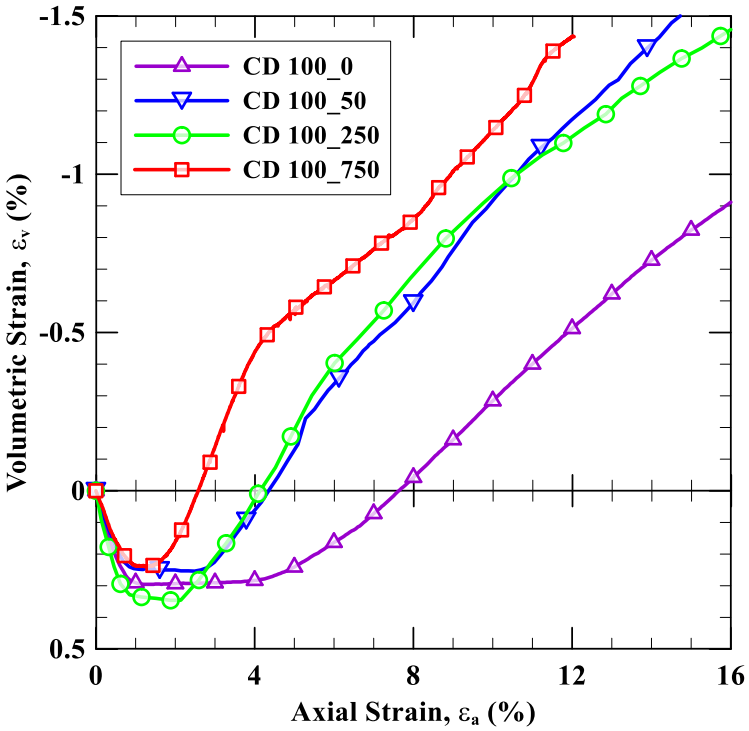

Figure 3.43 Volumetric strain response of specimen consolidated to a net confining pressure of 100 kPa under drained condition

The response of deviatoric stress for a net confining pressure of 200 kPa with varying induced matric suction is shown in Fig. 3.44. It presents the additional test for induced matric suction of 500 kPa for a net confining pressure of 200 kPa. Figure 3.44 shows an important detail. The critical state strength for a specimen having an induced matric suction 500 kPa or 750 kPa is lower than that of a specimen having 250 kPa induced matric suction. This mainly occurred due to the brittleness of the specimen at suction above 500 kPa. The brittleness induced strain

localization resulted in the formation of a distinct failure plane and localized slip failure occurred.

The deviator stress response at the net confining pressure of 200 kPa (Fig. 3.44), also demonstrated similar features, like an increase in stiffness, peak deviator stress and post-peak softening with an increase in induced matric suction, as that obtained at the net confining pressure of 100 kPa (Fig. 3.42). Additionally, the peak deviator stress at the net confining pressure of 200 kPa is attained at a smaller axial strain with an increase in matric suction, which is similar for the net confining pressure of 100 kPa.

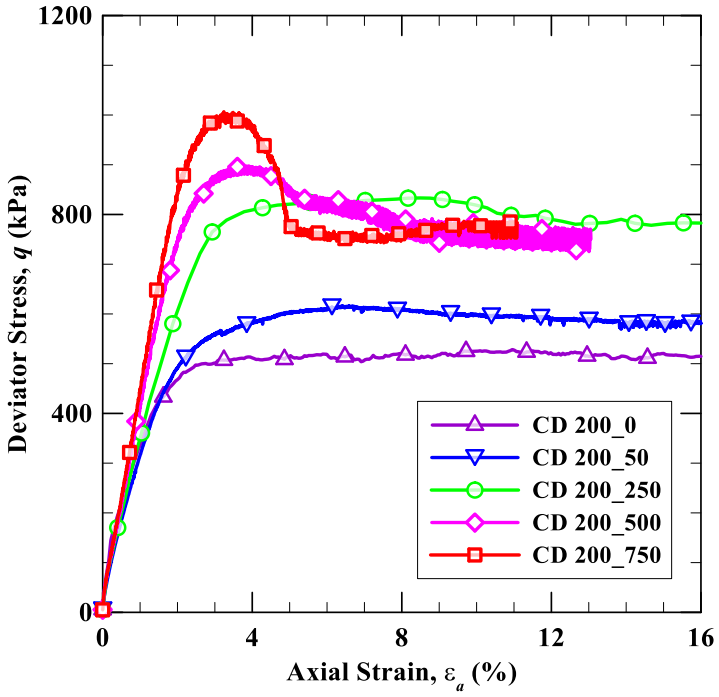

Figure 3.44 Deviator stress response of specimen consolidated to a net confining pressure of 200 kPa under drained condition

Figure 3.45 shows that the increase in suction has a negligible effect of the compression of the soil specimen, while the dilation is enhanced with an increase in suction. When Figs. 3.44 and Fig. 3.45 are compared, it can be observed that the peak deviator stress is attained near the strain at which dilation initiates, which coincides for specimens subjected to a matric suction of 500 and 750 kPa. The test at 500 and 750 kPa induced matric suction were stopped after reaching axial strain of 11% and 12% respectively, due to clear indication that the specimen had sheared along a distinct plane and the presence of the latex membrane introduced the 'membrane effect', after which the true volumetric strain response was not represented by the triaxial test.

The 'membrane effect' is the error introduced in the measurement of volume of soil when a gap or a crack within the soil specimen is concealed by the membrane, which is supposed to be filled with the confining fluid, i.e. water from cell pressure. The 'membrane effect' occurs mainly in case of planer failure or wedge type of failure, where the two wedges of soil have a gap between the shear failure surface. The reference to 'membraned effect' is different from the generally used term 'membrane penetration effect'. The 'membrane penetration effect' is the introduction of errors in volume change measurements of granular soils in triaxial testing due to the effect of penetration of the latex membrane enclosing the soil into the voids between the particles (Frydman et al., 1973).

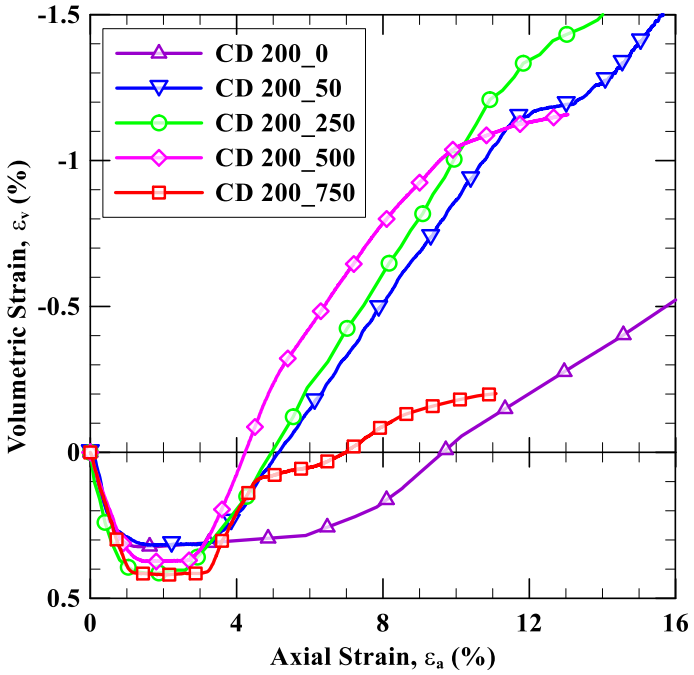

Figure 3.45 Volumetric strain response of specimen consolidated to a net confining pressure of 200 kPa under drained condition

Figure 3.46 showed higher deviator stress at critical state for increasing matric suction. This is due to a net confining pressure of 400 kPa, which increases the ductility of the soil at any given matric suction when compared to lower net confining pressures of 100 and 250 kPa.

The remaining trends are similar to that observed in Figs. 3.44 and 3.46, which include the increase in stiffness, peak deviator stress and post-peak softening, with an increase in suction. The peak deviator stress is attained at a smaller axial strain with an increase in suction.

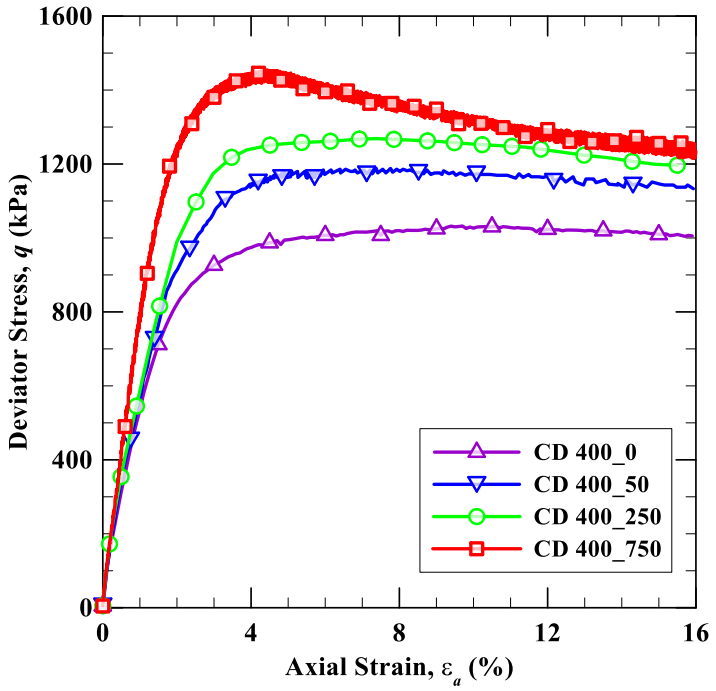

Figure 3.46 Deviator stress response of specimen consolidated to a net confining pressure of 400 kPa under drained condition

Figure 3.47 shows a similar response as compared to the net confining pressure of 100 and 200 kPa. It was observed that the compression of soil is independent of the induced suction. The dilation increased with increase in suction. Also, the peak deviator stress is attained near the axial strain value at which the dilation initiates.

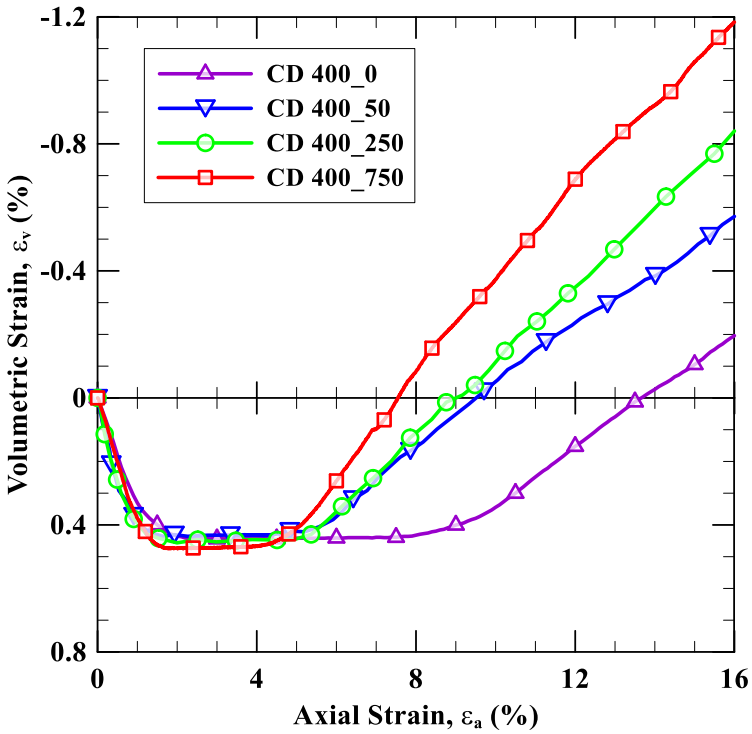

Figure 3.47 Volumetric strain response of specimen consolidated to a net confining pressure of 400 kPa under drained condition

3.10.3 *Analyses of Suction-Controlled Shearing at Critical State*

The Mohr's stress circle is plotted at the net confining pressure of 100, 200 and 400 kPa for varying suction levels of 50, 250 and 750 kPa. The Mohr's stress circle is used to determine the shear strength parameters (i.e. cohesion intercept and angle of internal friction) of the soil specimen at each suction level.

The modified Mohr-Coulomb Failure criterion was assumed to draw a common tangent to the three-Mohr's circle, from which the slope of the line is determined to be the angle of internal friction, while the y-axis intercept is determined to be the cohesion intercept for that suction level.

The Mohr's stress circle for the net confining pressure of 100, 200 and 400 kPa at matric suction of 50, 250 and 750 kPa is shown in Figs. 3.48, 3.50 and 3.52. The angle of internal friction, φ′ was observed to be almost constant (φ′ ≈ 33.6°), which is in accordance with Fredlund and Morgenstern (1977). A non-linear increase in cohesion intercept was observed from Figs. 3.48, 3.50 and 3.52.

The value of the angle of internal friction due to the influence of matric suction, φ^b was computed using the following expression:

$$\varphi^b = tan^{-1}\left(\frac{c''}{u_a - u_w}\right) \tag{3.10}$$

where $c'' = (c - c')$ is the apparent cohesion, c is the cohesion intercept and c' is the effective cohesion for saturated soil.

The critical state line (CSL) and the stress paths for the net confining pressure of 100, 200 and 400 kPa at the suction of 50, 250 and 750 kPa is shown in Figs. 3.49, 3.51 and 3.53. The slope of the CSL was calculated to be constant (M = 1.355) for all suction levels. This validates the assumption made in Barcelona Basic Model (BBM) as postulated by Alonso et al. (1990), that the slope of the critical slope line is independent of matric suction.

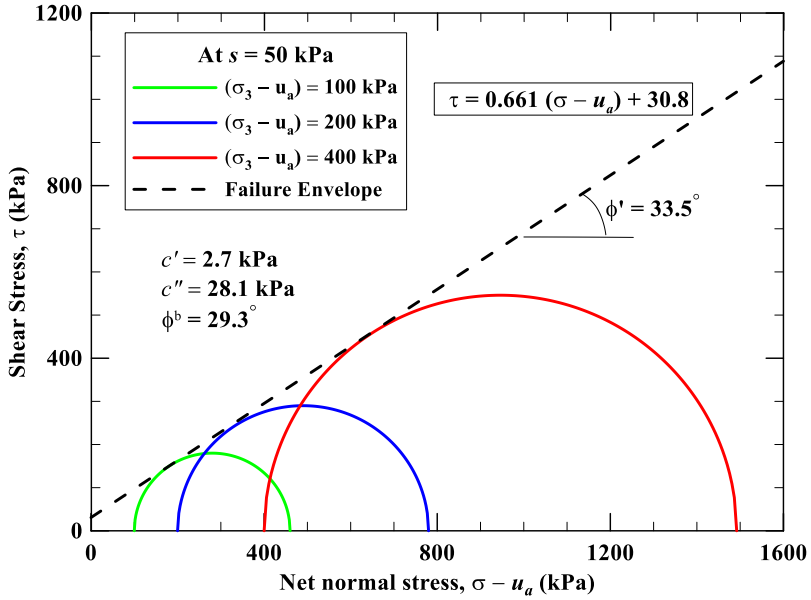

Figure 3.48 Mohr's stress circle at varying net confining pressure and at s = 50 kPa

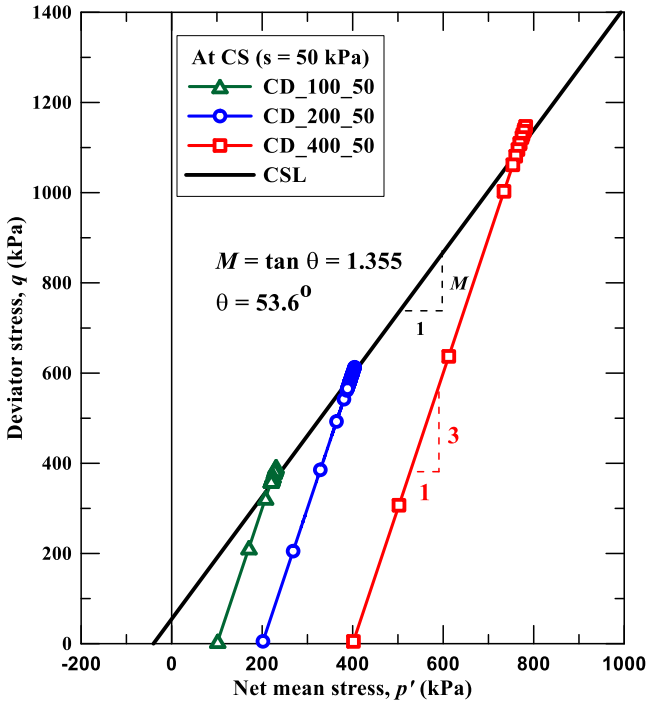

Figure 3.49 CSL and stress paths in p'-q space at s =50 kPa

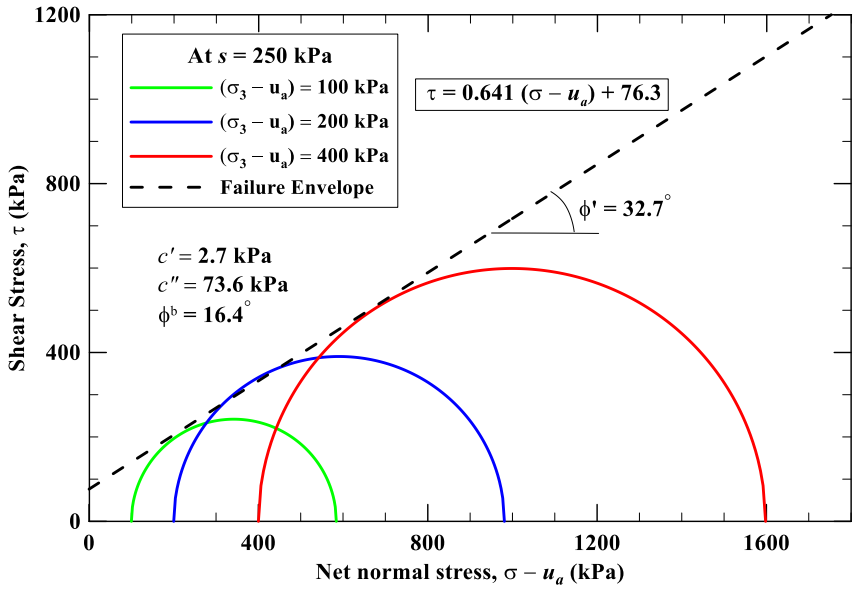

Figure 3.50 Mohr's stress circle at varying net confining pressure and at s = 250 kPa

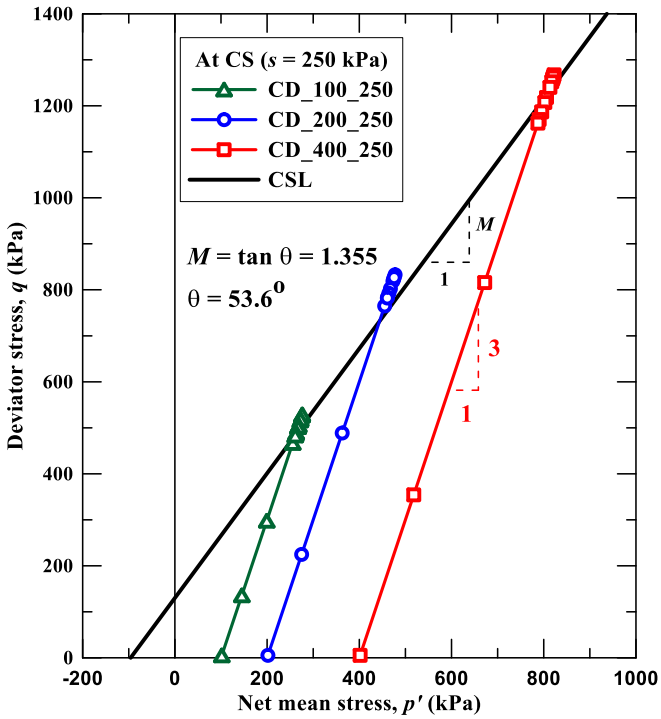

Figure 3.51 CSL and stress paths in p'-q space at s = 250 kPa

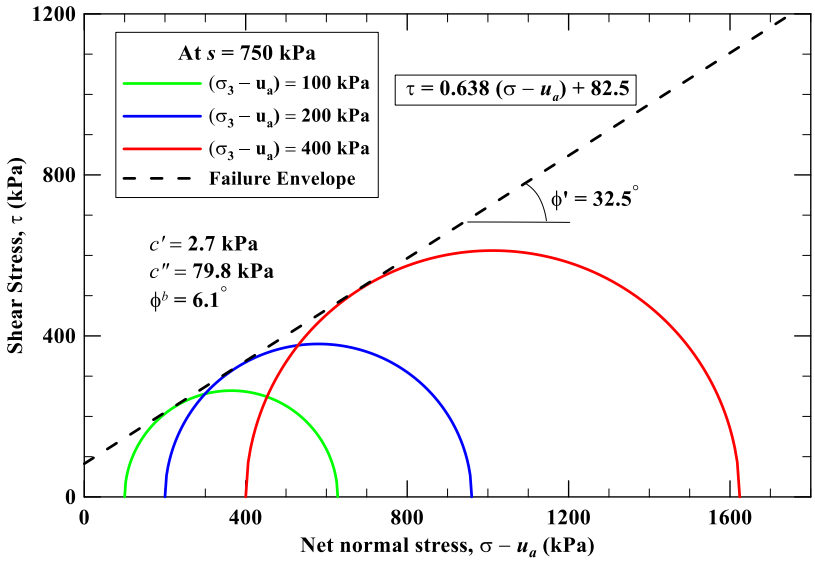

Figure 3.52 Mohr's stress circle at varying net confining pressure and at s = 750 kPa

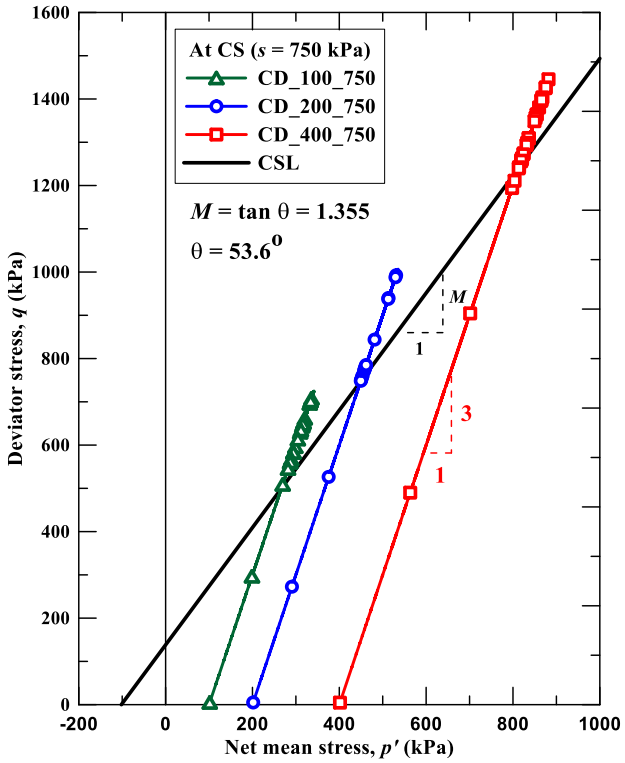

Figure 3.53 CSL and stress paths in p'-q space at s = 750 kPa

It is evident from Fig. 3.53 that the peak deviator stress is high as compared to the deviator stress at the critical state. Due to post-peak softening, the stress path crosses the CSL and then returns due to decrease in strength at critical strength.

The CSL obtained from the Figs. 3.49, 3.51 and 3.53 have been integrated along with the CSL obtained from tests on the saturated specimen. The resultant plot is shown in Fig. 3.54. It can be that the slope of the CSL at all suction levels are the same, while the y-axis intercept is different, and it increased with increasing matric suction.

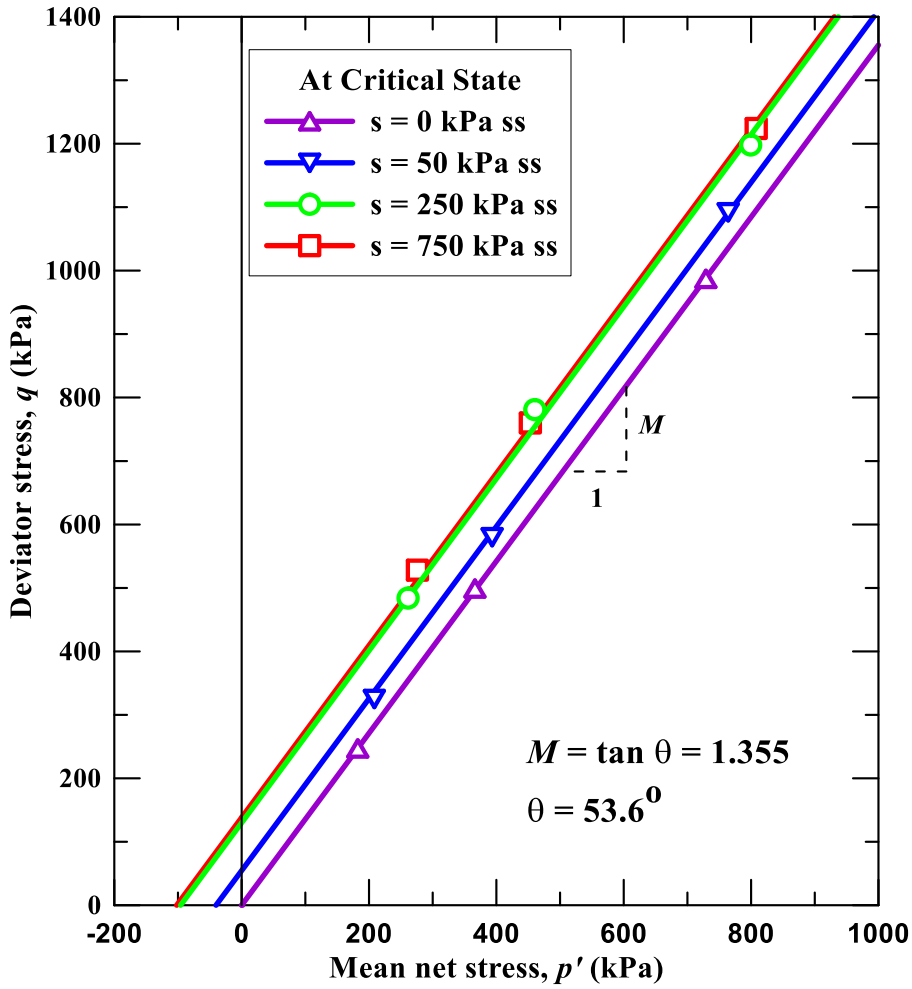

Figure 3.54 CSL in *p′*-*q* space at varying suction levels (*s* = 0, 50, 250, 750 kPa)

3.10.4 *Matric Suction Variation during Shearing*

The control of matric suction is pivotal to maintain a constant suction level throughout the test and to ensure the excess pore water pressure is not generated during the shearing. Figs. 3.55 and 3.56 demonstrate the negligible variation (less than ± 0.5 kPa) for both the suction levels (*s* = 50 kPa and *s* =750 kPa). If excess

pore water would have been generated, then there would have been a larger variation in suction levels during shearing.

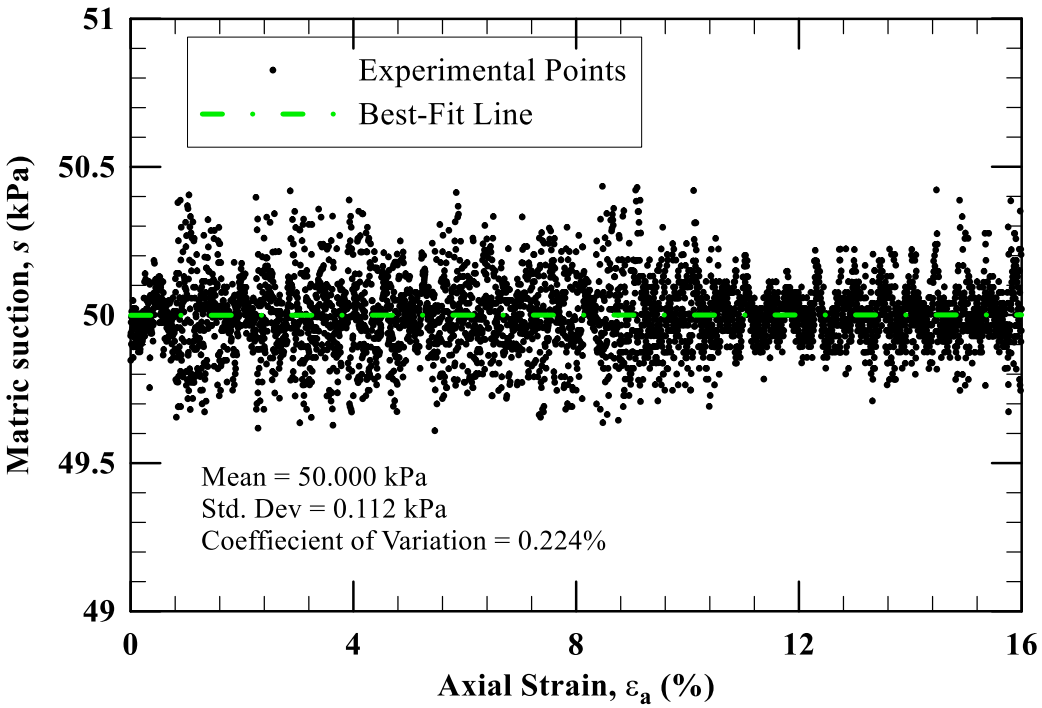

Figure 3.55 Variation of matric suction with axial strain during shearing for CD_100_50

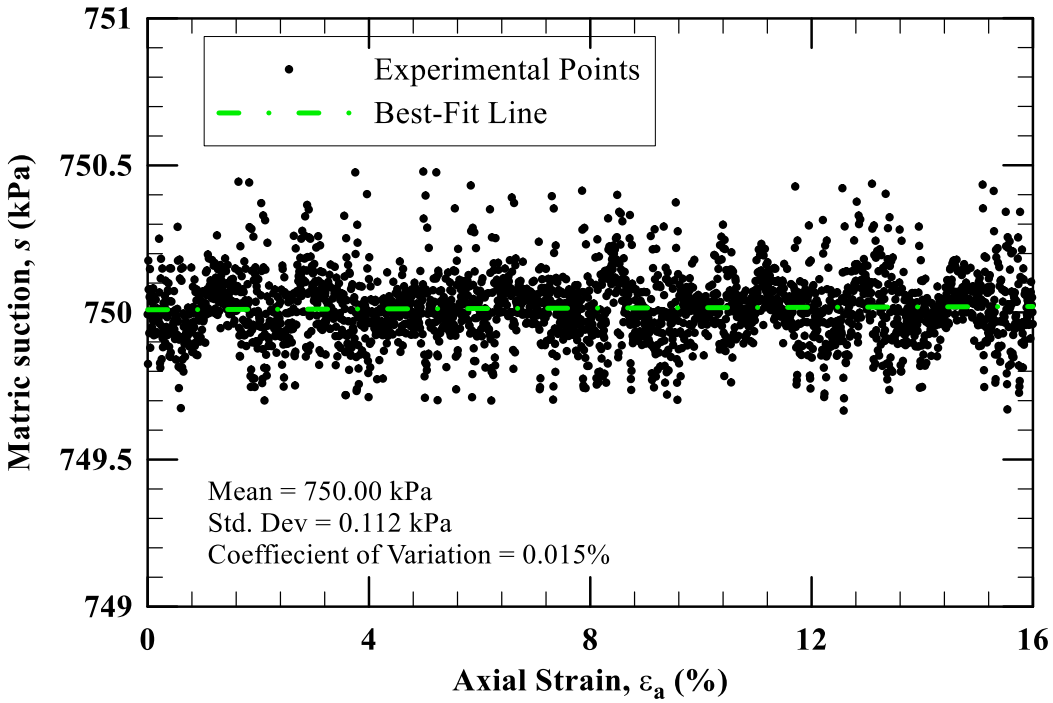

Figure 3.56 Variation of matric suction with axial strain during shearing for CD_400_750

3.10.5 *Analyses of Suction-Controlled Shearing at Peak State Failure*

The line joining the peak stress on *p'-q* space for the net confining pressure of 100, 200 and 400 kPa at a suction of 0 (saturated), 50, 250 and 750 kPa is shown in Fig. 3.57. The slope of the peak stress state line was obtained to be approximately 1.37 for all suction levels. The comparison between Figs. 3.54 and 3.57 show that the peak strength of the soil increased significantly from suction of 250 to 750 kPa, whereas, for strength at the critical state, the corresponding increase was negligible.

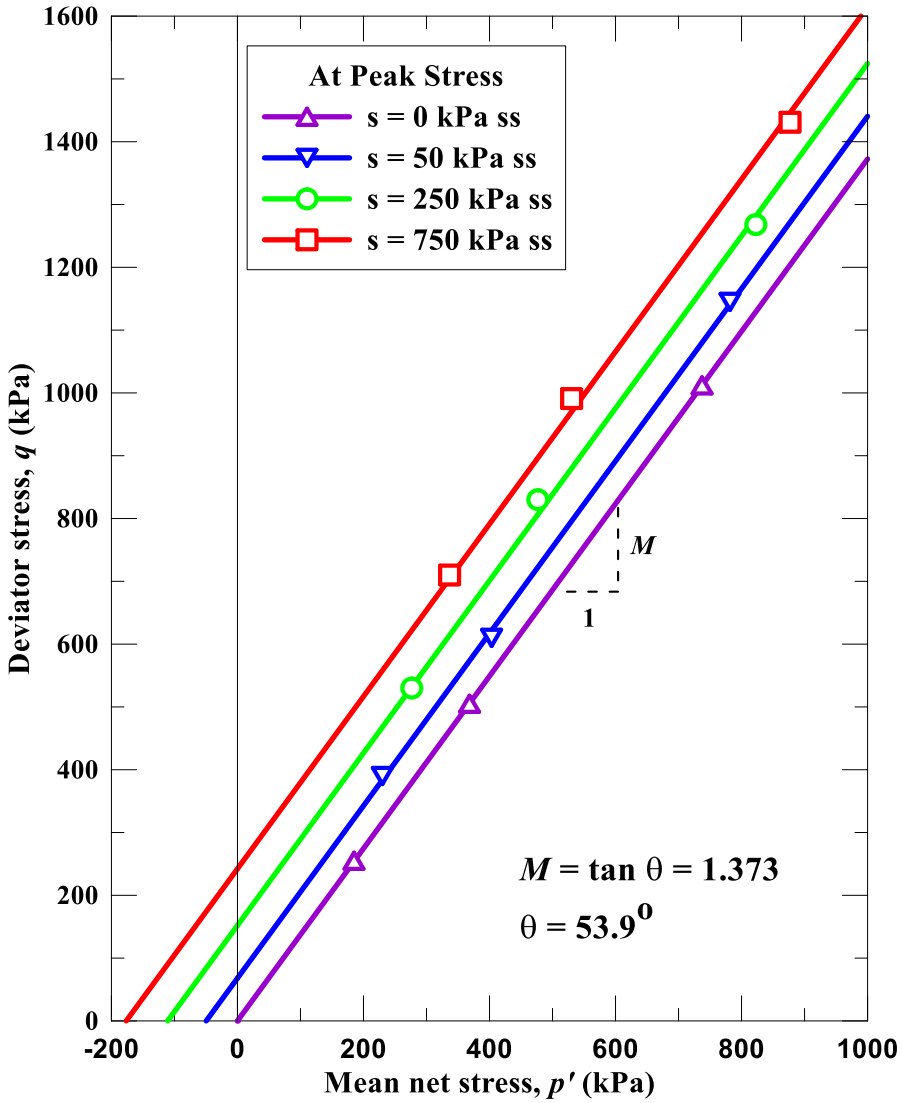

Figure 3.57 Peak state line in *p′*-*q* space at varying suction levels (*s* = 0, 50, 250, 750 kPa)

3.10.6 *Suction Stress Variation with Matric Suction*

The effective stress approach postulated by Bishop (1959) has been utilized by Lu and Likos (2006) to introduce the concept of suction stress. Suction stress

refers to the net interparticle force generated within a matrix of unsaturated soil particles due to the combined effects of negative pore water pressure and surface tension (Lu and Likos, 2004). At the macroscopic level, the suction stress generates a tensile force which pulls the soil particles towards each other, thereby increasing the effective stress of the soil. The suction stress can represent the state of stress for unsaturated soil using a single stress variable, which could be determined using the SWCC of a soil (Song et al., 2012). The results of the triaxial tests have been used to validate the suction stress determined from the SWCC of the soil.

Lu and Likos (2006) proposed the concept of suction stress using the following relationship of effective stress:

$$\sigma' = (\sigma - u_a) - \sigma^s \tag{3.11}$$

where $\sigma_s = (u_a - u_w)\,\chi$ = suction stress.

The suction stress was determined using the van Genuchten (1980) SWCC model, which is as follows:

$$S_e = \left\{\frac{1}{1+[\alpha(u_a-u_w)]}\right\}^{1-1/n} \tag{3.12}$$

Lu et al. (2010) suggested the following closed-form expression for suction stress for the entire range of matric suction:

$$\sigma^s = (u_a - u_w), \qquad \text{for } (u_a - u_w) \leq 0 \tag{3.13}$$

$$\sigma^s = \frac{(u_a-u_w)}{\{1+[\alpha(u_a-u_w)]^n\}^{(n-1)/n}}, \qquad \text{for } (u_a - u_w) > 0 \tag{3.14}$$

Additionally, Lu et al. (2010) had compiled the suction stress data from 14 different soils for the semi-quantitative validation using the results from triaxial tests and the following relationship was suggested:

$$\sigma^s = \frac{(\sigma_1 - u_a)_f - (\sigma_3 - u_a)_f tan^2\left(\frac{\pi}{4} + \frac{\varphi'}{2}\right) - 2c' \tan\left(\frac{\pi}{4} + \frac{\varphi'}{2}\right)}{2\tan\left(\frac{\pi}{4} + \frac{\varphi'}{2}\right) tan\varphi'} \qquad (3.15)$$

The suction stress was determined by two methods developed by Lu et al. (2010). Method 1 refers to the determination of suction stress using Eq. 3.14, which utilizes the van Genuchten (1980) SWCC model parameters (α and *n*). Since the additional parameter *m* was not used independently in Eq. 3.13, but was used in section 3.44 (Table 3.5). Henceforth, the new calibrated parameters for SWCC using Eq. 3.13 are α = 0.07 and *n* = 1.3.

Method 2 refers to the computation of suction stress using Eq. 3.15, which is for semi-quantitative validation using triaxial test results obtained in this research. Figure 3.58 and 3.59 show the variation of suction stress with matric suction. The suction stress was also determined form the experimental results, by using the following relationship:

$$\sigma^s = \frac{c''}{\tan \varphi'} \qquad (3.16)$$

where, c'' = apparent cohesion, and

φ' = angle of internal friction of the saturated specimen.

The apparent cohesion was obtained from the Mohr-Coulomb failure envelope at each suction level, as shown in Figs. 3.48, 3.50 and 3.52 for matric suction of 50, 250, and 750 kPa, respectively. The comparison of values of suction stress obtained from Method 1 shows that the actual suction stress obtained from the experimental results were much higher than that predicted by Eq. 3.14 for suction level 50 and 250 kPa (Fig. 3.58). However, for matric suction of 750 kPa, the suction stress values are quite similar. Since the SWCC model was utilized in the determination of suction stress, the limitations of the model also affected the values of suction stress. It can also be observed that the experimental value of suction stress increases rapidly with an increase in matric suction up to 250 kPa, however, the subsequent increase in suction stress almost negligible.

The determination of suction stress from the experimental results using Method 2 (Eq. 3.15; Fig. 3.59) are similar, which is expected since both set of values of suction stresses were derived from the same triaxial tests.

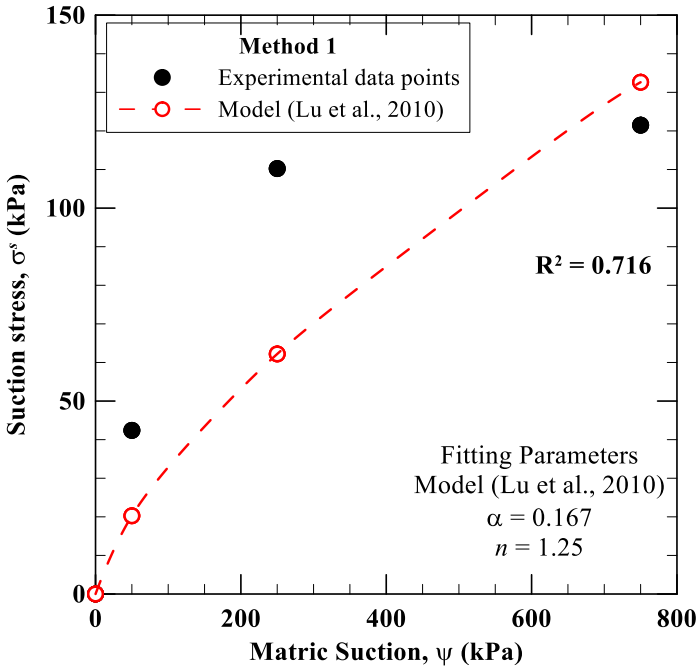

Figure 3.58 Variation of suction stress with matric suction using Method 1

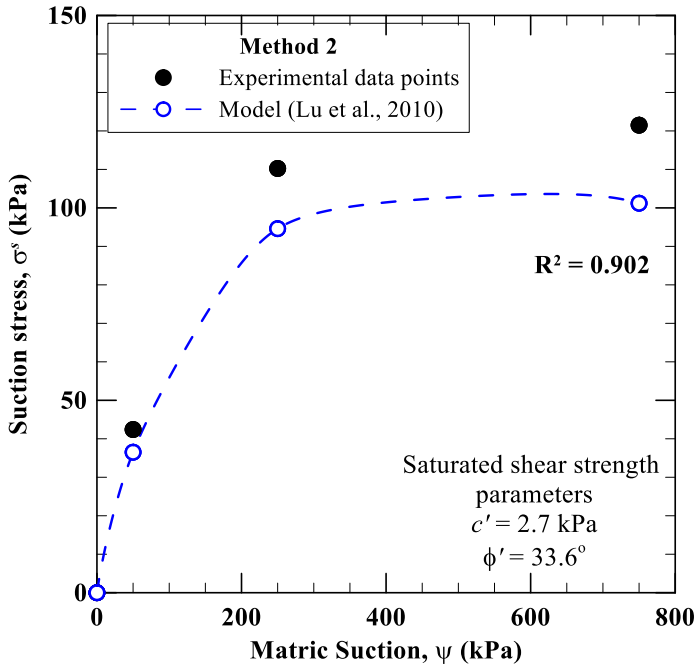

Figure 3.59 Variation of suction stress with matric suction using Method 2

Figures 3.60 and 3.61 show the variation of Bishop's effective stress parameter, χ by using the values of suction stress obtained from Method 1 and Method 2 described above. The following expression is used to determine the value of χ from suction stress:

$$\chi = \frac{\sigma^s}{(u_a - u_w)} \tag{3.17}$$

The experimental values depict a relatively slower decrease in values of χ with an increase in matric suction as compared to the prediction obtained from Method 1 and Eq. 3.17 (Fig. 3.60).

The experimental values and the values obtained from Method 2 and Eq. 3.17, show similarity, primarily due to the use of same series of triaxial test results to arrive at the results (Fig. 3.61).

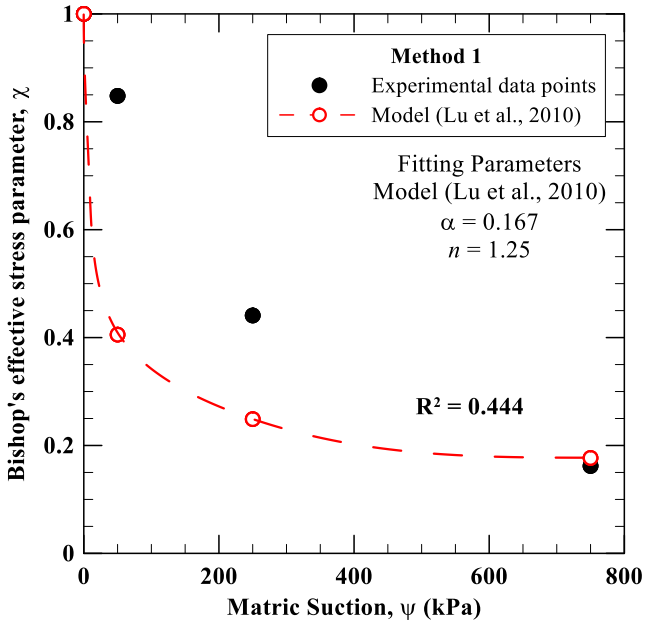

Figure 3.60 Variation of Bishop's effective stress parameter, χ with matric suction using Method 1

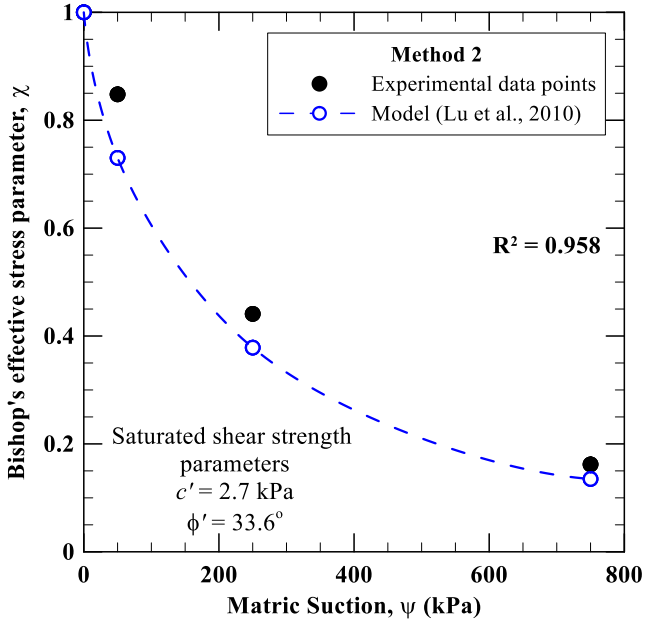

Figure 3.61 Variation of Bishop's effective stress parameter, χ with matric suction using Method 2

The shear strength of unsaturated soil could be determined using the Bishop's effective stress parameter, χ, which is as follows:

$$\tau_f = c' + [(\sigma - u_a) + \chi(u_a - u_w)] \tan \varphi' \quad (3.18)$$

The shear strength of unsaturated soil could also be defined using the suction stress by the following relationship:

$$\tau_f = c' + [(\sigma - u_a) + \sigma^s] \tan \varphi' \quad (3.19)$$

The comparison between the shear strength of unsaturated soil with an increase in matric suction using Eq. 3.19 is shown in Figs. 3.62 and 3.63. The computation of suction stress, which is a component of Eq. 3.19, was done using Methods 1 and 2 developed by Lu et al. (2010). The experimental determination of shear strength was done using the experimental values of apparent cohesion (c'') for each suction level (as shown in Figs. 3.48, 3.50, and 3.52) and substituting their values in the following equation:

$$\tau_f = c' + c'' + (\sigma - u_a) \tan \varphi' \quad (3.20)$$

The shear strength determination using the suction stress from Method 1 (Fig. 3.62) underestimated their values for suction level of 50 and 250 kPa for all values of initial net confining pressure ($\sigma - u_a$ = 100, 200, and 400 kPa), however, the predicted values of shear strength at matric suction of 750 kPa were identical.

The shear strength determined using the suction stress computed from the triaxial test (using Eq. 3.15; Fig. 3.63) were quite similar to the experimentally values, which was expected since the same series of triaxial tests were utilized to

determine the values of suction stress. Hence, the use of Eq. 3.15 for determination of suction stress is validated.

Additionally, the effect of suction stress on the overall shear strength of unsaturated soil was demonstrated in Figs. 3.62 and 3.63.

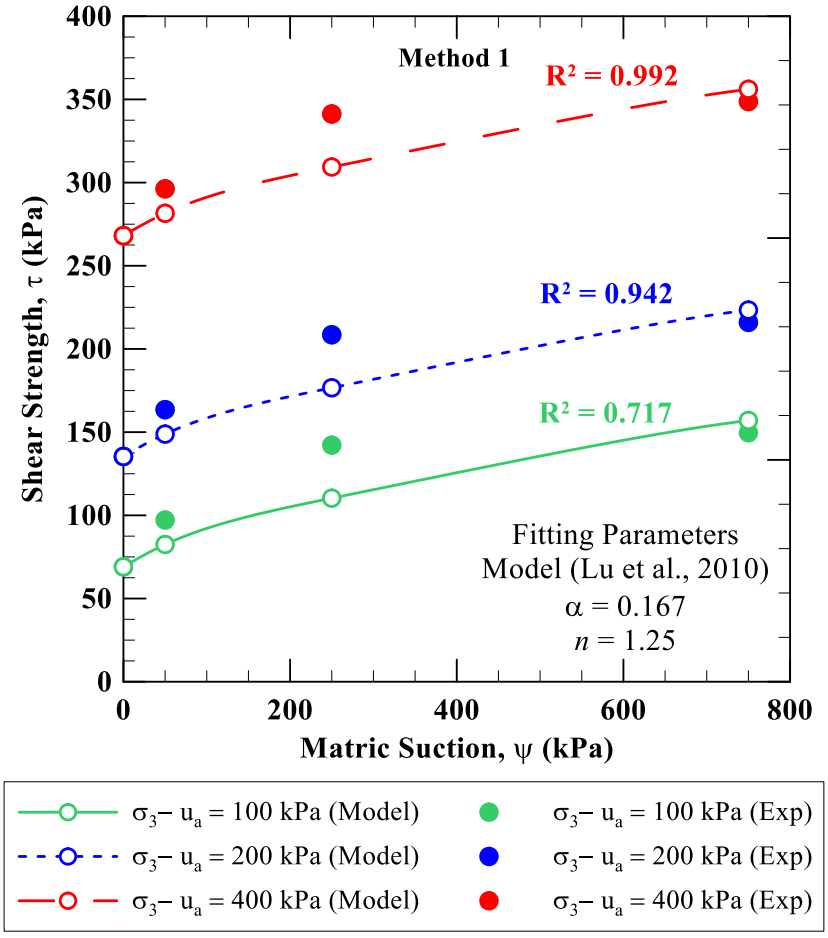

Figure 3.62 Variation of shear strength of unsaturated soil at varying net confining pressure of 100, 200, and 400 kPa using Method 1

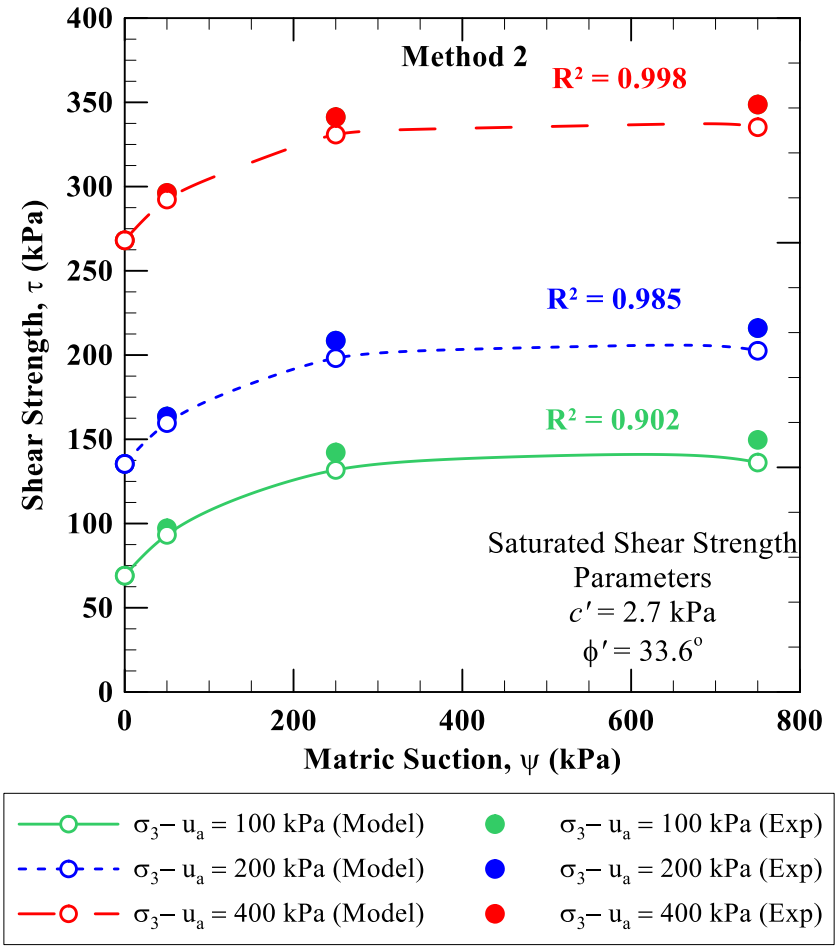

Figure 3.63 Variation of shear strength of unsaturated soil at varying net confining pressure of 100, 200, and 400 kPa using Method 2

3.10.7 *Effect of Suction and Net Confining Pressure on the Post-Peak Softening*

The post-peak softening of a soil at a suction level can be quantified by calculating the ratio of the difference between the peak deviator stress and the deviator stress at critical state to the peak deviator stress. The variation of this ratio with net confining pressure for varying suction levels is shown in Fig. 3.64. It can

be observed that the ratio decreases with increase in net confining pressure for a constant suction level. On the other hand, the ratio increases with increase in suction for a constant net confining pressure.

This clearly identifies the decrease in post-peak softening with an increase in net confining pressure. Also, the rate of decrease of post-peak softening ($-\Delta\eta/\Delta(\sigma_3 - u_a)$) increases with increase in suction. The parameter, η denotes the ratio of the difference between the peak deviator stress and the deviator stress at critical state to the peak deviator stress. The negative sign signifies the decrease in the value of η with an increase in net confining pressure (σ_3-u_a).

In addition, the post-peak softening (explained in section 2.11.1) increases with increase in suction for any given value of net confining pressure, especially when the suction increases from 250 kPa to 750 kPa.

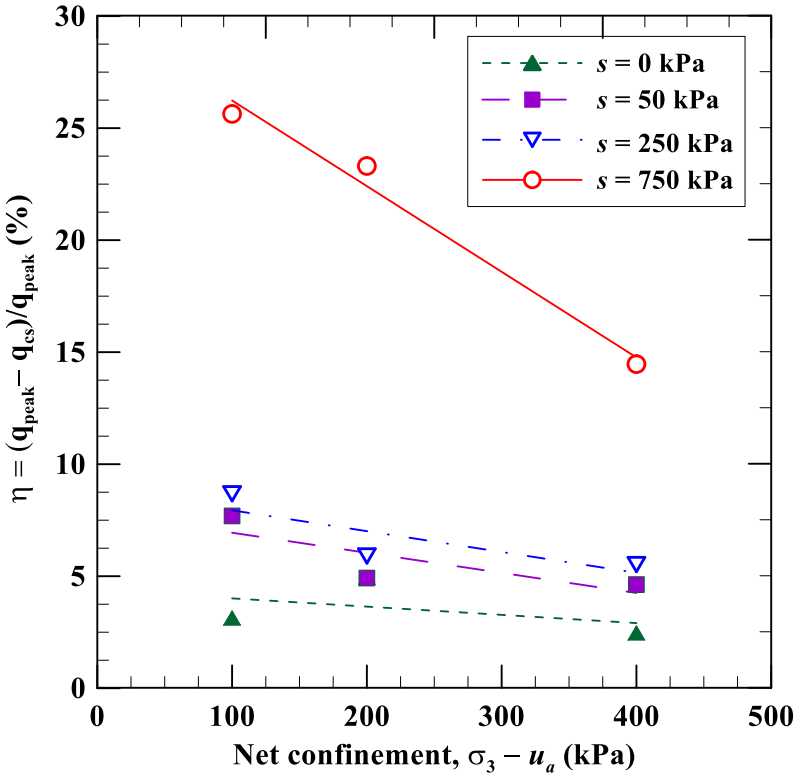

Figure 3.64 Effect of net confining pressure on the difference between deviatoric stress at peak stress and critical state for varying suction

3.10.8 *Effect of Suction on Stiffness of Soil*

The stiffness of the soil is compared using four different references. First, the initial stiffness of the soil is calculated using the criteria of secant modulus at 1% axial strain, $E_{1\%}$. Second, the modulus at peak stress is computed using the secant modulus at the strain corresponding to the peak deviator stress, E_{peak}. Third, the modulus at critical state is computed using the secant modulus at strain corresponding to deviator stress at the critical state, E_{cs}. Finally, the secant modulus

at 10% strain is computed, $E_{10\%}$. Since the strain at critical state depends on the suction level and the net confining pressure, for uniformity, the value of $E_{10\%}$is preferred over that of E_{cs}. The values of these stiffness moduli were obtained from the deviator stress response at the net confining pressure of 100, 200 and 400 kPa for saturated (s = 0 kPa) and unsaturated specimens (s = 50, 250 and 750 kPa).

The comparison among the values of these stiffness moduli with varying suction are shown in Figs. 3.65 – 3.69. It can be observed that there is a significant increase in the secant stiffness modulus at peak strength and 1% strain with an increase in matric suction. While the increase in matric suction results in a marginal increase in the secant stiffness modulus for critical state and 10% strain.

Henceforth, the contribution of matric suction is primarily limited to the initial stiffness and the strain corresponding to the peak strength of the soil.

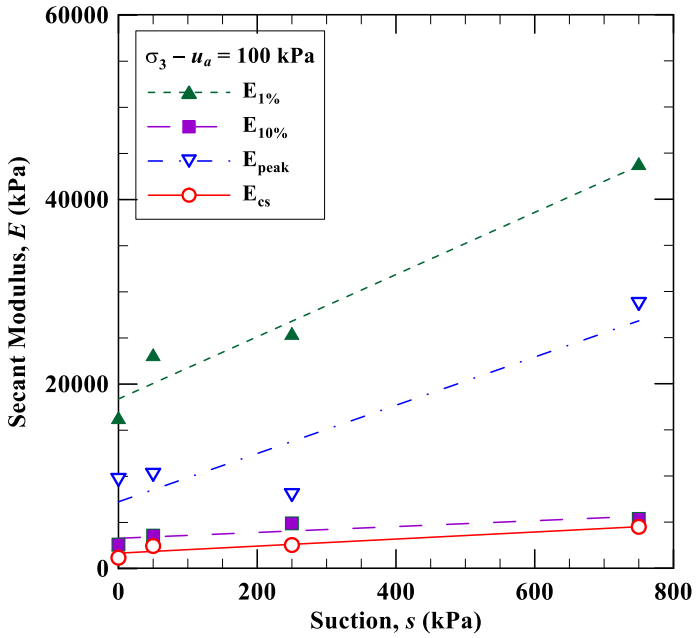

Figure 3.65 Secant stiffness moduli, $E_{1\%}$, $E_{10\%}$, E_{peak}, and E_{cs} variation at $\sigma_3 - u_a$ = 100 kPa

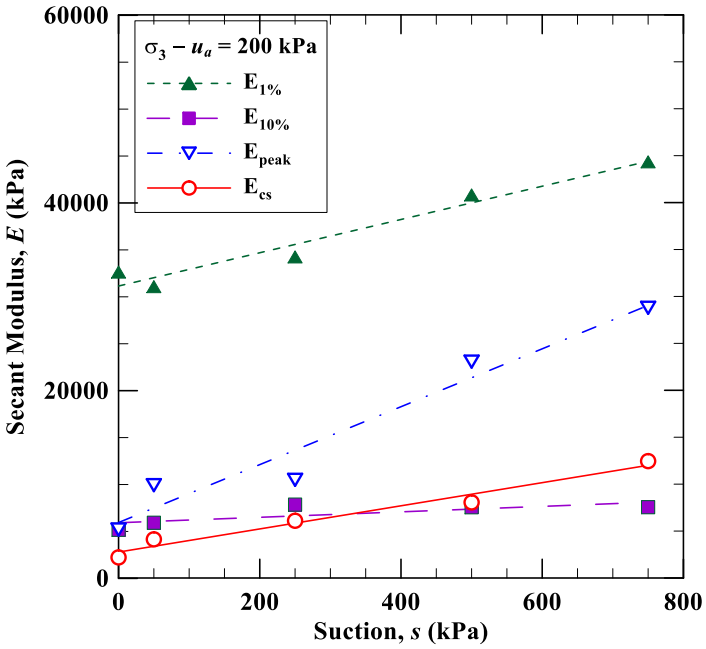

Figure 3.66 Secant stiffness moduli, $E_{1\%}$, $E_{10\%}$, E_{peak}, and E_{cs} variation at $\sigma_3 - u_a$ = 200 kPa

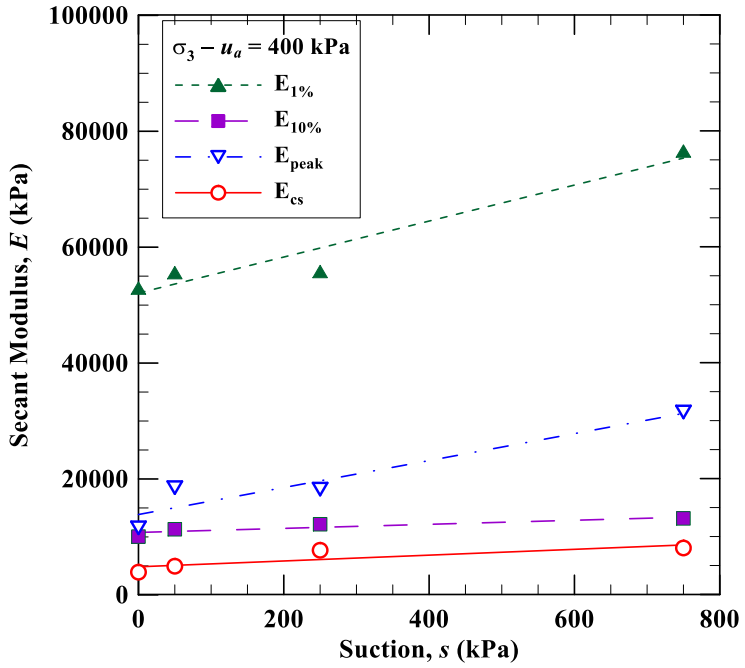

Figure 3.67 Secant stiffness moduli, $E_{1\%}$, $E_{10\%}$, E_{peak}, and E_{cs} variation at $\sigma_3 - u_a$ = 400 kPa

Figures 3.68 and 3.69 show the variation of $E_{1\%}$ and $E_{10\%}$ with suction for varying net confining pressure. It can be observed that the stiffness modulus for 1% strain has a linear variation with suction, whereas the secant stiffness modulus for 10% strain has a non-linear behavior, which initially increases rapidly till 250 kPa, and then it almost remains constant.

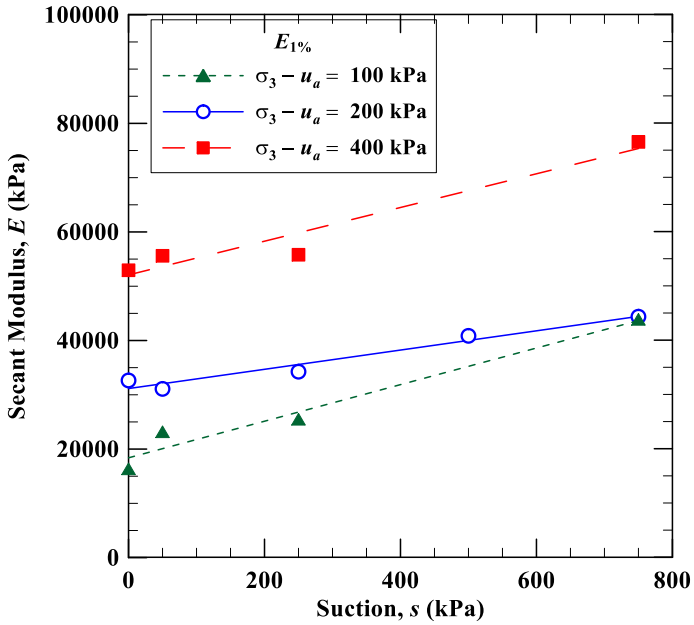

Figure 3.68 Variation of $E_{1\%}$ with suction for varying net confining pressure

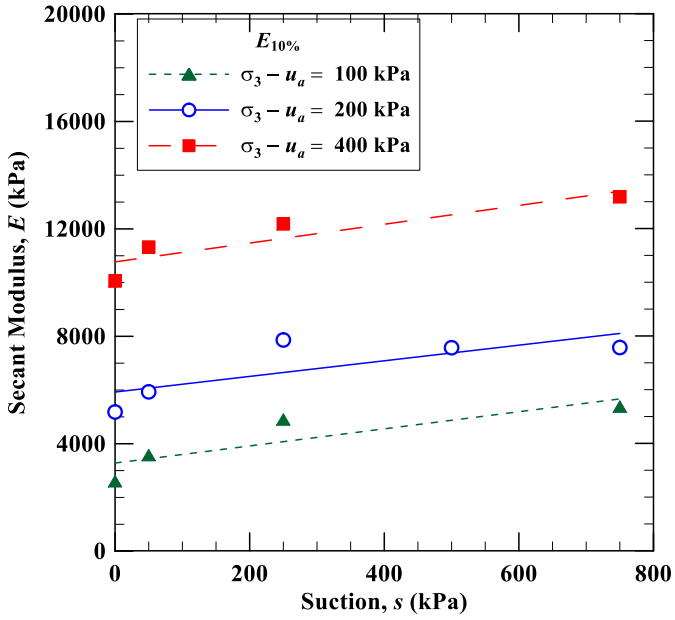

Figure 3.69 Variation of $E_{10\%}$ with suction for varying net confining pressure

3.10.9 *Effect of Net Confining Pressure on Stiffness of Soil*

Figures 3.70 – 3.73 show the variation of secant stiffness moduli with net confining pressure for suction levels of 0 kPa (saturated), 50 kPa, 250 kPa and 750 kPa, respectively. It can be observed that in all cases the increase in $E_{1\%}$ with net confining pressure is very high, as compared to that for the other secant stiffness moduli. Therefore, the initial stiffness of the soil is highly dependent on the net confining pressure applied. The initial stiffness occurs when the specimen is mostly within its elastic limit. The elastic modulus is highly dependent on the confining pressure, whereas the modulus after reaching plastic state is almost independent of the confining pressure.

It is also well-known that the orientation of the soil fabric gets disturbed or re-oriented with increasing axial strains. The initial stiffness (computed at an axial strain of 1%) occurs when the original soil fabric is barely re-oriented. However, the other secant stiffness moduli, especially at critical state and at an axial strain of 10%, have re-oriented soil fabric.

Figure 3.73 shows that the secant modulus for peak strength and the critical state is practically independent of the applied net confining pressure for s = 750 kPa, which may be due to the combination of an increase in strength and ductility with an increase in net confining pressure.

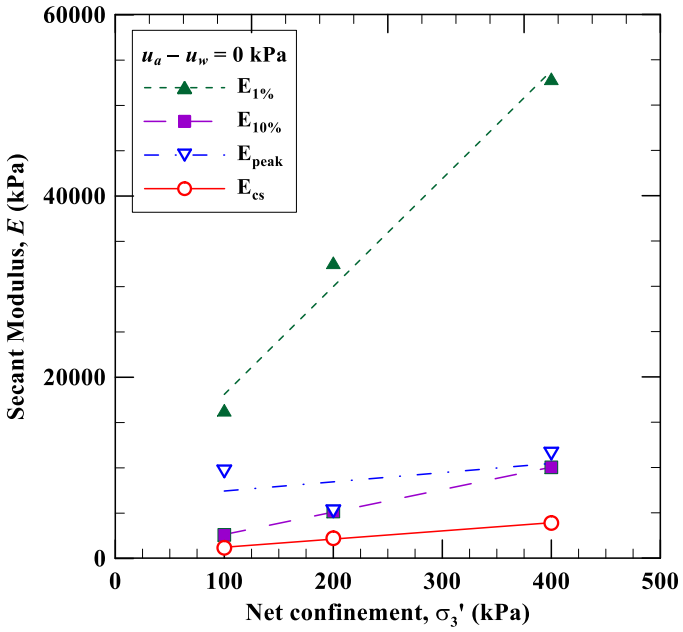

Figure 3.70 Secant stiffness moduli, $E_{1\%}$, $E_{10\%}$, E_{peak}, and E_{cs} variation for saturated soils

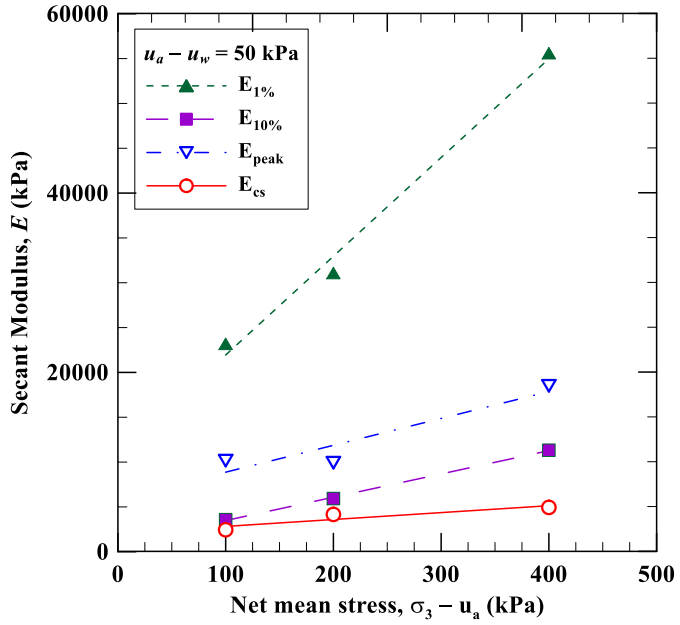

Figure 3.71 Secant stiffness moduli, $E_{1\%}$, $E_{10\%}$, E_{peak}, and E_{cs} variation for s = 50 kPa

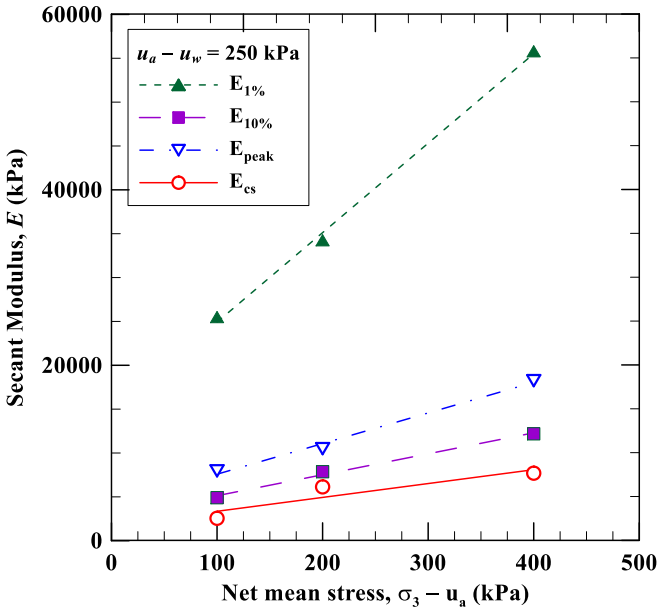

Figure 3.72 Secant stiffness moduli, $E_{1\%}$, $E_{10\%}$, E_{peak}, and E_{cs} variation for s = 250 kPa

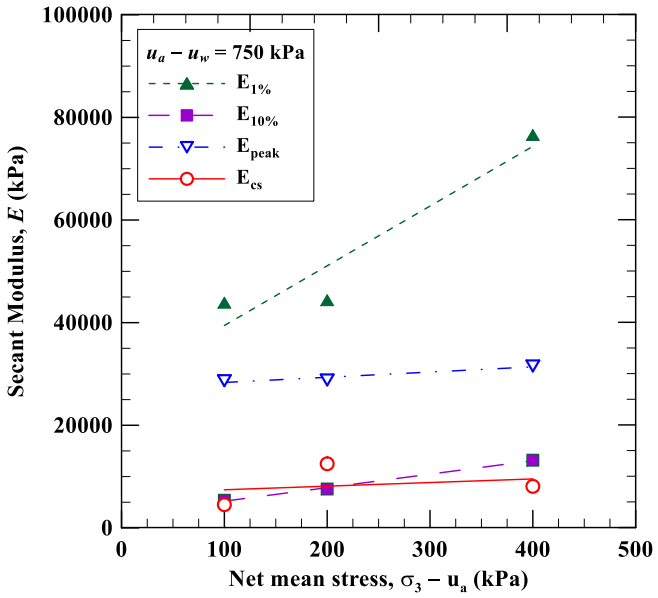

Figure 3.73 Secant stiffness moduli, $E_{1\%}$, $E_{10\%}$, E_{peak}, and E_{cs} variation for s = 750 kPa

Figures 3.74 and 3.75 show the variation of $E_{1\%}$ and $E_{10\%}$ with net confining pressure for varying suction. It can be observed that the slope of the lines is identical for all the suction levels.

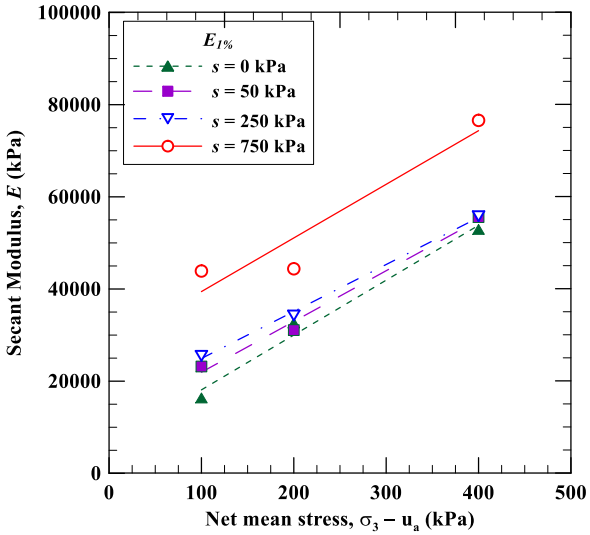

Figure 3.74 Variation of $E_{1\%}$ with net confining pressure for varying suction

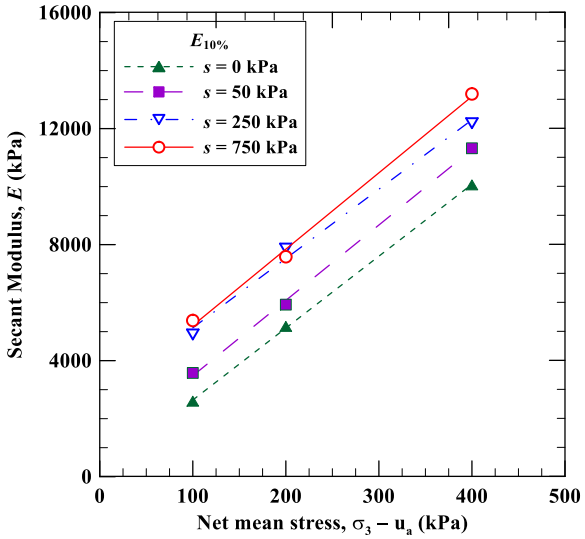

Figure 3.75 Variation of E_{cs} with net confining pressure for varying suction

3.10.10 *Effect of Suction on Cohesion Intercept*

Total cohesion is the sum of effective cohesion and apparent cohesion. The difference between the shear strength of saturated and unsaturated soil is mainly due to the variation in the value of apparent cohesion intercept. Vilar et al. (2006) had proposed a hyperbolic equation that estimates the value of total cohesion intercept based on the suction and effective cohesion of the saturated soil. The model uses a pair of curve-fitting parameters (i.e. *a* and *b*), which is determined by plotting $\psi/(c(\psi) - c')$ for unsaturated soils ($\psi > 0$).

The hyperbolic equation is as follows:

$$c(\psi) = c' + \frac{\psi}{(a+b\psi)} \tag{3.21}$$

where, $c(\psi)$ is the cohesion intercept, which is a function of suction, $\psi = (u_a - u_w)$ and *a* and *b* are the curve fitting parameters. Figure 3.76 shows the best-fit line for the experimental data points. The values of cohesion intercept were obtained from the Mohr's stress circle for *s* = 50, 250 and 750 kPa. The variation of cohesion intercept using Vilar et al. (2006) model and the experimental data are shown in Fig. 3.77. It can be observed that the model shows a good fit with the experimental data.

Figure 3.78 shows the shear strength prediction by using the shear strength parameters of saturated soil (c' and φ') and the cohesion intercept variation with suction using Vilar et al. (2006) model. The shear strength of unsaturated soil was

computed using the modified Mohr-Coulomb Failure Criterion by Fredlund and Morgenstern (1977). The actual experimental points were also plotted and the shear strength values were shown in Fig. 3.78. It can be observed that the prediction is quite close to the actual observed strength.

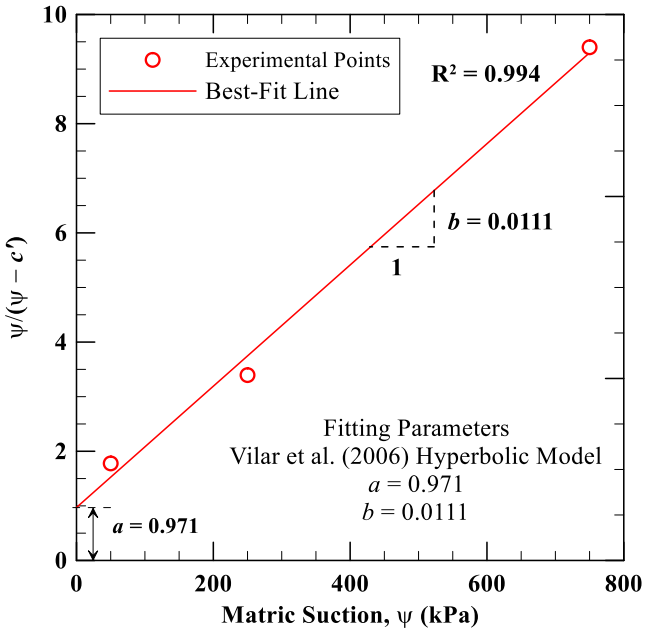

Figure 3.76 Evaluation of best-fitting parameters for Vilar et al. (2006) model

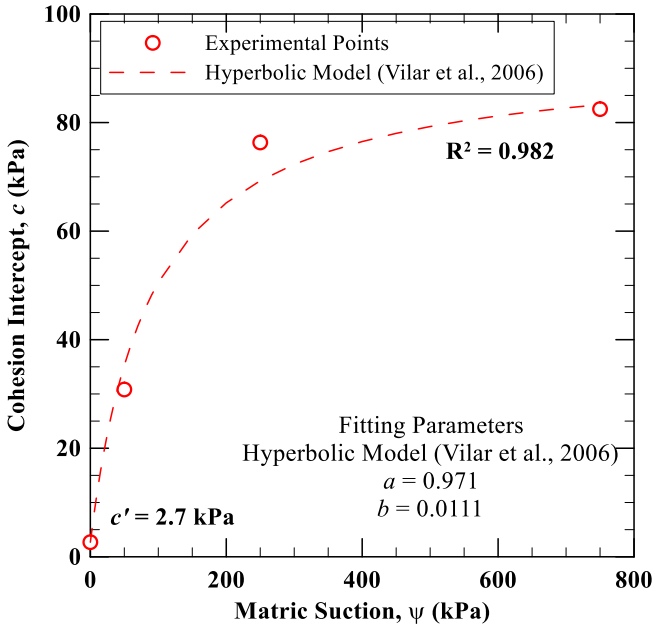

Figure 3.77 Variation of the cohesion intercept with matric suction using Vilar et al. (2006) model

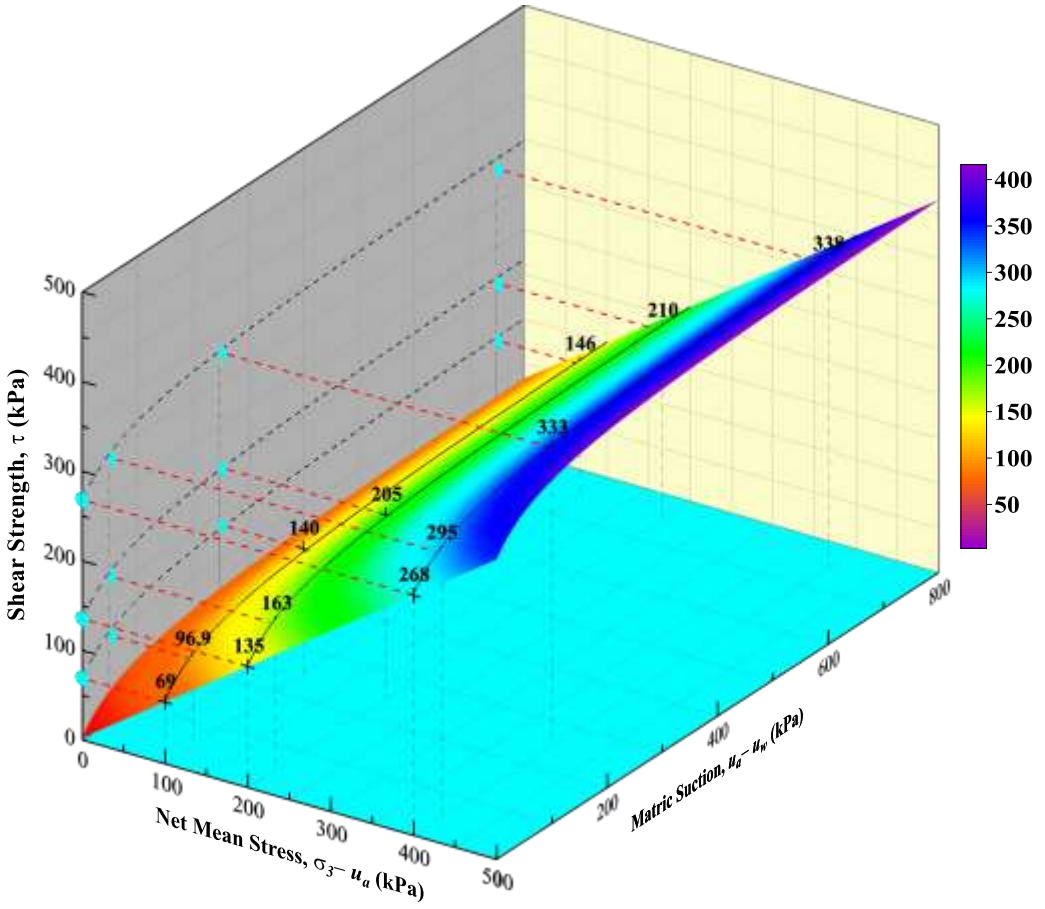

Figure 3.78 The prediction of strength from shear strength parameters of saturated soil and the cohesion intercept variation with matric suction using Vilar et al. (2006) model

3.10.11 *Variation of Angle of Internal Friction due to Suction*

Houston et al. (2008) postulated a hyperbolic relation to estimate the value of the angle of internal friction due to suction, φ^b. The hyperbolic equation is as follow:

$$\varphi^b = \varphi' - \left(\frac{\psi^*}{a+b\psi^*}\right) \tag{3.22}$$

where, φ' = angle of internal friction

$\psi^* = \psi - \text{AEV} = (u_a - u_w) - \text{AEV}$

and *a* and *b* are the fitting parameters.

The fitting parameters, *a* and *b* are obtained by plotting ψ^* against $\psi^*/(\phi' - \phi^b)$ and determining the y-axis intercept (*a*) and slope (*b*) of the best-fit line. The experimental data, obtained from the series of triaxial tests, has been used to determine fitting parameters, *a* and *b*, as shown in Fig. 3.79. The variation of ϕ^b with suction and the experimental data is shown in Fig. 3.80. It shows reasonable fit with the experimental data. Also, the behavior of experimental value of ϕ^b is in correspondence with that of Fredlund and Morgenstern (1977). If the air-entry value (AEV) of the soil is known, Eq. 3.22 could be used to estimate the shear strength of unsaturated soils for varying matric suction.

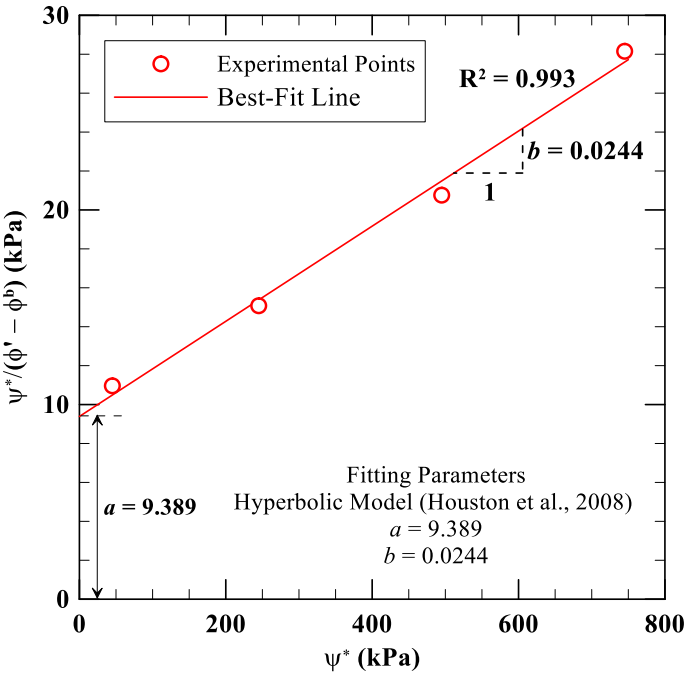

Figure 3.79 Evaluation of best-fitting parameters for Houston et al. (2008) model

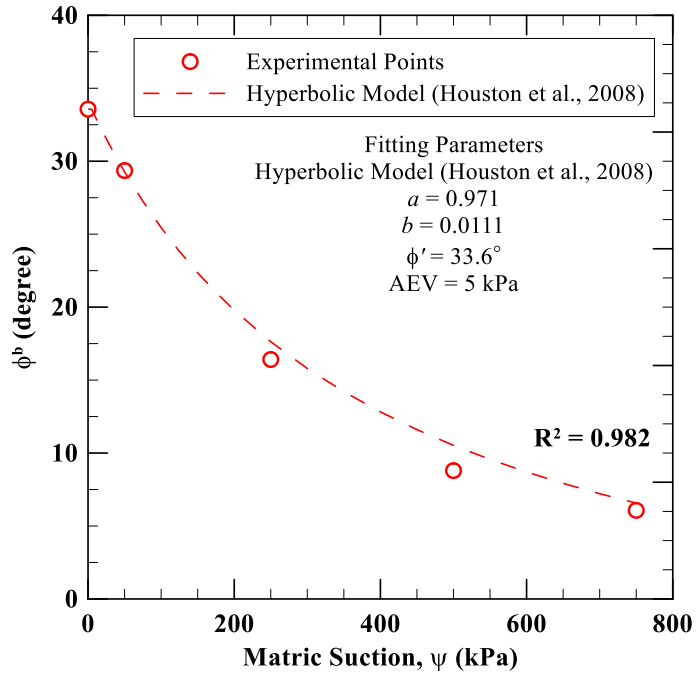

Figure 3.80 Variation of ϕ^b with matric suction using Houston et al. (2008) model

3.10.12 *Shear Strength Prediction based on SWCC*

The prediction of the shear strength of unsaturated soil using triaxial tests is an elaborate process, which requires expensive instruments and is time-consuming. Therefore, several researchers have attempted to use the SWCC and the shear strength parameters of saturated soils to predict the shear strength of unsaturated soils (Vanapalli et al., 1996; Fredlund et al., 1996; Oberg and Sallfors, 1997; Khalili and Khabbaz, 1998; Bao et al., 1998; Han and Vanapalli, 2016).

Fredlund et al. (1996) proposed the following equation to predict the shear strength of unsaturated soil from saturated shear strength parameters (c' and φ') and the SWCC of the soil.

$$\tau = c' + (\sigma - u_a)tan\ \varphi' + (u_a - u_w)[\Theta(u_a - u_w)]^{\kappa} \tan\ \varphi' \qquad (3.23)$$

where Θ = normalized volumetric water content = θ/θ_s and κ = fitting parameter used for obtaining best-fit curve between the observed and predicted values.

Vanapalli and Fredlund (1996) (Method I) proposed a non-linear relationship for estimating the shear strength of unsaturated soil using the following expression:

$$\tau_f = c' + (\sigma - u_a)\ tan\varphi' + [(u_a - u_w)\ \Theta^{\kappa}\ tan\varphi'] \qquad (3.24)$$

Vanapalli et al. (1996) (Method II) proposed the following model to predict the shear strength of unsaturated soil by eliminating the fitting parameter, κ and modifying Eq. 3.24,

$$\tau_f = c' + (\sigma - u_a)tan\varphi' + (u_a - u_w)\left[\left(\frac{\theta-\theta_r}{\theta_s-\theta_r}\right)tan\emptyset'\right] \qquad (3.25)$$

where, θ = volumetric water content,

θ_s = saturated volumetric water content, and

θ_r = residual volumetric water content that can be estimated from the soil water characteristic curve.

Oberg and Sallfors (1997) suggested a similar model involving the degree of saturation (*S*) for sands and silts, which is as follows:

$$\tau_f = c' + (\sigma - u_a)\, tan\varphi' + (u_a - u_w)(S \tan \varphi') \qquad (3.26)$$

Bao et al. (1998) extended the modified shear strength equation (Fredlund and Morgenstern, 1977) for predicting the shear strength of unsaturated soils. The equation suggested is as follows:

$$\tau_f = c' + (\sigma - u_a) \tan \varphi' + (u_a - u_w)\left(\frac{\log(u_a-u_w)_r - \log(u_a-u_w)}{\log(u_a-u_w)_r - \log(u_a-u_w)_b}\right)(\tan \varphi') \qquad (3.27)$$

where, $(u_a - u_w)_r$ = residual suction and $(u_a - u_w)_b$ = air-entry value (AEV).

Khalili and Khabbaz (1998) proposed a model by using the Bishop's effective stress parameter, χ to predict the shear strength of the soil

$$\tau_f = c' + (\sigma - u_a) \tan \varphi' + (u_a - u_w)(\chi \tan \varphi') \qquad (3.28)$$

where,

$$\chi = \left[\frac{(u_a-u_w)_f}{(u_a-u_w)_b}\right]^{-\eta} \qquad (3.29)$$

The slope of the calibration lines, which were determined from a set of 14 soils, was observed to be 0.4 for clayey soils to 0.65 for sandy soils, but there were a few exceptions. An average value for fitting parameters, $\eta = 0.55$ was suggested for all soils.

The experimental results obtained from the series of triaxial tests have been used to investigate the performance of these above-mentioned models for the test soil. The predictions from the above models have been shown in Table 3.6, along with the experimental data, obtained from this research. The fitting parameter, η for the Khalili and Khabbaz (1998) model was assumed as 0.45 for silts, to appropriately fit the data, instead of the generic fitting value of 0.55 for all soils.

The predictions of the above models have been shown in Fig. 3.81 – 3.86. The predictions have been compared with the experimental results for $(\sigma - u_a) = 200$ kPa. It is observed that the Bao et al. (1998) provided the best prediction for the silty soil. However, the remaining models performed satisfactorily for matric suction less than 250 kPa.

Table 3.6 Shear strength predictions from SWCC

Matric suction, *s* (kPa)	τ_{exp} (kPa)	τ_{model} (kPa)					
		Fredlund (1996)	Vanapalli and Fredlund (1996) - I	Vanapalli and Fredlund (1996) - II	Oberg and Sallform (1997)	Khalili and Khabbaz (1998)	Bao et al. (1998)
0	135.39	135.38	135.38	135.38	135.38	135.38	135.38
50	163.02	155.22	154.68	152.24	155.27	147.15	155.69
250	204.53	193.16	193.39	179.99	202.56	163.9	192.00
750	210.06	250.85	254.13	218.38	295.53	187.57	213.24

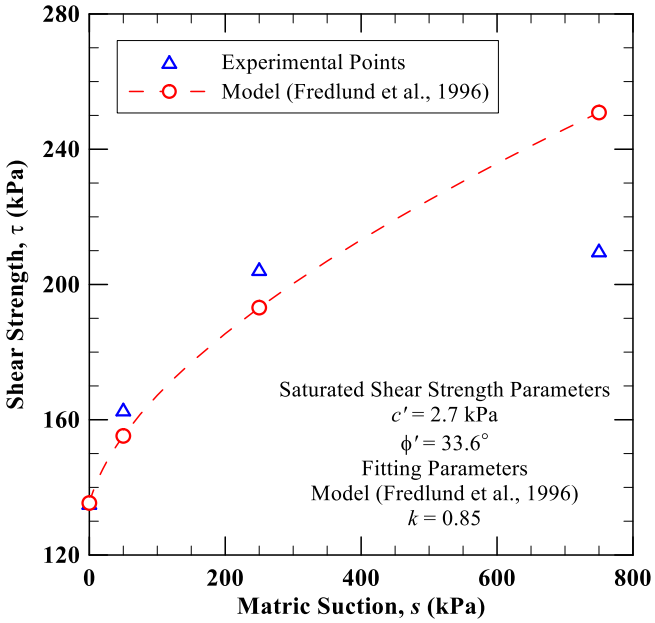

Figure 3.81 Experimental and predicted shear strength from SWCC using Fredlund et al. (1996)

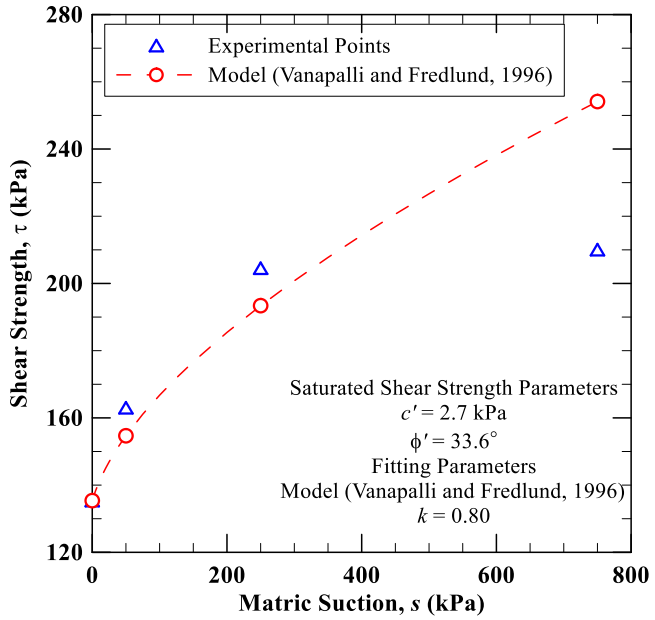

Figure 3.82 Experimental and predicted shear strength from SWCC using Vanapalli and Fredlund (1996) model (Method I)

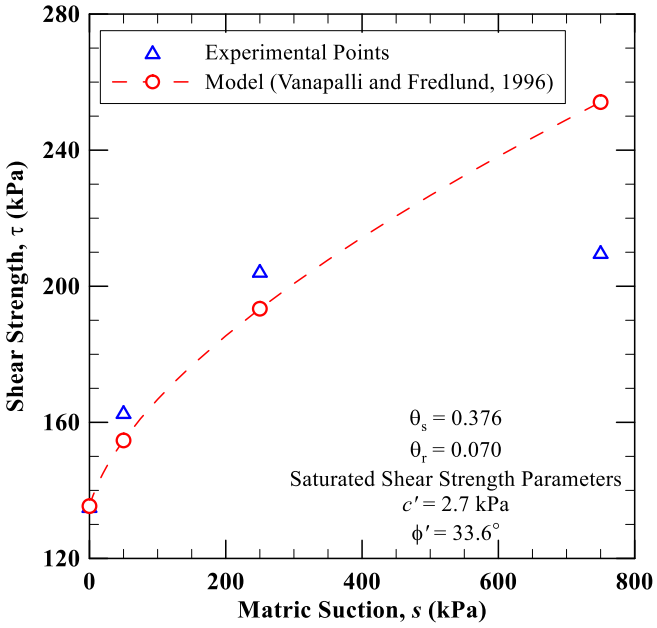

Figure 3.83 Experimental and predicted shear strength from SWCC using Vanapalli and Fredlund (1996) model (Method II)

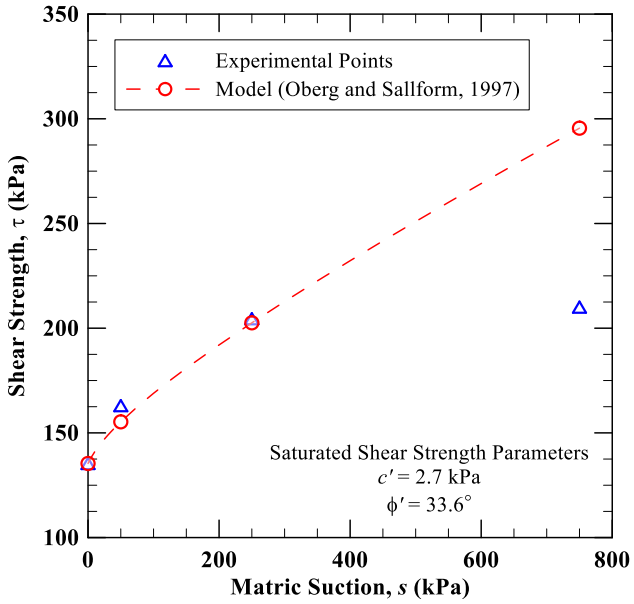

Figure 3.84 Experimental and predicted shear strength from SWCC using Oberg and Sallfors (1997) model

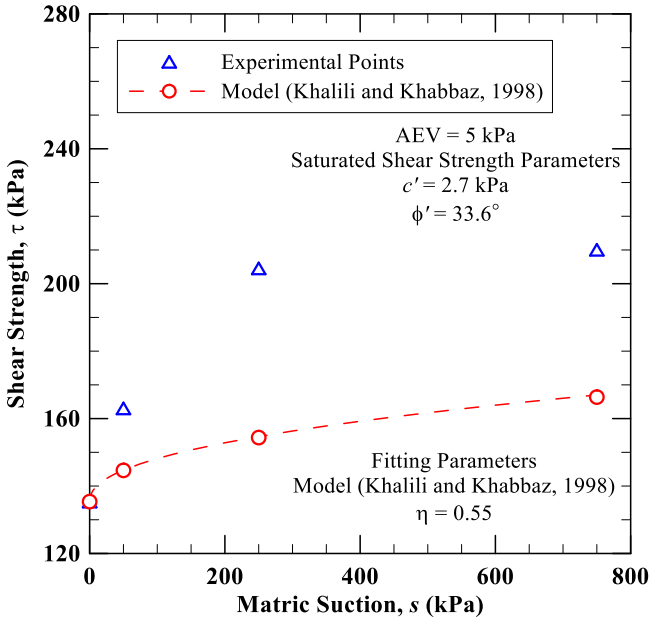

(a.)

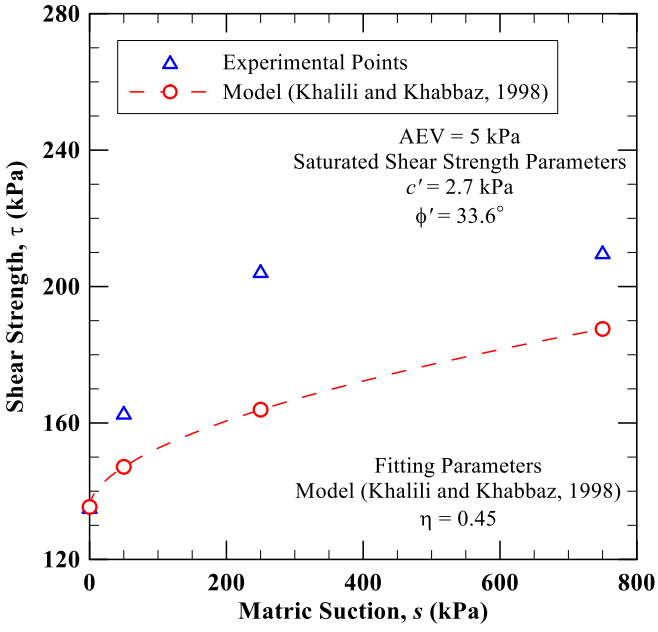

(b.)

Figure 3.85 Experimental and predicted shear strength from SWCC using Khalili and Khabbaz (1998) model for (a) η = 0.55, and (b) η = 0.45

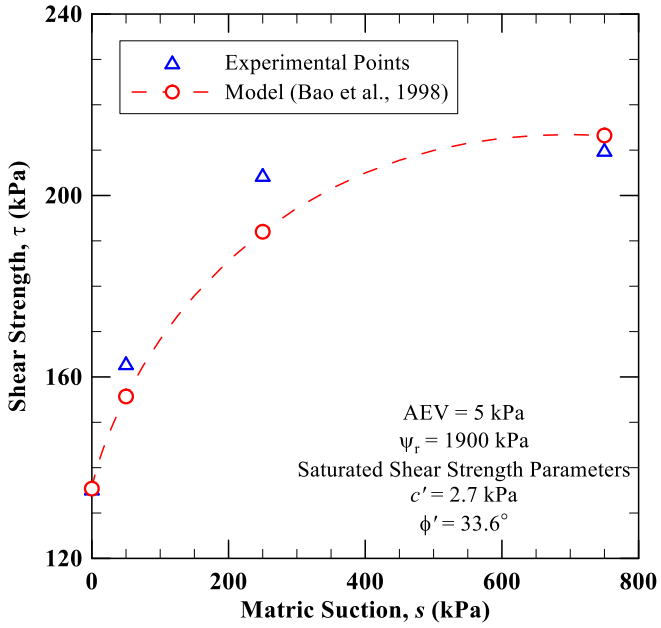

Figure 3.86 Experimental and predicted shear strength from SWCC using Bao et al. (1998) model

3.10.13 *Effect of Suction on Dilation Angle*

Dilatancy of soils is a phenomenon by which the volume of the soil increases during shearing. Dilatancy generally occurs in dense sands and silts (Holtz and Kovacs, 1981). Theoretically, a material showing dilatancy may behave as a compressive material if the confining pressure is increased beyond its pre-consolidation pressure (Holtz and Kovacs, 1981). The term dilatancy of soils was initially identified by Reynolds (1885) and it influences the shear strength of soil. Hence, the study of dilatancy is important for the development of accurate models for predicting the behavior of dense soil. Also, the dilation represents the plastic

behavior of the soil (Salgado, 2006). This indicates that determination of dilatancy is essential for predicting the elasto-plastic behavior of the soils.

Rowe (1962) defined dilatancy of a soil specimen as the magnitude of the ratio of increase in volumetric strain to the corresponding increase in major principal strain. Generally, the dilatancy is characterized by the dilation angle, ψ. Therefore,

$$\psi = \ tan^{-1}\left(\frac{d\varepsilon_v}{d\varepsilon_1}\right) = \ tan^{-1}\left(\frac{\dot{\varepsilon_v}}{\dot{\varepsilon_1}}\right) \tag{3.30}$$

where, ε_v = volumetric strain, ε_1 = major principal strain

Bolton (1984) suggested an empirical expression for determining the peak dilatancy angle of soils, ψ_p:

$$\varphi_p - \varphi_c = 0.8(\psi_p) \tag{3.31}$$

where, ϕ_p and ϕ_c are the peak and critical state friction angle of soil.

Equation 3.31 is modified to the following expression, for triaxial compression:

$$\varphi_p - \varphi_c = 0.5(\psi_p) \tag{3.32}$$

Since the angle of dilation is expected to vary with suction and net confining pressure, the Eqs. 3.31 and 3.32 are not used in this study. The research of unsaturated soils undergoing dilative behavior during shearing is rare. Hence, the development of advanced computational models to predict the behavior of

unsaturated soils demonstrating dilation has been impeded, due to lack of experimental data to calibrate the predictive models.

In this research, the angle of dilation, ψ has been investigated using the experimental data obtained from the series of triaxial tests. Few of the most common methods for determination of dilation angle have been considered.

Method 1: The dilation angle, ψ, defined by Rowe (1962):

$$\psi = \tan^{-1}\left(\frac{\dot{\varepsilon_v}}{\dot{\varepsilon_1}}\right) \tag{3.33}$$

Method 2: Been and Jefferies (2004) defined the dilatancy angle as:

$$\psi = \tan^{-1}\left(\frac{\dot{\varepsilon_v}}{\dot{\gamma}}\right) \tag{3.34}$$

where, γ = shear strain.

Method 3: Vermeer and de Borst (1984) and later, Schanz and Vermeer (1996) defined dilatancy angle as:

$$\psi = \sin^{-1}\left(-\frac{\dot{\varepsilon}_v/\dot{\varepsilon}_1}{2-\dot{\varepsilon}_v/\dot{\varepsilon}_1}\right) \tag{3.35}$$

Recently, Strahler et al. (2016) and Esposito and Andrus (2017) had used Method 3 to compute the dilation angle.

The peak dilation angles were computed using the above methods and tabulated in Table 3.7 for all the triaxial tests. The peak dilation angle was generally observed to occur when the peak stress is achieved, and the time of development of

peak stress, coincides with the initiation of dilation, especially for suction greater than 250 kPa.

The peak dilation angles were predicted to be the highest by Method – I, while the Method – III predicted the least values.

Table 3.7 Experimental values of peak dilation angle

σ_3-u_a (kPa)	Suction (kPa)	Method 1		Method 2		Method 3	
		$\frac{\dot{\varepsilon_v}}{\dot{\varepsilon_1}}$	ψ (°)	$\frac{\dot{\varepsilon_v}}{\dot{\varepsilon_\gamma}}$	ψ (°)	$\frac{\dot{\varepsilon_v}/\dot{\varepsilon_1}}{2-\dot{\varepsilon_v}/\dot{\varepsilon_1}}$	ψ (°)
100	0	0.1250	7.13	0.0810	4.63	0.0588	3.37
	50	0.2041	11.54	0.1250	7.13	0.0926	5.31
	250	0.2541	14.26	0.1566	8.90	0.1127	6.47
	750	0.3600	19.80	0.2025	11.45	0.1525	8.77
200	0	0.1240	7.07	0.0760	4.35	0.0584	3.35
	50	0.1895	10.73	0.1286	7.33	0.0865	4.97
	250	0.2600	14.57	0.1590	9.03	0.1150	6.61
	500	0.3110	17.28	0.1870	10.59	0.1346	7.73
	750	0.3140	17.43	0.1890	10.70	0.1357	7.80
400	0	0.1125	6.42	0.0650	3.72	0.0533	3.05
	50	0.1263	7.20	0.0740	4.23	0.0594	3.41
	250	0.1542	8.77	0.0990	5.65	0.0716	4.10
	750	0.1826	10.35	0.1127	6.43	0.0837	4.80

Figures 3.87 – 3.89 show the variation of peak dilation angle with matric suction for the net confining pressure of 100, 200 and 400 kPa, respectively, using all the three methods. Second-order polynomials were used to best-fit each curve. The Method-I showed very high values of dilation angle as compared to Methods-II and III. However, all the methods showed a similar general trend for variation of dilation angle with suction. It was observed that the dilation angle generally

increased with increasing suction till a suction of 500 kPa, beyond which the peak dilation angle remained constant.

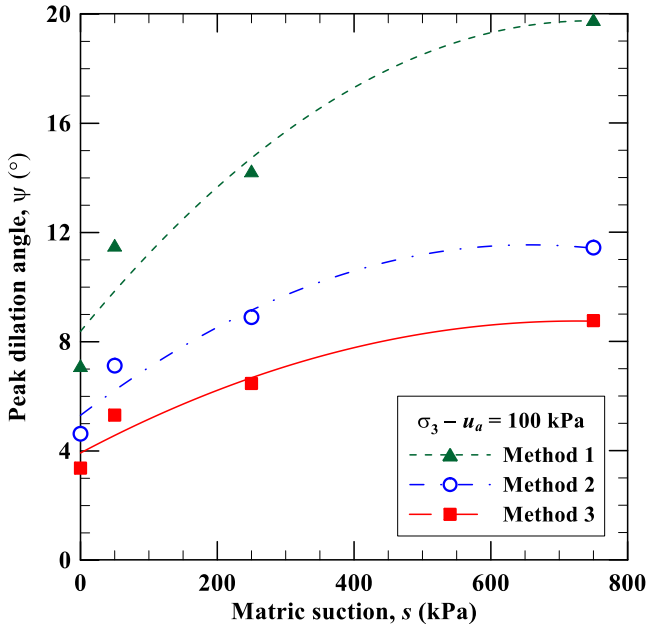

Figure 3.87 Effect of matric suction on dilation angles at net confining pressure of 100 kPa

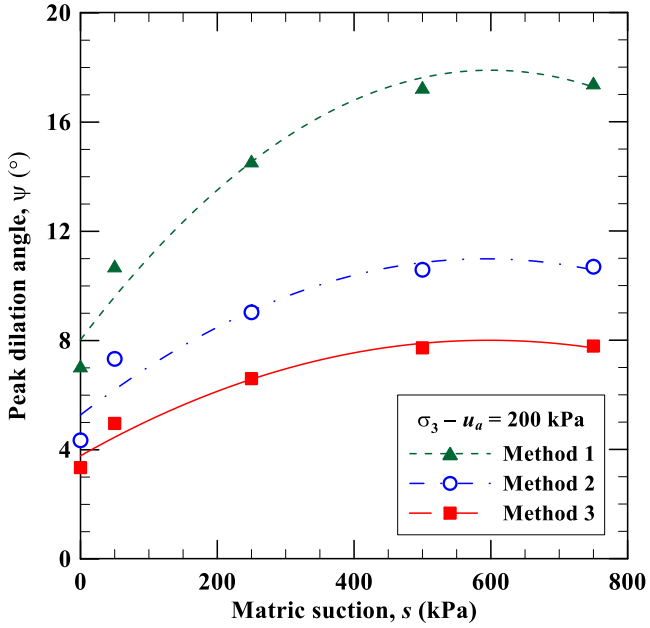

Figure 3.88 Effect of matric suction on dilation angles at net confining pressure of 200 kPa

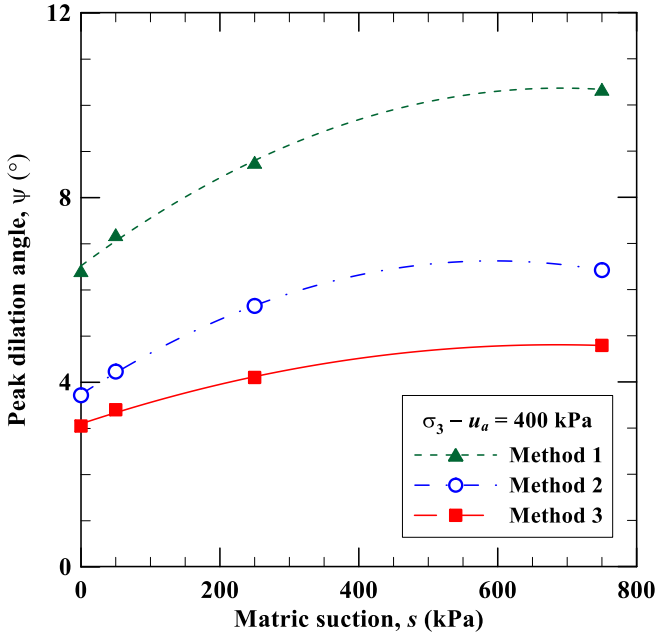

Figure 3.89 Effect of matric suction on dilation angles at net confining pressure of 400 kPa

3.10.14 *Effect of Confining Pressure on Dilation Angle*

The variation of dilation angle with net confining pressure for varying matric suction using Methods-I, II and III, were shown in Figs. 3.90, 3.91, and 3.92, respectively. It was observed that for all the three methods, the increase in net confining pressure resulted in the decrease of peak dilation angle, especially for an increase of net confining pressure from 200 kPa to 400 kPa. The magnitude of the slope of peak dilation angle curve, with respect to net confining pressure, increases with increase in matric suction. It was also observed that for low net confining pressure the influence of matric suction on the dilation angle was significant, however, at high net confining pressure the dilation angles are quite similar for varying suction levels.

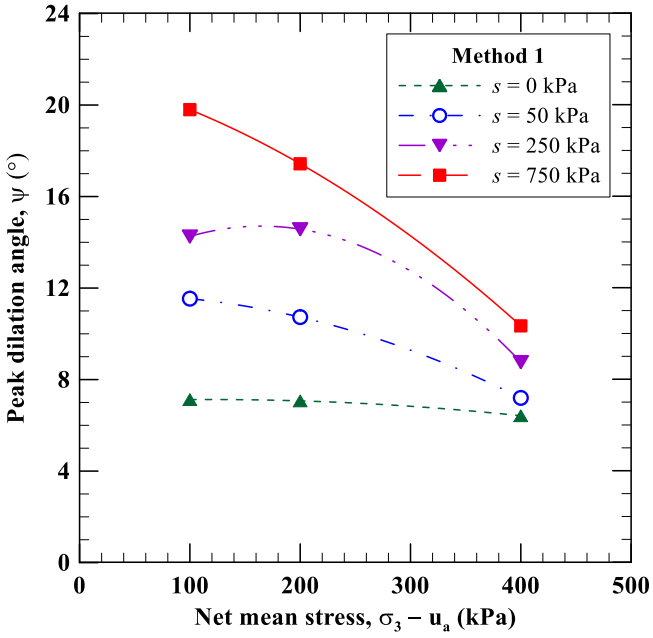

Figure 3.90 Effect of net confining pressure on dilation angles using Method I

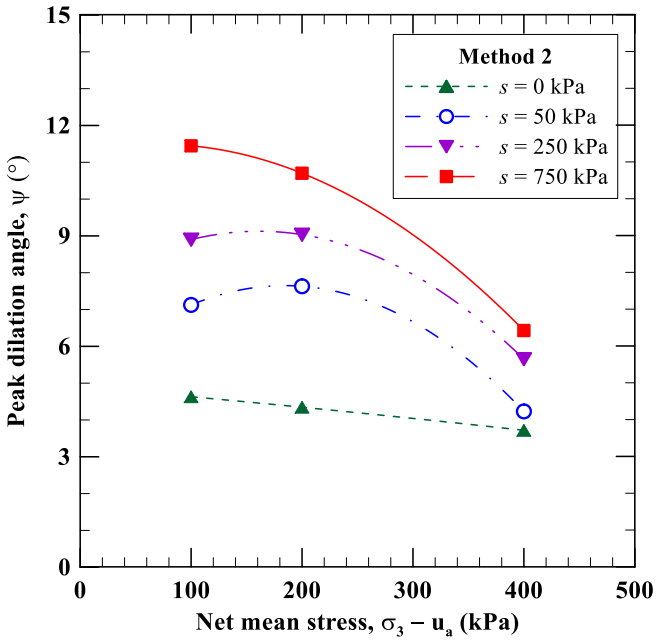

Figure 3.91 Effect of net confining pressure on dilation angles using Method II

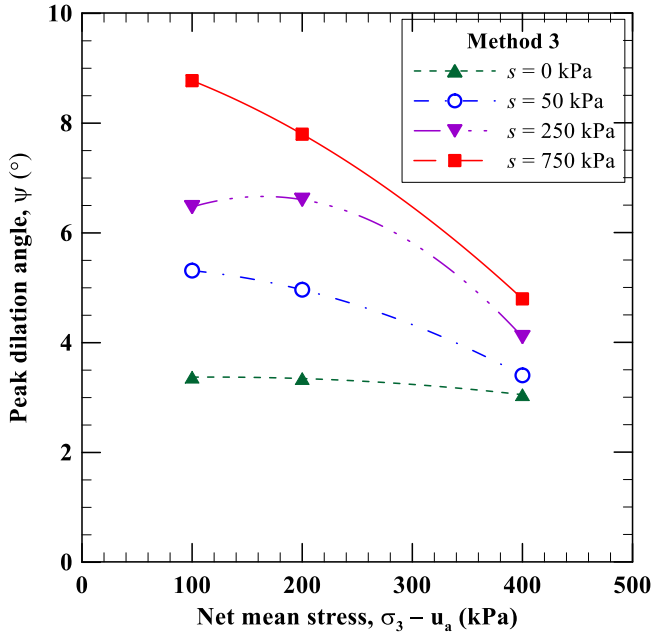

Figure 3.92 Effect of net confining pressure on dilation angles using Method III

3.11 Summary

The basic laboratory test results including, soil classification, determination of the maximum dry density and the optimum moisture content, selection of compaction technique to obtain consistent replicates and soil water characteristics curve are discussed. The modifications to a conventional triaxial setup and its advanced features are presented. The procedure to conduct a suction-controlled triaxial test on compacted soil specimen using axis-translation technique is described.

A series of consolidated drained triaxial tests on saturated and unsaturated specimens were conducted at the same net confining pressure and matric suction, but varying axial strain rate for shearing, to determine the appropriate strain rate for shearing. Subsequently, an elaborate test series were conducted on saturated and unsaturated specimens at the net confining pressure of 100, 200, and 400 kPa over a suction range of 0 to 750 kPa, using the axis-translation technique. A total of 3 saturated and 10 unsaturated specimens were tested as a part of this series of tests.

The suction-controlled isotropic consolidation, deviator stress and volumetric strain responses for each test were studied in detail, to analyze the variation of stiffness and dilation angle with varying suction and net confining pressure. All the tests were conducted by following the conventional triaxial compression (CTC) stress path to obtain the shear strength parameters of the test soil over the varying suction range.

The major findings are presented in this Chapter. One of the findings which should be specifically mentioned is that at critical state, the increase in strength of the soil with suction may cease to exist after reaching moderate values of suction (s = 250 to 750 kPa), however, for the same range of increase in suction (s = 250 to 750 kPa), the peak strength may increase significantly. The non-linear variation of the angle of internal friction due to suction (φ^b) and the variation of cohesion intercept with matric suction were predicted satisfactorily using well-known models. Additional models were used to compare the experimental results with shear strength predictions using SWCC.

Chapter 4

MONOTONIC MULTISTAGE TRIAXIAL TESTS AND CONSTITUTIVE MODELING

4.1 Introduction

The lack of availability of replicating soil specimens for determination of shear strength using triaxial testing is a common problem which has been attempted to be addressed for years. For unsaturated soil specimen, an additional problem arises due to the complexities involved in its behavior and the enormous time required to perform each suction-controlled triaxial test. These problems, along with the need for sophisticated and expensive equipment to perform triaxial tests on the unsaturated soil specimen, warrant the necessity to develop a testing procedure which could mitigate some of these problems to facilitate the determination of shear strength of unsaturated soil.

Multistage triaxial tests of saturated specimens primarily refer to the loading/unloading of the same specimen over varying confining pressures, to obtain the shear strength parameters from a single test. The review of literature for the multistage triaxial test for saturated and unsaturated soils has been described in section 2.11.

Typically, suction-controlled multistage triaxial tests are performed by loading/shearing the specimen prior to failure at the constant net confining pressure ($\sigma_3 - u_a$), but increasing matric suction ($u_a - u_w$) in subsequent stages by Ho and

Fredlund (1982), Rahardjo et al. (1995), Khalili and Zargarbashi (2010), Khosravi et al. (2011), Leong et al. (2013), Handoko et al. (2013), and Rahardjo et al. (2013, 2014). However, the suction equalization for each new suction level requires additional time, which results in a further delay in the completion of the test. Instead, new specimens could be utilized for each new suction level, while the suction equalization could be carried out outside the triaxial cell to hasten the suction equalization process.

Overall, the time required to complete the triaxial tests is reduced drastically using this approach. Henceforth, in this study, the matric suction is kept constant for each multistage test and the net confining pressure is increased after each loading/unloading sequence, an approach followed by Rahardjo et al. (1995) and Rosone et al. (2016). A similar approach of multistage testing at constant suction but varying net confining pressure was performed using a multi-axial or true triaxial testing device by Macari and Hoyos (2001). However, discussion regarding multi-axial triaxial device is beyond the scope of this research.

In this study, an attempt has been made to conduct a series of suction-controlled multistage triaxial tests under drained conditions and validate these results against conventional (or single-staged) triaxial tests. Moreover, the effect of using multistage triaxial tests on the constitutive modeling for determination of shear strength of unsaturated soils has been investigated in this study. The original framework of the Barcelona Basic Model (BBM) postulated by Alonso et al. (1990)

has been considered to be one of the most popular constitutive models for simulating the behavior of unsaturated soil, especially for normally and lightly overconsolidated soils of low-plasticity. The results from the suction-controlled tests were analyzed and the elastoplastic behavior of the silty soil, like the suction-induced variation in stiffness, pre-consolidation pressure, apparent tensile strength, apparent cohesion, and critical state line (CSL), were studied. These results, and dilatant behavior of soil, would also augment the rather limited research (Ng and Chiu, 2003; Manzanal et al., 2011; Tsiampousi et al., 2013; Solowski and Sloan, 2015; Zhou and Sheng, 2015; Xiong et al., 2016) available on such geomaterials. Thereby, enabling the development of elaborate constitutive models in future.

4.2 Test Program

In this research, all the triaxial tests were performed on consolidated drained specimens of silty soil (ML), which were compacted at the same dry density and moisture content, following CTC stress path. The properties of the soil have been discussed in section 3.2. A multistage test was performed on a saturated specimen at effective confining pressures of 100, 200, and 400 kPa. Two multistage triaxial tests were conducted on unsaturated specimens at the induced suction of 50 kPa and 250 kPa for net confining pressure of 100, 200, and 400 kPa each. Figure 4.1 shows the stress paths followed during the multistage triaxial tests.

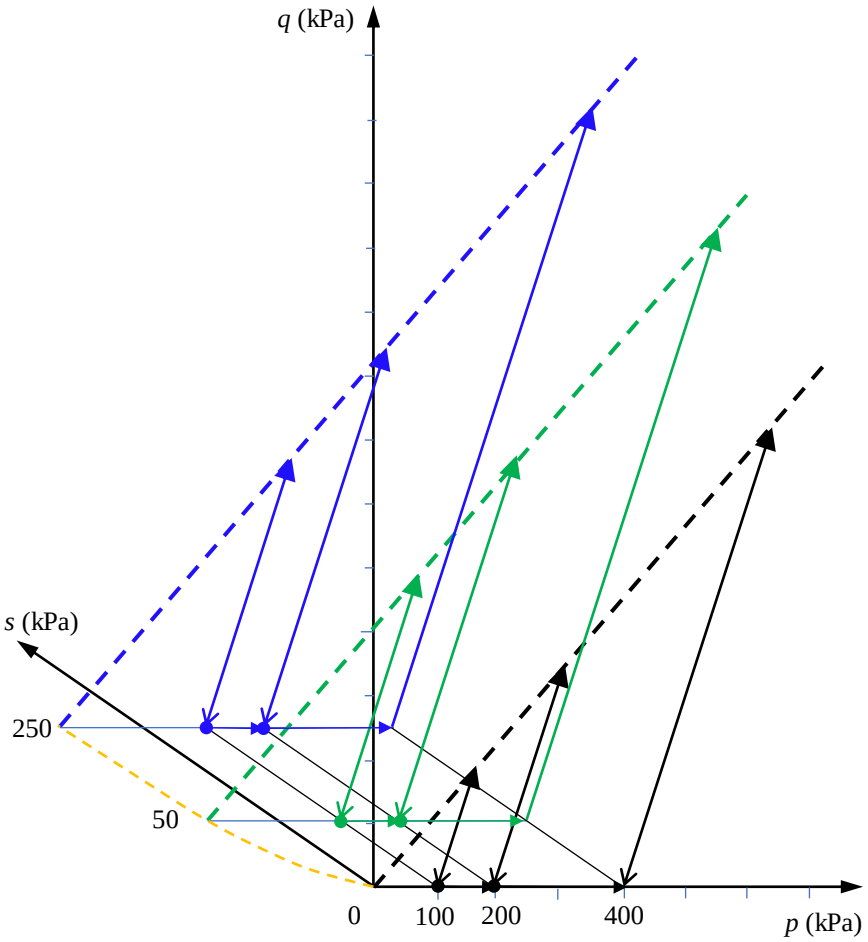

Figure 4.1 Stress path followed during multistage triaxial tests for saturated (s = 0) and unsaturated specimens (s = 50 and 250 kPa)

4.3 Testing Procedure

4.3.1 *Saturated Soil Specimens*

The experimental setup, specimen preparation, and saturation of specimen using back pressure technique for the multistage triaxial tests were the same as that for the single-stage triaxial tests, which have been described in Chapter 3. The

application of the first effective confining pressure (σ_3' = 100 kPa) and subsequent consolidation was also the same as that for the single-stage test.

The saturated specimen was consolidated at an effective confining pressure of 100 kPa by ramping the cell pressure to its target value within 30 seconds. After the consolidation was completed, the specimen was sheared monotonically under drained conditions at a strain rate of 0.05%/min, which was selected based on the independent strain rate studies (mentioned in section 3.9.2). The shearing was stopped before the failure of the specimen, which was based on the criteria for termination of shearing. The details regarding the criteria are provided in section 4.3.3. As soon as the shearing was stopped, the deviator stress was gradually reduced to 5 kPa (i.e., the seating stress). This was done to avoid changes in the volume of the specimen due to sustained stresses near failure, also known as creep (Ho and Fredlund, 1982).

Subsequently, the same specimen was subjected to the next effective confining pressure of 200 kPa by increasing the cell pressure in 30 seconds. The drainage valves were opened during consolidation, to allow for the dissipation of excess pore water pressure. After the volume change of the specimen reaches a constant value, which was equal to the water flowing out of the specimen, the consolidation was assumed to be completed. A minimum of 24 hours was provided for consolidation to occur. The consolidated specimen was loaded monotonically until just before its failure. The termination point for stopping the shearing stage

was based on the criteria mentioned in section 4.3.3. The deviator stress was then reduced gradually to the seating stress of 5 kPa.

Finally, the same specimen was subjected to the highest effective confining pressure of 400 kPa by increasing the cell pressure in 30 seconds and allowing the specimen to consolidate till the volume change of the specimen became constant and was equal to the outflow of water from the specimen. Subsequently, the specimen was sheared till the specimen failed. The stress path of a multistage triaxial test of a saturated specimen was similar to that of an unsaturated specimen (shown in Fig. 4.2), except for the application of suction.

4.3.2 *Unsaturated Soil Specimens*

The entire procedure for suction equalization is the same for both conventional and multistage triaxial tests. The process of suction equilibration is explained in detail in section 3.7.3. The stress path followed during a typical multistage triaxial test on a specimen at an induced suction of 50 kPa is shown in Fig. 4.2. The point 'A' in Fig. 4.2 denotes the point in the p'-q-s space which corresponds to the suction equilibrated soil specimen ($\sigma_3 - u_a = 10$ kPa and $s = u_a - u_w = 50$ kPa).

After equilibration of suction was achieved, the first isotropic net confining pressure ($\sigma_3 - u_a = 100$ kPa) was applied by increasing the cell pressure (σ_3) at the rate of 5 kPa/h (stress path 'A' to 'B' in Fig. 4.2). The consolidation was completed after 24 h or when the water content change was less than 0.04%/day, whichever

occurred later (Point ‘B’ in Fig. 4.2). Subsequently, the sample was loaded (stress path ‘B’ to ‘C’ in Fig. 4.2) before its failure was reached (Point ‘C’ in Fig. 4.2), which was decided based on the variation of tangent modulus of the stress-strain response and the volumetric strain response.

Subsequently, the approach used by Ho and Fredlund (1982) was followed to minimize the creep in the soil, where the deviator stress was gradually reduced to a seating stress of 5 kPa (Point ‘B′’ in Fig. 4.2). The second isotropic net confining pressure ($\sigma_3 - u_a$= 200 kPa) was applied by increasing the cell pressure (σ_3) at a rate of 5 kPa/h (stress path ‘B′’ to ‘D’ in Fig. 4.2) and after consolidation was completed (Point ‘D’ in Fig. 4.2), the specimen was again loaded (stress path ‘D’ to ‘E’ in Fig. 4.2). The loading was stopped prior to failure (Point ‘E’ in Fig. 4.2) and the deviator stress was again gradually reduced to the seating stress equal to 5 kPa (Point ‘D′’ in Fig. 4.2).

Finally, the last isotropic net confining pressure ($\sigma_3 - u_a$= 400 kPa) was applied, by increasing the cell pressure (σ_3) at a rate of 5 kPa/h (stress path ‘D′’ to ‘F’ in Fig. 4.2) and after consolidation (Point ‘F’ in Fig. 4.2), the specimen was loaded monotonically (stress path ‘F’ to ‘G’ in Fig. 4.2) and sheared to failure (Point ‘G’ in Fig. 4.2). Meanwhile, the matric suction was maintained at a constant value, throughout the test. For the sake of uniformity, the rate of cell pressure increase during all phases of isotropic consolidation was kept constant (5 kPa/h),

which was the same as that for the conventional triaxial testing. Moreover, for all stages, the consolidation was allowed for a minimum of 24 hours and the shearing rate for all specimens was 0.003%/min, as obtained from the independent strain rate studies (described in section 3.9.3).

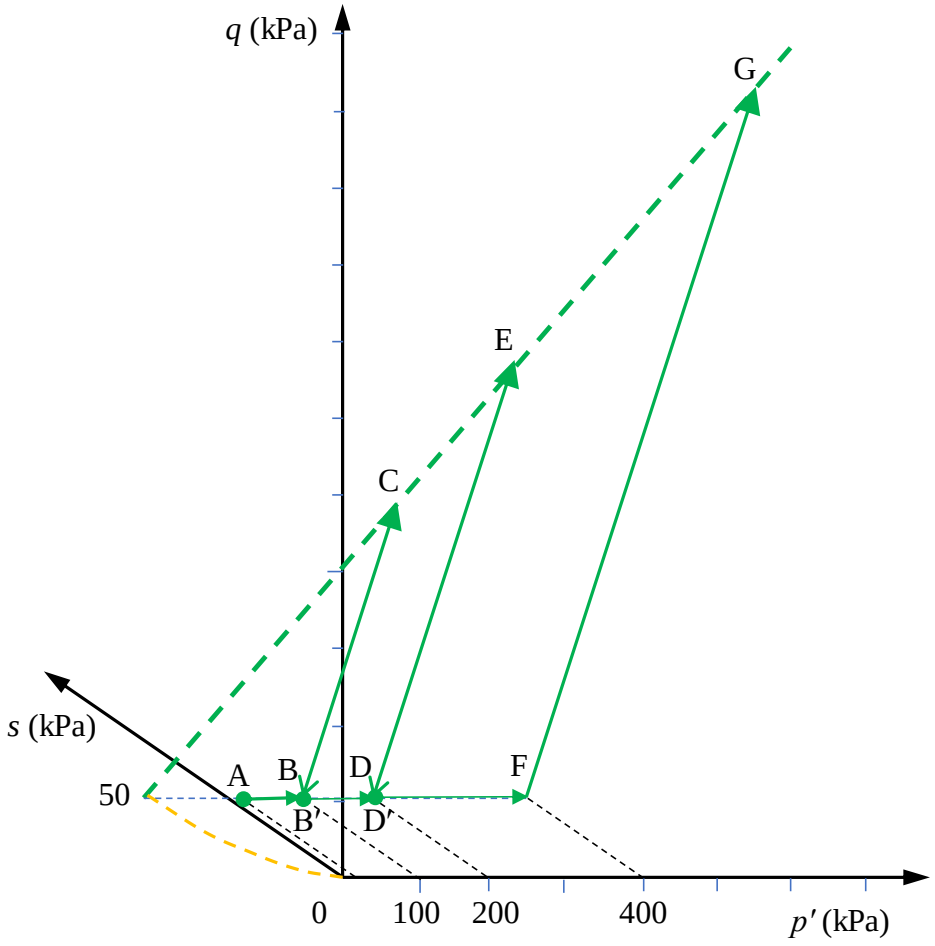

Figure 4.2 Illustration of stress path followed during multistage triaxial test at a suction of 50 kPa

4.3.3 *Selection of Termination Point for Shearing*

One of the most important aspects of the success of multistage testing is the selection of the predefined criterion for stopping a loading stage (Khosravi et al., 2011; Sharma et al., 2012). Any premature stoppage or delay in stoppage may result in under-prediction of deviator stress or failure of the specimen. In the case of under-prediction of deviator stress, the analysis for shear strength parameters may be erroneous. Whereas, the failure of the specimen in the initial confining pressure would result in lower values of deviator stress for any latter confining pressures, which would again result in lower shear strength parameters.

Henceforth, the criterion which is convenient to compute during testing and does not compromise the accuracy of the test has been defined and validated in this research. The tangent modulus of elasticity and the volumetric strain is monitored closely throughout the test. Initially, the modulus of elasticity is very high. After the linear portion of the stress-strain curve, the modulus of elasticity decreases gradually. The criterion for the ratio of the initial modulus (determined by the tangent modulus at an axial strain of 0.25%) to the tangent modulus (E_i/E_r) were 25 and 15 for the net confining pressures of 100 kPa and 200 kPa, respectively (Fig. 4.2a). For the net mean stress of 200 kPa, the selected ratio is lower to prevent accumulation of high plastic strains, as the specimen has been loaded, unloaded, and reloaded by that stage.

Also, the moment at which the volumetric strain becomes negative, which indicates the initiation of dilation was considered as the alternative criterion (Fig. 4.2b). Whenever either of the criteria was satisfied, the shearing for the initial two stages was stopped. Subsequently, the specimen was gradually unloaded and the next confining pressure was applied.

The advantage of having two-fold criteria is that in case the specimen does not dilate, then the relative stiffness criterion can prevent the failure of the specimen. On the other hand, if the material is too brittle, then the specimen suddenly reaches its failure and the tangent modulus might decrease too sharply to terminate the test before failure. In these cases, mostly, it had been observed from conventional (single-stage) triaxial tests that the volume change response shows earlier indications of failure by monitoring the dilation of the soil (Figs. 3.42 – 3.47).

In this chapter, a modified nomenclature system (as compared to Chapter 3) is followed. For the single-stage test, the nomenclature in the form of "CD_*x*_*y*_ss" is followed. Whereas, for multistage tests, "CD_*x*_*y*_ms" is the preferred nomenclature. 'CD' denotes the Consolidated Drained test; '*x*' and '*y*' represent the net confining pressure ($\sigma_3 - u_a$) and the matric suction ($u_a - u_w$) applied in kPa during the test, respectively; and 'ss' and 'ms' represent the single-stage and multistage tests, respectively. Throughout this study, the Cambridge notations were

used for determination of net mean stress $\left(p = \frac{(\sigma_1 + 2\sigma_3)}{3} - u_a\right)$ and deviator stress ($q = \sigma_1 - \sigma_3$).

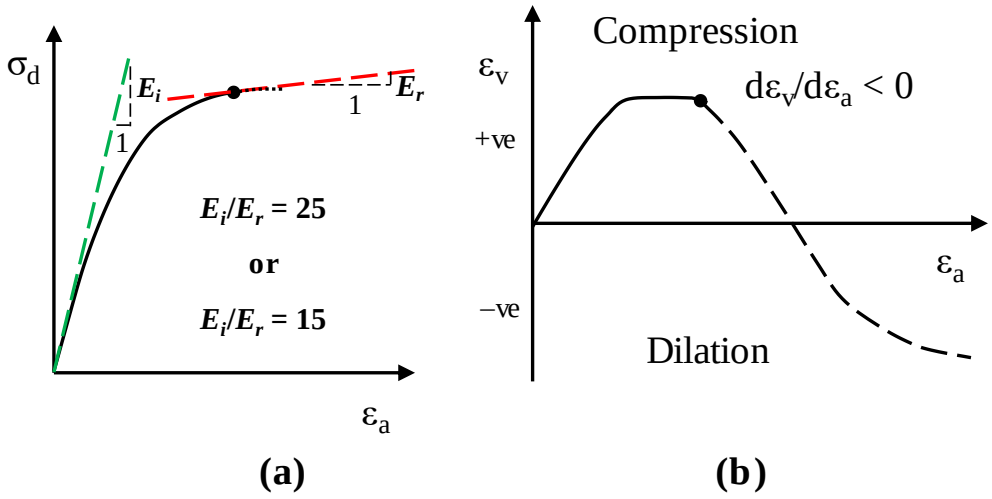

Figure 4.3 Graphical representation of termination point for shearing during multistage triaxial test

4.4 Mechanical Response of Soils subjected to Monotonic Loading using Multistage Test

4.4.1 *Response of Saturated Soil Specimens*

The multistage test was performed on a saturated specimen at three effective confining pressures of 100, 200, and 400 kPa. The initial tangent modulus refers to the tangent modulus determined at an axial strain of 0.25% from the start of shearing stage. The stress-strain response from the shearing stages for the multistage triaxial test at varying effective confining pressure is shown in Fig. 4.4. The stress-strain response shows the increase in deviator stress with an increase in

effective confining pressure. The unloading curves are also shown for the initial two confining pressures of 100 and 200 kPa.

For the initial effective confining pressure of 100 kPa, as the initial tangent modulus of 25 MPa decreases to a constant positive value of 1 MPa (E_i/E_r = 25), the loading was stopped. At this moment, the change in volumetric strain with axial strain was nearly zero ($d\varepsilon_v/d\varepsilon_a \approx 0$ in Fig. 4.5). In this case, the criterion of the relative stiffness of soil (E_i/E_r; described in section 4.3.3) was the critical factor in deciding the stoppage of shearing. Subsequently, the specimen was gradually unloaded, while maintaining the same effective confining pressure.

The next loading stage was initiated and it was stopped when the tangent modulus decreased from 60 MPa to 4 MPa (E_i/E_r = 15), while the change in volumetric strain with axial strain was nearly zero ($d\varepsilon_v/d\varepsilon_a \approx 0$ in Fig. 4.5). Finally, after consolidation at 400 kPa, the specimen is sheared beyond its peak strength.

The volume change response during shearing is shown in the form of volumetric strain response of saturated soil during the shearing stage in Fig. 4.5. The cumulative axial and volumetric strains are shown in Fig. 4.5. Due to the decrease in axial strain during unloading, the starting of the plot for the next shearing stage initiates from a lower value of axial strain as compared to the axial strain corresponding to the moment when the shearing was stopping. Similar observations were made by Rahardjo et al. (1995). It can be observed that at each

new effective confining pressure the soil initially compresses and then for a significant portion of shearing there is no change in the overall volume change of the specimen. However, the specimen dilates if the shearing is continued, as in the case when the effective confining pressure was 400 kPa.

The comparison between the responses observed for single-stage and multistage triaxial tests for saturated soil specimens are discussed later, in section 4.5.1.

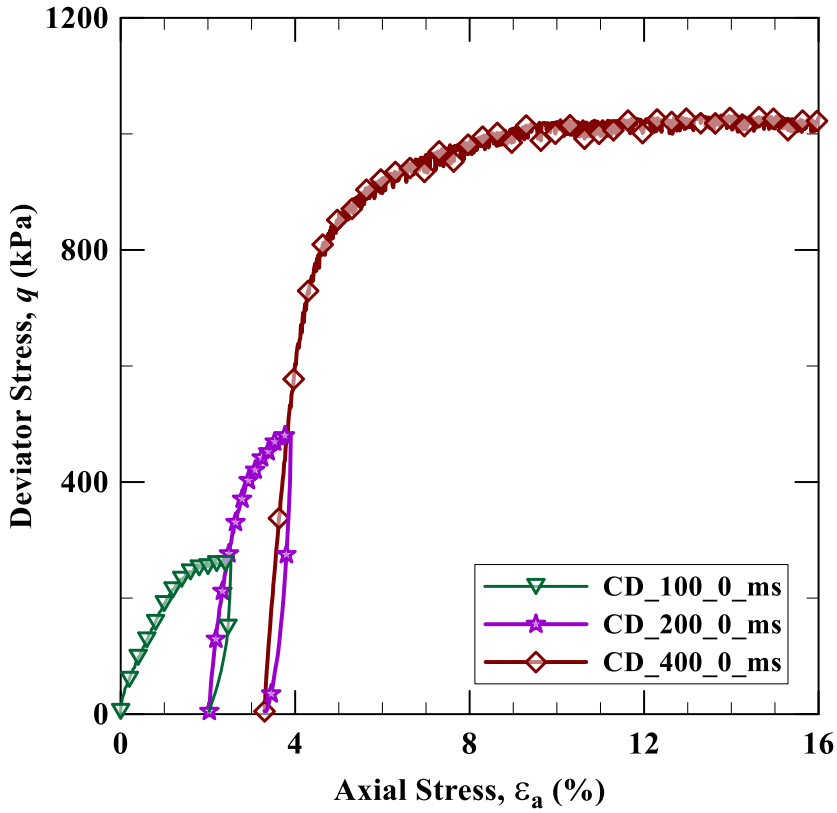

Figure 4.4 Deviator stress response of saturated soil specimen obtained from a multistage triaxial test

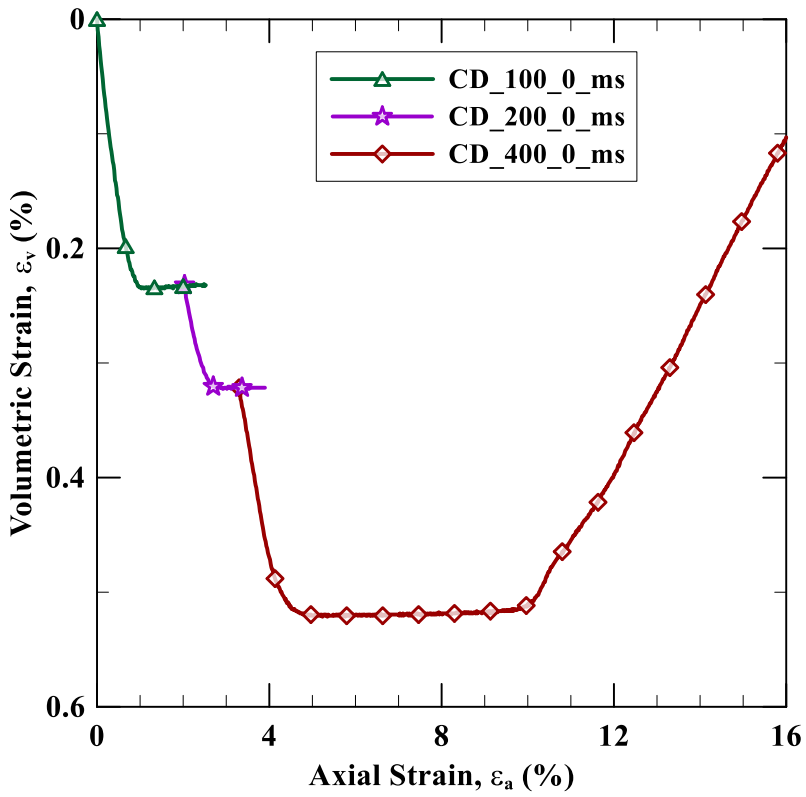

Figure 4.5 Volumetric strain response of saturated soil specimen obtained from a multistage triaxial test

The strength of the soil in saturated condition was determined by plotting the Mohr's circle at the maximum deviator stress obtained during shearing at the initial two effective confining pressures of 100 and 200 kPa. While for the final effective confining pressure of 400 kPa, the deviator stress corresponding to the critical state was considered for plotting the Mohr's circle. The Mohr's circle and the Mohr-Coulomb Failure Envelope are shown in Fig. 4.6. The Mohr-Coulomb Failure Envelope (MCFE) was obtained by plotting the common tangent to the

three Mohr's circles. The effective cohesion (c') and the effective angle of friction angle (φ') were determined to be 3.5 kPa and 33.4°, respectively.

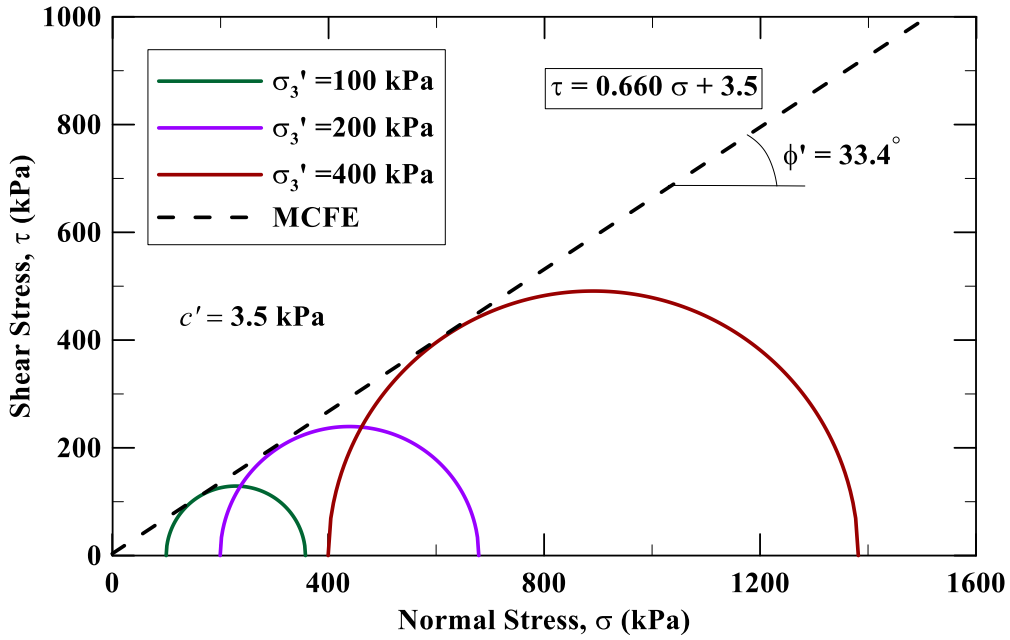

Figure 4.6 Determination of critical shear strength parameters for saturated silt specimen using Mohr-Coulomb failure criterion

4.4.2 *Response of Unsaturated Soil Specimens*

The deviator stress response of the consolidated specimen at constant matric suction of 50 kPa during shearing in drained conditions using multistage triaxial test is shown in Fig. 4.7. The corresponding volumetric strain response for the specimen at constant matric suction of 50 kPa using multistage triaxial test is shown in Fig. 4.8.

The shearing for the first net confining pressure of 100 kPa was stopped when the change in volumetric strain with axial strain decreased to a negative value

($d\varepsilon_v/d\varepsilon_a < 0$ in Fig. 4.8). While the tangent modulus decreased from 24.7 MPa to 1.2 MPa ($E_i/E_r = 20 < 25$, in Fig. 4.7). Hence, the criterion of the relative stiffness of soil (described in section 4.3.3) was not the critical factor in deciding the stoppage of shearing. Instead, the criteria for prevention of dilation of the specimen was the decisive factor.

The second shearing stage at a net confining pressure of 200 kPa was stopped when the tangent modulus decreased from 72.7 MPa to 4.8 MPa (E_i/E_r = 15.1 in Fig. 4.7), while the change in volumetric strain with axial strain was nearly zero ($d\varepsilon_v/d\varepsilon_a \approx 0$ in Fig. 4.8). Hence, for the second shearing stage, the relative stiffness of the soil was the critical factor in deciding the stoppage of shearing. Finally, after consolidation at a net confining pressure of 400 kPa, the specimen was sheared beyond its peak strength. The increase of initial tangent modulus with subsequent stages was also observed by Rahardjo et al. (1995).

Figure 4.7 shows that at each new effective confining pressure the soil initially compresses and then for a substantial portion of shearing there is no change in the overall volume change. However, the specimen showed dilation if the shearing was continued further, as in the case when the net confining pressure was 100 kPa and 400 kPa.

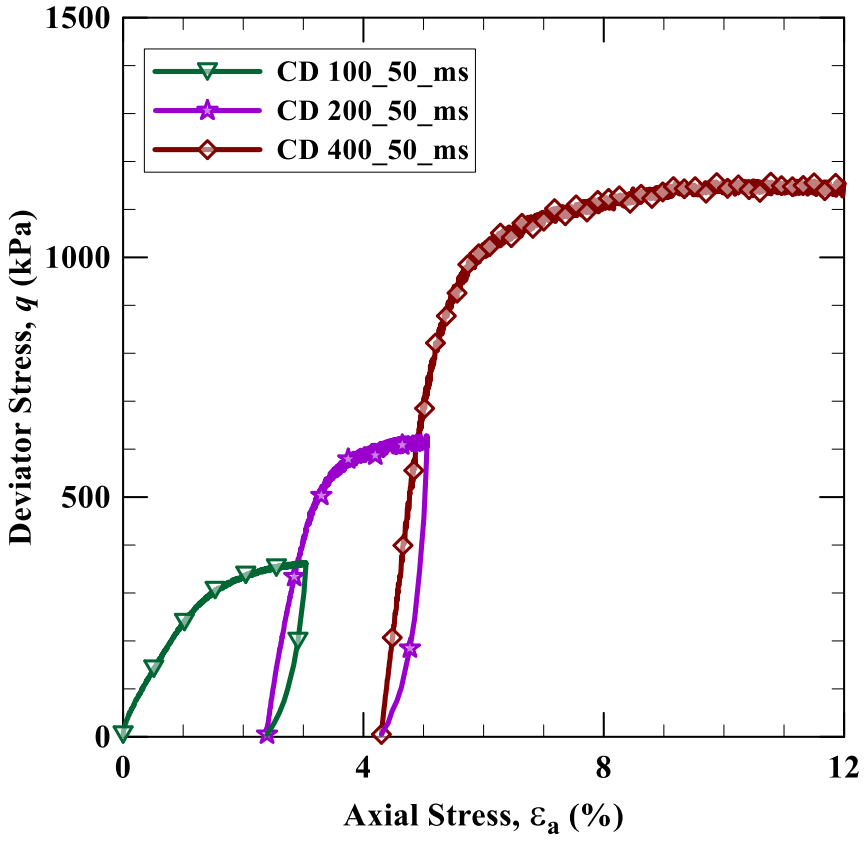

Figure 4.7 Deviator stress response of consolidated specimen at induced matric suction of 50 kPa under drained conditions obtained from a multistage triaxial test

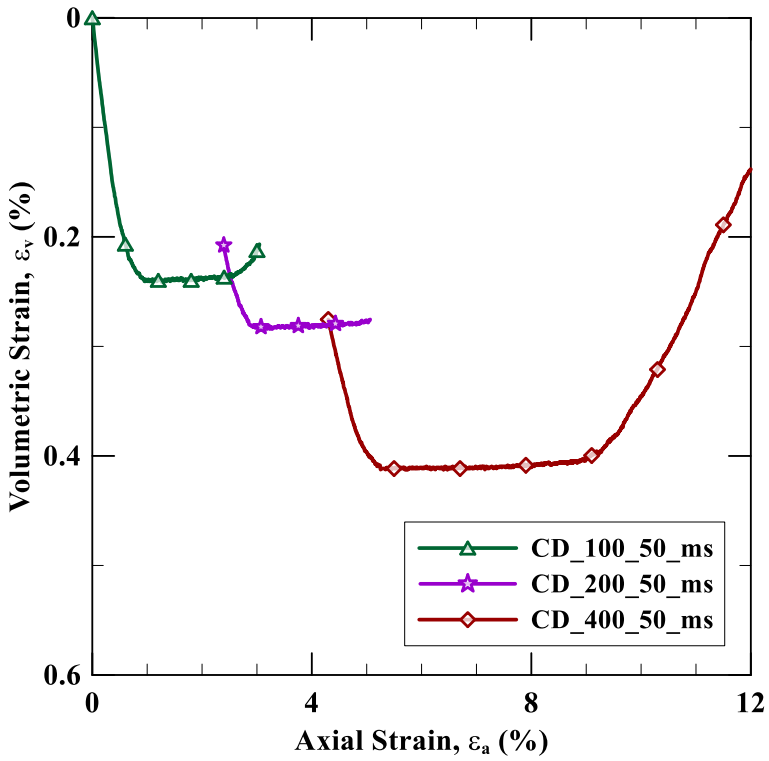

Figure 4.8 Volumetric strain response of consolidated specimen at induced matric suction of 50 kPa under drained conditions obtained from a multistage triaxial test

Figure 4.8 shows the Mohr's circles for a specimen at varying net confining pressures of 100, 200, and 400 kPa and at a constant matric suction of 50 kPa. The maximum deviator stresses obtained from the initial two net confining pressures of 100 and 200 kPa were utilized to plot the Mohr's circles, along with the deviator stress at critical state for net confining pressure of 400 kPa.

The common tangent to the Mohr's circles defines the modified Mohr-Coulomb Failure Criterion by Fredlund and Morgenstern (1977). The cohesion

intercept (c) was obtained as 32.6 kPa, which is the sum of effective cohesion of saturated soil (c' = 3.5 kPa) and apparent cohesion (c'' = 29.1 kPa). The effective cohesion of saturated soil was obtained from the multistage test of the saturated specimen and its results have been discussed earlier in section 4.4.1. The angle of internal friction (φ') of the unsaturated soil was determined to be 33.2°, which is practically the same as the value obtained for saturated specimen (φ' = 33.4°). The angle of internal friction due to matric suction (φ^b) was calculated to be 30.2°.

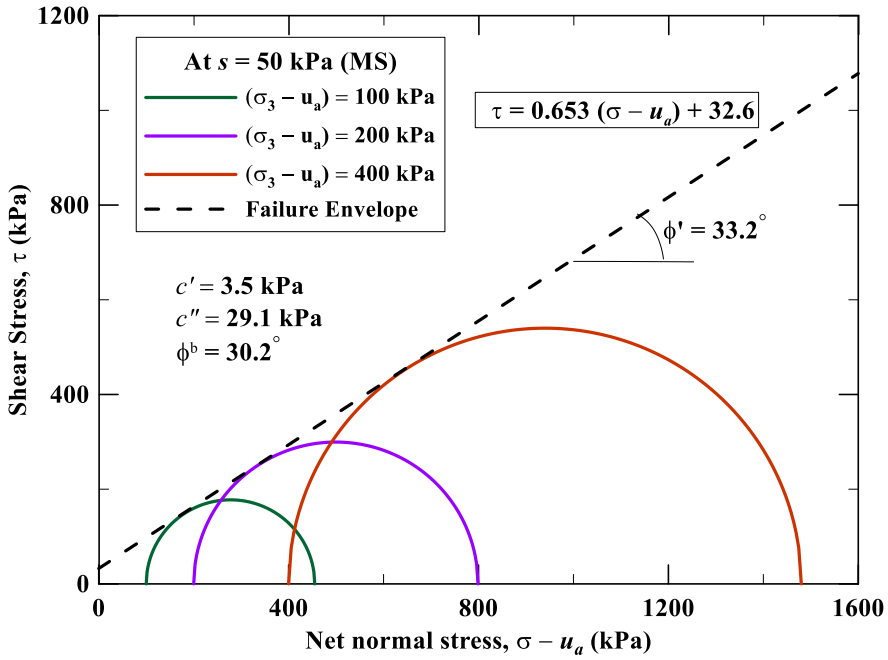

Figure 4.9 Mohr's stress circle at varying net confining pressure and at s = 50 kPa

Similarly, the deviator stress response of the specimen at constant matric suction of 250 kPa during shearing in drained conditions using multistage triaxial

test is shown in Fig. 4.10. The corresponding volumetric strain response for the specimen at constant matric suction of 250 kPa using multistage triaxial test is shown in Fig. 4.11.

The first stage of shearing at the net confining pressure of 100 kPa was stopped when the change in volumetric strain with axial strain decreased to a negative value ($d\varepsilon_v/d\varepsilon_a < 0$ in Fig. 4.11). Meanwhile, the tangent modulus diminished from 26.7 MPa to 6.5 MPa ($E_i/E_r = 4.1 < 25$, in Fig. 4.10). Hence, the criterion for prevention of dilation of the specimen was the critical factor in determining the termination of the first shearing stage. In this case, the relative stiffness factor was too low ($E_i/E_r = 4.1$). This might be due to the increase in brittleness of the soil with increasing suction and decrease in net confining pressure. As the specimen become more brittle (defined in section 2.11), the dilation initiates at a smaller axial strain (as observed in section 3.10). It is to be noted that for brittle materials the multistage tests are very sensitive to the application of additional axial strain near failure (Sharma et al., 2012).

The second shearing stage at a net confining pressure of 200 kPa, was also stopped when the change in volumetric strain with axial strain decreased to a negative value ($d\varepsilon_v/d\varepsilon_a < 0$ in Fig. 4.11). However, the tangent modulus reduced from 97 MPa to 8 MPa ($E_i/E_r = 12.2$ in Fig. 4.10). Hence, the criteria for prevention of dilation of the specimen was also, the critical factor in determining the

termination of the second shearing stage. Since the net confining pressure was higher than in the previous case, it might have resulted in the delay of initiation of dilation (as observed for single stage tests in Figs. 3.37, 3.39 and 3.41), which indirectly caused the relative stiffness ratio E_i/E_r to be higher in this case. However, due to the suction induced brittleness, the prevention of dilation criterion was the determining factor in the termination of shearing.

Finally, after consolidation at 400 kPa, the specimen was sheared beyond its peak strength, and the highest deviator stress and post-peak softening (defined in section 2.11) were clearly observed.

Figure 4.11 shows that at each new effective confining pressure the soil initially compresses and then for a substantial portion of shearing there is no change in the overall volume change of the specimen. However, with continuous shearing, the specimen dilates, as seen in all the shearing stages.

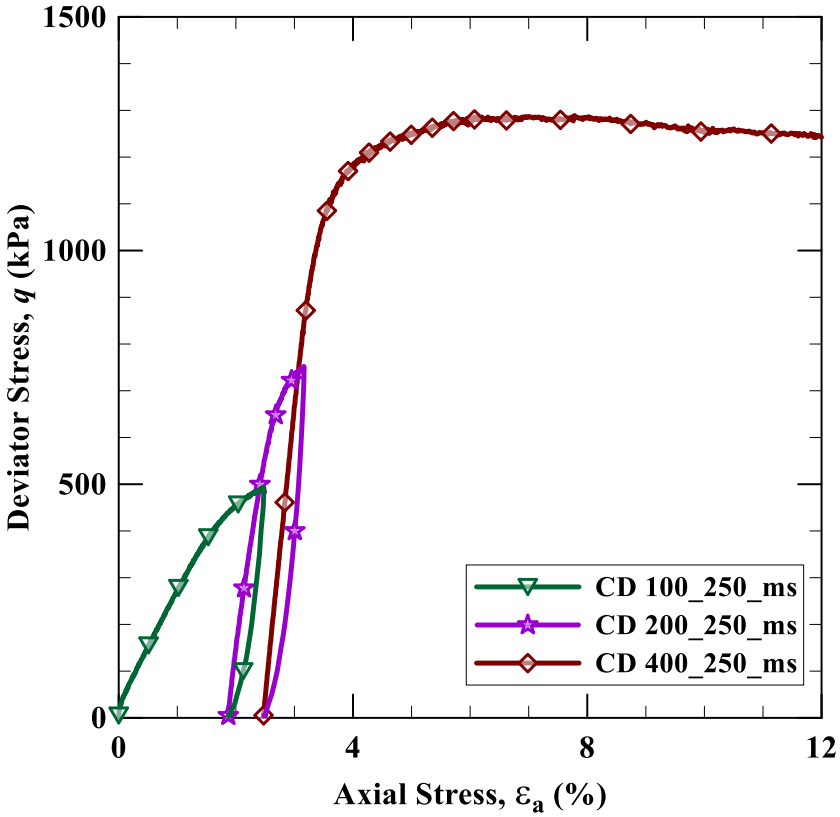

Figure 4.10 Deviator stress response of consolidated specimen at induced matric suction of 250 kPa under drained conditions obtained from a multistage triaxial test

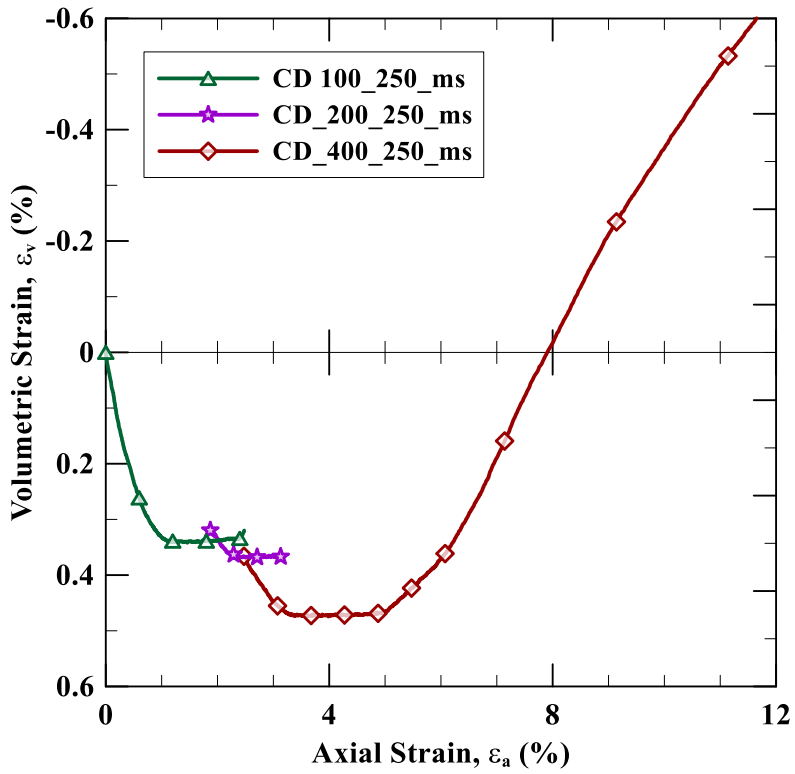

Figure 4.11 Volumetric strain response of consolidated specimen at induced matric suction of 250 kPa under drained conditions obtained from a multistage triaxial test

Figure 4.12 shows the Mohr's circles for a specimen at varying net confining pressures of 100, 200, and 400 kPa and at a constant matric suction of 250 kPa. The maximum deviator stresses obtained from the initial two net confining pressures of 100 and 200 kPa were utilized along with the deviator stress at critical state for net confining pressure of 400 kPa, to plot the Mohr's circles (similar to the cases of saturated specimen and specimen at induced matric suction 50 kPa).

In the Fig. 4.12, the common tangent defines the modified Mohr-Coulomb Failure Criterion as proposed by Fredlund and Morgenstern (1977). The cohesion intercept (c) was obtained as 76.8 kPa, which is the sum of effective cohesion of saturated soil (c' = 3.5 kPa) and apparent cohesion (c'' = 73.3 kPa). The angle of internal friction (φ') of the unsaturated soil was obtained to be 32.1°, which is practically similar to the value obtained for saturated specimen (φ' = 33.4°). The angle of internal friction due to matric suction (φ^b) was calculated to be 16.3°. The variation of the value of φ^b with suction shows that the contribution of suction towards the strength of the soil decrease with increase in suction.

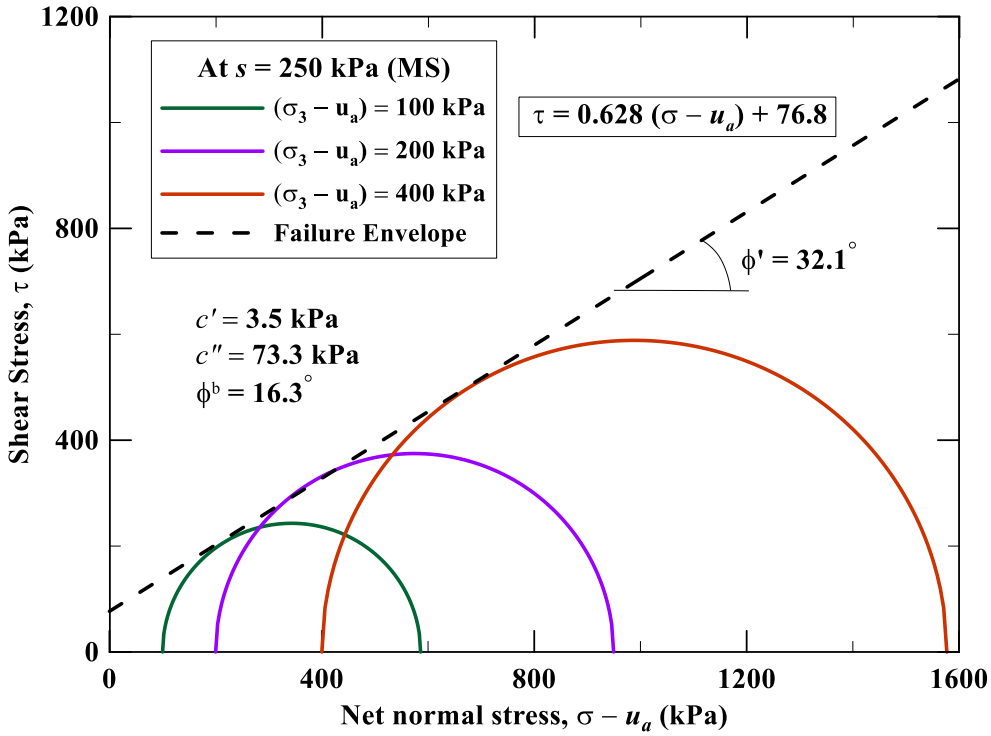

Figure 4.12 Mohr's stress circle at varying net confining pressure and at s = 250 kPa

4.5 Comparison between the Conventional and Multistage Triaxial Test

4.5.1 *Saturated Soil Specimens*

One of the primary objectives of performing the multistage triaxial test on compacted specimens of silty soil was to verify if the results obtained by multistage test were comparable to that by single-stage tests.

The comparison of the deviator stress responses of the single-stage and multistage triaxial tests on a saturated specimen is demonstrated in Fig. 4.13. It is evident that the deviator stresses for each effective confining pressure are nearly the same. The small variation between the results obtained from these tests, especially for the second confining pressure, may be attributed to two possible reasons. Firstly, it may be due to the premature termination of the loading sequence, prior to reaching the peak and the critical state for the initial two confining pressures. Secondly, the variability of soil specimen might have caused the subtle difference in deviator stress response. Nevertheless, these variations in the results are generally acceptable as soil behavior is quite complex and usually has a lot of uncertainty. Henceforth, the shear strength parameters (c' = 3.5 kPa and φ' = 33.4°) obtained from multi-stage tests would be nearly similar to that obtained from single-stage tests (c' = 2.7 kPa and φ' = 33.6°).

The initial stiffness of the specimen obtained using a multistage test at the higher effective confining pressure (σ_3' = 200 and 400 kPa) is significantly higher that the initial stiffness obtained using the single-stage test. It might be due to the

rearrangement of the soil particles during the first stage of shearing, which caused the densification of the particles (as observed in the volumetric strain response in Fig. 4.5). Similar observations were made by Rosone et al. (2016), where only the initial stiffness of the final shearing stage (at the highest confining pressure) were compared.

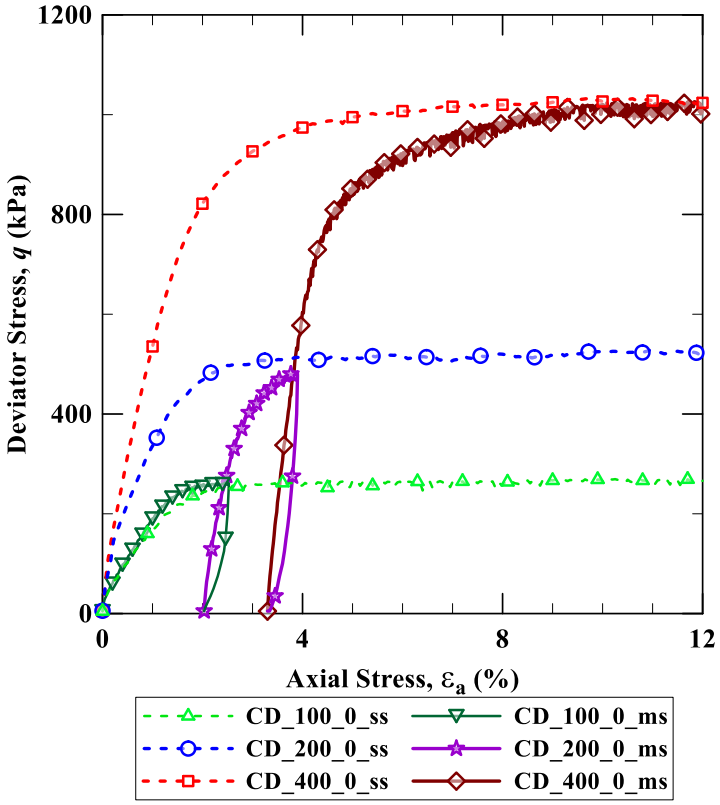

Figure 4.13 Comparison of deviator stress responses of saturated soil specimen obtained from single-stage and multistage triaxial tests

4.5.2 *Unsaturated Soil Specimens*

The comparison between single-stage and multistage triaxial test for unsaturated soil specimens at matric suction of 50 kPa and 250 kPa is shown in Fig. 4.14 and Fig. 4.15, respectively. It is evident that for both cases the deviator stress response obtained from multistage tests are quite similar to that obtained from single-stage tests.

However, when the deviator stress responses of the soils are compared for the specimen at a net confining pressure of 200 kPa (second shearing stage for multistage test) and an induced matric suction of 250 kPa, it is observed that the deviator stress at the termination point is significantly lower (9.7%) than the peak deviator stress obtained from the single-stage test at the same net confining pressure and suction level. This might be primarily due to the premature termination of the shearing stage during the multistage test. However, the difference between the deviator stresses at the critical state was 4.0%, which is generally considered to be within the acceptable range of error for experimental soil mechanics.

Figures 4.14 and 4.15 show that the initial tangent modulus was observed to be higher in the case of the second and the final shearing stage of the multistage triaxial test ($\sigma_3 - u_a$ = 200 and 400 kPa) as compared to that of the single-stage triaxial test at the same net confining pressure. These observations are in concordance with that of Rosone et al. (2016).

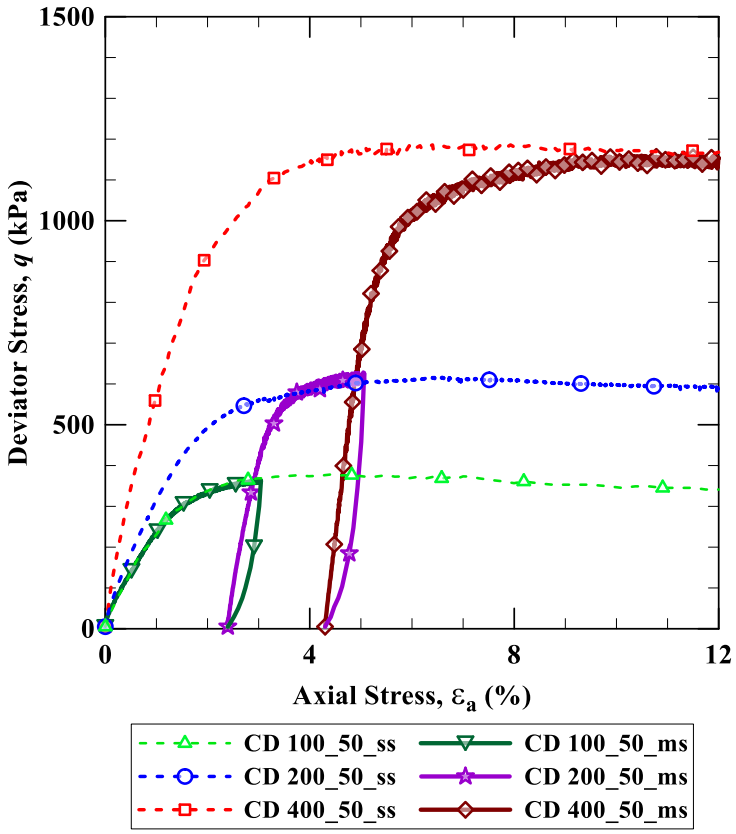

Figure 4.14 Comparison between the deviator stress responses of unsaturated soil specimen at matric suction of 50 kPa obtained from single-stage and multistage triaxial tests

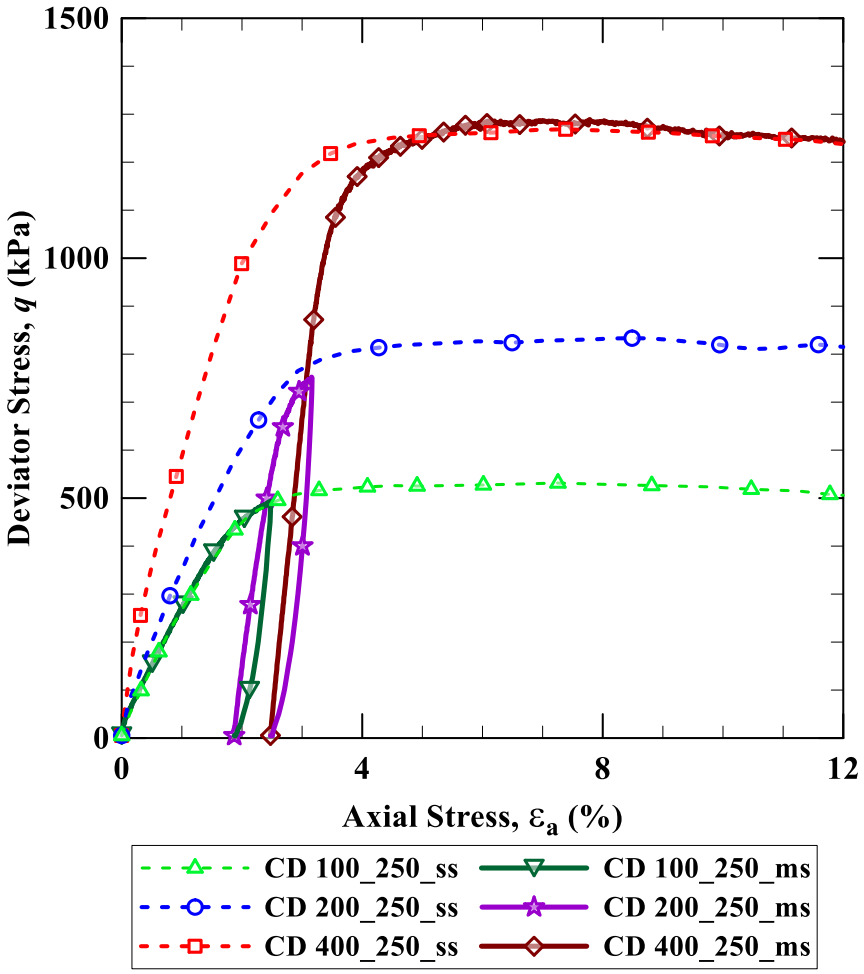

Figure 4.15 Comparison between the deviator stress responses of unsaturated soil specimen at matric suction of 250 kPa obtained from single-stage and multistage triaxial tests

The variation of deviator stress obtained from single-stage and multistage tests at peak and critical states were computed and shown in Table 4.1. It is observed that the variation at peak stress state was in the range of -1.2% to -9.7%, while at critical state the range was between -4.5% to 4.0%. Since the soil

demonstrates slight post-peak softening, the deviator stress at the termination of shearing during the multistage test was near the critical state than that at peak state stress.

The final shearing stage of a multistage test allows the shearing to continue till the specimen reaches its critical state. Hence, the comparison of the deviator stress response for the final stage (net confining pressure of 400 kPa) would be helpful in determining the effect of shearing the same specimen at varying net confining pressures on the critical state strength. Since the variation at critical state between single-stage and multistage tests is less than 2% for net confining pressure of 400 kPa for all the suction levels (s = 0, 50 and 250 kPa), the procedure followed during the multistage test has a negligible impact on the critical state. Moreover, the variation at peak stress state for the final net confining pressure of 400 kPa between single-stage and multistage tests varies between 3.0% and 7.2%.

The comparison of the shear strength parameters obtained from single-stage and multistage tests have been listed in Table 4.2. It lucidly shows that practically both the types of tests yield similar shear strength parameters. Similar conclusions were drawn by Ferreira et al. (2016) where the angle of internal friction of granular material obtained from single-stage and multistage triaxial test varied by less than 2° on an average. This is a further validation of the effectiveness of the procedure developed to determine the termination of the shearing stage using multistage triaxial tests. Moreover, the approximate time required to complete the tests

(assuming maximum axial strain of 20% during shearing) to obtain the shear strength parameters is shown in Table 4.2. It is observed that the multistage test required less than half of the time needed by single-stage tests to determine the shear strength parameters of the soil for all the suction levels (s = 0, 50, and 250 kPa).

Table 4.1 Variation of deviator stress at peak and critical state for single-stage and multistage triaxial tests

Suction, s (kPa)	Net confining pressure, $(\sigma_3 - u_a)$ (kPa)	$\frac{q_{ss,\,peak} - q_{ms}}{q_{ss,\,peak}}$	$\frac{q_{ss,\,cs} - q_{ms}}{q_{ss,\,cs}}$
0	100	-1.18%	-4.45%
0	200	8.76%	4.01%
0	400	2.96%	0.51%
50	100	8.97%	1.39%
50	200	1.80%	-3.28%
50	400	5.68%	1.10%
250	100	8.30%	-0.41%
250	200	9.70%	4.03%
250	400	7.18%	1.75%

$q_{ss,\,peak}$ is the deviator stress at peak stress state for single-stage tests

$q_{ss,\,cs}$ is the deviator stress at critical state for single-stage tests

q_{ms} is the deviator stress at the point of termination of shearing for multistage tests

Table 4.2 Comparison between the results obtained from the single-stage and the multistage triaxial tests

Test Type	Suction, s (kPa)	#Tests	Cohesion Intercept, c (kPa)	φ' (°)	φ^b (°)	Approximate completion time (ε_a = 20%) (days)
Single-stage	0	3	2.7	33.6	-	16
Multistage	0	1	3.5	33.4	-	7.5
Single-stage	50	3	30.8	33.5	29.3	58
Multistage	50	1	32.6	33.2	30.2	24
Single-stage	250	3	76.3	32.7	16.4	68
Multistage	250	1	76.8	32.1	16.3	27

The experimental data points obtained from multistage triaxial tests in p'-q space, along with the critical state lines (CSLs) for varying suction states obtained from single-stage triaxial tests have been shown in Fig. 4.16. It highlights the accuracy of the multistage triaxial tests to mimic the single stage tests. The slope of the CSLs for varying suction have a similar slope. Hence, the CSLs for all the suction states have been assumed to have the same slope of 1.355 as that obtained for saturated specimens.

Figures 4.17 and 4.18 show prediction of strength of unsaturated soil based on the integration of Vilar et al. (2006) model for cohesion intercept and the modified Mohr-Coulomb Failure Envelope by Fredlund and Morgenstern (1977). The cohesion intercept was computed by using the Vilar et al. (2006) model as

described in 3.10.9 (Eq. 3.11) for both single-stage and multistage triaxial tests. For Fig. 4.17, the three-dimensional surface (or equation) is based on the equation (Eq. 2.14) of unsaturated shear strength of unsaturated soil by Fredlund and Morgenstern (1977) with shear strength parameters of saturated specimen obtained from single-stage triaxial test ($c' = 2.7$ kPa and $\varphi' = 33.6°$).

Similarly, for Fig. 4.18, the shear strength parameters on saturated specimen obtained from multistage triaxial test ($c' = 3.5$ kPa and $\varphi' = 33.4°$) were used to generate the three-dimensional shear strength equation. The experimental values from single-stage and multistage tests were utilized to compute the shear strength at individual suction level by using the actual experimental cohesion intercept. These experimental shear strength values were also plotted and labelled.

For clarity in comparison, the projections of the three-dimensional surface for net mean stress of 100, 200, and 400 kPa (shown by dotted lines) and the experimental points were extended to the τ-s plane (represented as cyan colored dots). It is observed that the results from both the type of tests were quite similar and the three-dimensional surface for single-stage and multistage triaxial test appear to be identical.

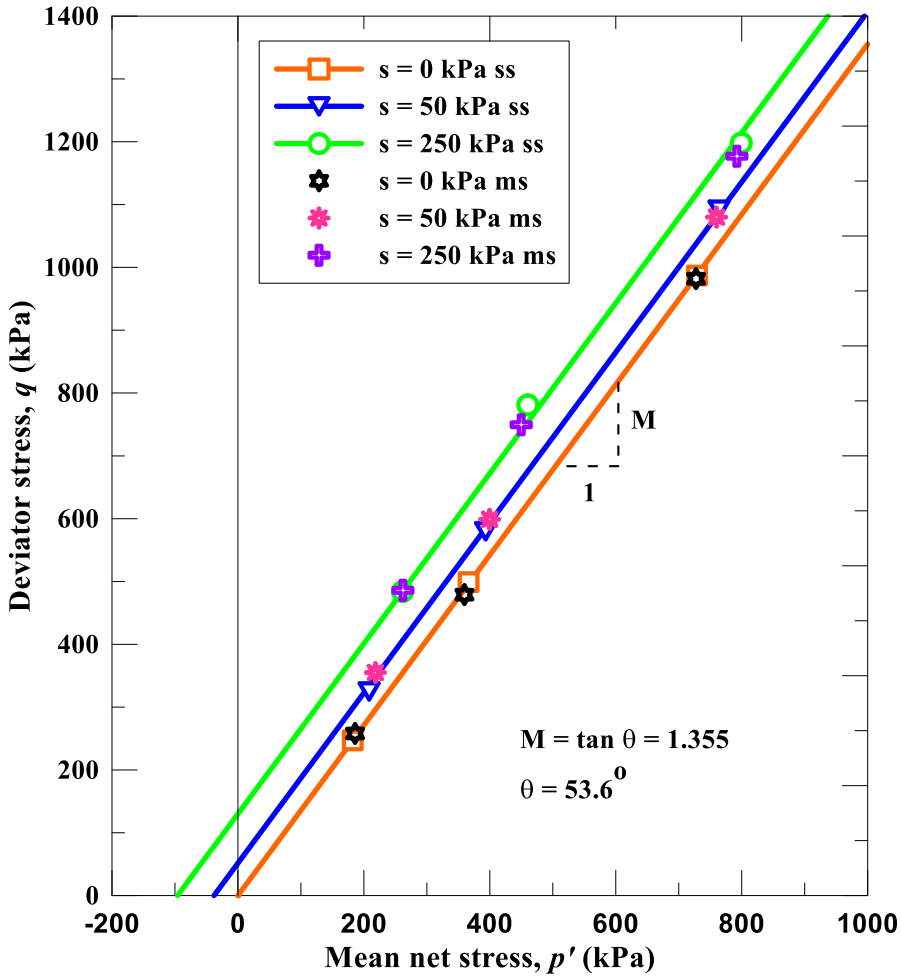

Figure 4.16 CSL in p'-q space at varying suction levels (s = 0, 50, 250, 750 kPa) for single-stage and multistage tests

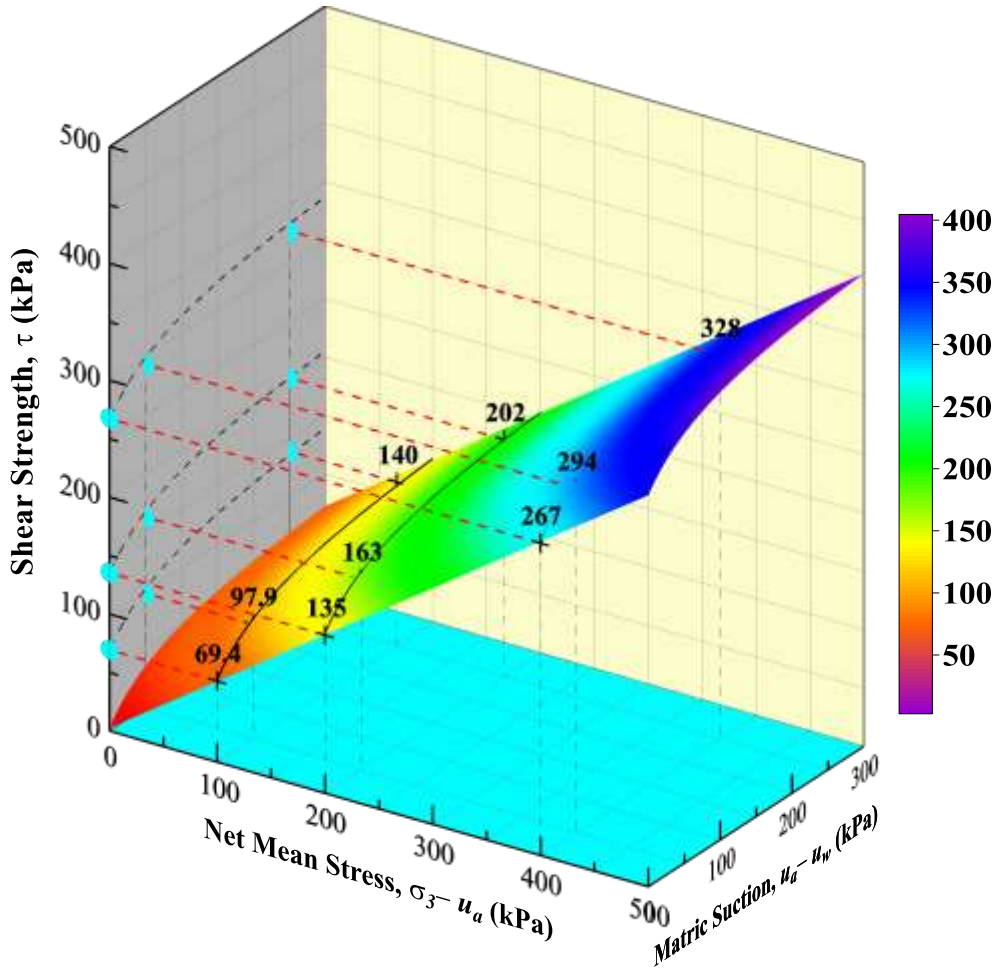

Figure 4.17 A three-dimensional surface for shear strength of unsaturated soil developed from multistage triaxial tests and the cohesion intercept variation with matric suction using Vilar et al. (2006) model

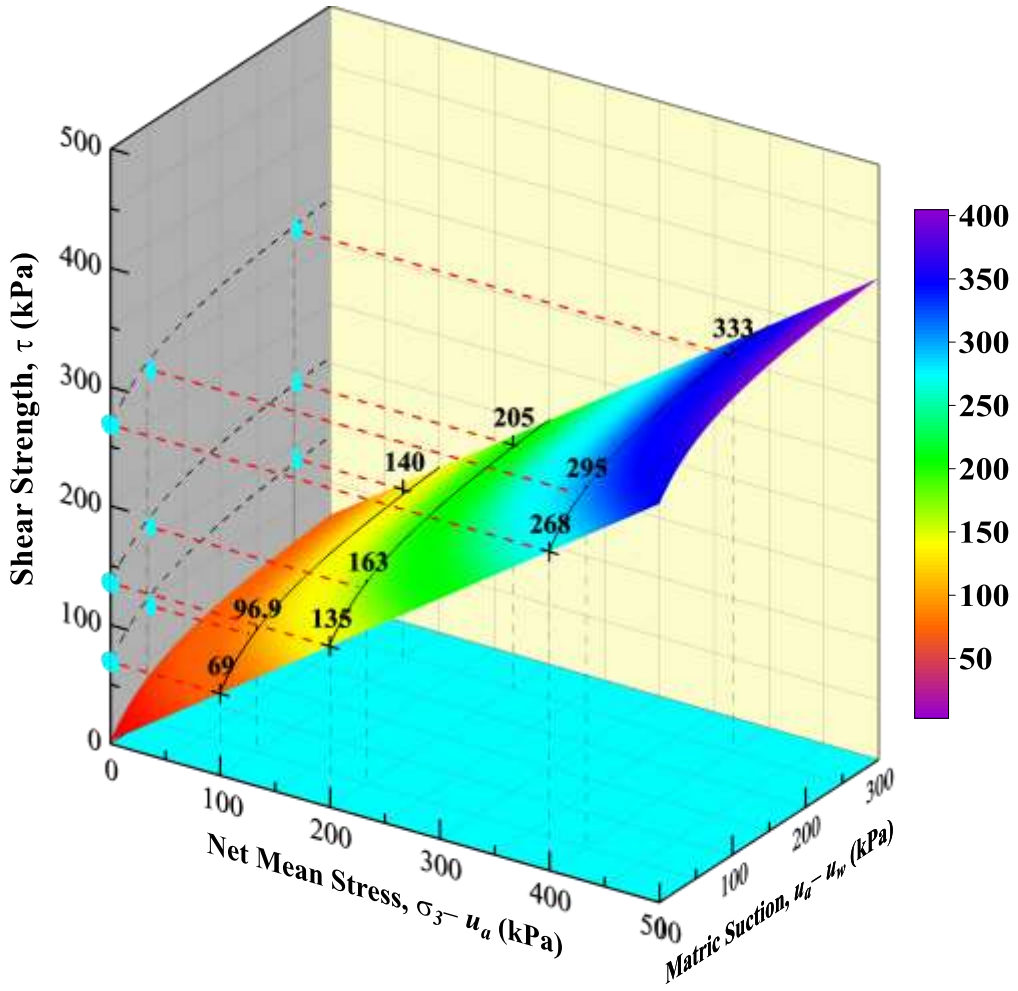

Figure 4.18 A three-dimensional surface for shear strength of unsaturated soil developed from single-stage triaxial tests and the cohesion intercept variation with matric suction using Vilar et al. (2006) model

4.5.3 *Summary*

The multistage test had previously shown promising results as an alternative for conventional or single-stage triaxial test on saturated specimens to address the issues of soil variability, lack of replicating soil specimens and the time required to complete a full series of test to determine the shear strength parameters (Kenney and Watson,1961; Sridharan and Rao, 1972; Parry and Nadarajah, 1973; Saeedy and Mollah 1988; Sharma et al., 2011). The comparison presented in section 4.5.2 shows that the procedure adopted for appropriately selecting the termination point for the initial two shearing stages (as mentioned in section 4.3.3) is adept at preventing the failure of the saturated and unsaturated specimen, which is essential for the satisfactory performance of the multistage test. The comparison also demonstrated the practical utility of the multistage tests (at constant suction) in providing similar results (less than 5% variation at critical state) as obtained by single-stage tests, but in less than half the time required.

4.6 Modeling Soil Response Under Monotonic Loading

4.6.1 *General*

The complex behavior of unsaturated soils has resulted in hurdles in modeling its behavior. Additional complications arise due to the different approaches employed by various researchers, like the use of total stress, or the use of Bishop's stress coupled with other variables to simulate the collapse of soils

(Solowski and Sloan, 2015). The number of constitutive models for unsaturated soils is also increasing rapidly, which use different approaches.

The widely known specialized constitutive models for unsaturated soils include those postulated by Alonso et al. (1990), Cui and Delage (1996), Alonso et al. (1999), Wheeler et al. (2003), Gallipoli et al. (2003), Tamagnini (2004), Georgiadis et al. (2005), Russell and Khalili (2006), Kimoto et al. (2007), Thu et al. (2007), Sheng et al. (2008), Kohler and Hofstetter (2008), Romero and Jommi (2008), Buscarnera and Nova (2009), Zhang and Lytton (2009a, b), Koliji et al. (2010), Manzanal et al. (2011), Liu and Muraleetharan (2012), Sun and Sun (2012), Casini (2012), Kodikara (2012), Guimãres et al. (2013), Tsiampousi et al. (2013), Solowski and Sloan (2015), Zhou and Sheng (2015), and Xiong et al. (2016). The presence of so many models with different approaches results in difficulties to comprehend the difference between each of them (Zhang and Li, 2010; Zhou et al., 2012; Solowski and Sloan, 2015).

The behavior of the silty soil tested in this research shows slight post-peak softening (defined in section 2.11) and stress-induced-dilatancy. Many constitutive models have been developed for dilatant geomaterials by Ng and Chiu (2003), Manzanal et al. (2011), Tsiampousi et al. (2013), Solowski and Sloan (2015), Zhou and Sheng (2015), and Xiong et al. (2016). Moreover, other models were also developed for unsaturated soils demonstrating compressive behavior by Alonso et al. (1990), Toll (1990), Josa et al. (1992), Wheeler and Sivakumar (1995), Cui and

Delage (1996), Houlsby (1997), Chiu and Ng (2003), Gallipoli et al. (2003), Datcheva and Schanz (2003); Khalili et al. (2005), Russell and Khalili (2006), Kohler and Hofstetter (2008), Yang et al. (2008), Buscarnera and Nova (2009), Zhang and Lytton (2009a, b), Koliji et al. (2010), Sun and Sun (2012), Kodikara (2012), Guimãres et al. (2013), and Zhou and Sheng (2015).

However, the Barcelona Basic Model (BBM) by Alonso et al. (1990) forms the basis for most of the elasto-plastic constitutive modeling of unsaturated soils (Gens, 2010) and it has been the most widely used model for unsaturated soils. Henceforth, the BBM was used to compare the results obtained from suction-controlled single-stage and multistage triaxial tests.

4.6.2 *Barcelona Basic Model*

The Barcelona Basic Model (BBM) proposed by Alonso et al. (1990) utilizes a critical state framework for predicting the behavior of unsaturated soils. It is an elasto-plastic constitutive model developed to incorporate hardening plasticity. It was ideally suited for slightly to moderately expansive clayey soils showing compressive behavior upon shearing; though it can also predict the behavior of sand, silt, clayey sand, and sandy clay. The basic framework of the model is an extension of the Modified Cam Clay (MCC) model (Roscoe and Burland, 1968). The BBM was defined in terms of the three state variables, i.e., the net mean stress, p; the deviator stress, q; and the matric suction, s.

4.6.3 *Calibration of Barcelona Basic Model parameters*

The BBM requires the determination of various model parameters associated with the changes in isotropic stress, deviator stress, shear strength and matric suction (Alonso et al., 1990). The following variables are used to predict the change in soil behavior: (*i*) net mean stress, $p = (\sigma_1 + 2\ \sigma_3)/3 - u_a$; (*ii*) deviator stress, $q = (\sigma_1 - \sigma_3)$; (*iii*) matric suction, $s = (u_a - u_w)$; (*iv*) total volumetric strain, $\varepsilon_v = (\varepsilon_1 + 2\varepsilon_3)$; (*v*) total shear strain, $\varepsilon_q = (2/3)(\varepsilon_1 - \varepsilon_3)$ and (*vi*) specific volume, $v = (1 + e)$.

The yield function defines the yield surface, which delineates the plastic behavior from the elastic behavior. The BBM recommends an elliptical shaped yield surface in *p*-*q* space, as shown in Fig. 4.19 and is determined by Eq. 5.1. The variation of stresses results in the expansion of the yield surface in the *p*-*q*-*s* space.

$$f(p, q, s) = q^2 - M^2(p + p_s)[p_o(s) - p] = 0 \tag{4.1}$$

where M = slope of the critical state line in the *p*-*q* plane;

$$p_s = ks \tag{4.2}$$

k = slope of the apparent tensile strength line in *p*-*s* plane.

s = soil suction.

Another yield function is recommended in the *p*-*s* space which characterizes the suction increase (SI) yield loci. This yield function signifies the plastic

compression which occurs due to an increase in suction, and is determined by the following expression:

$$f(s, s_o) = s - s_o = 0 \tag{4.3}$$

where s_o is the maximum suction experienced by the soil.

The BBM assumes that the increase in matric suction results in a decrease in the volumetric stiffness parameter, $\lambda(s)$. Henceforth, the yield surface in *p*-*q*-*s* space expands with an increase in suction. The variation of $\lambda(s)$ with suction, *s* is as follows:

$$\lambda(s) = \lambda(0)\left[(1 - r)e^{(-\beta s)} + \mathrm{r}\right] \tag{4.4}$$

where $r = \frac{\lambda(s \to \infty)}{\lambda(0)}$;

β = parameter controlling the rate of increase of soil stiffness with matric suction.

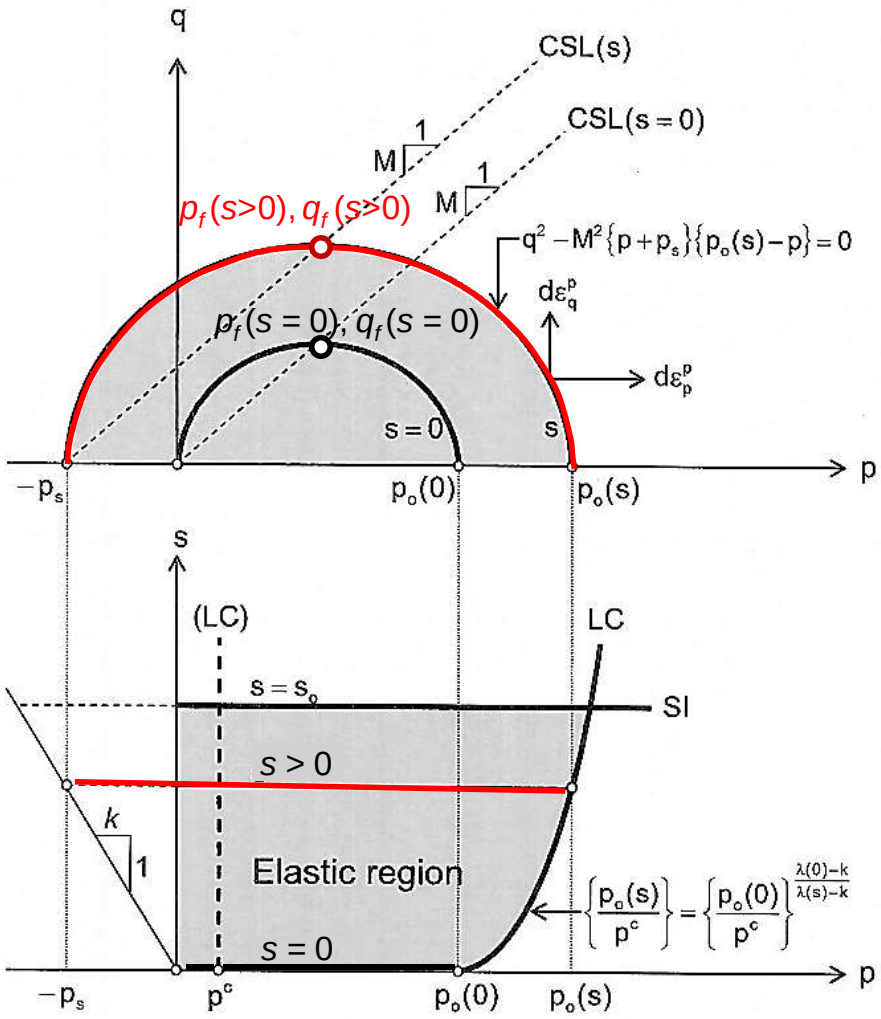

Figure 4.19 Yield surfaces in *p*-*q*-*s* space (modified from Alonso et al., 1990 and Macari et al., 2003)

At constant suction, the yield surface in the *p*-*s* space is defined by the Loading Collapse (LC) curve. The values of isotropic stress, $p_o(s)$ defines the LC curve in the *p*-*s* space and is expressed as (Alonso et al., 1990):

$$\frac{p_o(s)}{p^c} = \left[\frac{p_o(0)}{p^c}\right]^{\frac{\lambda(0)-\kappa}{\lambda(s)-\kappa}} \quad (4.5)$$

where, $p_o(s)$ = yield stress as a function of matric suction, s

$p_o(0)$ = preconsolidation stress at saturated condition (s = 0)

p^c = reference/preconsolidation stress at which the LC becomes a straight line (i.e., $p_o(s) = p^c$)

$\lambda(0)$ = compressibility coefficient at saturated condition along the virgin loading

$\lambda(s)$ = soil stiffness parameter that varies with matric suction, s

κ = elastic rebound index

The BBM assumes a linear increase in cohesion with an increase in suction and is defined as the value of $-p_s = -ks$ in the p-s space when q = 0 (shown in Fig. 4.19). The major axis of the ellipse extends from $-p_s$ to $p_o(s)$, as shown in Fig. 4.19. The failure of the soil is characterized by the critical state and is defined by the values of p_f and q_f in p-q space, which is dependent of the induced matric suction.

4.6.3.1 Calibration of BBM parameters from experimental results

A series of isotropic consolidation tests were performed on statically compacted specimens of silty soil at constant suction levels of 50 kPa, 250 kPa, and 750 kPa (as mentioned in section 3.8). The net mean stress was increased at a constant rate of 5 kPa/h to attain the required level at constant suction.

Figure 4.20 shows the change in specific volume with the variation of net mean stress from all suction controlled hydrostatic compression (HC) tests. The slope of the virgin curve or the volumetric stiffness parameter, $\lambda(s)$ were determined to be $\lambda(50) = 0.011$, $\lambda(250) = 0.009$, and $\lambda(750) = 0.006$. It could be observed that the slope of the virgin curve or the volumetric stiffness parameter, $\lambda(s)$ decreases with increases in suction. In other words, the stiffness of the soil increases with increase in suction, which is consistent with the BBM framework.

While the elastic rebound index, κ shows an increase, from 0.0012 at 50 kPa matric suction to 0.0019 at 750 kPa matric suction. However, an average value of $\kappa = 0.0016$ was selected for modeling based on BBM framework. Additionally, the preconsolidation pressure or yield stress were calculated to be $p_o(50) = 51$ kPa, $p_o(250) = 62$ kPa and $p_o(750) = 70$ kPa, from HC tests performed at matric suction of 50 kPa, 250 kPa and 750 kPa, respectively. Similar observations and assumptions were made by Patil et al. (2016a) for developing the BBM from suction-controlled triaxial tests.

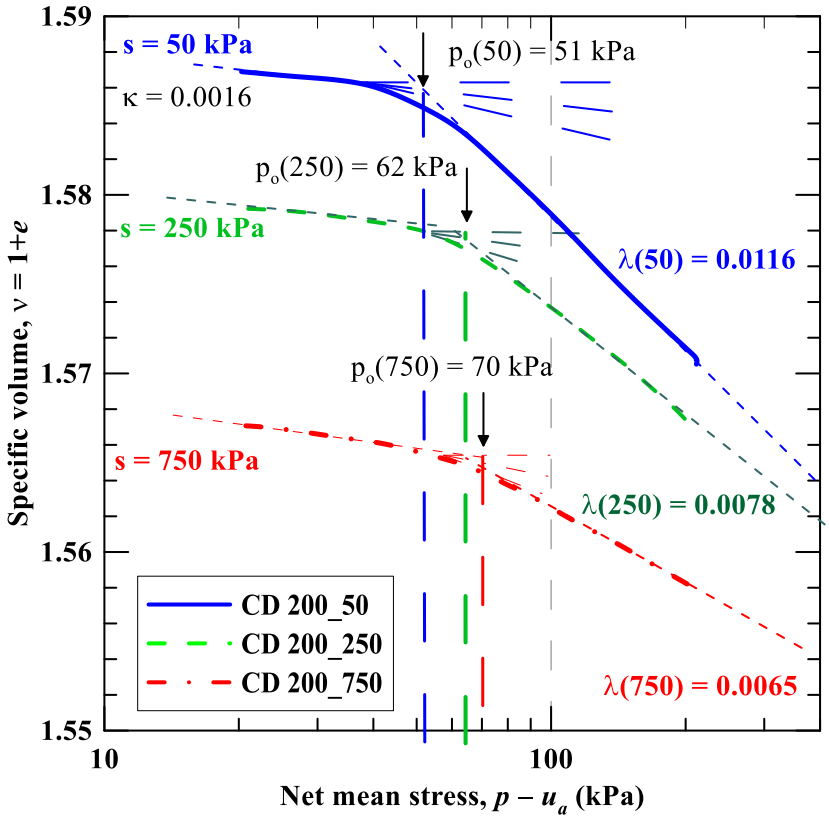

Figure 4.20 Response of silty soil from suction-controlled HC test at s = 50, 250 and 750 kPa

The Generalized Reduced Gradient (GRG) method (available in "Solver add-in" for a standard spreadsheet like Microsoft Excel) was adopted to solve the overdetermined system of nonlinear equation (Eq. 4.4). The experimental data for values of $\lambda(s)$ were used to determine the BBM parameters, which are as follows: $\lambda(0) = 0.014$, $r = 0.4655$, and $\beta = 0.0074$ kPa^{-1}. The effect of the values of β and r on the stiffness parameter $\underline{\lambda}(s)$ are shown in Figs. 4.21 and 4.22, respectively.

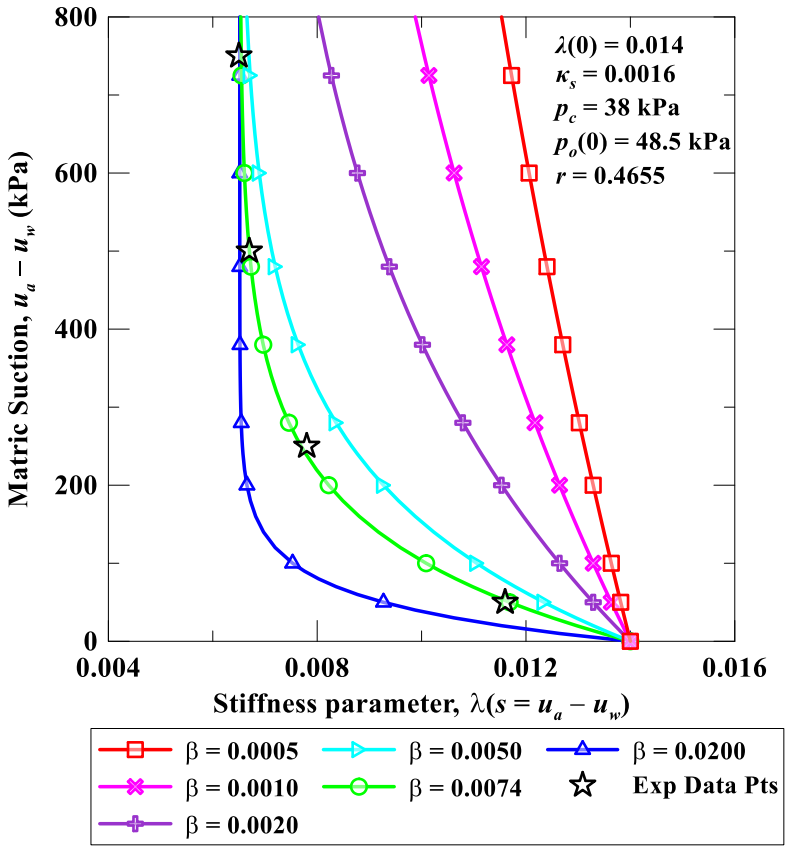

Figure 4.21 Variation of stiffness parameter $\underline{\lambda}(s)$ for different values of β

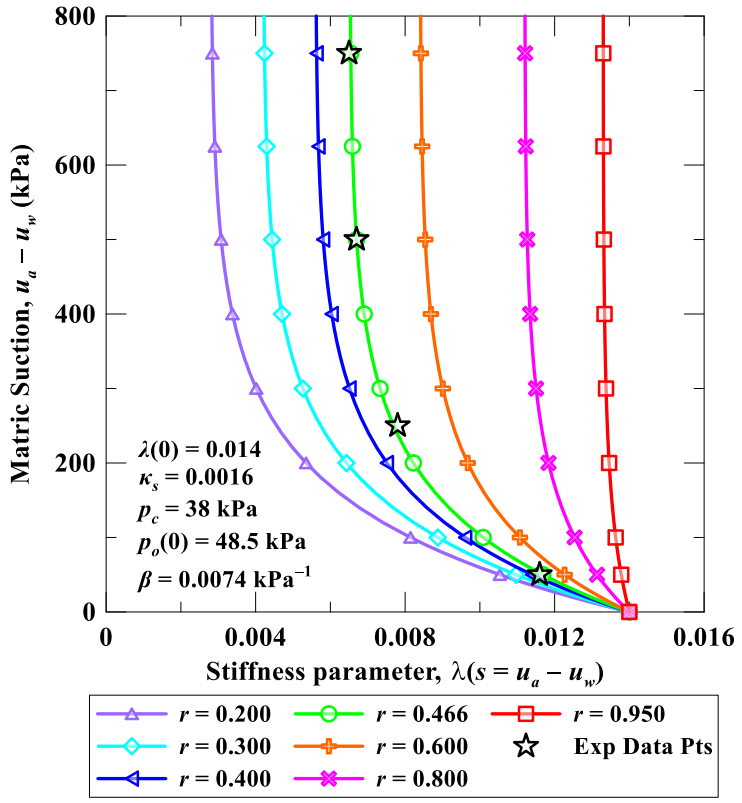

Figure 4.22 Variation of stiffness parameter $\underline{\lambda}(s)$ for different values of r

The same method was utilized to calibrate the parameters p^c and $p_o(0)$ using the known values of $p_o(s)$ and Eq. 4.5. The following best-fit values were obtained: $p^c = 38$ kPa and $p_o(0) = 48.5$ kPa. The influence of the value of $p_o(0)$ on the loading collapse (LC) curve is shown in Fig. 4.23.

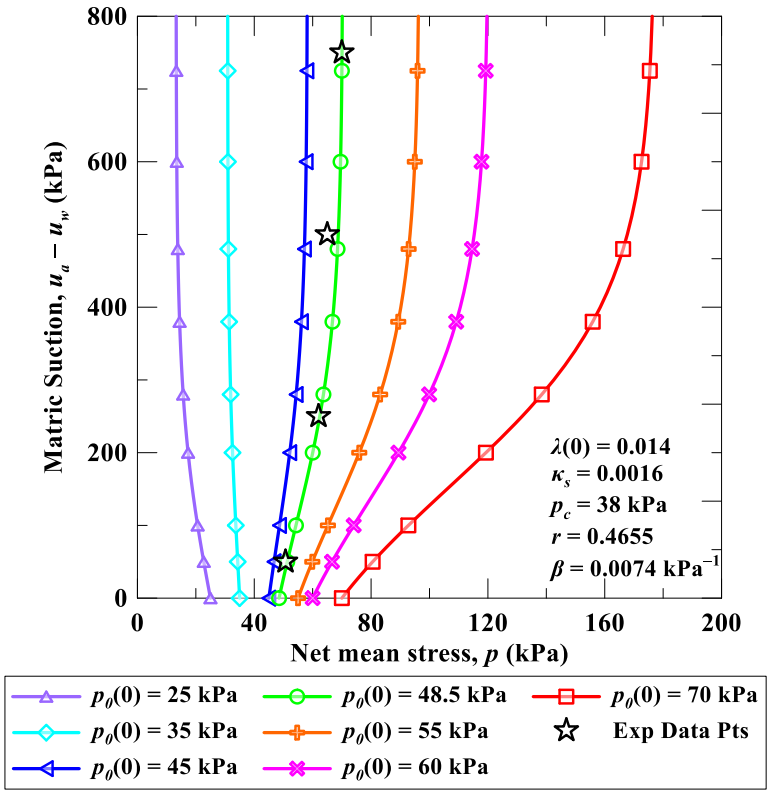

Figure 4.23 Variation of net mean stress for different values of $p_o(0)$

The BBM formulation postulates a constant value of k, which denotes the increase in cohesion intercept due to suction. However, it was observed that the present set of experimental data points suggests a nonlinear or bilinear trend for the value of k with suction. The variation in the value of k appeared to change drastically at the suction of 250 kPa. Henceforth, the following values were used:

$$k = \begin{cases} 0.4914, & s \le 250 \\ 0.0222, & s > 250 \end{cases} \tag{4.6}$$

Figure 4.24 shows the Loading Collapse (LC) yield curve and the Apparent Tensile Strength (ATS) locus in *p*-*s* space as determined from the experimental results. The ATS was determined from the x-axis intercept of the CSLs at varying suction states from the suction-controlled CTC tests. The rate of increase of ATS with suction is determined to be 0.4914, for suction below 250 kPa, and 0.0222, for suction beyond 250 kPa (from Eq. 4.6). The behavior of LC yield curve is similar to the trend expected from BBM framework. The use of non-plastic silt resulted in a smaller range of LC yield curve, due to the lack of significant influence of induced matric suction on the volume change of the soil, as compared to soft clays.

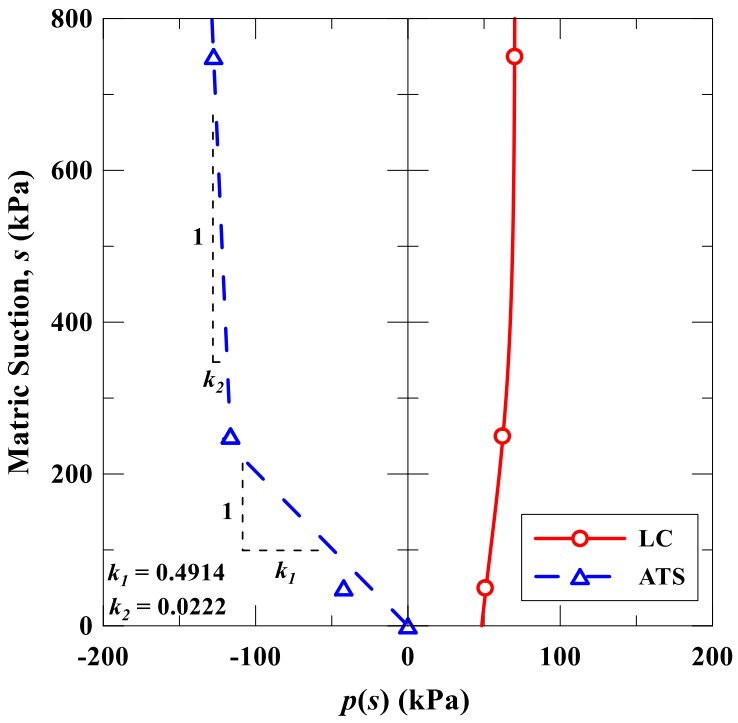

Figure 4.24 Loading Collapse and Apparatus Tensile Strength of the silty soil on *p*-*s* space

The Loading Collapse (LC) yield curves for various intermediate geomaterials are plotted in Fig. 4.25. It was observed that the LC yield curve for the current study is within the expected range.

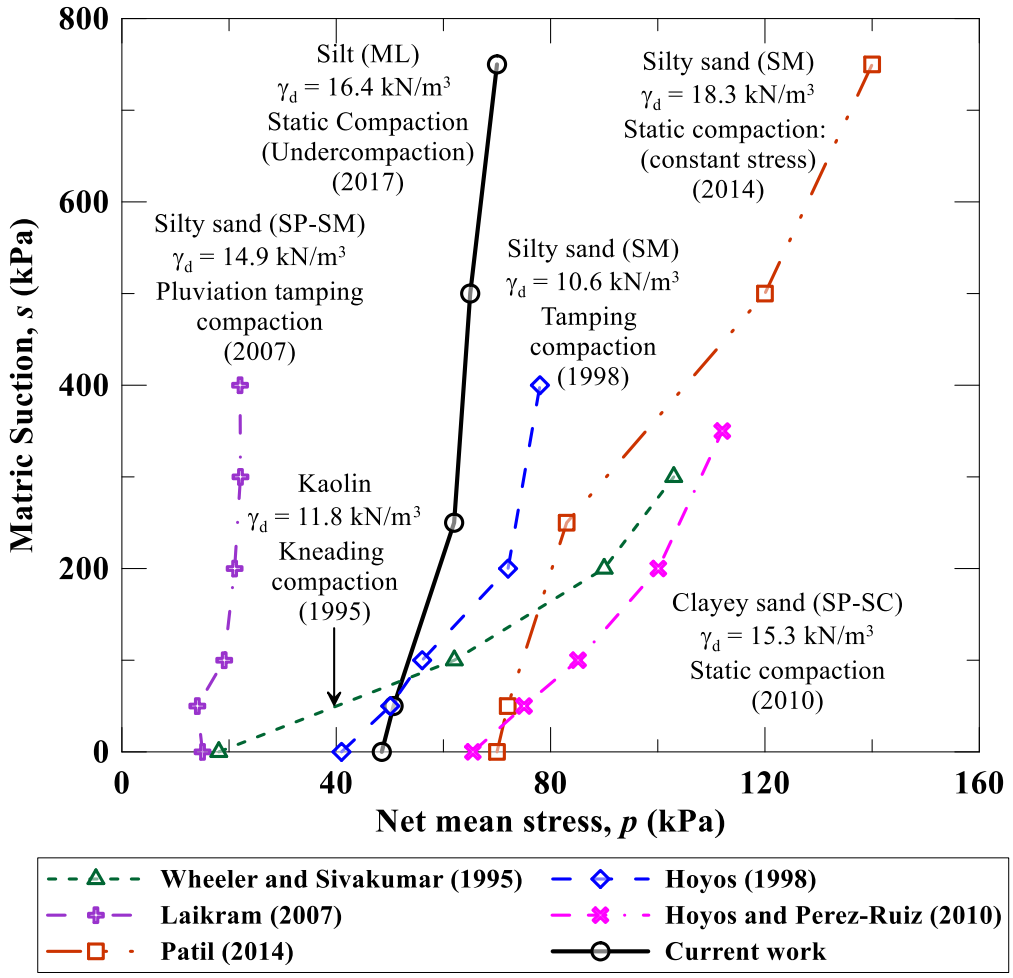

Figure 4.25 Current and previously reported LC curves for varying soil types, compaction technique, and soil conditions

4.6.4 *Constitutive Behavior under Shear Loading*

The experimental data (presented in Chapter 3) for shearing were utilized to obtain the strength at the critical state for varying net confining pressure and suction levels. The BBM formulation postulates that the slope of the critical state line, M remains constant irrespective of the induced matric suction. The experimental data for strength at critical state (section 3.10) shows that the values of the slope of CSL at varying suction levels are similar to that in the saturated condition. Hence the slope of CSL was assumed to be same at all suction levels, i.e., M = 1.3555. The calibrated values of the BBM parameters are listed in Table 4.3.

Table 4.3 Calibrated parameters for BBM for silty soil

Parameter	Calibrated Value	Units
$\lambda(0)$	0.014	–
κ	0.0016	–
r	0.4655	–
β	0.0074	kPa^{-1}
p^c	38	kPa
G	18000	kPa
M	1.3555	–
k	0.4914 ($s \leq 250$ kPa) 0.0222 ($s > 250$ kPa)	–
$p_o(0)$	48.5	kPa

The variation of deviator stress, q at critical state for different values of initial net mean stress and matric suction could be expressed by the Eq. 4.7. Eq. 4.7 represents the three-dimensional surface with net mean stress, p and suction, s as variables and the BBM parameters M and k. The non-linearity of cohesion intercept with suction is accounted for by approximating the value of k as a bi-linear function, as shown in Eq. 4.6. The surface, Eq. 4.8 and it simplified form (Eq. 4.9), is determined within the domain of net mean stress of 100 to 400 kPa and matric suction of 0 to 750 kPa.

$$q = Mp + Mks \tag{4.7}$$

$$q = \begin{cases} -1.356p + 1.356\times0.4914s, s \leq 250\ kPa \\ 1.356p + 0.6663\times250 + 1.356\times0.02218\times(s-250), s > 250\ kPa \end{cases} \tag{4.8}$$

$$q = \begin{cases} 1.356p + 0.6663s,\ s \leq 250\ kPa \\ 1.356p + 159.06 + 0.02218s,\ s > 250\ kPa \end{cases} \tag{4.9}$$

The predictions of the BBM framework (Eq. 4.9) was compared with the experimental results (Section 3.10), as shown in Figs. 4.26 and 4.27. The BBM predictions for the strength at critical state for varying suction levels and initial net mean stress forms a close correlation with that of the experimental observations for both single-stage and multistage triaxial tests.

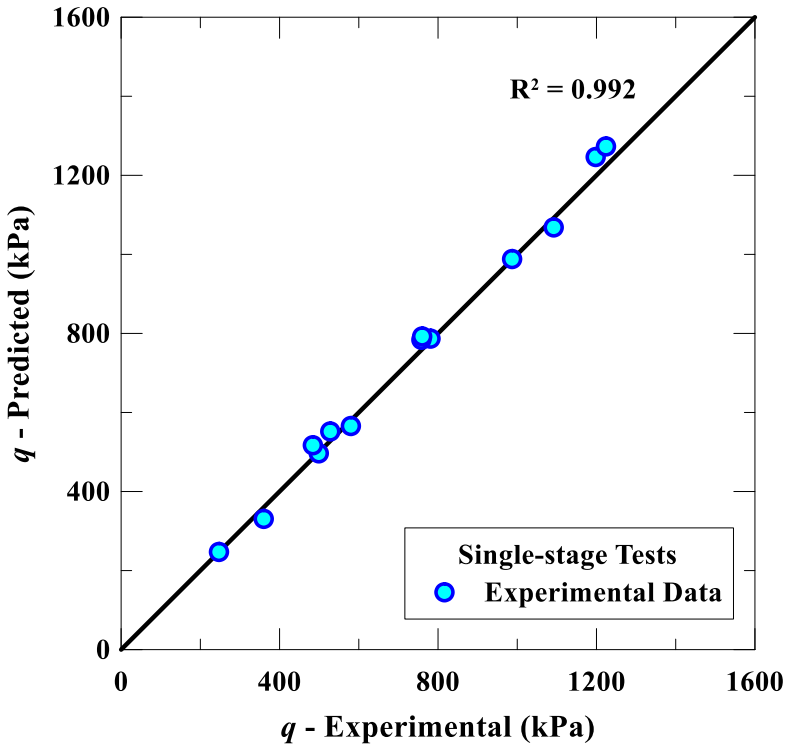

Figure 4.26 Comparison of predicted and experimental values of deviator stress at critical state using single-stage tests (s = 0 to 750 kPa) as postulated by the BBM framework

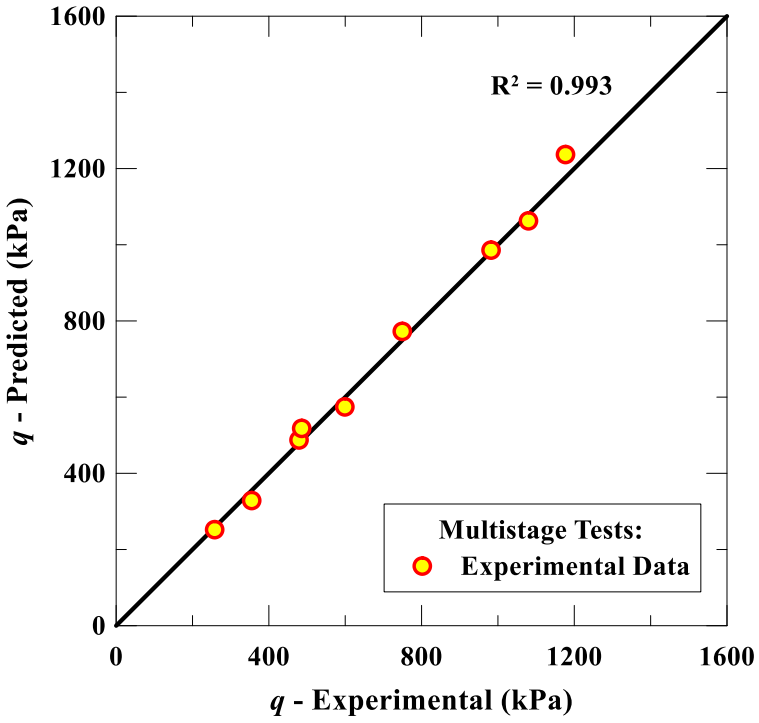

Figure 4.27 Comparison of predicted and experimental values of deviator stress at critical state using multistage tests (s = 0 to 250 kPa) as postulated by the BBM framework

4.6.5 *Implementation of Barcelona Basic Model*

The original BBM framework follows the Cam-clay framework by assuming that any change in net mean stress, p induces elastic or recoverable changes in the volume of the soil. The elastic volume strain increment is expressed by:

$$d\varepsilon_{vp}^{e} = -\frac{dv}{v} = \frac{\kappa}{v}\frac{dp}{p} \tag{4.10}$$

Eq. 4.10 implies a linear relationship exists between the specific volume, *v*, and the logarithm of mean stress, ln (*p*), which is represented by the elastic unloading-reloading line (url) of the soil (Alonso et al., 1990).

The changes in deviator stress, *q*, which induces elastic shear strains can be utilized to determine the elastic shear strain increment, by using the following expression:

$$d\varepsilon_q^e = \frac{2}{3}(d\varepsilon_1^e - d\varepsilon_3^e) = \frac{1}{3G}dq \tag{4.11}$$

The BBM assumes that the yield surface in the *p*-*q* space is defined by an ellipse (Eq. 4.1). The size of the elliptical-shaped yield surface is defined by the value of yield stress, $p_o(s)$. The yield surface expansion and soil hardening are associated with the normal compression of the soil. The relationship between specific volume, $v = 1+e$, and the logarithm of net mean stress, ln(*p*), during isotropic normal compression along the iso-ncl is governed by:

$$v = N(s) - \lambda(s) ln \frac{p}{p^c} \tag{4.12}$$

The magnitude of the plastic volumetric strain is computed as:

$$d\varepsilon_{vp}^p = \left[\frac{\lambda(s)-\kappa}{v}\right]\frac{dp_o(s)}{p_o(s)} \tag{4.13}$$

In a CTC test, the value of deviator stress, q is computed by

$$q = 3(p - p_{ini}) \tag{4.14}$$

where p_{ini} is the initial value of net mean stress prior to shearing.

During a CTC test, the deviator stress is monotonically increased with a shear loading ratio, $dq = 3\,dp$, until the critical state line (CSL) was reached. At this point, the soil becomes fully plastic and plastic shear strain develops with no plastic volumetric strain, which results in no change in stress path for the given sample.

4.6.5.1 Explicit Integration of Constitutive Relations

The step-wise integration scheme of shearing a lightly overconsolidated soil specimen using the BBM framework is demonstrated by using Fig. 4.28. It shows the response of soil in the p-q and v-ln p space, along with the deviator stress and specific volume responses with respect to induced shear strain.

The values of the following parameters, $\lambda(0)$, κ, β, r, p_c, G, M, k, $p_o(0)$, and $s = (u_a - u_w)$, are calibrated to be utilized in the explicit integration. The general case of lightly overconsolidated soil is used, since points, A and B (in Fig. 4.28) are identical for normally consolidated soil. Additionally, for normally consolidated soils $p_{ini} = p_o^B(s)$.

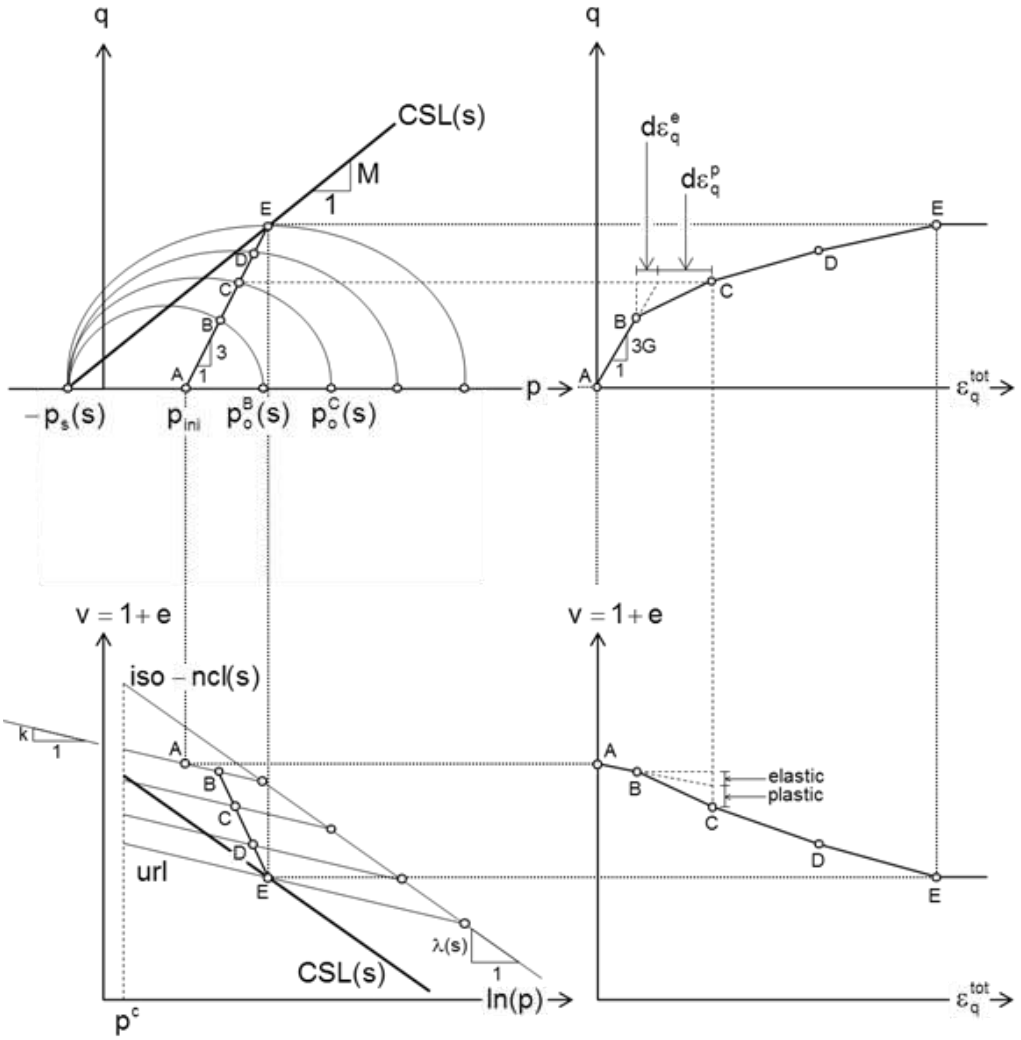

Figure 4.28 Schematic of BBM response for a constant suction CTC test under drained conditions on a lightly-overconsolidated specimen (after Hoyos, 1998)

The step-wise explicit integration procedure for BBM as described by Hoyos (1998) is as follows:

Step 1. The value of $\lambda(s)$ is computed using Eq. 4.4.

Step 2. The value of $p_o^B(s)$ is calculated as:

$$p_o^B(s) = p^c \left[\frac{p_o(0)}{p^c}\right]^{\frac{\lambda(0)-\kappa}{\lambda(s)-\kappa}} \tag{4.15}$$

Step 3. In the case of a lightly overconsolidated soil, the intersection of the CTC stress path and the initial yield surface could be computed by using Eq. 4.1 and Eq. 4.14 and solving for the value of q_B, which is as follows:

$$q_B = \frac{-b+\sqrt{b^2-4ac}}{2a} \tag{4.16}$$

where,

$$a = 1 + \left(\frac{1}{9}\right) M^2,$$

$$b = \left(\frac{1}{3}\right) M^2[2P_{ini} - p_o^B(s) + p_s], \text{ and}$$

$$c = M^2[p_{ini} + p_s][p_{ini} - p_o^B(s)] \tag{4.17}$$

Hence, for a CTC stress path,

$$p_B = p_{ini} + \frac{1}{3} q_B \tag{4.18}$$

Step 4: The specific volume, v_B at the point B on the unloading-reloading line (url) corresponding to the net mean stress, p_B is computed as:

$$v_B = v_{ini} - \kappa \ln\left[\frac{p_B}{p_{ini}}\right] \tag{4.19}$$

Step 5. The elastic shear strain increment (which is recoverable) can be calculated for stress path AB using the following expression:

$$d\varepsilon_q^e = \frac{1}{3G} q_B \tag{4.20}$$

Step 6. The coordinates of the ultimate point or failure point E on the CSL is computed as:

$$q_E = \left[\frac{3M}{3-M}\right](p_{ini} + p_s) \tag{4.21}$$

$$p_E = p_{ini} + \frac{1}{3}q_E \tag{4.22}$$

The yield surface at failure can be determined by replacing $p_o(s)$ and p_s in Eq. 4.1 and solving by substituting the value of deviatoric stress, q_E or net mean stress, p_E obtained from Eq. 4.21 or Eq. 4.22.

Step 7. The interval between q_B to q_E is divided into equal deviatoric stress increments *dq*.

Step 8. The specific volume, v_o^B on the isotropic normal consolidation line (iso-ncl), corresponding to $p_o^B(s)$, is calculated using the following expression:

$$v_o^B = v_{ini} - \kappa \ln\left[\frac{p_o^B(s)}{p_{ini}}\right] \tag{4.23}$$

Step 9. The first increment of stress path BC is considered as a result of step 7. The coordinates of point C is as follows:

$$q_C = q_B + dq \tag{4.24}$$

$$p_C = p_B + \frac{1}{3}dq \tag{4.25}$$

Step 10. The value of $p_o^C(s)$ for the expanded yield locus through the intermediate point C is computed by the following expression:

$$p_o^C(s) = p_C + \frac{(q_C)^2}{M^2(p_C + p_s)} \tag{4.26}$$

Step 11. Since the specific volume on the iso-ncl, v_o^B, corresponding to p_o^B(s) is calculated from Step 8, it is feasible to compute the specific volume on the iso-ncl associated to any value of p_o(s) i.e. $p_o^C(s)$, $p_o^D(s)$, and $p_o^E(s)$. The specific volume v_o^C on the iso-ncl corresponding to p_o^c(s) is computed as:

$$v_o^C = v_o^B - \lambda(s) \ln\left[\frac{p_o^C(s)}{p_o^B(s)}\right] \tag{4.27}$$

Step 12. The specific volume, v_C at point C on the url corresponding to p_C is computed as:

$$v_C = v_o^C + \kappa \ln\left[\frac{p_o^C(s)}{p_C}\right] \tag{4.28}$$

Step 13. Shearing a specimen along the CTC stress path in drained condition allows the volume changes within the specimen. These volume changes between stress path BC consists of both elastic and plastic components. The elastic deformations are due to the change in net mean stress, *p*. However, the plastic deformations are caused due to the expansion of the elliptical-shaped yield surface and are computed in step 15.

The elastic volumetric and shear strain increments, $d\varepsilon_{vp}^e$ and $d\varepsilon_q^e$, along stress path BC can be computed as follows:

$$d\varepsilon_{vp}^e = \frac{\kappa}{v}\frac{dp}{p} = \frac{\kappa}{v_B}\left[\frac{p_C - p_B}{p_B}\right] \tag{4.29}$$

$$d\varepsilon_q^e = \frac{1}{3G}[q_C - q_B] = \frac{1}{3G}dq \tag{4.30}$$

Step 14. The total volumetric strain increment, $d\varepsilon_{vp}^{tot}$ developed along the stress path BC is computed as:

$$d\varepsilon_{vp}^{tot} = \frac{-dv_{BC}}{v_B} = \frac{v_B - v_C}{v_B} \tag{4.31}$$

Step 15. The plastic volumetric strain increment $d\varepsilon_{vp}^{p}$, developed along stress path BC is computed as:

$$d\varepsilon_{vp}^{p} = d\varepsilon_{vp}^{tot} - d\varepsilon_{vp}^{e} \tag{4.32}$$

Step 16. Finally, by assuming that the soil follows the non-associative flow rule for the direction of plastic shear strain increments, $d\varepsilon_q^p$, the plastic shear strain increment developed along the stress path BC can be computed by using the following expression:

$$d\varepsilon_{q}^{p} = \frac{2\alpha q_C}{M^2\left[2p_C + p_s - p_o^C(s)\right]} d\varepsilon_{vp}^{p} \tag{4.33}$$

where α is a constant and is defined as:

$$\alpha = \frac{M(M-9)(M-3)}{9(6-M)}\left[\frac{1}{1-\frac{\kappa}{\lambda(0)}}\right] \tag{4.34}$$

Step 17. The total shear strain increment is computed using: $d\varepsilon_q^{tot} = d\varepsilon_q^{e} + d\varepsilon_q^{p}$, for the stress path BC.

Step 18. The steps 8-17 are repeated for point D, and for all subsequent points along the stress path DE.

Step 19. Finally, the plots of *q-p*, *v-p*, $q\text{-}\varepsilon_q^{tot}$, and $v\text{-}d\varepsilon_q^{tot}$ are plotted as demonstrated in Fig. 4.28.

The original BBM framework was postulated for predicting the strength and volume change of soft clays, where the soil compresses upon shearing, with no dilation. Therefore, the deviator stress response gradually increases and finally attains a steady state, also known as the critical state. However, for soils showing dilatancy, the BBM framework is not expected to predict the soil response accurately. Although, the predictions for stress-strain response at the critical state were observed to be near to the experimental data from the single-stage and multistage triaxial tests. The subsequent section devotes to the comparison of experimental results and the BBM predictions.

4.6.5.2 Comparison between single-stage results and BBM predictions

The comparison between the predictions from BBM framework and experimental data of the deviator stress response with monotonic shearing for varying initial net mean stress (100, 200 and 400 kPa) and matric suction levels (50, 250 and 750 kPa) under drained condition following CTC stress path are shown in Fig. 4.29 to Fig. 4.31.

The results from the BBM demonstrated moderately close predictions at the critical state. However, as expected the BBM predictions were not able to capture the post-peak softening response, as its assumption is based on the strain hardening.

The BBM predictions for the response of the soil at initial net mean stress of 100 kPa and a matric suction of 50 kPa had the least similarity with the observed response, as seen in Fig. 4.29. The difference in deviator stress at the critical state

between the BBM prediction and experimental observation was approximately 50 kPa (or 13.8%). This might be due to the underestimation of the ATS (difference of 18 kPa or 42% in the value of $p_s(s = 50)$) at the suction of 50 kPa, as seen in Fig. 4.24. If the actual experimental values were used, the value of k would have been 0.8432 for the suction level of 50 kPa. The results, in that case, showed good coherence with the experimental results (shown in Appendix B). The difference at the peak stress would be 38 kPa (or 9.9%), while at the critical state the difference would have been 8.5 kPa (or 2.4%). Hence the use of a non-linear variation of k with respect to the matric suction would be optimal for BBM predictions.

An interesting observation was made for the BBM prediction at a matric suction of 250 kPa and net mean stress of 400 kPa (Fig. 4.30). The BBM predictions were observed to be close to the peak stress level of the experimental results, which may partly be due to overprediction (by 6%) of ATS at the suction of 250 kPa.

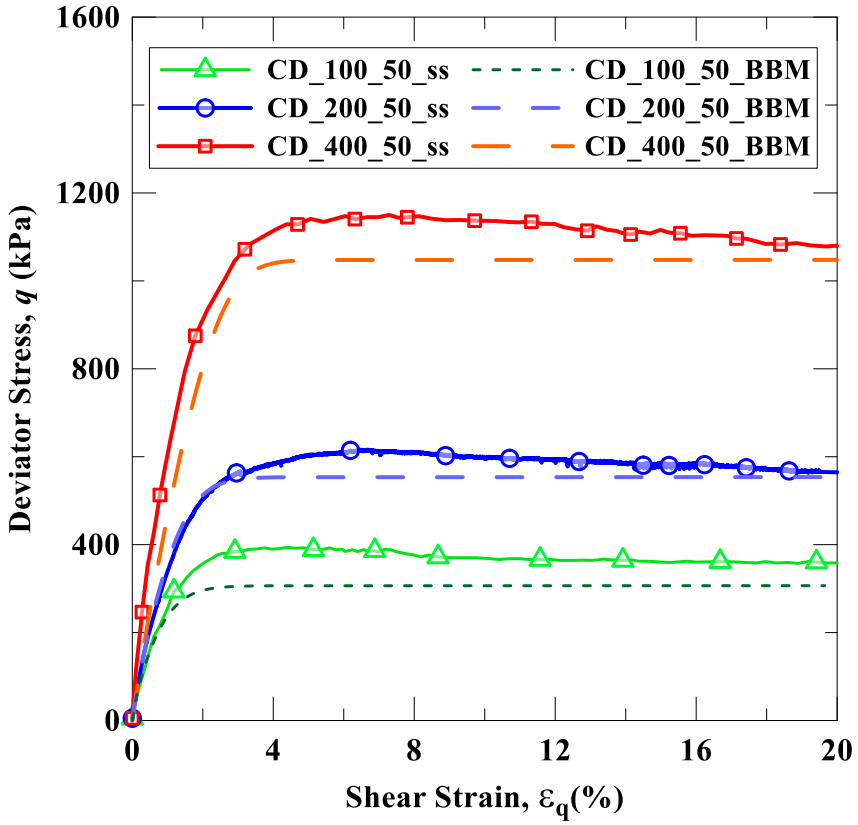

Figure 4.29 Experimental and BBM predicted response from suction-controlled CTC test under drained conditions at initial net mean stress of 100 kPa, 200 kPa, and 400 kPa and matric suction of 50 kPa

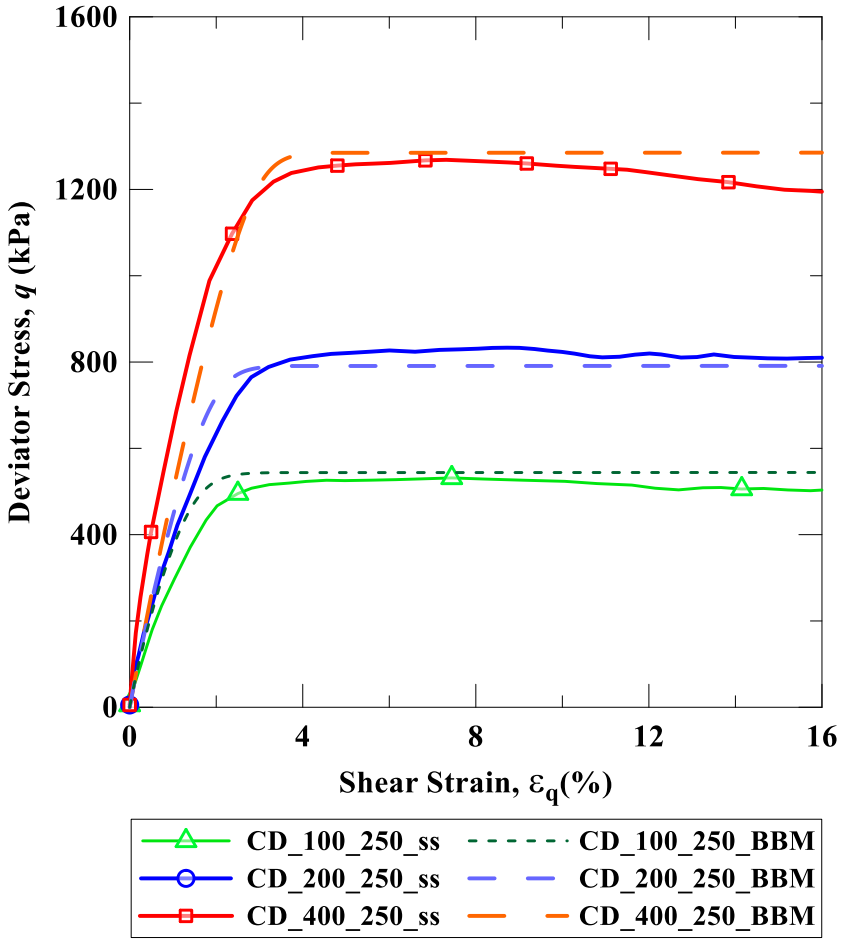

Figure 4.30 Experimental and BBM predicted response from suction-controlled CTC test under drained conditions at initial net mean stress of 100 kPa, 200 kPa, and 400 kPa and matric suction of 250 kPa

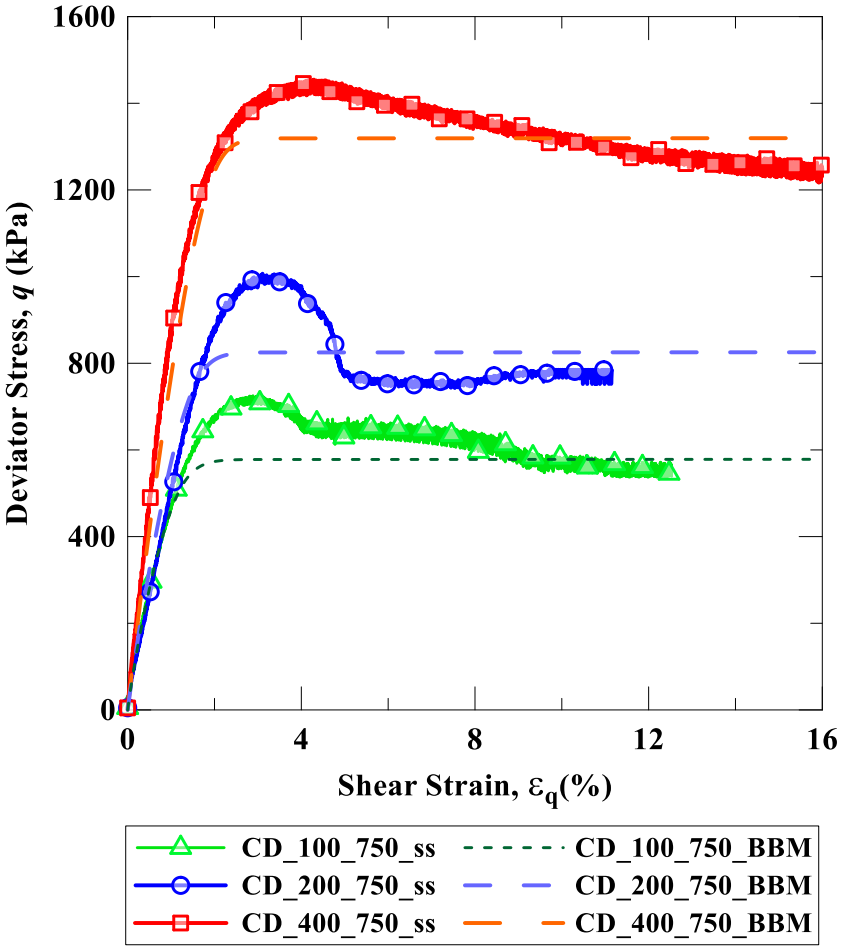

Figure 4.31 Experimental and BBM predicted response from suction-controlled CTC test under drained conditions at initial net mean stress of 100 kPa, 200 kPa, and 400 kPa and matric suction of 750 kPa

4.6.5.3 Comparison between multistage results and BBM predictions

Figures 4.32 and 4.33 show the comparison between the stress-strain response obtained from the multistage triaxial tests at varying initial net mean stress of 100, 200, and 400 kPa and at a matric suction of 50 kPa and 250 kPa, respectively. The stress-strain response (Fig. 4.32) from multistage triaxial test shows good correlation with the predictions from BBM framework at the critical state for an initial net mean stress of 400 kPa and matric suction of 50 kPa.

However, since the ATS and the value of *k* were underestimated (by 42%), as in the case of single-stage tests, at the matric suction of 50 kPa, the difference between the BBM predictions and experimental observations seem to be distinct. If the value of *k* at matric suction of 50 kPa was 0.8432 (which forms the best-fit line from *s* = 0 to s = 50 kPa) the predictions would be close to the observed experimental results (shown in Appendix B). The deviator stress response from the multistage tests also shows the unloading sequence for net mean stress of 100 and 200 kPa.

The deviator stress at the initial net mean stress of 100 and 200 kPa were not allowed to reach the failure state and stopped when the dilation was initiated (as described in section 4.4.2). Hence the predictions (as shown in Fig. 4.33) appear to be slightly higher than the experimental observations. Additionally, the ATS was overestimated, due to the constant value of $k = 0.4914$, instead of 0.466 which is suited for suction at 250 kPa.

After reviewing the comparisons between the BBM predictions and the experimental observations from single-stage and multistage triaxial tests (Figs. 4.29, 4.30, 4.32, and 4.33), it could be mentioned that the use of multistage tests results in negligible errors in the BBM predictions. Hence, the BBM generated by calibrating the parameters using single-stage and multistage tests produce similar predictions.

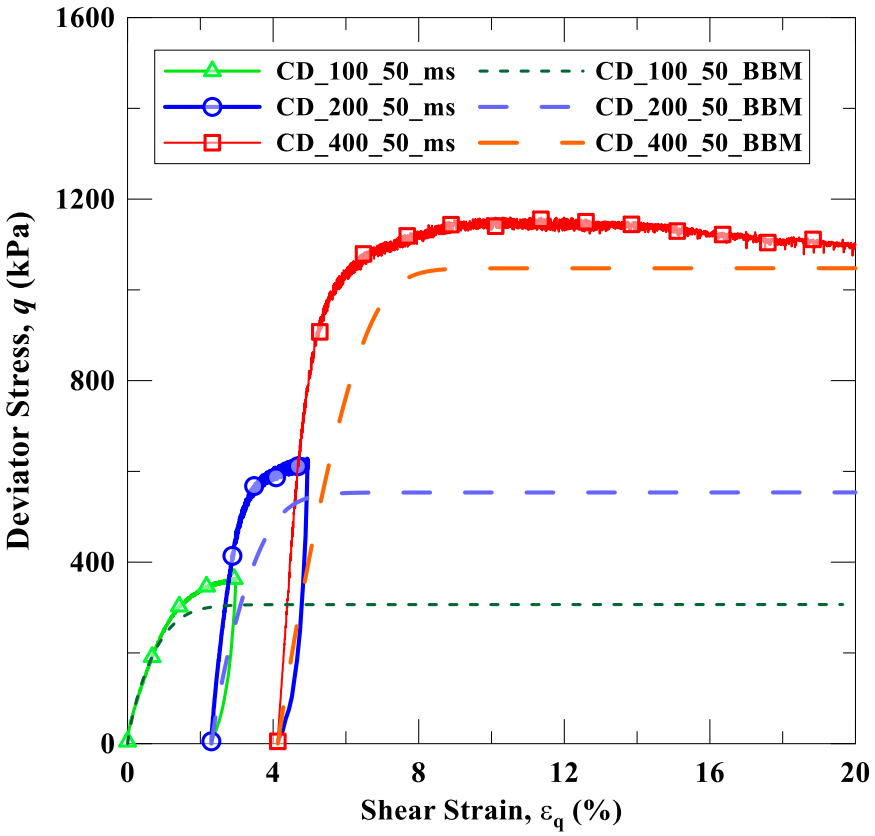

Figure 4.32 Comparison between predictions from BBM framework and multistage triaxial test at a constant matric suction of 50 kPa and varying net mean stress of 100, 200, and 400 kPa

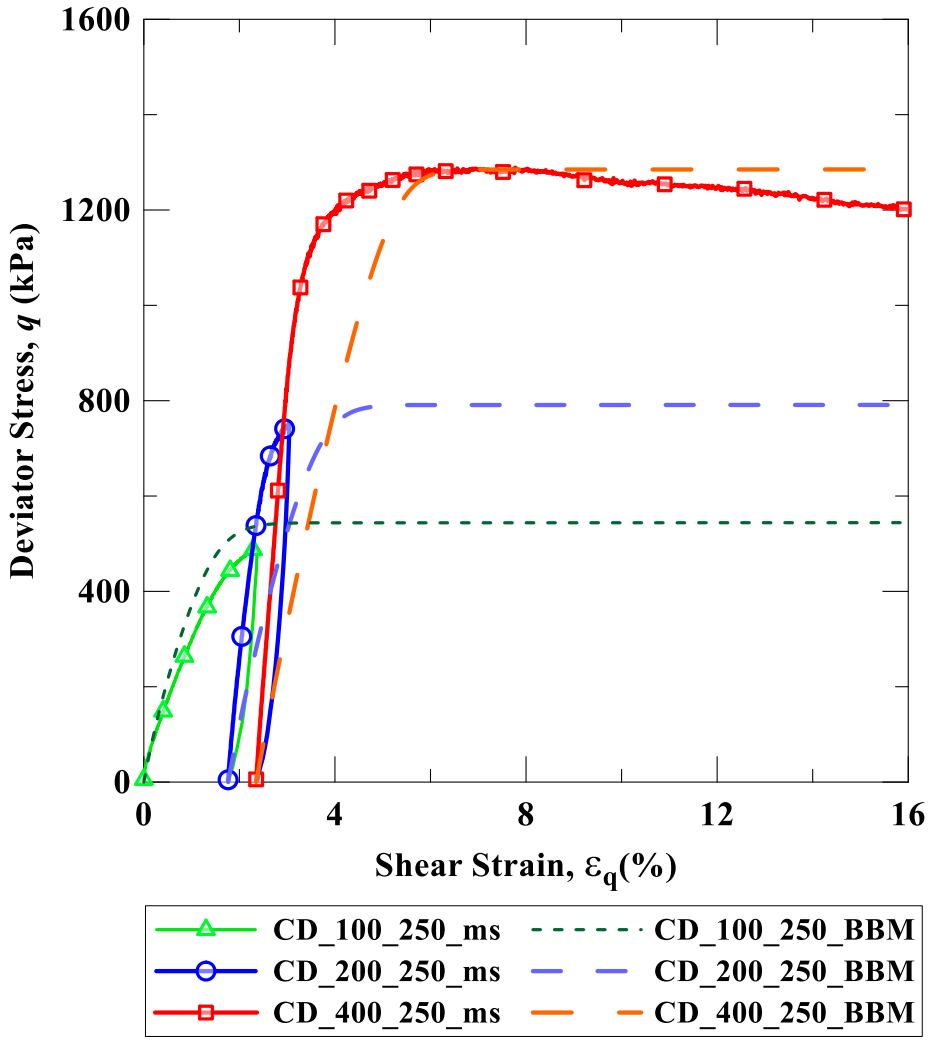

Figure 4.33 Comparison between predictions from BBM framework and multistage triaxial test at a constant matric suction of 250 kPa and varying net mean stress of 100, 200, and 400 kPa

The shear-induced expansion of the yield surfaces at initial net mean stress of 100, 200, and 400 kPa and induced matric suction of 50, 250 and 750 kPa are shown in Fig. 4.34 to Fig. 4.36. Figures 4.34 and 4.35 shows the comparison between the single-stage and multistage triaxial test at critical state on *p*-*q* space and its proximity to the expanded yield surface at the critical state. The yield surface is assumed to be an ellipse as postulated by the BBM framework (Eq. 4.1).

The "YS" in the Fig. 4.34 to Fig. 4.36 denotes yield surface and the term "Ini" represents the initial state. Hence, "YS CD_100_50_Ini" denotes the yield surface prior to the initiation of shearing at a net mean stress of 100 and matric suction of 50 kPa (CD_100_50 test). Whereas, "YS CD_100_50_Final" represents the expanded yield surface at critical state due to the shearing of the specimen for CD_100_50 test. Additionally, "SP" denotes the CTC stress path under drained conditions predicted by the BBM framework at any given initial net mean stress, *p* and matric suction, *s*. The experimental points at the critical state are shown in the *p*-*q* space and for example represented by "CD_100_50_ss" (for single-stage triaxial test) or "CD_100_50_ms" (for multistage triaxial test).

For single-stage tests, the initial and final yield surfaces for each initial net mean stress are shown in Fig. 4.34 to Fig. 4.36. For each initial net mean stress, the soil is assumed to be normally consolidated prior to the commencement of

shearing. Hence, for all the values of net mean stress, the increase in deviator stress results in subsequent enlargement of the yield surface till the CSL is intercepted.

For multi-stage tests (Figs. 4.34 and 4.35), the initial yield surface post-consolidation at a net mean stress of 100 kPa expands with increase deviator stress, as it is normally consolidated. After unloading and consolidation at a net mean stress of 200 kPa, the soil is slightly over-consolidated, as the yield surface generated during loading at 100 kPa net mean stress is larger than that at the second stage of consolidation. Therefore, in this case, the yield surface remains constant and no additional plastic deformations are developed during the initial loading sequence for the net mean stress of 200 kPa. However, once the stress path intersects the yield surface, elasto-plastic deformations are developed for additional loading. Similar observations are made from shearing at the net mean stress of 400 kPa, where the soil is moderately over-consolidated. However, in all cases, a significant portion of the loading occurs in the virgin state of the soil. Hence, the residual shear stresses and strains induced due to the loading in the previous stages would not have a significant effect on the critical state of the current stage of testing.

The recommendations from this study are that the ratio between the net consolidation stress of the subsequent stages in a multistage triaxial test should be greater than 2 or 3 for low matric suction (less than 250 kPa) and should be greater than 4 for higher suction range (more than 750 kPa) to decrease the overlapping of the yield surfaces from subsequent stages.

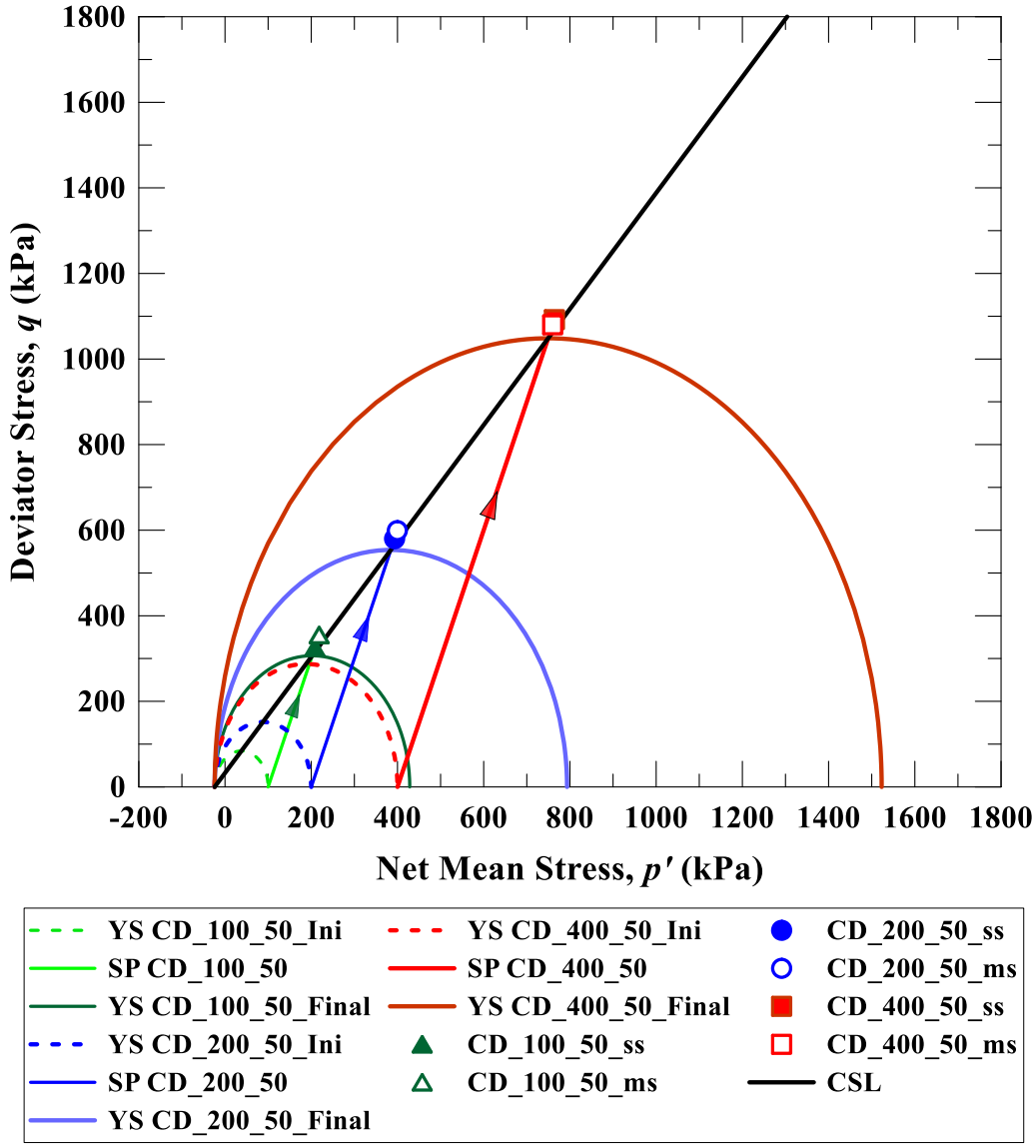

Figure 4.34 Variation of yield surface during single-stage and multistage triaxial testing at matric suction of 50 kPa

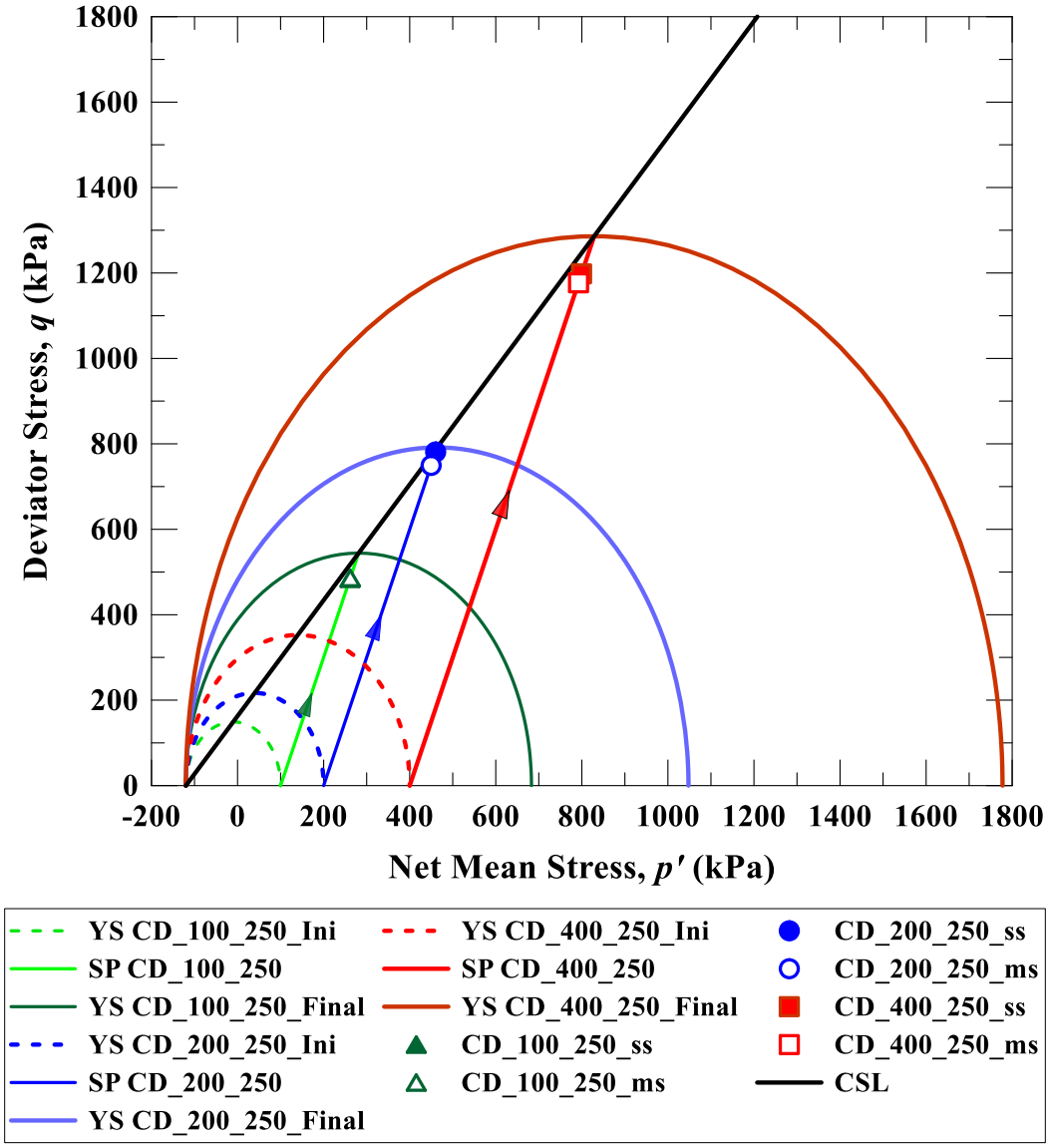

Figure 4.35 Variation of yield surface during single-stage and multistage triaxial testing at matric suction of 250 kPa

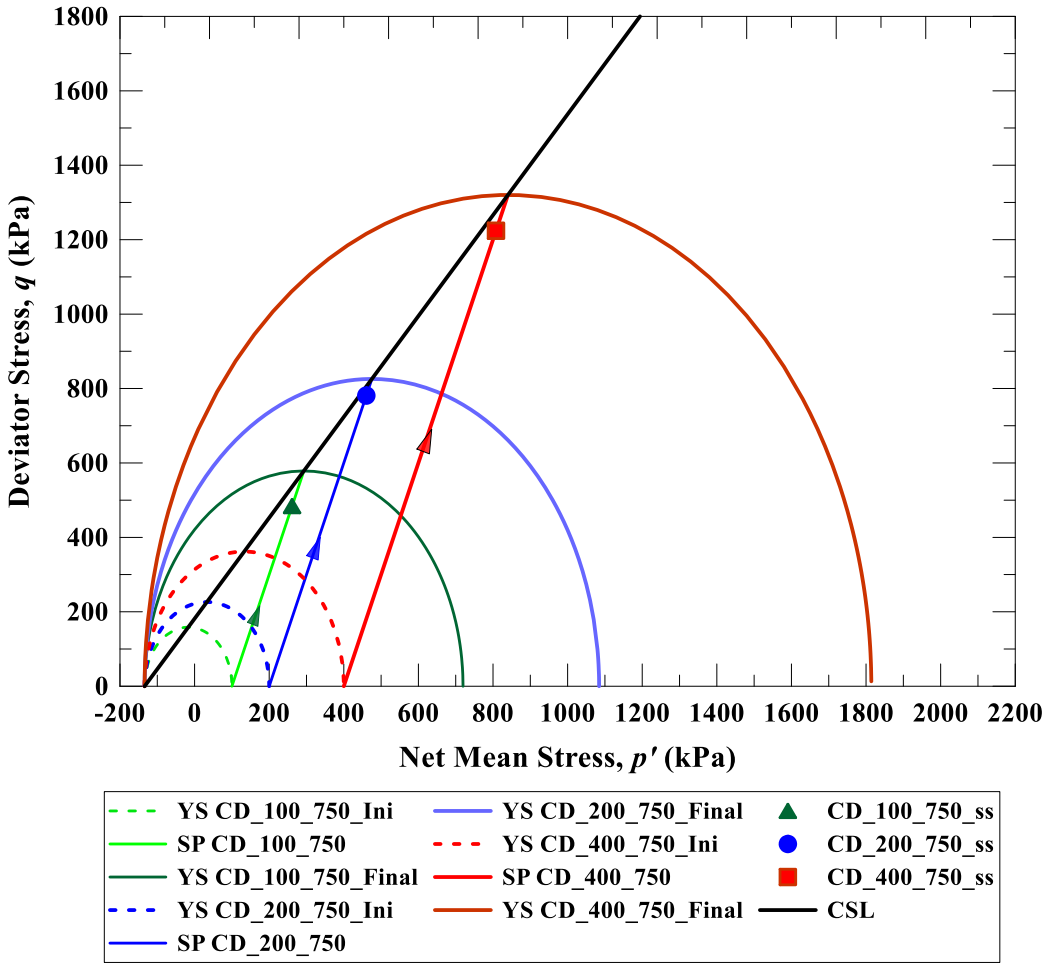

Figure 4.36 Variation of yield surface during single-stage triaxial testing at matric suction of 750 kPa

4.6.6 *Summary for BBM and its Application to Multistage Testing*

The compacted silty soil specimen demonstrated a small magnitude of post-peak softening, even for saturated and low suction state (less than 250 kPa), henceforth the BBM framework is not suitable to determine the peak strength. However, the strengths at critical state are fairly predicted by the BBM framework

for low to moderate suction states. It was also observed that the use of the constant value of *k*, which denotes the increase in cohesion with suction, is a major limitation of the BBM framework and a nonlinear function of *k* with respect to matric suction was determined to be most suited to be for the BBM predictions.

The variation in the results from single-stage and multistage triaxial tests had negligible influence on the validation for predictions based on BBM framework. Additionally, it was observed that if the subsequent initial net mean stress were in multiples of 2 or greater, for low suction range ($s<250$ kPa) and 4 or greater, for high suction range ($s>750$ kPa), the corresponding strength at critical states for single-stage and multistage triaxial tests were identical, due to the small portion of overlapped yield surfaces.

4.7 Summary

The procedure to conduct the multistage triaxial stage at constant suction and varying initial net mean stress using the new two-fold criteria for determination of termination point during the initial two shearing stage (when initial net mean stress was 100 and 200 kPa) is described. It is to be noted that the advantages of the two-fold criteria are applicable to the generic behavior of soils and are not limited to soils depicting dilatant behavior upon shearing.

The mechanical response of the series of multistage triaxial tests at constant suction, but varying initial net mean stress (100, 200, and 400 kPa) were conducted on saturated and unsaturated specimens over a suction range of 0 to 250 kPa, using

axis translation technique. The deviator stress and volumetric strain responses for each test were studied in detail and compared with that for single-stage triaxial tests, to validate the approach used for multistage triaxial tests. The variation of the critical criterion for termination of shearing with matric suction is also demonstrated.

The main features of the Barcelona Basic Model (BBM) framework for unsaturated soils by Alonso et al. (1990) are listed. The calibration of the various parameters was conducted using the results from suction-controlled triaxial tests. The prediction models for varying suction levels (s = 50 to 750 kPa) were developed based on the BBM framework and comparisons were made with the stress-strain response of single-stage and multistage triaxial tests. It was observed that the post-peak softening was not captured by the BBM, as the BBM framework is based on concept of strain hardening. However, the strength at critical state was adequately predicted by the BBM for both single-stage and multistage triaxial tests. Moreover, the initial (prior to shearing) and final (after reaching the critical state) yield surface were plotted using the BBM, for studying the minimum ratio of confining stress to be applied to subsequent stages in the multistage triaxial test.

Chapter 5

EFFECT OF SUCTION ON RESILIENT MODULUS OF SOIL USING SUCTION-CONTROLLED TESTS

5.1 General

The flexible pavements are widely constructed as a mode of transportation system throughout the world. The foundation of a pavement consists of compacted granular material, which lies over compacted subgrade soil (Brown, 1996). The traffic loads from the surface are transferred to the subgrade soil and cause elastic and plastic deformations in the subgrade, which results in stresses being developed in the various layers of a flexible pavement (Puppala et a., 1999; Kim and Siddiki, 2006).

The design of pavement is dependent primarily on the fatigue cracking at the bottom of the surface layer and the permanent (i.e., plastic) deformation at the surface of subgrade soil (Han and Vanapalli, 2016). The fatigue cracking occurs due to the repeated loading and unloading of the flexural stresses on the pavement structure, which develops due to the elastic deformations of the layers beneath the top surface, including the subgrade soil. Hence, the fatigue cracking is dependent on the resilient behavior of the pavement materials when subjected to traffic loading (Seed et al., 1962; Puppala et al., 1999). The permanent or plastic deformations

could be determined by performing tests under repeated cycles of deviator loads at varying confining pressure and was observed to be predominant in specimens compacted and tested at wet of optimum moisture content (Puppala et al, 2009).

Additionally, the failure of flexible pavements occurs typically due to the excessive rutting or cracking of pavement layers due to fatigue, temperature changes, and/or softening because of cracking in the surface layer (Barksdale, 1972; Brown, 1974, 1996; Puppala et al., 1996; Puppala, 2008). Since, the failure of flexible pavements does not occur due to the criteria of soil strength, the 1993 AASHTO guide for design of pavement structures and its subsequent version in 1998 and the AASHTO Mechanistic-Empirical Pavement Design Guide (M-EPDG) in 2004, recommended the use of resilient modulus, instead of soil strength parameters (Brickman, 1989; Mohammad et al. 1994; Maher et al., 2000; Puppala, 2008; Zapata et al., 2009). Hence, the resilient modulus of the soil subgrade is a key design parameter for the flexible pavement systems.

Subgrade soils are generally compacted at or near the optimum moisture content, and it mostly stays in unsaturated condition throughout its service period (Han and Vanapalli, 2015). It is well-known that the moisture regime change greatly influences the resilient modulus of the soil (Puppala, 2008). The moisture regime change in the subgrade soil is directly related to the soil suction in the subgrade. Therefore, the soil suction affects the resilient modulus of the subgrade. Additionally, the AASHTO Mechanistic-Empirical Pavement Design Guide (M-

EPDG) has emphasized the influence of environmental factors, especially the effect of moisture regime, on the performance of the pavement (Cary and Zapata, 2011).

Sauer and Monismith (1968), Edris and Lytton (1976), Fredlund et al. (1977), and Edil and Motan (1979) introduced the prediction of resilient modulus using suction as a dependent parameter.

5.2 Review of Literature: Resilient Modulus of Soils

5.2.1 *Definition of Resilient Modulus*

The resilient modulus (M_R) of a material, introduced by Seed et al. (1962), is defined as the ratio of applied deviator stress (σ_d) to the recoverable or resilient strain (ε_r) experienced by the material, due to the loading and unloading of the applied deviator stress. Resilient modulus (M_R) is expressed as:

$$M_R = \frac{\sigma_d}{\varepsilon_r} \tag{5.1}$$

Figure 5.1 shows the schematic representation of the time-dependent applied load and stress-strain response of the subgrade material.

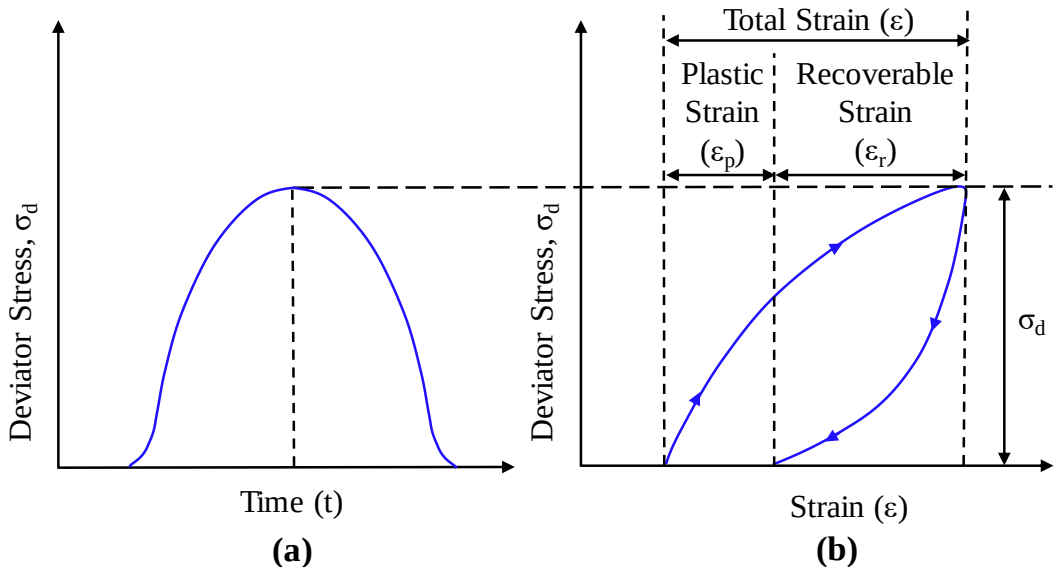

Figure 5.1 Illustration for definition of resilient modulus

5.2.2 *Factors influencing the Resilient Modulus of Subgrade Soils*

The factors affecting the resilient modulus of the soils had been reviewed in depth by Lekarp (2000) and Puppala (2008), which have been described below:

1. Applied stress: The applied stress level has been reported to have the most influence on the resilient modulus of the soil (Williams, 1963; Kolisoja, 1997; Lekarp, 2000). The effect of confining pressure was observed to have a high degree of influence on the resilient modulus of various types of soils, including treated soils (Mitry, 1964; Hicks, 1967; Smith and Nair, 1973; Uzan, 1985; Lekarp, 2000; Potturi, 2006; Puppala, 2008; Saride et al., 2010; Rout et al., 2012; Rout, 2012; Ruttanaporamakul, 2012; Ng et al., 2013; Ruttanaporamakul et al., 2014; Salour et al., 2014). The deviator stress was observed to have a lesser influence on the resilient modulus as compared to

that of the confining pressure (Lekarp, 2000). Malla and Joshi (2006). In addition, Ruttanaporamakul (2012) had observed that the resilient modulus increased with an increase in deviator stress for cohesionless soils; while the resilient modulus decreased with an increase in deviator stress for cohesive soils.

2. Density of subgrade soil: Generally, it has been observed that the resilient modulus increases with a corresponding increase in density (Hicks, 1970; Kolisoja, 1997).
3. Gradation of soil and particle shape: The increase in fines content has been observed to decrease the stiffness or the resilient modulus of the soil, which was initially studied by Hicks (1970) and Thom and Brown (1987). Jorenby and Hicks (1986) had observed an initial increase in stiffness and later reduction, as clayey fines were added to crushed aggregate. The influence of particle shape was observed to be the highest for aggregates. The angular to subangular shaped aggregates demonstrated higher resilient modulus than that of subrounded to rounded aggregate (Thom and Brown, 1989; Barksdale and Itani, 1989). Additionally, the curing time of treated soils significantly affect the resilient modulus (Zhang et al., 2015).
4. Moisture content, soil suction and climatic conditions: The decrease in moisture content (or increase in soil suction) has been considered intuitively and determined experimentally to increase the resilient modulus of soils

(Haynes and Yoder, 1963; Elliot et al., 1988; Wilson et al, 1990; Jin et al., 1994; Mohammed et al., 1999; Witczak et al., 2000; George, 2004; yang et al., 2005; Gupta et al., 2007; Puppala, 2008; Ng et al., 2013). The environmental conditions have a significant influence on the resilient modulus of the soils (Puppala, 2008; Zapata et al., 2009, Salour et al., 2014).

5. Stress history and compaction technique: The stress history and the soil fabric have been observed to have some influence on the resilient modulus of soils (Boyce et al., 1976). However, Hicks (1970) noted that after application of approximately 100 cycles of same stress amplitude, the effect of stress history is negligible. Allen (1973), Brown and Hyde (1975), and Mayhew (1983) made similar observations and recommended that this observation was valid till the applied stress has negligible permanent deformations. Lee (1993) observed that the clayey specimens compacted at a high degree of saturation (wet of optimum moisture content) showed high sensitivity to the type of compaction used.
6. Load duration, frequency, number of load cycles, and load sequence: Seed et al. (1965) had observed small influence of the load duration and frequency of the applied deviator stress, which was validated by various researchers (Hicks, 1970; Boyce et al., 1976; Thom and Brown, 1987). Hicks (1970) and Allen (1973) observed no significant impact on the resilient modulus of granular materials due to the number of loading cycles

(Lekarp et al., 2000). Hicks and Allen (1974) observed a negligible influence due to the number of load cycles after 50-100 cycles. Ng et al. (2013) concluded that the resilient modulus increases with an increase in the number of load cycles when the soils tend to contract under cyclic loads. However, Ng et al. (2013) observed that for dilative soils, the resilient modulus decreased slightly under cyclic loads. After 100 cycles, this effect was observed to be negligible for both types of soils (Ng et al., 2013).

5.2.3 *Determination of Resilient Modulus of Soils*

The resilient modulus of soils is determined using mostly the triaxial setup by performing the repeated load triaxial test (RLTT). However, other laboratory devices to determine the resilient modulus include resonant column, simple shear, hollow cylinder test, and cubical triaxial test.

The resilient modulus is analogous to the modulus of elasticity employed in the theory of elasticity (Puppala, 2008). Since the traffic load is a moving load, the individual points of the subgrade soil experience discrete loading and unloading at intermittent intervals, which is conventionally simulated by a cyclic loading sequence (Han and Vanapalli, 2016).

The repeated load triaxial testing setup is designed to simulate the stress increase due to traffic load on the subgrade soils by applying a predefined cyclic loading sequence at varying confining stress, which simulates the in-situ overburden pressure (Puppala, 2008).

The AASHTO T-307-99 (2003) is one of the most common standard testing protocol followed in determining the resilient modulus of subgrade soils. The axial deviator stress comprises of two components: (*i*) seating/contact stress, and (*ii*) cyclic deviator stress. The seating stress constitutes 10% of the total deviator stress to be applied, which is applied for proper contact of the load actuator with the top surface of the specimen. The cyclic deviator stress is applied in the form of the haversine-shaped waveform (specified by AASHTO and NCHRP). The haversine-shaped waveform (Fig. 5.2) is a function of the phase angle (θ) and is defined as:

$$\text{haversine}\,(\theta) = \frac{(1+\cos(\theta))}{2} \tag{5.2}$$

where θ is the phase angle, which defines the number of cycles (1 cycle = 360° = 2π radians).

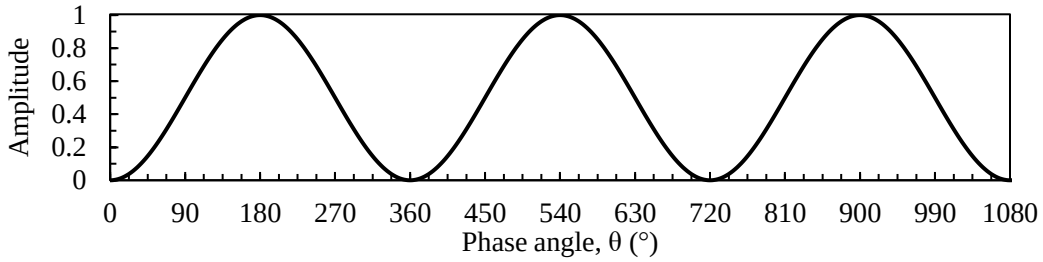

Figure 5.2 Illustration of haversine-shaped waveform

Each loading and unloading sequence of the cyclic load is applied in 0.1 s and a relaxation period is 0.9 s, which is recommended by the AASHTO T-307-99 (2003). Figure 5.3 shows a hypothetical sequence of application of

loading/unloading for 3 cycles if the applied cyclic stress has an amplitude of 1 unit.

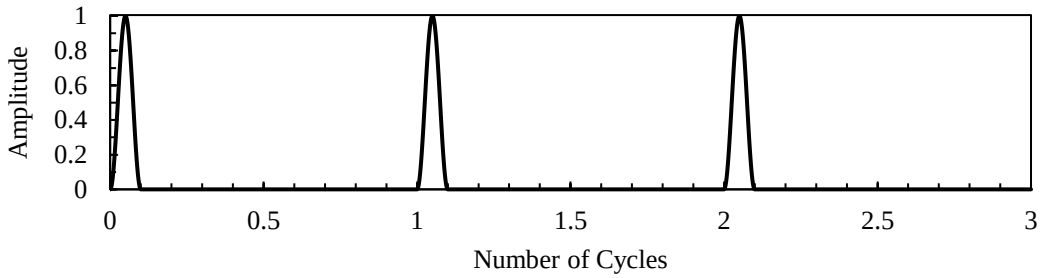

Figure 5.3 Illustration of cyclic stress applied during the resilient modulus test using RLTT

The factors affecting the resilient modulus of soils have been addressed partly by the standardization of testing protocol by AASHTO, i.e., AASHTO T292-91, AASHTO T294, AASHTO T307-99 (AASHTO, 2003); and NCHRP suggested method namely NCHRP 1-28A (Witczak, 2003). Henceforth, the effect of confining stress, deviator stress, loading sequence, number of load cycles and frequency of applied cyclic load has been mitigated using a standardized testing protocol. The standardized loading sequences have been developed to facilitate the comparison of results obtained from various sources. The detailed information regarding the various testing protocols had been summarized by Puppala (2008).

The resilient modulus of subgrade soils using the RLTT has been conducted by many researchers. Seed et al. (1962) was one of the pioneers to study the resilient modulus of soils, which focused on the effect of compaction and soil type on the resilient modulus. Others studied the influence of factors influencing the resilient

modulus, which are described in Section 5.2.2. Most of the previous studies mainly catered to the approach of performing RLTT on unsaturated specimens without controlling or measuring the suction within the soil specimen. Since the primary objective of this research is to study the effect of suction on the resilient modulus of soils, the studies similar to the main objective are discussed.

The experimental study demonstrated significant influence of suction on the resilient modulus of various pavement materials (Khoury and Zaman, 2004; Yang et al., 2008; Thom et al., 2008; Khoury et al., 2011; Ng et al., 2013; Sivakumar et al., 2013; Ng and Zhou, 2014; Salour et al., 2014; Abu-Farsakh et al., 2015; Salour and Erlingsson, 2015).

Khoury and Zaman (2004) performed a series of the resilient modulus test on specimens of sandy and clayey soils. The AASHTO T-307-99 testing protocol was used to apply the loading sequence. The soil suction was determined using the filter paper technique after the conclusion of each test. The variation of resilient modulus with moisture content and soil suction was plotted. It was concluded that the wetting and drying process had a greater influence on the resilient modulus of clayey soil than that of sandy soil.

Yang et al. (2005) performed a similar study on the effect of soil suction on resilient modulus of clayey soil using the AASHTO T 292-91 testing protocol, without directly controlling or measuring the soil suction before or during the test. It was observed that the resilient modulus increased with an increase in matric

suction and total suction. However, the scatter in the values of soil suction were very high. A model was developed to predict the resilient modulus by using the deviator stress, soil suction, and Bishop's effective stress parameter, χ.

Yang et al. (2008) performed suction-controlled RLTT to determine the effect of soil suction on the resilient modulus of clayey soils. The specimens were initially equilibrated using independent control of pore air pressure and pore water pressure. However, during the loading sequence of RLTT, the pore air pressure line was drained, while the pore water pressure line was undrained. In other words, the resilient modulus was determined using the constant water (CW) test (explained in section 2.8). It was observed that the soil suction decreased slightly during the testing sequence (Fig. 5.4). The water content of each test, shown in Fig. 5.4 were 23.4% ($S \approx 72\%$), 20.2% ($S \approx 64\%$), and 19.1% ($S \approx 54\%$).

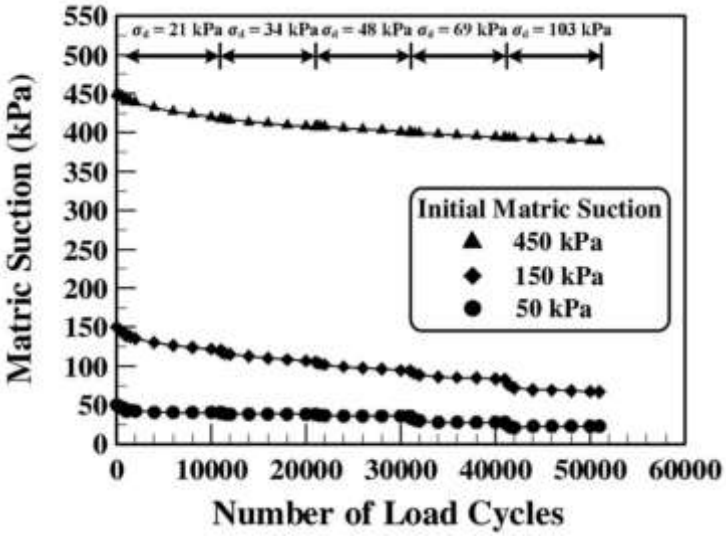

Figure 5.4 Variation of matric suction with number of cycles during the resilient modulus test (after Yang et al., 2008)

Thom et al. (2008) performed repeated load triaxial test on specimens of kaolin while measuring suction throughout the duration of the test using a thermocouple psychrometer. A non-standard loading sequence was applied, which comprised of three deviator stresses, a quarter (200 cycles), half (100 cycles), and three-quarter (100 cycles) of the failure deviator stress (determined from the monotonic triaxial test), for constant confining stress of 50 kPa. Additional specimens were used for confining stress of 100 and 150 kPa. A total of nine loading sequences were tested. Figure 5.5 shows the variation of suction with the number of load cycles. The decrease in suction during testing was observed to be synchronized with the application of deviator stress, which might be due to the increase in the degree of saturation with additional loading.

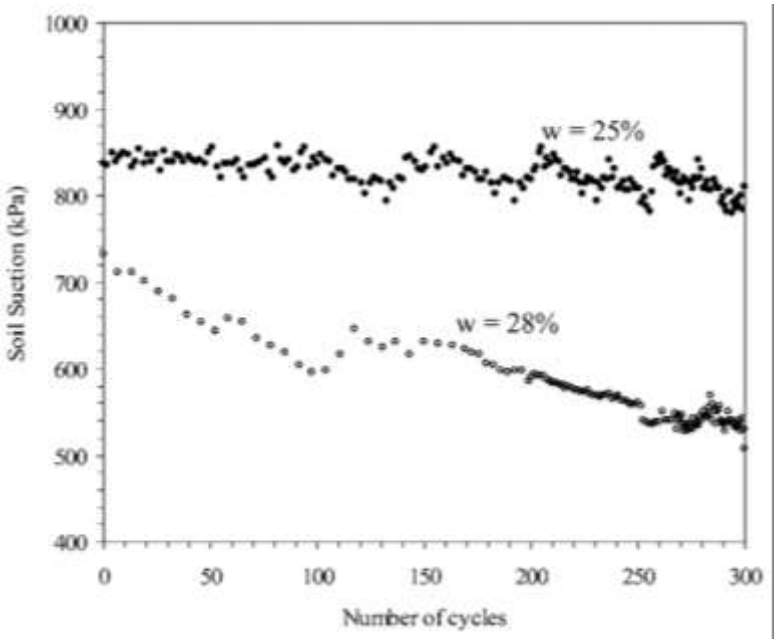

Figure 5.5 Variation of matric suction with number of cycles during the resilient modulus test (after Thom et al., 2008)

Khoury et al. (2011) performed suction-controlled RLTT to determine the resilient modulus of sandy silt specimens using the AASHTO T 307-99 testing protocol. The modification in the testing protocol was introduced, in the form of change in confining pressure to net confining pressure and an independent application of pore air and pore water pressure, to perform suction-controlled testing. The tests were conducted at varying suction levels from 25 kPa to 100 kPa. It was observed that the resilient modulus increased with suction. Additionally, the resilient modulus of specimens tested at only a given net confining pressure and suction showed lower values as compared to the ones on which continuous varying load sequences were applied. This indicated the influence of loading history on the resilient modulus of the soil.

Rout (2012) and Rout et al. (2012) performed suction-controlled RLTT on base materials like poorly graded gravelly soil. The specimens were prepared at varying suction levels of s = 50, 100 and 150 kPa. It was concluded that for base materials like gravelly soils, the suction-controlled M_R tests yielded similar results as compared to the traditional moisture-controlled M_R tests.

Ng et al. (2013) performed suction-controlled RLTT to determine the resilient modulus of soil using the axis-translation technique. The soil deformation at the mid-height of the specimen was monitored using three Hall-effect transducers developed by Clayton et al. (1989). A suction probe (Xu, 2011) was used to determine the suction at the mid-height of the specimen. The repeated loads were

applied in constant water (CW) test. It was justified that as the permeability of the unsaturated fine-grained soil is low and the rate of loading is very high, the resilient modulus obtained using the CW test and the drained test as recommended by AASHTO (2003) would be identical. A modified loading sequence was also used. As mentioned earlier in section 5.2.2, the resilient modulus was observed to increase with an increase in the number of loading cycles for the contractive behavior of soil, whereas for the dilative response, the resilient modulus values decreased with increasing loading cycles. The resilient modulus was also observed to decrease with an increase in applied cyclic stress for all confining pressures over both wetting and drying cycles. On the other hand, resilient modulus increased with an increase in suction, which had been observed in all the studies performed.

Similar observations were made from studies conducted by Sivakumar et al. (2013). Ng and Zhou (2014) performed a study on the effect of suction and temperature on the resilient modulus of soils by using a modified version of the setup as used by Ng et al. (2013).

Salour et al. (2014); and Salour and Erlingsson (2015) performed suction-controlled RLTT on compacted specimens of two types of non-plastic silty sand from Sweden. The modified version of NCHRP 1-28A (2004) test protocol was followed to account for applying pore air pressure (similar to the approach used by Khoury et al., 2011). The experimental results were used to calibrate and later validate a model for predicting the resilient modulus of soils from its induced

suction. The conclusions drawn from the study were similar to that of Khoury et al. (2011), where resilient modulus was observed to increase with an increase in applied deviator stress and matric suction.

Although the relationship between resilient modulus and soil suction has been investigated for many years, the issue of repeatability and reliability of resilient moduli is still a concern. Henceforth, in this research, the influence of dry unit weight of soil and the soil suction was investigated by performing an elaborate series of RLTT tests on specimens at varying dry density and a wide range of suction values.

5.2.4 *Prediction of Resilient Modulus*

Reliable determination of the resilient modulus of soils using experimental methods like suction-controlled, repeated load triaxial tests (RLTT) are time-consuming, expensive, and require advanced laboratory equipment with trained professionals (Han and Vanapalli, 2016). These are the main reasons for the development of prediction models and empirical relations, which could determine the resilient modulus of soils.

Empirical relations are often used by engineers for determination of resilient modulus using static load tests like CBR test, R-value test, Texas triaxial value, and SSV test (Puppala, 2008). Additional correlations have been established for determining the resilient modulus of a variety of soils using cone penetration test (CPT) data by Mohammed et al. (2007) and Lui et al. (2016). Geotechnical

engineers often use the existing correlations with unconfined compressive strength (UCS) tests. However, the major limitations arise when the stiffness of the soil are predicted using its strength because the latter is mostly determined at failure, while the resilient modulus is mostly dependent on the initial stiffness of the soil. The degree of influence of each factor, which influences the resilient modulus and strength, might vary significantly.

Correlations were also established to determine the resilient modulus from the parameters obtained from the non-destructive field testing methods, like the cone penetration test, the dynamic cone penetration test, the falling weight deflectometer, and the plate load test (Kim and Siddiki, 2006).

Many researchers had utilized the correlation between resilient modulus and suction to develop models or equations for predicting the resilient modulus at varying suction values. The initial relations were developed by Fredlund et al. (1977), Johnson et al. (1986), and Loach (1987). Later, researchers suggested many models like Jin et al. (1994), Lytton (1995), Oloo and Fredlund (1998), Parreira and Gonçalves (2000), Ceratti et al. (2004), Heath et al. (2004), Yang et al. (2005), Gupta et al. (2007), Liang et al. (2008), and Sawangsuriya et al. (2009). Recently, researchers had developed advanced models and calibrated them by using data from suction-controlled or suction measured during RLTTs (Cary and Zapata, 2011; Ng et al., 2013; Azam et al., 2013; Ba et al., 2013; Nokkaew et al., 2014; Salour, et al., 2014; Han and Vanapalli, 2015; Salur and Erlingsson, 2015).

The Mechanistic-Empirical Pavement Design Guide (M-EPDG, 2004) recommended the use of the following relation for determining the resilient modulus (M_R):

$$M_R = k_1 p_a \left(\frac{\theta_b}{p_a}\right)^{k_2} \left(\frac{\tau_{oct}}{p_a}+1\right)^{k_3} \quad (5.3)$$

where p_a = atmosphere pressure at mean sea level (≈ 101.3 kPa); θ_b = bulk stress;

τ_{oct} = octahedral shear stress; and k_1, k_2, and k_3 = model parameters. For calibrating the model by using the resilient modulus at the optimum moisture content, M_{ROPT} the following relation was provided:

$$\log\left(\frac{M_R}{M_{RSAT}}\right) = a + \frac{b-a}{1+\exp\left[\ln\left(-\frac{b}{a}\right)+k_m(S-S_{OPT})\right]} \quad (5.4)$$

where a = fitting parameter = minimum of log (M_R/ M_{ROPT}); b = fitting parameter = maximum of log (M_R/ M_{ROPT}); k_m = regression parameter; S = degree of saturation (in decimal); and S_{OPT} = degree of saturation corresponding to the optimum moisture content (in decimal). The values of the fitting and regression parameters were suggested to be a = –0.5934, b = 0.4, and k_m = 6.1324 for fine-grained soils; whereas, a = –0.3123 b = 0.3, and k_m = 6.8157 were suggested for coarse-grained soils.

Sawangsuriya et al. (2009) proposed the following empirical relations for fine-grained soils:

$$\frac{M_R}{M_{RSAT}} = -5.61 + 4.54 \log(\psi) \quad (5.5)$$

$$\frac{M_R}{M_{ROPT}} = -0.24 + 0.25 \log(\psi) \quad (5.6)$$

where M_{RSAT} = Resilient modulus (M_R) at saturated condition, and ψ = suction (in kPa).

Recently, Ba et al. (2013) suggested an $M_R - \psi$ relationship for granular base materials for a suction range of 0-100 kPa, which was as follows:

$$\frac{M_R}{M_{ROPT}} = 0.385 + 0.267 \log(\psi) \quad (5.7)$$

where ψ = suction (in kPa).

Cary and Zapata (2011) postulated Eq. (5.8) for granular soil and clayey sand for a soil suction range of 0 to 250 kPa, which was later verified by Salour et al. (2014) for sandy subgrade soil over a soil suction range of 0 to 450 kPa.

$$M_R = k_1 p_a \left(\frac{\theta_{net} - 3\Delta u_{w-net}}{p_a}\right)^{k_2} \left(\frac{\tau_{oct}}{p_a} + 1\right)^{k_3} \left(\frac{\psi_o - \Delta\psi}{p_a} + 1\right)^{k_4} \quad (5.8)$$

Recently, Han and Vanapalli (2014, 2015) had proposed Eq. (5.9), which was developed, calibrated, and validated using the test results from 11 different compacted, fine-grained subgrade soils (silty and clayey soils).

$$M_R = M_{RSAT} + \zeta \psi S^{\xi} \quad (5.9)$$

where

$$\zeta = \frac{M_R - M_{RSAT}}{\psi S^{\xi}} \quad (5.10)$$

and ξ = fitting parameter; S = degree of saturation. The calibration of the parameter, ζ is performed by replacing the value of $M_R = M_{ROPT}$, which is the resilient modulus at OMC having a suction of ψ_{OPT} and degree of saturation, S_{OPT}. Equation (5.9) can be estimated by using the SWCC of the soils, for which the value of the degree of saturation (S) is replaced by the fitting parameters for SWCC model, like Fredlund and Xing (1994) SWCC model. The following equation is derived by substituting the SWCC model fitting parameters in place of the degree of saturation (S) in Eq. (5.9):

$$\frac{M_R - M_{RSAT}}{M_{ROPT} - M_{RSAT}} = \frac{\psi}{\psi_{OPT}} \left[\frac{ln\left\{2.718 + \left(\frac{\psi_{OPT}}{a}\right)^n\right\}}{ln\left\{2.718 + \left(\frac{\psi}{a}\right)^n\right\}} \right]^{m\xi} \tag{5.11}$$

where a, m, and n are the fitting parameters of the SWCC model by Fredlund and Xing (1994). The value of the fitting parameter, ξ was observed to be approximately equal to 2 for most soils. Equation (5.11) can be used to predict the resilient modulus of soils at varying suction states using the values of M_{RSAT}, M_{ROPT}, ψ_{OPT}, and the SWCC of the compacted soil, which are relatively easy to obtain.

5.2.5 *Synopsis of Literature Review*

This section explained the utility of resilient modulus in the design of flexible pavements. The definition and the concept of resilient modulus were described. The factors affecting the resilient modulus of subgrade soils were discussed, along with the techniques to mitigate some of these factors which negatively influence the repeatability of these tests. The laboratory tests to

determine the resilient modulus of soils were mentioned. Special attention was given to the repeated load triaxial test (RLTT), which is the most commonly used test to determine the resilient modulus of subgrade soils. The past and recent advances in the determination of resilient modulus using RLTT were discussed in detail, with a special focus on the suction-controlled RLTTs. The recent prediction models and relations between resilient modulus and soil suction were explained in brief, to highlight the approaches by which cost-efficient and reliable values of resilient modulus could be obtained in a short span of time.

5.3 Experimental Program

A series of suction controlled repeated load triaxial tests (RLTTs) were performed on compacted silty soil (ML) specimens at varying density and matric suction. The soil properties have been discussed in section 3.2. One of the objectives of this dissertation study was to determine the effect of using suction-controlled RLTTs in determining the resilient modulus of subgrade soil. Additionally, the influence of density and matric suction on the resilient modulus of the soil was to be studied. An attempt was also made to determine the influence the wetting and drying of the soil specimen compacted at the same dry density, but varying suction levels, which corresponds to the Proctor compaction curve (as shown in Fig. 5.6).

The list of all the RLTT tests performed is shown in Table 5.1. Several specimens were prepared and tested at a dry density of 1.67 g/cm^3 and varying

moisture content to study the effect of a wide range of suction (0 to 100 MPa) on the resilient modulus of soil. Additionally, the effect of density was studied by testing specimens at constant suction but varying dry density of the specimen.

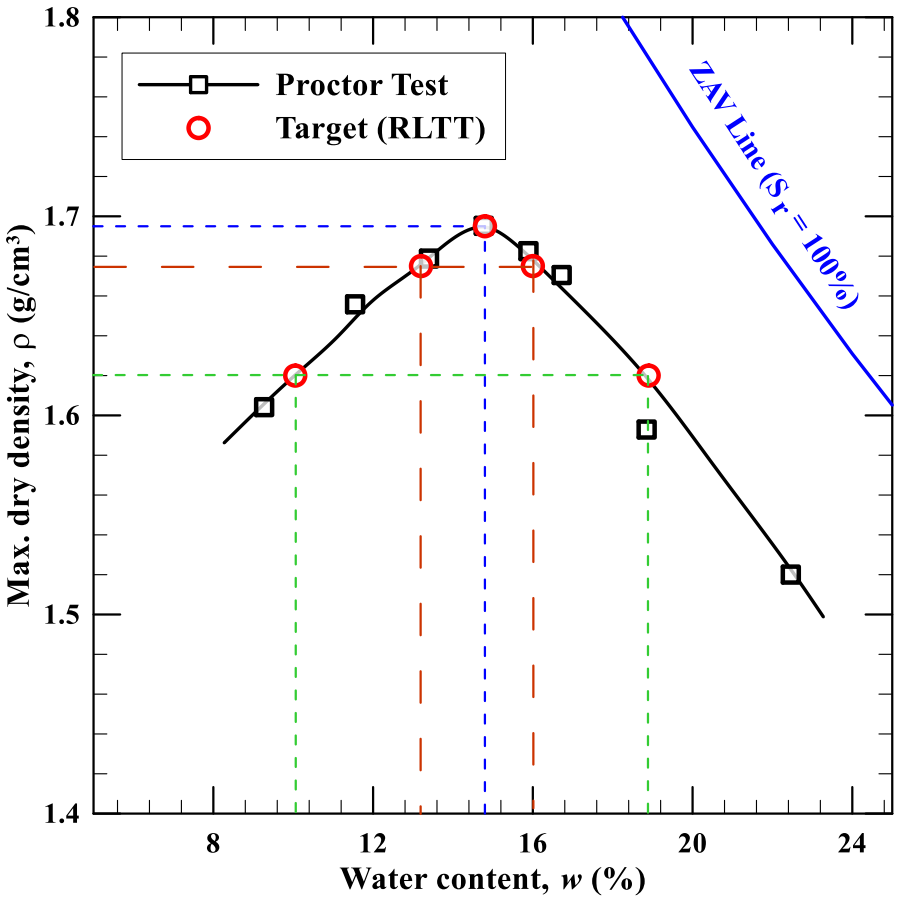

Figure 5.6 Compression curve for silty soil showing the target density and water content for the RLTT specimens

Table 5.1 Series of suction-controlled RLTT tests performed in this research

Sl. #	Density, ρ (g/cm^3)	Water Content, *w* (%)	Suction, ψ (kPa)	# of Tests (including repetitions)
1	1.67	22.5, 21.2*, 18.6*, 16.0*, 15.0*, 13.2*, 11.8, 8.9, 3.1*, 2.5	0, 2*, 10*, 26*, 36*, 65*, 100, 300, 30000*, 100000	16
2	1.70	21.8, 14.8, 8.6	0, 36, 300	3
3	1.62	23.4, 18.9, 10.1	0, 10, 200	3
4	1.67	16.2 (W), 13.1 (D)	26 (W), 65 (D)	2
5	1.62	19.2 (W), 10 (D)	10 (W), 200 (D)	2

* represents the tests which were conducted twice

5.4 Specimen Preparation

The static compaction technique was used to prepare specimens (similar to triaxial test) at the target density and moisture content of 16%. All the specimens were compacted at the same moisture content to negate the effect of variation of the specimen, due to moisture content present in the soil during compaction. Khoury and Zaman (2004) had earlier observed that the moisture content at compaction significantly affects the resilient modulus of soils. The effect of variation of moisture content during specimen preparation is explained in section 3.3.1. The details regarding the specimen preparation are explained in section 3.3

After specimen preparation, they were equilibrated to the required suction level using either only axis-translation technique, for specimens in the suction range

of 0 to 65 kPa, or a combination of drying the specimen outside the triaxial cell and later equilibrating suction by applying axis-translation technique (for specimens in the suction range of 100 kPa to 300 kPa) or by applying vapor pressure technique (for specimens in the suction range of 30 MPa and 100 MPa).

5.5 Experimental Procedure

5.5.1 *General*

The simulation of various traffic loads on the subgrade soil at different overburden pressures is conducted in the laboratory by application of series of varying confining pressure and deviator stress. Based on the application of suction or back pressure during the testing sequence, the RLTTs are characterized into two categories: (*i*) conventional RLTTs, and (*ii*) suction-controlled RLTTs.

5.5.2 *Conventional RLTT*

The conventional RLTT refers to the application of confining pressure and deviator stress without controlling or measuring the suction within the specimen. These tests are performed in drained conditions without application of back pressure. The standard testing protocols for the loading sequence are available from AASHTO and NCHRP, which have been discussed by Puppala (2008).

One of the most common standards for subgrades soil is the AASHTO T-307-99 (2003). It consists of a preconditioning sequence and 15 sequences of varying deviator stresses and confining pressures (Table 5.2).

Table 5.2 Loading sequence for performing an RLTT as recommended by AASHTO T307-99 (2003)

Sequence #	Confining Pressure		Max. Deviator Stress		Peak Cyclic Stress		Seating/Contact Stress		No. of Load Cycles
	kPa	psi	kPa	psi	kPa	psi	kPa	psi	
0	41.4	6	27.6	4	24.8	3.6	2.8	0.4	500 – 1000
1	41.4	6	13.8	2	12.4	1.8	1.4	0.2	100
2	41.4	6	27.6	4	24.8	3.6	2.8	0.4	100
3	41.4	6	41.4	6	37.3	5.4	4.1	0.6	100
4	41.4	6	55.2	8	49.7	7.2	5.5	0.8	100
5	41.4	6	68.9	10	62	9	6.9	1	100
6	27.6	4	13.8	2	12.4	1.8	1.4	0.2	100
7	27.6	4	27.6	4	24.8	3.6	2.8	0.4	100
8	27.6	4	41.4	6	37.3	5.4	4.1	0.6	100
9	27.6	4	55.2	8	49.7	7.2	5.5	0.8	100
10	27.6	4	68.9	10	62	9	6.9	1	100
11	13.8	2	13.8	2	12.4	1.8	1.4	0.2	100
12	13.8	2	27.6	4	24.8	3.6	2.8	0.4	100
13	13.8	2	41.4	6	37.3	5.4	4.1	0.6	100
14	13.8	2	55.2	8	49.7	7.2	5.5	0.8	100
15	13.8	2	68.9	10	62	9	6.9	1	100

The deviator stress is applied as a combination of seating/contact stress (10% of maximum deviator stress) and a cyclic stress. The cyclic stress varies in a haversine-shaped waveform, as discussed in section 5.2.3. Table 5.2 shows the loading sequence recommended by AASHTO T307-99 (2003). The cyclic stress is

applied for 0.1 seconds, while only the seating/contact stress is applied for 0.9 seconds in the form of a haversine-shaped waveform.

5.5.3 *Suction-controlled RLTT*

The suction-controlled RLTT refers to the test conducted under application of varying net confining pressure and deviator stress on suction-controlled specimens. The suction may be controlled using axis-translation technique or vapor pressure technique. In this research, the suction-controlled technique using axis-translation technique was used for specimens subjected to a matric suction of 0 to 300 kPa; while the vapor pressure technique was used for specimens subjected to a total suction of 30 and 100 MPa.

5.5.3.1 Suction Equalization

The specimens were prepared at a moisture content of 16% (mentioned in section 5.4), which corresponds to a matric suction of 26 kPa. The specimens which were to be saturated were placed in the triaxial cell with porous stones placed at the top and the bottom of the specimen. A back-pressure saturation technique was employed to saturate the specimen. Meanwhile, the cell pressure was kept 15 kPa greater than the back pressure, thereby maintaining an effective confining pressure of more than 15 kPa, throughout the test.

The specimen which was to be subjected to a matric suction in the range of 2 to 65 kPa were directly placed in the triaxial cell, fitted with High-Air Entry (HAE) disk in the base pedestal and a porous stone in the top cap. A cell pressure

of 15 kPa was first applied and the back pressure (or pore water pressure) was then increased to 5 kPa. An air pressure of 5 kPa was also applied. Gradually, the cell pressure and the air pressure were increased to reach the target matric suction. The suction equalization was assumed to be complete when less than 0.5 cm^3/day of water entered or came out of the specimen (Sivakumar, 1993; Ng et al., 2013).

However, the specimens subjected to a suction higher than 65 kPa till 300 kPa, were initially air-dried outside the cell, by using the same technique as explained in section 3.7.3. Once the specimens reached near their respective target matric suction levels, the specimen were placed in the triaxial cell and were subjected to axis translation technique to induce the target matric suction.

The specimens to be tested at high suction states (s = 30 and 100 MPa), were initially prepared at a water content of 16%, which corresponds to a matric suction of 26 kPa. Subsequently, these specimens were partially dried outside the triaxial cell till the water content decreased to 5%, using a procedure similar to that explained in section 3.7.3. Later, the specimen was placed in an acrylic chamber with an attached relative humidity (RH) and temperature probe (auto-RH apparatus), and by using Kelvin's equation (Eq. 5.12, Sposito, 1981), the required relative humidity was computed for standard operating temperature of 23.5 to 24.5 °C (shown in Fig. 5.7).

$$\psi = -\frac{RT}{\nu_{wo}\,\omega_v}\ln\left(\frac{u_v}{u_{vo}}\right) = -\frac{RT}{\nu_{wo}\,\omega_v}\ln(RH) \tag{5.12}$$

where,

ψ = total suction, kPa,

T = Absolute temperature, K,

R = Universal gas constant (8.31432 J mol^{-1} K^{-1}),

v_{wo} = Specific volume of water (i.e. reciprocal of density, m^3/kg),

ω_v = molecular mass of water vapor (18.016 kg/kmol),

u_v = partial pressure of water (or pore-water) vapor (kPa), and

u_{vo} = saturation pressure of pure water vapor (kPa).

The elaborate working principle for the same automatic relative humidity (Auto-RH) apparatus is explained by Patil (2014). This experimental setup was validated for monotonic triaxial tests by Patil et al. (2016b).

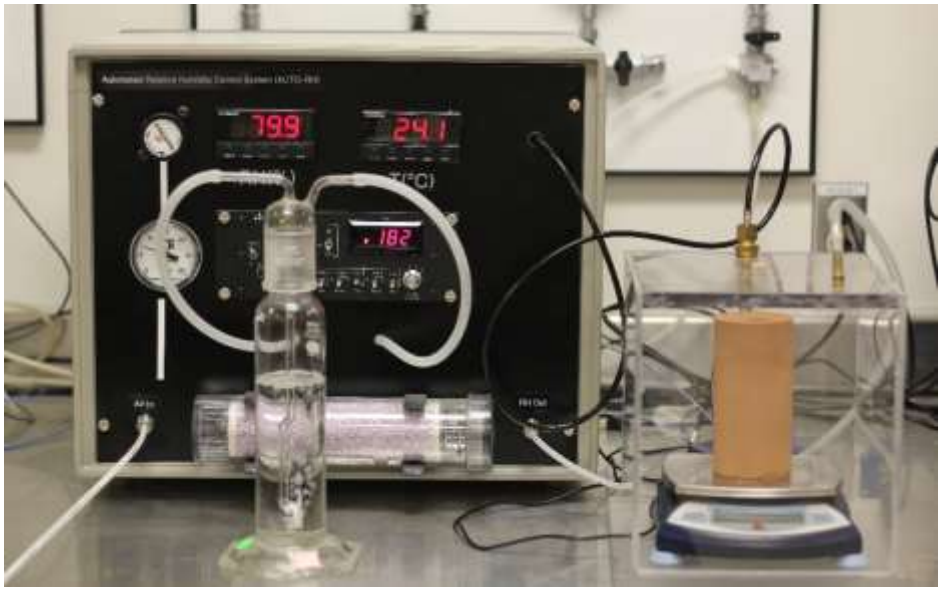

Figure 5.7 Suction equilibration using an Auto-RH apparatus

5.5.3.2 Suction-controlled RLTT

Once the specimen reached its target suction, the loading sequence recommended by AASHTO T307-99 (2003) was used to determine the resilient modulus of the saturated soil. The only difference in the loading sequence (shown in Table 5.2) being that the net confining pressures of 13.8, 27.6, and 41.4 kPa were used, instead of confining pressures for suction-controlled tests (from matric suction of 2 to 300 kPa), since the pore air and pore water pressures were also applied. Throughout the test, the suction was controlled by maintaining the pore air and pore water pressures at the desired levels, thereby maintaining drained conditions.

The specimens which were equilibrated to a total suction of 30 and 100 MPa using the Auto-RH apparatus, were placed in the triaxial cell after suction equalization, which approximately took a month. The top cap and the bottom pedestal, both fitted with porous stones, were connected to the Auto-RH apparatus as shown in Fig. 5.8 and the relative humidity was maintained at the desired level to maintain the target total suction within the soil specimen. Since the external pore air and pore water pressures are not applied during the vapor pressure technique, the effective confining pressure is the same as confining pressure (Table 5.2).

The axial deformations were measured and recorded using a pair of Linear Variable Displacement Transducers (LVDTs) having an accuracy of 0.001 mm over a range of 5 mm (shown in Fig. 5.9). Additionally, since the contact/seating

stresses and cyclic deviator stress are mostly too low, ball bearings and matching sockets were used to prevent the eccentric application of axial loads or deviatoric stresses (shown in Fig. 5.9).

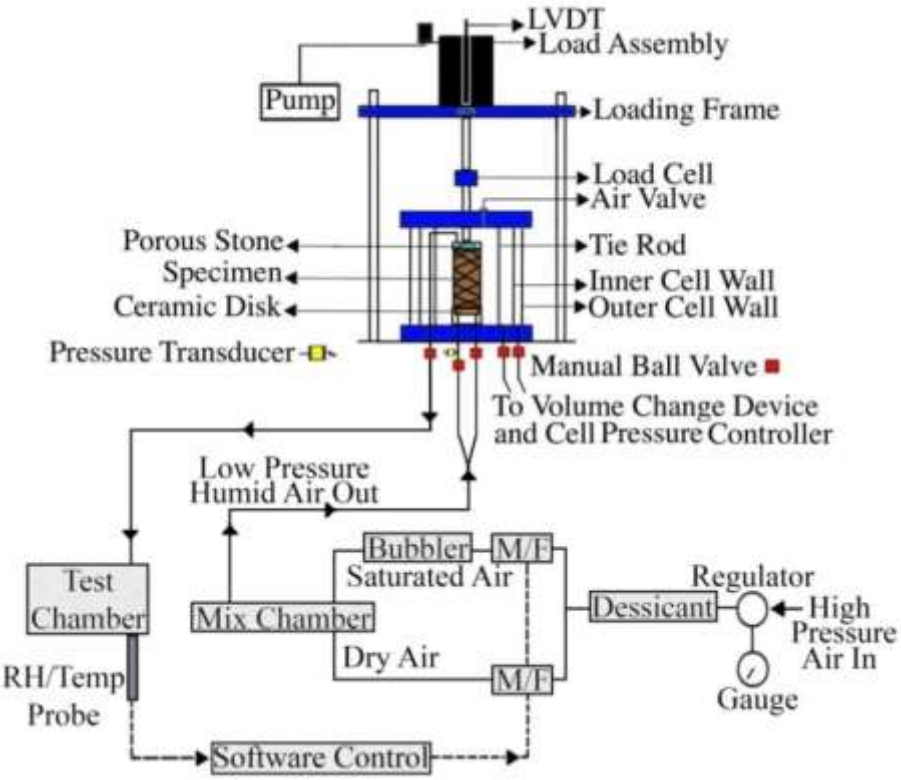

Figure 5.8 Schematic diagram of the triaxial setup for performing suction-controlled RLTT on soils under high total suction using automatic relative humidity (Auto RH) apparatus (after Patil, 2014)

Figure 5.9 Modifications to the triaxial device for performing suction-controlled RLTTs

5.5.4 *Unconfined Compression Strength Test*

The specimens were tested for their unconfined compressive strength (UCS) after the completion of the RLTTs. The purpose of UCS test is to quickly obtain the compressive strength for soils that possess sufficient cohesion to allow testing in the unconfined state (ASTM D2166-16). All the UCS tests were performed at an axial displacement rate of 0.5 mm/min, to negate the effect of axial displacement rate of shearing on the response of the soil specimen.

5.6 Experimental Results

5.6.1 *Resilient Modulus of Saturated and Unsaturated Specimens under Low to Moderate Suction State*

A series of suction-controlled repeated load triaxial tests were performed on specimens having varying densities (1.62 to 1.70 g/cm^3) and matric suction (0 to 300 kPa) using the axis-translation technique. The results obtained from the RLTTs have been discussed in this section. The resilient modulus value mentioned at each net confining pressure and deviator stress corresponds to the average of the resilient moduli obtained in the last five cycles (96th to 100th cycles).

5.6.1.1 Variation of resilient modulus with net confining pressure and deviator stress

The resilient moduli for the specimens compacted at a dry density of 1.67 g/cm^3 are shown in Figs. 5.10 to 5.17, for varying induced matric suction of 0 (saturated) to 300 kPa. It was observed that the resilient modulus decreases with an increase in deviator stress for all values of matric suction. Such a trend is typical of the silty or clayey soils (Ruttanaporamakul, 2012; Ng et al., 2013). The resilient modulus was observed to increase with an increase in net confining pressure, which is the expected trend.

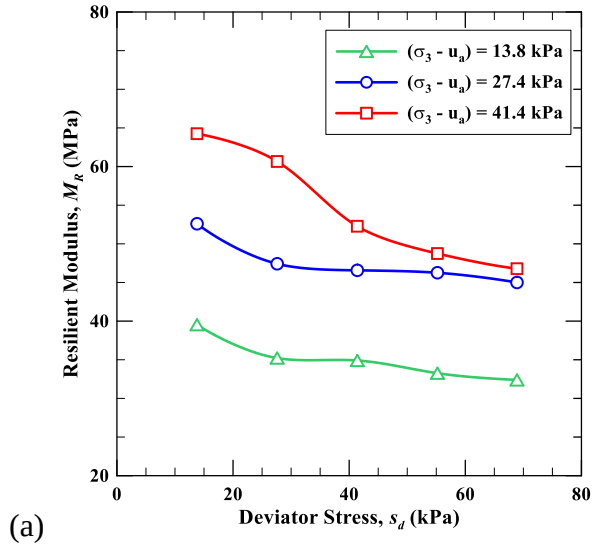

(a)

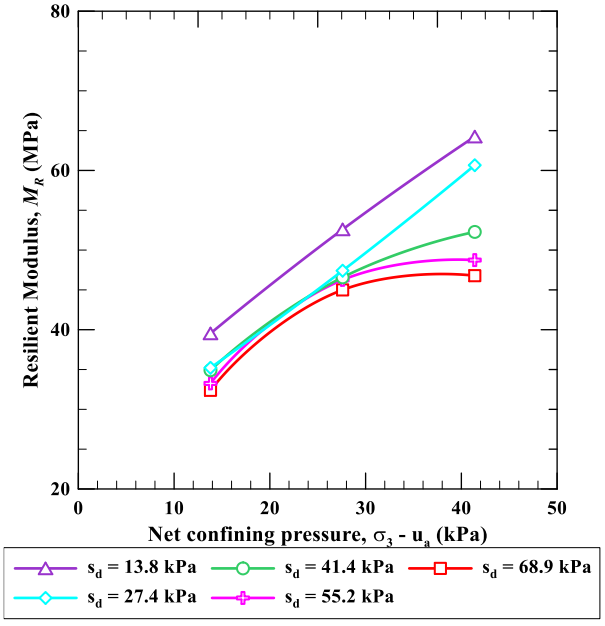

(b)

Figure 5.10 Variation of resilient modulus with (a) deviator stress, and (b) net confining pressure for a saturated specimen at a dry density of 1.67 g/cm^3

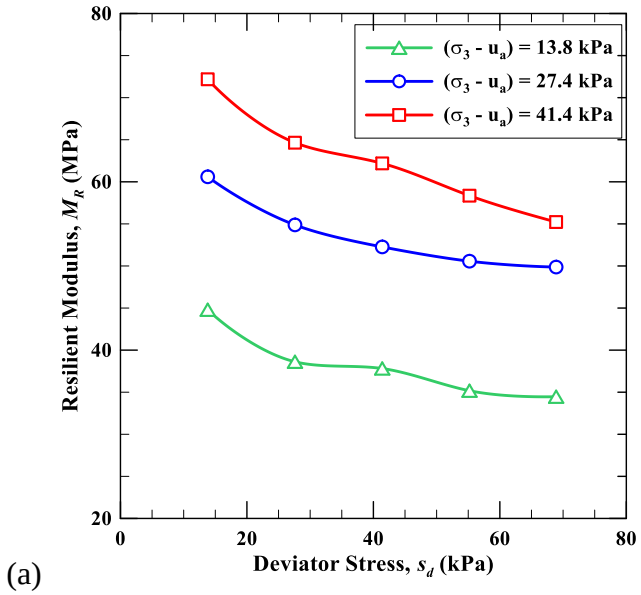

(a)

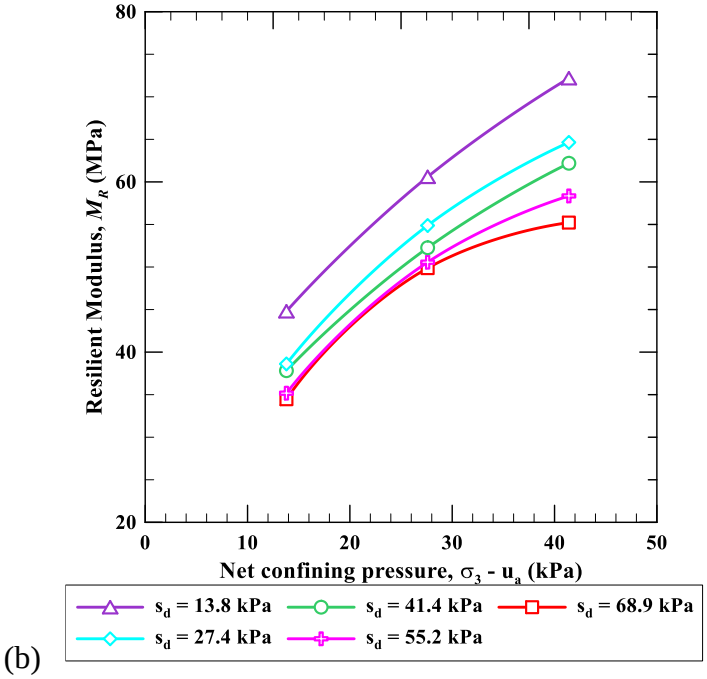

(b)

Figure 5.11 Variation of resilient modulus with (a) deviator stress, and (b) net confining pressure for a specimen at a dry density of 1.67 g/cm^3 and s = 2 kPa

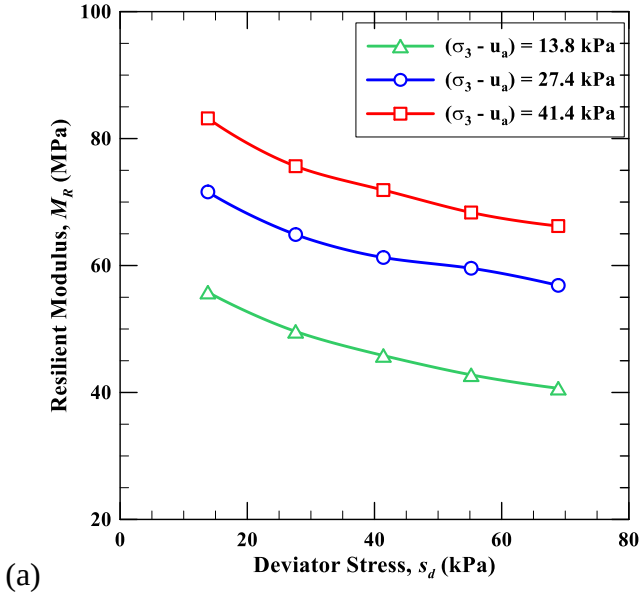

(a)

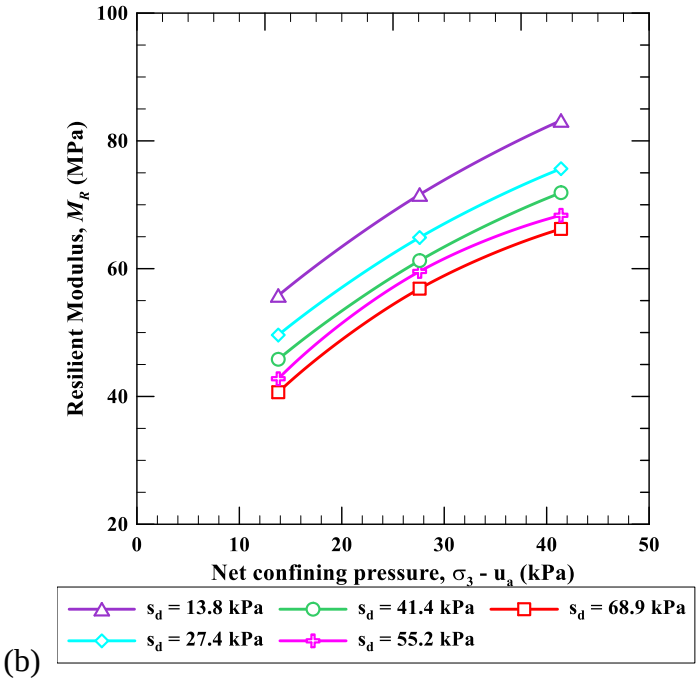

(b)

Figure 5.12 Variation of resilient modulus with (a) deviator stress, and (b) net confining pressure for a specimen at a dry density of 1.67 g/cm^3 and s =10 kPa

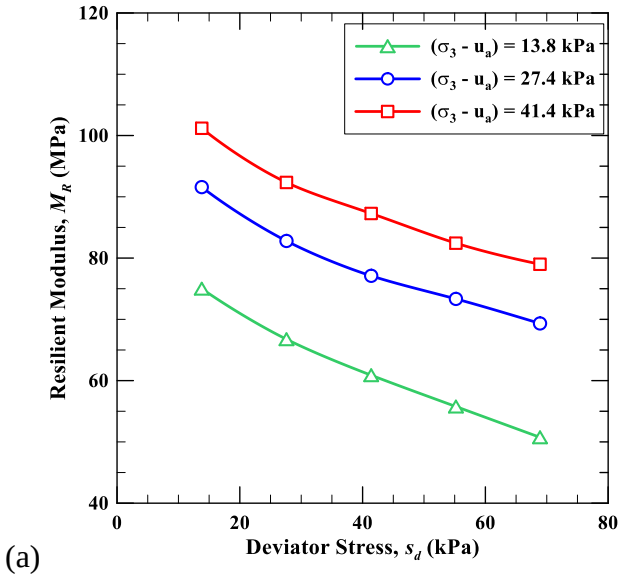

(a)

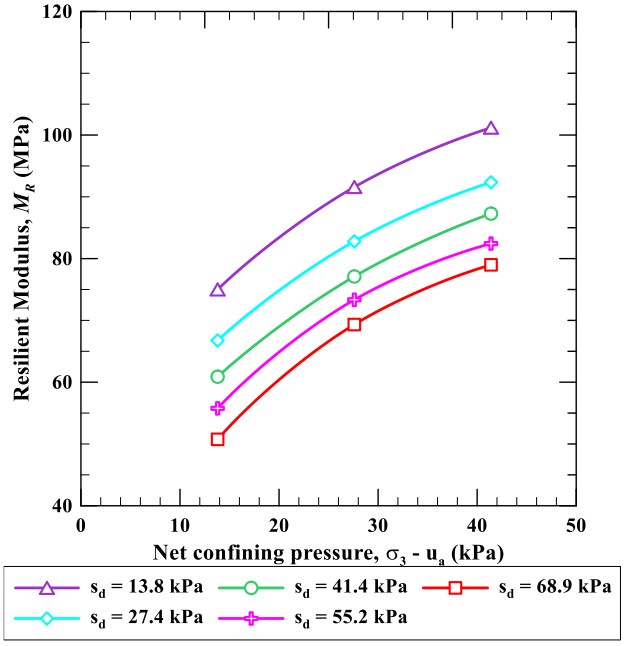

(b)

Figure 5.13 Variation of resilient modulus with (a) deviator stress, and (b) net confining pressure for a specimen at a dry density of 1.67 g/cm^3 and s = 26 kPa

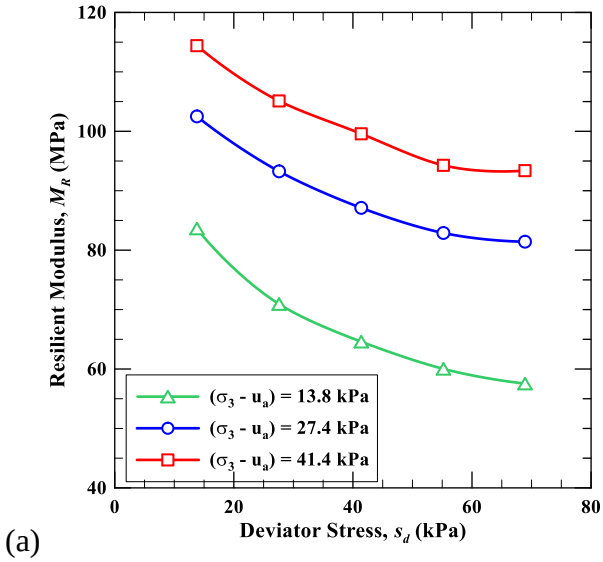

(a)

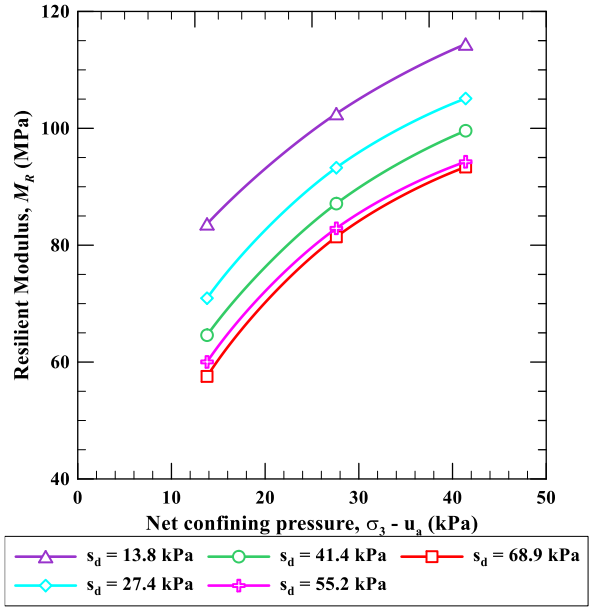

(b)

Figure 5.14 Variation of resilient modulus with (a) deviator stress, and (b) net confining pressure for a specimen at a dry density of 1.67 g/cm^3 and s = 36 kPa

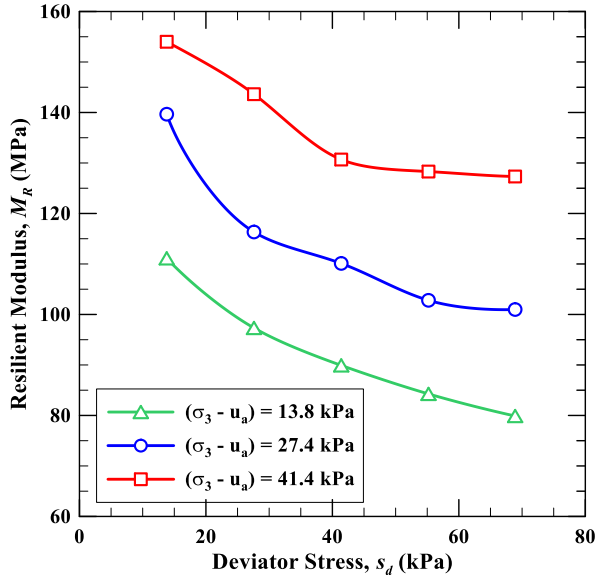

(a)

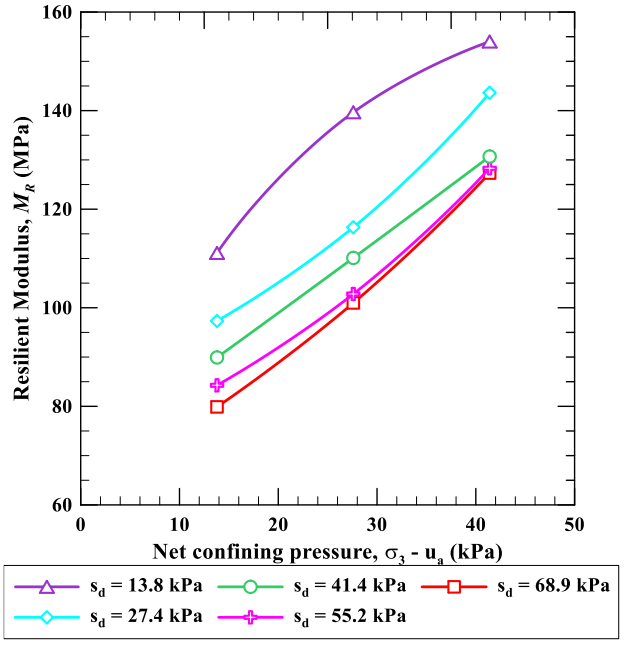

(b)

Figure 5.15 Variation of resilient modulus with (a) deviator stress, and (b) net confining pressure for a specimen at a dry density of 1.67 g/cm^3 and s = 65 kPa

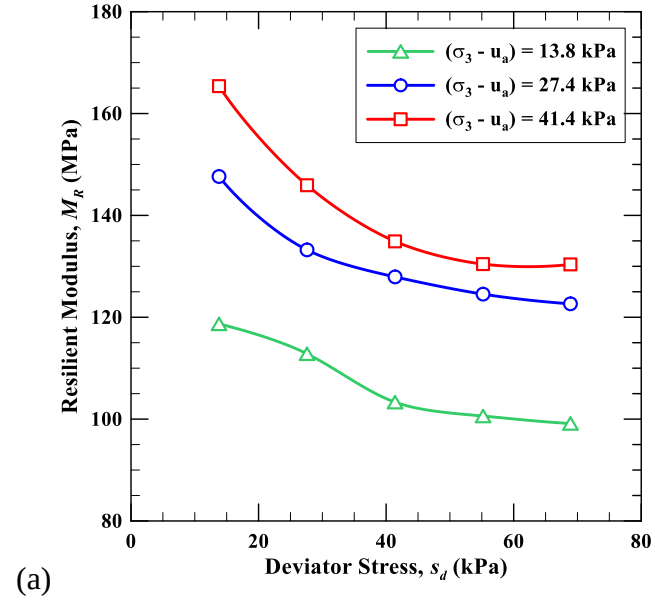

(a)

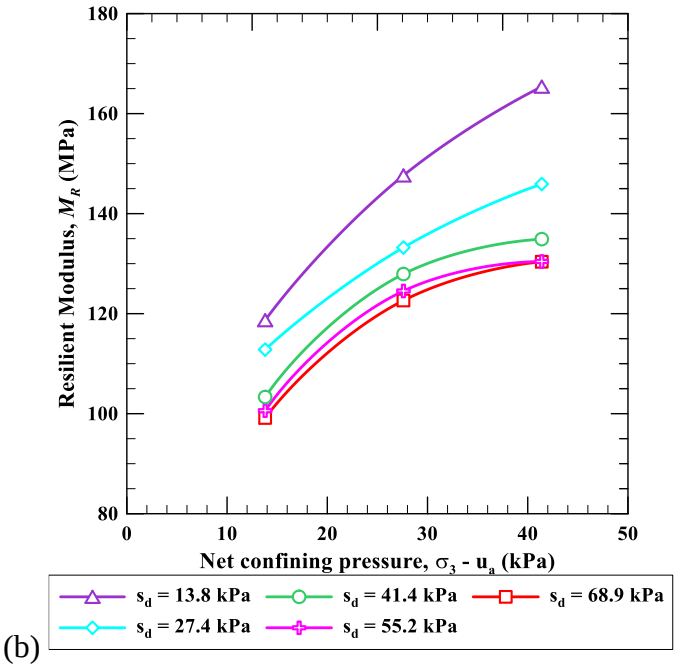

(b)

Figure 5.16 Variation of resilient modulus with (a) deviator stress, and (b) net confining pressure for a specimen at a dry density of 1.67 g/cm^3 and s = 100 kPa

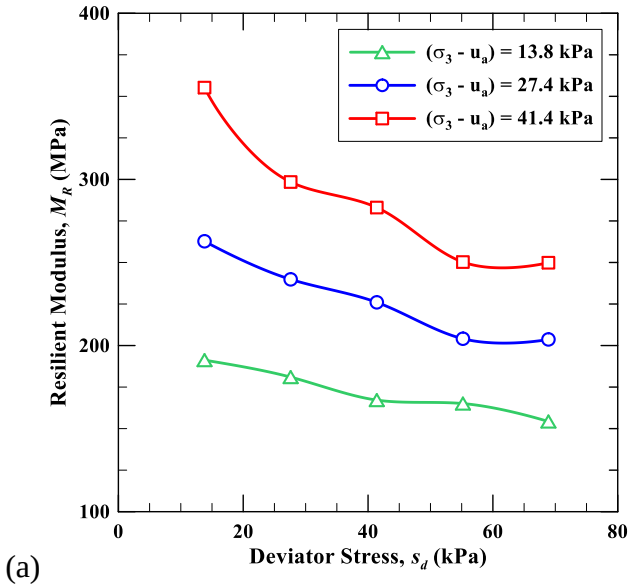

(a)

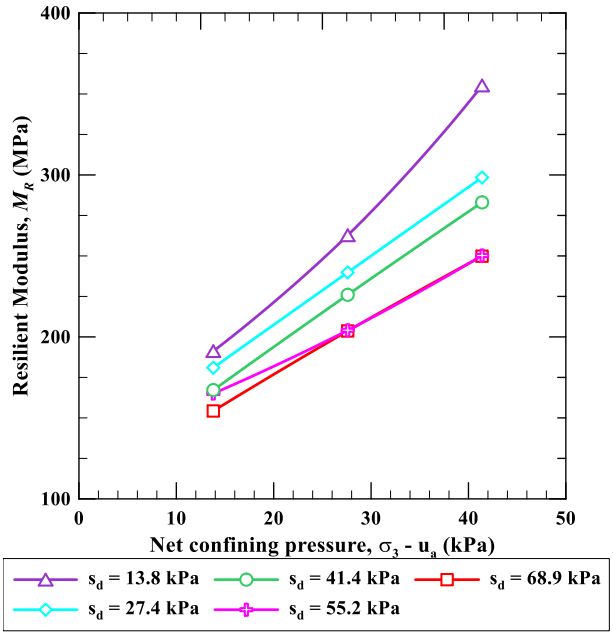

(b)

Figure 5.17 Variation of resilient modulus with (a) deviator stress, and (b) net confining pressure for a specimen at a dry density of 1.67 g/cm^3 and s = 300 kPa

Figures 5.18, 5.19, and 5.20 show the variation of resilient modulus with net confining pressure and deviator stress for a specimen prepared at a dry density of 1.7 g/cm^3 and at three matric suctions of 0 (saturated), 36, and 300 kPa, respectively. It is interesting to note that the specimen at a dry density of 1.7 g/cm^3 and a matric suction of 36 kPa, corresponds to the maximum dry density (MDD) at optimum moisture content (OMC) of 14.8%. The response of the soil specimen at a higher dry density is similar to that at 98% of MDD (i.e., dry density of 1.67 g/cm^3). It was observed that the resilient modulus decreases with an increase in deviator stress for all matric suction levels. While, the resilient modulus increases with an increase in net confining pressure, which is an expected response.

The tests were also conducted at a lower dry density of 1.62 g/cm^3, which corresponds to 95% of MDD. The specimens were subjected to a matric suction of 0 (saturated), 10, and 200 kPa. The specimens at matric suction of 10 and 200 kPa correspond to a moisture content of 18.9% and 10.1%, respectively, and they lie on the compaction curve for a standard Proctor test (as shown in Fig. 5.6). The results of these tests are shown in Figs. 5.21 to 5.23. A similar trend of variation of resilient modulus with an increase in net confining pressure and deviator stress is observed, as in the case of specimens at a dry density of 1.67 and 1.70 g/cm^3.

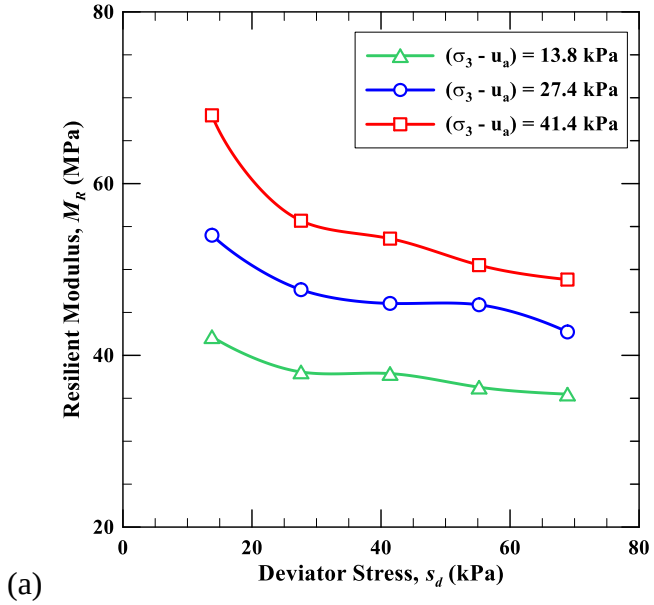

(a)

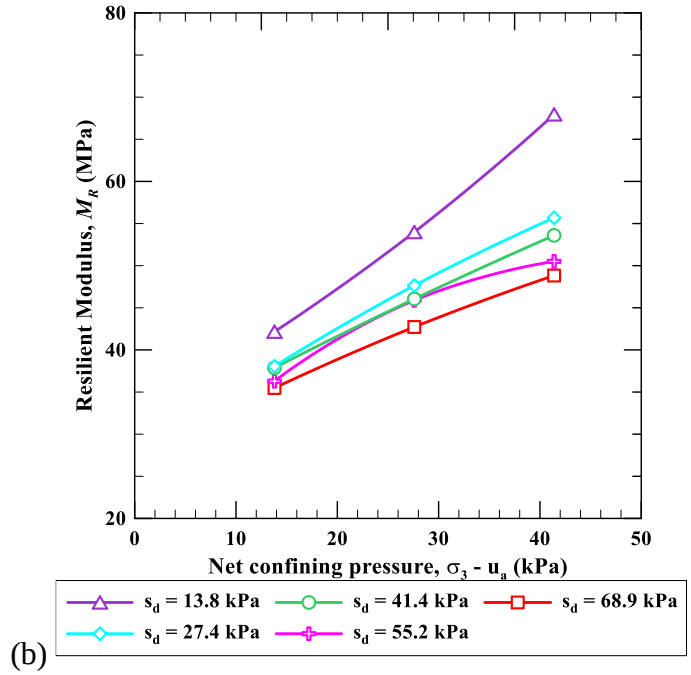

(b)

Figure 5.18 Variation of resilient modulus with (a) deviator stress, and (b) net confining pressure for a saturated specimen at a dry density of 1.70 g/cm^3

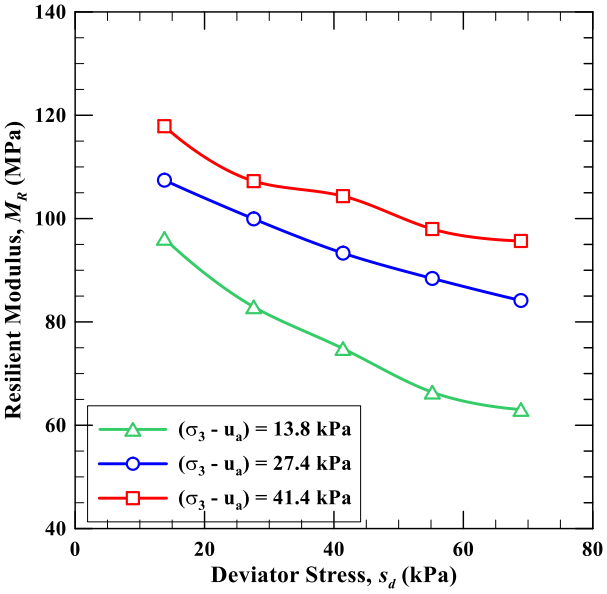

(a)

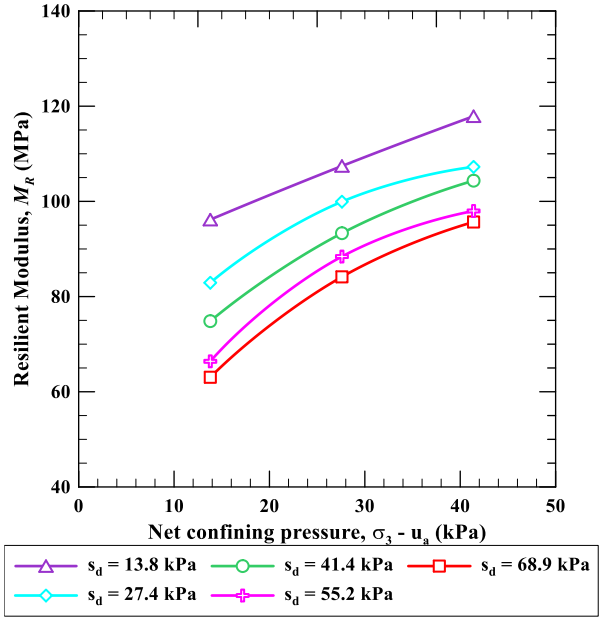

(b)

Figure 5.19 Variation of resilient modulus with (a) deviator stress, and (b) net confining pressure for a specimen at a dry density of 1.70 g/cm^3 and s = 36 kPa

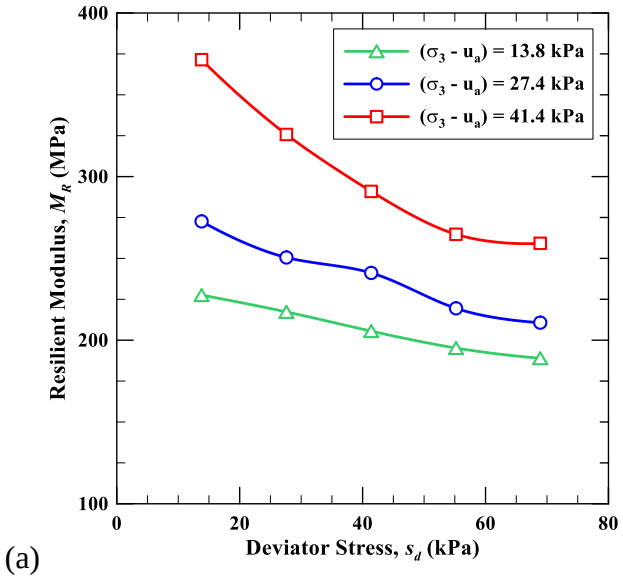

(a)

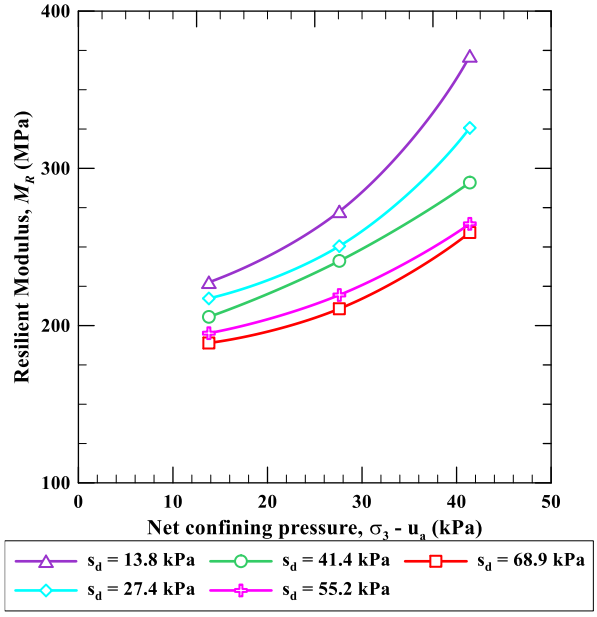

(b)

Figure 5.20 Variation of resilient modulus with (a) deviator stress, and (b) net confining pressure for a specimen prepared at a dry density of 1.70 g/cm^3 and s = 300 kPa

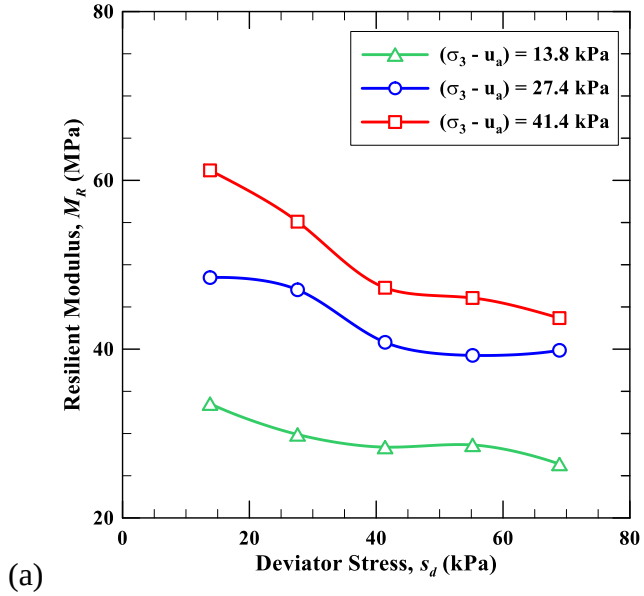

(a)

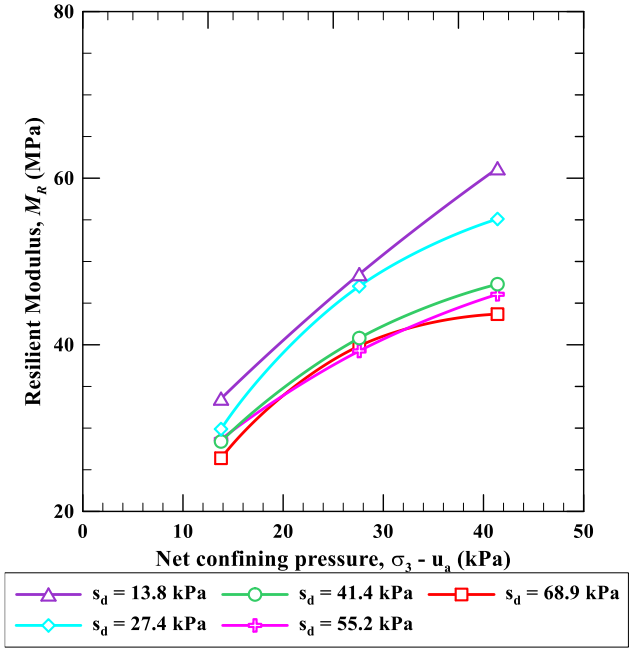

(b)

Figure 5.21 Variation of resilient modulus with (a) deviator stress, and (b) net confining pressure for a saturated specimen prepared at a dry density of 1.62 g/cm^3

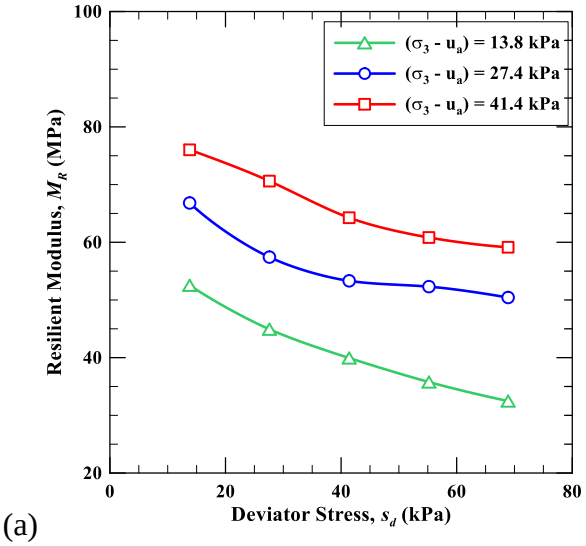

(a)

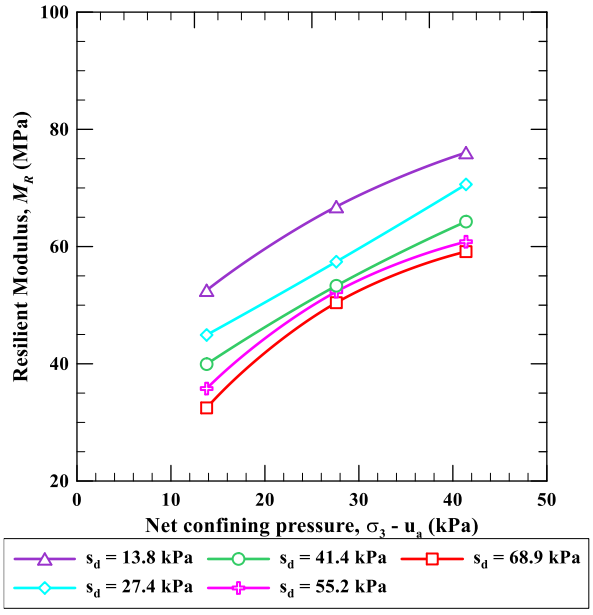

(b)

Figure 5.22 Variation of resilient modulus with (a) deviator stress, and (b) net confining pressure for a specimen prepared at a dry density of 1.62 g/cm^3 and s = 10 kPa

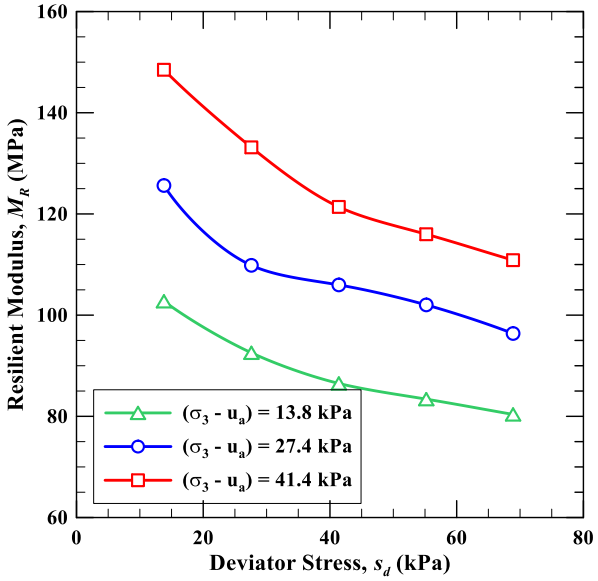

(a)

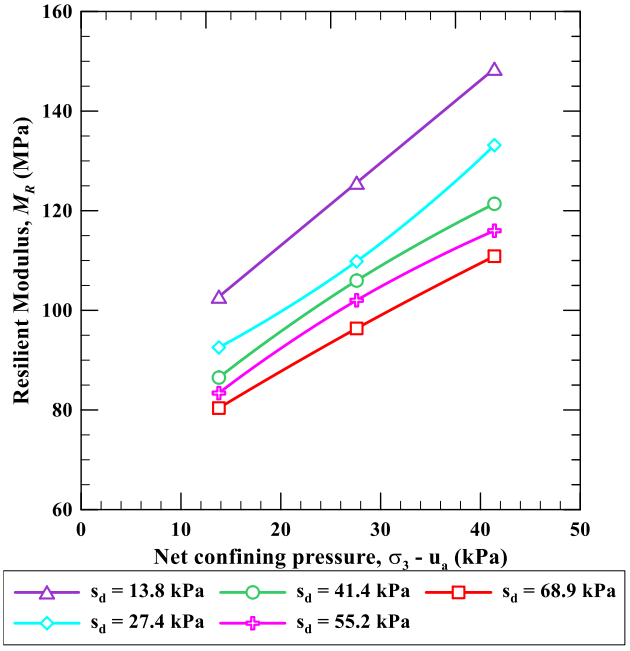

(b)

Figure 5.23 Variation of resilient modulus with (a) deviator stress, and (b) net confining pressure for a specimen prepared at a dry density of 1.62 g/cm^3 and s = 200 kPa

5.6.1.2 Influence of wetting or drying of soil specimens on the resilient modulus

The effect of drying or wetting of a specimen on its resilient modulus, when compared to that for another specimen at the same dry density and moisture content (or suction level) is investigated in this research. The results of the resilient moduli obtained from various specimens at different dry densities and matric suction (discussed in section 5.6.1.1) were utilized in this research. Additionally, a new series of tests was conducted. The specimens were compacted and equilibrated to the wetter (points 'D' or 'E' in Fig. 5.24) or the drier (points 'A' or 'B' in Fig. 5.24) side of the OMC and then by using axis-translation technique, the specimens were subjected to a new matric suction which corresponds to the other side of OMC (as shown in Fig. 5.24).

Figure 5.25 shows the variation of the resilient modulus of a specimen compacted and equilibrated at a suction of 65 kPa and then gradually the induced suction was reduced to 26 kPa (wetting path 'B' to 'D' in Fig. 5.24). Figure 5.25 compares the resilient modulus of a wetted specimen with that of another specimen compacted and equilibrated directly to a matric suction of 26 kPa (point 'D' in Fig. 5.24; results were previously shown in Fig. 5.13). In Fig. 5.25 the nomenclature used includes a letter 'W', which denotes that the specimen was gradually wetted to reach the required suction. The drying of the soil specimen was the denoted by the letter 'D' (as shown in Figs. 5.26 and 5.28).

It was observed from Fig. 5.25 that the wetted specimen demonstrated slightly lesser resilient moduli as compared to the specimen which was directly compacted and equilibrated to a matric suction of 26 kPa, by more than 10% on an average. On closer inspection, it was observed that the difference was amplified in the case of lower net confining pressure and higher deviator stress. For instance, the difference during the last sequence of loading (having lowest net confining pressure and highest deviator stress) was 21%, whereas the difference in the first sequence (having highest net confining pressure and lowest deviator stress) was only 4%.

This shows the effect of hysteresis in the resilient modulus and suction (M_R-s) relationship due to wetting-drying process. The subsequent drying and wetting of the soil might have resulted in the rearrangement of the soil particles, which might have caused the decrease in resilient modulus values. It was observed by Khoury and Zaman (2004) that specimens after drying to a moisture content showed higher resilient modulus (approximately 25% higher) than specimens compacted to the same moisture content. This increase in resilient modulus also includes the effect of moisture content during compaction. Nevertheless, the hysteresis behavior due to wetting and drying process was concluded to be dominant in the clayey soils as compared to the sandy soils (Khoury and Zaman, 2004).

On the other hand, the drying of a soil specimen by inducing a change in matric suction from 26 kPa to 65 kPa (converse of the previous case; drying path 'D' to 'B' in Fig. 5.24), resulted in slightly higher values of resilient modulus (6% on an average) as compared to that of a specimen compacted and equilibrated directly to a matric suction of 65 kPa (point 'B' in Fig. 5.24; comparison shown in Fig. 5.26). Since the repeatability of the resilient modulus tests is generally considered to be quite poor, the increase in resilient modulus (varying from 3% to 13%) may fall within the margin of error. Additionally, apart from the first sequence in the RLTT, the difference for the rest of the sequences was less than 9%. No significant trend in the variation of the difference between the resilient moduli values with the change in the net confining pressure and the deviator stress was obtained from the response of the soil specimens.

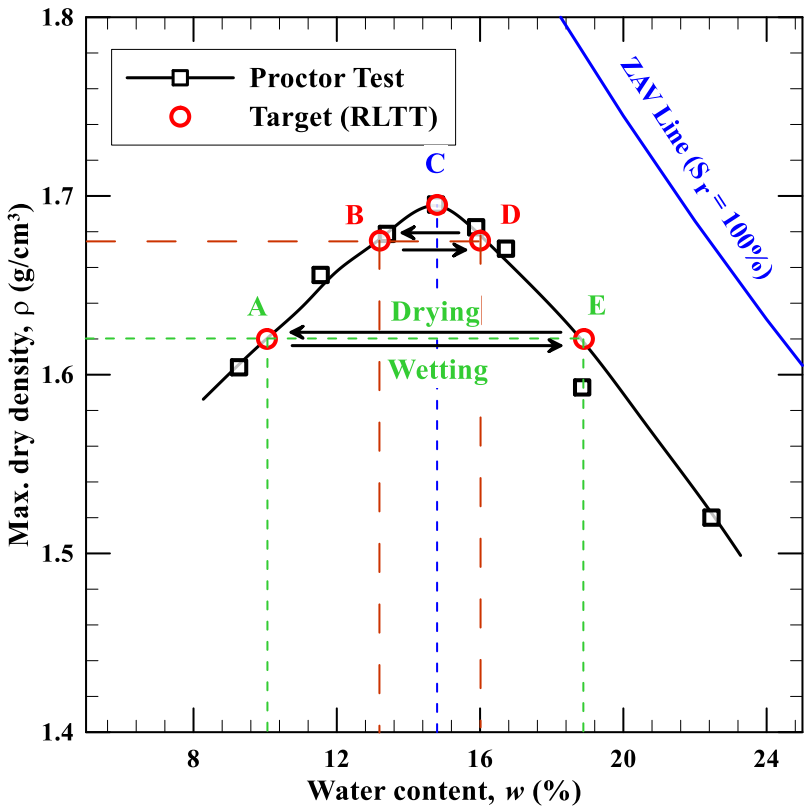

Figure 5.24 Compaction curve and demonstration of drying or wetting of a specimen at the same dry density

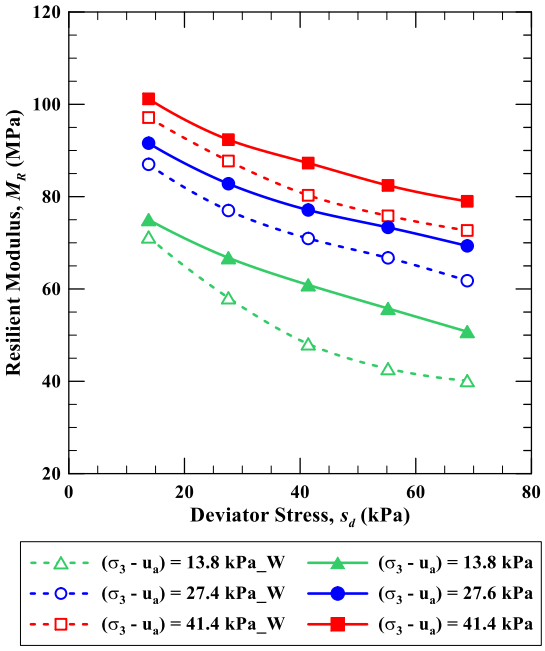

(a)

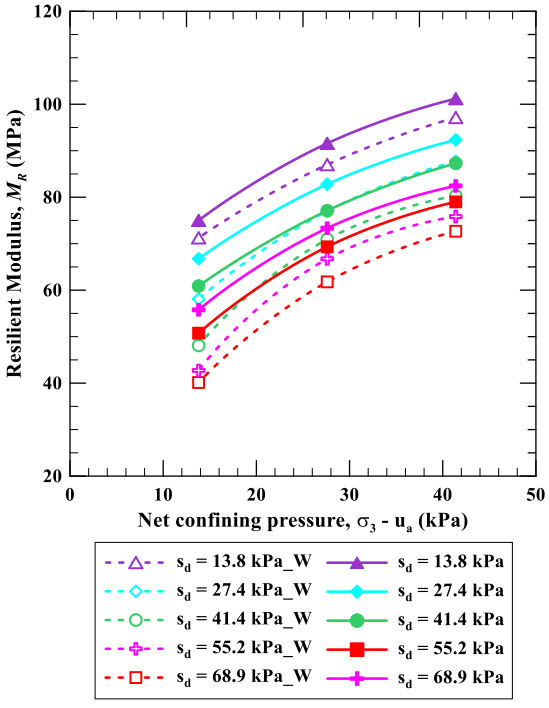

(b)

Figure 5.25 (a) and (b) Comparison of resilient moduli for wetted specimen (s = 65 to 10 kPa), and another specimen at s = 10 kPa and prepared at a dry density of 1.67 g/cm^3

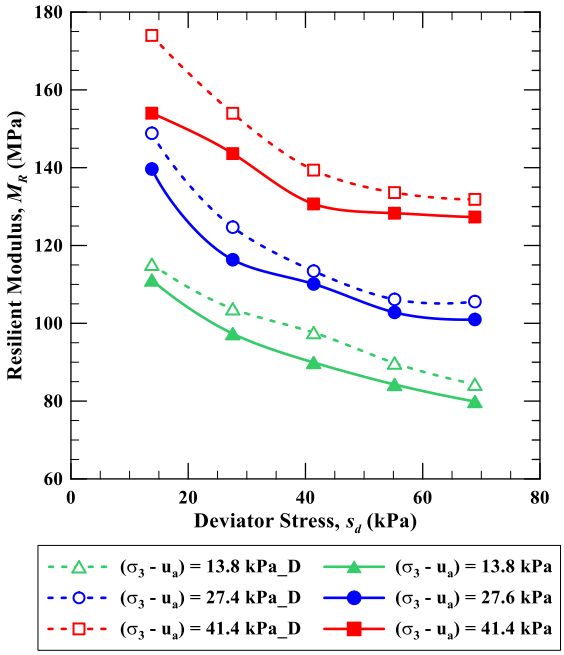

(a)

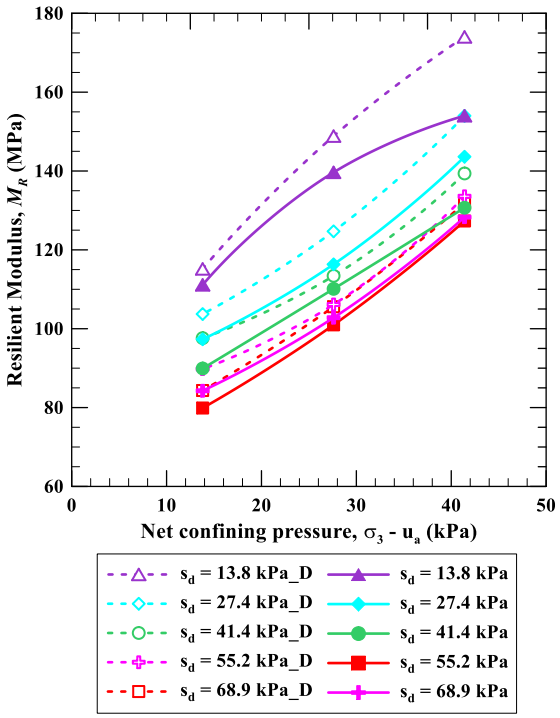

(b)

Figure 5.26 (a) and (b) Comparison of resilient moduli for dried specimen (s = 26 to 65 kPa), and a specimen at s = 65 kPa and prepared at a dry density of 1.67 g/cm^3

When the specimen was wetted, or moistened by inducing a change of matric suction from 200 kPa to 10 kPa (wetting path ‘A’ to ‘E’ in Fig. 5.24), the resilient moduli for the various sequences were observed to be significantly higher (3.5 % to 20%; average being 11%) than that of the specimen compacted and directly subjected to a matric suction of 10 kPa (point ‘E’ in Fig. 5.24). Similar observations, as discussed for the specimen at matric suction of 26 kPa (Fig. 5.25), were made regarding the variation of the difference in resilient moduli with net confining pressure and deviator stress. It is evident from Fig. 5.27(a) that as the deviator stress was increased the differences between the resilient moduli values were increased. While the difference in resilient modulus was higher for the lowest (13.8 kPa; a difference of 11%) and intermediate (27.6 kPa; a difference of 14%) net confining pressures as compared to highest net confining pressure (41.4 kPa; a difference of 7%).

The combined evidence of the decrease in resilient modulus (Fig. 3.25 and 3.27) when the specimens are wetted from a higher matric suction value to a lower as compared to the resilient modulus of the specimen compacted and equilibrated directly to the same value of the lower matric suction shows that the hysteresis of SWCC affects the resilient modulus of soils.

Figure 5.28 shows the effect of drying a specimen from an initially induced matric suction of 10 kPa to 200 kPa (drying path ‘E’ to ‘A’ in Fig. 5.24) on the

resilient modulus of the soil, as compared that of a specimen compacted and equilibrated directly to the matric suction of 200 kPa (point ‘A’ in Fig. 5.24).

The values of resilient modulus for each sequence were identical for both the specimens. The difference in the values of the resilient moduli varied from a range of –10% to 8%. However, the average of the differences in resilient moduli between the two specimens was only -1.6%, which shows that on an average the resilient modulus of a specimen upon drying is similar to that of the specimen which was directly equilibrated to the same value of matric suction. The variation of the difference between the resilient modulus of the two soil specimens reverses its trend with an increase in net confining pressure and deviator stress. The dried specimen shows a higher resilient modulus at lower values of deviator stress than the specimen directly equilibrated to the matric suction of 200 kPa; however, the trend reverses at higher values of deviator stress. The difference in values of resilient moduli was observed to have an incoherent trend for an increase in net confining pressure.

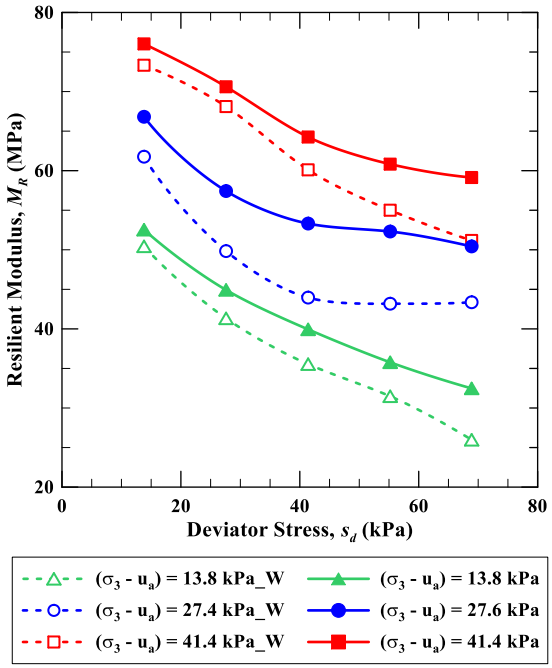

(a)

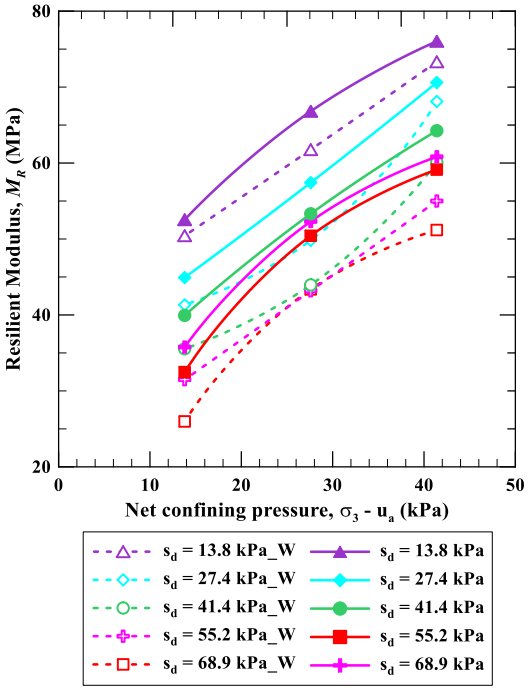

(b)

Figure 5.27 (a) and (b) Comparison of resilient moduli for wetted specimen (s = 200 to 10 kPa), and a specimen at s = 10 kPa and prepared at a dry density of 1.62 g/cm^3

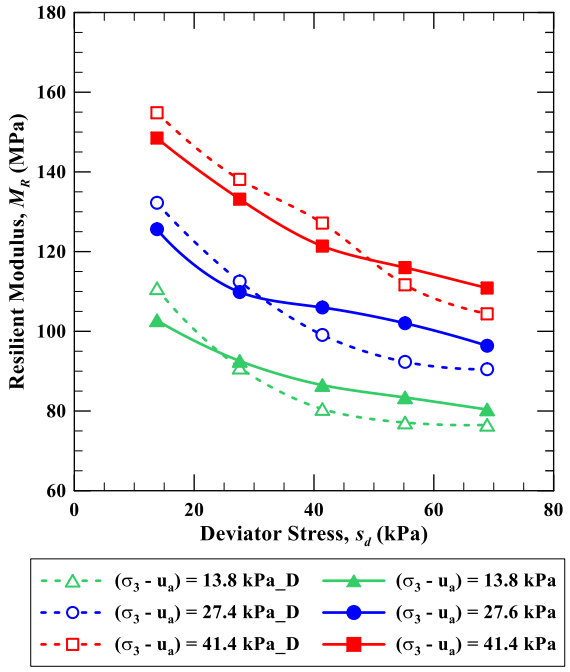

(a)

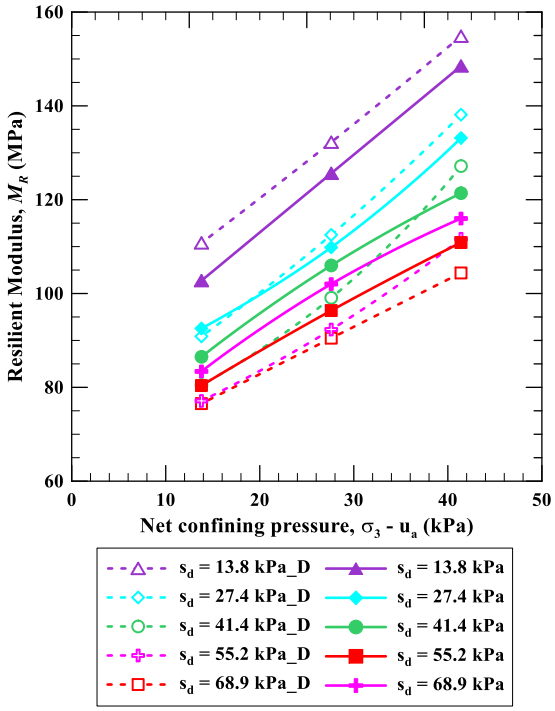

(b)

Figure 5.28 (a) and (b) Comparison of resilient moduli for dried specimen (s = 10 to 200 kPa), and a specimen at s = 200 kPa and prepared at a dry density of 1.62 g/cm^3

5.6.1.3 Variation of resilient modulus with suction

Figures 5.29 and 5.30 show the variation of resilient modulus with an increase in matric suction at a constant dry density of 1.67 g/cm^3 for the eighth sequence, which has a net confining pressure of 27.6 kPa and a maximum deviator stress of 41.4 kPa, and the last sequence, which has a net confining pressure of 13.8 kPa and a maximum deviator stress of 68.9 kPa. In both the cases, it was observed that the resilient modulus increases rapidly till 65 kPa, and subsequently, the increase in resilient modulus with an increase in suction decreased slightly.

The overall behavior follows a non-linear trend, which is similar to the trend of suction stress, apparent cohesion and the value of the angle of internal friction which is dependent on suction, φ^b (discussed in section 3.10). Though these parameters correspond to the strength of unsaturated soils, however, the strength and stiffness of soils are interdependent. Henceforth, as the apparent cohesion of the soil increases rapidly till 50 kPa (Fig. 3.77), so does the value of resilient modulus. Thereafter, the apparent cohesion gradually increases to a matric suction of 250 kPa. The values of apparent cohesion in Chapter 3 were based on the values at the critical state, however, the resilient modulus was determined at very low stress and strain levels. Therefore, the apparent cohesion reached a constant value after a matric suction of 500 kPa, while the value of resilient modulus showed a consistent increasing trend at matric suction of 300 kPa.

Similar values of resilient moduli were observed (M_R = 28.1 MPa to 114.1 MPa for s = 8 to 100 kPa for the 8th sequence) by Khoury et al. (2011) for manufactured silt specimens compacted at 93% of MDD and 0.7% wet of optimum moisture content.

However, the peak strength of the unsaturated soil specimen was observed to increase even at matric suction of 750 kPa (Fig. 3.57). The variation of resilient modulus with suction is similar to that of the initial stiffness determined from a conventional triaxial compression test (shown in Fig. 3.57). Since the initial stiffness and resilient modulus are both computed by inducing small strains, their variation with induced soil suction might be identical.

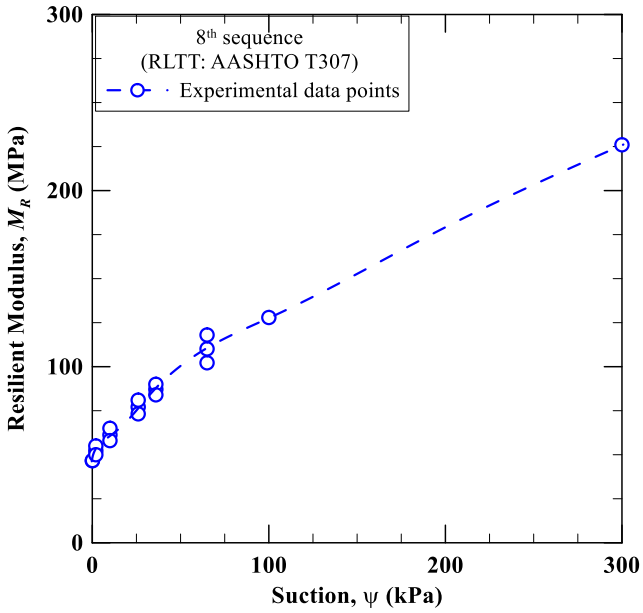

Figure 5.29 Variation of resilient modulus (for the eighth sequence of loading) with matric suction for specimens at a dry density of 1.67 g/cm^3

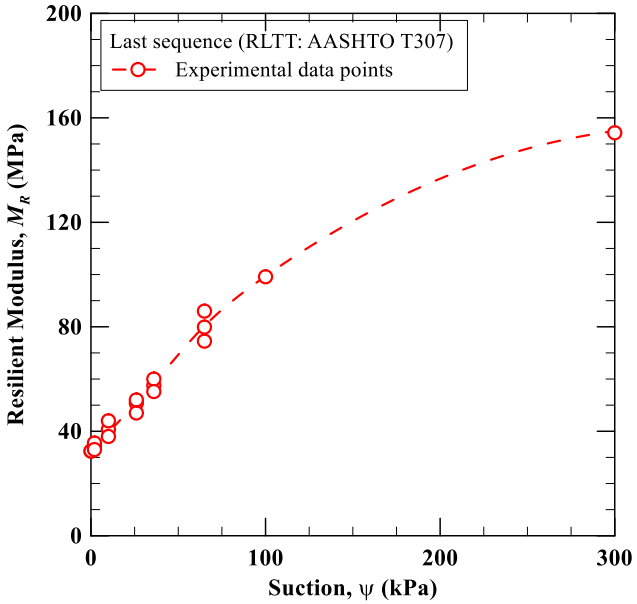

Figure 5.30 Variation of resilient modulus (for the last sequence of loading) with matric suction for specimens at a dry density of 1.67 g/cm^3

5.6.1.4 Variation of resilient modulus with dry density of specimen

The resilient modulus is expected to vary with changes in dry density of the soil specimen. When the values of resilient moduli of various specimens at constant suction and varying dry densities were compared (Figs. 5.8, 5.18, and 5.21; or Figs. 5.14 and 5.19), it was observed that the resilient modulus was higher for the soil specimen prepared with the highest dry density. Similar conclusions were drawn by Trollope et al. (1962), Hicks (1970), Robinson (1974), Rada and Witczak (1981), and Kolisoja (1997). However, the effect of dry density was more predominant for the lower values of net confining pressures. Similar observations were made by Barksdale and Irani (1989).

The resilient moduli values for net confining pressure of 13.8 kPa showed upto 30% increase for saturated specimens compacted at 98% of MDD, as compared to that at 95% of MDD. While, for the same net confining pressure (13.8 kPa), the increase in resilient modulus with an increase in density from 95% to 98% of MDD was upto 20% for specimens equilibrated at a matric suction of 10 kPa.

The resilient moduli values for the lowest net confining pressure were observed to increase by 10% and 16%, for specimens compacted at MDD as compared to those compacted at 98% of MDD, at the lower suction levels (s = 0 and 36 kPa) and at higher matric suction of 300 kPa, respectively.

However, other researchers (Thom and Brown, 1988; Brown and Selig, 1991) concluded that stated that the effect of density and state of compaction on resilient modulus of soils were relatively insignificant.

5.6.2 *Resilient Modulus of Specimens under High Suction State*

5.6.2.1 Variation of resilient modulus with net confining pressure and deviator stress

Figures 5.31 and 5.33 show the resilient modulus of soil specimen subjected to total suction of 30 MPa and 100 MPa. Figure 5.32 shows the resilient modulus of another soil specimen subjected to a total suction of 30 MPa. Since the suction-controlled RLTT of specimens at high suction states were rarely determined, the results of the RLTT of a replicate specimen at the induced total suction of 30 MPa is shown in Fig. 5.32. It was observed by comparing the resilient moduli from Figs.

5.31 and 5.32 that the variation in resilient modulus of the replicates at an induced total suction of 30 MPa was in the range of –5% to 12%, with an average of 5%, which is generally acceptable, considering that the repeatability of RLTTs is quite poor.

It was observed that the specimens at high suction states of 30 and 100 MPa show a very high resilient modulus at the lowest deviator stress (s_d = 13.8 kPa). This is due to the very high stiffness of the soil specimen. The low deviator stress results in very small axial deformations in the specimen, thereby increasing the resilient modulus. As the deviator stress increases, the deformations increase rapidly, resulting in a decrease of resilient modulus. The resilient modulus of the soil specimen increases with an increase in net confining pressure, however, the increase is quite small (less than 10% for an increase of net confining pressure from 13.8 kPa to 27.6 kPa for 30 and 100 MPa total suction). For a similar increase in net confining pressure for specimens at lower suction levels (s = 0 to 65 kPa), the corresponding increase in resilient modulus is nearly 30% for all values of deviator stress.

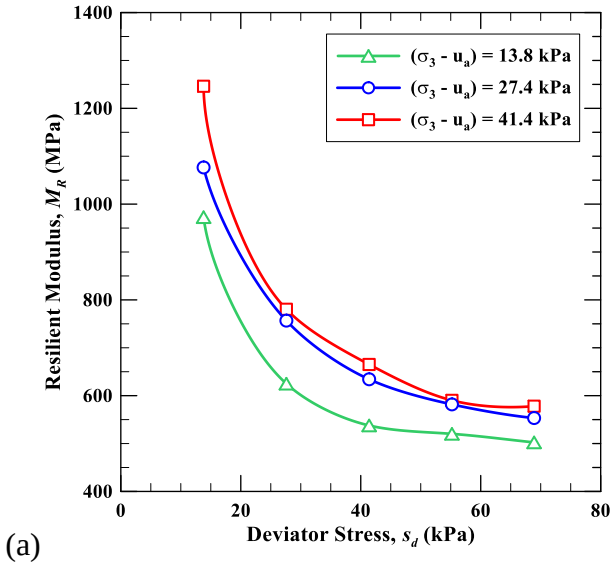

(a)

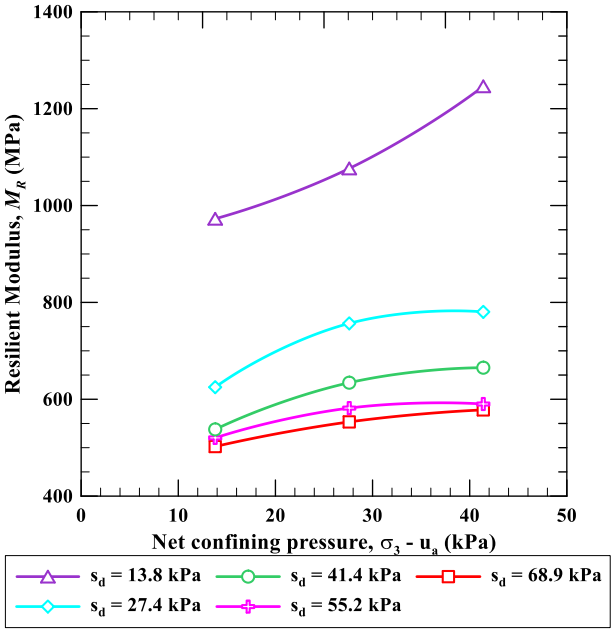

(b)

Figure 5.31 Variation of resilient modulus with (a) deviator stress, and (b) net confining pressure for a specimen prepared at a dry density of 1.67 g/cm^3 and equilibrated to total suction of 30 MPa

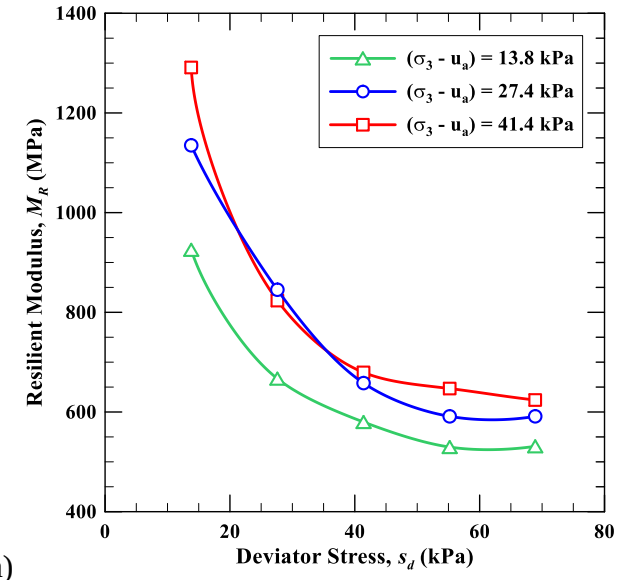

(a)

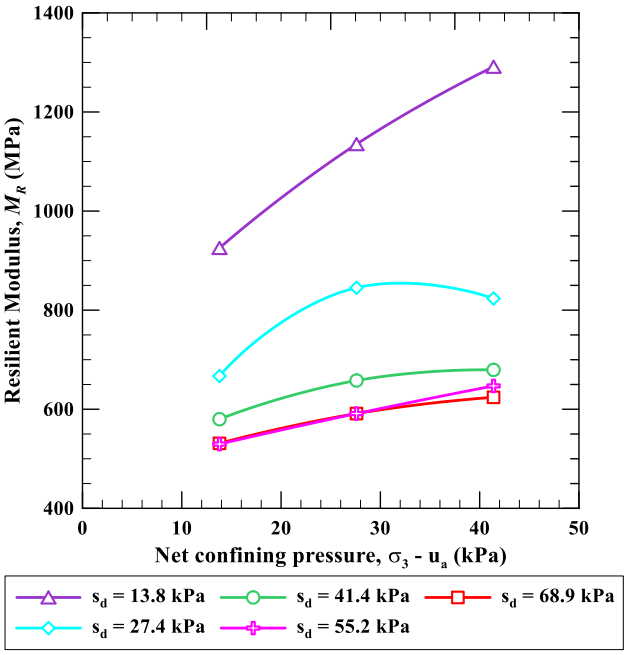

(b)

Figure 5.32 Variation of resilient modulus with (a) deviator stress, and (b) net confining pressure for a replicate specimen prepared at a dry density of 1.67 g/cm^3 and equilibrated to a total suction of 30 MPa

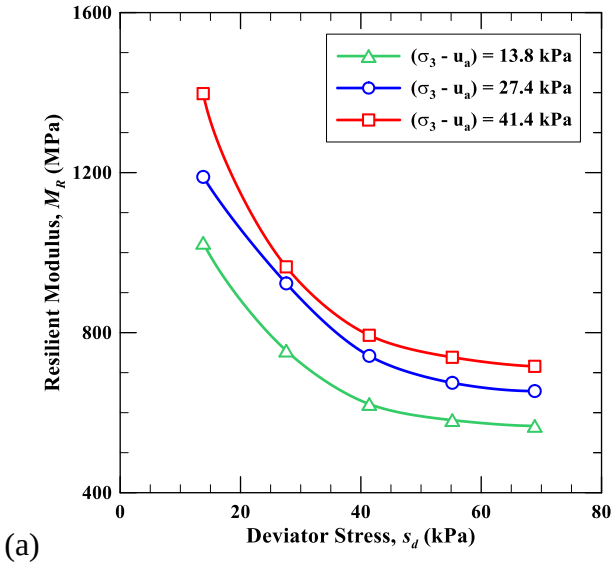

(a)

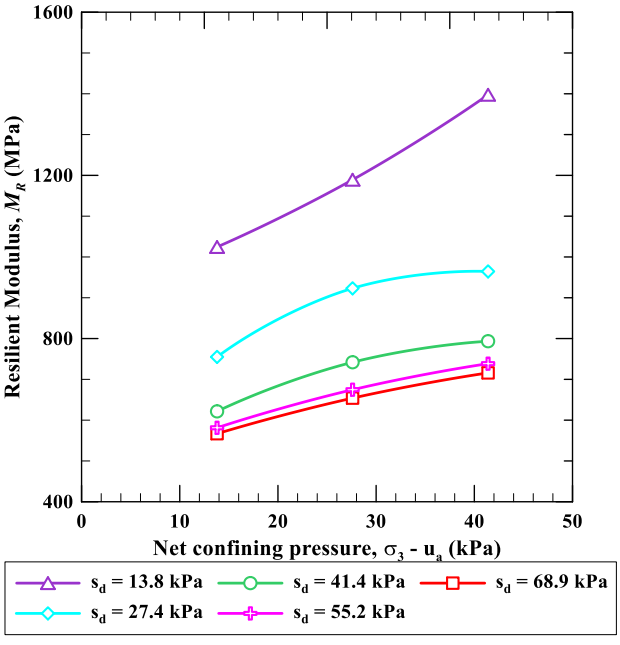

(b)

Figure 5.33 Variation of the resilient modulus with (a) deviator stress, and (b) net confining pressure for a specimen at a dry density of 1.67 g/cm^3 and total suction of 100 MPa

5.6.3 *Variation of Resilient Modulus under Wider Suction State*

The results of suction-controlled RLTTs using vapor pressure technique was utilized to enhance the variation of resilient modulus over a wide range of suction states, as shown in Figs. 5.34 and 5.35. Figures 5.34 and 5.35 show the variation of resilient modulus for specimens a constant dry density of 1.67 g/cm^3 (98% of MDD) for the eighth sequence, which has a net confining pressure of 27.6 kPa and a maximum deviator stress of 41.4 kPa, and the last sequence, which has a net confining pressure of 13.8 kPa and a maximum deviator stress of 68.9 kPa.

Since the suction varies from a low value to very high values; and to study the effect of low and high suction states, simultaneously, the suction was plotted in logarithmic scale, instead of arithmetic scale as used earlier in Figs. 5.29 and 5.30. However, the slopes of increase in resilient modulus with an increase in suction were computed in arithmetic scale, hereby referred to as by the rate of increase of resilient modulus with suction, denoted by η. The value of η is computed with reference to saturated condition and expressed by the following relationship:

$$\eta = \frac{M_{R,\psi} - M_{R,\psi=0}}{\psi} \tag{5.13}$$

Figure 5.36 shows the variation of η with suction for the eighth and last sequences of the suction-controlled RLTTs. It can be observed from Fig. 5.36 that the rate of increase of resilient modulus with suction (η) was quite high (above 100 x 1000 =10^5) till a suction of 300 kPa, thereafter, the value of η started to decrease exponentially, to reach an approximate value of 1500 to 2000 at 30 MPa suction.

Finally, it reduced to approximately 50 (≈ 0.5% of initial values of η) at 100 MPa suction. Henceforth, beyond 300 kPa suction, the increase resilient modulus with suction follows a similar trend as in the case of apparent cohesion or the suction stress of unsaturated soils (discussed in section 3.10).

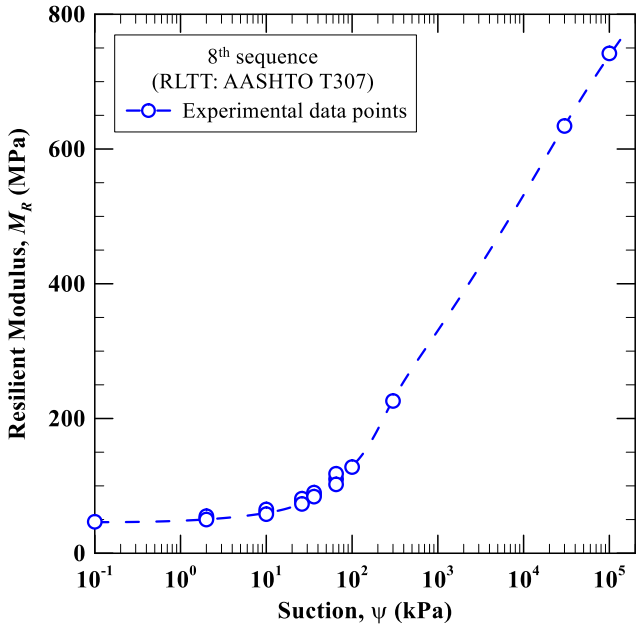

Figure 5.34 Variation of resilient modulus (for the eighth sequence of loading) with suction for specimens prepared at a dry density of 1.67 g/cm^3

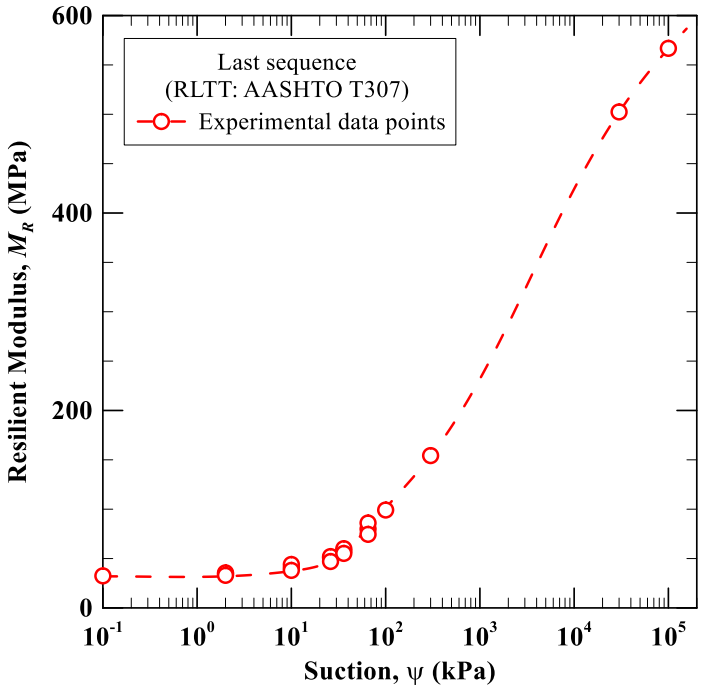

Figure 5.35 Variation of resilient modulus (for the last sequence of loading) with suction for specimens prepared at a dry density of 1.67 g/cm^3

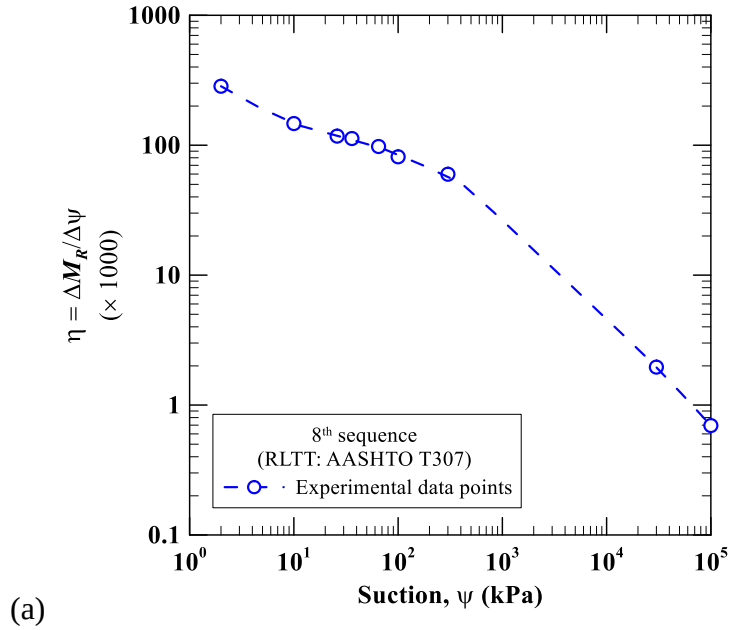

(a)

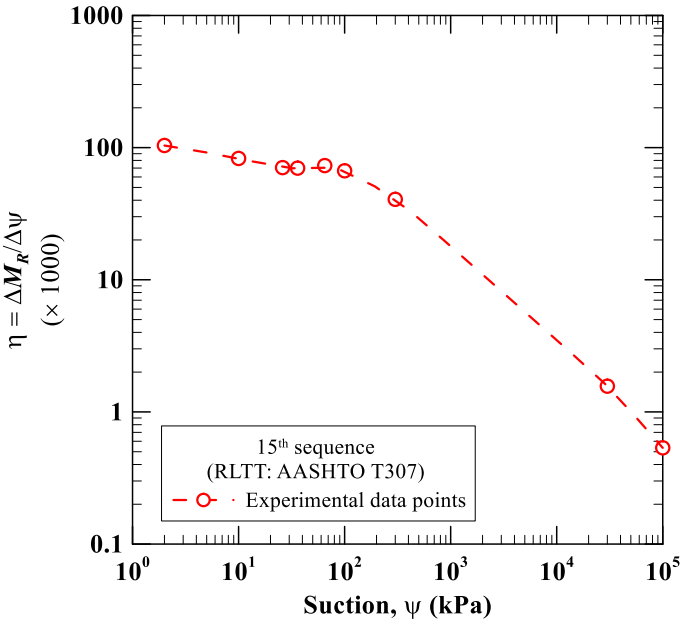

(b)

Figure 5.36 Variation of rate of increase of resilient modulus with suction for (a) eighth sequence, and (b) last sequence of RLTTs for specimens prepared at a dry density of 1.67 g/cm^3

5.6.4 *Variation of Soil Suction during the RLTT*

The variation of suction during the RLTT was determined by plotting the values of matric suction throughout the test. Figures 5.37 and 5.38 show the variation of suction during the last five cycles of the sequences with the highest confining pressure of 41.4 kPa, including the preconditioning sequence (labeled as "Seq# 0") for target matric suction of 26 and 100 kPa, respectively. The variation was observed only during the application of the cyclic load, especially for low suction states (s = 0 to 26 kPa). Once the cyclic load was removed the suction measured would return to its target value.

When another non-suction controlled RLTT was conducted on a specimen, it was observed that during the pre-conditioning sequence, the target suction reduced by approximately 3 kPa when the target suction was 26 kPa after applying 200 cycles of cyclic stresses. However, after the application of 200 cycles of cyclic stress, the decreased suction reached a constant value. Similar observations were made by Yang et al. (2008), where the suction was observed to decrease by 10% after application of 500 cycles of deviator stress for a matric suction of 50 kPa and remained almost constant beyond 500 cycles.

Since the tests used in this research were conducted in suction-controlled conditions, the overall reduction in suction level was almost negligible. However, the suction equilibration requires a considerable amount of time, due to the low permeability of unsaturated soils and the RLTT is a rapid test, where the loading

and unloading occur in only 0.1 second. Although the soil specimen might not be ideally equilibrated, but since the applied stresses and strains are low, it was assumed that the soil specimen is under suction-equilibrium at the macro level for practical purposes.

Figures 5.37 and 5.38 show the temporary increase in suction due to the application of cyclic stresses, which might be due to the compression of pore-air for a short duration, resulting in higher values of suction. Figure 5.37 also shows that the temporary increase in suction is dependent on the magnitude of cyclic deviator stress, which varies from 8% (for Seq# 1) to 11% (Seq# 4 and 5) of the applied cyclic deviator stress.

Figure 5.38 shows the variation of suction for a target suction of 100 kPa. The temporary increase in suction due to the application of the same magnitude of cyclic deviator stress, for a target suction of 100 kPa, was calculated to be lower (varies from 3.5% to 7.5% of cyclic deviator stress) than that for a target suction of 26 kPa. Henceforth, it was concluded that the influence of cyclic loads on the matric suction decreased with increase in target suction (or desaturation) of the soil specimen.

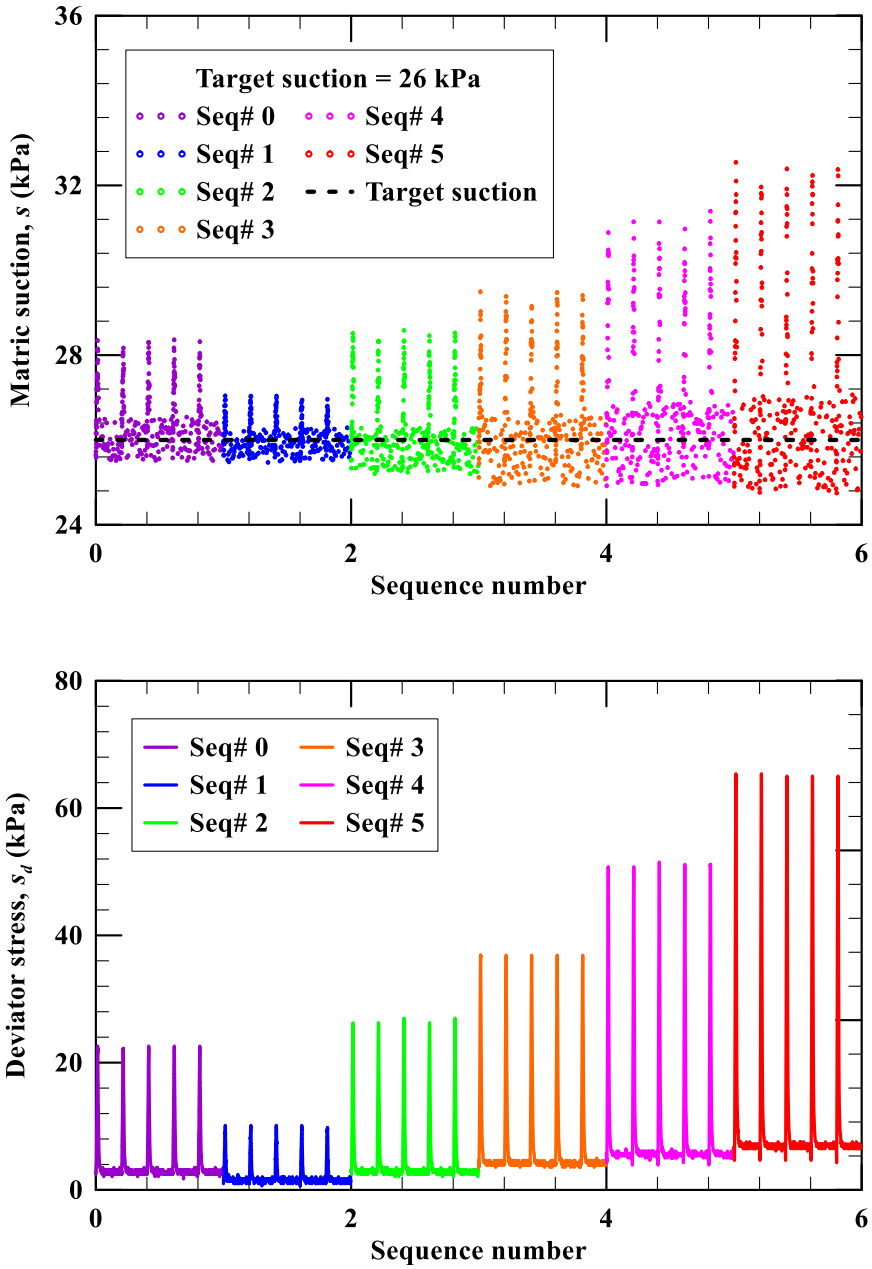

Figure 5.37 Variation of suction during the last five cycles of the pre-conditioning sequence and initial five sequences of an RLTT test for a specimen at a dry density of 1.67 g/cm^3 and induced matric suction of 26 kPa

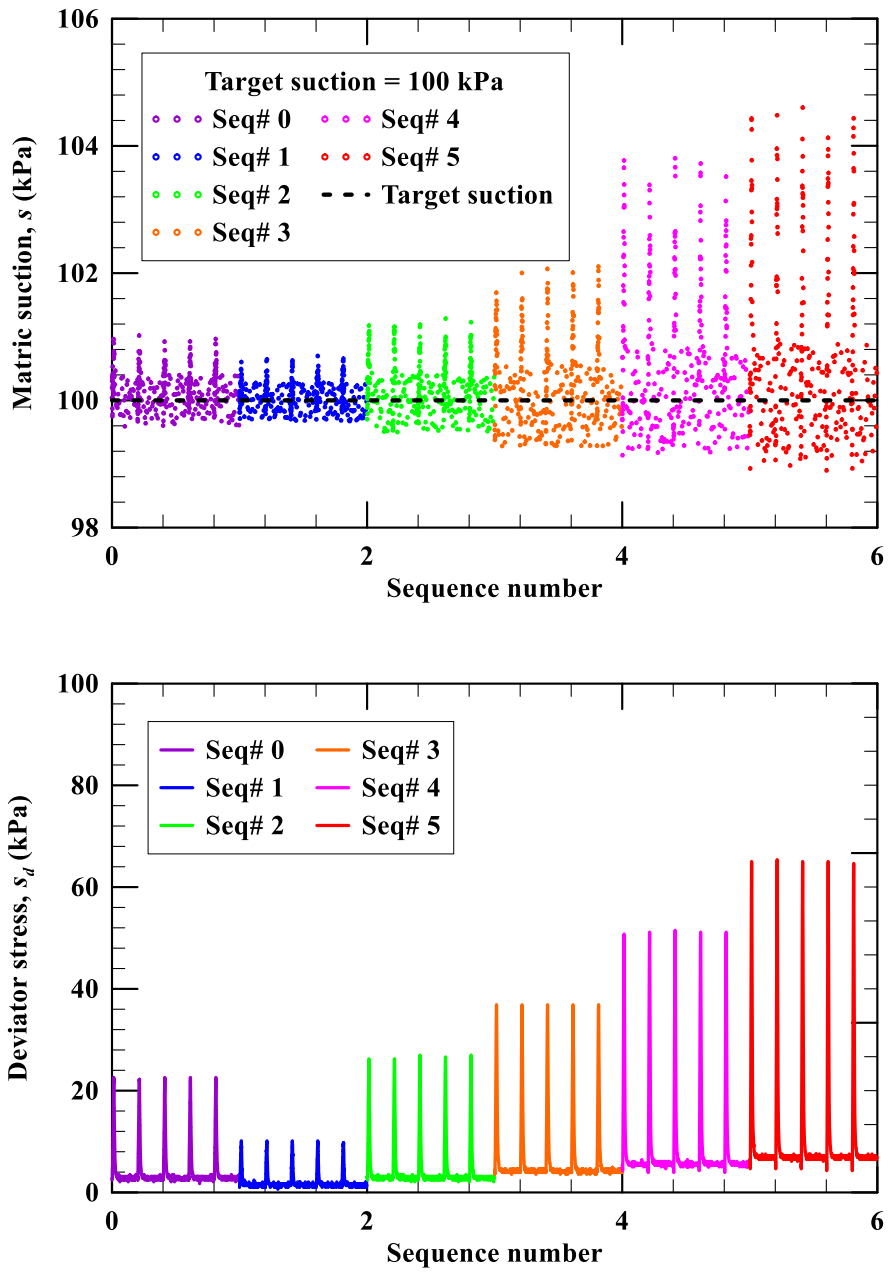

Figure 5.38 Variation of suction during the last five cycles of the pre-conditioning sequence and initial five sequences of an RLTT test for a specimen at a dry density of 1.67 g/cm^3 and induced matric suction of 100 kPa

5.7 Prediction Models for Determination of Resilient Modulus

5.7.1 *General*

The resilient modulus of subgrade soils is sensitive to many factors, including applied stress level, moisture regime, type of soil, and testing protocol (Puppala, 2008). Subgrade soils are usually compacted and typically exist in unsaturated conditions. The soil suction has a significant influence of the resilient modulus of soils, however, the experimental testing for determining the resilient modulus at varying suction levels needs sophisticated equipment, trained personnel and is time-consuming (Han and Vanapalli, 2016).

Henceforth, many researchers had conducted tests to determine the resilient modulus-suction relationship and attempted in developing models for predicting the behavior (Khoury and Zaman, 2004; Yang et al., 2008; Sawangsuriya et al., 2009; Cary and Zapata, 2011; Ba et al., 2013; Ng. et al., 2013; Sivakumar et al., 2013; Salour et al., 2014; Han and Vanapalli, 2015). Nevertheless, most of these models require elaborate experimental data to determine the model parameters (Han and Vanapalli, 2014). However, the model by Han and Vanapalli (2015) follows a simplified approach and requires only a few uncomplicated tests to establish a resilient modulus-suction relationship.

5.7.2 *Model by Han and Vanapalli (2015)*

The model was developed by studying the resilient modulus – suction relationship of 11 different types of compacted soils. A brief description of the model, along with the equations for establishing the relationship are presented in section 5.2.4.

5.7.2.1 Model parameters and its calibration

The general equation for the model (Eq. 5.9 and Eq. 5.10) has the fitting parameter, ξ; the degree of saturation, S; soil suction corresponding to the optimum moisture content, ψ_{OPT}; and the resilient modulus values at the saturated condition, M_{RSAT}, and at optimum moisture content, M_{ROPT}. However, the degree of saturation could be substituted by using the SWCC model, like the Fredlund and Xing (1994) SWCC model. In this research, the SWCC specimen for the silty soils were compacted at a dry density of 1.67 g/cm^3 and moisture content of 16% and the best-fit model were generated over a wide range of suction, as shown in Fig. 3.10. The parameters for the best-fit Fredlund and Xing (1994) SWCC model are shown in Table 5.3.

The following equation, which was derived by substituting the parameters from the Fredlund and Xing (1994) SWCC model, was used in this research:

$$\frac{M_R - M_{RSAT}}{M_{ROPT} - M_{RSAT}} = \frac{\psi}{\psi_{OPT}} \left[\frac{ln\left\{2.718 + \left(\frac{\psi_{OPT}}{a}\right)^n\right\}}{ln\left\{2.718 + \left(\frac{\psi}{a}\right)^n\right\}} \right]^{m\xi} \tag{5.14}$$

Equation 5.14 was utilized to predict the resilient modulus at any suction level by using the values of M_{RSAT}, M_{ROPT}, ψ_{OPT}, and the SWCC model parameters of the compacted soil and the fitting parameter, ξ.

Table 5.3 Calibrated parameters for Fredlund and Xing (1994) SWCC models

Parameters	Calibrated values
α	18
n	0.8
m	1.0
θ_s	0.376
Ψ_r	1900 kPa

Han and Vanapalli (2015) observed that the value of the fitting parameter, ξ is mostly within the range of 1 to 3. For fine-grained soils, ξ was observed to be near 2, while for cohesionless soils a value of 1 was suggested by Han and Vanapalli (2015).

The value of resilient modulus at saturated condition was obtained from the RLTT test conducted on a saturated specimen (Fig. 5.9 shows the results of the test).

The value of M_{ROPT} might be obtained experimentally or by using empirical relations. In this research, both the methods are used to determine the value of resilient modulus at optimum moisture content (M_{ROPT}).

Method 1 refers to the determination of M_{ROPT} using experimental results. The results of the suction-controlled RLTT of a specimen at an induced matric suction of 36 kPa (shown in Fig. 5.14) were used to obtain the value of M_{ROPT} for

any given sequence. The experimentally determined value of M_{ROPT} is used to predict the value of resilient modulus at any suction level.

Since the motive behind the development of a prediction model is to minimize the number of tests to be performed, the Method 2 was devised to empirically access the value of M_{ROPT}, instead of performing an RLTT on a specimen at optimum moisture content. For this purpose, the relationship postulated by Sawangsuriya et al. (2009) was utilized (Eq. 5.5), which is explained in section 5.2.4. The value of M_{ROPT} was determined by substituting the experimentally determined values of M_{RSAT} and the suction corresponding to the optimum moisture content (ψ = 36 kPa). The value of resilient modulus at any suction level was determined by substituting these values, along with the SWCC model parameters in Eq. 5.14.

5.7.2.2 Comparison of Results

Figures 5.39 and 5.40 show the comparison between the resilient modulus obtained from the model using Method 1 and the experimental values for the eighth and the last sequence of loading, respectively. It is observed that the prediction is similar to the experimentally obtained values till a matric suction of 300 kPa. However, at the higher values of suction, the prediction overestimates the resilient modulus by approximately 14 times, for a suction of 30 MPa and 35 times for a

suction of 100 MPa. This shows that the model is limited to work within the moderate suction range.

Similarly, Figs. 5.41 and 5.42 show the comparison between the resilient modulus determined from the model using Method 2 and the experimental values for the eighth and the last sequence of loading, respectively. It is observed that the predictions for resilient modulus are quite different from that of the experimental results. The predicted value of M_{ROPT} was significantly lower (using Eq. 5.5) than the experimentally observed values. Hence, even the use of a much lower value of the fitting parameter ($\xi = 0.2$), satisfactory predictions for resilient modulus could not be established (for low to moderate suction state). Additionally, the issue of overpredicting the resilient modulus for specimens at high suction state still exists.

Therefore, it could be concluded that due to the consistent increase of resilient modulus with suction, even at high suction states, the model is not suitable for predicting the resilient modulus beyond the medium suction state.

Additionally, empirical relations for determining the resilient modulus at the optimum moisture content (OMC) is not advised as the resilient modulus at suction higher than that at OMC is very sensitive, to the accuracy of the resilient modulus at OMC.

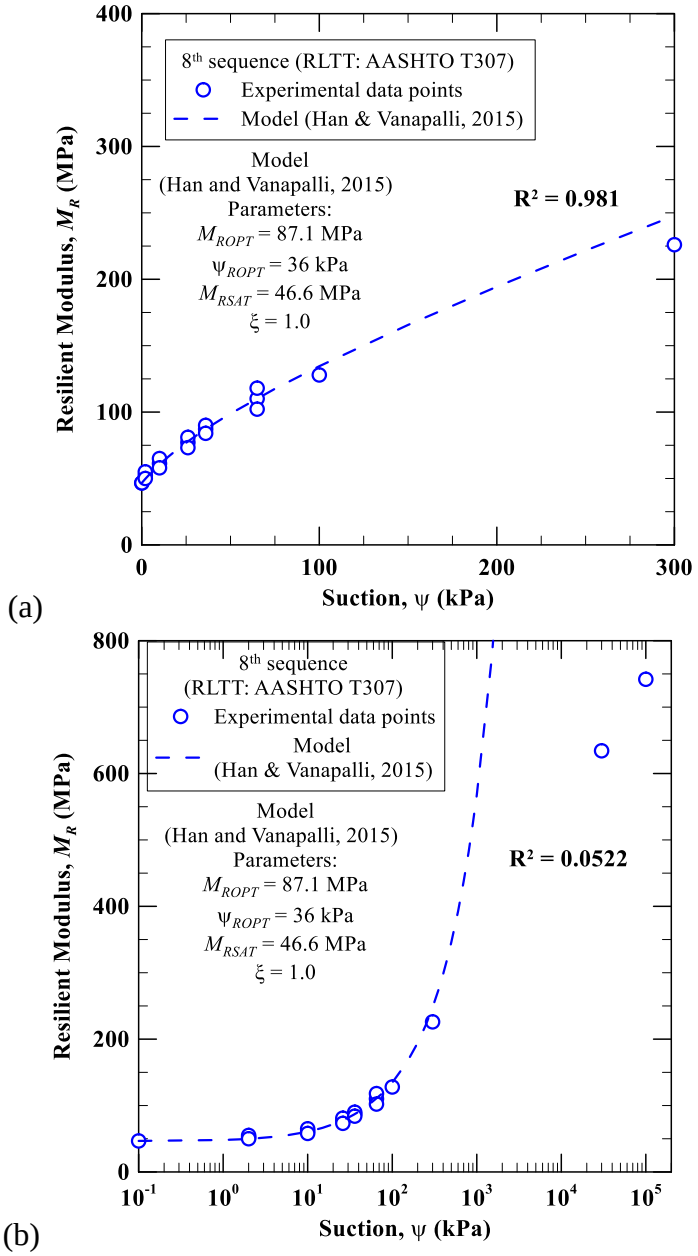

Figure 5.39 Comparison of resilient moduli (8th sequence) obtained from experimental results and the prediction model using Method 1 for a specimen at a dry density of 1.67 g/cm^3 over (a) moderate suction range, and (b) wide suction range

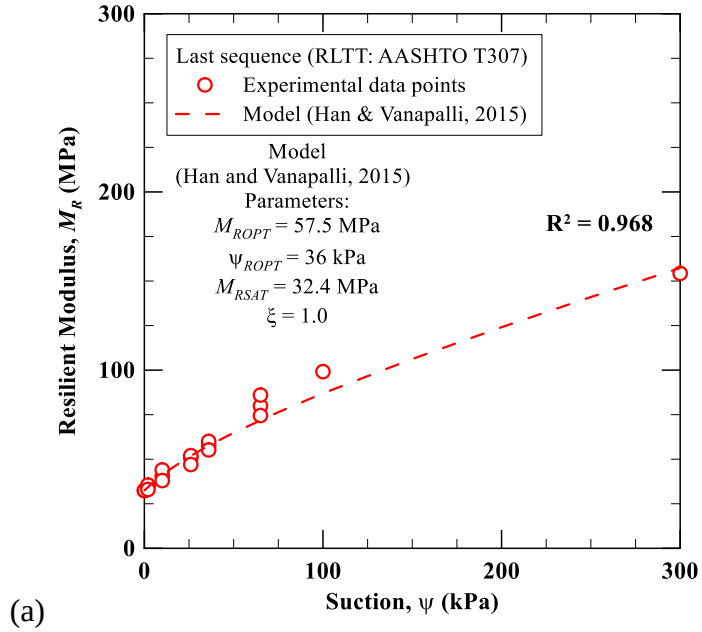

(a)

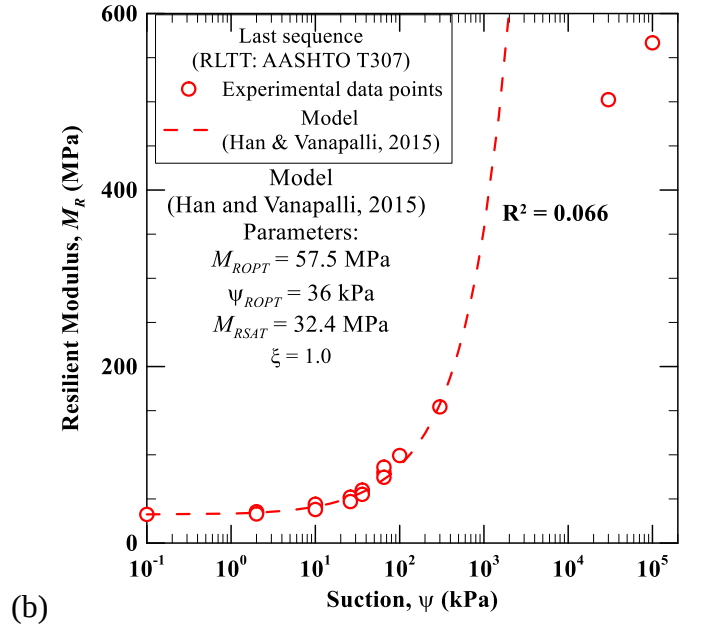

(b)

Figure 5.40 Comparison of resilient modulus (last sequence) obtained from experimental results and the prediction model using Method 1 for a specimen at a dry density of 1.67 g/cm^3 over (a) moderate suction range, and (b) wide suction range

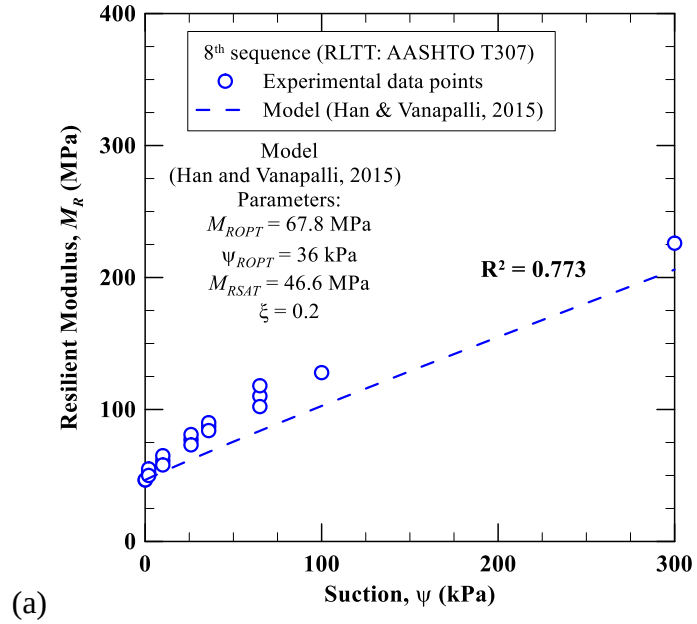

(a)

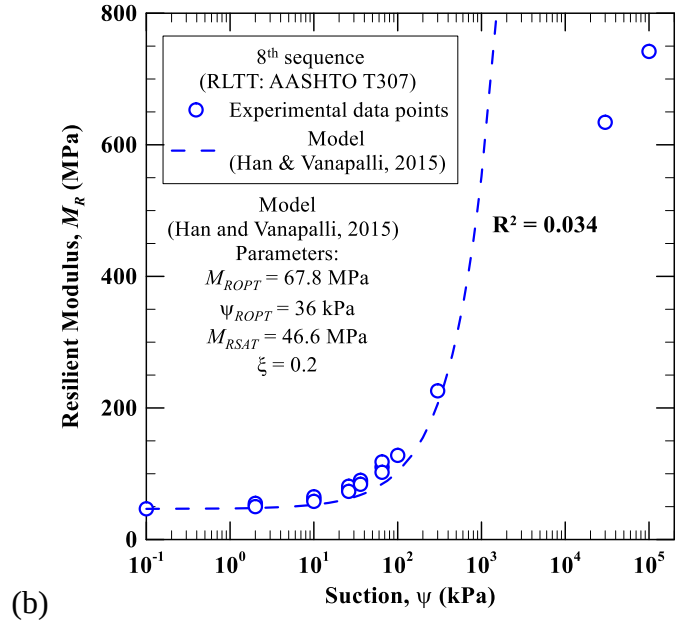

(b)

Figure 5.41 Comparison of resilient modulus (8th sequence) obtained from experimental results and the prediction model using Method 2 for a specimen at a dry density of 1.67 g/cm^3 over (a) moderate suction range, and (b) wide suction range

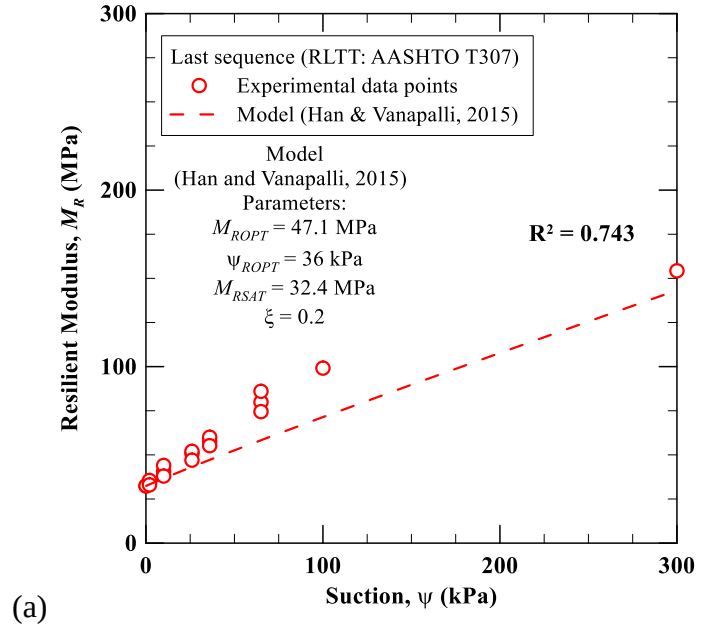

(a)

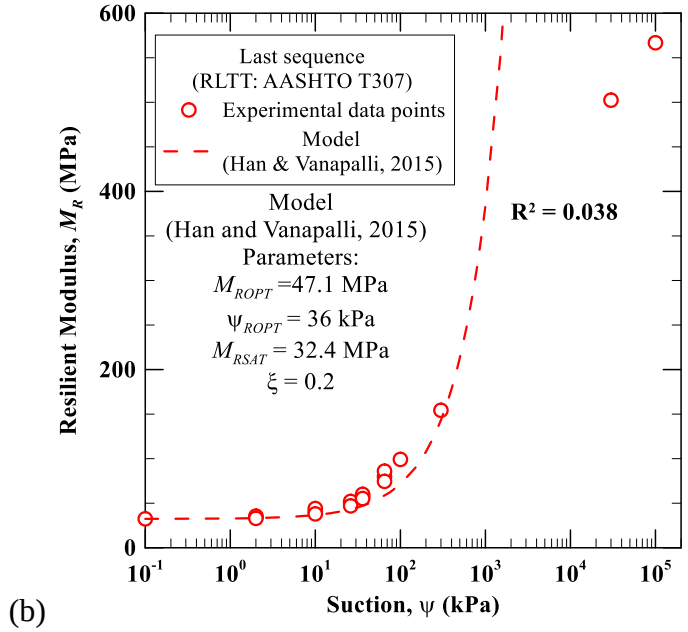

(b)

Figure 5.42 Comparison of resilient modulus (last sequence) obtained from experimental results and the prediction model using Method 2 for a specimen at a dry density of 1.67 g/cm^3 over (a) moderate suction range, and (b) wide suction range

5.8 Summary

This chapter introduces the concept of resilient modulus of unsaturated soils and its utility in the design of flexible pavements. The factors affecting the resilient modulus of unsaturated subgrade soils are presented. The methods to determine the resilient modulus of soils are described in brief. A review of the past and the recent advances in repeated load triaxial tests for determination of resilient modulus of unsaturated soils is discussed. The use of models for predicting the variation of resilient modulus with suction is introduced and a few recent models and equations are discussed.

The experimental program for studying the influence of suction and dry density of soil on the resilient modulus is described. The specimen preparation and suction equilibration are also explained and demonstrated. The procedure followed to perform suction-controlled repeated load triaxial test under varying suction states is also described.

The experimental results, including the variation of resilient modulus with net confining pressure, deviator stress, suction, and dry density of soil specimen, are studied in detail. The influence of wetting and drying cycles on the resilient modulus of the soil specimen is demonstrated. The important findings and the trends are discussed and compared to the available literature.

Finally, the calibration and validation of a recent and simplified model postulated by Han and Vanapalli (2015) were done using the experimental results

from this research. This model appears to provide reasonable resilient moduli predictions for low to moderate soil suction states. Also, the limitations of the model are discussed.

Chapter 6

LIQUEFACTION RESISTENCE IN UNSATURATED SOILS

6.1 Introduction

The problem of liquefaction has been considered very seriously due to the excessive damage it causes within a short span of time. The liquefaction phenomenon is manifested through sand boils and ground crack, excessive settlement of buildings, flow failures, and lateral spreading and subsequent cracking (Boulanger and Idriss, 2006, USGS, 2006a). Figures 6.1, 6.2, and 6.3 show some of the damages caused due to liquefaction during major earthquakes.

Liquefaction had been observed during the earthquakes in San Francisco, California, 1906; Niigata, Japan and Alaska in 1964; San Fernando Dam, California in 1971; Loma Prieta, California in 1989; Bhuj, India in 2001; Christchurch, New Zealand in 2011; and Tokyo Bay area, Japan in 2011 (Youd and Hoose, 1978; USGS, 2006b; Das and Ramana, 2011; Bhattacharya et al., 2011; Green et al., 2014). Generally, liquefaction occurs due to significant seismic activity and is associated with mainly cohesionless soils. However, studies have been conducted to determine the liquefaction potential in cohesive soils.

(a)

(b)

Figure 6.1 Photographs of damages caused due to liquefaction during Niigata Earthquake in 1964: (a) Bearing capacity failure in Kawagishi-cho; (b) Failure of Showa Bridge (Kramer, 1996; USGS, 2006a)

The saturation of soil is considered to be a pre-requisite for liquefaction. The main reason for this general conception is due to the presence of highly compressible pore-air in unsaturated soils. However, a drastic reduction in the shear strength and stiffness of the unsaturated soil may result in excessive deformation, which could trigger the failure of structures. Henceforth, in this chapter, the liquefaction potential of soil, which is not fully saturated, is investigated in detail.

(a)  (b) 

Figure 6.2 Photographs of damages caused due to liquefaction during the Loma Prieta earthquake in 1989: (a) Formation of sand boils; (b) Lateral spreading near the Pajaro River (USGS, 2006a).

Figure 6.3 Lower San Fernando Dam Failure due to liquefaction in 1971 (Seed, n.d.)

6.2 Review of Literature: Liquefaction

6.2.1 *Definition of Liquefaction*

The term ‘liquefaction’ was originally coined by Mogami and Kubo (1953). The definition of liquefaction has been debated upon for years. The liquefaction of soils traditionally referred to the loss of strength in saturated cohesionless soils due to the generation of excess pore water pressure during dynamic loading (Rauch, 1997; Coduto, 1999). The liquefaction of soil is associated with the deformation caused when the saturated soil is subjected to monotonic, transient, or cyclic stresses (Rauch, 1997; Jefferies and Been, 2006). All liquefaction phenomena include the generation of excess pore water pressure under undrained loading conditions (Kramer, 1996).

6.2.2 *Types of Liquefaction*

The various types of liquefaction are classified into two major categories: (*i*) flow liquefaction; and (*ii*) cyclic mobility (Coduto, 1999).

Flow liquefaction refers to the reduction of shear strength of the soil due to the generation of excess pore water pressure and subsequent ‘flow failure’. After the reduction of shear strength, due to cyclic stress, the existing static shear stress may cause the flow failure. Flow liquefaction can cause sudden catastrophic failures, as observed during earthquakes in the Sheffield Dam (California) in 1925 and lower San Fernando Dam (California) in 1971.

Cyclic mobility is described as the tendency of dense, saturated sands to gradually soften when subjected to cyclic shear stresses in undrained condition (Castro, 1975; Castro and Poulos, 1977). The cyclic mobility may occur in dense or loose cohesionless soils, when the static shear stress is less than the shear stress of liquefied soil (Kramer, 1996; Rauch, 1997). The deformation caused by cyclic mobility is known as lateral spreading, which can occur on level surfaces or gentle slopes (having an inclination less than 3°). Although cyclic mobility might not be as catastrophic as flow liquefaction, however, they might result in significant deformations, which cause failures resulting in substantial damages (Jefferies and Been, 2006).

Although the liquefaction initiation due to flow liquefaction and cyclic mobility has traditionally not been considered separately, since they are different phenomena, it is essential to study them distinctly. Flow liquefaction could be caused due to monotonic loading and cyclic loading from seismic activity, and vibrations from pile driving, train traffic, geophysical explorations, and blasting (Kramer, 1996). However, the seismic activities may solely initiate the cyclic mobility.

The possibility of soil to liquefy by flow liquefaction or cyclic mobility could be determined by considering the initial stress condition and the stress path followed by similar specimens during monotonic loading (Kramer, 1996). Figure 6.3 shows the response of five soil specimens, having the same void ratio when

subjected to undrained shearing. The specimens ‘A’ and ‘B’ directly reach the peak strength at the steady state point. While, the specimens ‘C’, ‘D’ and ‘E’ reach their respective peak strength, marked as x, in the *p′-q* space (Fig. 6.3a). Subsequently, the shearing of the specimens ‘C’, ‘D’ and ‘E’, beyond their respective peak strengths results in a decrease in deviator stress and increase in pore water pressure. Finally, the stress paths for all the five specimens reach the steady state point.

The specimens having the same void ratios, but varying initial stress conditions, after shearing in undrained condition reach the same value of deviator stress at a constant effective mean stress, resulting in constant stress condition. This forms a point in the *p′-q* space, known as the steady state point (Fig. 6.4a and Fig. 6.5). Similarly, specimens at another initial void ratio and varying initial stress condition, after shearing would reach a different steady state point. The locus of various steady-state points obtained from shearing the specimens at varying initial void ratios form the steady state line (SSL) (Fig. 6.5).

Figure 6.5 shows the approach used by Vaid and Chern (1983) to identify the zone of the possible development of flow liquefaction or cyclic mobility. The flow liquefaction surface (FLS) defines the initiation of flow liquefaction in the *p′-q* space. The FLS can be plotted by joining the points at which the specimen reaches its peak undrained shear strength, which has been marked as ‘x’ in Fig. 6.4a. The FLS demarcates the boundary between stable and unstable states during undrained shearing.

Since the flow liquefaction does not initiate if the stress path is below the steady state point, the FLS is curtailed at the same deviator stress as that of the steady state point (Kramer, 1996).

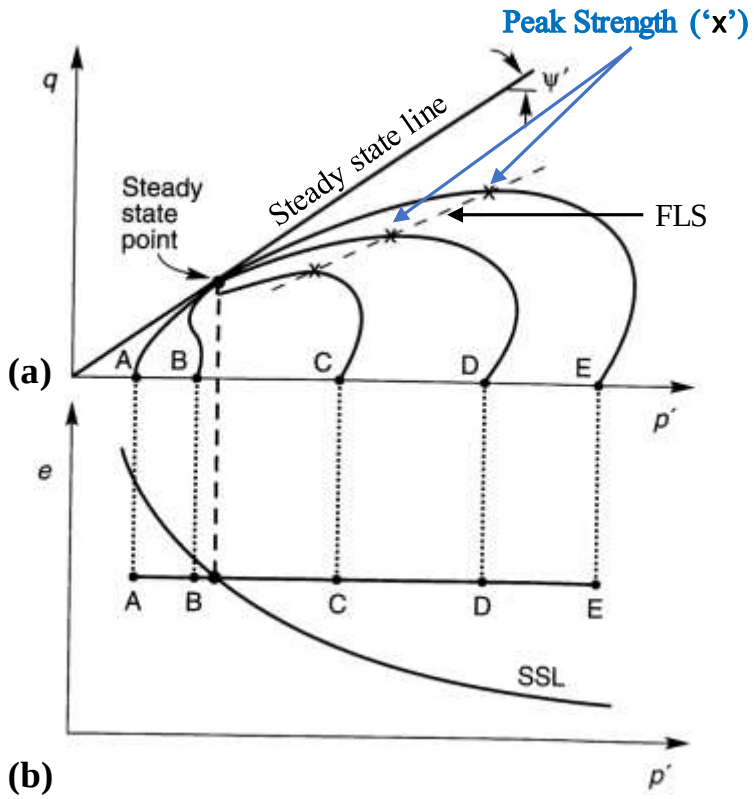

Figure 6.4 Response of isotropically consolidated specimens subjected to monotonic shearing in undrained condition (modified from Kramer, 1996)

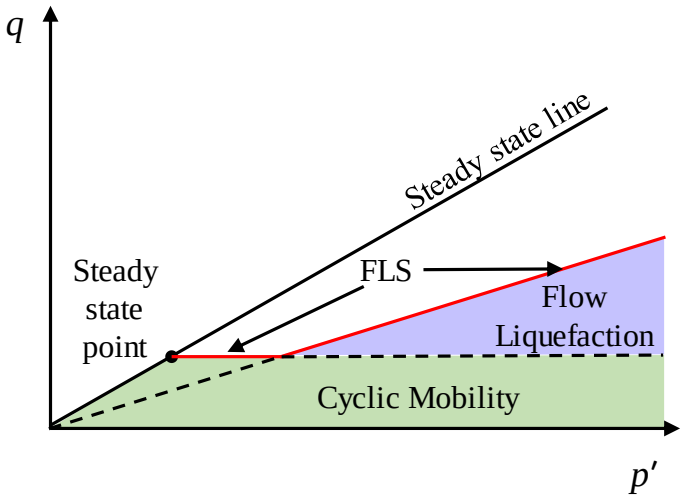

Figure 6.5 Zone of susceptibility to flow liquefaction and cyclic mobility and the orientation of flow liquefaction surface in p'-q space

Figure 6.5 illustrates that lesser cyclic shear stresses are required to initiate cyclic mobility than flow liquefaction. Hence, the static shear stresses required to initiate flow liquefaction by cyclic loading is greater than the steady state shear strength. Conversely, cyclic mobility may be initiated when the static shear stress is less than the steady state shear strength.

The soils at a very low confining pressure behave as dense soils (Holtz and Kovacs, 1983) and flow liquefaction occurs exclusively in loose soils (Kramer, 1996). The flow liquefaction zone (Fig. 6.5) does not start from a very low effective mean stress. However, the zone of susceptibility for cyclic mobility extends from a very low to a very high value of effective mean stress (Fig. 6.5).

In a cyclic triaxial test, the initiation of cyclic mobility is not as well-defined as in the case of flow liquefaction. Hence, the criterion of some limiting cyclic

strain amplitude (like double amplitude strain of 5%) is often selected as a pre-defined point to indicate liquefaction failure due to cyclic mobility (Kramer, 1996).

6.2.3 *Liquefaction in Saturated Soils*

Laboratory tests to investigate the cyclic loading or liquefaction of saturated cohesionless soils have been performed using triaxial, simple shear or torsional ring shear test devices. Cyclic triaxial tests have been most prominently used to characterize the behavior of cohesionless soils, after the pioneering work of Seed and Idriss (1966).

The results from cyclic triaxial and simple shear tests showed that as the shear stress amplitude (also known as, the cyclic stress ratio) increased, the number of cycle required to initiate liquefaction decreased for different types of soils (Seed and Lee, 1965; Silver et al., 1976; Ishihara et al., 1980; Garga and Mckay, 1984; Toki et al., 1986; Prakash and Sandoval, 1992; Evans and Zhou, 1995; Thevanayagam et al., 2000; Xenaki and Athanasopoulos, 2003, 2008; Sitharam et al., 2004; Ghionna and Porcino, 2006; Boulanger and Idriss, 2007; Boominathan et al., 2010; Rees, 2010; Dash and Sitharam, 2011; Tsukamoto et al., 2014; Wang et al., 2016). When the CSR was plotted against the number of cycles required to induce liquefaction in logarithmic scale, the curve followed a non-linear function, which was asymptotic to the x-axis.

The effect of relative density has a significant effect on the resistance to liquefaction. An increase in relative density required a higher CSR to liquefy the

specimen at the same number of cycles (Sitharam et al., 2004). Since the relative density and void ratio of soil are related, a decrease in void ratio required higher CSR to initiate liquefaction at the same number of cycles (Seed and Lee, 1965).

The liquefaction of cohesive soils had also been established by various researchers (Anderson et al., 1980, 1988; Hyodo et al., 1994; Lefebvre and Pfendler, 1996; Perlea, 2000; Moses et al., 2003; Boulanger and Idriss, 2006, 2007; Li et al., 2011). The liquefaction studies on gravels were initially conducted in the field by Coulter and Migliaccio (1966), Wang (1984), and Youd et al. (1985) and in the laboratory by Wong et al. (1974), Banerjee et al. (1979), and Evans and Seed (1987). However, it was observed that the effect of membrane penetration for gravel specimens had a significant effect on the higher liquefaction resistances observed in the laboratory (Kramer, 1996).

The following factors had been observed to influence the liquefaction resistance of saturated soils: (*i*) soil type; (*ii*) density or void ratio of the soil; (*iii*) initial stress condition of the soil; (*iv*) soil gradation; (*v*) particle shape of soil; (*vi*) over-consolidation ratio of the soil; (*vii*) specimen preparation (*viii*) age of soil deposit (Townsend, 1978; Youd and Perkins, 1978; Kramer, 1996; Jefferies and Been, 2004).

Most of the cyclic triaxial tests in past had been conducted on isotropically consolidated cohesionless specimens having a relative density of 30% to 80% (Seed and Lee, 1965; Ladd, 1977; Vaid and Sivathayalan, 1996; Sitharam et al., 2004).

The applied shear stress is generally defined as the ratio of deviator stress to twice the effective confining pressure, and is known as cyclic stress ratio (CSR),

$$\text{CSR} = \frac{\sigma_d}{2\sigma_3'} \tag{6.1}$$

where σ_d is the deviator stress, and σ_3' is the effective confining pressure. From the past literature, it had been observed that the cyclic triaxial tests on cohesionless soil specimens had been conducted on varying values of CSR mostly in the range of 0.1 to 0.5 to initiate liquefaction (Seed and Lee, 1965; Silver et al. 1976; Ladd, 1977; Singh et al., 1982; Kutter et al., 1994; Boulanger and Truman, 1996; Vaid and Sivathayalan, 1996; Gallagher and Mitchell, 2002; Sitharam et al., 2004; Ghionna and Porcino, 2006; Xenaki and Athanasopoulos, 2008; Das and Sitharam, 2011; Wang et al., 2016; Markham et al., 2016).

The cyclic triaxial tests do not simulate the exact ground motion during a seismic activity. The application of shear stress in the simple shear device provides the most accurate simulation of the in-situ shear stress applied during an earthquake (Seed et al., 1975). Seed et al. (1975) suggested that the CSR required to initiate liquefaction in the field was nearly 10% less than that obtained in the simple shear device. Also, the definition of CSR for the triaxial test is different from that for the simple shear device. The correction factor, c_r is used to convert the CSR of triaxial and simple shear device. Finn et al. (1971) defined the value of c_r using the following expression:

$$c_r = \frac{1+K_o}{2} \tag{6.2}$$

Castro (1975) had suggested the following expression for the correction factor, c_r:

$$c_r = \frac{2(1+2K_o)}{3\sqrt{2}} \tag{6.3}$$

Thus, the following relation may be used to convert the CSR obtained from the field to that for the triaxial device:

$$(CSR)_{field} = \frac{\tau_{cyclic}}{\sigma'_{vo}} = 0.9c_r(CSR)_{triaxial} \tag{6.4}$$

6.2.4 *Liquefaction in Unsaturated Soils*

The analysis for liquefaction in soils has been conducted with the basic assumption that the soil needs to be saturated (Kramer, 1996). However, soils which are near saturation may generate enough excess pore water pressure during cyclic shearing to result in significant reduction in the shear strength and stiffness of unsaturated soil. This may result in limited, but significant deformation, which is known as cyclic mobility, which has been explained in section 6.2.2.

The presence of pore air in unsaturated soils is considered to be the major factor which prevents liquefaction. Since air is highly compressible as compared to water, the generation of excess pore water pressure is expected to be hindered, due to the volume change of pore air with an increase in pressure. However, recently it has been proven from suction-controlled triaxial tests that soils in unsaturated condition have undergone liquefaction due to excessive deformation, without

reaching zero net mean stress (Unno et al., 2008; Okamura and Noguchi, 2009; Tsukamoto et al., 2014; Wang et al., 2016; Zhang et al., 2016).

Initial studies included the effect of saturation on liquefaction resistance of cohesionless soils (Sherif et al., 1977; Yoshimi et al., 1989; Xia and Hu, 1991, Ishihara and Tsukamoto, 2004; Yang et al., 2004). These studies mainly relied on the value of Skempton's pore pressure parameter, *B* for demonstrating the increase of liquefaction resistance with desaturation or decrease in *B*-value.

Recently, the suction-controlled specimens were subjected to cyclic loading in undrained conditions to determine the response of unsaturated soils (Unno et al., 2008; Okamura and Noguchi, 2009; Tsukamoto et al., 2014; Liu and Xu, 2015; Wang et al., 2016; Zhang et al., 2016). These limited studies had shown that liquefaction occurred under higher values of cyclic stresses for a small decrease in the degree of saturation. However, an elaborate series of cyclic triaxial tests are required to establish the effect of suction on liquefaction resistance of cohesionless soils tested at varying relative densities.

The effect of various parameters on the liquefaction resistance is generally considered by performing a parametric study and selecting a predefined number of cycles (say 20 or 25) to define the liquefaction caused due to the applied CSR. Okamura and Noguchi (2009) suggested the use of liquefaction resistance ratio to study the effect of saturation, which is defined as follows:

$$\text{Liquefaction resistance ratio, LRR} = \frac{CSR_{N=x}}{CSR_{sat,N=x}} \qquad (6.5)$$

where, $CSR_{N = x}$ is the cyclic stress ratio required to liquefy the soil at any degree of saturation in x number of cycles, and $CSR_{sat, N = x}$ is the cyclic stress ratio required to liquefy the saturated soil in x number of cycles.

6.2.5 *Synopsis of Literature Review*

The liquefaction of soils has been a major concern for geotechnical engineers and researchers, due to the extensive damages caused by it. Over the last five decades of elaborate research on the study of liquefaction, only recently few researchers have started to focus on the study of liquefaction in unsaturated soils. The general perception still exists that complete saturation (S = 100%) is required to cause liquefaction.

This section dealt with the definition of liquefaction in soils and discussed the ambiguity in its definitions. The main types of liquefaction, i.e. flow liquefaction and cyclic mobility were defined and the conditions conducive to both the types of liquefaction are presented. The past and recent findings for liquefaction in saturated soils were elaborated. Finally, the outcomes of the limited studies on liquefaction in unsaturated soils are discussed.

6.3 Basic Properties of Test Soil

The fine sands are predominantly susceptible to liquefaction. Hence, a sandy soil was selected to perform the study of the liquefaction of unsaturated soils. From the sieve analysis and hydrometer tests, it was determined that the soil primarily comprised of sand (52%) and silt (41%), with a small amount of clay

(7%). The grain size distribution is shown in Fig. 6.6. The soil was found out to be non-plastic from Atterberg Limit tests, which were conducted in accordance to ASTM D4318-10e1. The soil was classified as silty sand (SM) as per the Unified Soil Classification system (USCS). The specific gravity of the soil solids was obtained to be 2.67, by conducting specific gravity test using a pycnometer, as per ASTM D854-14. The standard Proctor tests were conducted as per ASTM D698-12e2 (shown in Fig. 6.7), and the maximum dry density of 1.87 g/cm^3 was obtained at an optimum moisture content of 12.2%. The physical and mechanical properties of the soil are listed in Table 6.1.

Table 6.1 Properties of the silty sand used in the study

Parameters	**Value**
Sand (%)	52
Silt (%)	41
Clay (%)	7
USCS classification	SM
Maximum dry unit weight, $\gamma_{d,\,max}$, (kN/m^3)	18.4
Optimum moisture content, w_{opt} (%)	12.2
Plasticity Index, PI (%)	NP (Non-Plastic)
Specific Gravity, G_s	2.67

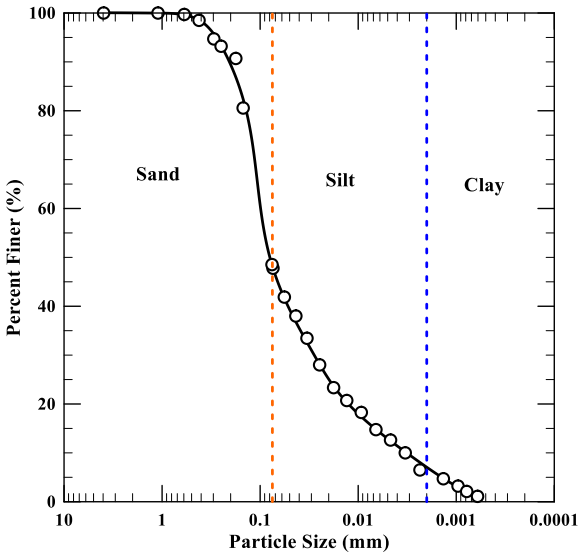

Figure 6.6 Grain size distribution of the silty sand used in the study

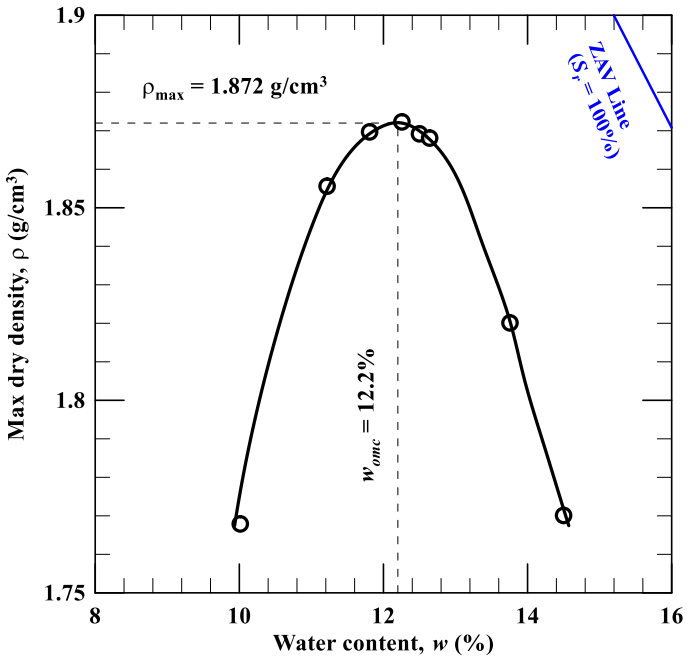

Figure 6.7 Standard Proctor compaction curve for the silty sand used in the study

6.4 Specimen Preparation

The liquefaction predominantly occurs in loose soils at relatively low confining pressures (Kramer, 1996). Hence, the heavily compacted soils were not required in this study. Undrained triaxial compression tests were performed on cylindrical specimens having a height of 142 mm and a diameter of 71 mm. Thereby, the height to diameter (*H*/*D*) ratio was 2.0, as recommended by ASTM D5311/D5311M-13. Additional specimens of height of 25.4 mm and diameter of 63.5 mm were prepared for obtaining the SWCC of the silty sand specimen at varying densities.

Various methods were considered for preparing loose specimens, like the dry funnel deposition, water sedimentation, slurry deposition, mixed dry deposition, and air pluviation. Previous studies (Oda, 1972a, 1972b; Ladd, 1974; Mulilis, et al. 1977; Tatsuoka, et al. 1979, 1986; Miura and Toki, 1982; Zlatovic and Ishihara, 1997; Jang and Frost, 1998; Vaid et al., 1999; Wood and Yamamuro, 1999; Høeg et al., 2000; Wood et al., 2008) had reported that the response of sands to shearing could be influenced by the specimen deposition or reconstitution method. A detailed effect of specimen preparation technique on response of silty sands to undrained triaxial compression had been conducted by Wood et al. (2008)

The specimen was expected to undergo further compaction (i.e., increase in relative density) with an increase in confining pressure prior to consolidation. Since the final target relative densities for undrained shearing lie in the range of 40 to

75%, the target relative densities after specimen preparation was around 20% to 50% (obtained by a series of trial tests). Hence, the methods capable of generating low to medium relative density specimens were selected for the study. The moist tamping technique along with the mixed dry deposition (MDD) and dry funnel deposition (DFW) were the only methods capable of preparing of specimens at a low relative density (Wood et al., 2008).

The specimens prepared by moist tamping technique showed flocculation or formation of "honeycomb structure" during saturation. Similar observations were made by Casagrande (1975), where "honeycombed structure" was predicted to undergo premature liquefaction. Hence, the moist tamping method was not used in this study.

Additionally, it was observed that the grain size distribution was identical throughout the height of the specimen, which was prepared by the dry funnel deposition method. Wood et al. (2008) had warned that the dry funnel deposition method may result in higher silt content in the outer region and a higher concentration of sand in the core of the specimen. However, the sieve analysis of the specimens prepared using this method for silty sand used in the study showed a uniform distribution of sand and silt throughout the specimen, which may be due to the absence of coarser sand particles. Henceforth, the dry funnel deposition method was used to prepare all the specimens of silty sand in this study.

The specimens for target relative density of 75% were prepared by using a variation of the dry funnel method. The dry soil was poured through a funnel in 10 layers, with a light block being placed after each layer. An additional load was placed on the block to partially compact the soils. The load applied was gradually increased (from 250 g to 1.5 kg; selected on the basis of multiple trials) as the higher layers are reached, to prepare specimens of the same density, which is known as undercompaction principle (explained in section 3.3), proposed by Ladd (1978).

The membrane penetration effect (explained in section 3.10) was considered to be insignificant since fine sandy soil was used in this study (D_{50} = 0.1 mm; Raju and Sadasivan, 1974; Vaid and Negussey, 1984; Kuerbis, 1989; Wood et al., 2008).

6.5 Soil Water Characteristic Curve

The drying cycle of the soil-water characteristic curve (SWCC) of the test soil at its target dry density was obtained by using the Fredlund device, commonly known as Tempe Cell, and the relative humidity apparatus. The Tempe Cell was used for matric suction below 500 kPa. The experimental points in the residual zone of the SWCC were obtained from the automatic relative humidity apparatus, which works on the principle of vapor pressure technique (explained in section 3.4.2).

The specimens at relative densities of 50% and 75% were tested for their soil suction-water content relationship. The experimental data points were joined using the best-fit curves using the Fredlund and Xing (1994) SWCC model and are

shown in Fig. 6.8. The model parameters for specimens at both the relative densities (D_r = 50% and 75%) has been tabulated in Table 6.2.

Table 6.2 Model Parameters for selected silty sand specimens at relative density of 50% and 75%

Fredlund and Xing (1994)	Values	
	D_r = 50%	D_r = 75%
a	33	40
n	0.72	0.72
m	1.85	1.85
θ_s	0.357	0.344
Ψ_r (kPa)	750	800

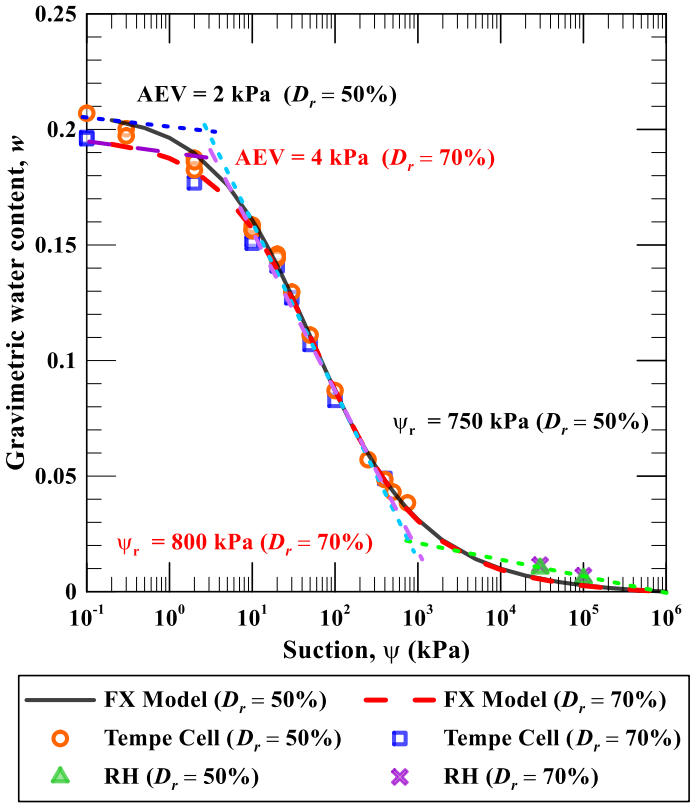

Figure 6.8 SWCC of silty sand specimens (D_r = 50% and 75%) used in the study

6.6 Experimental Program

In this research, a series of cyclic triaxial tests were performed on consolidated undrained specimens of silty sand (SM) of varying relative densities (D_r = 50% and 75%) under low net confining pressure of 50 kPa and at varying suction levels (s = 0 to 30 kPa) by applying varying cyclic stresses (CSR = 0.15 to 0.45). The cyclic load was applied in the form of a sinusoidal waveform as recommended by ASTM D5311-13. Additional monotonic triaxial tests were conducted on silty sand specimens of 50% relative density at varying net mean stress of 50 and 100 kPa and at saturated and unsaturated conditions (s = 25 kPa) to determine the variation of Bishop's effective stress parameter, χ with an increase in suction.

The frequency of loading within a range of 0.001 Hz to 0.1 Hz were observed not to influence the response of the soil, however the presence of high-air entry (HAE) disks of 1-bar (= 100 kPa) in unsaturated soil testing required a slow frequency rate to allow proper response of excess pore water pressure to be captured by the pore pressure transducer. Hence, all the cyclic triaxial tests on unsaturated soil specimens were performed at a frequency of 0.001 Hz. While all the cyclic triaxial tests on saturated soil specimens were performed at a frequency of 0.1 Hz since the porous stone allows free movement of water from the base of the specimen to the pore water pressure transducer.

Table 6.3 Series of cyclic triaxial tests performed in this dissertation research

Test #	Matric Suction (kPa)	Relative Density, D_r (%)	Cyclic Stress Ratio (CSR)	Degree of Saturation, S_r (%)	*B*-value
1-4	0	49 – 51	0.15, 0.20, 0.25, 0.35	100	0.96 – 0.97
5-6	0.1 – 0.2[(1)]	52 – 54	0.25	96 – 98	0.50, 0.70
7-9	2	50 – 53	0.15, 0.25, 0.30	89 – 90	0.28 – 0.29
10-13	10	49 – 54	0.15, 0.20, 0.25, 0.35	75 – 77	0.06 – 0.07
14-16	20	52 – 53	0.25, 0.35, 0.45	70 – 71	0.04 – 0.05
17	30	54	0.35	63	0.02
18-19	0	74 – 76	0.15, 0.20	100	0.96
20	2	74	0.35	90	0.32
21-22	10	72 – 74	0.25, 0.45	77 – 78	0.07 – 0.08
23	20	74	0.35	73	0.03

(1) – approximate value of suction (Test# 5 & 6)

6.7 Modifications for Performing Cyclic Triaxial Tests on Unsaturated Specimens

The calibration of the experimental setup was initially performed. Since the specimen is subjected to tensile forces, a coupler (shown in Fig. 6.9a) was attached to the loading shaft to allow the axial actuator to apply tensile forces to the top cap and indirectly to the specimen.

Additionally, the suction applied during the cyclic triaxial tests are low. Hence, it is important to maintain accurate values of cell pressure, air pressure, and pore-water pressure. The U-tube manometer (shown in Fig. 6.9b), having a range of 10 kPa with a resolution of 0.1 kPa, was used to achieve this objective.

Prior to starting any test, each pressure line was connected to one end of the manometer and the other end is kept open to the atmospheric pressure. A series of

small values of pressures, ranging from 0 to 10 kPa) were applied to the manometer and proper adjustments were made when necessary. Subsequently, only the pore air pressure line from the pressure volume controller (PVC) was connected and a parallel connection was used to apply the pore air pressure to the specimen during the suction equilibration phase of the test (shown in Fig. 6.9).

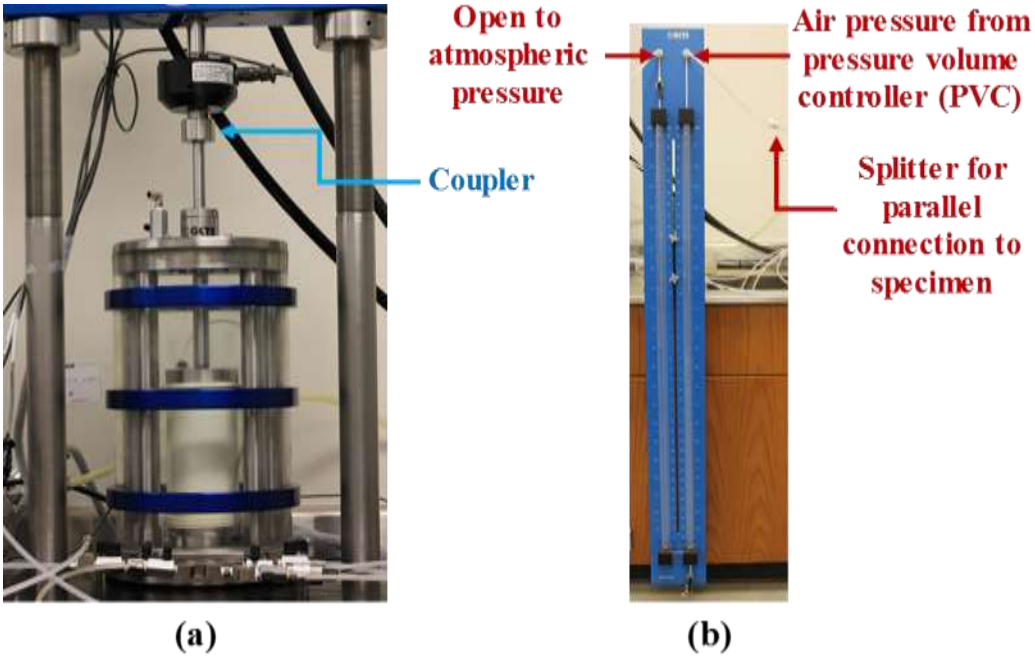

Figure 6.9 Modifications to the experimental setup for performing cyclic triaxial tests

6.8 Testing Procedure

6.8.1 *Saturated Test*

A series of cyclic triaxial tests were performed on saturated specimens of silty sand at varying cyclic stress ratio (CSR = 0.15, 0.2, 0.25, and 0.35) and relative density (D_r = 50% and 74%). The experimental procedure was slightly different as

compared to that of monotonic triaxial tests, due to the difference in specimen preparation technique (as explained in section 6.4).

The base pedestal fitted with a saturated porous stone was attached to the base plate of the triaxial setup and the pore pressure lines were saturated using manual control. A moist filter paper was placed on the previously saturated porous stone to prevent migration of fine particles into the pore water pressure line. Additionally, the filter paper prevented the clogging of the porous stone. The soil specimen was prepared by pouring soil through a funnel into a split mold placed on the base pedestal fitted with a latex membrane. The soil was leveled after each layer (as explained in section 6.4) and finally, the top cap fitted with dry porous stone was placed on the top surface of the dry specimen with a dry filter paper to prevent clogging of the porous stone. The soil specimen, the base pedestal and the top cap assembly was sealed using a latex membrane and "O"-rings (similar to the assembly as described in section 3.6.1).

A small suction (magnitude of 10 kPa) is applied to the specimen through the top cap, to prevent the specimen from bulging due to its self-weight. The double-walled cells were placed and the entire chamber was sealed. Initially, the outer cell and later the inner cell was filled with de-aired water by applying a 15 kPa pressure from the pressure control panel. Since the air release valve was open, the soil specimen did not experience any confining pressure, apart from the applied suction, which is independent of the cell pressure applied to fill the cells. Once the

inner cell was almost filled, the pressure was reduced to 5 kPa and after it was filled, the air release valve was closed. Subsequently, the suction was decreased gradually to zero. Immediately, the cell pressure was increased to 15 kPa and a back pressure of 5 kPa was introduced. Thus, an effective confining pressure of 10 kPa was maintained throughout the process of filling the cell. A seating stress of 5 kPa was applied to the axial actuator to maintain proper contact with the top surface of the specimen.

6.8.1.1 Saturation of the specimen

The saturation process is similar to that explained in section 3.6.2 for monotonic triaxial tests. A small back pressure of 5 kPa was applied from the base of the specimen and a suction of 10 kPa is applied from the top of the specimen to allow the water-front to slowly move towards the top the specimen. This procedure was conducted as per the guidelines of ASTM D5311-13. After the water-front reached near the top of the specimen, the applied suction was removed. When the water came out through the top porous stone, due to the back pressure of 5 kPa, the valve to the top cap was closed.

Subsequently, the specimen was saturated using back-pressure approach, which has been explained in section 3.6.2. The specimen was considered to be fully saturated when the Skempton's pore-water pressure parameter, *B*, is greater than 0.95. The details regarding the *B*-value test have been provided in section 3.6.2.

The silty sand specimen was observed to reach a *B*-value of greater than 0.95 at back pressure of 580 kPa.

Additional cyclic triaxial tests (Test # 5 and 6 in Table 6.3) were performed on specimens having lower *B*-values to study the effect of variation of liquefaction resistance with a decrease in the degree of saturation and the *B*-value. Hence, the increase back pressure was stopped after reaching *B*-values of 0.50 and 0.70.

6.8.1.2 Isotropic consolidation

The consolidation stage involves the dissipation of excess pore water pressure generated due to the application of the target effective pressure at which the shearing would be conducted (explained in section 3.6.3). During consolidation, the volume of the soil specimen undergoes changes due to the dissipation of excess pore water pressure. The target consolidation stress was achieved by ramping up the cell pressure while maintaining a constant back pressure. The target cell pressure was reached in 30 seconds and the change in the volume of the soil specimen and the volume of water flowing out of the specimen was recorded and plotted. The consolidation was continued for 24 hours to ensure primary consolidation of both saturated and unsaturated specimens and to allow the same amount of time for consolidation to occur for all the specimens.

6.8.1.3 Monotonic loading in drained conditions

Two monotonic triaxial tests were performed to determine the slope of the critical state line and the shear strength parameters of saturated specimens of silty

sand at a relative density of 50%. The test procedure for conducting these triaxial tests under drained conditions was similar to that used for monotonic triaxial tests on compacted specimens of silty soil in saturated condition (explained in section 3.6.4).

6.8.1.4 Cyclic loading in undrained conditions

The cyclic loading was applied using a sinusoidal waveform having constant amplitude and frequency throughout the loading and unloading sequence. The mean value of the cyclic deviator stress was zero. Hence the amplitudes of deviator stresses during the application of compression and tension are equal. During the application of cyclic load, the cell pressure was maintained at a constant value, while the drainage valve was closed to simulate undrained conditions. Hence, the back pressure was not controlled and the pore water pressure was measured using the pore water pressure transducer connected to the base of the specimen.

The axial strains and the excess pore water pressure generated with increasing cycles of deviator stress were closely monitored. The effective stress path followed during the test was computed. Generally, the point at which the effective confining stress reaches a value of zero is considered as the initiation of liquefaction. However, in this study, the undrained cyclic loading of unsaturated soil was not expected to result in an effective confining stress of zero. Hence, the number of cycles required to achieve an axial strain of 5% was considered as the

point of liquefaction for all cases. A similar assumption was made by other researchers (Okamura and Soga, 2006; Okamura and Noguchi, 2009; Tsukamoto et al., 2014).

6.8.2 *Unsaturated Tests*

For cyclic triaxial tests on unsaturated specimen, the same procedure for sample preparation and initial wetting of soil specimen was followed as in the case of the saturated test, explained in section 6.7.1. However, instead of using the porous stone in the base pedestal, high-air entry (HAE) ceramic disks of 1-bar (100 kPa) air-entry value were used. The soil specimen was in direct contact with the HAE disks to enable the flow of water from the specimen to the pore water pressure line through the HAE disks. The soil specimen was allowed to achieve near saturated condition, but the back-pressure saturation approach was not used. Instead, the specimens were equilibrated to the required matric suction level by using the axis-translation technique (explained in section 2.9.1).

6.8.2.1 Suction equilibration

The independent control of pore air pressure and pore water pressure allowed the application of the required suction level. The *B*-value test (explained in section 3.6.2) was conducted to indirectly check the degree of saturation. Additionally, the water flowing into or out of the specimen enabled the determination of the degree of saturation of the specimen. In this research, the suction was considered to be equilibrated when the change in water content was

less than 0.04%/day, as suggested by Sivakumar (1993). Throughout the suction equilibration process, the net confining pressure was kept at 15 kPa to prevent accidental swelling of the specimen.

6.8.2.2 Suction-controlled isotropic consolidation

The suction-equilibrated specimen was subjected to the required net confining pressure of 50 kPa by increasing the cell pressure while maintaining constant pore air and pore water pressures (similar to monotonic triaxial tests; explained in section 3.7.3). The cell pressure was increased at the rate of 5 kPa/hr. The volume change of the specimen was monitored using the volume change device. The volume of water flowing out of the specimen was recorded using the pressure volume controller. The consolidation was assumed to be complete when the volume change of the specimen attains a constant value and is equal to the volume of water flowing out of the specimen. Each specimen was consolidated for more than 24 hours to ensure complete dissipation of pore air and water pressure throughout the specimen.

6.8.2.3 Monotonic loading in drained conditions

The monotonic loading of the silty sand specimens at a net confining pressure of 50 and 100 kPa and at matric suction of 25 kPa was performed in a similar manner as described in section 3.7.3. These tests were carried out to determine the variation of the Bishop's effective stress parameter, χ for the silty

sand specimen, which would enable the reasonably accurate computation of the effective stress of unsaturated soil during cyclic loading in undrained conditions.

6.8.2.4 Cyclic loading in undrained conditions

The cyclic loading in unsaturated soil is similar to the procedure explained for saturated soils, except for the measurement of air pressure during the entire duration of the test. Both the pore air and pore water pressure lines are closed and the pore air and pore water pressures were recorded independently. The cyclic loading was stopped when either the specimen reached an axial strain greater than 5% or the total number of cycles of deviator stress exceeded 500. The frequency of cyclic deviator stress was kept constant at 0.001 Hz, for proper capture of pore water pressure response.

6.9 Experimental Results

6.9.1 *Saturated Specimens*

The results for the series of cyclic triaxial tests performed on saturated (*B*-value > 0.95) and near-saturated (*B*-value = 0.50 and 0.70) soil specimens have been discussed in this section. Figure 6.10 shows the specimen before, during and after the application of cyclic load. The specimen after preparation and under the application of suction (10 kPa) is shown in Fig. 6.10(a). The specimen after isotropic consolidation is shown Fig. 6.10(b). The compression of the specimen under the application of peak compressive deviator stress is shown Fig. 6.10 (c) and (e). The extension of the specimen under the application of peak tensile deviator

stress is shown in Fig. 6.10 (d) and (f). The specimen after removing the pressures and the triaxial cells is shown in Fig. 6.10(g). The specimen after removing the latex membrane and subjected to light disturbance is shown in the Fig. 6.10(f). It was observed that the specimen undergoes higher axial strains with increasing cycles of deviator stress. Additionally, it was observed that the specimen (after the test; Fig. 6.10f) had negligible resistance to disturbance and started to flow.

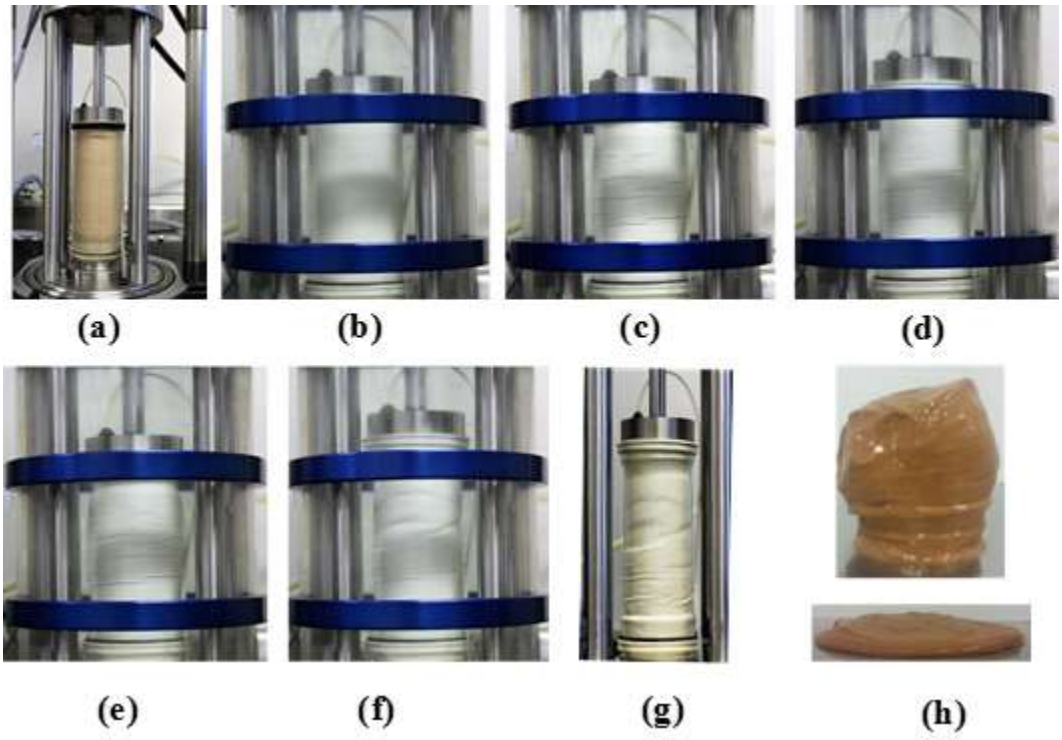

Figure 6.10 A typical cyclic triaxial test on saturated specimen under undrained conditions (Test# 18)

The response of the saturated specimen prepared at a relative density of 51% on being subjected to a sinusoidal cyclic deviator stress (peak amplitude of 20 kPa)

with a frequency of 0.1 Hz is shown in Figs. 6.11 – 6.16. It was observed that the excess pore water pressure or the pore water pressure ratio, r_u increases rapidly with the number of cycles. The magnitude of axial strain increases swiftly as the excess pore water pressure reaches 70% of the initial effective confining pressure (r_u = 0.7).

Figure 6.15 shows the deviator stress – axial strain relationship for the test conducted. It was observed that the stiffness of the soil specimen is almost constant during the initial loading cycles. However, as the effective stress (Fig. 6.16) decreases and reaches near zero and the stress path intersects the CSL (M = 1.15 in compression), the softening behavior of the soil specimen is observed. This behavior is known as "cyclic liquefaction" condition (Robertson and Wride, 1997). The "cyclic liquefaction" condition is characterized by the "transient excursion" of the effective stress path through the origin (Ghionna and Porcino, 2006). The axial strain reaches a value of 5% in tension after 18 cycles (Fig. 6.12). It was also observed that the effective stress reaches zero for the saturated soil specimen subjected to cyclic stress ratio (*CSR*) of 0.20.

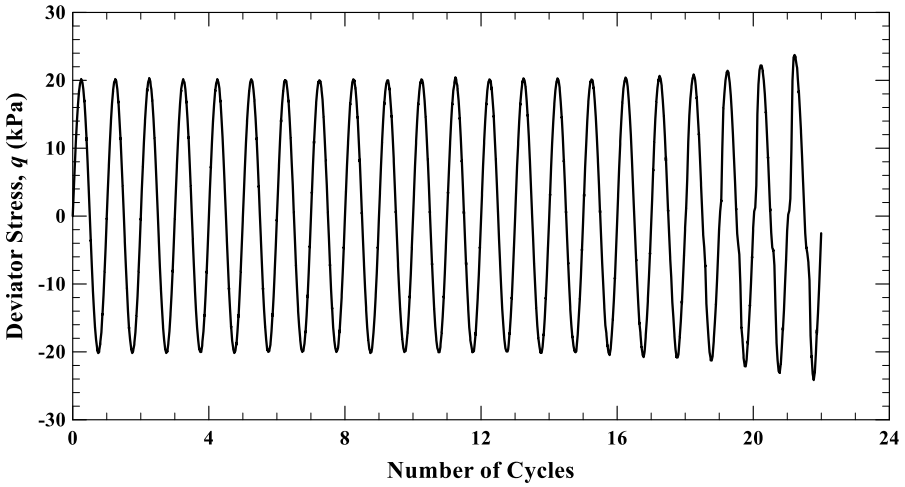

Figure 6.11 Sinusoidal deviator stress applied during the cyclic test on saturated specimen (Test# 2; CSR = 0.20; D_r = 51%)

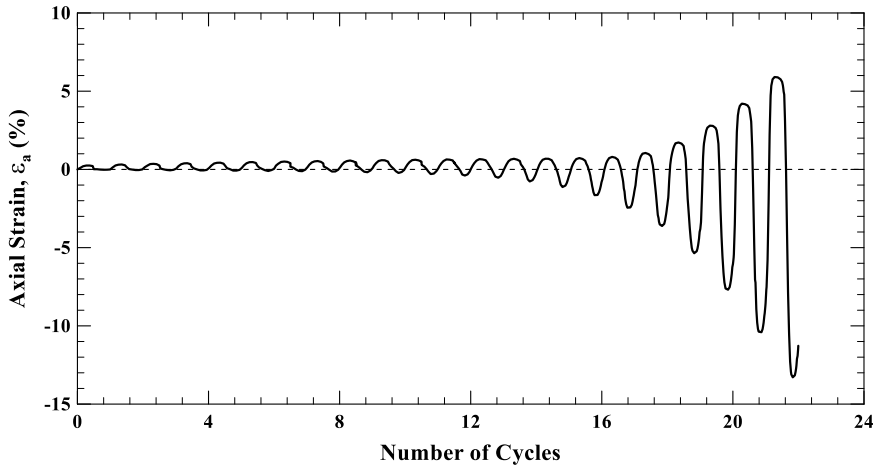

Figure 6.12 Variation of axial strain with applied cyclic deviator stresses on saturated specimen (Test# 2; CSR = 0.20; D_r = 51%)

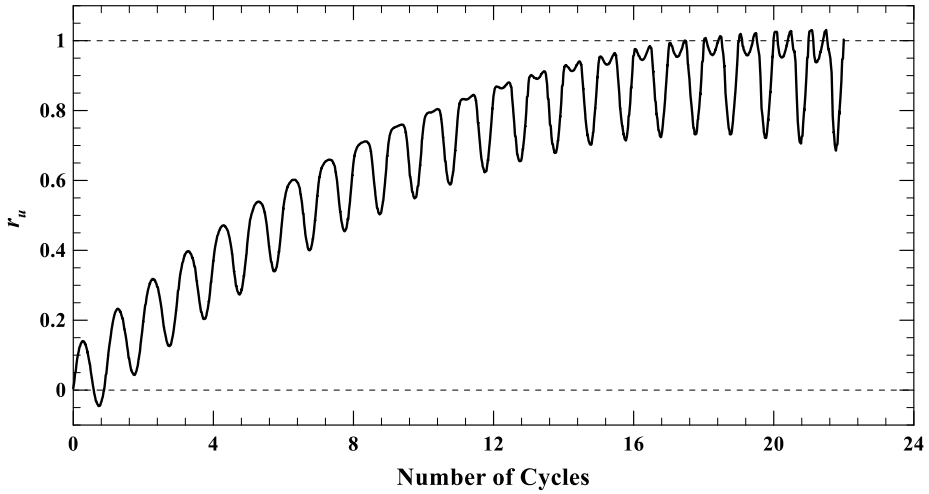

Figure 6.13 Variation of pore water pressure ratio with applied cyclic deviator stresses on saturated specimen (Test# 2; CSR = 0.20; D_r = 51%)

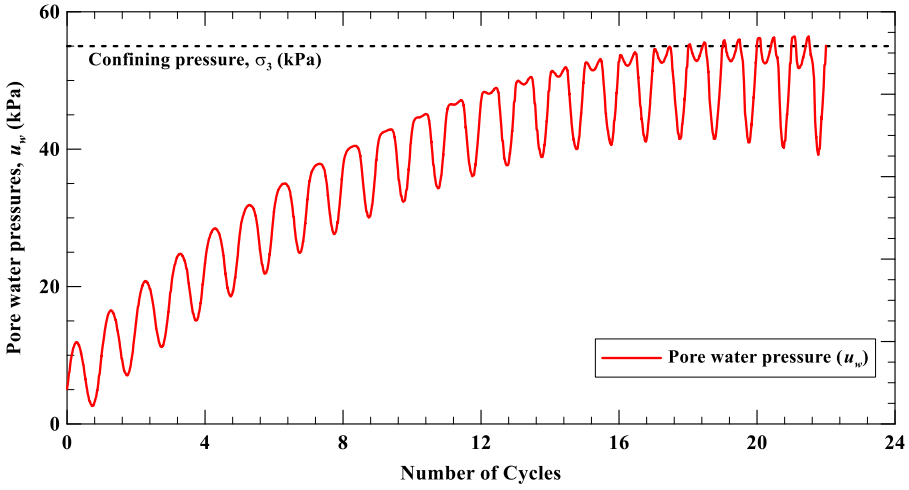

Figure 6.14 Pore water pressure response of saturated soil on being subjected to a cyclic deviator stress (Test# 2; CSR = 0.20; D_r = 51%)

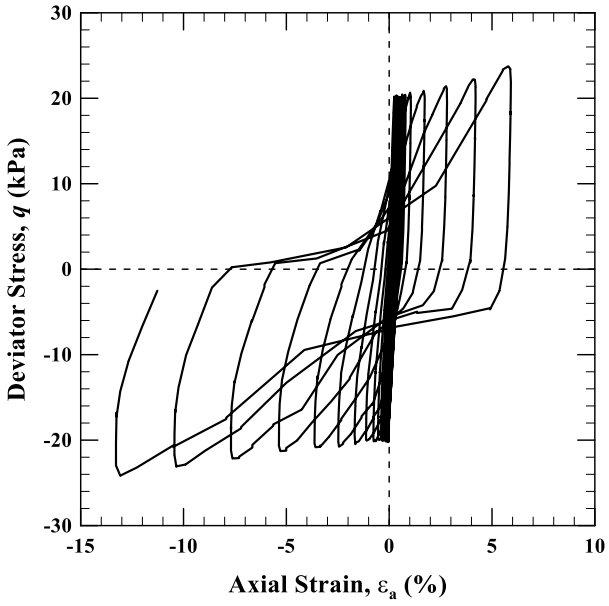

Figure 6.15 Stress-strain response of saturated soil when subjected to cyclic deviator stress (Test# 2; CSR = 0.20; D_r = 51%)

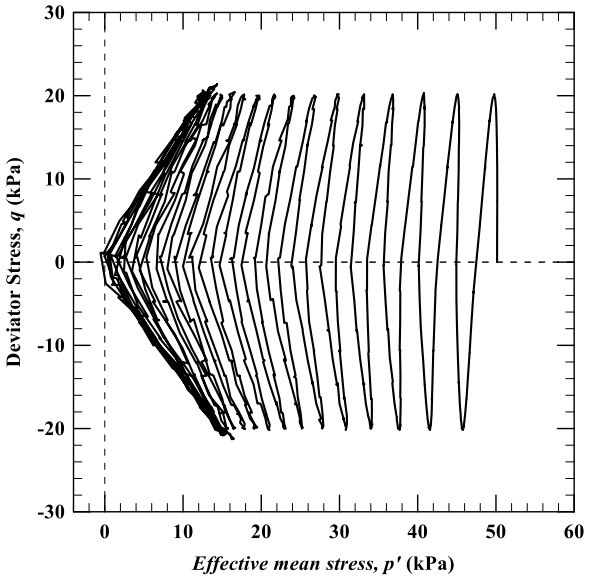

Figure 6.16 Effective stress path followed during cyclic triaxial test of saturated soil in undrained conditions (Test# 2; CSR = 0.20; D_r = 51%)

Similar tests on saturated specimens prepared at a relative density of 48% to 51 % were performed for CSR of 0.15, 0.25, and 0.35, where the axial strain reached 5% after 56, 7, and 3 cycles, respectively.

Additional tests were performed on saturated specimens prepared at a relative density of 76% and 74% for CSR of 0.15 and 0.20, where the specimen failed after 154 and 142 cycles, respectively.

The tests on specimens having *B*-value of 0.50 and 0.70 (not fully saturated, S_r = 98% and 96%) were also performed at CSR of 0.25 and it was observed that the specimens failed after 16 and 19 cycles respectively, which is much higher than that for saturated specimen having B-value of 0.97, which was also subjected to CSR of 0.25.

Similar results for cyclic liquefaction for loose cohesionless soils were observed by other researchers (Yoshimi et al., 1989; Kutter et al., 1994; Ghionna and Porcino, 2006; Unno et al., 2006; Okamura and Noguchi, 2009; Das and Sitharam, 2011; Liu and Xu, 2015; Wang et al., 2016; Markham et al., 2016), where the saturated soils failed by cyclic softening.

Figure 6.17 shows the variation of number of cycles required to liquefy a specimen for different cyclic stress ratio (CSR). It also compares the curve obtained from the present study to that obtained from other studies on similar type of soil. The present results are within those reported in the literature and any variations

noted are attributed to differences in soil types and testing parameters used in respective research studies.

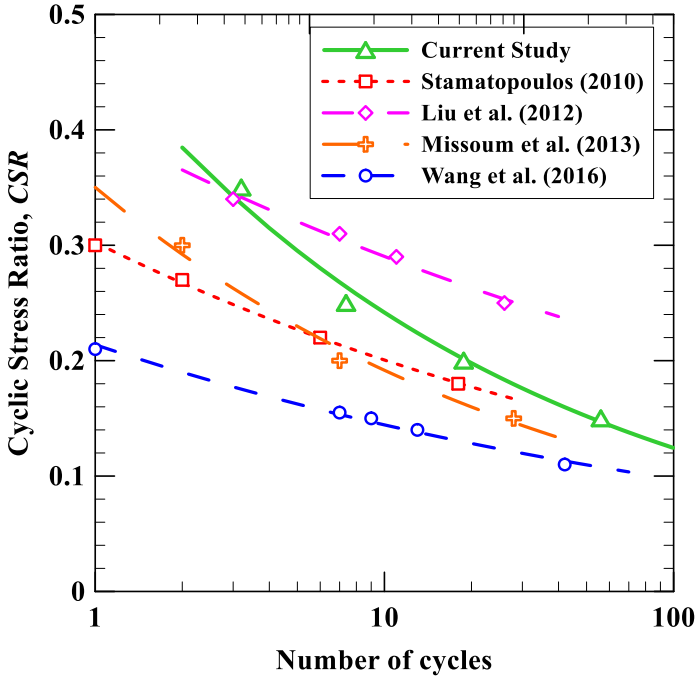

Figure 6.17 Comparison of experimental results for liquefaction obtained from various studies on saturated specimens of sands with fines

6.9.2 *Unsaturated Specimens*

6.9.2.1 General

The results of the cyclic triaxial tests on unsaturated specimens (s = 2 to 30 kPa) in undrained conditions have been discussed in this section.

6.9.2.2 Bishop's effective stress parameter

The effective stress of unsaturated soil during cyclic triaxial tests have been estimated by using the following relationship based on Bishop's approach (1959):

$$\sigma' = (\sigma - u_a) + \chi(u_a - u_w) \quad (6.6)$$

where,

σ is the total stress,

u_a is the pore air pressure,

u_w is the pore water pressure, and

χ is a soil parameter related to the degree of saturation of the soil and the wetting or drying cycle.

The previous studies have shown that contrary to the proposal by Bishop (1959), the relationship between χ and degree of saturation, *S* is not unique; and the soil type and stress path had a noteworthy effect on the relationship (Jennings and Burland, 1962; Bishop and Blight, 1963; Burland, 1964; Blight, 1967; Fang, 1977; Matyas and Radhakrishna, 1968; Aitchison and Woodburn 1969; Barden et al., 1969; Brackely, 1971; Escario and Juca, 1989). Hence, the results from monotonic triaxial tests of silty sand specimens (D_r = 50%) at saturated and unsaturated conditions (*s* = 25 kPa) for net confining pressures of 50 and 100 kPa were utilized to determine the value of χ at the suction of 25 kPa.

Furthermore, it was assumed that the value of χ varies linearly between saturated condition and suction of 30 kPa, as the degree of saturation is high in this range and the suction level is low. From the monotonic tests, it was determined that the effective cohesion was zero and the angle of internal friction of the silty sand was 28.4°, which is consistent with the shear strength parameters of loose

cohesionless soils. The slope of critical state line was obtained as 1.15. The apparent cohesion (c′′) at matric suction of 25 kPa was computed to be 12.4 kPa. Therefore, the value of χ was determined to be 0.915 at matric suction of 25 kPa, by using Eq. (6.7).

$$\chi = \frac{c''}{(u_a - u_w)\tan\varphi'} \tag{6.7}$$

Hence, the following values of χ were used for various suction levels (as shown in Table 6.4).

Table 6.4 Variation of χ with suction

Matric suction, *s* (kPa)	χ
0	1.0000
0.15	0.9995
2	0.9930
10	0.9660
20	0.9320
25	0.9145
30	0.8980

6.9.2.3 Response of unsaturated soils subjected to cyclic loading in undrained conditions

The response of unsaturated soil at matric suction of 2 kPa when subjected to cyclic deviator stresses (CSR = 0.25) is shown in Figs. 6.18 – 6.23. It was observed that the behavior of unsaturated soils is similar to that of the saturated soil. It is to be noted that the air-entry value of the specimen prepared at a relative

density of 50% is 2 kPa. Hence, it is expected that the response of the soil would not vary significantly.

The variation of pore air and pore water pressures in Fig. 6.21 shows that the initial matric suction decreases as the excess pore water pressure increases. This might be due to the dissolution of air into the solution due to increased stresses and also might be as a result of increase in the pore water pressure, which in turn decreases the volume of pore air. Hence at excess pore water pressure ratio of 0.9, the air pressure becomes almost equal to the pore water pressure and the matric suction drops to 0.4 kPa. Similar observations were made by researchers like Okumura and Noguchi (2009), where a significant decrease in matric suction levels was observed during the application of cyclic loading in undrained conditions.

From Fig. 6.19, it was observed that the axial strain reaches a value of 5% in tension after 28 cycles. Hence, the soil specimen at a matric suction of 2 kPa required 4 times higher number of cycles to induce an axial strain of 5% as compared to the saturated soil specimen for the same applied cyclic deviator stress (CSR = 0.25). It is also higher than the number of cycles required to fail specimens at B-value of 0.70 and 0.50 (Test # 5 and 6), where 16 and 19 cycles were required, respectively, to achieve an axial strain greater than 5% in magnitude for the same value of CSR.

The stress path (Fig. 6.23) shows that the effective stress almost reached a value of zero. Hence, the presence of pore air pressure prevented the effective stress

to reach and then drop below zero, as seen in saturated soil specimens. However, the specimen failed due to lower stiffness at very low effective stresses and the stress path intersected the critical state line, thereby inducing plastic strains, which also resulted in excessive deformations.

Similar tests were performed on soil specimens prepared at a relative density of 50% and at a matric suction of 2 kPa for CSR of 0.15 and 0.30. These specimens reached an axial strain of 5% after 144 cycles (for CSR = 0.15) and 12 cycles (for CSR = 0.30). A specimen at matric suction of 2 kPa was also prepared at a higher relative density of 75% and was tested by applying cyclic deviator stresses (CSR = 0.35), which reached the criteria of an axial strain of 5% after 19 cycles.

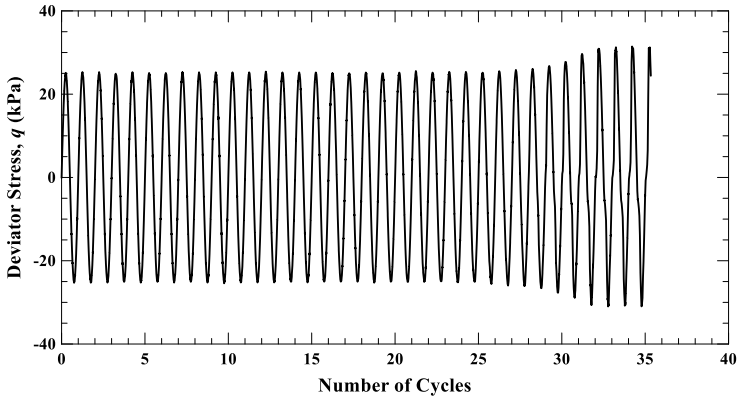

Figure 6.18 Sinusoidal deviator stress applied during the cyclic test on unsaturated specimen at matric suction of 2 kPa (Test# 8; CSR = 0.25; D_r = 53%)

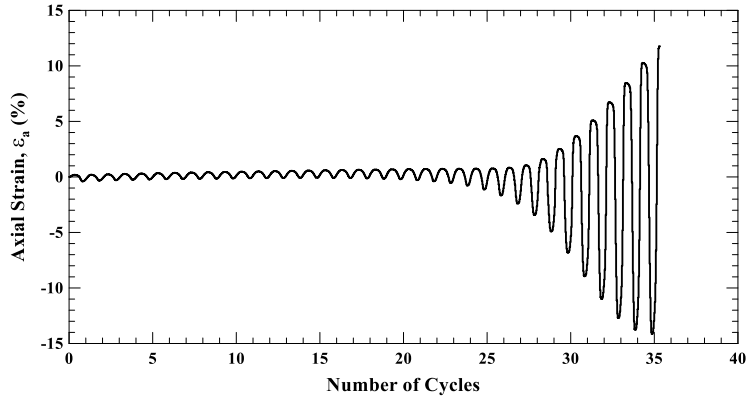

Figure 6.19 Variation of axial strain with applied cyclic deviator stresses on unsaturated specimen at matric suction of 2 kPa (Test# 8; CSR = 0.25; D_r = 53%)

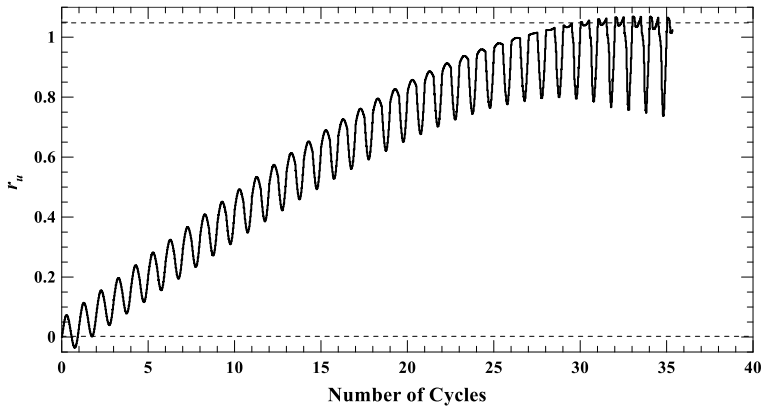

Figure 6.20 Variation of pore water pressure ratio with applied cyclic deviator stresses on unsaturated specimen at matric suction of 2 kPa (Test# 8; CSR = 0.25; D_r = 53%)

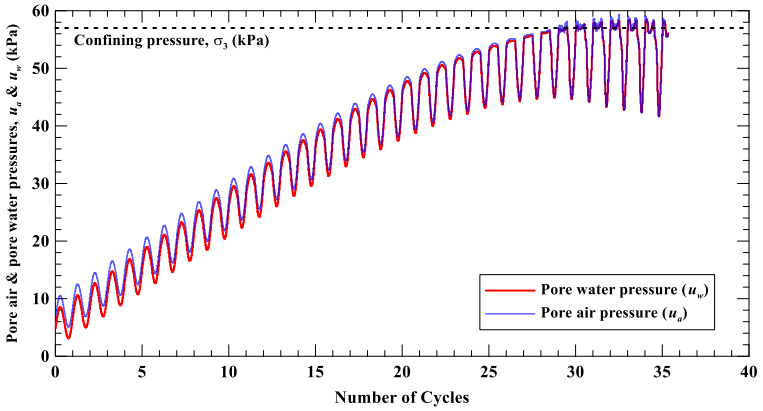

Figure 6.21 Pore water and pore air pressure response of unsaturated soil at a matric suction of 2 kPa on being subjected to a cyclic deviator stress (Test# 8; CSR = 0.25; D_r = 53%)

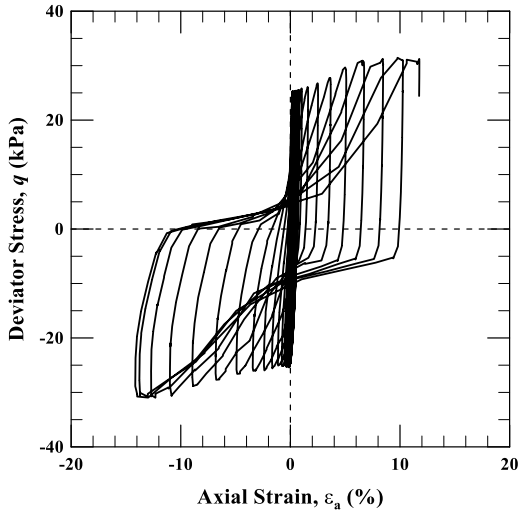

Figure 6.22 Stress-strain response of unsaturated soil at a matric suction of 2 kPa when subjected to cyclic deviator stress (Test# 8; CSR = 0.25; D_r = 53%)

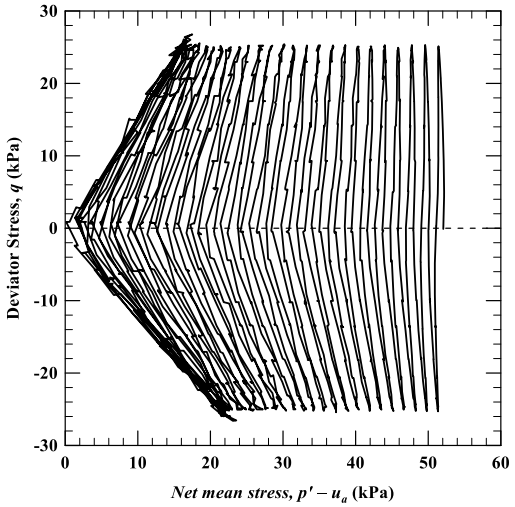

Figure 6.23 Effective stress path followed during cyclic triaxial test of unsaturated soil at a matric suction of 2 kPa in undrained conditions (Test# 8; CSR = 0.25; D_r = 53%)

The response of soil specimen prepared at a relative density of 54% and equilibrated to a matric suction of 10 kPa when subjected to a cyclic deviator stress of 35 kPa (amplitude; CSR = 0.35) is shown in Fig. 6.24 – 6.29. The specimen does not attain the condition of "cyclic softening" condition, as seen in specimens at lower values of matric suction. Instead, the specimen rarely undergoes compression, and fails in tension (Fig. 6.25). The net mean stress decreases gradually with increasing number of loading cycles to a value of 6 kPa prior to failure.

The matric suction was observed to decrease slightly (Fig. 6.27) as the higher excess pore water pressure is reached (r_u > 0.85). As the net mean stress decreases to less than 20% of its initial value, due to increase in the pore air and

pore water pressures, the effective stress path intersects the critical state line (M =1.15).

Although the net mean stress never reaches near zero, the liquefaction of the specimen occurs due to significant loss of stiffness and strength and it undergoes considerable deformations. This type of liquefaction is known as cyclic mobility (explained in section 6.2.2). In this case, the excess pore water pressure never becomes equal to the initial net confining pressure ($\sigma_3 - u_a$). Hence, it was observed that as the matric suction was increased the flow liquefaction ceases to occur due to the presence of pore air, but liquefaction due to cyclic mobility may still occur, depending upon the degree of saturation and the value of CSR. This specimen reached an axial strain of 5% in tension after 12 cycles of deviator stress.

Similarly, specimens prepared at a relative density of 50% and equilibrated to a matric suction of 10 kPa, were subjected to varying peak amplitude of cyclic deviator stresses having CSR of 0.15, 0.20, and 0.25. It was observed that the specimen subjected to cyclic deviator stress of 0.15, did not undergo significant deformation (maximum magnitude of axial strain was less than 0.5%), while the pore water pressure ratio increased gradually till 0.60 and then reached a constant value. Since the net mean stress ($p' - u_a$) did not decrease significantly and the peak amplitude of the cyclic deviator stress was low, the effective stress path did not reach the critical state line and hence the soil specimen did not fail.

An important aspect is required to be noted here, due to the presence of apparent cohesion and positive y-axis intercept of unsaturated soil in *p*-*q* space, the critical state line of unsaturated soil is well above the CSL of saturated soil. Hence, significantly higher amplitudes of deviator stresses are required to reach the CSL of unsaturated soils. Hence, unsaturated soils with higher induced matric suction are less susceptible to liquefaction.

The other specimens at matric suction of 10 kPa and relative density of 50%, which were subjected to cyclic deviator stress with CSR = 0.20 and 0.25 reached an axial strain of 5% after 124 and 48 cycles, respectively.

The specimens prepared at a relative density of 74% and matric suction of 10 kPa and subjected to cyclic deviator stresses with CSR of 0.25, did not liquefy after application of 500 cycles of deviator stress. However, a similar specimen when subjected to cyclic deviator stresses with CSR of 0.45 failed (reached axial strain of 5%) after 26 cycles.

When the cyclic deviator stress is defined by a CSR of 0.5 and above, the top cap starts to lose contact with the specimen during the application of the negative cycle (tensile stresses) of deviator stresses. This occurs due to the total axial stress reaching negative values when the magnitude of the negative values of deviator stress becomes greater than the confining pressure. Thereby, a CSR of 0.45 is very high, considering that the maximum limit of the value of CSR is 0.5.

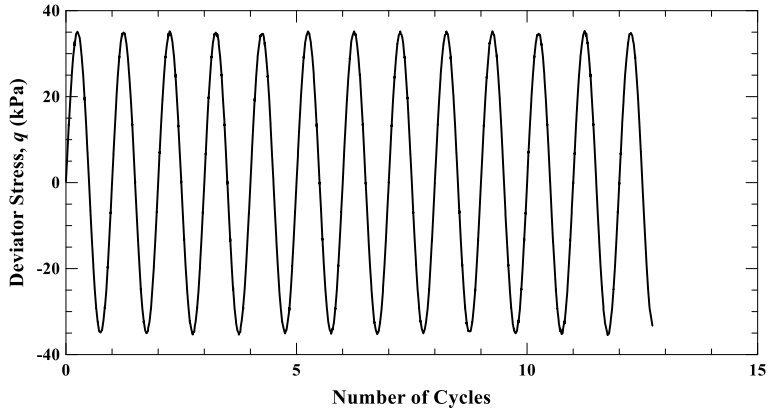

Figure 6.24 Sinusoidal deviator stress applied during the cyclic test on unsaturated specimen at matric suction of 10 kPa (Test# 13; CSR = 0.35; D_r = 54%)

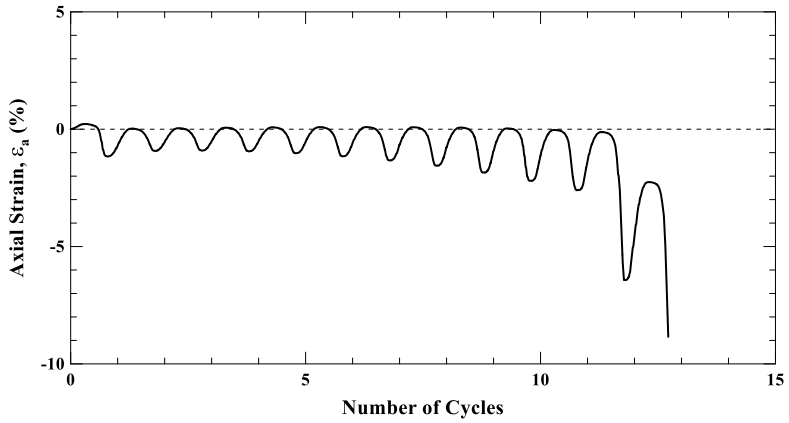

Figure 6.25 Variation of axial strain with applied cyclic deviator stresses on unsaturated specimen at matric suction of 10 kPa (Test# 13; CSR = 0.35; D_r = 54%)

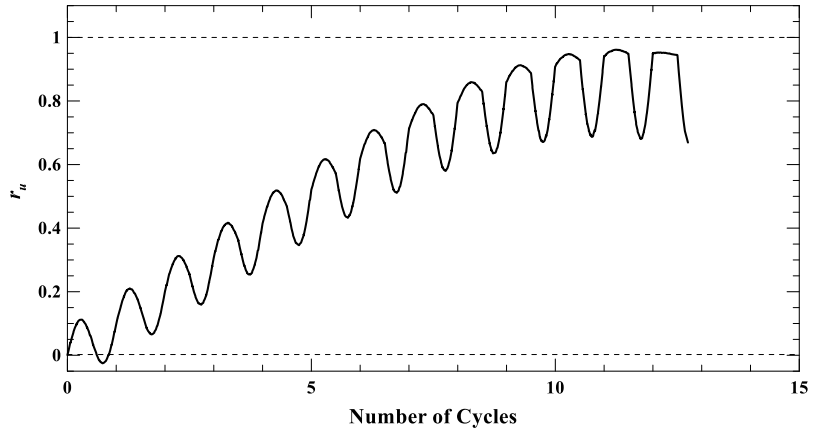

Figure 6.26 Variation of pore water pressure ratio with applied cyclic deviator stresses on unsaturated specimen at matric suction of 10 kPa (Test# 13; CSR = 0.35; D_r = 54%)

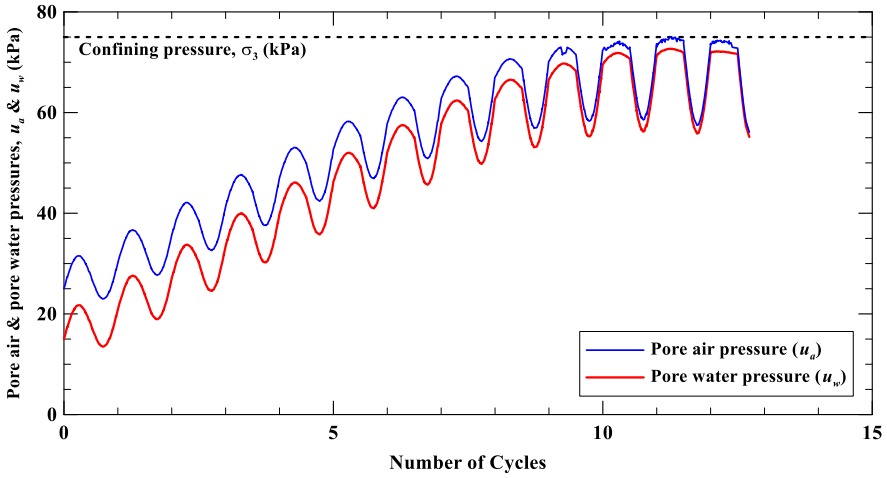

Figure 6.27 Pore water and pore air pressure response of unsaturated soil at a matric suction of 10 kPa on being subjected to a cyclic deviator stress (Test# 13; CSR = 0.35; D_r = 54%)

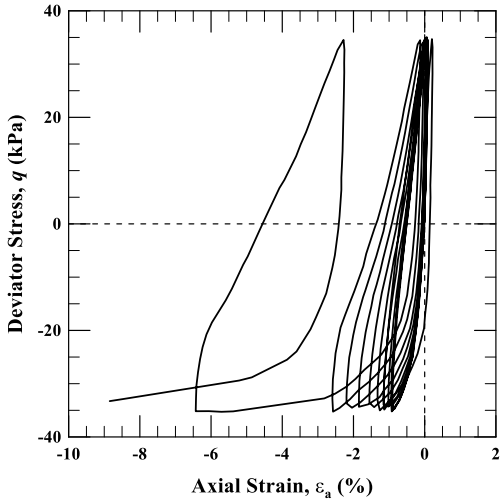

Figure 6.28 Stress-strain response of unsaturated soil at a matric suction of 10 kPa when subjected to cyclic deviator stress (Test# 13; CSR = 0.35; D_r = 54%)

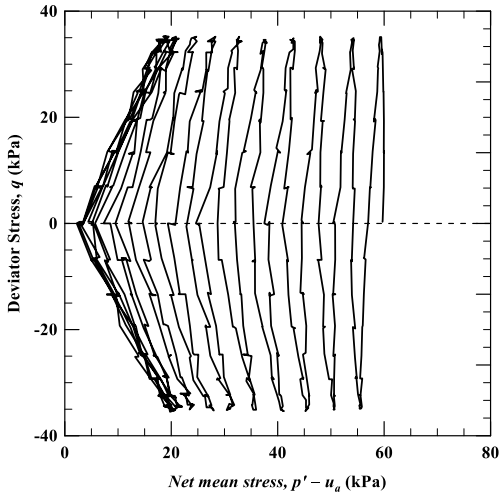

Figure 6.29 Effective stress path followed during cyclic triaxial test of unsaturated soil at a matric suction of 10 kPa in undrained conditions (Test# 13; CSR = 0.35; D_r = 54%)

The response of soil specimen prepared at a relative density of 53% and equilibrated to a matric suction of 20 kPa when subjected to a cyclic deviator stress of 35 kPa (amplitude; CSR = 0.45) is shown in Figs. 6.30 – 6.35. It was observed that the specimen undergoes gradual increase in excess pore water pressure or pore water pressure ratio (r_u) and reaches a constant peak value of r_u = 0.9. The matric suction reduced by less than 50% with increasing cycles of deviator stress. Figure 6.34 shows that the stiffness of the specimen decreased gradually, due to the application of high amplitude of deviator stress. Hence the specimen failed by cyclic mobility. The specimen reached an axial strain of 5% in tension, after 8 cycles.

Another specimen prepared at a relative density of 54% and equilibrated at matric suction of 30 kPa had been tested by applying a cyclic deviator stress having CSR of 0.35, but due to the presence of high amount of pore air and higher apparent cohesion, the specimen did not fail. Similarly, a denser specimen (D_r = 74%) at matric suction of 20 kPa did not fail when subjected to cyclic deviator stress of CSR = 0.35.

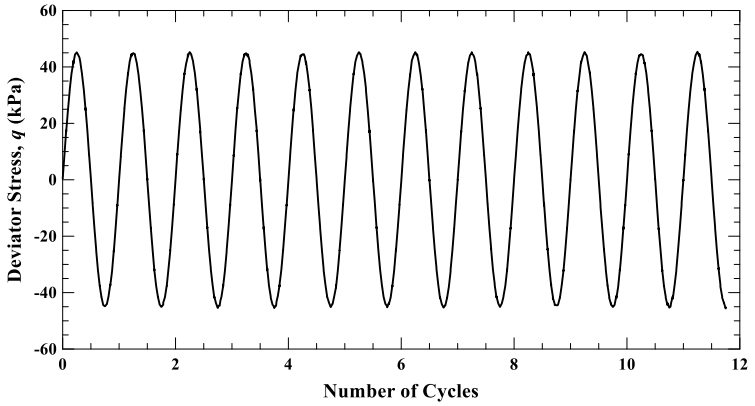

Figure 6.30 Sinusoidal deviator stress applied during the cyclic test on unsaturated specimen at matric suction of 20 kPa (Test# 16; CSR = 0.45; D_r = 53%)

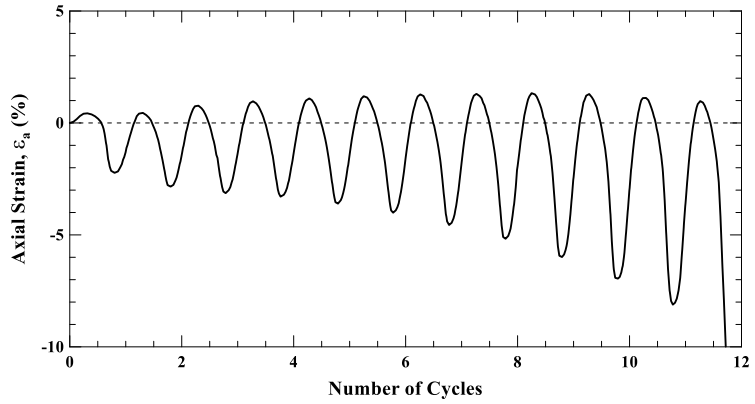

Figure 6.31 Variation of axial strain with applied cyclic deviator stresses on unsaturated specimen at matric suction of 20 kPa (Test# 16; CSR = 0.45; D_r = 53%)

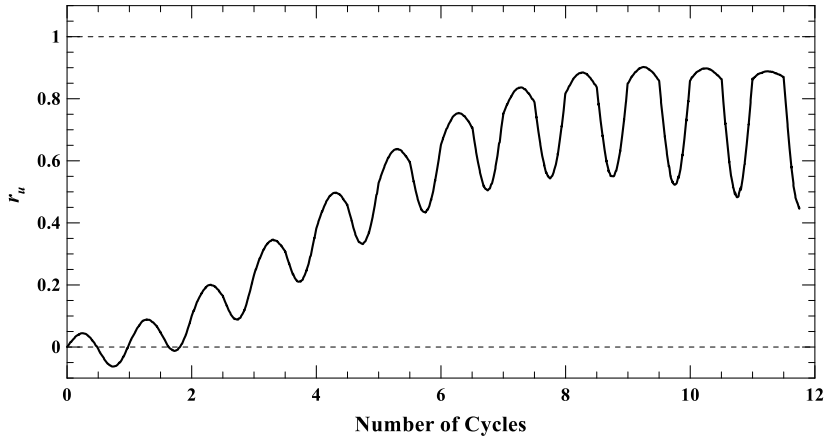

Figure 6.32 Variation of pore water pressure ratio with applied cyclic deviator stresses on unsaturated specimen at matric suction of 20 kPa (Test# 16; CSR = 0.45; D_r = 53%)

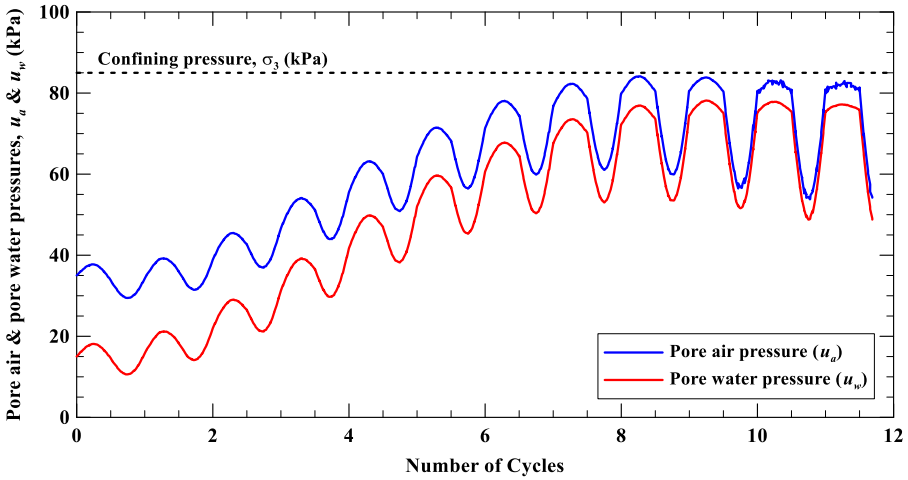

Figure 6.33 Pore water and pore air pressure response of unsaturated soil at a matric suction of 20 kPa on being subjected to a cyclic deviator stress (Test# 16; CSR = 0.45; D_r = 53%)

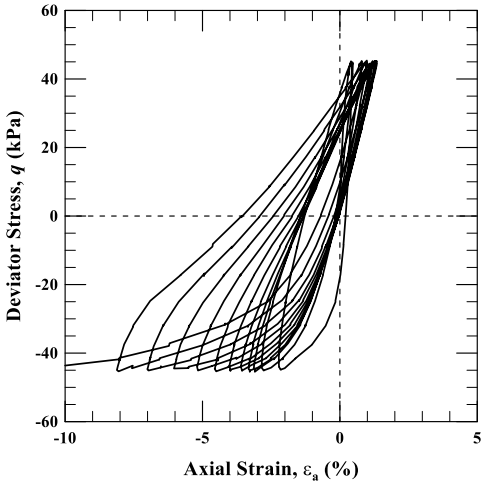

Figure 6.34 Stress-strain response of unsaturated soil at a matric suction of 20 kPa when subjected to cyclic deviator stress (Test# 16; CSR = 0.45; D_r = 53%)

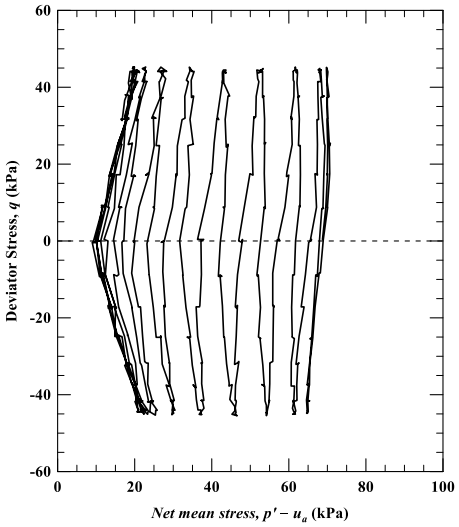

Figure 6.35 Effective stress path followed during cyclic triaxial test of unsaturated soil at a matric suction of 20 kPa in undrained conditions (Test# 16; CSR = 0.45; D_r = 53%)

6.9.3 *Liquefaction Resistance Ratio*

Okamura and Noguchi (2009) had recommended the use of the term ‘Liquefaction Resistance Ratio’, abbreviated as LRR (defined in section 6.2.4), to demonstrate the effect of desaturation on the susceptibility of liquefaction of unsaturated soils. In this study, the cyclic stress ratio (CSR) required to cause an axial strain of 5% in 20 cycles is termed as liquefaction resistance. The Liquefaction Resistance Ratio (LRR) is the ratio of liquefaction resistance of unsaturated soil to that of saturated soil.

The relationship between the CSR and the number of cycles for tests on saturated and unsaturated specimens at a relative density of approximately 50% is shown in Fig. 6.36. It is evident that as the soil suction increases, higher cyclic deviator stresses and/or greater number of cycles of deviator stresses are required to fail the specimen (axial strain of 5%). Since the specimen at matric suction of 30 kPa did not fail when subjected to cyclic deviator stress having CSR of 0.35, it is tacitly safe to assume that specimens of silty sand at a moderate relative density of 50% are not susceptible to liquefy beyond a suction of 30 kPa. Additionally, significant seismic stresses would be required to liquefy similar type of soils at matric suction beyond 20 kPa.

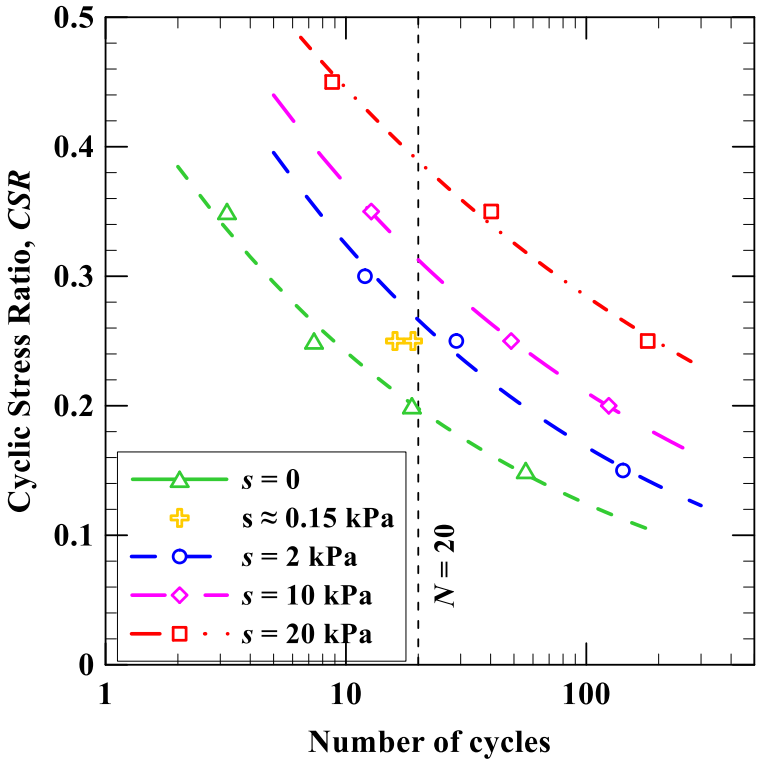

Figure 6.36 Effect of soil suction on the liquefaction resistance of unsaturated silty sand specimen.

The variation of LRR with the soil suction, the degree of saturation, and the *B*-value (Skempton's pore water pressure parameter) is shown in Fig. 3.37, 3.38, and 3.39, respectively. It was observed that the LRR increases rapidly with a small increase in soil suction or a small decrease in the degree of saturation. As the degree of saturation decreases beyond 75%, the value of LRR increases rapidly with desaturation. Zhang et al. (2016) had performed similar tests on cohesionless soils from a degree of saturation of 75% to 100% and the variation of liquefaction

resistance with the degree of saturation were observed to be similar to that in the present study.

From Fig. 3.39, it was observed that the LRR initially increases linearly with an increase in *B*-value, but as the *B*-value reaches below 0.06, the LRR increases exponentially. When the triaxial test results presented by Ishihara et al. (2001) were utilized to plot a curve between LRR and *B*-value, a similar trend was observed.

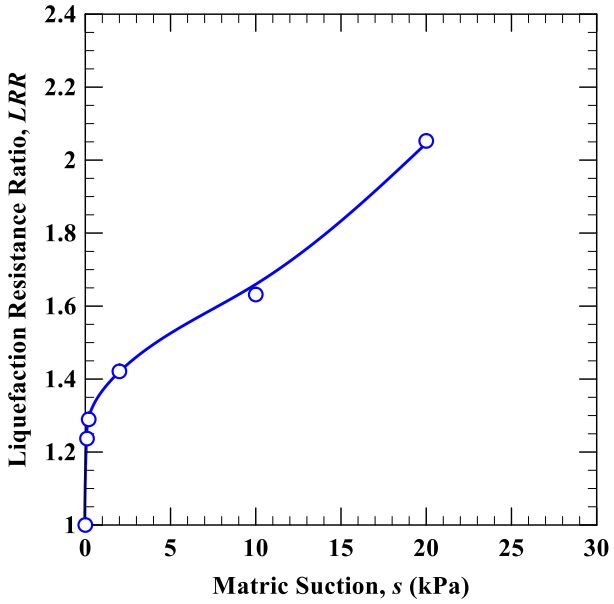

Figure 6.37 Effect of soil suction on the Liquefaction Resistance Ratio (LRR) of silty sand

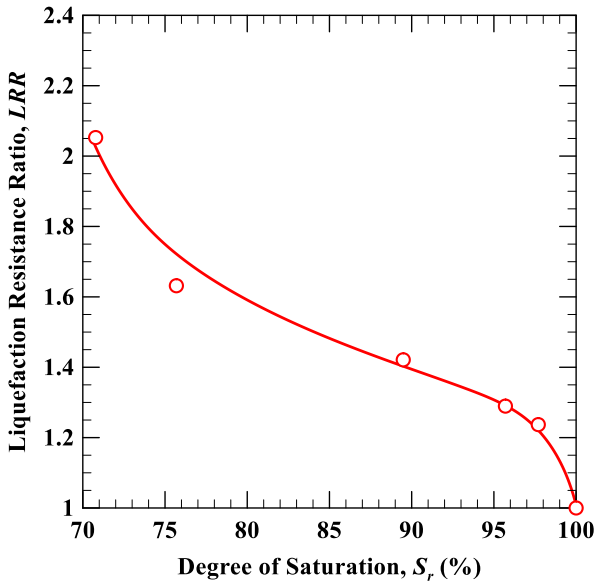

Figure 6.38 Effect of degree of saturation on the Liquefaction Resistance Ratio (LRR) of silty sand

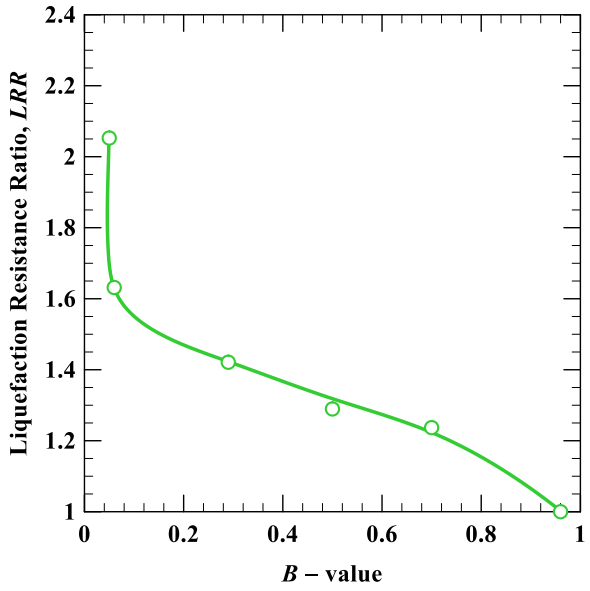

Figure 6.39 Effect of B-value on the Liquefaction Resistance Ratio (LRR) of silty sand

6.10 Summary

The concept of liquefaction in saturated and unsaturated soils is presented in this chapter. The types of liquefaction and the necessity to study the liquefaction of unsaturated soils are described.

The basic laboratory test results including, soil classification, determination of the maximum dry density and the optimum moisture content, selection of compaction technique to obtain consistent replicates and soil water characteristics curve are discussed. The experimental program for this study is listed and the modifications to the experimental setup required to perform cyclic triaxial tests on saturated and unsaturated specimens in undrained conditions are presented. The experimental procedure followed to perform these tests is described.

An elaborate series of cyclic triaxial tests were performed at varying cyclic stress ratio (*CSR* = 0.15 to 0.45) and induced matric suction (s = 0 to 30 kPa) at constant net confining pressure ($\sigma_3 - u_a$ = 50 kPa). The results of these tests are discussed in detail and the essential findings are presented. One of the major findings was the cyclic liquefaction of specimens at an initial degree of saturation of 75%. Though higher stresses were required to fail the specimen, however, it was interesting to note that the specimen liquefied even when the net mean stress ($p' - u_a$) was significantly greater than zero.

Additional analysis of the experimental data provided the relationship between cyclic stress ratio (*CSR*) and the number of cycles required to fail the

specimen (axial strain = 5%) for varying matric suction values (s = 0 to 20 kPa). Moreover, the variation of Liquefaction Resistance Ratio (LRR) with an increase in the matric suction, and a decrease in the degree of saturation and the B-value is presented.

Chapter 7

CONCLUSIONS AND RECOMMENDATIONS

7.1 Introduction

The main objective of this dissertation research was to characterize the mechanical response of unsaturated soils subjected to monotonic and dynamic loads under varying levels of soil suction, using a modified triaxial setup.

The study focused on the response of silty soils to monotonic suction-controlled triaxial testing at varying matric suction levels. A series of 6 triaxial tests on saturated specimens and 12 suction-controlled triaxial tests on unsaturated specimens at varying matric suctions in the range of 50 to 750 kPa, were performed.

These tests facilitated the determination of appropriate shearing rate for specimens under drained condition. The test results provided insight into the suction induced increase in yield stress and apparent tensile strength of unsaturated soils. A parametric evaluation of angle of friction due to matric suction (φ^b), shear strength at critical and peak states, and peak dilation angle with soil suction, could be accomplished. The parameters for the Barcelona Basic Model (BBM) were also calibrated using the test results. Subsequently, BBM prediction models were developed.

A substantial portion of this work deals with the determination of resilient modulus of soils using suction-controlled repeated load triaxial tests (RLTTs). An attempt was made to devise a relationship between the resilient modulus and soil

suction. Twenty-six suction-controlled RLTTs were conducted on silty soil specimens of varying dry unit weights over a wide range of induced suction. The influence of wetting and drying of the soil specimens on the resilient moduli was studied. A resilient modulus – suction relationship was established by calibrating and validating the model by Han and Vanapalli (2015) using the present experimental data from the RLTTs.

The effect of suction on the dynamic or cyclic response of loose silty sand specimens under undrained conditions has been probed in detail. The study addresses the susceptibility of silty sand specimens to liquefy under unsaturated conditions. Twenty-three cyclic triaxial tests were performed on consolidated undrained specimens of silty sand (SM) at different relative densities (D_r = 50% and 75%) under a low net confining pressure of 50 kPa and at multiple suction levels (s = 0 to 30 kPa) by applying varying cyclic deviator stresses (CSR = 0.15 to 0.45). The relationship between the cyclic stress ratio (CSR) and the number of loading cycles required to reach 5% axial strain (which is assumed to indicate failure of the specimen) was developed for varying values of matric suction. The experimental data was utilized to examine the variation of Liquefaction Resistance Ratio (LRR) with matric suction, degree of saturation and *B*-value of the specimen.

The secondary objective of the dissertation was to develop a test protocol to determine the strength of unsaturated soils using lesser number of soil specimens and to significantly reduce the time for testing without affecting the reliability of

test results. As part of this testing procedure, a two-fold criterion for termination of shearing during initial stages, has been outlined for the multistage triaxial tests. The secondary objective was aimed at addressing the issue of soil variability in replicates, and decreasing the testing cost and time required for performing suction-controlled triaxial tests on unsaturated specimens. Each suction-controlled multistage triaxial test was performed at constant matric suction and varying net confining pressures. The response of the soil specimens and the shear strength parameters obtained from the multistage triaxial tests were compared to those obtained from conventional single-stage triaxial tests to validate the procedure adopted for multistage triaxial tests.

The major conclusions from the dissertation have been described in the next section.

7.2 Major Conclusions

Several conclusions could be drawn from the dissertation research. They are:

1. The stress-strain response of saturated and unsaturated silty soil when subjected to drained shearing showed post-peak softening with volumetric dilative behavior at all matric suction levels (s = 0 to 750 kPa).
2. The variation of friction angle with matric suction (φ^b) was found to be highly non-linear. The slope of the critical state line (M) was observed to be practically constant for all the suction levels.

3. An increase in the rate of shearing under drained conditions resulted in a significant increase in the peak deviator stress of saturated and unsaturated soil. The deviator stress at critical state increased slightly with a similar increase in the axial strain rate. Henceforth, for comparative analysis, it is essential to perform all the triaxial tests on a single soil type at the same axial strain rate.
4. The *y*-intercept of the CSL (critical state line) and the PSL (peak state line) in $p' - q$ space is dependent on the induced soil suction. However, any increment in *y*-intercept of the CSL in $p' - q$ space with soil suction is limited by the suction cutoff value (s_{cutoff}), beyond which it practically remained constant. The suction cutoff value is much lower for CSL as compared to PSL. Therefore, the increase in shear strength of soil with suction virtually ceases after reaching a much lower value of suction for the critical state ($s_{cutoff} \approx 500$ kPa) as compared to that at the peak state. This could be attributed to an enhanced brittleness and post-peak softening behavior in the soil specimens at increased suction state.
5. The stiffness of the soil increased with soil suction till a cut-off value of suction, beyond which only a small increase in stiffness was observed. The rate of increase of stiffness with an increase in suction, at critical state or at high value of strain, were observed to decrease significantly after reaching a soil suction of approximately 500 kPa. However, no apparent suction-cutoff value was observed until a suction of 750 kPa for initial stiffness and secant stiffness at the peak state.

6. The post-peak softening was observed to increase exponentially with an increase in suction, which is also due to the increase in the brittleness of the soil with an increase in soil suction. However, the post-peak softening was observed to decrease with an increase in net confining pressure, which is due to the decrease in the value of over-consolidation ratio (OCR) of the soil with an increase in net confining pressure. Similar trend was observed for the variation of the peak dilation angle with increasing net confining pressure and soil suction.
7. The multistage triaxial tests were capable of producing almost identical responses of saturated and unsaturated soils when subjected to monotonic loading at varying suction levels of 0, 50, and 250 kPa. The two-fold criterion for termination of shearing included firstly, the ratio of the initial tangent modulus to the tangent modulus at the point of termination (E_i/E_r) of 25 and 15 for the first two shearing stages; and secondly, the volumetric strain of greater than zero. This criterion served as an appropriate condition to terminate the shearing for the initial stages of the test.
8. The shear strength parameters obtained from multistage triaxial tests were similar to those obtained from single-stage triaxial tests. It was also observed that the multistage triaxial tests required less than half of the time needed by single-stage tests to determine the shear strength parameters of the soil for all the suction levels (s = 0, 50, and 250 kPa).

9. It is recommended that for multistage triaxial tests, the subsequent initial net mean confining pressures are in multiples of 2 or greater for low suction range (s<250 kPa) and 4 or greater for high suction range (s>750 kPa). This would result in a small portion of overlapped yield surfaces from consecutive stages which would result in identical determination of shear strengths at the corresponding critical states for single-stage and multistage triaxial tests.
10. The use of a non-linear function of k (parameter for demonstrating the increase of cohesion intercept with suction) is ideally suited for making accurate predictions instead of a constant value as proposed by the Barcelona Basic Model (BBM) framework by Alonso (1990).
11. The variation in the results from single-stage and multistage triaxial tests had negligible influence on the validation for predictions based on BBM framework. Therefore, the multistage triaxial tests are also suitable for validation of constitutive models.
12. The experimental setup enabled the determination of resilient modulus (M_R) over a wide range of suction (s = 0 to 100 MPa) using a combination of axis-translation technique and vapor pressure technique to perform suction-controlled RLTTs. These tests aided in improving the repeatability in determination of resilient modulus.
13. The resilient modulus was observed to increase with the net confining pressure, and this effect is pronounced at lower suction levels. However, the resilient

modulus of the silty soil decreased with increase in deviator stress, which is typical of fine-grained soils. The resilient modulus was also observed to increase (up to 20% to 30%) with an increase in the dry density of soil (from 95% to 98% of MDD at OMC). The effect of dry density of soil on the resilient modulus of soil specimen is more pronounced at low values of net confining pressure and matric suction.

14. The effect of hysteresis in the resilient modulus and suction ($M_R - s$) relationship was observed, during the wetting-drying process. The wetted specimen demonstrated slightly lesser resilient moduli (decrease by 10% to 20%) as compared to the specimen which was directly compacted and equilibrated to the same matric suction. However, the specimens tested after bringing them to the desired matric suction value by imposing the drying cycle showed negligible change in the resilient moduli as compared to a specimen directly compacted and equilibrated to the same matric suction condition.
15. The values of resilient moduli remained virtually constant till the air entry value of the soil and increased linearly with an increase in suction until s = 100 kPa (in this study). At higher suction levels (s > 100 kPa), the rate of increase of resilient moduli with suction gradually decreased. At the high suction states (s >1 MPa), there was insignificant increase of resilient modulus with an increase in suction.

16. The prediction of resilient modulus at any suction level was done using the model by Han and Vanapalli (2015). It is based on the resilient moduli at the saturated condition and at optimum moisture content, and it provided reasonably good estimation until moderate suction levels (s = 300 kPa). However, at higher suction states, the model overestimated the value of resilient modulus due to lack of a bounding function which limits the increase of resilient modulus with suction beyond the residual suction level.
17. The experimental setup with the required modifications was able to perform cyclic triaxial tests on saturated and unsaturated silty sand specimens under undrained conditions at varying amplitudes of cyclic deviator stress having CSR values of 0.15 to 0.45.
18. The introduction of low value of matric suction required higher cyclic deviator stresses to be applied in the form of higher CSR values and/or higher number of loading cycles to liquefy the soil specimens. The increase in number of loading cycles resulted in a volumetric transformation of soil response from compressive to dilative. All the soil specimens that failed could be attributed to cyclic mobility condition which is typical of liquefaction in moderately dense cohesionless soils.
19. The non-linear relationship between the CSR and the number of loading cycles for tests on saturated and unsaturated soil specimens at varying matric suction

values (s = 0 to 20 kPa) demonstrated the influence of matric suction and CSR on the number of cycles required to fail the specimen.

20. The variation of Liquefaction Resistance Ratio (LRR) with soil suction, degree of saturation and *B*-values showed that desaturation or increase in soil suction results in higher resistance to liquefaction. As the degree of saturation reduces to 97%, the LRR value was increased by almost 25% which indicates that slight desaturation may significantly reduce the susceptibility of soils to liquefy.

7.3 Future Scope for Research

1. The effect of hysteresis of the soil water characteristic curve (SWCC) on the shear strength of unsaturated soils may be studied in future to understand the influence of climatic conditions on the behavior of the soil.
2. In the current research, the average volume change of the entire specimen was recorded using the volume of water surrounding the soil specimen. However, it would be interesting to study the effect of suction on volume change during monotonic shearing at various locations on the soil specimen, which could be achieved by photogrammetric or imaging techniques.
3. A modified top cap and base pedestal having both HAE ceramic disk and porous stone at each end of the specimen may be utilized to decrease the suction equalization time during testing of unsaturated soils. However, caution must be exercised to avoid air getting trapped at the middle of the specimen during the wetting process.

4. The experimental data from the current research could be utilized to develop, calibrate and validate an advanced constitutive model which is capable of predicting the suction-induced post-peak softening and dilatancy of soils.
5. The loading collapse curve used in the constitutive modeling of unsaturated soils may be validated experimentally by performing tests simulating the wetting-induced collapse of soil at varying initial net mean stresses and suction levels.
6. The influence of compaction energy and compaction technique on the yield stress or preconsolidation pressure of compacted unsaturated specimens could be probed further.
7. The variation of plastic deformation of soils compacted at different dry densities over a wider range of suction needs to be investigated by using the suction-controlled RLTTs.
8. An independent study with an aim to assess the liquefaction of very loose specimens of cohesionless soils is recommended, to capture the transition of flow liquefaction to cyclic liquefaction with increasing matric suction.

APPENDIX – A

Variation of Soil Stiffness with Matric Suction

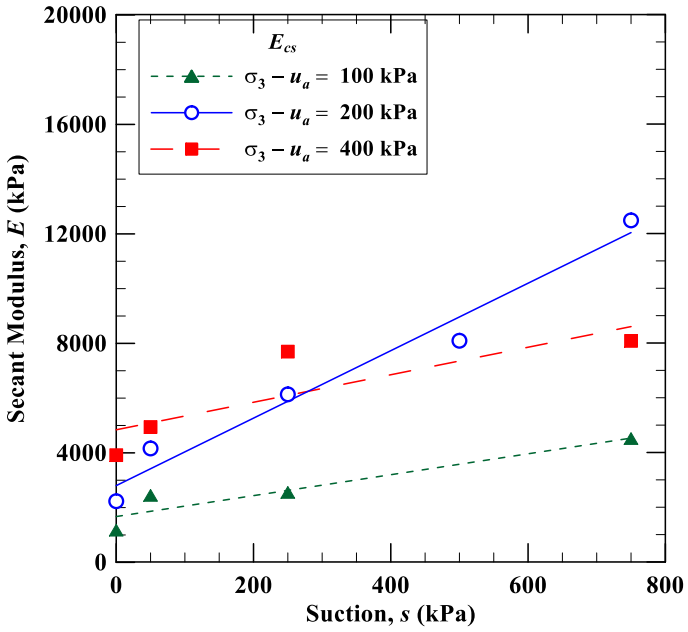

Figure A.1 Variation of E_{cs} with suction for varying net confining pressure

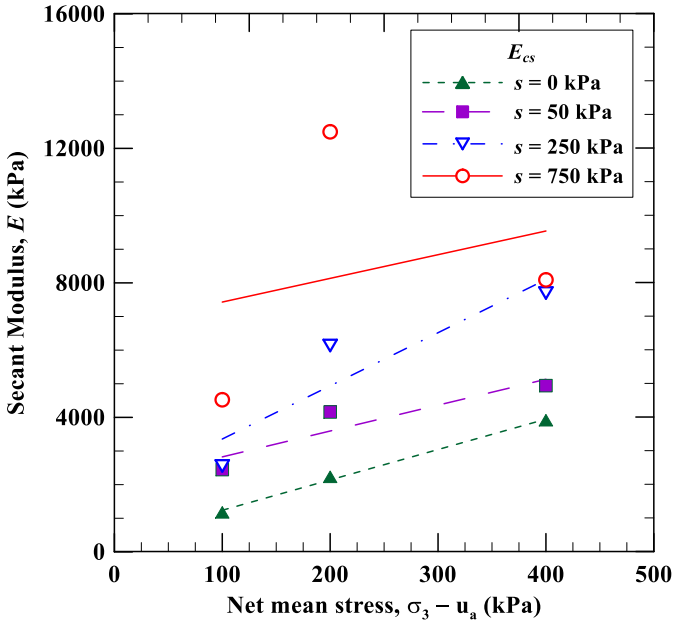

Figure A.2 Variation of E_{cs} with net confining pressure for varying suction levels

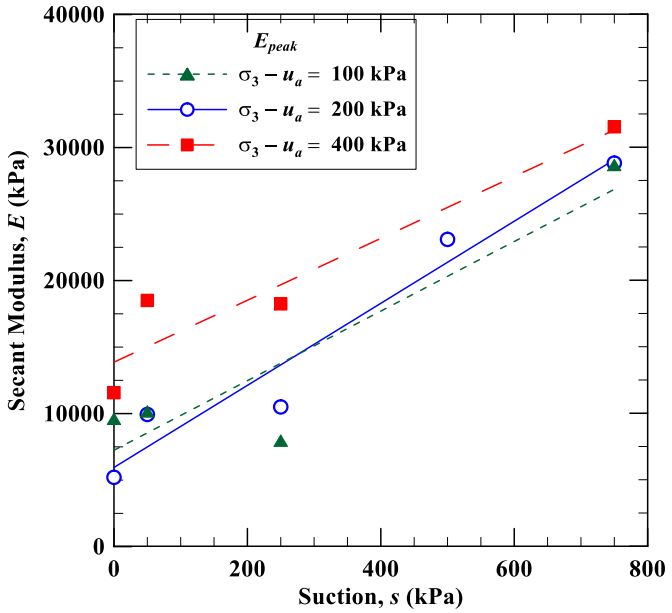

Figure A.3 Variation of E_{peak} with suction for varying net confining pressure

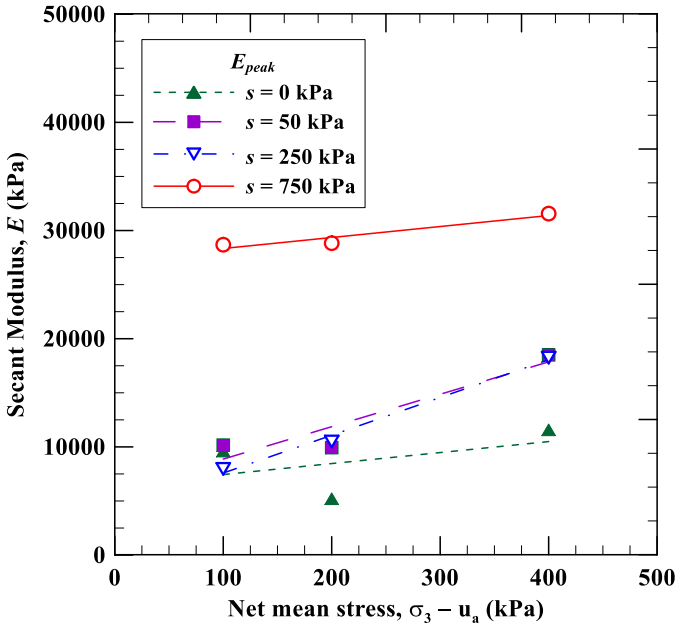

Figure A.4 Variation of E_{peak} with net confining pressure for varying suction levels

REFERENCES

AASHTO T 307-99 (2003). Determining the Resilient Modulus of Soils and Aggregate Materials, *American Association of State Highway and Transportation Officials*, Washington, D.C.

Abu-Farsakh, M. Y., Mehrotra, A., Mohammad, L., and Gaspard, K. (2015). Incorporating the effect of moisture variation on resilient modulus for unsaturated fine-grained subgrade soils. *Proc., Transportation Research Board 94th Annual Meeting (No. 15-1149)*, Washington, DC.

Ahangar-Asr, A., Johari, A., and Javadi, A. A. (2012). An evolutionary approach to modelling the soil–water characteristic curve in unsaturated soils. *Computers and Geosciences*, Elsevier, 43, 25–33.

Allaby, M. (2004). *A Dictionary of Earth Sciences*. Oxford University Press, Oxford, U.K.

Allen, J. (1973). *The effect of non-constant lateral pressures of the resilient response of granular materials*. Doctoral Dissertation, University of Illinois at Urbana-Champaign, Urbana, IL.

Allen, J. J., and Thompson, M. R. (1974). Resilient response of granular materials subjected to time dependent lateral stresses. *Transp. Res. Rec. 510*, Transportation Research Board, Washington, D.C., 1–13.

Alonso, E. E., Gens, A., and Josa, A. (1990). A constitutive model for partially saturated soils. *Geotechnique*, 40(3), 405–430.

Andersen, K., Kleven, A., and Heien, D. (1988). Cyclic soil data for design of gravity structures, *Journal of Geotechnical Engineering*, 1145, 517–539.

Andersen, K.H., Pool, J.H., Brown, S.F., Rosenbrand, W.F. (1980). Cyclic and static laboratory tests on Drammen clay. *Journal of Geotechnical Engineering Division*, 106 (5), 499–529.

Arenson, L. U., and Springman, S. M. (2005). Triaxial constant stress and constant strain rate tests on ice-rich permafrost samples. *Canadian Geotechnical Journal*, 42(2), 412–430.

ASTM D2325-03. (2000). Standard Test Method for Capillary-Moisture Relationships for Coarse and Medium Textured Soils by Porous-Plate Apparatus. ASTM International, West Conshohocken, PA.

ASTM D2487-00. (2003). Standard classification of soils for engineering purposes (unified soil classification system) . ASTM International, West Conshohocken, PA.

ASTM D2488-03. (2001). Standard Practice for Description and Identification of Soils (Visual-Manual Procedure). ASTM International, West Conshohocken, PA.

ASTM D2850-15. (2015). Standard Test Method for Unconsolidated-Undrained Triaxial Compression Test on Cohesive Soils. ASTM International, West Conshohocken, PA.

ASTM D422-07 (2007): Standard Test Method for Particle-Size Analysis of Soils. ASTM International, West Conshohocken, PA.

ASTM D4318-05. (2003). Standard test method for liquid limit, plastic limit, and plasticity index of soils. ASTM International, West Conshohocken, PA.

ASTM D4767-11. (2011). Standard Test Method for Consolidated Undrained Triaxial Compression Test for Cohesive Soils. ASTM International, West Conshohocken, PA.

ASTM D5298-03. (2003). Standard Test Method for Measurement of Soil Potential (Suction) Using Filter Paper. ASTM International, West Conshohocken, PA.

ASTM D5311/D5311M-13. 2013. Standard Test Method for Load Controlled Cyclic Triaxial Strength of Soil. ASTM International, West Conshohocken, PA.

ASTM D6836-02. (2003). Standard test method for liquid limit, plastic limit, and plasticity index of soils. ASTM International, West Conshohocken, PA.

ASTM D698-00 (2003). Standard test methods for laboratory compaction characteristics of soil using standard effort (12,400 ft-lbf/ft^3 (600 kN/m^3)). ASTM International, West Conshohocken, PA.

ASTM D7181-11. (2011). Method for Consolidated Drained Triaxial Compression Test for Soils. ASTM International, West Conshohocken, PA.

ASTM D854-06. (2003). Standard Test Methods for Specific Gravity of Soil Solids by Water Pycnometer. ASTM International, West Conshohocken, PA.

Banerjee, N.G., Seed, H.B., and Chan, C.K. (1979). Cyclic Behavior of Dense Coarse-Grained. Materials in Relation to the Seismic Stability of Dams, Earthquake Engineering Research center (EERC), Report No. UCB/EERC-79/13, University of California, Berkeley, California.

Bao, C. G., Gong, B., and Zhan, L. (1998). Properties of unsaturated soils and slope stability of expansive soil. *Keynote lecture: UNSAT 98*, 2nd International Conference on Unsaturated Soils, Beijing.

Barbour, S. L. (1998). The soil-water characteristic curve: a historical perspective. *Canadian Geotechnical Journal*, 35(5), 873–894.

Barfknecht, J.E. (2001). *Characterization of the Strength and Plastic Deformation Properties of Unsaturated Soils*. Doctoral Dissertation, Texas A&M University, College Station, Texas.

Barksdale, R. D., and Itani, S. Y. (1989). Influence of aggregate shape on base behaviour. *Transp. Res. Rec. 1227*, Transportation Research Board, Washington, D.C., 173–182.

Barrera M (2002). *Estudio experimental del comportamiento hidro-mecánico de suelos colapsables*. Doctoral Dissertation, Universitat Politècnica de Catalunya, Barcelona, Spain

Bear, J. (1979). *Hydraulic of groundwater*. McGraw-Hill, New York, 190-224.

Bhattacharya, S., Hyodo, M., Goda, K., Tazoh, T., and Taylor, C. A. (2011). Liquefaction of soil in the Tokyo Bay area from the 2011 Tohoku (Japan) earthquake. *Soil Dynamics and Earthquake Engineering*, 31(11), 1618–1628.

Bishop, A. W. (1959). The principle of effective stress. *Teknisk Ukeblad I Samarbeide Med Teknikk*, 106(39), 859–863.

Bishop, A. W. and Green, G. E. (1965). The influence of end restraints on the compressive strengths of cohesionless soil. *Geotechnique*, 15(3), 243-266.

Bishop, A. W. and Henkel, D. J. (1957). *The measurement of soil properties in the triaxial test.* Edward Arnold, Ltd, London.

Bishop, A. W. and Henkel, D. J. (1962). *The measurement of soil properties in the triaxial test.* 2nd Edition, Edward and Arnold Publishers, London, UK.

Bishop, A.W. and Blight, G.E. (1963). Some Aspects of Effective Stress in Saturated and Unsaturated Soils. *Geotechnique*, 13(3), 177-197.

Bishop, A.W. and Donald, I.B. (1961). The Experimental Study of Partly Saturated Soils in the Triaxial Apparatus. *Proceedings of 5th ICSMFE*, Paris, France, 1, 13-21.

Bishop, A.W., and Wesley, L.D. (1975). A hydraulic triaxial apparatus for controlled stress path testing. *Géotechnique*, 25(4): 657–670.

Blatz, J. A., and Graham, J. (2000). A method for controlled suctions in triaxial testing. *Geotechnique*, 50(4), 465-470.

Blatz, J. A., Cui, Y-J., and Oldecop, L. (2008). Vapour equilibrium and osmotic technique for suction control. *Geotechnical and Geological Engineering*, 26, 661-673.

Blight, G.E. (1967). Effective stress Evaluation for Unsaturated Soils. *Journal of Soil Mechanics and Foundation Division*, ASCE, 93(SM2), 125-148

Bocking, K. A. and Fredlund, D. G. (1980). Limitations of the axis-translation technique. *Proc. 4th International Conference on Expansive Soils*, Denver, CO, June 16-18, D. Snethen, Ed., ASCE, NY, 1, 117-135.

Bolton, M. D. (1986). The strength and dilatancy of sands. *Geotechnique*, 36(1), 65-78.

Boominathan, A., Rangaswamy, K., and Rajagopal, K., (2010). Effect of Non-Plastic Fines on Liquefaction Resistance of Gujarat Sand. *International Journal of Geotechnical Engineering*, 4(2), 241–253.

Boulanger, R. W., and Idriss, I. M. (2006). Liquefaction Susceptibility Criteria for Silts and Clays. *Journal of Geotechnical and Geoenvironmental Engineering*, 132(11), 1413–1426.

Boulanger, R. W., and Idriss, I. M. (2007). Evaluation of cyclic softening in silts and clays. *Journal of Geotechnical and Geoenvironmental Engineering*, 133(6), 641-652.

Boulanger, R. W., and Truman, S. P. (1996). Void redistribution in sand under post-earthquake loading. *Canadian geotechnical journal*, 33(5), 829-834.

Boyce, J. R., Brown, S. F., and Pell, P. S. (1976). The resilient behavior of a granular material under repeated loading. *Proc. 8th ARRB Conf. Mat. Constr. and Maintenance*, 8, Part 3, 1–12.

Bray, J. D., and Sancio, R. B. (2006). Assessment of the liquefaction susceptibility of fine-grained soils. *Journal of Geotechnical and Geoenvironmental Engineering*, 132(9), 1165-1177.

Brickman, A. (1989). An Overview of Resilient Modulus Test Systems, *Workshop on Resilient Modulus*, Corvallis, OR.

Brooks, R. H., and Corey, A. T. (1964). Hydraulic properties of porous media and their relation to drainage design. *Transactions of the ASAE, 7*(1), 26-0028.

Brown, S.F., Repeated Load Testing of a Granular Material, *Journal of the Geotechnical Engineering Division*, 100(7), 1974, 825–841.

Brown, S. F. (1996). Soil mechanics in pavement engineering. *Geotechnique*, 46(3), 383–426

Brown, S. F., and Hyde, A. F. L. (1975). Significance of cyclic confining stress in repeated-load triaxial testing of granular material. *Transp. Res. Rec. 537*, Transportation Research Board, Washington, D.C., 49–58.

Burland, J.B. (1964). Some Aspects of Effective Stress in Saturated and Unsaturated Soils. *Geotechnique,* 14(1), 65-68.

Cabarkapa, Z., and Cuccovillo, T. (2006). Automated triaxial apparatus for testing unsaturated soils. *Geotechnical Testing Journal*, 29(1), 21-29.

Cary, C. E., and Zapata, C. E. (2011). Resilient modulus for unsaturated unbound materials. *Road Mater. Pavement Des.*, 12(3), 615–638.

Casagrande, A. (1975). Liquefaction and cyclic deformation of sands – a critical review. *Proc.: 5th Pan-American Conference on Soil Mechanics and Foundation Engineering*, Buenos Aires, Argentina, A.A. Balkema, Rotterdam, The Netherlands. 5, 79-133.

Castro, G. (1969). *Liquefaction of Sands*. Doctoral Dissertation, Harvard University, Cambridge, MA.

Castro, G. (1975). Liquefaction and Cyclic Mobility of Saturated Sands. *Journal of Geotechnical Engineering Division*, ASCE, 101(GT6), 551-570.

Castro, G. (1975). Liquefaction and cyclic mobility of saturated sands. *Journal of Geotechnical Engineering Division*, 101, GT6, 551-569.

Castro, G. and Poulos, S.J. (1977). Factors Affecting Liquefaction and Cyclic Mobility. *Journal of Geotechnical Engineering Division*, ASCE, 103(GT6), 501-516.

Chiu, C. F., and Ng, C. W. W. (2003). A state-dependent elasto-plastic model for saturated and unsaturated soils. *Géotechnique*, 53(9), 809–829.

Clayton, C. R. I., Khatrush, A. S., Bica, A. V. D., and Siddique, A. (1989). The use of hall effect semiconductors in geotechnical instrumentation. *Geotechnical Testing Journal*, 12(1), 69-76.

Coduto, D. P., (1999). *Geotechnical Engineering Principles and Practices*. New Jersey: Prentice-Hall.

Coleman, J.D. (1962). Stress strain relations for partly saturated soil. *Geotechnique*, 12(4), 348-350.

Coulomb, C.A. (1776). Sur une application des regles maximis et minimis a quelques problemes de statique, relatifs a l'architecture, *Acad. Sci. Paris Mem. Math. Phys.*, 7, 343-382.

Coulter, H.W., and Migliaccio, R.R. (1966). *Effect of earth quake of March 27, 1964 at Valdez, Alaska.* U.S. Geological Survey Professional Paper 542-C, U.S. Dept. of the Interior, Washington, D.C.

Cox, D. W. (1978). Volume Change of Compacted Clay Fill. *Clay Fills*, Institution of Civil Engineers, London, 79–86.

Crawford, A., and Wylie, D. (1987). A modified multiple failure state triaxial testing method. *28th U.S. Symp. on Rock Mechanics*, Taylor & Francis, London, 133–140.

Croney, D., and Coleman, J. D. (1954). Soil structure in relation to soil suction (pF). *European Journal of Soil Science*, 5(1), 75-84.

Cui Y.J. (1993). *Etude du comportement d'un limon compacté non saturé et de sa modelisation dans un cadre élasto-plastique*. Doctoral Dissertation, Ecole Nationale des Ponts et Chaussées, Paris, France.

Cui, Y. J. and Delage, P. (1996). Yielding and plastic behaviour of an unsaturated compacted silt. *Geotechnique*, 46(2), 291-311.

Das, B. M., and Ramana, G. V. (2011). *Principles of Soil Dynamics*. Cengage Learning, Stamform, CT.

Dash, H. K., and Sitharam, T. G. (2011). Undrained cyclic and monotonic strength of sand-silt mixtures. *Geotechnical and Geological Engineering*, 29(4), 555-570.

Datcheva, M. and Schanz, T. (2003). Anisotropic bounding surface plasticity with rotational hardening for unsaturated frictional material. *Journal de Physiqye iv*, 105, 305-550.

Delage, P., Howat, M. D., and Cui, Y. J. (1998). The relationship between suction and swelling properties in a heavily compacted unsaturated clay. *Engineering Geology*, 50, 31-48.

Delage, P., Suraj De Silva, G. P. R., and De Laure, E. (1987). Un nouvel appareil triaxial pour les sols non satures. *Proc. 9th European Conference on SMFE*, Dublin, 25-28.

Delage, P., Suraj De Silva, G. P. R., and Vicol, T. (1992). Suction controlled testing of non saturated soils with an osmotic consolidometer. *Proc. 7th International Conference on Expansive Soils*, Dallas, 206-211.

Drumm, E. C., Boateng-Poku, Y. and Pierce, T. J. (1990). Estimation of Subgrade Resilient Modulus from Standard Tests. *Journal of Geotechnical Engineering*, ASCE, 116, No. 5, 774-789.

Drumm, E. C., Reeves, J. S., Madgett, M.R. and Trolinger, W. D. (1997). Subgrade Resilient Modulus Correction for Saturation Effects. *Journal of Geotechnical and Geoenvironmental Engineering*, ASCE, 123, No. 7, 663-670.

Drumright E.E. (1989). *The Contribution of Matric Suction to the Shear Strength of Unsaturated Soils*. Doctoral Dissertation, Colorado State University, Fort Collins, Colorado.

Edil, T.B. and Motan, S.E. (1979). Soil-water potential and resilient behavior of subgrade soils. *Transportation Research Record*, 705, Washington, D.C., 54–63.

Edlefsen, N. E., and Anderson, A. B. C. (1943). Thermodynamics of soil moisture. *Hilgardia*, 15(2), 31–298.

Edris, E.V., and Lytton, R.L. (1976). *Dynamic properties of subgrade soils, including environmental effects*. Report Number: TTI-2-18-74-164-3, Texas A&M University, College Station, Texas.

Elliott, R. P., and Thornton, S. I. (1988). Resilient Modulus and AASHTO Pavement Design. *Transportation Research Record*, 1196, TRB, National Research Council, Washington, D.C., 116-124.

Elliott, R. P., Dennis, N. and Qiu, Y. (1999). *Permanent Deformation of Subgrade Soils, Phase II: Repeated Load Testing of Four Soils*. Report No. MBTC FR-1089, Final Report, National Technical Information Service, Springfiled, VA, 1-85.

Escario, V., and Juca, J.F.T. (1989). Shear strength and deformation of partly saturated soils, Proc. Twelfth International Conference on Soil Mechanics and Foundation Engineering, Rio de Janeiro, 1, 43-46.

Escario, V., and Saez, J. (1986). The shear strength of partly saturated soils, *Geotechnique*, 36(3), 453-456.

Evans, M. D., and Seed, H. B. (1987). *Undrained Cyclic Triaxial Testing of Gravels: The Effect of Membrane Compliance*. Earthquake Engineering Research Center, Report No. UCB/EERC-87/08, University of California, Berkeley, California,

Evans, M. D., and Zhou, S. (1995). Liquefaction behavior of sand-gravel composites. *Journal of Geotechnical Engineering*, 121(3), 287-298.

Ferreira, S. M. R., Correia, A. G., and Roque, A. J. (2016). Strength of Non-traditional Granular Materials Assessed from Drained Multistage Triaxial Tests. *Procedia Engineering*, Elsevier B.V., 143, 67–74.

Finn, W. D. L., Pickering, D. J., and Bransby, P. L. (1971). Sand liquefaction in triaxial and simple shear tests. *Journal of Soil Mechanics and Foundations Division*, 97(4), 639–659.

Fleming, H. O. (1952). Undrained triaxial compression tests on a decomposed phyllite. First Australia New Zealand Conference on Soil Mechanics and Foundation Engineering, 1952, 112-122.

Fredlund, D. G., and Morgenstern, N. R. (1977). Stress State Variables for Saturated and Unsaturated Soils. *Journal of Geotechnical and Geoenvironmental Engineering*, 103(5), 447–466.

Fredlund, D. G., and Rahardjo, H. (1993). *Soil Mechanics for Unsaturated Soils*. Wiley, New York.

Fredlund, D. G., and Xing, A. (1994). Equations for the soil-water characteristic curve. *Canadian Geotechnical Journal*, *31*(4), 521-532.

Fredlund, D. G., Rahardjo, H., and Fredlund, M. D. (2012). *Unsaturated Soil Mechanics in Engineering Practice*. John Wiley and Sons, Inc., Hoboken, New Jersey.

Fredlund, D. G., Xing, A., Fredlund, M. D., and Barbour, S. L. (1996). The relationship of the unsaturated soil shear strength to the soil-water characteristic curve. *Canadian Geotechnical Journal*, 33, 440-448.

Fredlund, D.G., Bergan, A.T., and Wong, P.K. (1977). Relation between resilient modulus and stress research conditions for cohesive subgrade soils. *Transportation Research Record*, 642, Washington, D.C., 73–81.

Gallagher, P. M., and Mitchell, J. K. (2002). Influence of colloidal silica grout on liquefaction potential and cyclic undrained behavior of loose sand. *Soil Dynamics and Earthquake Engineering*, *22*(9), 1017-1026.

Gallagher, P.M., James, M. 2002. Influence of colloidal silica grout on liquefaction potential and cyclic undrained behavior of loose sand. *Soil Dynamics and Earthquake Engineering*, 22, 1017-1026.

Gallipoli, D., Gens, A., Sharma, R., and Vaunat, J. (2003). An elasto-plastic model for unsaturated soil incorporating the effects of suction and degree of saturation on mechanical behavior. *Geotechnique*, 53, 123-135.

Gan, J. K. M., Fredlund, D. G. and Rahardjo, H. (1988). Determination of shear strength parameter for unsaturated soil using direct shear test. *Canadian Geotechnical Journal*, 25(3), 500-510.

Garga, V. K., and McKay, L. D. (1984). Cyclic triaxial strength of mine tailings. *Journal of Geotechnical Engineering*, 110(8), 1091-1105.

Gaskin, P. N., Raymond, G. P. and Addo-Abedi, F. Y. (1979). Repeated Compressive Loading of a Sand. *Canadian Geotechnical Journal*, National Research Council of Canada, 16, 798-802.

GCTS. (2010). *CATS Triaxial Test Manual users guide and manual*. Geotechnical Consulting & Testing Systems. Tempe, Arizona.

Geiser, F. (1999). *Comportement mécanique d'un limon non saturé: étude expérimentale et modélisation constitutive*. Doctoral Dissertation, Ecole Polytechnique Fédérale de Lausanne, EPFL, Switzerland

Geiser, F., Laloui, L. and Vulliet, L. (2000). On the Volume Measurement in Unsaturated Triaxial Test. *Proc. Asian Conference on Unsaturated Soils*, Singapore, 669-674

George, K. P. (2004). Prediction of resilient modulus from soil index properties. *Rep. No. FHWA/MS-DOT-RD-04-172*, Federal Highway Administration, U.S. Department of Transportation, Washington, D.C.

Georgiadis, K., Potts, D. M., and Zdravkovic, L. (2005). Three-dimensional constituitive model for partially and fully saturated soils. *International Journal of Geomechanics*, 5(3), 244-255.

Ghazzaly, O. and Ha, H. (1975). Pore Pressures and Strains After Repeated Loading of Saturated Clay: Discussion. *Canadian Geotechnical Journal*. National Research Council of Canada, 12, 265-267.

Ghionna, V. and Porcino, D., (2006). Liquefaction Resistance of Undisturbed and Reconstituted Samples of a Natural Coarse Sand from Undrained Cyclic Triaxial Tests, *Journal of Geotechnical and Geoenvironmental Engineering*, 132(2), 194–202.

Giancoli, D. C. (1985). *Physics: Principles with Applications*. Prentice-Hall, Englewood Cliffs, N.J.

Gibbs, J. (1873). A Method of Geometrical Representation of the Thermodynamic Properties of Substances by Means of Surfaces. *Transactions of the Connecticut Academy of Arts and Sciences*, 382–404.

Gould, S., Rajeev, P., Kodikara, J., Zhao, X.-L., Burn, S., and Marlow, D. (2012). A New Method for Developing Equations Applied to the Water Retention Curve. *Soil Science Society of America Journal*, The Soil Science Society of America, Inc., 6(3), 806–814.

Green, R.A. (2001). *Energy Based Evaluation and Remediation of Liquefiable Soils*. Doctoral Dissertation, Virginia Polytechnic Institutive and State University, Blacksburg, VA

Gulhati, S. K., and Satija, B. S. (1981). Shear Strength of Partially Saturated Soils. *Proc. 10th International Conference on Soil Mechanics and Foundation Engineering*, 1, 609-612.

Gupta, S. C., Ranaivoson, A., Edil, T. B., Benson, C. H., and Sawangsuriya, A. (2007). *Pavement design using unsaturated soil technology*, Minnesota Dept. of Transportation, St. Paul, MN.

Hall, D. K. and Thompson, M. R. (1994). Soil-Property-Based Subgrade Resilient Modulus Estimation for Flexible Pavement Design. *Transportation Research Record*, 1449, TRB, National Research Council, Washington, D.C., 30-38.

Han, Z., and Vanapalli, S. K. (2015). Model for predicting resilient modulus of unsaturated subgrade soil using soil-water characteristic curve. *Canadian Geotechnical Journal*, 52(10), 1605–1619.

Han, Z., and Vanapalli, S. K. (2016). State-of-the-Art: Prediction of Resilient Modulus of Unsaturated Subgrade Soils. *International Journal of Geomechanics*, 2016, 16(4).

Handoko, L., Yasufuku, N., Oomine, K., and Hazarika, H. (2013). Suction Controlled Triaxial Apparatus for Saturated-Unsaturated Soil Test. *International Journal of GEOMATE*, 4(1), 466–470.

Haynes, J. G., and Yoder, E. J. (1963). Effects of repeated loading on gravel and crushed stone base course materials used in the AASHO Road Test. *Hwy. Res. Rec. 39*.

Hicks, R. G. (1970). *Factors influencing the resilient properties of granular materials*. Doctoral Dissertation, University of California, Berkeley, Berkeley, California.

Hicks, R. G., and Monismith, C. L. (1971). Factors Influencing the Resilient Response of Granular Materials. *Highway Research Record*, 345, Highway Research Board, Washington, D.C., 15-31.

Hilf, J. W. (1956). *An investigation of pore-water in compacted cohesive soils*. Doctoral Dissertation, Technical Memo. No. 654, U. S. Department of the

Interior, Bureau of Reclaimation, Design and Construction Division, Denver, CO.

Ho, D. Y. F., and Fredlund, D. G. (1982). Multi-stage triaxial tests for unsaturated soils. *Geotechnical Testing Journal*, 5(1), 18–25.

Høeg, K., Dyvik, R., and Sandbækken, G. (2000). Strength of undisturbed versus reconstituted silt and silty sand specimens. *Journal of Geotechnical and Geoenvironmental Engineering*, 126(7). 606–617.

Holtz, R.D., and Kovacs, W.G. (1981). *An introduction to Geotechnical Engineering, Prentice-Hall*, Eaglewood Cliffs, N.J.

Houlsby, G. T. (1997). The work input to an unsaturated granular material. *Geotechnique*, 47, 193-196.

Houston, S. L., Houston, W. N., and Wagner, A. M. (1994). Laboratory filter paper suction measurements. *Geotechnical Testing Journal*, 17(2), 185-194.

Houston, S. L., Perez-Garcia, N., and Houston, W. N. (2008). Shear Strength and Shear-Induced Volume Change Behavior of Unsaturated Soils from a Triaxial Test Program. *Journal of Geotechnical and Geoenvironmental Engineering*, 134(11), 1619–1632.

Houston, W. N., Dye, H. B., Zapata, C. E., Perera, Y. Y., and Harraz, A. (2006). Determination of SWCC Using One Point Suction Measurement and Standard Curves. *Unsaturated Soils 2006*, American Society of Civil Engineers, Reston, VA, 1482–1493.

Hoyos L.R., and Macari E.J. (2001). Development of a stress/suction-controlled true triaxial testing device for unsaturated soils. *Geotechnical Testing Journal*, 24(1):5–13.

Hoyos L.R., Laikram A, and Puppala A.J. (2005). A novel true triaxial apparatus for testing unsaturated soils under suction-controlled multi-axial stress states. *Proc. of the 16th international conference on soil mechanics and geotechnical engineering*, Osaka, Japan, 387–390

Hoyos LR, Arduino P (2005) Modeling response of unsaturated silty sand in three-invariant stress space. *Proc. of the 3rd MIT conference on computational fluid and solid mechanics*, Boston, Massachusetts, 256–260

Hoyos, L. R. (1998). *Experimental and computational modeling of unsaturated soil behavior under true triaxial stress states*. Doctoral Dissertation, Georgia Institute of Technology, Atlanta.

Hoyos, L. R., Diego, D. Perez-Ruiz., and Puppala, A. J. (2012). Modeling unsaturated soil response under suction-controlled true triaxial stress paths. *International Journal of Geomechanics*, 12(3), 292-308.

Hoyos, L. R., Laloui, L., and Vassallo, R. (2008). Mechanical testing in unsaturated soils. *Geotechnical Geology Engineering*, 26, 675-689.

Hoyos, L. R., Thudi, H. R., and Puppala, A. J. (2007). Soil-water retention properties of cement treated clay. *Problematic Soils and Rocks and In Situ Characterization*, 1-8.

Hyde, A. F. L. (1974). *Repeated load triaxial testing of soils*. Doctoral Dissertation, University of Notingham, U.K.

Hyodo, M., Tanimizu, H., Yasufuku, N., and Murata, H. (1994). Undrained cyclic and monotonic triaxial behaviour of saturated loose sand. *Soils and foundations*, 34(1), 19-32.

Ishihara, K. 1993. Liquefaction and flow failure during earthquakes. *Geotechnique* 43, 351-415.

Ishihara, K. and Tsukamoto, Y. (2004). Cyclic strength of imperfectly saturated sands and analysis of liquefaction, *Proc. Japan Academy Ser. B*, 80(8), 372 – 391.

Ishihara, K., Troncoso, J., Kawase, Y., and Takahashi, Y. (1980). Cyclic strength characteristics of tailings materials. *Soils and Foundations*, 20(4), 127-142.

Ishikawa, T., Tokoro, T., Ito, K., and Miura, S. (2010). Testing methods for hydro-mechanical characteristics of unsaturated soils subjected to one-dimensional freeze-thaw action. *Soil Science Society of America Journal*, 50(3), 431–440.

Ishikawa, T., Zhang, Y., Segawa, H., Miura, S., and Tokoro, T. (2012). Developement of medium-size triaxial apparatus for unsaturated granular base course material. *Advances in Transportation Geotechnics II: 2nd International Conference on Transportation Geotechnics (ICTG)*, Japan, 534-540.

Ishikawa, T., Zhang, Y., Tokoro, T., and Miura, S. (2014). Medium-size triaxial apparatus for unsaturated granular subbase course materials. *Soils and Foundations*, 54(1_, 67-80.

Jang, D.J., and Frost, J.D. (1998). Sand structure differences resulting from specimen preparation procedures. *Proc.: Specialty Conference on Geotechnical Earthquake Engineering and Soil Dynamics*, Seattle, Washington, 1, 234–245.

Jefferies, M., and Been, K. (2006). *Soil Liquefaction: A Critical State Approach*. Taylor and Francis, New York, NY.

Jennings, J. E. and Burland, J. B. (1962). Limitations to the use of effective stresses in partly saturated soils. *Geotechnique*, 2, 125-144.

Jennings, J. E. B. and Knight, K., 1957, The Additional Settlement of Foundation Due to a Collapse of Structure of Sandy Subsoil on Wetting. *Proc. 4th International Conference on Soil Mechanics and Foundation Engineering*, 2, Butterworths, London, 316–319.

Jin, M. S., Lee, K. W., and Kovacs, W. D. (1994). Seasonal variation of resilient modulus of subgrade soils. *J. Transp. Eng.*, 603–616.

Johari A, Javadi AA. (2011). Prediction of soil-water characteristic curve using neural network, *Unsaturated Soils - Proceedings of the 5th International Conference on Unsaturated Soils*, 1, 461-466.

Johnson, T. C., Berg, R. L., and Dimillio, A. (1986). Frost action predictive techniques: An overview of research results. *Transp. Res. Rec. 1089*, Transportation Research Board, Washington, D.C., 147–161.

Jones, D.E., and Holtz, W.G. (1973). *Expansive Soils – The Hidden Disaster, Civil Engineering*, American Society of Civil Engineers, New York, 139-153.

Jorenby, B. N., and Hicks, R. G. (1986). Base course contamination limits. *Trans. Res. Rec. 1095*, Transportation Research Board, Washington, D.C., 86–101.

Josa, A., Balmaceda, A., Gens, A., and Alonso, E. E. (1992). An elastoplastic model for partially saturated soils exhibiting a maximum of collapse. *Proc. 3rd International Conference on Computational Plasticity*, Barcelona, 1, 815-826.

Jotisankasa, A., (2005). *Collapse Behaviour of a Compacted Silty Clay*. Doctoral Dissertation, Imperial College London, London.

Kenney, T. C., and Watson, G. H. (1961). Multiple-stage triaxial tests for determining c and φ of saturated soils. *Proc. Fifth Int. Conf. on Soil Mechanics and Foundation Engineering*, Paris, 1, 191–195.

Khalili, N., and Khabbaz, M. H. 1998. A unique relationship for χ for the determination of shear strength of unsaturated soils. *Geotechnique*, 48(5), 681–688.

Khalili, N., and Zargarbashi, S. (2010). Influence of hydraulic hysteresis on effective stress in unsaturated soils. *Géotechnique*, 60(9), 729–734.

Khalili, N., Geiser, F., and Blight, G. E. (2004). Effective Stress in Unsaturated Soils: Review with New Evidence. *International Journal of Geomechanics*, 4(2), 115–126.

Khalili, N., Witt, R., Laloui, L., Vulliet, L., and Koliji, A. 2005. Effective stress in double porous media with two immiscible fluids. *Geophys. Res. Lett*., 32, 13539–13544.

Khosravi, A., Alsherif, N., Lynch, C., and Mccartney, J. (2011). Multistage Triaxial Testing to Estimate Effective Stress Relationships for Unsaturated Compacted Soils. *Geotechnical Testing Journal*, 35(1), 128-134.

Khoury, C. N., Khoury, N. N., and Miller, G. A. (2011). Effect of cyclic suction history (hydraulic hysteresis) on resilient modulus of unsaturated fine-grained soil. *Transportation Research Record*, 2232, TRB, Washington, DC, 68–75.

Khoury, N. N., and Zaman, M. M. (2004). Correlation between resilient modulus, moisture variation, and soil suction for subgrade soils. *Transportation Research Record*, 1874, TRB, Washington, DC, 99–107.

Kim, T.-H., and Sture, S. (2008). Capillary-induced tensile strength in unsaturated sands. *Canadian Geotechnical Journal*, 45(5), 726–737.

Kodikara, J. (2012). New framework for volumetric constitutive behavior of compacted unsaturated soils. *Canadian Geotechnical Journal*, 49, 1227-1243.

Kodikara, J., Barbaour, S. L., Fredlund, D. G. (2000). Desiccation cracking of soil layers. *Proc. Asian conference in unsaturated soils, UNSAT ASIA*, Singapore, 693-698.

Kolisoja, P. (1997). *Resilient deformation characteristics of granular materials.* Doctoral Dissertation, Tampere University of Technology, Publ. No. 223, Tampere, Finland.

Kondner, R. L. (1963). Hyperbolic stress-strain response, cohesive soils. *J. Soil Mech. Found. Div.*, 89(1), 115–143.

Krahn, J., and Fredlund, D.G. (1972). On total matric and osmotic suction, *Journal of Soil Science Journal*, 114(5), 339-348.

Kramer, S. L. (1996). *Geotechnical earthquake engineering*. Prentice Hall, Upper Saddle River, N.J.

Kuerbis, R. (1989). *The undrained loading response of sand*. M.S. Thesis, University of British Columbia, B.C.

Kutter, B. L., Chen, Y. R., and Shen, C. K. (1994). *Triaxial and torsional shear test results for sand*. Report No. NFESC-CR-94.003-SHR. California Univ Davis.

Ladd, R. S. (1974). Specimen preparation and liquefaction of sands. *Journal of Geotechnical Engineering*, 100(GT10), 1180–1184.

Ladd, R. S. (1977). Specimen preparation and cyclic stability of sands. American Society of Civil Engineers, *Journal of the Geotechnical Engineering Division*, 103, 535-547.

Ladd, R. S. (1978). Preparing Test Specimens Using Undercompaction. *Geotechnical Testing Journal*, 1(1), 16–23.

Laikram, A. (2007). *Modeling Unsaturated Soil Response under Suction-Controlled Multi-Axial Stress States*. Doctoral Dissertation, University of Texas at Arlington, Arlington, Texas.

Lawton, E. C., Fragaszy, R. J., and Hardcastle, J. H. (1989). Collapse of compacted clayey sand. *Journal of Geotechnical Engineering*, 115(9), 1252–1267.

Lee, W. (1993). *Evaluation of In-Service Subgrade Resilient Modulus with Consideration of Seasonal Effects*. Doctoral Dissertation, Purdue University, West Lafayette, IN.

Lefebvre, G., and Pfendler, P. (1996). Strain rate and preshear effects in cyclic resistance of soft clay. *Journal of Geotechnical Engineering*, *122*(1), 21-26.

Lekarp, F., Isacsson, U. and Dawson, A. (2000). State of The Art. I: Resilient Response of Unbound Aggregates, *Journal of Transportation Engineering*, 126, 66-75.

Leong E.C., Agus S.S., Rahardjo H. (2004) Volume change measurement of soil specimen in triaxial test. *Geotechnical Testing Journal* , 27(1):47–56

Leong, E. C., and Rahardjo, H. (1997). Review of Soil-Water Characteristic Curve Equations. *Journal of Geotechnical and Geoenvironmental Engineering*, 123(12), 1106–1117.

Leong, E. C., Nyunt, T. T., and Rahardjo, H. (2013). *Triaxial Testing of Unsaturated Soils*. Multiphysical Testing of Soils and Shales, Springer Series in Geomechanics and Geoengineering, L. Laloui and A. Ferrari, eds., Springer Berlin Heidelberg, Berlin, Heidelberg, 33–44.

Leong, E.C., Tripathy, S., and Rahardjo, H. (2003). Total suction measurement of unsaturated soils with a device using the chilled-mirror dew-point technique, *Geotechnique*, 53(2), 173-182.

Li, L. L., Dan, H. B., and Wang, L. Z. (2011). Undrained behavior of natural marine clay under cyclic loading. *Ocean Engineering*, 38(16), 1792-1805.

Li, L., and Zhang, X. (2015). A new triaxial testing system for unsaturated soil characterization. *Geotechnical Testing Journal*, 38(6), 823–839.

Liang, R. Y., Rabab'ah, S., and Khasawneh, M. (2008). Predicting moisture-dependent resilient modulus of cohesive soils using soil suction concept. *J. Transp. Eng.*, 34–40.

Likos, W. J. (2012). User Manual automated relative humidity control system.

Likos, W. J. and Lu, N. (2002). Filter paper technique for measuring total suction. *Transportation Research Record: Journal of the Transportation research Board*, 1786, 120-128.

Likos, W. J., and Lu, N. (2003). Automated humidity system for measuring total suction characteristics of clay. *Geotechnical Testing Journal*, 26(2), 179–190.

Liu, C., and Xu, J. (2015). Experimental study on effects of initial conditions on liquefaction of saturated and unsaturated sand. *International Journal of Geomechanics*, 15(6).

Loach, S.C. 1987. Repeated loading of fine grained soils for pavement design. Ph.D. thesis, University of Nottingham, Nottingham, U.K.

Lowe, J. and Johnson, T. C. (1960). Use of back pressure to increase degree of saturation of triaxial test specimens. ASCE Research Conference on Shear Strength of Cohesive Soils, Boulder, Colorado, USA, 819-836.

Lu, N., and Likos, W. J. (2004). *Unsaturated Soil Mechanics*. J. Wiley, Hoboken.

Lu, N., and Likos, W. J. (2006). Suction Stress Characteristic Curve for Unsaturated Soil. *Journal of Geotechnical and Geoenvironmental Engineering*, 132(2), 131–142.

Lu, N., Godt, J., and Wu, D., (2010). A Closed-Form Equation for Effective Stress in Unsaturated Soil, *Water Res.*, 46, W05515.

Lu, N., Kim, T.-H., Sture, S., and Likos, W. J. (2009). Tensile Strength of Unsaturated Sand. *Journal of Engineering Mechanics*, 135(12), 1410–1419.

Lumb, P. (1964). Multi-stage triaxial tests on undisturbed soils Civil Engineering and Public Works Review, 591-595.

Lytton, R. L. (1995). Foundations and pavements on unsaturated soils. Keynote Address, Proc. 1st Int. Conf. on Unsaturated Soils, 3, Balkema, Rotterdam, the Netherlands, 1201–1220.

Ma, T., Wei, C., Wei, H., and Li, W. (2016). Hydraulic and Mechanical Behavior of Unsaturated Silt: Experimental and Theoretical Characterization. International Journal of Geomechanics, 16(6).

Madabhushi, S. P. G., (2007). Ground improvement methods for liquefaction. *Proceedings of the Institution of Civil Engineers* - Ground Improvement, 195-206.

Maher, M.H., T. Bennett, W.J. Papp, Jr., and N. Gucunski, *Resilient Modulus Properties of New Jersey Subgrade Soils*, FHWA NJ 2000-01, Rutgers University, Piscataway,

Malla, R.B. and S. Joshi, *Establish Subgrade Support Values for Typical Soils in New England*, Report No. NETCR 57, New England Transportation Consortium, Fall River, Mass., Apr. 2006.

Manzanal, D., Fernández Merodo, J. A., and Pastor, M. (2011). Generalized plasticity state parameter-based model for saturated and unsaturated soils. Part II: Unsaturated soil modeling. International Journal for Numerical and Analytical Methods in Geomechanics, 35, 1899–1917.

Marinho, F.A.M., and Oliveira O.M. (2006). The Filter Paper Method Revisited, *Geotechnical Testing Journal*, 29(3), 250-258.

Markham, C. S., Bray, J. D., Riemer, M. F., and Cubrinovski, M. (2016). Characterization of Shallow Soils in the Central Business District of Christchurch, New Zealand. *Geotechnical Testing Journal*, 39(6), 922–937.

Matsuoka H., Sun D.A., Kogane A., Fukuzawa N., Ichihara W. (2002) Stress–strain behaviour of unsaturated soil in true triaxial tests. Can Geotech Journal, 39, 608–619.

Matyas, E. L. and Radhakrishna, H. S. (1968). Volume Change Characteristics of Partially Saturated Soils. Geotechnique, 18(4), 432–448.

Mayhew, H. C. (1983). Resilient properties of unbound road base under repeated triaxial loading. *Lab. Rep. 1088*, TRRL, Crowthorne, U.K.

Missoum, H., Belkhatir, M., Bendani, K., and Maliki, M. (2013). Laboratory investigation into the effects of silty fines on liquefaction susceptibility of Chlef (Algeria) sandy soils. *Geotechnical and Geological Engineering*, 31(1), 279-296.

Mitchell, J. K., and Soga, K. (2006). Fundamentals of soil behavior, Wiley, New York.

Mitry, F. G. (1964). *Determination of the modulus of resilient deformation of untreated base course materials*. Doctoral Dissertation, University of California, Berkeley, Berkeley, California.

Miura, S., and Toki, S. (1982). A sample preparation method and its effect on static and cyclic deformation-strength properties of sand. *Soils and Foundations*, 22(1), 61–77.

Mogami, T., and Kubo, K. (1953). The behavior of soil during vibration. *Proc. 3rd International Conference on Soil Mechanics and Foundation Engineering*, Zurich, 1, 152-155.

Mohammad, L. N., Puppala, A. J. and Alavilli, P. (1995). Resilient Properties of Laboratory Compacted Subgrade Soils, Transportation Research Record, 1196, TRB, National Research Council, Washington, D.C., 87-102.

Mohammad, L. N., Titi, H. H. and Herath, A. (1999). Evaluation of Resilient Modulus of Subgrade Soil by Cone Penetration Test, Transportation Research Record, 1652, TRB, National Research Council, Washington, D.C., 236-245.

Mohammad, L.N., Puppala, A.J. and Alavilli, P. (1994). Influence of Testing Procedure and LVDTs Location on Resilient Modulus of Soils, *Transportation Research Record 1462*, Transportation Research Board, National Research Council, Washington, D.C., 91–101. N.J.

Mohr, O. (1914). Die Spannungszustand einer Staumauer. *Abhandlungen aus dem Gebiete der technischen Mechanik*, 284-308.

Moses, G. G., Rao, S. N., and Rao, P. N. (2003). Undrained strength behaviour of a cemented marine clay under monotonic and cyclic loading. *Ocean engineering*, 30(14), 1765-1789.

MSU (N.d.) Where does groundwater come from? Retrieved from http://www.orcbs.msu.edu/environ/programs_guidelines/wellhead/glossary_faq/where_groundwater_comes_from.htm (Accessed on: 07/01/2015)

Mulilis, J.P., Seed, H.B., Chan, C.K., Mitchell, J.K., and Arulanandan, K. (1977). Effects of sample preparation on sand liquefaction. *Journal of Geotechnical Engineering*, 103(GT2), 91–108

Muraleetharan, K. K., and Wei, C. 1999. Dynamic behaviour of unsaturated porous media: Governing equations using the theory of mixtures with interfaces TMI. Int. J. Numer. Analyt. Meth. Geomech., 23, 1579–1608.

Murray, E. J. 2002. An equation of state for unsaturated soils. *Can. Geotech. J*., 39, 125–140.

Murray, E. J. and Sivakumar, V. (2010). *Unsaturated soils: A fundamental interpretation of soil behavior*. Wiley-Blackwell, A John Wiley & Sons, Ltd, Publication.

Nambiar, M. R. M., Rao, G. V., and Gulhati, K. S. (1985). Multistage triaxial testing: A rational procedure. *ASTM STP 883*, 274–293.

Ng C. W. W, Zhan L. T., Cui Y. J. (2002) A new simple system for measuring volume changes in unsaturated soils. *Can Geotech J*., 39:757–764

Ng, C. W. W. and Pang, Y. W., (2000). Experimental Investigations of the Soil–Water Characteristics of a Volcanic Soil. *Can. Geotech. J.*, 37(6), 1252–1264.

Ng, C. W. W., and Zhou, C. (2014). Cyclic behaviour of an unsaturated silt at various suctions and temperatures. *Geotechnique*, 64(9), 709–720.

Ng, C. W. W., and Zhou, R. Z. B. (2005). Effects of soil suction on dilatancy of an unsaturated soil. Proceedings of the 16th International Conference on Soil Mechanics and Geotechnical Engineering in Harmony with the Global Environment, 2, 559-562.

Ng, C. W. W., Cui, Y., Chen, R., and Delage, P. (2007). The axis-translation and osmotic techniques in shear testing of unsaturated soils: A comparison. Soils and Foundations, 47(4), 675–684.

Ng, C. W. W., Xu, J., and Yung, S. Y. (2009). Effects of Imbibition-Drainage and Stress Ratio on Anisotropic Stiffness of an Unsaturated Soil at Very Small Strains, Can. Geotech. J., 46(9), 1062–1076.

Nishimura, T. and Fredlund, D. G. (2003). A new triaxial apparatus for high total suction using relative humidity control. 12th Asian Regional Conference on Soil Mechanics and Geotechnical Engineering, Leung et al. (eds), World Scientific Publishing.

Nishimura, T. and Vanapalli, S. K. (2005). Volume change and shear strength behavior of an unsaturated soil with high soil suction. 16th International Conference on Soil Mechanics and Geotechnical Engineering. 563-566.

Nishimura, T., Toyota, H. and Koseki, J. (2010). Evaluation of apparent cohesion of an unsaturated soil. Unsaturated soils - Experimental studies in unsaturated soils and expansive soils, Buzzi, Fityus & Sheng (eds), Taylor and Francis group, London, 109-114.

Nishimura, T., Toyota, H., Vanapalli, S. K. and Won, O. T. (2008). Determination of the shear strength behavior of an unsaturated soil in the high suction range using vapor pressure technique. Proc. Of the Ist European Conference on Unsaturated Soils. Unsaturated Soils: Advances in Geo-Engineering, Toll et al. (eds) CRC Press: Taylor and Francis Group, 441-447.

Noor, M., and Jais, I. (2014). Prediction of stress strain response by rotational multiple yield surface framework for unsaturated granite residual soil. Unsaturated Soils: Research & Applications, N. Khalili, A. Russell, and A. Khoshghalb, eds., CRC Press, 425–431.

Nyunt, T. T., Leong, E.-C., and Rahardjo, H. (2011). Stress-strain behavior and shear strength of unsaturated residual soil from triaxial tests. Proc. of Fifth Asia-Pacific Conference on Unsaturated Soils: Theory and Practice 2011, Pattaya, Thaliand, November 14-16, 1, A. Jotisankasa, A. Sawangsuriya, S.

Soralump, and W. Mairaing, eds., Kasetsart Univeristy, Bangkock, Thailand, 221–226.

Oberg, A. and Sallfors, G. (1997). Determination of shear strength parameters of unsaturated silts and sands based on the water retention curve. Geotechnical Testing Journal, 20(1), 40-48.

Oda, M. (1972a). Initial fabrics and their relations to mechanical properties of granular material. *Soils and Foundations*, 12(1), 17–36.

Oda, M. (1972b). The mechanism of fabric changes during compressional deformation of sand. *Soils and Foundations*, 12(2), 1–18

Oh, S., and Lu, N. (2015). Slope stability analysis under unsaturated conditions: Case studies of rainfall-induced failure of cut slopes. Engineering Geology, Elsevier B.V., 184, 96–103.

Okamura, M., and Noguchi, K. (2009). Liquefaction resistances of unsaturated non-plastic silt. *Soils and Foundations*, 49(2), 221-229.

Oloo, S. Y., and Fredlund, D. G. (1998). The application of unsaturated soil mechanics theory to the design of pavements. Proc. 5th Int. Conf. on the Bearing Capacity of Roads and Airfields, Tapir Academic Press, Trondheim, Norway, 1419–1428.

Olson, R.E. and Langfelder, L.J. (1965). Pore-Water Pressures in Unsaturated Soils. *Journal Soil Mechanics and Foundation Division*, ASCE, 91(SM4), 127-160.

Omidi, G. H., Thomas, J. C., and Brown, K. W. (1996). Effect of desiccation cracking on the hydraulic conductivity of a compacted clay liner. *Water, Air and Soil Pollution*, 89, 91-103.

Paddy, J. F. (1969). Theory of surface tension. *Surface and Colloid Science*, 1.

Padilla, J. M., Perera, Y. Y., Houston, W. N. and Fredlund D. G. (2005). A new soil-water characteristic curve device. *Advanced Experimental Unsaturated Soil Mechanics* – Tarantino, Romero & Cui (eds), Taylor and Francis Group, London, 15-22.

Pagoulatos, A. (2004). Evaluation of multistage triaxial testing on Berea sandstone. M.S. thesis, Univ. of Oklahoma, Norman, OK.

Patil, U.D. (2014). Response of Unsaturated Silty Sand over a Wider Range of Suction States Using a Novel Double-Walled Triaxial Testing System. Doctoral Dissertation, University of Texas at Arlington, Arlington, Texas.

Patil, U. D., Hoyos, L. R., and Puppala, A. J. (2016a). Modeling essential elastoplastic features of compacted silty sand via suction-controlled triaxial testing. *International Journal of Geomechanics*, 16(6).

Patil, U. D., Puppala, A. J., and Hoyos, L. R. (2016b). Characterization of compacted silty sand using a double-walled triaxial cell with fully

automated relative humidity control. *Geotechnical Testing Journal*, 39(5), 742-756.

Perez-Ruiz, D.D. (2009). A Refined True Triaxial Apparatus for Testing Unsaturated Soils under Suction-Controlled Stress Paths. Doctoral Dissertation, University of Texas at Arlington, Arlington, Texas.

Perlea, V. G. (2000). Liquefaction of cohesive soils. *Proc.: Soil Dynamics and Liquefaction 2000*, GSP 107. 58-76.

Pham, H. Q., and Fredlund, D. G. (2008). Equations for entire soil-water characteristic curve on volume change soils. *Canadian Geotechnical Journal*, 45, 443-453

Pham, H. Q., Fredlund, D. G., and Barbour, S. L. (2002). A simple soil-water hysteresis model for predicting the boundary wetting curve. *Proceedings of the 55th Canadian Geotechnical Conference: Ground and Water-Theory to Practice*, Niagara Falls, Ontario, 1261–1267.

Pham, H. Q., Fredlund, D. G., and Barbour, S. L. (2003a). A practical hysteresis model for the soil – water characteristic curve for soils with negligible volume change. *Geotechnique*, 53(2), 293–298.

Pham, H. Q., Fredlund, D. G., and Barbour, S. L. (2003b). Estimation of the Hysteretic Soil-Water Characteristic Curves from the Boundary Drying Curve. *Proceedings of the 56th Canadian Geotechnical Conference*, Winnipeg, MB, 115–121.

Pietsch, W., and Rumpf, H. (1967). Haftkraft, Kapillardruck, Flüssigkeitsvolumen und Grenzwinkel einer Flüssigkeitsbrücke zwischen zwei Kugeln. *Chemie Ingenieur Technik*, 39(15), 885–893.

Polito, C.P. (1999). The Effects of Non-Plastic and Plastic Fines on the Liquefaction of Sandy Soils. Doctoral Dissertation, Virginia Polytechnic Institute and State University, Blacksburg, Virginia.

Potturi. A.K. (2006). Evaluation of Resilient Modulus of Cement and Cement-Fiber Treated Reclaimed Asphalt Pavement (Rap) Aggregates using Repeated Load Triaxial Test, Master's Thesis, University of Texas at Arlington, Arlington, Texas.

Prakash, S., and Sandoval, J. A. (1992). Liquefaction of low plasticity silts. *Soil Dynamics and Earthquake Engineering*, 11(7), 373-379.

Puppala, A. J. (2008). *Estimating stiffness of subgrade and unbound materials for pavement design*. NCHRP Synthesis 382, Transportation Research Board, Washington, DC.

Puppala, A. J., Konnamas, P. and Vanapalli, S. K. (2006). Soil-water characteristic curves of stabilized expansive soils. Journal of Geotechnical and Geoenvironmental Engineering, 132(6), 736-751.

Puppala, A. J., Manosuthkij, T., Nazarian, S., Hoyos, L. R., and Chittoori, B. (2012). In situ matric suction and moisture content measurements in

expansive clay during seasonal fluctuations. Geotechnical Testing Journal, 35(1), 1-9.

Puppala, A. J., Mohammad, L. N. and Allen, A. (1996). Non-Linear Models for Resilient Modulus Characterization of Granular Soils, Proceedings of Engr. Mechanics, ASCE, New York, N.Y., USA, 1, 559-562.

Puppala, A. J., Mohammad, L. N. and Allen, A. (1999). Permanent Deformation Characterization of Subgrade Soils from RLT Test, Journal of Materials in Civil Engineering Eng., 1999, 11(4): 274-282.

Puppala, A. J., Saride, S., and Chomtid, S. (2009). Experimental and Modeling studies of permanent strains of subgrade soils. ASCE, Journal of Geotechnical and Geoenvironmental Engineering, 135(10), 1379-1389.

Rahardjo, H., Lim, T. T., Chang, M. F., and Fredlund, D. G. (1995). Shear strength characteristics of a residual soil with suction.pdf. *Canadian Geotechnical Journal*, 32, 60–77.

Rahardjo, H., Satyanaga, A., D' Amore G. A. R., and Leong, E. (2012). Soil-water characteristic curves of gap-graded soils. Engineering Geology, 125, 102-107.

Rahardjo, H., Satyanaga, A., Leong, E. C., and Wang, J. Y. (2014). Characterization of unsaturated properties of recycled materials. Unsaturated Soils: Research & Applications, N. Khalili, A. R. Russell, and A. Khoshghalb, eds., CRC Press, 81–91.

Rahardjo, H., Satyanaga, A., Leong, E.-C., and Wang, J.-Y. (2013). Unsaturated properties of recycled concrete aggregate and reclaimed asphalt pavement. Engineering Geology, 161, 44–54.

Raju, V. S., and Sadasivan, S. K. (1974). Membrane penetration in triaxial tests on sand. *Journal of the Geotechnical Engineering Division*, 100(4), 482-489.

Rampino, C., Mancuso, C., and Vinale, F. (1999). Laboratory testing on an unsaturated soil: equipment, procedures, and first experimental results. Canadian Geotechnical Journal, 36(1), 1–12.

Rampino, C., Mancuso, C., and Vinale, F. (2000). Experimental behaviour and modelling of an unsaturated compacted soil. Canadian Geotechnical Journal, 37(4), 748–763.

Rauch, A.F. (1997). *An Empirical Method for Predicting Surface Displacements Due to Liquefaction-Induced Lateral Spreading in Earthquakes*. Doctoral Dissertation, Virginia Polytechnic Institute and State University, Blacksburg, VA.

Rees, S. (2010). *Effects of Fines on the Undrained Behaviour of Christchurch Sandy Soils*. Doctoral Dissertation, University of Canterbury, Christchurch, New Zealand.

Robertson, P. K., and Wride, C. E. (1997). Cyclic liquefaction and its evaluation based on the SPT and CPT. *Proc. NCEER workshop on Evaluation of*

Liquefaction Resistance of Soils, Technical Report NCEER-97-0022, 41-88.

Rojas, J. C., Mancuso, C. and Vinale, F. (2008). A modified triaxial apparatus to reduce testing time: Equipment and preliminary results. Unsaturated Soils: Advances In Geo-Engineering, Toll et al. (eds), Taylor and Francis Group, London.

Roscoe, K. H., and Burland, J. B. (1968). On the generalized stress-strain behavior of Wet Clay, In Engineering Plasticity. J. Heyman and F. Leckie (Ed.), Cambridge University Press, Cambridge, 535-609.

Rosone, M., Airò Farulla, C., and Ferrari, A. (2016). Shear strength of a compacted scaly clay in variable saturation conditions. *Acta Geotechnica*, 11(1), 37–50.

Rout. R. K. (2012), Resilient Properties of Unsaturated Base Materials, Master's Thesis, University of Texas at Arlington, Arlington, Texas.

Rout, R. K., Ruttanapormakul, P., Valluru, S., and Puppala, A. J. (2012). Resilient moduli behavior of lime-cement treated subgrade soils. Proc. *GeoCongress 2012: State of the Art and Practice in Geotechnical Engineering*, 1428-1437.

Rowe, P. W. (1962). The stress-dilatancy relation for static equilibrium of an assembly of particles in contact. *Proc. Royal Society. A.*, 269, 500-527.

Russel, A. R. and Khalili, N. (2006). A unified bounding surface plasticity model for unsaturated. *International Journal of Numerical and Analytical Methods in Geomechanics*, 30(3), 181-212

Russell A.G., Cubrinovski, M., Cox, B., Wood, C., Wotherspoon, L., Bradley, B., and Maurer B. (2014). Select Liquefaction Case Histories from the 2010–2011 Canterbury Earthquake Sequence. *Earthquake Spectra*, 30 (1), 131-153.

Ruttanaporamakul. P. (2012), Resilient Moduli Properties of Compacted Unsaturated Subgrade Materials, Master's Thesis, University of Texas at Arlington, Arlington, Texas.

Saeedy, H. S., and Mollah, M. A. (1988). Application of multistage triaxial test to Kuwaiti soils. *ASTM STP 977*, 363–375.

Salgado, R. (2006). *The engineering of foundations*. McGraw-Hill publishing company.

Salour, F., Erlingsson, S., and Zapata, C.E. (2014). Modelling resilient modulus seasonal variation of silty sand subgrade soils with matric suction control. Canadian Geotechnical Journal, 51(12): 1413–1422.

Sauer, E.K., and Monismith, C.L. (1968). Influence of soil suction on behavior of a glacial till subjected to repeated loading. Highway Research Record, 215, Highway Research Board, Washington, D.C., 8–23.

Sawangsuriya, A., Edil, T. B., Bosscher, P. J. (2008). Modulus-suction-moisture relationship for compacted soils. Canadian Geotechnical Journal, 45, 973-983.

Schoenemann, M. R., and Pyles, M. R. (1988). Stress path considerations in multistage triaxial testing. ASTM STP 977, 732–739.

Schubert, H. (1984). Capillary Forces—Modeling and Application in Particulate Technology. Powder Technology, 37(1), 105–116.

Schuurman, I. E. (1966). The Compressibility of an Air/Water Mixture and a Theoretical Relation kimBetween the Air and Water Pressures. Géotechnique, 16(4), 269–281.

Seed, H. B. and Chan, C.K. (1957). Thixotropic Characteristics of Compacted Clays, Journal of Soil Mechanics and Foundation Engineering Division, ASCE, 83(6), 31-47.

Seed, H. B. and Chan, C.K. (1959). Structure and Strength Characteristics of Compacted Clays, Journal of Soil Mechanics and Foundation Engineering Division, ASCE, 85, No. 5, 87-128.

Seed, H. B., and Chan, C. K. (1958). Effect of Stress History and Frequency of Stress Application on Deformation of Clay Subgrades Under Repeated Loading, Proc., Highway Research Record, 37, Highway Research Board, Washington, D.C., 555-575.

Seed, H. B., and Idriss, I. M. (1971). Simplified Procedure for Evaluating Soil Liquefaction Potential. *Journal of the Soil Mechanics and Foundations Division*, 97(9), 1249–1273.

Seed, H. B., and Lee, K. L. (1965). *Studies of the liquefaction of sands under cyclic loading conditions*. Soil Mechanics and Bituminous Materials Laboratory, University of California.

Seed, H. B., Chan, C. K., and Lee, C. E. (1962). Resilience characteristics of subgrade soils and their relation to fatigue failures in asphalt pavements. Proc., Int. Conf. on the Structural Design of Asphalt Pavements, ASCE, Reston, VA, 611–636.

Seed, H.B. and Lee, K.L. (1966). Liquefaction of Saturated Sands During cyclic loading. *Journal of the Soil Mechanics and Foundations Division*, ASCE 92, 105-134.

Seed, H.B. (N.d.). Liquefaction – Lower San Fernando Dam. Retrieved from https://research.engineering.ucdavis.edu/gpa/earthquake-hazards/liquefaction-lower-san-fernando-dam (Accessed on: 04/02/2017)

Sharma R.S. (1998). Mechanical behaviour of unsaturated highly expansive clays. Ph.D. Thesis, University of Oxford, UK

Sharma, M. S. R., Baxter, C. D. P., Moran, K., Vaziri, H., and Narayanasamy, R. (2011). Strength of Weakly Cemented Sands from Drained Multistage

Triaxial Tests. *Journal of Geotechnical and Geoenvironmental Engineering*, 137(12), 1202–1210.

Sherif, M. A., Tsuchiya, C., and Ishibashi, I. (1977). Saturation effects on initial soil liquefaction. *Journal of the Geotechnical Engineering Division*, 103(8), 914–917.

Sillers, W. S. and Fredlund, D. G. (2001). Statistical assessment of soil-water characteristic curve models for geotechnical engineering. *Canadian Geotechnical Journal*, 38, 1297-1313.

Silver, M.L., Chan, C.K., Ladd, R.S., Lee, K.L., Tiedemann, D.A., Townsend, F.C., Valera, J.E., Wilson, J.H. (1976). Cyclic Triaxial Strength of Standard Test Sand. American Society of Civil Engineers, *Journal of the Geotechnical Engineering Division*, 102, 511-523.

Silver, M.L., Chan, C.K., Ladd, R.S., Lee, K.L., Tiedemann, D.A., Townsend, F.C., Valera, J.E., Wilson, J.H. (1976). Cyclic Triaxial Strength of Standard Test Sand. *Journal of the Geotechnical Engineering Division*. 102, 511-523.

Sitharam, T.G., Govindaraju, L., and Murthy, B.R.S. (2004). Evaluation of Liquefaction Potential and Dynamic Properties of Silty Sand Using Cyclic Triaxial Testing, *Geotechnical Testing Journal*, 27(5), 423-429,

Sivakumar V. (1993). *A critical state framework for unsaturated soils*. Doctoral Dissertation, University of Sheffield, U.K.

Sivakumar, V., and Wheeler, S. J. (2000). Influence of Compaction Procedure on the Mechanical Behaviour of an Unsaturated Compacted Clay Part 1: Wetting and Isotropic Compression, *Geotechnique*, 50(4), 359–368.

Sivakumar, V., Kodikara, J., O'Hagan, R., Hughes, D., Cairns, P., and McKinley, J. D. (2013). Effects of confining pressure and water content on performance of unsaturated compacted clay under repeated loading. *Geotechnique*, 63(8), 628–640.

Smith, W. S., and Nair, K. (1973). Development of procedures for characterization of untreated granular base coarse and asphalt-treated base course materials. *Rep. No. FHWA-RD-74-61*, Federal Highway Administration, Washington, D.C.

Sposito, G. (1981). *The Thermodynamics of Soil Solutions*, Oxford Clarendon Press, London.

Sridharan, A., and Narasimha Rao, S. (1972). A new approach to multistage triaxial test. *Journal of Soil Mechanics and Foundation Division*, 98(11), 1279–1286.

Stamatopoulos, C. A. (2010). An experimental study of the liquefaction strength of silty sands in terms of the state parameter. *Soil Dynamics and Earthquake Engineering*, 30(8), 662-678.

Sun, D. A., Matsouka, H., and Xu, Y. F. (2004). Collapse Behavior of Compacted Clays in Suction-Controlled Triaxial Tests, ASTM Geotech. Test. J., 27(4), 362–370.

Tami, D., Rahardjo, H., and Leong, E.-C. (2004). Effect of Hysteresis on Steady-State Infiltration in Unsaturated Slopes. *Journal of Geotechnical and Geoenvironmental Engineering*, 130(9), 956–967.

Tarantino, A. and Mongiovi, L. (2000). Experimental investigations on the stress variables governing unsaturated soil behavior at medium to high degrees, *Proc. Experimental Evidence and Theoretical Approaches in Unsaturated Soils*, Trento, 3-19.

Tatsuoka, F., Iwasaki, T., Yoshida, S., Fukushima, S., and Sudo, H. (1979). Shear modulus and damping by drained tests on clean sand specimens reconstituted by various methods. *Soils and Foundations*, 19(1), 39–54.

Tatsuoka, F., Ochi, K., Fujii, S., and Okamoto, M. (1986). Cyclic undrained triaxial and torsional shear strength of sands for different sample preparation methods. *Soils and Foundations*, 26(3), 23–41.

Taylor, D. W. (1950). A triaxial shear investigation on a partially saturated soil, Triaxial Testing of Soils and Bituminous Mixtures, ASTM STP 106, 180-191.

Terzaghi, K. (1936). The shear resistance of saturated soils. Proceedings of Ist International Conference *Soil Mechanics and Foundation Engineering*, Cambridge, MA, 1, 54-56.

Terzaghi, K. (1943). *Theoretical Soil Mechanics*, John Wiley & Sons, Inc., New York.

Thakur, V. K., Sreedeep, S., and Singh, D. N. (2005). Parameters affecting soil–water characteristic curves of fine-grained soils. *Journal of Geotechnical and Geoenvironmental Engineering*, 131(4), 521-524.

Thevanayagam, S., Fiorillo, M., and Liang, J. (2000). Effect of non-plastic fines on undrained cyclic strength of silty sands. *Proc.: Soil Dynamics and Liquefaction 2000*, GSP 107, 77-91.

Thom, N. H., and Brown, S. F. (1987). Effect of moisture on the structural performance of a crushed-limestone road base. *Transp. Res. Rec. 1121*, Transportation Research Board, Washington, D.C., 50–56.

Thom, N. H., and Brown, S. F. (1989). The mechanical properties of unbound aggregates from various sources. *Unbound aggregates in roads*, R. H. Jones and A. R. Dawson, eds., 130–142.

Thom, R., Sivakumar, V., Brown, J., and Hughes, D. (2008). A simple triaxial system for evaluating the performance of unsaturated soils under repeated loading. Geotech. Testing J., 31(2), 1–8.

Thompson, M. R. and Robnett, Q.L. (1979). Resilient Properties of Subgrade Soils. *Journal of Transportation Engineering*, ASCE, 105, No. 1, 71-89.

Toki, S., Tatsuoka, F., Miura, S., Yoshimi, Y., Yasuda, S., and Makihara, Y. (1986). Cyclic undrained triaxial strength of sand by a cooperative test program. *Soils and Foundations*, 26(3), 117-128.

Toll, D. G. (1990). A framework for unsaturated soil behaviour. *Geotechnique*, 40(1), 31-44.

Townsend, F. (1978). A Review of Factors Affecting Cyclic Triaxial Tests. *Dynamic Geotechnical Testing*, STP35686S, ASTM International, West Conshohocken, PA, 356-383.

Tsukamoto, Y., Kawabe, S., Matsumoto, J., and Hagiwara, S. (2014). Cyclic resistance of two unsaturated silty sands against soil liquefaction. *Soils and Foundations*, 54(6), 1094–1103.

Unno, T., Kazama, M., Uzuoka, R., and Sento, N. (2008). Liquefaction of unsaturated sand considering the pore air pressure and volume compressibility of the soil particle skeleton. *Soils and Foundations*, 48(1), 87–99.

USGS. 2006a. About Liquefaction. San Francisco Bay Region Geology and Geologic Hazards. Retrieved from https://geomaps.wr.usgs.gov/sfgeo/liquefaction/aboutliq.html

USGS. 2006b. Earthquakes That Have Caused Liquefaction in the San Francisco Bay Area. San Francisco Bay Region Geology and Geologic Hazards. Retrieved from https://geomaps.wr.usgs.gov/sfgeo/liquefaction/eq_caused.html

Uzan, J. (1985). Characterization of granular material. *Transp. Res. Rec. 1022*, Transportation Research Board, Washington, D.C., 52–59.

Vaid, Y. P., and Chern, J. C. (1983). Mechanism of deformation during cyclic undrained loading of saturated sands. *Soil Dynamics and Earthquake Engineering*, 2(3), 171–177.

Vaid, Y. P., and Sivathayalan, S. (1996). Static and cyclic liquefaction potential of Fraser Delta sand in simple shear and triaxial tests. *Canadian Geotechnical Journal*, 33(2), 281-289.

Vaid, Y.P., and Negussey, D. (1984). A critical assessment of membrane penetration in the triaxial test. *Geotechnical Testing Journal*, 7(2), 70–76

Vaid, Y.P., Sivathayalan, D.S., and Stedman, D. (1999). Influence of specimen reconstituting method on the undrained response of sand. *Geotechnical Testing Journal*, 22(3), 187–195

Van Genuchten, M. T. (1980). A closed-form equation for predicting the hydraulic conductivity of unsaturated soils. *Soil science society of America journal*, 44(5), 892-898.

Vanapalli, S. K., and Fredlund, D. G. (2000). Comparison of different procedures to predict unsaturated soil shear strength. *Advances in Unsaturated Geotechnics*, 195-209.

Vanapalli, S. K., Fredlund, D. G., and Pufahl, D. E. (1999). The influence of soil structure and stress history on the soil–water characteristics of a compacted till. *Geotechnique*, 49(2), 143–159.

Vanapalli, S. K., Fredlund, D. G., Pufahl, D. E. and Clifton, A. W. (1996). Model for the prediction of shear strength with respect to soil suction. *Canadian Geotechnical Journal*, 33, 379-392.

Vanapalli, S. K., Sillers, W. S. and Fredlund, M. D. (1998). The meaning and relevance of residual state to unsaturated soils. *51st Canadian Geotechnical Conference*, Edmonton, Alberta, October 4-7, 1-8.

Vanapalli, S.K. (1994). *Simple Test Procedures and their Interpretation in Evaluating the Shear Strength of an Unsaturated Soil*. Doctoral Dissertation, University of Saskatchewan, Saskatoon, Canada.

Vilar, O. M. (2006). A simplified procedure to estimate the shear strength envelope of unsaturated soils. *Canadian Geotechnical Journal*, 43(10), 1088-1095.

Wang, H., Koseki, J., Sato, T., Chiaro, G., and Tan Tian, J. (2016). Effect of saturation on liquefaction resistance of iron ore fines and two sandy soils. *Soils and Foundations*, 56(4), 732–744.

Wang, W. (1984). Earthquake Damages to Earth Dams and levees in Relation to Soil Liquefaction. Proceedings of the International Conference on case Histories on Geotechnical Engineering, 1984.

Wheeler S.J. (1988). The undrained shear strength of soils containing large gas bubbles. *Géotechnique*, 38(3):399–413.

Wheeler, S. J., and Sivakumar, V. (1995). An elastic-plastic critical state framework for unsaturated soil. *Geotechnique*, 451, 35–53.

Wheeler, S. J., and Sivakumar, V. (2000). Influence of Compaction Procedure on the Mechanical Behaviour of an Unsaturated Compacted Clay, Part 2: Shearing and Constitutive Modeling, *Geotechnique*, 50(4), 369–376.

Wilson, B. E., Sargand, S. M., Hazen, G. A., and Green, R. (1990). Multiaxial Testing of Subgrade, Transportation Research Record, 1278, TRB, National Research Council, Washington, D.C., 91-95.

Witczak, M. W., and Uzan, J. (1988). The universal airport pavement design system, Report I of IV: Granular material characterization. University of Maryland, College Park, MD.

Witczak, M.W. (2003). NCHRP 1-28A: Harmonized test method for laboratory determination of resilient modulus for flexible pavement design. Final Report, TRB, National Research Council, Washington, D.C.

Wong, R. T., Seed, H. B., and Chan, C. K. (1974). Liquefaction of gravelly soils under cyclic loading conditions. Report No. UCB/EERC-74/11, Earthquake

Engineering Research Center, College of Engineering, University of California, Berkeley, California.

Wood, D. M. (2004). *Geotechnical modelling*. Spon Press, New York.

Wood, D.M. (1990). *Soil Behavior and Critical State Soil Mechanics*, Cambridge University Press, New York.

Wood, F. M., Yamamuro, J. A., and Lade, P. V. (2008). Effect of depositional method on the undrained response of silty sand. *Canadian Geotechnical Journal*, 45(11), 1525–1537.

Wood, F.M., and Yamamuro, J.A. (1999). The effect of depositional method on the liquefaction behavior of silty sand. *Proc.: 13th ASCE Engineering Mechanics Conference*, Johns Hopkins University, Baltimore, Maryland

Xenaki, V. C., and Athanasopoulos, G. A. (2003). Liquefaction resistance of sand–silt mixtures: an experimental investigation of the effect of fines. *Soil Dynamics and Earthquake Engineering*, 23(3), 1-12.

Xenaki, V. C., and Athanasopoulos, G. A. (2008). Dynamic properties and liquefaction resistance of two soil materials in an earthfill dam—Laboratory test results. *Soil Dynamics and Earthquake Engineering*, 28(8), 605-620.

Xia, H., and Hu, T. (1991). Effects of saturation and back pressure on sand liquefaction. *Journal of Geotechnical Engineering*, 1347–1362.

Xu, J. (2012). Liquefaction Potential of Unsaturated Nevada Sand at Different Initial Conditions, Master's Thesis, University of South Carolina, Columbia, SC.

Yamamuro, J. A., Wood, F. M., and Lade, P. V. (2008). Effect of depositional method on the microstructure of silty sand. Canadian Geotechnical Journal, 45(11), 1538–1555.

Yang, J., Savidis, S., and Roemer, M. (2004). Evaluating liquefaction strength of partially saturated sand. *Journal of Geotechnical Engineering Division*, 130(9), 975–979.

Yang, S. R., Huang, W. H., and Tai, Y. T. (2005). Variation of resilient modulus with soil suction for compacted subgrade soils. Transportation Research Record,1913, Transportation Research Board, Washington, D.C., 99–106.

Yang, S. R., Lin, H. D., Kung, J. H., and Huang, W. H. (2008). Suction-controlled laboratory test on resilient modulus of unsaturated compacted subgrade soils. *Journal of Geotechnical and Geoenvironmental Engineering*, 134(9): 1375–1384.

Yoshimi, Y., Tanaka, K., and Tokimatsu, K. (1989). Liquefaction resistance of a partially saturated sand. *Soils and Foundations*, 29(3), 157–162.

Youd, T. L., and Hoose, S. N. (1978). *Historic ground failures in northern California triggered by earthquakes.* U.S. Geological Survey professional paper 993, U.S. Govt. Printing Office, Washington, D.C., 1-177.

Youd, T. L., and Perkins, D. M. (1978). Mapping liquefaction-induced ground failure potential. *Journal of the Soil Mechanics and Foundations Division*, *104*(4), 433-446.

Youd, T. L., Harp, E. L., Keefer, D. K., and Wilson, R. C. (1985). The Borah Peak, Idaho earthquake of October 28,1983 – Liquefaction. *Earthquake Spectra*, 2(1), 71–89.

Youd, T.L., Idriss, I.M., Andrus, R.D., Arango, I., and Castro, G. et al. (2001). Liquefaction Resistance of Soils: Summary Report from the 1996 NCEER and 1998 NCEER/NSF Workshops on Evaluation of Liquefaction Resistance of Soils *Journal of Geotechnical and Geoenvironemntal Eng*., ASCE, 127(10), 817-833.

Yu, H. S. (2006). *Plasticity and geotechnics*. Springer, New York.

Zhang, B., Muraleetharan, K. K., and Liu, C. (2016). Liquefaction of Unsaturated Sands. *International Journal of Geomechanics*, 16(3).

Zhang, L. L., Fredlund, D. G., Zhang, L. M., and Tang, W. H. (2004). Numerical study of soil conditions under which matric suction can be maintained. *Canadian Geotechnical Journal*, 41, 569-582.

Zhang, L., and Chen, Q. (2005). Predicting bimodal soil-water characteristic curves. *Journal of Geotechnical and Geoenvironmental Engineering*, 131(5), 666-670.

Zhang, Y., Ishikawa, T., Tokoro, T., and Nishimura, T. (2014). Influences of degree of saturation and strain rate on strength characteristics of unsaturated granular subbase course material. *Transportation Geotechnics*, 1(2), 74–89.

Zlatovic, S., and Ishihara, K. (1997). Normalized behavior of very loose non-plastic soils: effects of fabric. *Soils and Foundations*, 37(4), 47–56.

BIOGRAPHICAL INFORMATION

Aritra Banerjee was born on December 30, 1987 in Asansol, West Bengal, India. He graduated from National Institute of Technology (NIT) Calicut, Kerala, India, with a Bachelor's degree in Civil Engineering in May 2011. After working in Jindal Steel and Power Limited as a Graduate Engineer, he pursued Master's in Civil Engineering with a specialization in Geotechnical Engineering from Indian Institute of Technology (IIT) Roorkee, Uttarakhand, India. In IIT Roorkee, he examined on the influence on the construction of twin tunnels on ground subsidence and building distress by using Finite Element Methods.

In 2014, he joined the doctoral program in Department of Civil Engineering at University of Texas at Arlington. He studied the influence of suction on the behavior of soils when subjected to monotonic and dynamic loading, under the guidance of Prof. Anand J. Puppala. He successfully defended his dissertation in April 2017.